ISTANBUL RUMELI UNIVERSITY 1ST INTERNATIONAL SCIENTIFIC RESEARCH CONFERENCE ON SUSTAINABLE ENGINEERING AND TECHNOLOGY

PROCEEDING BOOK

ISBN: 978-605-73381-1-2

T.C. İSTANBUL RUMELİ ÜNİVERSİTESİ

University of BONAB

30 years Varna Free University

The University Of Sheffield.

UAEU

جامعة الإمارات العربية المتحدة
United Arab Emirates University

rumeliconferences@gmail.com

RUMELI 1ST INTERNATIONAL SCIENTIFIC RESEARCH CONFERENCE ON SUSTAINABLE ENGINEERING AND TECHNOLOGY (ISRCSET'22)

MAY 13- 15, 2022 - ISTANBUL

Issued: 25.05.2022

ISBN: 978-605-73381-1-2

CONFERENCE ID

RUMELI 1ST INTERNATIONAL SCIENTIFIC RESEARCH CONFERENCE ON SUSTAINABLE ENGINEERING AND TECHNOLOGY (ISRCSET'22)

DATE – PLACE

MAY 13- 15, 2022
ISTANBUL

ORGANIIZATION

International Scientific Research and Strategy Development Association
T.C. Istanbul Rumeli University.

EVALUATION PROCESS

All applications have undergone a double-blind peer review process.

PRESENTATION

Poster and Oral Presentation

PERCENTAGE OF PRESENTATION

40% form Turkey and 60% from other Countries

PARTICIPATED COUNTRIES

Turkey – Iran – India- Tunisia- Germany – Poland- Uganda- Ghana - Senegal- Greece- KSA- UK- Egypt- Colombia- Algeria- Philippines – Czech Republic- UAE- Amman- Morocco- Japan- Libya- Kosovo – Bangladesh – Indonesia - Saudi Arabia

Scientific & Review Committee

Prof. Dr. Hasan ARMAN

United Arab Emirates University - UAE

Prof. Dr. Omer YUKSEK

Karadeniz Technical University, Türkiye

Prof. Dr. Ahmet CAN

Istanbul Rumeli University, Türkiye

Prof. Dr. Yusuf AYVAZ

Yildiz Technical University, Türkiye

Prof. Dr. Suat AKBULUT

Yildiz Technical University, Türkiye

Prof. Dr. Barış SEVİM

Yildiz Technical University, Türkiye

Prof. Dr Yasar NUHOGLU

Yildiz Technical University, Türkiye

Prof. Dr. Hüseyin SERENCAM

Trabzon University, Türkiye

Prof. Dr. Beyhan BOLAK HISARLIGIL

Istanbul Rumeli University, Türkiye

Prof. Dr. İlyas Erdal KEREY

Istanbul Rumeli University, Türkiye

Prof. Dr. İlhan OSMANŞAHİN

Istanbul Rumeli University, Türkiye

Prof. Dr. Hakan HISARLIGIL

Istanbul Rumeli University, Türkiye

Assist. Prof. Dr. Kemal Hakan TEKIN

Istanbul Rumeli University, Türkiye

Assist. Prof. Dr. Hatice GUNER

Istanbul Rumeli University, Türkiye

Assist. Prof. Dr. Cenk GUNGOR

Istanbul Rumeli University, Türkiye

Assist. Prof. Dr. Ali COSAR

Yildiz Technical University, Türkiye

Assist. Prof. Dr. M. Sinan Yardım

Yildiz Technical University, Türkiye

Assist. Prof. Dr. S.Ayhan GAZIOGLU

Yildiz Technical University, Türkiye

Assist. Prof. Dr. Gulmira ABDİRASULOVA

Kazakh State Kizlar University, Kazakhstan

Assist. Prof. Dr. Omid AFGHAN

Kabul University, Afghanistan

Assist. Prof. Dr. Maha Hamdan ALANAZİ

Riyad Kral Abdulaziz Technology Instıtute, S, Arabia

Assist. Prof. Dr. Dzhakipbek Altaevich ALTAYEV

Al – Farabi Kazak Milli Üniversity, Kazakhstan

Assist. Prof. Dr. Amina Salihi BAYERO

Yusuf Maitama Sule University, Nigeria

Assist. Prof. Dr. Karligash BAYTANASOVA

Al – Farabi Kazak University, Kazakhstan

Assist. Prof. Dr. Baurcan BOTAKARAEV

Hoca Ahmet Yesevi University, Kazakhstan

Assist. Prof. Dr. Ahmad Sharif FAKHEER

Jordanian State University, Jordan

Assist. Prof. Dr. Bazarhan İMANGALİYEVA

K.Zhubanov Aktobe State University, Kazakhstan

Assist. Prof. Dr. Keles Nurmaşulı JAYLIBAY

Kazakh State Kizlar University, Kazakhstan

Assist. Prof. Dr. Mamatkuli Jurayev

Science Academy of Ozbekistan

Assist. Prof. Dr. Kalemkas KALIBAEVA

Kazakh State Kizlar University, Kazakhstan

Assist. Prof. Dr. Bouaraour Kamel

Ghardaia University, Algeria

Assist. Prof. Dr. Sonali MALHOTRA

Delhi Balbahtri Academy, India

Assist. Prof. Dr. Alia R. MASALİMOVA

Al – Farabi Kazak University, Kazakhstan

Assist. Prof. Dr. Amanbay MOLDIBAEV

Taraz State University, Kazakhstan

Assist. Prof. Dr. Gulşat ŞUGAYEVA

Dosmukhamedov Atyrau State University, Kazakhstan

Assist. Prof. Dr. K.A. TLEUBERGENOVA

Kazakh State Kizlar University, Kazakhstan

Assist. Prof. Dr. Cholpon TOKTOSUNOVA

Rasulbekov Kırgız University, Kyrgyzstan

Assist. Prof. Dr. Botagul TURGUNBAEVA

Kazakh State Kizlar University, Kazakhstan

Assist. Prof. Dr. Dinarakhan TURSUNALİEVA

Rasulbekov Kırgız University, Kyrgyzstan

Assist. Prof. Dr. Yang ZİTONG

Wuhan University, China

Rumeli 1ST International Scientific Research Conference On Sustainable Engineering And Technology (ISRCSET'22) MAY 13 - 15, 2022 - ISTANBUL

CONGRESS PROGRAM

Online (with Video Conference) Presentation

Meeting ID: 853 4114 7994
Passcode: 140522

IMPORTANT, PLEASE READ CAREFULLY

- To be able to make a meeting online, login via https://zoom.us/join site, enter ID instead of "Meeting ID
- or Personal Link Name" and solidify the session.
- The Zoom application is free and no need to create an account.
- The Zoom application can be used without registration.
- The application works on tablets, phones and PCs.
- Speakers must be connected to the session **10 minutes before** the presentation time.
- All congress participants can connect live and listen to all sessions.
- During the session, your camera should be turned on **at least** %70 of session period
- Moderator is responsible for the presentation and scientific discussion (question-answer) section of the session.

TECHNICAL INFORMATION

- Make sure your computer has a microphone and is working.
- You should be able to use screen sharing feature in Zoom.
- Attendance certificates will be sent to you as pdf at the end of the congress.
- Moderator is responsible for the presentation and scientific discussion (question-answer) section of the session.
- Before you login to Zoom please indicate your name surname and hall number,

exp. H-2, S- 1 NAME SURNAME

Opening Speach 10 : 00 – 10 : 25 (Turkey Local Time)

Prof. Dr. Ibrahim YUKSEL - Chairman of the Conference

10:00 – 10:10

Prof. Dr. Hazım Tamer DODURKA - Istanbul Rumeli University -Rector

10:15 – 10:25

Rumeli 1ST International Scientific Research Conference On
Sustainable Engineering And Technology (ISRCSET'22)
MAY 13- 15 , 2022 - ISTANBUL

HALL 1 – SESSION 1	Meeting ID: 853 4114 7994	Passcode: 140522
14.05.2022 10:30- 12:00 (Turkey Local Time)	INVITED SPEAKER : PROF. DR. SUAT AKBULUT	
	MODERATOR: ASST. PROF., ELIF EBRU ERMIS	

Authors	Topic Title
PROF. DR. SUAT AKBULUT	**Nanotechnological Modification of Clay Soil in geotechnical Engineering.**
OKTAY ÇAVUŞOĞLU HAKAN AYDIN HALUK DİNKCİ AHMET GÜRKAN YILMAZOĞLU UĞUR ÜZEL	Yeni Nesil Birleştirme Teknolojileri Kendinden Kilitlemeli Perçinleme
OKTAY ÇAVUŞOĞLU HAKAN AYDIN AHMET GÜRKAN YILMAZOĞLU UĞUR ÜZEL SÜLEYMAN İNCE	**AISI 304 Kalite Östenitik Paslanmaz Çeliğin Kaynak Parametrelerinin Mekanik Özelliklere Etkisi**
ASST. PROF. DR. SERTAÇ TUHTA	Determination Of Jacketing Of Beams On Dynamic Parameters Of RC Structure
ASST. PROF. DR. SERTAÇ TUHTA	**Effect Of Wing Wall On Dynamic Parameters Of Reinforced Concrete Chimney**
MOHAMMAD REZA AKHTARI SEYED AMIN TABATABAEI YAMCHI MIR SHAHRIAR HASHEMI ZONOZI SALAR SHATERI AMIR AMINZADEH GHAVIFEKR	Optimal Mixing Design of Fiber Self-Compacting Concrete and its Effect on the Compressive Strength of Concrete for Different Grades
ASST. PROF., ELIF EBRU ERMIS PROF. DR., CUNEYT CELIKTAS	Revealing 137Cs Photopeak By Multi-Pixel Photon Counter
ASST. PROF. DR. FURKAN GÜNDAY	Investigation Of Jacketing Of Columns Effect On Dynamic Parameters Of Reinforced Concrete Building
ASST. PROF. DR. FURKAN GÜNDAY	**Research Of Jacketing Of Shear Walls On Dynamic Parameters Of RC Structure**

HALL 2 – SESSION 1 Meeting ID: 853 4114 7994 Passcode: 140522

14.05.2022 10:30- 12:00 (Turkey Local Time) INVITED SPEAKER : Assoc. Prof. Dr. Iman HAJIRASOULIHA

MODERATOR: DR. ÖĞR. ÜYE. BANU BULUT ACAR

Authors	Topic Title
ASSOC. PROF. DR. IMAN HAJIRASOULIHA	Recent Advances In Optimum Seismic Design Of Structures Equipped With Energy Dissipation Devices
SENA NUR ASLAN DR. ÖĞR. ÜYESI TÜLAY KORKUSUZ POLAT	**Treyler Üretimi Yapan Bir İşletmede Üretim Planlama İçin İyileştirme Çalışması**
MİHRİCAN ERDOĞAN DR. ÖĞR. ÜYESI TÜLAY KORKUSUZ POLAT	Bir Döküm Fabrikasında Üretim Kapasitesini Ve Verimliliğini Arttırma Çalışması
EMRE YUMURTACI ALTUĞ BAKIRCI SEVDA TELLİ ÇETİN	**Bir Otomobil Motor Alt Braket Sacının Kabartma Tiplerine Bağlı Olarak Doğal Frekansının Artırılması**
AYSUN ŞENGÜL SONER ÇELEN HERKAİL ÖZEN	Kuvars Kumunun Akışkan Yataklı Kurutucuda Kurutulmasının Deneysel İncelenmesi
AMIT KUMAR	**Power Quality Improvement For Non Linear Load Using Six Pulse Converter With Passive Shunt Filter**
ASSOC. PROF. DR. İLKER ÖRS LECTURER SAVAŞ YELBEY ASSOC. PROF. DR. SELÇUK SARIKOÇ	Environmental Impacts Of Use Of Biodiesel Produced From Waste Cooking Oils In Diesel Engines
ARŞ. GÖR. YETKİN KARABULUT DR. ÖĞR. ÜYESİ YILDIZ KOÇ	**Spin-On Tipi Yağ Filtresinin Hesaplamalı Akışkanlar Dinamiği Yöntemiyle Analizi**
DR. ÖĞR. ÜYE. BANU BULUT ACAR	FeCrAl/U3Si2 Yakıtın Standart UO2 /Zr Yakıtı İle Aynı Yanma Oranına Ulaşması İçin Gerekli Zenginliğinin Belirlenmesi

SAYED AMIR HAMZEH MIRKHESHTI	**Economic Evaluation Offshore Wind Project under Uncertainly and Risk Circumstances**

HALL 3 – SESSION 1 Meeting ID: 853 4114 7994 Passcode: 140522

14.05.2022 10:30- 12:00 (Turkey Local Time) INVITED SPEAKER : PROF. DR. HASAN ARMAN

MODERATOR: DOÇ. DR. GÜRDAL KANAT YÜKSEK

Authors	Topic Title
PROF. DR. HASAN ARMAN PROF. DR. ALA ALDAHAN ASSOC. PROF. DR. OSMAN ABDELGHANY MSC. SAFWAN PARAMBAN	Evaluating Geoengineering Properties Of Evaporitic Rocks From The City Of Abu Dhabi, United Arab Emirates (UAE): Overview And Data Base Generation
NURTEN DEVA **MUHARREM ZABELI**	**Utilization Of Wastes As Alternative Raw Material In Cement Industry**
HARİTA MÜHENDİSİ GÜRHAN DEMİRTAŞ PROF. DR. HEDİYE ERDOĞAN	Kadastro Paftalarının Yenileme Sonrası Değerlendirilmesi
MD. SHARAFAT CHOWDHURY **ASSIS. PROF. BIBI HAFSA**	**Performance of Binary Logistic Regression and Random Forest Model in Creating GIS based Landslides Susceptibility Map at Rangamati Metropolitan Area, Bangladesh**
ASSOC. PROF. KHANDAKAR HASAN MAHMUD RAJU AHMED MD. ABU SAYEID JANNATUN HUSSNA TUYA	Earthquake Spatial Zoning Of Bangladesh: A Study On The Spatial Autocorrelation Between Earthquake Epicenters And Geo-Tectonic Fault Lines
MÜH. MERVE ÖZGEL **DOÇ. DR.,GÜRDAL KANAT YÜKSEK** **MÜH. BEKİR TOMBUL**	**Pb Ağır Metali İçeren Baca Gazı Tozunun Solidifikasyon/Stabilizasyon Prosesiyle Bertaraf Edilebilirliğinin İncelenmesi**
HARİTA MÜHENDİSİ FURKAN KOCAMAN PROF. DR. HEDİYE ERDOĞAN	Coğrafi Bilgi Sisteminde Kanalizasyon Ve İçme Suyu Altyapı Bilgi Sistemi Oluşturulması
PROF. DR. IBRAHİM YUKSEL	Hydroelectric Potentials Of Small Streams Without Flow Measurement Stations In The Euphrates And Tigris Basins: A Case Study In Batman Basin

HALL 4 – SESSION 1 Meeting ID: 853 4114 7994 Passcode: 140522

14.05.2022 10:30- 12:00 (Turkey Local Time)

MODERATOR: DR. ÖĞR. ÜYESİ TUBA ÖZTÜRK

Authors	Topic Title
ASSOC. PROF. EHSAN SHAHGHASEMI	Human Sustainable Development: Welfare and Happiness in Iran
MBA, OKECHUKWU JOSHUA	**An Overview on Metaverse Tourism and Blockchain Technology and How It Can Revolutionize the Hospitality Industry**
HAYRİ YIGIT ALİ RİFAT BOYNUEGRI	Design And Implementation Of A Low-Cost Laser Diode Driver For Wireless Power Transmission
DR. ÖĞR. ÜYESİ, İSMAİL AKGÜL DR. ÖĞR. ÜYESİ, VOLKAN KAYA	**Review On Artificial Neural Networks**
DR. ÖĞR. ÜYESİ TUBA ÖZTÜRK	Evaluation Of Technological Development Within The Contex Of Environmental Sustainability Approach
AYHAN TOKMAK DOÇ. DR. ÖVGÜ CEYDA YELGEL	**Yapay Sinir Ağları İle Rüzgar Gücü Tahmini**
TADASHI WATANABE	Numerical Simulation of the Transient Shape Variation of a Rotating Liquid Droplet
ARŞ. GÖR., BELKIZ TORĞUL PROF. DR., TURAN PAKSOY	**Blok Zincir Uygulamaları İle Kapalı Döngü Tedarik Zincirinde Bilgi Yönetiminin Değeri**
UMUT BABAYİĞİT ASSOC. PROF. ALİ GEZER	DNS Based Scanning Approach For Trickbot Banking Trojan Detection
RECEP YILDIRIM DR. ÖĞR. ÜYESI, SINEM AKYOL	**Doğal Dil İşleme Yöntemleri ile Sosyal Medya Paylaşımlarında Depresyon Tespiti**
NORAZAM ARBIN ISHAK HASHIM	**Double-Diffusive Natural Convection with Marangoni and Cooling Effects**

HALL 5 – SESSION 1 Meeting ID: 853 4114 7994 Passcode: 140522

14.05.2022 10:30- 12:00 (Turkey Local Time)

MODERATOR: ABDULLAH ÖZKÖSE

Authors	Topic Title
PETR HOMOLA ROMAN RŮŽEK	Laser Beam Micro-Drilling Effect on Ti-6Al-4V Titanium Alloy Sheet Properties
ARITRAS ROY **RINKU MUKHERJEE**	**Unsteady 3D Post-Stall Aerodynamics Accounting for Effective Loss in Camber Due to Flow Separation**
NISRIN R. ABDELAL STEVEN L. DONALDSON	The Effect of Nylon and Kevlar Stitching on the Mode I Fracture of Carbon/Epoxy Composites
ASSEM M. F. SALLAM **AH. EL-S. MAKLED**	**Two-Stage Launch Vehicle Trajectory Modeling for Low Earth Orbit Applications**
ABDULLAH ÖZKÖSE AHMET TAMKOÇ	Determination of Agricultural Characteristics of Smooth Bromegrass (Bromus inermis Leyss) Lines under Konya Regional Conditions
SHASHI SHARMA **V. K. KATIYAR** **UADAY SINGH**	**Mathematical Modeling on Capturing of Magnetic Nanoparticles in an Implant Assisted Channel for Magnetic Drug Targeting**
HAITHEM ELDERRAT **HUW DAVIES** **EMMANUEL BROUSSEAU**	Improving the Exploitation of Fluid in Elastomeric Polymeric Isolator
YOUSSEF KHMOU SAID SAFI MILOUD FRIKEL	Generalized Maximum Entropy Method for Cosmic Source Localization
PRAVEEN SARASWAT **RUDRAMAN SINGH**	**MHD Unsteady Free Convection of Heat and Mass Transfer Flow through Porous Medium with Time Dependent Suction and Constant Heat Source/Sink**
MOHAMMAD HASSAN HEIDARI AMIR HOSSEIN GOODARZI MAJID AZARNIUSH	Evolution of Cord Absorbed Dose during of Larynx Cancer Radiotherapy, with 3D Treatment Planning and Tissue Equivalent Phantom

ARESH VIKRAM SINGH **SARIKA NAGAR**	**Synthesis and Application of Tamarind Hydroxypropane Sulphonic Acid Resin for Removal of Heavy Metal Ions from Industrial Wastewater**

HALL 6 – SESSION 1 Meeting ID: 853 4114 7994 Passcode: 140522

14.05.2022 10:30- 12:00 (Turkey Local Time)

MODERATOR: SAFAK ISIK

Authors	Topic Title
SANDHYA DIXIT TILAK RAJ	A TISM Model for Structuring the Productivity Elements of Flexible Manufacturing System
NAMEESH MIGLANI RAJEEV SAHA R. S. PARIHAR	**A Graph Theoretic Approach for Quantitative Evaluation of NAAC Accreditation Criteria for the Indian University**
SAFAK ISIK OZALP VAYVAY	Selection of Strategic Suppliers for Partnership: A Model with Two Stages Approach
NAVEEN VIRMANI RAJEEV SAHA RAJESHWAR SAHAI	**Identifying and Ranking Critical Success Factors for Implementing Leagile Manufacturing Industries Using Modified TOPSIS**
AMIR HADI ZIAIE	682 Non-Singular Gravitational Collapse of a Homogeneous Scalar Field in Deformed Phase Space
EL-SADEK H. NOUR EL-DEEN K. HARBY	**Solar-Powered Adsorption Cooling System: A Case Study on the Climatic Conditions of Al Minya**
ABBAS AL-REFAIE	Cluster Analysis of Customer Churn in Telecom Industry
AHMED NOUAINIA MOHAMED HAJJI TAOUFIK AGUILI	**Application of MoM-GEC Method for Electromagnetic Study of Planar Microwave Structures: Shielding Application**
EMAD ALENANY M. ADEL EL-BAZ	Modelling a Hospital as a Queueing Network: Analysis for Improving Performance
HUBERT KLAR	**Dominant Correlation Effects in Atomic Spectra**
AVDHESH K. SHARMA	Modeling Drying and Pyrolysis of Moist Wood Particles at Slow Heating Rates

HALL 1 – SESSION 2	Meeting ID: 853 4114 7994	Passcode: 140522
14.05.2022 **14:00 – 16:00 (Turkey Local Time)**		
		MODERATOR: CENK GÜNGÖR
Authors	**Topic Title**	
PROF. DR. ERGÜN ERÇELEBI İBRAHIM HALIL POLAT	Gerçek Zamanlı Plaka Tanıma Sistemi (Raspberry PI Ve Phyton İle)	
YUSUF TUNÇAY **CENK GÜNGÖR**	**Application Of Radial Basis Functions Method To Advection- Diffusion Problem**	
CHEMICAL ENGINEER, ÖZGE DOYRANLI ASSOC. PROF. DR. HASAN ŞILDIR	Techno-Economic Analysis Of FDCA Production From Biomass And Bioethanol As A Co-Product	
ARŞ. GÖR. DR. ERMAN ÇELİK	**Investigation Of Biomimicry Approaches On Design Of Energy Harvesting Devices From Water Motion**	
ORHAN URAS KURTULUŞ	Challenge of Matrix-Light Technology on Automotive Exterior Lighting	
ELNAZ LASHGARI **EMEL DEMIRCAN**	**Electromyography Pattern Classification with Laplacian Eigenmaps in Human Running**	
FURKAN YANIK DR. ALİ RIFAT BOYNUEĞRİ DR. YAVUZ EREN	Delivery Operations In Warehouses By Ultracapacitor Powered Drones	

HALL 2 – SESSION 2 Meeting ID: 853 4114 7994 Passcode: 140522

14.05.2022 14:00 – 16:00 (Turkey Local Time)

MODERATOR: ARMAN ATASOY

Authors	Topic Title
PROF. DR. İSMET SEZER	A Review Study On The Effects Of Dimethyl Ether On NOx Emissions In Diesel Engines
PROF. DR. İSMET SEZER	**A Review Study On The Effects Of Dimethyl Ether On PM Emissions In Diesel Engines**
FATEMEH MEHRI ARMAN ATASOY SOMAYEH MOLLAEI MEHDI BABAEI FAKHRADDIN GHAHRAMANI	Application Of Grasshopper Optimization Algorithm In Design Process Of Lead Rubber Bearing Seismic Isolator
DR. HALE BAKIR	**The Detection Of Deteriorated PV Modules In Turkey**
DR. HALE BAKIR	FV Panellerde Arıza Tespiti Ve Analizi
YUNUS SEVİM	A Study of an Improvement Median Filter for Impulse Noise
MELİKE KOCA CEYHUN YILDIZ Ö. FATİH KEÇECİOĞLU	Sayısal Hava Tahmin Verileri Ve Makine Öğrenmesi Algoritmalarının Türkiye'de Gün Öncesi Güneş Enerji Tahmini İçin Kullanılması: Eskişehir İlinde Şebekeye Bağlı Bir Güneş Enerjisi Santralinde Örnek Uygulama
ÖĞR. GÖR. EMRE YILMAZ	**Eksenel Yük Etkisindeki Aramid Fiber Takviyeli Epoksi Matris Kompozit Plakların Farklı Fiber Açılarının Deformasyon Değişimine Etkilerinin İncelenmesi**
FATIMA ZOHRA RAHOU A. GUEN BOUAZZA B. BOUAZZA	Simulation of High Performance Nanoscale Partially Depleted SOI n-MOSFET Transistors

HALL 3 – SESSION 2	Meeting ID: 853 4114 7994	Passcode: 140522
14.05.2022 14:00 – 16:00 (Turkey Local Time)		
	MODERATOR: PROF. DR. AYDIN BAŞARIR	
Authors	Topic Title	
KEMAJL ZEQIRI	**The Indirect Impact Of Mining On Social-Wellbeing - Case Of Kosovo's Surface Coal Mines**	
PROF. DR. AYDIN BAŞARIR PROF. DR. HASAN ARMAN	The Impacts Of Climate Change And Socio-Economic Factors On Food Security: A Case Study Of United Arab Emirates	
PROF. DR. AYDIN BAŞARIR **MUMIN DAYAN**	**Factors Affecting Sustainable Food Innovations of Manufacturers: A Case Study of United Arab Emirates Food Industry**	
DR. ŞAKIR YILMAZ	Degradation Of Toxic Pollutant Catalyzed By Silver Nanoparticles Supported On Aloe Vera Leaves	
DR.ÖĞR.ÜYESİ GAMZE BİLGEN **MURAT DUYSAK**	**Türkiye Deprem Ve Kurtarma Çalışmaları**	
MURAT DUYSAK DR.ÖĞR.ÜYESİ GAMZE BİLGEN	Türkiye Sel Felaketleri: Giresun Örneği	
PROF.DR. ABDULLAH KAYGUSUZ **DOÇ.DR. ALAADDIN VURAL**	**Budak (Torul / Gümüşhane) Ve Çevresindeki Geç Kretase Yaşlı Volkanik Kayaçların Petrografik Ve Jeokimyasal Özellikleri**	
DOÇ.DR. ALAADDIN VURAL PROF.DR. ABDULLAH KAYGUSUZ	Yumrudağı Volkaniklerinin (Çanakkale/Türkiye) Genel Jeolojisi, Petrografisi Ve Jeokimyası	

HALL 4 – SESSION 2	Meeting ID: 853 4114 7994	Passcode: 140522
14.05.2022 14:00 – 16:00 (Turkey Local Time)		
	MODERATOR: AYMEN LAADHARI	
HAMDY M. YOUSSEF **EMAN A. AL-LEHAIBI**	**Adomian's Decomposition Method to Generalized Magneto-Thermoelasticity**	
MADHU ANEJA SAPNA SHARMA	Numerical Approach to a Mathematical Modeling of Bioconvection Due to Gyrotactic Micro-Organisms over a Nonlinear Inclined Stretching Sheet	
YİANNİS G. SMİRLİS	**Classifying and Predicting Efficiencies Using Interval DEA Grid Setting**	
MAATOUG HASSİNE MOURAD HRİZİ	Topological Sensitivity Analysis for Reconstruction of the Inverse Source Problem from Boundary Measurement	
R. SEKULA	**Material Concepts and Processing Methods for Electrical Insulation**	
ALLURU GOPALA KRİSHNA THELLA BABU RAO	Performance Assessment of Carbon Nano Tube Based Cutting Fluid in Machining Process	
AYHAN AYDOĞDU **ERCAN CEYHAN** **ALİ KAHRAMAN** **NURSEL ÇÖL**	**Effects of Plant Densities on Seed Yield and Some Agricultural Characteristics of Jofs Pea Variety**	
AYMEN LAADHARİ	An Implicit Methodology for the Numerical Modeling of Locally Inextensible Membranes	
AHMAD H. ABDELGWAD	**Microstrip Patch Antenna Enhancement Techniques**	
LOCHAN BASYAL	Email Based Global Automation with Raspberry Pi and Control Circuit Module: Development of Smart Home Application	

LOCHAN BASYAL	**Email Based Global Automation with Raspberry Pi and Control Circuit Module: Development of Smart Home Application**

HALL 5 – SESSION 2 Meeting ID: 853 4114 7994 Passcode: 140522

14.05.2022 14:00 – 16:00 (Turkey Local Time)

MODERATOR: NURLIANI, IDA ROSADA

Authors	Topic Title
SHAIBU BAANNI AZUMAH WILLIAM ADZAWLA	Effect of Urea Deep Placement Technology Adoption on the Production Frontier: Evidence from Irrigation Rice Farmers in the Northern Region of Ghana
NURLIANI, IDA ROSADA	**Strategy in Controlling Rice-Field Conversion in Pangkep Regency, South Sulawesi, Indonesia**
AYUKO ITSUKI SACHIYO ABURATANI	Comparative Analysis of Soil Enzyme Activities between Laurel-Leaved and Cryptomeria japonica Forests
GERALD AMATRE JULIUS BUNNY LEJJU MORGAN ANDAMA	**Jigger Flea (Tunga penetrans) Infestations and Use of Soil-Cow Dung-Ash Mixture as a Flea Control Method in Eastern Uganda**
KRISHAN LAL ANISH DUA	Fish Catch Composition from Gobind Sagar Reservoir during 2006-2012
ALI RABIEE HESSAM GHASEMNEJAD	Effect of Stitching Pattern on Composite Tubular Structures Subjected to Quasi-Static Crushing
AHMAD AMIRI HAMED K. ARZANI S. N. KAZI B. T. CHEW	Numerical Heat Transfer Performance of Water-Based Graphene Nanoplatelets
HAJJI LOBN CHATTAOUI MAYSSA REGAIEG HAJER	**Biocontrol Effectiveness of Indigenous Trichoderma Species against Meloidogyne javanica and Fusarium oxysporum f. sp. radicis lycopersici on Tomato**

M'HAMDI-BOUGHALLEB NAIMA **RHOUMA ALI** **HORRIGUE-RAOUANI NAJET**	
GÜRCAN D. BAYSAL ALI TANIŞ	Plant Supporting Units (Ekobox) Application Project for Increasing Planting Success in Arid and Semi-Arid Areas

HALL 6 – SESSION 2 Meeting ID: 853 4114 7994 Passcode: 140522

14.05.2022 14:00 – 16:00 (Turkey Local Time)

MODERATOR: BADR M. ALSHAMMARI

Authors	Topic Title
MAHA BENHAMAD ALI SNOUSSI AMMAR BEN BRAHIM	A Simulation Model and Parametric Study of Triple-Effect Desalination Plant
NUR SARMA **PAUL M. TUOHY** **SINIŠA DJUROVIĆ**	**Investigation of Grid Supply Harmonic Effects in Wound Rotor Induction Machines**
JOSE D. HERRERA MARIO A. RIOS	A Multiobjective Damping Function for Coordinated Control of Power System Stabilizer and Power Oscillation Damping
IDRIS A. ELFEITURI	**Exergy Based Performance Analysis of a Gas Turbine Unit at Various Ambient Conditions**
AHMAD K. JASSIM RAHEEM KH. AL-SUBAR	Studying the Possibility to Weld AA1100 Aluminum Alloy by Friction Stir Spot Welding
EKOW A. KWOFIE **EMMANUEL K. ANTO** **GODFRED MENSAH**	**Determination of the Optimal DG PV Interconnection Location Using Losses and Voltage Regulation as Assessment Indicators Case Study: ECG 33 kV Sub-Transmission Network**
BADR M. ALSHAMMARI T. GUESMI	Optimal Design of Multimachine Power System Stabilizers Using Improved Multi-Objective Particle Swarm Optimization Algorithm

MOSES C. SIAME **KAZUTOSHI HAGA** **ATSUSHI SHIBAYAMA**	**Treatment of Low-Grade Iron Ore Using Two Stage Wet High-Intensity Magnetic Separation Technique**
PETR MOHYLA IVO HLAVATÝ JIŘÍ HRUBÝ LUCIE KREJČÍ	Investigation of Heat Affected Zone of Steel P92 Using the Thermal Cycle Simulator

CONTENT

NANOTECHNOLOGICAL MODIFICATION OF CLAY SOILS IN GEOTECHNICAL ENGINEERING

Suat AKBULUT*

*Yıldız Technical University, Civil Engineering Faculty, Civil Eng. Department, Istanbul, Turkey

Summary

Nanotechnology is the redesign, remanufacture and reimplementation of structures, devices and systems with shape and size control at the nanoscale. Therefore, materials obtained by nanotechnology are called nanomaterials. Thanks to nanotechnology, materials can be redesigned and changed at atomic, molecular and macromolecular scales. When substances are reduced to nano sizes, they acquire properties that are very different from macro sizes. The stronger, the lighter, different heat and electrical conductivities, magnetic and optical properties, color changes, friction, adhesion, hydrophobic or hydrophilic, biological interaction and surface properties of materials are determined by the chemical composition and morphology of nanometer-sized layers. Nowadays, the control of these nano surface properties and development of smart materials are provided by nanotechnology.

Clay soils, which have an important place in geotechnical engineering, are widely used in the production of nanomaterials, especially in the field of nanotechnology, due to its nano-sized particles, the other hand, nanotechnological methods are promising for the modification of the engineering properties of clay soils. The main purpose of this study is to draw attention to the use of nanotechnology in the solution of problems encountered in clay soils in geotechnical engineering by briefly discussing nanotechnology.

Keywords: Nanotechnology, nanogeotechnique, clay minerals, nanocomposites, soil improvement

1. Introduction

Thanks to nanotechnology, the changes in physical properties caused by the addition of atoms to a nanoscale structure become evident depending on the type of atom, and the geometry of the nanostructure. For example, the conductivity of a nanostructure can be changed even if a single atom is added to that structure. Friction, adhesion, hydrophobicity/hydrophilicity, biological interaction and surface properties of materials are determined by the chemical composition and morphology of nanometer layers. Therefore, the controlled and intelligent use of these surface properties are important to nanotechnology. Building materials from within the atomic and molecular dimension allows for stronger and lighter materials to emerge. These materials have lower defect levels and lead to the development of new manufacturing methods and techniques with their unique and unusual properties. The physical properties, bond structure, and therefore strength of a nanostructure can vary significantly depending on its size and shape. Similarly, the bond structure between atoms can also change at the nanoscale; whether the material is mechanically strengthened or weakened, its electronic conductivity can completely change strength (Jerez et al. 2006; Hollaway and Hackmen, 2005; LeBaron et al., 1999). Materials produced with nanotechnology can be used in almost every field: structural applications, body care products, electronic components, biotechnology or medicine, environmental protection, civil engineering, etc. (Goddard and et al., 2007).

Clays are substances that are smaller than 2 microns in size and can swell when exposed to water, unlike the other soil minerals. The formation of clay, which is a natural secondary mineral composed of hydrated aluminum and magnesium silicates, can occur by crystallization from solution, decomposition of primary minerals, change of these minerals in the hydrothermal environment, diagenesis and restructuring, even under laboratory conditions (Önalp, 2002).

It can be easily said that the type of primary minerals (parent rock), ion content of the environment, temperature and pH effect are important in the formation of clay minerals, which generally have a bar/twiggy or layered structure. Most of the clay minerals are compounds of a layered structure formed by silica tetragon (tetrahedral) coming together. This structure is infinitely repeatable and appears in the form (Si4O10)4-. The electrical balance is provided by the replacement of the four oxygens by the hydroxyl or by combining them with another positively charged layer (Erkan, 1978; Karacan and Gurkan, 2002). In some cases, silica tetrapods (Si4O11)6- can be found in the form of bands (silica chains). These bands are combined by providing electrical balance aluminum and/or magnesium ions. In addition, clays Mg+2 or Al+3 ions are found in octagonal layers in which oxygen and hydroxyls are bonded in an octagonal coordination (Moore and Reynolds, 1989). The presence of weak bonds between these layers can allow the water and other ions to settle there. The water molecules and/or cation type entering between the layers give each clay mineral a different name and feature (Karacan and Gürkan, 2002).

The surface of clay minerals in octahedral and tetrahedral crystal structure has negative (anion) charge. Because negatively charged crystals tend to become electrically neutral, cations in water are strongly held by the clay surface due to the negative charge present. These cations are electorally attached to the clay surface, and when the chemical content of water changes, these cations are replaced by cations with greater valence. This displacement is called "cation Exchange" (Rhoades, 1982; Moore and Reynolds, 1989; Grim, 1974) and they are called "exchangeable cations" (Holtz and Kovaks, 1981). All clays carry a net negative charge at the crystal surfaces, which means that foreign cations are attached to the surfaces to ensure neutrality;, in other words, cation exchange of clays is an important feature of clays. The fact that clays have nano size, surface charge, the need for electrical balance of clay minerals and Van der Waals forces between other charged particles, its abundance in nature and economical attribute make clays important in terms of nanocomposite production (Akbulut et al., 2010; Akbulut et al., 2013). Studies on improving the properties of clays with the effect of cation exchange are carried out with inorganic (lime, cement, etc.) and organic materials (surfactants). It has been shown in some studies that as a result of the interaction of clays with inorganic substances, clays retain high valence cations in their structures with the effect of cation exchange capacity, and the swelling, hydraulic conductivity and strength properties of clay change accordingly (Akbulut et al., 2012; Alawaji, 1999; Stern and Shackelford, 1998; McRory and Ashmawy, 2004). Other studies on clays are those with organic substances such as surfactants and polymers. In these studies, it was observed that the type, cation exchange capacity, grain size, additive type and properties of

the clay (Ruhl and Daniel 1997; Irene et al. 1997; Mathew and Rao, 1997; Kaya and Frang, 2003). In recent years, organic-inorganic nanocomposites have attracted the attention of researchers due to their unexpected hybrid properties. Many researches have reported that especially organic-inorganic composites have high strength, high modulus, high impermeability and thermal strength (Jerez et al. 2006; Hollaway and Hackmen, 2005; LeBaron et al., 1999; Aranda and Hitzky, 1999; Xiao and Cezar, 2003).

Various applications of clay-polymer interactions are seen in civil and environmental engineering such as stabilization of soil structures, drilling mud, interaction with water etc. (Hollaway and Hackman, 2005; Akbulut and Pamukcu, 2010). A wide variety of additives (polypropylene, polyacrylamide, epoxy resin, poly caprolactan, acrylic polymer, polyvinyl alcohol and polyethylene oxide), clay types and surfactants are used to produce nanocomposites in very different combinations. Changing loads of clay layers, layer distribution structure, properties of clay-polymer composites with other factors are important research topics today and in the future. Along with these, it is important to answer questions of what developments in this field need such as: i) which resins yield more suitable nanocomposites and which polymers can currently be achieved in civil and environmental engineering, ii) what properties can improve the support of clay layers at the nanoscale, iii) whether it is currently possible to manufacture nanocomposite materials in civil engineering, (Hollaway and Hackman, 2005). In this study, summary information about nanotechnology and clay minerals is given and the importance of clays in terms of nanocomposite production is revealed. In addition, it was pointed out that new nanocomposites could be obtained by changing the surface properties of clay minerals at the nanoscale, and it was tried to create a vision for the researchers in the field of Geotechnical Engineering.

2. Nanotechnology and Its Uses

Nano literally means one billionth of a physical size. A nanometer is a unit of length equal to one billionth of a meter (1 nm = 10^{-9} m =10^{-6} mm). Nanoparticles, which are specified as powders or particles with sizes in the range of 1-100 nm, form the basis of nano-sized materials and nanotechnology (Ates and Bahceci, 2015). The nanoscale means it is only a tens or hundreds atom in size. Nano, micro and macro dimensions are shown in Figure 1 and 2.

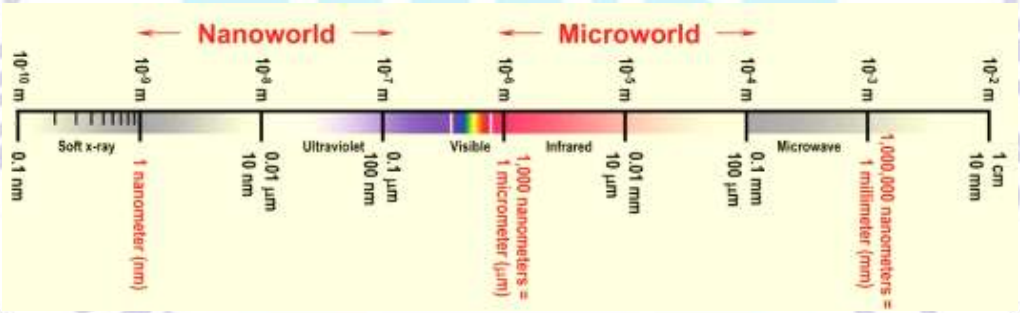

Figure 1. Nano, micro and Macro Dimensions (Web 1)

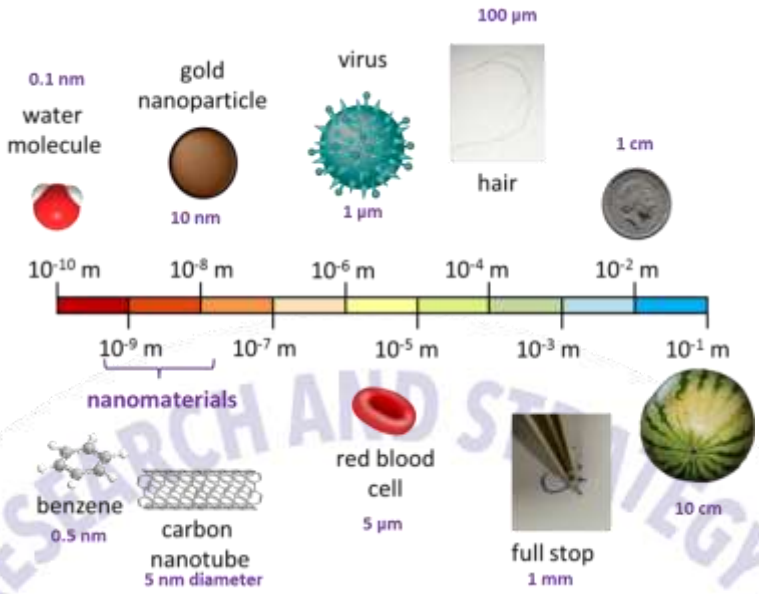

Figure 2. Shape representation of nano, micro and macro structures (Web 2)

Nanotechnology first described in 1959 by physicist Richard Feynman (Bhattacharyya and Gupta, 2008) is the ability to understand, to control and to manipulate matter at the level of individual atoms and molecules (Goddard and et al., 2007). Nanotechnology is the redesign and reproduction of structures, devices and systems at the nanoscale with shape and size control. It is well known that when substances are reduced to nano sizes they acquire physical or chemical properties that are much different from macroscale. The changes in physical properties caused by each new atom added to a nanoscale structure become evident depending on the type of this atom, the type and geometry of the nanostructure (Kurt, 2009). Building materials from atomic and molecular dimensions allows for stronger and lighter materials to emerge. These materials have lower defect levels and lead to the development of new manufacturing methods and techniques with their unique and unusual properties. Similarly, the bond structure between atoms can also change at nanoscales, while the material is mechanically strengthened or weakened, its electronic conductivity can completely change (Yazıcı, E., 2009; Lines M.G., 2008**;** Doğan, G., 2007**).** Materials may have stronger, lighter or more different ways of conducting heat and electricity, their magnetic and optical properties may increase or decrease significantly, and their colors may change. A wide range of nanomaterials or particles can be found naturally on Earth, such as photochemical products, volcanic products, and exhaust fumes (Enderby and Dowling, 2004; Ates and Bahçeci, 2015).

Surface and interfacial properties can be improved by using surfactants known as chemical agents. With these additive additions, the surface properties and behavior of the particles are changed.

2.1. Nanotechnological Methods

There are two general approaches to the production of nanomaterials and structures, which are top-down and bottom-up applications shown in Figure 3 (Enderby and Dowling, 2004; Menceloğlu and Kırca, 2008)

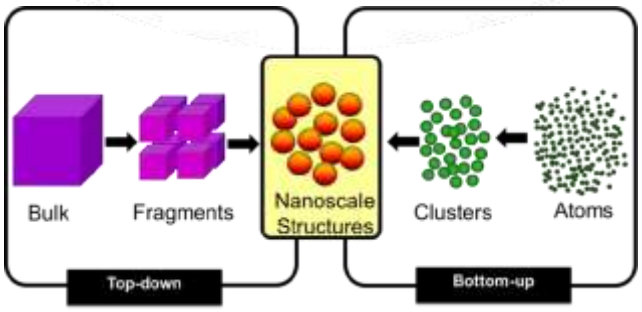

Figure 3. "Top-down" and "bottom-up" synthesis of nanofabrication (Rawat, 2015)

The top-down approach relies on the successive fragmentations or processing of macro-scale materials to smaller nano-sized objects (Rawat, 2015), and the process starts with the whole material and the material is divided into small pieces. In this main approach, the structural dimensions of microscopic elements are reduced to the nanometer scale, with special processing and chemical etching techniques, lithography, and extremely flawless surface shaping. Mechanical abrasion, electro blast, cauterization, thermal method, gas atomizer, lithograph, extreme ultraviolet, solidification method on the rotating cold surface can be represented like top-down methods.

In the bottom-up approach, the material is synthesized as a result of the growth of atoms and molecules in size through chemical reactions. Bottom-up manufacturing is to process atoms and molecules one by one and create a nanostructure. The formation of nanoparticles from atoms is a chemical process and solutions are used as starting materials (Vandana, 2005; Ates and Bahçeci, 2015). Bottom-up methods are inert gas condensation, flame synthesis, chemical vapor condensation, combustion, wet chemical synthesis, electro-explosion, ultrasonic spray pyrolysis, and sol-gel method.

2.2. Sol-Gel method

Sol-Gel method is based on hydrolysis and condensation reactions of initial solutions such as metal oxide and inorganic salt (Figure 4). In this method, materials of desired size and shape can be produced from minerals and chemicals in a controlled manner, homogeneously on a molecular scale (Lee et al., 2004; Sadeghzadeh-Attar et al., 2007).

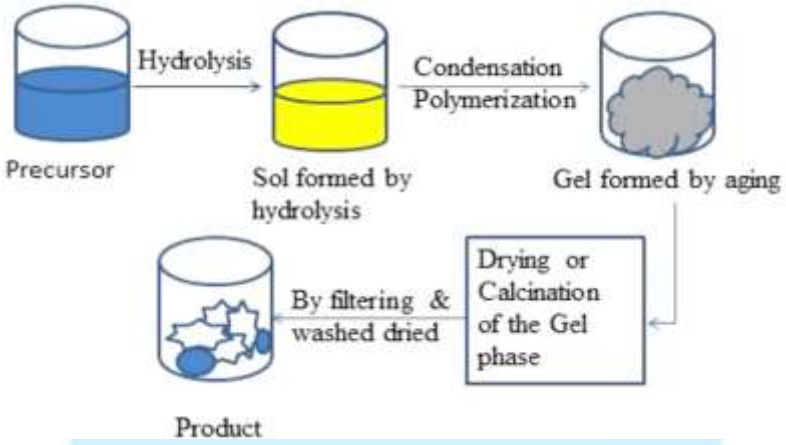

Figure 4. Processing of the "sol-gel" method (Cui et al., 2018)

Sol consists of solid particles several hundred nanometers in diameter suspended in the liquid phase. These solid particles then condense as a new phase (gel) in the liquid phase (solvent) into which the solid macromolecules are immersed and nano structures are formed (Chen and Soutar, 2009; Brinker and Scherer, 1990).

3. Mineralogical properties of clays

Clay, which generally means clay soil in civil engineering, is a soil with plasticity and cohesiveness properties that contains some clay minerals as well as other mineral contents. In clayey soils, the effect of the particle size distribution on the engineering behavior is quite small, whereas the clay mineral types have a more significant effect on the behavior of the clay. Clay minerals are active electrochemical particles with grain sizes smaller than 2 microns. This means that even if the clay is present in very small amounts in the soil mass, it will affect the engineering properties of the soil mass. Clay minerals are very fine crystalline elements that result from the chemical weathering of rock-form minerals; they can only be seen with an electron microscope. There are many clay minerals and the main ones are kaolinite, montmorillonite, illtite

and chlorite. Kaolinite is a 1:1 clay mineral formed by repeated bedding of 1 tetrahedral (silica) and 1 octahedral (alumina or gibbsite) layers in Figure 5.

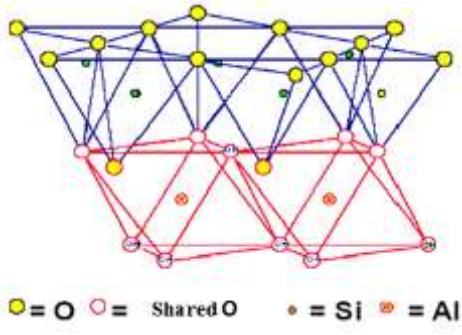

Figure 5. Structure of kaolinite, 1:1 layered silicate (Bhattacharyya et al, 2008)

Montmorillonite, which is mostly called smectite, is 2:1 layered and consists of a combination of 2 silica layers and 1 alumina layer as illustrated in Figure 6. The Van der Waals forces on the silica layers are weak and there is a net charge gap in the octahedral layer, water and exchangeable ions can enter between the layers and separate the layers.

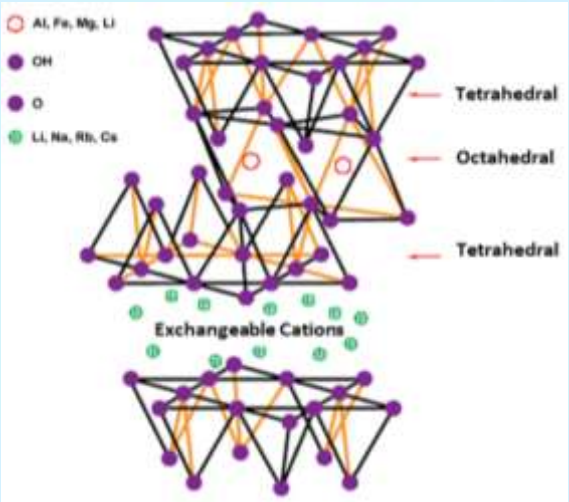

Figure 6. Structure of montmorillonite, 2:1 layered silicate (Beyer, 2002)

The very small montmorillonite minerals have a strong interaction with water. Soils containing montmorillonite are susceptible to swelling. The illite mineral is also in a 2:1 layer structure similar to montmorillonite. The intermediate layer contains potassium ions. Vermiculite is commonly trioctahedral as in smectite and the 2:1 layers are separated by hydrated cations occupying the interlayer space (Brigatti et al., 2013). The chlorite mineral has a 2:1:1 layer and is composed of a silica layer, an alumina layer, another silica layer, and a gibbsite (Al) or brucide (Mg) layer. Chlorite mineral is suitable for swelling and is less active than montmorillonite (Holtz and Kovacs, 1981). Different clay minerals structures are shown in Figure 7.

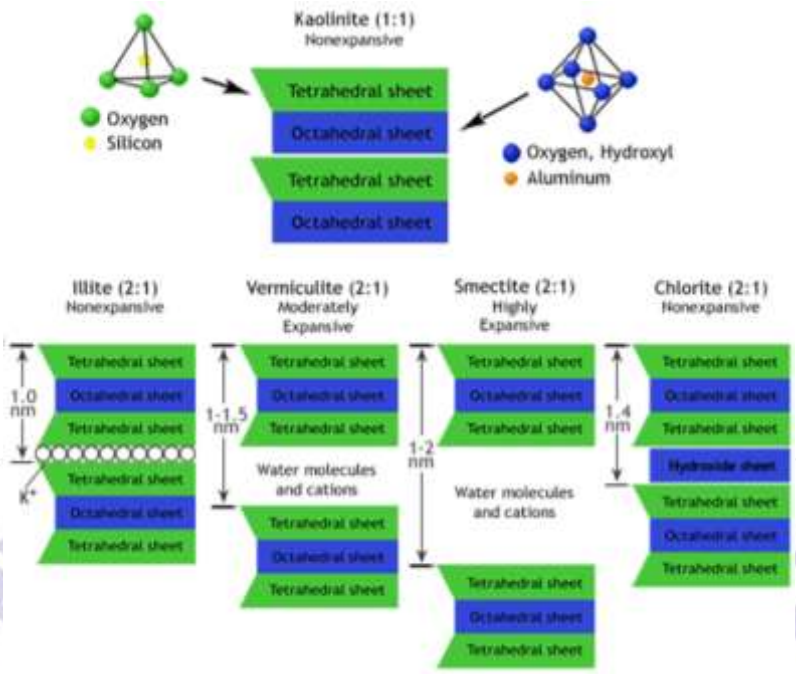

Figure 7. Diagrammatic representation of different clay mineral structures (Web 3)

3.1. Clay as Nanomaterial

Clay minerals modified with different chemicals (surfactant, polymers) to make clay complexes with organic monomers and polymers suitable are called nanoclay (organoclay, inorganoclay) structures. The most important nanoclay material is montmorillonite, a 2:1 layered smectite clay (Crainic and Marquez, 2002). These clays have a large surface area, which makes them privileged in changing their properties with the polymer. In addition, clays are characterized as naturally hydrophilic (water loving). The structural representation of the Montmorillonite clay layers is given in Figure 8. The thickness of the montmorillonite mineral is approximately 1 nm, and it has interlayer spaces and is a feature that takes cations into these spaces.

Figure 8. The structure of montmorillonite clay layers (Hollaway and Hackman, 2005)

The new nanoclay modified with surfactant is used in different engineering applications such as plastic materials, automotive parts, production of light, effective and scratch resistant, high temperature resistant nanocomposites. Although organoclays are not yet used in civil engineering, they have the ability to increase the service life of materials (Hollaway and Hackman, 2005). While long chain surfactants are added to the hydrophilic structure of natural clay, the interfacial distance increases and the surface chemistry of the clay is changed (LeBaron et al., 1999). By changing the surface chemistry of the clay mineral in accordance with the purpose, some engineering (settlement/swelling, hydraulic conductivity (water-proof feature), damping rate) properties of the clays can be improved (Akbulut et al., 2012; Akbulut, et al., 2013; Majedi et al, 2019).

4. Other chemicals

4.1. Surfactants

Surfactants are substances that increase or decrease surface tension containing a hydrophilic (water-loving) and a hydrophobic (water-loving) part/edge. Surfactants are divided into four groups as described below: anionic, cationic, nonionic and amphoteric (Kurt, 2009).

Anionic surfactants: A lipophilic (oil-loving) hydrocarbon group is surfactants associated with one or two hydrophilic (water-loving) groups. They dissociate in solution to yield a negative ion to a positively charged ion. The anionic part shows surface active properties.

Cationic surfactants: While a lipophilic hydrocarbon group contains one or more hydrophilic groups, they dissolve in solution as cations and anionic. The cationic portion shows surfactant property.

Nonionic surfactants: In the nonionic group of these non-ionic molecules, there are often many oxygen, nitrogen or sulfur atoms. They do not dissociate into ions in solution.

Amphoteric surfactants: The active group of the same molecule in solution contains both positive and negative charge. They can have anionic or cationic properties according to their structure and ambient conditions.

Figure 6 shows a surfactant schematically. As shown here, the surfactant molecule has a water-loving group (hydrophilic) at one end and a hydrophobic group at the other end (Figure 9).

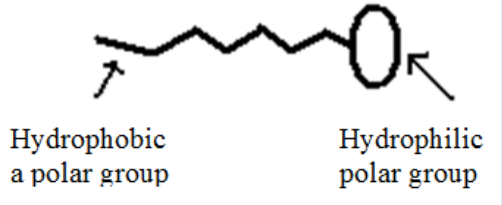

Figure 9. Representative picture of surfactant (Kurt, 2009)

4.2. Polymers

Monomer is defined for chemicals of small molar mass that can form large molecules by covalent bonds to each other, while polymers are large molecules formed by the bonding of many monomers together by covalent bonds.

Classification of polymers

As listed below, polymers can be classified in different ways (Saçak, 2004).

-Natural, semi-synthetic and synthetic polymers according to their sources,

-Organic and inorganic polymers in terms of the type of atoms that make up the main chains of the polymer,

-Linear, branched and cross-linked polymers by looking at the physical forms of the polymer chains,

-High density and low density polymers according to the size of their molar masses,

-Thermoplastics and thermosets according to their behavior against heat.

5. Polymer Composites

Composite materials are prepared by mixing two or more materials for the purpose of use or bringing them together in a certain order. The main purpose of composite preparation is to gather the valuable properties of different materials under one material (Saçak, 2004; Celik, et al., 2019). If composite materials are

formed by dispersing the nano-sized filler in the polymer matrix, that is called the nanocomposite materials. Polymer nanocomposites are composite materials consisting of nanoparticles in nanometer size. These are reproduced from direct mixing, solution mixing and in situ polymerization methods (Saçak, 2004; Bensadoun et al., 2011; Ajayan et al., 2003).

Direct mixing is the obtaining of material by direct mixing of polymer and nanoparticle in different phases or in solution. If the traditional solution-mixing method can be applied, the direct mixing method is the fastest method to produce new products.

Solution mixing is a method of material preparation by dissolving and dispersing both polymer and nanoparticle in solution.

In situ polymerization: The nanoscale particles are dispersed in the monomer or monomer solution and the resulting mixture is polymerized by standard polymerization methods. The most useful part of this method is that it allows the polymer to be grafted onto the particle surface. Many types of nanocomposites can be produced by in situ polymerization (Ajayan et al., 2003). The representation of the formation of the polymer molecule is given in Figure 10, and the schematic representation of three different silicate layered nanocomposites is given in Figure 11.

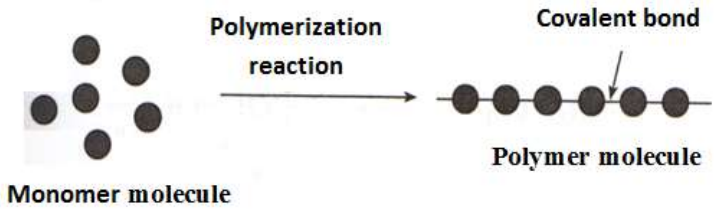

Figure 10. Formation of polymer molecules (Saçak, 2004)

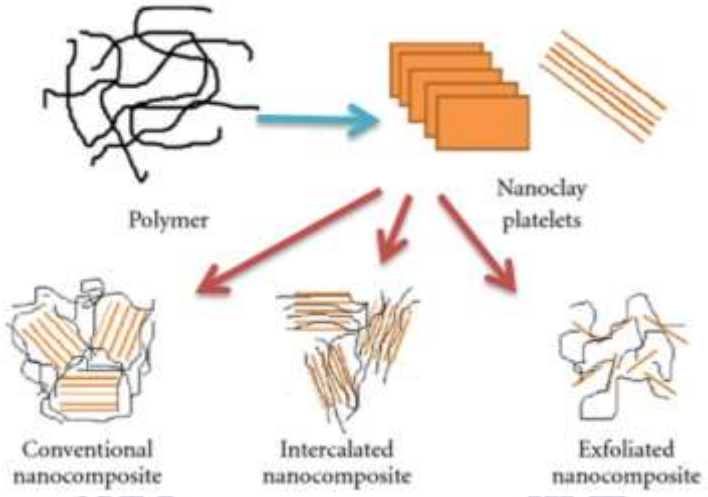

Figure 11. Schematic representation of three different polymer/silicate nanocomposites; (a)conventional, (b) intercalated, (c) exfoliated. Image modified from (Bensadoun et al., 2011)

6. Nanotechnological Solutions in Geotechnical Engineering

There are many application areas for nanomaterials used in civil engineering. These are nano paints, nano floor-concrete coatings, nanoglass and ceramic coatings, nano aluminum composite panels, facade protection, cold storage depot, construction molds, nanoconcrete, nanoconcrete additives, reinforcement of concrete with fiber-reinforced polymers, light-permeable property.

In addition, decorative and self-cleaning wall paints and paints resistant to Ultraviolet rays are manufactured using nanomaterials. The production of bacteria-proof sinks, self-cleaning windows and bathroom ceramics, catalytic cement and concrete products coated with titanium dioxide (preventing air

pollution and preventing dirt), metal fatigue resistance, manufacturing coating materials that prevent rusting of iron are also the results of nanotechnology. The products produced by applying chemicals to the fabric thanks to nanotechnology are used as insulation materials in construction.

Today, with the help of carbon nanotubes, the construction of light construction materials, plastic buildings more durable than concrete, production of light and flexible concrete 100 times more durable than steel, roads consisting of highly efficient and self-reproducing solar cells instead of asphalt, the cross-sections of reinforced concrete columns in buildings decreasing in size and gaining elastic properties are available; In this way, studies are carried out to cause less damage to buildings from earthquakes (Jerez et al. 2006; Hollaway and Hackmen, 2005; LeBaron et al., 1999).

On the other hand, different natural disasters such as landslides, ground deterioration caused by the effect of earthquakes, deterioration of soil structures working as engineering structures (earth fill dams, waste storage area mattresses, roads, protective layers for nuclear power plants, etc.) occur in various parts of the world every year. It is known that an important contributing factor to these fundamental problems arise from changes that occur in the clays over time, which are defined as soil in geotechnical engineering (Aranda and Hitzky, 1999; Xiao and Cezar, 2003; Kurt, 2009).

The "clay minerals", which behave differently from other soil groups, carry a negative charge on their edges, allowing foreign cations to bind to the crystal surfaces to neutralize/balance this situation. In general, it is possible to overcome these problems in clay soils by stabilizing the clays with organic and inorganic additives. It is possible to improve the engineering properties of clays (bearing strength, settling-swelling, permeability, damping, etc.) or to gain new properties (water-resistant, antibacterial, catalytic, heat-retaining) to clays with nanotechnological methods (Kurt and Akbulut, 2014).

7. Application

Under this title, it has been shown how organoclays called hydrophobic clay are produced by using different types of clays and surfactants, and nanoclay composites called seismic dampers are produced using hydrophobic clays and polymers.

7.1. Organoclay: Hydrophobic Clay

In this research study, a natural clay sample composed of smectite (56%), kaolinite (34%), illite (3%) minerals and non-clay minerals quartz (4%) and feldspar (3%) was used in order to modify different type of organoclays. Three cationic surfactants that are cetyl trimethyl ammonium chloride (CTAC), quatermised ethoxylated fatty amine (QEFA) and dialkyl ammonium meta sulfate (DAMS) were used in this study. The organoclays were produced by means of the sol gel method using natural clay and different chemical substances called surfactants. The mixture of suspension is 5% the surfactant by weight of clay (Kurt and Akbulut, 2014). It was seen that CTAC and QEFA decreased water affinity and also the liquid limit and plasticity index decreased when surfactant percentage was increased with cetyl trimethyl ammonium chloride CTAC and quatermised ethoxylated fatty amine QEFA in Figure 12.

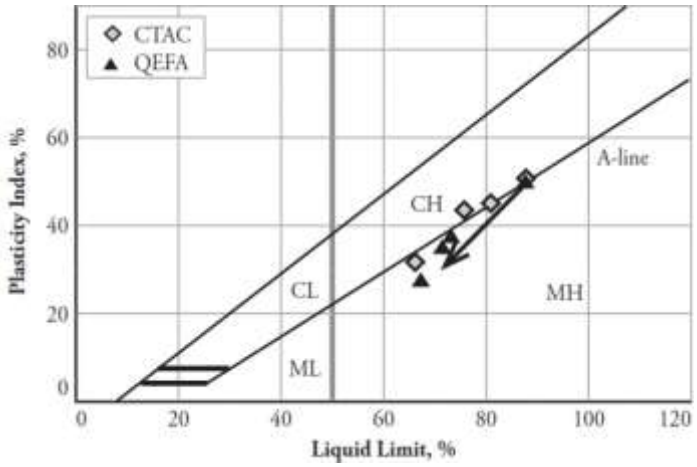

Figure 12. The changing of indexes properties of organoclays (Kurt and Akbulut, 2017)

Previously prepared surfactant solution (DAMS and deionized water) was added slowly to the clay suspension at 30ºC. The modified product (hydrophobic organoclay) was dried at room temperature. Dried hydrophobic clay samples were pressed to prepare the pallets for using water affinity tests. It can be seen in Figure 13, compacted samples has water proof specification as compared with natural clay samples Figure 14.

Figure 13. Water drops on the hydrophobic clay with modified DAMS (Kurt, 2009)

(a) (b)

Figure 14. Water drops on natural (a) and hydrophobic clays with DAMS (b)

7.2. Nanoclay Composite: Seismic Damper

In order to produce clay nanocomposites, the above mentioned hydrophobic clay, different types of polymers (locust bean gum, latex, glycerine, vinyl acrylic copolymer), and rubber powder were mixed by means of in situ polymerization. The nano claycomposite samples were prepared using the following procedure, as described by Kurt and Akbulut, 2014. First, LBG (0.5%) was added to 2 L of water and mixed using a mechanical stirrer at 4000 rpm until dissolved. During stirring, latex (10%) was added and mixed for 20 min. Then, glycerine (10%) was added and the solution was mixed for 10 min. Next, 2500 g of hydrophobic organo-clay and 1 L of water were added and mixed for 1 h. Finally, vinyl acrylic copolymer was added in different proportions and mixed with a mechanical stirrer (percentages by weight of clay).

Locust bean gum markedly increases gel strength and changes the gel character from brittle to elastic (Maier, et al., 1993) Latex is used in the experiments as an elastomer. The presence of glycerine is essential for preparing nanocomposites and it is used as plasticizer (de Carvalho, et al., 2001; Tang, et al., 2008). Vinyl acrylic copolymer as a water-based resin may be used as the adhesive component of the composition . The pigment binding and film forming of vinyl acrylic copolymer are significant, and its water stability is also notable. Vinyl acrylic copolymer was also used for its adhesive properties (Kurt and Akbulut, 2014). Due to its light-weight nature and its capacity for damping energy, the rubber powder can be used to mitigate seismic forces and to absorb earthquake vibrations (Nakhaei, et al., 2012) Polymers contents used in the tests and abbreviations are symbolized in Table 1.

Table 1. Content of polymers used in the tests and abbreviations (Kurt and Akbulut, 2014)

C	Natural clay
HOC	Hydrophobic clay
CNC0	HO-%0,5LBG-%10LTX-%10GLC
CNC5	HO-%0,5LBG -%10LTX-%10GLC-%5VA
CNC10	HO-%0,5LBG -%10LTX-%10GLC-%10VA
CNCR0	HO-%0,5 LBG -%10LTX-%10GLC-%5RP
CNCR5	HO-%0,5LBG-%10LTX-%10GLC-%5VA-%5RP
CNCR10	HO-%0,5LBG-%10LTX-%10GLC-%10VA-%5RP

In order to understand waterproof and the dynamic properties (secant shear modulus and damping ratio) of the nano claycomposites, the specimens were subjected to Goniometer tests and the dynamic simple shear tests (Kurt and Akbulut, 2014; Kurt and Akbulut, 2017). Based on the test results the following conclusions were made:

The contact angles of the clay-nanocomposites were increased with polymers contents as compared to that of the natural clay and hydrophobic clay (Figure 15). Contact angles of the natural clay, hydrophobic clay

(HOC) and nano claycomposite (CNCR10) sample are calculated as 37º, 88º, 106º, respectively. If the contact angle is less than 90 º, these types of materials are called hydrophilic or if it is greater than 90º, they are called hydrophobic. The consistency limits showed that clay-nanocomposites are non-plastic.

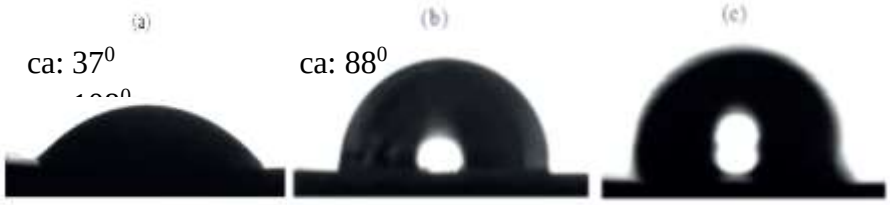

Figure 15. The contact angles of nano-claycomposite a) the natural clay (37º); b) hydrophobic clay HOC (88º); c) nanoclay composite CNCR10 (106º) (Kurt and Akbulut, 2017)

The dynamic simple shear test results revealed that the damping ratios of samples symbolized CNC and CNCR, which are compacted under E1 (Standard proctor) and E2 (modified proctor) energy levels, increased when compared with natural clay samples. Similarly, damping ratios of clay nanocomposites increased proportionally with VA percentage (Figure 16), in contrast to damping, the dynamic shear modulus was decreased by polymer content and percentages because of decreasing in dry unit weight of compacted nano claycomposites samples (Figure 16). As can be seen from Figure 16, Shear modulus decreased by % 50 compared to natural clay samples at different energy levels, while the Damping ratio increased by %150.

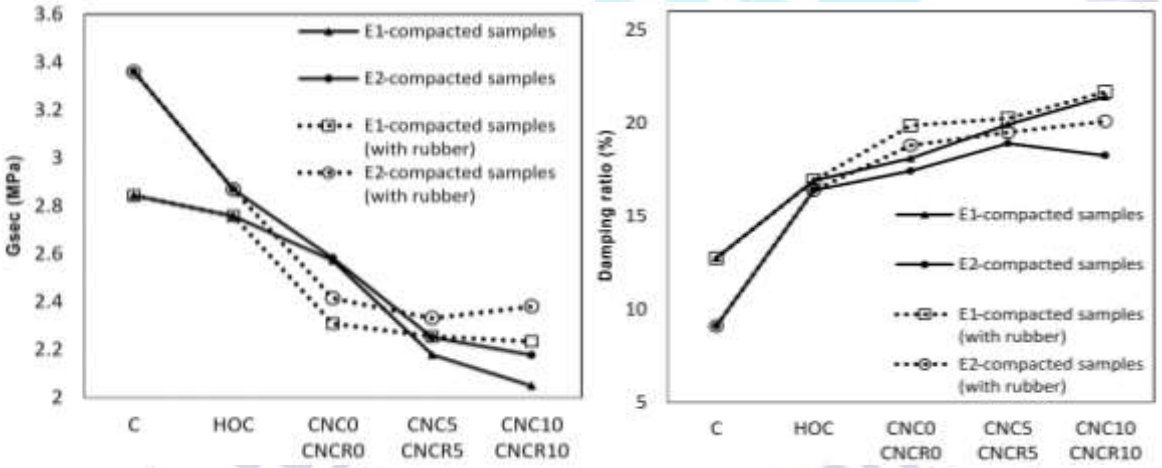

Figure 16. Damping rations of nanoclay composites as seismic damper (Kurt and Akbulut, 2014)

7.3. Possible use of these novel materials in geotechnical problems

These new hydrophobic clay materials can have alternative uses in different engineering applications to solve water permeability problems when used as a waterproof barrier for landfill sites, dams, water channels, around basements, under foundations and roof top in buildings (**Figure 17**).

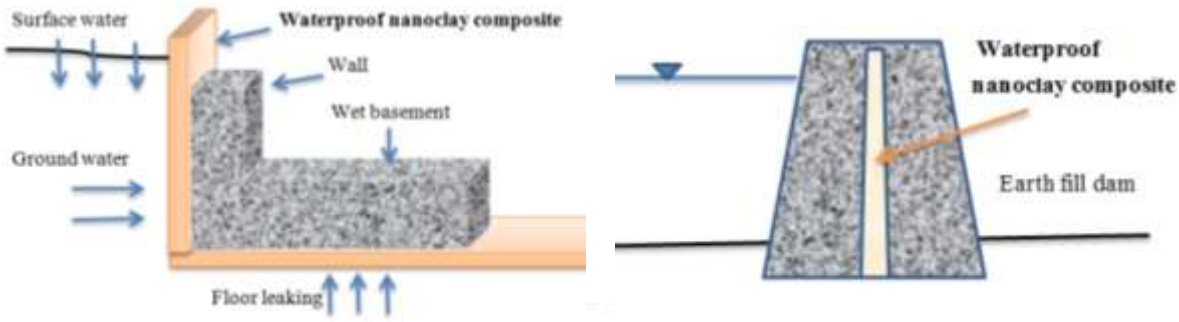

Figure 17. Possible applications of waterproof nanoclay composites in geotechnical engineering

On the other hand, nanoclay composite as a seismic isolator can be a useful agent for building foundations to mitigate earthquake hazards (Figure 18). These hydrophobic clay materials can be an alternative for geotechnical problems instead of the other geo-isolators because of their advantages such as it being impenetrable, puncture-proof, inflammable, inedible by insects, and abrasion resistant, but negative effects of these materials to human health and nature will need to be researched further.

Figure 18. Possible applications of nanoclay composite based seismic isolator

8. Conclusion

With the use of nanotechnology in every field, many engineering problems could be solved and the alternative nano materials can meet the desired engineering properties. In this research, it was pointed out that nanotechnological innovations create hope for the solution of the problems encountered in Geotechnical Engineering. The study can be summarized by the following conclusions .

- By giving brief information about nanotechnology, the use of nanotechnology in geotechnical engineering has been pointed out.

- Clay minerals were mentioned and the importance of clays as nanomaterials were briefly explained as well.

- Clay surfactants and clay polymer interactions and how to change the engineering properties of clays were discussed.

- Hydrophobic clay and nanoclay composites that were yielded from the research study and the consistency index, waterproof, dynamic modulus and damping ratios on these materials were defined respectively.

- It has been explained how this type of composites, called hydrophobic clay and nanoclay composite, can be used as a seismic damper in geotechnical applications.

- As a result, nanotechnology gives hope to researchers and engineers for solving different problems in all engineering fields.

Acknowledgments

The researcher would like to thank TUBITAK project numbered 2005/178 and the team involved in the research.

10. References

Ajayan P.M., Schadler L.S, and Braun P.V., 2003, Nanocomposite Science and Technology, John Wiley & Sons, pp.238

Akbulut S and Pamukcu S, 2010, Evaluation of dynamic properties of geosynthetic reinforced clay samples for environmental impact practices; Environmental Earth Sciences, Volume 61, Issue 7, pp. 1449-1456

Akbulut S, Nese Z, Arasan S, 2010, Electrokinetic properties of surfactant modified clays, International Journal of Civil and Structural Engineering, vol. 1 (3)

Akbulut S, Nese Z, Arasan S, 2012, Surfactant modified clays' consistency limits and contact angles, Earth Sciences Research Journal, Vol 16, No 2, pp.13-19

Akbulut S, Kurt Z.N., Arasan S, and Pekdemir P, 2013, Geotechnical properties of some organoclays, Sadhana-Academy Proceeding in Engineering Science, Vol. 38, Part 2, pp. 317-329

Akın Ö., 2002, Geoteknik Bilgisi I, Birsen Yayınevi, İstanbul

Alawaji H.A., 1999, Swell and compressibility characteristics of sand-betonies mixtures inundated with liquids, Applied Clay Science, 15, pp. 411-430

Aranda P., and Hitzky E.R., 1999, Poly (etilen oksit)/$NH4^{+}$ semektite nanocompozites, Applied Clay Sci., 15, pp. 119-135

Ates H and Bahçeci E, 2015, Nano Parçacıklar ve Nano Teller, GU J Sci Part:C , 3(1), pp. 437-442

Bensadoun F., Kchit N., Billotte C., Trochu F.O., and Ruiz E., 2011, A Comparative Study of Dispersion Techniques for Nanocomposite Made with Nanoclays and an Unsaturated Polyester Resin; Journal of Nanomaterials, V (6), pp. 12

Beyer G., 2002, Short communication: Carbon nanotubes as flame retardants for polymers, Fire and Materials, Volume 26, Issue 6, pp. 247-293

Bhattacharyya K.G. and Gupta S., 2008, Adsorption of a few heavy metals on natural and modified kaolinite and montmorillonite: A review, Advances in Colloid and Interface Science, Volume 140, Issue 2, pp. 114-131

Brigatti M.F., Galán E., and Theng B.K.G., 2013, Chapter 2, Structure and Mineralogy of Clay Minerals, Developments in Clay Science, V(5), pp. 21-81

Brinker, C. J. and Scherer, G.W., 1990, Sol-Gel Science - The Physics and Chemistry of Sol-Gel Processing, New York, Academic Press

Çelik S., Majedi P., and Akbulut S.,2019, Granular soil improvement by using polyester grouts, Iranian Journal of Science and Technology, Transactions of Civil Engineering, Vol 43 (3), pp.599-606

Chen, Q., and Soutar, A.M., 2009, Progress on Nanoceramics by Sol Gel Process, Key Engineering Materials, 391, pp. 79-95

Crainic N., and Marquez A.T., 2002, Nano-composites: a state of the art review, Key Engineering Materials, V:230-232, pp. 656

Cui S., Lin Yu, and Ding J., 2018, Semi-bald Micelles and Corresponding Percolated Micelle Networks of Thermogels, Macromolecules, Vol 51, 16, pp. 6405–6420

de Carvalho, A.J.F., Curvelo, A.A.S., and Agnelli, J.A.M., 2001, A first insight on composites of thermoplastic starch and kaolin, Carbohydrate Polymers. 45 (2), pp. 189-194

Doğan, G., 2007, Mikro ve Nano Hızlı Prototipleme, Yüksek Lisans Tezi, Y.T.Ü. Fen Bilimleri Enstitüsü, İstanbul

Enderby, J. and Dowling, A., 2004, Nanoscience and nanotechnologies: Opportunities and Uncertainties, The Royal Society & The Royal Academy of Engineering Report , London

Erkan Y., 1978, Kayaç oluşturan önemli minerallerin mikroskopta incelenmeleri, Hacettepe Üniv. Yayınları, A26, Ankara

Goddard III, W. A., Brenner, D., Lyshevski, S. E., and Iafrate, G. J. , 2007, Handbook of Nanoscience, Engineering, and Technology, CRC Press, 2nd edition

Grim R.E, 1974, Clay minerology 2nd ed. McGraw-hill, New York

Hollaway L, and Hackman I., 2005, Epoxy-layered silicate nanocomposites in civil engineering, Composites, Part A, pp.1-10

Holtz R.D., and Kovaks W.D., 1981; An introduction to geotechnical engineering, prentice-hall ınc., New Jersey

Irene M.C.I., Raymond K.M.M, and Samuel C.H.L., 1997, Modified clays for waste containment and pollutant attenuation, , J. Environmental Engineering, ASCE, Vol:123, No:1, pp. 25-32

Jerez J., Flury M., Shang J., and Deng Y., 2006, Coating of silica send with aluminosilicates clay, J. Colloid and Interface Science, 294, pp. 155-164

Karacan N., and Gürkan P., 2002, İnorganik Kimya (çeviri), Palme Yayıncılık, Ankara

Kaya A., and Fang H.Y, 2003, Experimental evidence of reduction in attractive and repulsive forces between clay particles permeated with organic liquids, Can. Geotech. Journal, 42, pp. 632-640

Kurt Z.N., and Akbulut S., 2014, The dynamic shear modulus and damping ratio of clay nanocomposites, Clays and Clay Minerals, vol. 62 (4), pp. 313-323

Kurt Z.N., and Akbulut S., 2017, Some Geotechnical Properties of Clay Nanocomposites, Periodica Polytechnica Civil Engineering, 61(3), pp. 381–388

Kurt Z.N., 2009, Yüzey Aktif Madde ile muamele Edilmiş Kilin Mukavemet Özellikleri, Atatürk Üniv. Fen Bil. Ens. Erzurum

Kurt Z.N., and Akbulut S., 2017, Some Geotechnical Properties of Clay Nanocomposites, Periodica Polytechnica Civil Engineering, 61(3), pp. 381–388

Kurt, Z. N., and Akbulut, S., 2014, The dynamic shear modulus and damping ratio of clay nanocomposites, Clays and Clay Minerals. 62 (4), pp. 313-323

LeBaron P.C., Wang Z., and Pinnavaia T.J, 1999, Polymer-layered silicate nanocomposite: an overview, Applied Clay Sci., 15, pp. 11-29

Lines M.G., 2008, Nanomaterials for Practical Functional Uses, Journal of Alloys and Compounds, 449, pp. 242-245

Maier, M., Anderson, M., Karl, C., and Magnuson, K., 1993, Guar, locust bean, tara, and fenugreek gums, In: Industrial Gums: Polysaccharides and their Derivatives (3rd edition). (Whistley, R. L., BeMiller, J. N. Eds), pp. 205-213. Academic Press, New York.

Majedi P., Akbulut S., and Kurt Z.N., 2019, Some geotechnical properties and damping ratio of clay nanocomposites, Journal of Engineering Research, vol. 7 (1)

Mathew P.K and Rao S.N., 1997, Influence of cations on compressibility behavior of a marine clay, J. Geotechnical and Geoenvironmental Engineering, ASCE, Vol:123, No:11, pp. 1071-1073

McRory J.A. and Ashmawy A.K, 2004, Polimer treatment of bentonite clay for contaminant resistant barriers, GSP 142, Waste Containment and Remediation, ASCE

Menceloğlu, Y. Z., and Kırca, M. B., 2008, Nanoteknoloji ve Türkiye, TÜSİAD, Yayın No -T/2008-11/474

Moore and Reynolds, 1989, Clay minerals, Oxford University Pres, Inc. New York

Nakhaei, A., Marandi, S. M., Sani Kermani, S., and Bagheripour, M. H., 2012, Dynamic properties of granular soils mixed with granulated rubber, Soil Dynamics and Earthquake Engineering. 43, pp. 124-132.

Rawat R.S., 2015, Dense Plasma Focus - From Alternative Fusion Source to Versatile High Energy Density Plasma Source for Plasma Nanotechnology, Journal of Physics Conference Series 591(1)

Rhoades J.D., 1982, Cation exchange capacity, Methods of Soil Analysis., Part 2. Chemical and Microbiological Properties (2nd ed.), American Society of Agronomy/Soil Science Society of America, Madison, WI, pp. 149–157.

Ruhl J.L. and Daniel D.E., 1997, Geosynthetic clay liners permeated with chemical solutions and leachates, J. Geotechnical and Geoenvironmental Engineering, ASCE, Vol:123, No:4, pp. 369-381

Saçak M., 2004, Polimer kimyası, Gazi kitabevi, Ankara

Sadeghzadeh-Attar A., Ghamsari S., Hajiesmaeilbaigi, M. F., and Mirdamadi, S., 2007, Template-Based Growth of TiO2 Nanorods by Sol-Gel Process, Semiconductor Physics, Quantum Electronics & Optoelectronics, 10, pp. 36-39

Stern R.T. and Shackelford C.D., 1998, Permeation of sand processed clay mixtures with calcium chloride solutions, J. Geotechnical and Geoenvironmental Engineering, ASCE, Vol:124, No:3, pp. 231-241

Tang, X., Alavi, S., and Herald, T. J., 2008, Effects of plasticizers on the structure and properties of starch–clay nanocomposite films, Carbohydrate Polymers. 74 (3), pp. 552-558.

Vandana, S. P., 2005, Nanometre Scale Surface Modification in a Needle–Plate Exploding System, J. Phys.: Condens. Matter, 17, pp. 5327-5334

Web 1, https://nanohub.org/resources/26676/download/Int_Scale_PK12_PG.pdf

Web 2, https://chembam.com/definitions/nanotechnology/

Web 3, https://news.soilobservation.com/clay-mineralogy

Xiao H. and Cezar N., 2003, Organo-modified cationic silica nanoparticles/anionic polimer as flocculants, J. Colloid and Interface Sci., 267, pp. 343-351

Yazıcı, E., 2009, Ultrasonik sprey piroliz tekniğiyle küresel gümüş nano-parçacıklarının üretimi, Yüksek Lisans Tezi, İ.T.Ü. Fen bilimleri Enstitüsü

AISI 304 KALİTE ÖSTENİTİK PASLANMAZ ÇELİĞİN KAYNAK PARAMETRELERİNİN MEKANİK ÖZELLİKLERE ETKİSİ

OKTAY ÇAVUŞOĞLU [1], HAKAN AYDIN [2] , AHMET GÜRKAN YILMAZOĞLU [3], UĞUR ÜZEL [4] , SÜLEYMAN İNCE [5]

[1]TOFAŞ, Türk Otomotiv Fabrikası, 0000-0002-2826-1814
[2]Bursa Uludağ Üniversitesi, 0000-0001-7364-6281
[3]TOFAŞ, Türk Otomotiv Fabrikası, 0000-0002-1811-7827
[4]TOFAŞ, Türk Otomotiv Fabrikası, 0000-0001-5819-6841
[5]Bursa Uludağ Üniversitesi, - 0000-0002-7340-5004

ÖZET

Bu çalışmada, paslanmaz çeliklerin Tungsten Inert Gaz (TIG) kaynak yöntemi ile birleştirilmesi esnasında kullanılan kaynak parametrelerinin mekanik özelliklere etkisi araştırılmıştır. Çalışmada AISI 304 kalite östenitik paslanmaz çelik plakalar TIG kaynağı ile alın kaynağı pozisyonunda birleştirilmiştir. Birleştirilen parçalar tahribatsız muayene yöntemlerinden sıvı penetrant testi yüzeydeki kaynak hatalarının bulunması için test edilmiştir. Sonrasında çekme testlerine tabi tutulmuş ve akma çekme ve uzama miktarları karşılaştırılmıştır. Değişen kaynak parametrelerinin mekanik özelliklere etkisi incelenmiş ve yorumlanmıştır.

Anahtar Kelimeler: Paslanmaz çelik, TIG, Kaynak, AISI 304

ABSTRACT

In this study, the effect of welding parameters used during the joining of stainless steels with Tungsten Inert Gas (TIG) welding method on mechanical properties was investigated. In the study, AISI 304 quality austenitic stainless steel plates were combined with TIG welding in the jumpweld welding position. The combined parts have been tested for non-destructive testing methods such as liquid penetrant testing to find welding defects on the surface. After that, it was subjected to tensile tests and yield tensile and elongation amounts were compared. The effect of changing welding parameters on mechanical properties has been studied and interpreted.

Keywords: Stainless steel, TIG, Welding, AISI 304

1. GİRİŞ

Günümüzde, otomotiv sektöründe en sık kullanılan birleştirme yöntemlerinin başında kaynak işlemi gelmektedir. 2 veya daha fazla katmanında efektif olarak birleştirilmesinde kısıtları bulunmasına rağmen tercih edilmektedir [1,2]. Yüksek kaynak kabiliyeti, her pozisyonda kaynak yapılabilmesi, sıçrama problemi olmaması, curuf temizliğine ihtiyaç duyumaması, metal ve metal dışı malzemelerin birleştirilmesine elverişli olmasından dolayı TIG kaynak yöntemi otomotiv sektöründe kullanılmaktadır [3]. Kaynak kalitesi, kaynak hızı, kaynak akımı, koruyucu gaz, kaynaklanacak malzeme türü, malzeme kalınlığı vb. parametrelerden etkilenmektedir. Otomotiv sektörü için uygun kaliteyi sağlamak için bu parametreleri optimize etmeye ihtiyaç duyulmaktadır [4-6].

Literatürde, Ahmed Khalid Hussain ve diğ. [7] AA6351 Alaşımlarında kaynak hızının kaynaklı bağlantının çekme mukavemeti üzerindeki etkisinin araştırmışlardır. Deneyler, farklı pah açısına ve pah yüksekliğine sahip tek v alın bağlantı numuneleri üzerinde yapılmıştır. Kaynaklı bağlantının mukavemeti üniversal bir çekme test cihazı ile test edilmiş ve sonuçlar yorumlanmıştır.

Ugur Esme ve diğ. [8] Gray ilişkisel analizi ve Taguchi yöntemini kullanarak kaynaklı bağlantıların uygun geometriyi elde etmek için optimal bir parametrik kombinasyon için tungsten soy gaz kaynağı (TIG) kaynak işleminin çoklu yanıt optimizasyonunu araştırmışlar. Ortogonal bir Taguchi yöntemi dizisine dayalı on altı deneysel çalışma, deney alanı içinde optimize edilecek amaç fonksiyonlarını türetmek için gerçekleştirilmiştir. Çok yanıtlı optimizasyon problemini çözmek için Taguchi yaklaşımı ve ardından Gray ilişkisel analizi kullanılmıştır. Faktörlerin kaynaklı birleştirmenin genel kalite özellikleri üzerindeki önemi de varyans analizi yöntemi (ANOVA) ile nicel olarak değerlendirilmiştir.

Bu çalışmada, AISI 304 kalite yaklaşık 2 mm et kalınlığına sahip östenitik paslanmaz çeliği farklı kaynak parametrelerinde kaynak yapılarak sıvı penetrant testi yapılmıştır. Daha sonra çekme testi numunesi haline getirilip çekme testinde mekanik özellikleri ölçülmüştür. Testler sonucunda elde edilen veri ve görseller çalışmamızda sunulmuş ve ulaşılan sonuçlar yorumlanmıştır.

2. DENEYSEL ÇALIŞMALAR

Çalışma kapsamında, 180 mm x 270 mm x 2 mm boyutlara sahip AISI 304 kaliteye sahip östenitik paslanmaz çelik farklı kaynak parametrelerinde TIG gaz altı kaynak yöntemi ile birleştirilmiştir. Birleştirilen plakalar 180 mm x 90 mm boyutlarında lazer ile kesilerek çekme testi için uygun boyutlara getirilmiştir. Deneylerde kullanılan malzemenin kimyasal kompozisyonu çizelge 1. 'de gösterilmiştir. Kaynak voltajı sabit tutularak, kaynak akımı ve kaynak hızının etkileri mekanik özelliklere etkileri araştırılmıştır. Birleştirilen parçalar kaynak yüzeyinde oluşabilecek kaynak kusurlarının değerlendirilmesi için tahribatsız muayene yöntemlerinden sıvı penetrant testine tabi tutulmuştur. Deney sırasında incelenen kaynak parametreleri çizelge 2 'de belirtilmiştir.

Çizelge 1. Kimyasal Kompozisyon (%) [9]

	Kimyasal Analiz Değerleri						
Malzeme	C	Mn	Si	Cr	Ni	P	S
AISI 304	0,08	2	1	18-20	8-10,5	0,045	0,03

Çizelge 2. Kaynak Parametreleri

KAYNAK AKIMI (I)	KAYNAK İLERLEME HIZI (mm/sn)
50 A	2.28 mm/sn
80 A	2.28 mm/sn
100 A	2.28 mm/sn
80 A	1.33 mm/sn
80 A	1.45 mm/sn
80 A	2.0 mm/sn

3. SONUÇLAR VE DEĞERLENDİRME

Kaynaklı numunelerini çekme deneyi yapılabilmesi için gerekli ölçülerde her parametrede 2 adet numune olacak şekilde lazerle kesim işlemi uygulanmıştır. Deneyin sonuçları çizelge 3'te gösterilmiştir. 304 kalite östenitik paslanmaz çeliklerin birleştirilmesinde TIG (Argon) kaynağı kullanılmıştır. Kaynak dikişi olarak alın kaynağı kullanılmıştır. Değişen parametreler amper ve ilerleme hızı olarak belirlenmiştir. İlk olarak ilerleme hızı sabitken 3 farklı akım değerinde 3 farklı kaynak yapılmıştır. Sonrasında amper değeri sabitken 3 farklı ilerleme hızında 3 farklı kaynak yapılmıştır. Çekme deneyi sonunda ulaşılan değerler her grupta 2 adet numune hazırlandığı için ortalama değerler kullanılmıştır. Görsel 1 ve görsel 2 'de kaynak akımına ve kaynak hızına bağlı olarak çekme dayanımları karşılaştırılmıştır. Kaynak akımının artmasıyla akma ve çekme dayanımı artarken, kaynak hızının artmasıyla akma ve çekme dayanımlarında azalma görülmüştür.

Çizelge 3. Çekme Deneyi Sonuçları

Akım Değeri (A)	Kaynak Hızı (mm/sn)	Akma Gerilmesi Re (Mpa)	Çekme Gerilmesi Rm (Mpa)	% Uzama Miktarı
50	2,28	221,3014	284,4443	2,36
80	2,28	248,3145	299,8556	6,50
100	2,28	284,2902	473,5925	11,97
80	1,33	241,2130	351,5346	4,64
80	1,45	245,275	333,1263	4,79
80	2,0	195,8152	238,0778	4,61

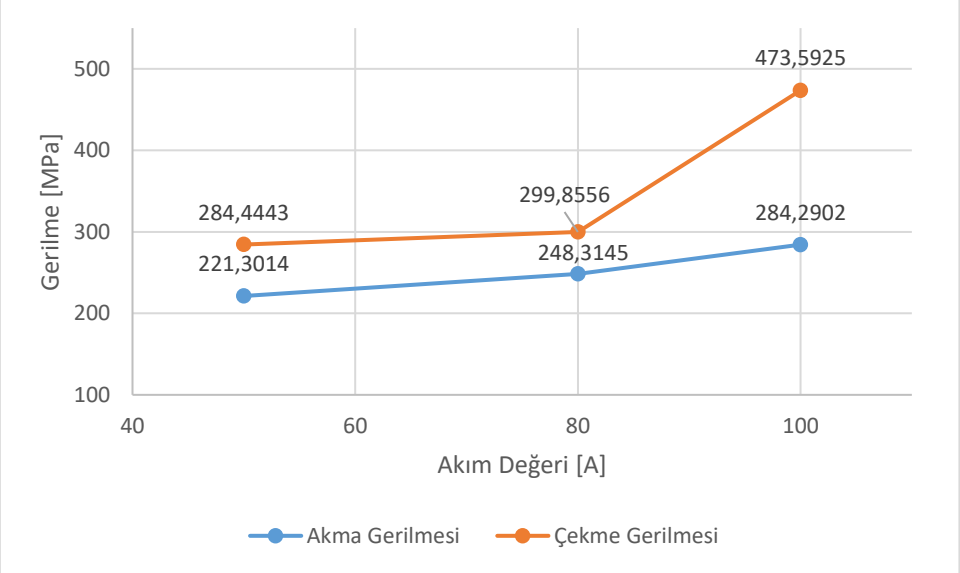

Görsel 1. Kaynak akımına bağlı gerilme değerleri

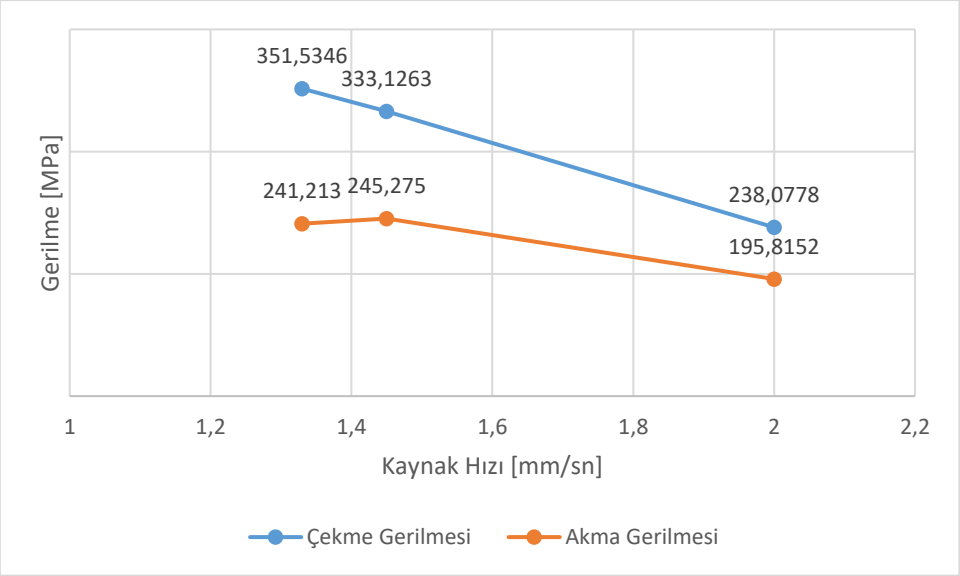

Görsel 2. Kaynak hızına bağlı gerilme değerleri

İlk olarak kaynaklı plakalarını temizleyici ile yüzey temizlenilmiştir. Temizledikten sonra kuruması için yaklaşık 8 dakika beklenilmiştir. Penetrant sıvısını kaynak bölgeleri yoğun olacak şekilde uygulanılmıştır (İşlem-1). Bu işlemden sonra penetrant sıvısının yüzeydeki kusurlu yerlere dolması yaklaşık 10 dakika beklenilmiştir. Yeterli süre bekledikten sonra temiz bir bez yardımıyla fazla penetrant sıvısını numunelerin üzerinden görülmeyecek şekilde temizlenilmiştir. Son olarak geliştirici, kaynak kusurlarını yüzeyde belirlemek için numunelerin üzerine sıkılmıştır (İşlem-2). Doğru sonuçlar alabilmemiz için yeterli süre beklenmiştir (5dk). 80 Amper – 2.28 mm/sn hızda kontrol sırasında gözenek tespit edilmiştir.

Görsel 4. Tahribatsız muayene görüntüsü 80 Amper – 2.28 mm/sn

4. SONUÇLAR

Gerçekleştirilen çalışma sonucuna göre, akım değeri arttıkça malzeme sünekleşmektedir. Akım değeri azaldıkça gevrekleştiği görülmüştür. İlerleme hızının en yüksek olduğu numunede gevrek bir kırılma meydana gelmiştir. Değerlere bakılarak sabit ilerleme hızında kaynak akım değeri arttıkça çekme ve akma dayanımlarında artış olduğu görülmüştür. Kaynak ilerleme hızındaki artışta akma gerilmesinde önemli bir artış veya azalış görülmeksizin çekme dayanımında düşüş olduğu görülmüştür. Elde edilen sonuçlara göre 100A ve 1.33 mm/sn ilerleme seçilmesi durumunda en mukavemetli kaynak sonuçları elde edilmiştir.

KAYNAKÇA

[1] Singh, A. K., Dey, V., & Rai, R. N. (2017). Techniques to improveweld penetration in TIG welding (A review). *Materials Today: Proceedings*, *4*(2), 1252-1259.

[2] Hong, K. M., & Shin, Y. C. (2017). Prospects of laser welding technology in the automotive industry: A review. *Journal of Materials Processing Technology*, *245*, 46-69.

[3] Huang, H. Y., Shyu, S. W., Tseng, K. H., & Chou, C. P. (2005). Evaluation of TIG flux welding on the characteristics of stainless steel. *Science and Technology of Welding and Joining*, *10*(5), 566-573.

[4] Kanemaru, S., Sasaki, T., Sato, T., Mishima, H., Tashiro, S., & Tanaka, M. (2014). Study for TIG–MIG hybrid welding process. *Welding in the World*, *58*(1), 11-18.

[5] Li, D., Lu, S., Dong, W., Li, D., & Li, Y. (2012). Study of the law between the weld pool shape variations with the welding parameters under two TIG processes. *Journal of Materials Processing Technology*, *212*(1), 128-136.

[6] Patel, N. S., & Patel, R. B. (2014). A review on parametric optimization of TIG welding. *International Journal of Computational Engineering Research*, *4*(1), 27-31.

[7] Hussain, A. K., Lateef, A., Javed, M., & Pramesh, T. (2010). Influence of welding speed on tensile strength of welded joint in TIG welding process. *International journal of applied engineering research*, *1*(3), 518.

[8] Greyjevo, O. G. T. V. Z., & Metodo, A. I. T. (2009). Optimization of weld bead geometry in TIG welding process using grey relation analysis and Taguchi method. *Materiali in tehnologije*, *43*(3), 143-149.

[9] Abuç, S., Östenitik Paslanmaz Çeliklerin Gazaltı Kaynak Yöntemi ile Kaynağında Koruyucu Gazın Mekanik Özelliklere Etkisi, Yüksek Lisans Tezi, Sakarya Üniversitesi, Fen Bilimler Enstitüsü, Sakarya, 2006.

Optimal Mixing Design of Fiber Self-Compacting Concrete and its Effect on the Compressive Strength of Concrete for Different Grades

Mohammad Reza Akhtari [1], Seyed Amin Tabatabaei Yamchi [2], Mir Shahriar Hashemi Zonozi [3], Salar Shateri [4], Amir Aminzadeh Ghavifekr[5]

[1] University of Tabriz, 0000 0003-1419-2317

[2] University of Tabriz, 0000-0001-6464-7207

[3] University of Tabriz, 0000-0003-3446-4930

[4] University of Tabriz, 0000-0001-7606-1545

[5] University of Tabriz, 0000-0002-0345-4150

ABSTRACT

Compressive strength is one of the most important and determining characteristics and mechanical properties of concrete, however, there are defects in concrete such as cracking, low hardness, and low tensile strength. In recent years, the fibers and additives (pozzolanic and superplasticizer) such as micro silica, and Nano-silica, have been used as an important material in the manufacture of concrete and reinforced concrete structures. The main purpose of this research is utilizing the biogeographical based optimization (BBO) algorithm as a meta-heuristic method to obtain the optimal mixing scheme for higher strength, which means that according to the valuesobtained from the algorithm, the lowest amount of consumables that caused the highest compressive strength can be obtained and calculated. According to the analysis of 219 pieces, the optimal compressive strength related to the analysis is 94 MPa, and in case of using 4 kg steel fibers, 21 kg glass fibers, 4 kg polypropylene fibers, 14 kg micro-silica , nano-silica 29 kg, fine grain 699 kg, coarse grain 711 kg, cement 332 kg and water 258 kg. Numerical results demonstrate that the combination of both micro-silica and nano-silica in concrete can have great effects on increasing the strength and reducing other materials which causes reduction in manufacturing costs.

Keywords: BBO Optimization Algorithm, Compressive Strength, Optimal Mixing, Self-Compacting Fiber Concrete

1. INTRODUCTION

Because civil researchers are looking for economic efficiency, lightening the weight of the structure, reducing the impact of forces caused by earthquakes, and increasing the strength of the structure attract much attention in recent years [1]. Therefore, increasing the strength and ductility

of the most widely used type of building materials, namely concrete, has become a major concern of researchers. Recently, artificial intelligence in civil engineering is moving towards sustainable development and is used in various parts of this field [2].

Due to the existence of defects in concrete such as tensile strength and low durability of concrete and also in some cases that require more strength, micro-nano silicon materials can be used to significantly reduce defects and achieve their goals of increasing resistance [3]. In flexural elements, the tensile strength parameter and the modulus of elasticity parameter play an important role in determining the amount of drift of the structure, and in the design and operation of them. In compressive elements, compressive strength is the main parameter to determine the characteristics of the concrete.

Due to the time-consuming experimental tests to achieve a mixing design in order to achieve the desired compressive strength, it is important to use theoretical methods to increase speed and reduce costs. But in the meantime, reducing the weight of materials used to make concrete and at the same time increase the resulting strength is very complicated [4]. Classical methods are not efficient to provide the optimal mixture design and do not take into account all of the vital characteristics. Therefore, utilizing methods based on meta-initiative algorithms reduces the amount of material to build concrete with compressive strength and their related costs.

In recent years, the use of meta-heuristic algorithms and intelligent processing to evaluate the optimal amounts of materials used in concrete production has been widely studied. In [5] a comprehensive research for concrete containing Metakaolin is proposed and artificial neural networks are utilized for estimation of the mechanical features of Metakaolin concrete. In [6] a combined multi-model approach is proposed to improve the accuracy of the prediction of the concrete compressive strength. Also, a genetic algorithm with multi-objective structure is utilized for mixture optimization regarding to the experimental constraints. 12 mixing designs with various amounts of mixtures and three types of cement strength classes (525,425,325) and 36 cubic samples (10 × 10 × 10) are taken into account in [7], and tested to estimate the compressive strength. The Taguchi approach is utilized for the optimal mixing plan. [8] proposed a mix design method based on integrated numerical simulation for heat transfer in concrete and utilized the genetic algorithm to minimize the danger of fast cracking within the specific conditions for the mechanical behavior of the concrete. In [9] total cost optimization of no-slump concrete regarding to some restrictions in compressive strength is studied and the overall cost is reduced by utilizing GA and particle swarm optimization (PSO). The proposed mixture includes Cement, silica fume,

water, fine aggregate, coarse aggregate and filler. In [10] an emerging method is proposed to optimize mixture proportion and modify the main features of concrete such as abrasion strength, flexural strength, slump, and drying shrinkage. GA, PSO, and differential evolution are utilized to scrutinize the model and solve the multi-objective problem.

The BBO algorithm is a relatively new algorithm that was introduced in 2008 [11] and is applied in this paper. BBO algorithm is utilized in [12] to solve reservoir operation problems and its results is compared with genetic algorithm. Considering the importance of the effects of mixing designs of concrete types on its mechanical properties, this paper investigates the optimal possible state for the type and amount of fibers (glass, pp). Also, the optimal ratio of fly-Ash and superplasticizer and the amount of its use in high-strength concretes have been studied.

To prepare a piece of concrete with a certain compressive strength, the mixing scheme is calculated and the mixing ratio of each of these materials is expressed to combine this amount of materials (sand, cement, and water) to obtain concrete with compressive strength. Due to the widespread use of concretes and the need to use them with different compressive strengths in different fields, the use of mixing designs has attracted much attention. Regrading to the widespread use of various fibers in the industry of reinforced concrete structures, in this study, the use of steel, glass, polypropylene fibers as well as the combination of nano-silica and micro-silica in a minimal way has been investigated and the optimal used Fibers and additives to improve compressive strength will be reported.

In this research, the BBO meta-heuristic algorithm is used to find the optimal values of the concrete mixing design for over-strengthening the 28-day compressive strength of self-compacting fiber concretes. The main goal in this research is to achieve an optimal state in the concrete mixing design with the maximum compressive strength of 28 days. The limitation of compressive strength of self-compacting concrete as the main step is formulated based on laboratory results and placement in statistical software and obtaining the coefficient by developing an analytical model and using meta-heuristic BBO algorithm. The results show that the proposed method, while providing compressive strength and other design limitations, has the ability to effectively reduce the cost of concrete construction. The rest of this paper is organized as follows: In section 2, mixing design of fiber compacting concrete is proposed. Cost function is defined in section 3. The structure of the BBO algorithm is described in section 4. Numerical simulations and conclusion are presented in section 5 and 6, respectively.

2. MIXING DESIGN OF FIBER COMPACTING CONCRTE

Fibers have been used to reinforce building materials since the 1960s. The brittle behavior of concrete and its weakness against tensile loads on concrete, forces civil engineers to use these materials that are available in natural and synthetic forms. The structures use steel reinforcements and fibers in an attempt to defeat tensile forces. According to the definition of ACI544, reinforced concrete or fiber concrete is concrete that is made with hydraulic cement and coarse-grained and fine-grained stone materials and sometimes from additives and separate and discontinuous fibers. It is made separately and discontinuously. These fibers are sometimes a good alternative to metal bars.

Adding fibers to concrete due to its randomness can prevent the growth of cracks in concrete, increase strength, improve stress and strain behavior, and increase the shape of concrete.

The most common type of fiber concrete in building structures is the use of steel fibers, but in this paper we seek to combine three types of fibers (steel, PP, glass) to achieve maximum strength with the optimal mixing design of these materials.

3. DEFINITION OF COST FUNCTION

Evolutionary algorithms include analyzing the old data and creating new data while preserving the old population and evolving the data, which suggests new solutions based on existing combinations and simple algorithm coding formulas. In meta-heuristic algorithms, the objective function is the main relation that optimizes using independent and dependent variables. The objective function acts as a black box that displays a solution by examining the variables.

The correct definition of the objective function formulation covers a large part of the optimization operation. Therefore, a proper process must be used to achieve the objective function. In this research, the independent variables of placement in the algorithm are water (w), cement (CE), coarse aggregate (CAG), fine aggregate (FAG), micro silica (MS), nano silica (NS), steel fibers (SF), glass fibers (GF), and polypropylene fibers (PPF) are considered a dependent variable of compressive strength. The objective function is derived from the above general elements.

4. Biogeography-BASED OPTIMIZATION ALGORITHM (BBO)

Optimization is a tool and method for selecting a member from a set of achievable members that are meta-heuristic (meta-exploratory) optimization for larger problems and continuous functions.

The BBO algorithm is an evolutionary and meta-innovative algorithm introduced by Dan Simon in 2008. This optimization algorithm is inspired by the spread and migration of living species in different habitats. This algorithm is based on how different species migrate from one island to another and create new species as well as the evolution of previous species, and there are several suitable and unsuitable habitats (islands) when the species from the habitats. Improperly migrate to suitable habitats, evolve and new species emerge.

Habitat characteristics index is denoted by HSI (habitat suitability index) and habitat suitability is determined by SIV (suitability index variables). In this study, SIV is considered as an independent habitat variable and HSI is considered as a habitat dependent variable. In this type of meta-heuristic evolutionary algorithms, the parameters or variables work together and the collective behavior of the parameters affects each other and causes a convergence.

5. NUMERICAL SIMULATION

A total of 109 pieces are entered into statistical software and fitted using the square (linear) regression function and the polynomial regression method.

Data errors are 0.5 times or less, that shows data are in a significant range. Tolerance and standard deviation of 3% for the data were controlled and no discrepancies or errors were observed according to the results. All steps and analyzes were performed on statistical software and the total results are presented in the form of statistical and graphical information.

General information from the data used (minimum and maximum) from the researchers' laboratory studies in the table below is that the objective function is extracted from this data using statistical software. Fisg [2-9] are obtained by statistical software as general data information.

TABEL.1. Statistical index of self-compacting fiber concrete constituents

Variables	Units	Min	Mean	Max
Water	kg/m^3	126	173.5	270
Cement	kg/m^3	274.5	449.3	540
Coarse - ag	kg/m^3	692	969.47	1150
Fine - ag	kg/m^3	625	861.41	1050
Micro-silica	kg/m^3	0	17.33	54
Nano-silica	kg/m^3	0	6.43	42.5
Steel-fiber	kg/m^3	0	2.45	25
Glass-fiber	kg/m^3	0	2.55	21.40
PP-fiber	kg/m^3	0	0.56	8.00

Using BBO meta-heuristic optimization algorithm and placing the mixing plan related to 109 pieces of concrete and the compressive strength of these concrete pieces in the algorithm, the following results are obtained. 10 times with maximum interaction are taken from the algorithm in order to test the accuracy of the data, the thigh algorithm was taken once with a maximum interaction of 100,000 and the data and mixing schemes and compressive strengths obtained from the optimization algorithm, which is a total of 10 mixing schemes with compressive strength, were predicted.

TABEL.2. Optimal concrete mixing design for 28-day strength utilizing BBO

N	W	Cement	Coarse ag	Fine ag	Micro Silis	Nano Silis	Steel Fiber	Pp Fiber	Glass Fiber	FC
1	184	294	802	677	10	10	10	0	19	79
2	258	332	711	699	14	29	4	4	21	94
3	241	283	1049	1006	22	7	18	0	13	92
4	253	284	1116	735	26	2	19	7	16	83.1
5	203	275	1031	986	10	9	11	6	10	93
6	260	236	768	932	3	16	5	1	19	85
7	242	279	694	1001	8	40	25	3	12	75
8	256	432	827	659	1	2	21	2	11	88
9	224	329	820	725	11	19	19	2	2	85.3
10	233	286	986	774	5	4	6	2	14	73.4

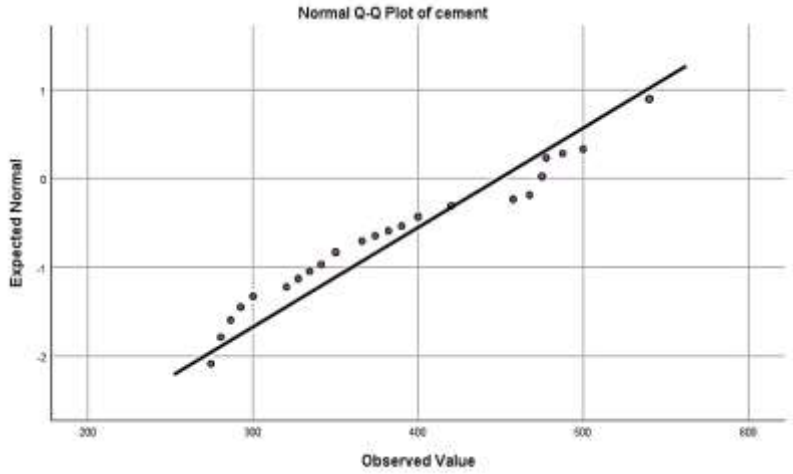

Fig 1. The degree of data scatter in Cement

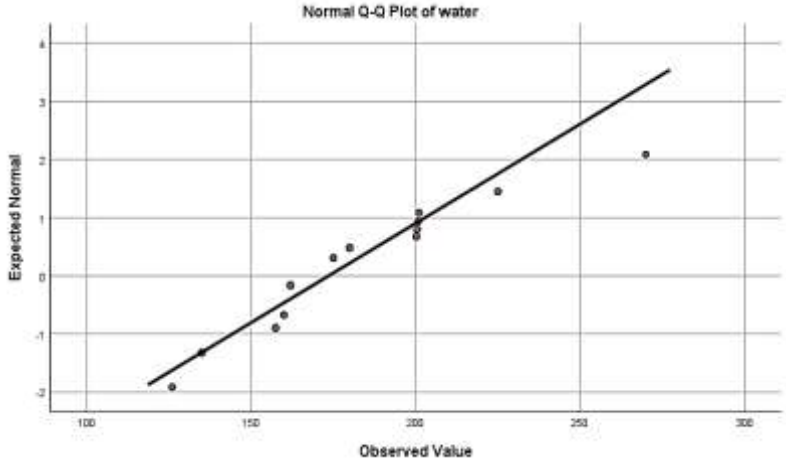

Fig 2 . The degree of data scatter in Water

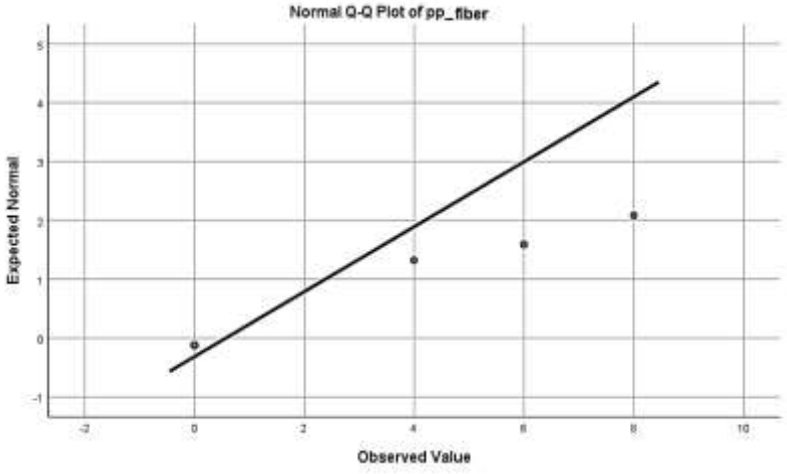

Fig 3. The degree of data scatter in Pp-fiber

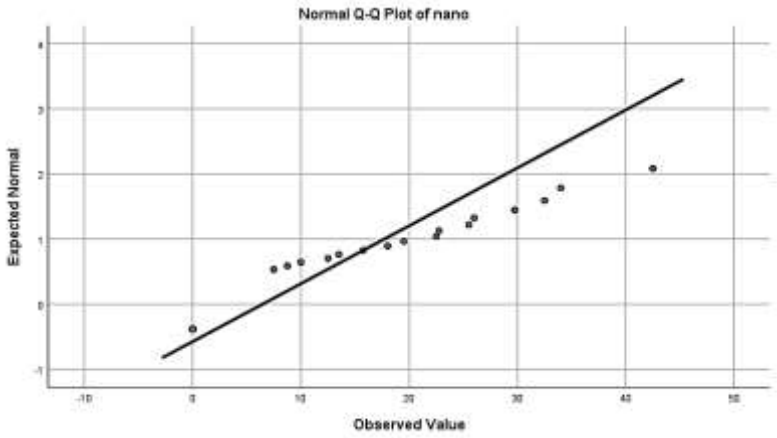

Fig 4 . The degree of data scatter in Nano

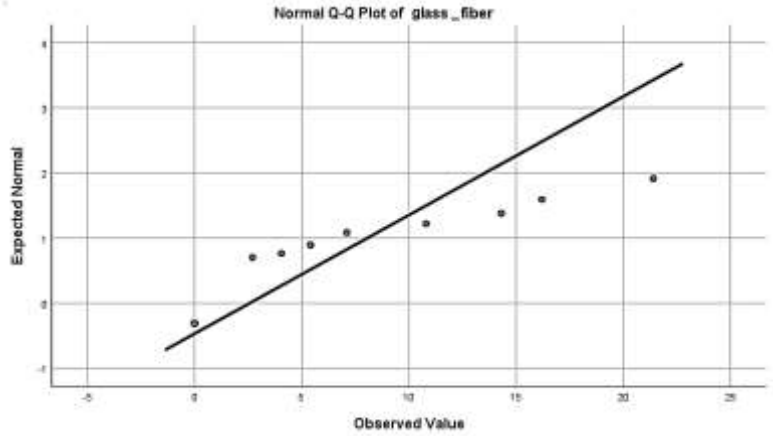

Fig 5. The degree of data scatter in Glass-fiber

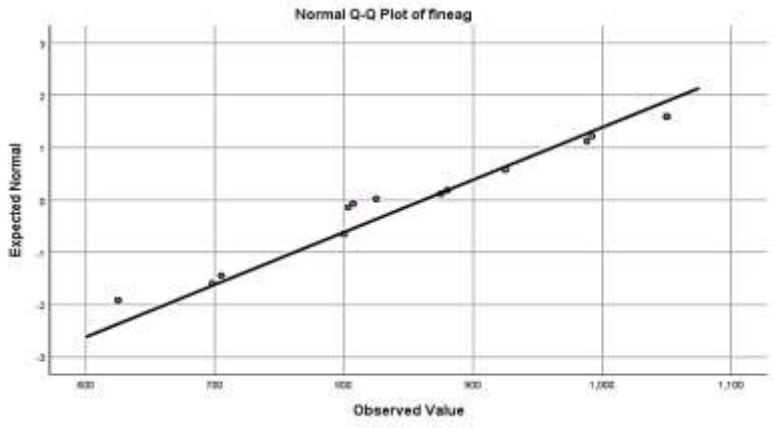

Fig 6. The degree of data scatter in Fine ag

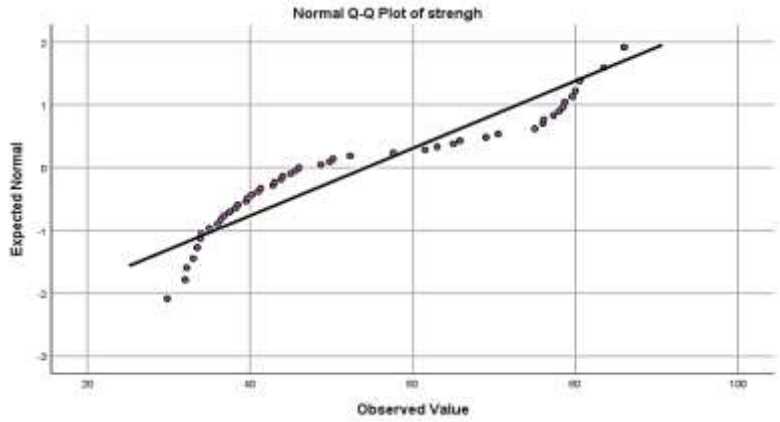

Fig 7. The degree of data scatter in Strengh

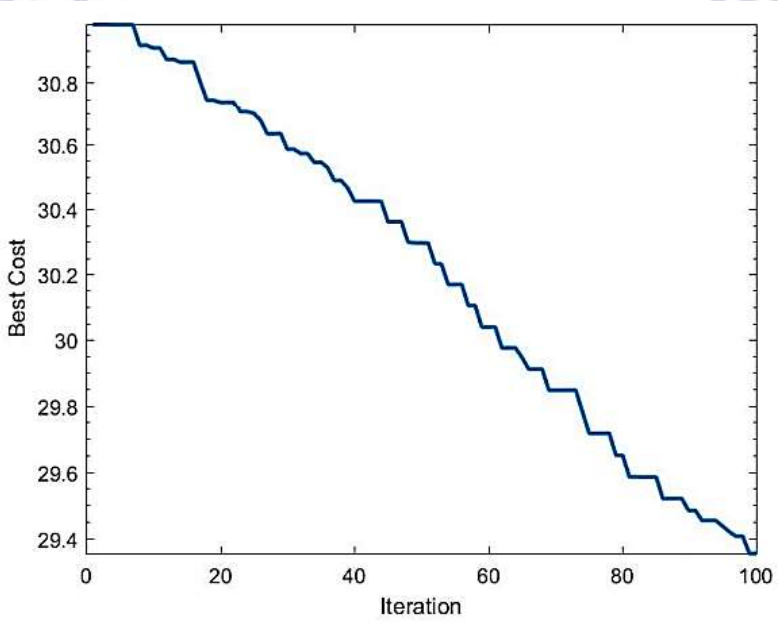

Fig. 8 . Evolution of optimal concrete mixing design for 28-day strength utilizing BBO

TABEL.3. Objective function coefficients

Coefficients						
Model		Unstandardized Coefficients		Standardized Coefficients	t	Sig.
		B	Std. Error	Beta		
1	(Constant)	40.408	8.352	------	-4.838	0
2	water	-0.143	0.027	-0.225	-5.234	0
3	cement	0.145	0.013	0.695	11.397	0
4	coarseag	0.033	0.006	0.178	5.364	0

5	fineag	0.017	0.006	0.091	2.94	0.005
6	micro	0.297	0.045	0.405	6.545	0
7	nano	0.55	0.059	0.332	9.343	0
8	Steel fiber	-0.157	0.075	-0.055	-2.085	0.043
9	Pp fiber	0.582	0.29	0.057	2.011	0.051
10	Glass fiber	-0.231	0.102	-0.068	-2.269	0.028

6. CONCLUSION

By utilizing large amounts of concrete materials, it is not necessarily possible to increase the compressive strength and it is useless and makes the weight of reinforced concrete structures heavier. The composition of self-compacting fiber-reinforced concrete materials must be composed of water, cement, micro silica and nano silica, and steel, glass, and polypropylene fibers. Utilizing BBO algorithm, leads to better compressive strength of the components, which reduces manufacturing costs and the weight of the concrete. As a result, it will reduce the weight of the structure and reduce the impact of the structure against earthquake forces.

7. REFERENCES

[1] Kang, D., Seo, K. S., Lee, H., & Chung, W. (2017). Experimental study on mechanical strength of GO-cement composites. Construction and Building Materials, 131, 303-308.

[2] Huang, Y., & Fu, J. (2019). Review on application of artificial intelligence in civil engineering. Computer Modeling in Engineering & Sciences, 121(3), 845-875.

[3] Yahyaei, B., Asadollahfardi, G., & Salehi, A. M. (2022). Study of using micro-nano bubble to improve workability and durability of self-compact concrete. Structural Concrete, 23(1), 579-592.

[4] Hameed, A. M., & Ahmed, B. A. F. (2019). Employment the plastic waste to produce the light weight concrete. Energy Procedia, 157, 30-38.

[5] Moradi, M. J., Khaleghi, M., Salimi, J., Farhangi, V., & Ramezanianpour, A. M. (2021). Predicting the compressive strength of concrete containing metakaolin with different properties using ANN. Measurement, 183, 109790.

[6] Motlagh, S. A. T., & Naghizadehrokni, M. (2022). An extended multi-model regression approach for compressive strength prediction and optimization of a concrete mixture. Construction and Building Materials, 327, 126828.

[7] Zarehparvar-Shoja, M., & Eskandari-Naddaf, H. (2017). Optimizing compressive strength of micro-and nano-silica concrete by statistical method. Civil Engineering Journal, 3(11), 1084-1096.

[8] Chiniforush, A. A., Gharehchaei, M., Nezhad, A. A., Castel, A., Moghaddam, F., Keyte, L., ... & Foster, S. (2021). Minimising risk of early-age thermal cracking and delayed ettringite formation in concrete–A hybrid numerical simulation and genetic algorithm mix optimisation approach. Construction and Building Materials, 299, 124280.

[9] Naseri, H. (2019). Cost optimization of no-slump concrete using genetic algorithm and particle swarm optimization. International Journal of Innovation, Management and Technology, 10(1), 33-37.

[10] Shirzadi Javid, A. A., Naseri, H., & Etebari Ghasbeh, M. A. (2021). Estimating the optimal mixture design of concrete pavements using a numerical method and meta-heuristic algorithms. Iranian Journal of Science and Technology, Transactions of Civil Engineering, 45(2), 913-927.

[11] Simon, D. (2008). Biogeography-based optimization. IEEE transactions on evolutionary computation, 12(6), 702-713..

[12] Haddad, O. B., Hosseini-Moghari, S. M., & Loáiciga, H. A. (2016). Biogeography-based optimization algorithm for optimal operation of reservoir systems. Journal of Water Resources Planning and Management, 142(1), 04015034.

REVEALING ^{137}Cs PHOTOPEAK by MULTI-PIXEL PHOTON COUNTER

Asst. Prof. Dr., ELIF EBRU ERMIS [1], Prof. Dr., CUNEYT CELIKTAS [2]

[1] Izmir Tinaztepe University, 0000-0001-6309-5973

[2]Ege University, Faculty of Science, 0000-0001-8608-066X

ABSTRACT

^{137}Cs gamma energy spectrum was examined by using a setup consisted of Multi-Pixel Photon Counter (MPPC) because the detector signals were vanished in the electronic noise signals. To obtain a noise free gamma energy spectrum, for this reason, the present study was performed. In the first part of the study, the energy spectrum of a solid ^{137}Cs radioisotope was achieved without any operation. In the second part, the noise was discriminated, and the photopeak of the radioisotope was unveiled by using a timing detection method (constant Fraction discrimination). Obtained spectra were compared with each other. The results showed that the proposed setup via the used method was successful in revealing the photopeak and enhancing the energy resolution.

Keywords: Multi-pixel photon counter, gamma energy spectrum, timing detection method.

1. INTRODUCTION

The MPPC (multi-pixel photon counter) is one of the devices called SiPM (silicon photomultiplier). It is a new type of photon-counting device using multiple APD (avalanche photodiode) pixels operating in Geiger mode. Although the MPPC is essentially an opto-semiconductor device, it has excellent photon counting capability and can be used in various applications for detecting extremely weak light at the photon counting level [1].

Zheng-Hua et al. studied the performance of the MPPC from room to liquid nitrogen temperatures [2] ; a study for testing gamma spectrometry performance of an MPPC with different types of scintillator performed by Grodzicka et al. [3]; the timing resolution of large size MPPC was investigated by Nagano et al. [4]; Kataoka et al. presented the current status and most recent progress of the MPPC-based scintillation detectors [5]; Ermis and Celiktas revealed the alpha peak of ^{226}Ra by the MPPC [6]; various characteristics of SiPMs that affect the use of SiPMs in gamma spectroscopy using scintillators reviewed by Grodzicka-Kobylka et al. [7]; Carnesecchi et al., investigated the time resolution capabilities of different kind of SiPMs coupled to the diffrent sizes of the scintillator [8]; the low-energy performances of three MPPCs coupled to different type of scintillators studied by Takahashi et al. [9]; Szawlowski et al. studied the performance of HAMAMATSU MPPC devices for scintillation light readout [10]; Light yields as a function of temperature were investigated by irradiation of LuAG:Pr, LuAG:Pr,Mo and LuYAG:Pr crystals with 662 keV gamma-rays from a ^{137}Cs source by Swiderski et al. [11]; Okazaki et al., developed a prompt gamma-ray imaging detector to measure ^{10}B distribution using a 50 mm times 50 mm times 10 mm $LaBr_3$(Ce) scintillator and an MPPC [12].

In the present study, an experimental setup consisted of the MPPC through constant fraction timing method was offered to eliminate the electronic noise for ^{137}Cs gamma energy spectrum since the spectrum was veiled by the electronic noise.

2. MATERIAL AND METHODS

In the spectrometer, a Hamamatsu MPPC module (C10507-11-100U type) was used. It is composed of a SiPM semiconductor sensor with an active area of 1 times 1 mm^2. The MPPC is consisted of a current to voltage converter circuit, a high-speed comparator circuit, (model no: TH27076), a high-voltage power supply circuit (model no: 12F-002), a temperature-compensation circuit, a counter circuit and a microcontroller (model no: HCE9S1043A), and also has an USB port connected to a PC for bias supply. These units were mounted on the HAMAMATSU K29-F40635 model readout board. The module has analog and comparator (digital) outputs (Fig. 1).

Figure 1. Photograph of the used MPPC module.

In the experimental study, CsI(Tl) inorganic scintillator (Epic-Crystal) was used. It has the dimensions of 10 times 10 times 30 mm^3, and coated with teflon tape. The scintillator was attached to the SiPM window by optical silicone gel (Silicone Technology, LS-3252). ^{137}Cs gamma radiation source was used in this work. Its shape is a point solid type and activity is 5 μCi (Spectrum Techniques).

A light-tight dark box was used to prevent the electronic noise due to the ambient light. The module, the scintillator and the source were put into this box. And also, the box was moved into a cooler to keep constant of the module temperature. Data acquisition time was chosen as 100 s during the measurements.

Block diagram of the setup is shown in Fig. 2.

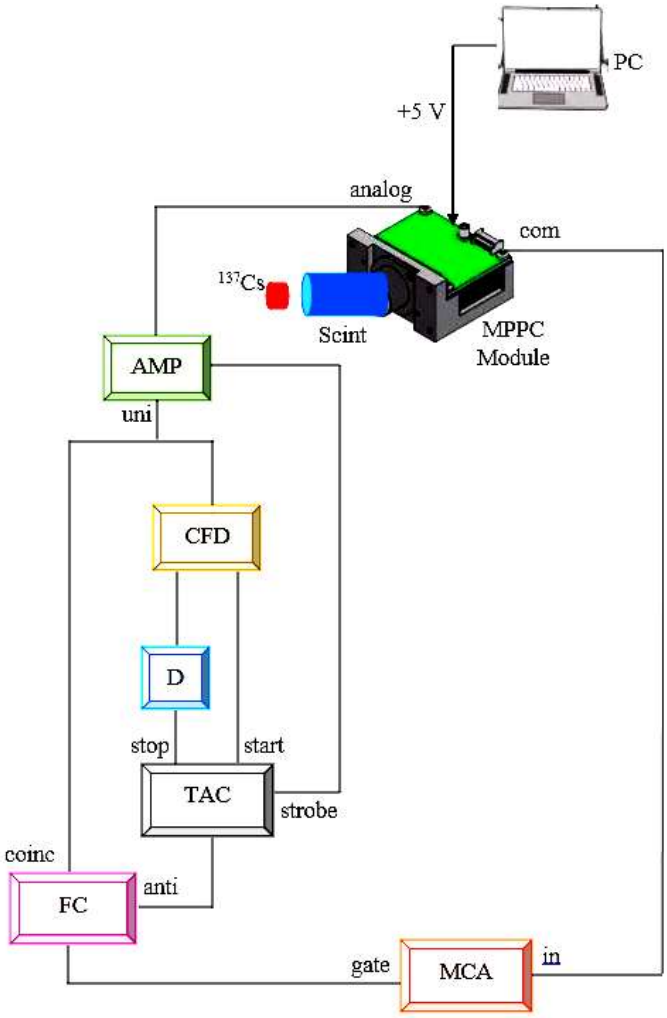

Figure 2. Block diagram of the used experimental setup. AMP: amplifier (ORTEC 671), CFD: constant fraction discriminator (ORTEC 584), TAC: time to amplitude converter (ORTEC 566), D: delay (ORTEC 425A, FC: coincidence module (ORTEC 414A), MCA: multichannel analyzer (ORTEC TRUMP 8k).

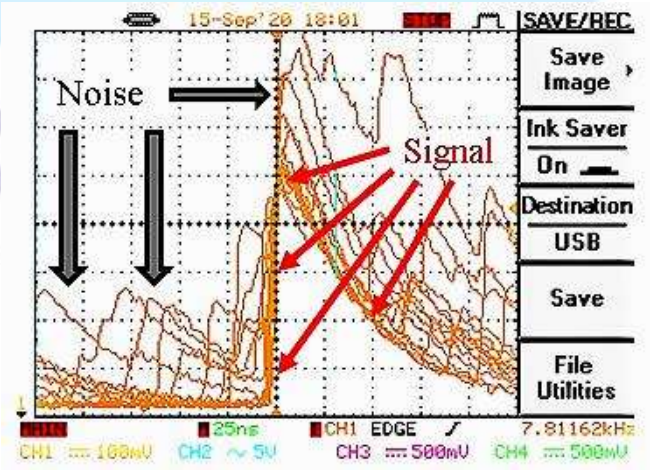

Figure 3. Analog output signal shape of the MPPC.

In Fig. 3, the analog output signal shape in a digital oscilloscope (GWINSTEK GDS-2204) of the used MPPC is shown. Since the output was too noisy, it was difficult to distinguish the original signal shape. The original signal shape was a bit sharper than the noise as can be seen in the figure. In order to see and evaluate how these signals gave an energy spectrum in an MCA, the spectra are given in the following figures; Fig. 4 for only noise signals, Fig. 5 for noise and source signals.

The output spectrum without the radioactive source i.e. the noise spectrum is given in Fig. 4 for the proper comparison.

Figure 4. MPPC module output spectrum without gamma source (MCA screen view).

For eliminating this negative effect on the gamma energy spectrum, constant fraction discrimination timing (CFDT) method was used. The analog output of the MPPC was sent to the amplifier (AMP) in the spectrometer in Fig. 2. The unipolar output of the AMP was connected to the constant fraction discriminator (CFD) to perform timing process. In CFDT method, the input signal to the constant fraction shaping circuitry is delayed, and a fraction of the undelayed pulse is subtracted from the input signal. A bipolar timing pulse is generated, and its zero-crossing is detected and used to produce an output logic pulse [13]. Timing outputs of the CFD were then sent to "start" and "stop" inputs of the time to amplitude converter (TAC) through delay (D) unit to constitute time difference between these outputs. The TAC device is used to generate a timing output that is proportional to the time interval between its start and stop signals. The timing output of the TAC and the AMP output were connected to fast coincidence (FC) to record the energy signals from the AMP triggered by the timing signal from the TAC.

The MPPC comparator (com) output generates a logic signal. Simultaneous connection of the MPPC com and FC outputs in the MCA gave the noise free energy spectrum, gating FC output with the MPPC output (Fig. 7).

3. RESULTS AND DISCUSSION

An experimental method through the CFDT was purposed here to unveil the ^{137}Cs gamma spectrum that remain in the noise spectrum by MPPC device. Direct gamma spectrum from the MPPC without using the timing method is shown in Fig. 5. Noise in the spectrometer negatively affected in ^{137}Cs gamma energy spectrum.

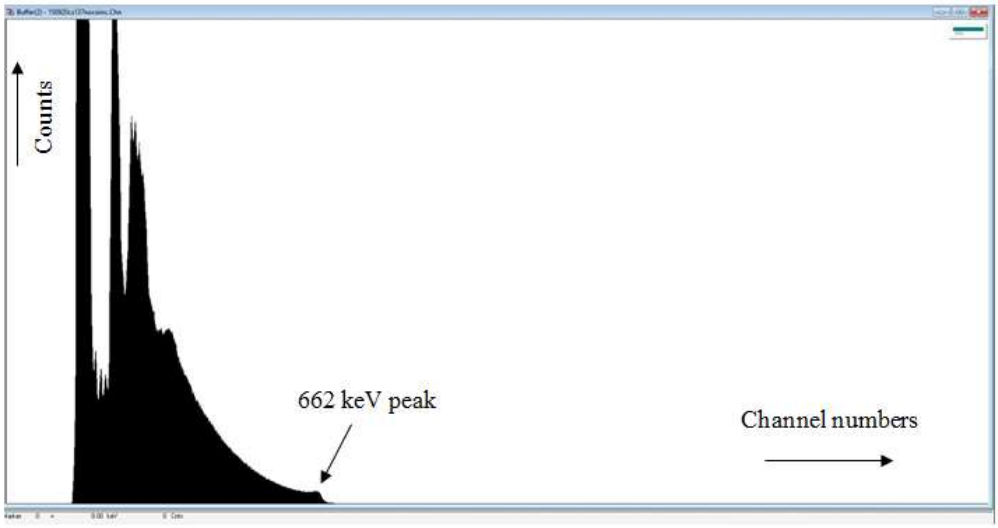

Figure 5. Gamma spectrum obtained directly from the MPPC module (MCA screen view).

As can be seen in Fig. 5, 662 keV-energy photopeak of the radioisotope cannot be distinguished. It is veiled by the noise in the whole spectrum. For this reason, in order to reveal the photopeak and eliminate the noise substantially, a spectrometer in Fig. 2 was offered using CFDT method. After applying the offered method to the MPPC signals, unveiled photopeak mostly free from the noise was obtained successfully as can be seen in Fig. 6. In addition, a reference ^{137}Cs gamma spectrum by a CsI(Tl) crystal in different dimensions and a different type MPPC (S11827-3344MG(x1)) is given in this figure for the comparison of the results. It can be noticed that the 662 keV-energy peak is more obvious than the reference one. Additionally, a quite good energy resolution value was obtained. This reflects the advantage of the used method here.

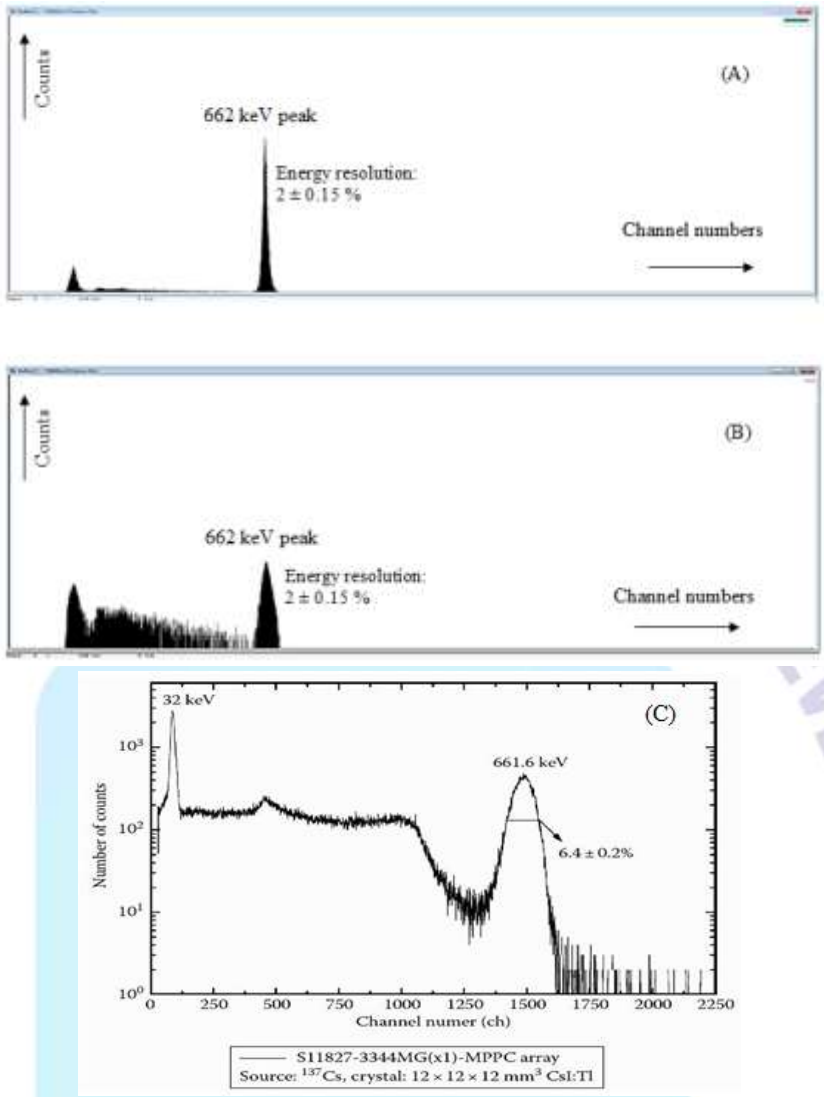

Figure 6. Comparison of the obtained noise free gamma spectrum with a reference spectrum (A) in linear scale (MCA screen view), (B) in log scale (MCA screen view), (C) gamma spectrum by a different type MPPC (Grodzicka, 2016).

In order to realize the difference between the spectra above, a comparison is given in Fig. 7, also.

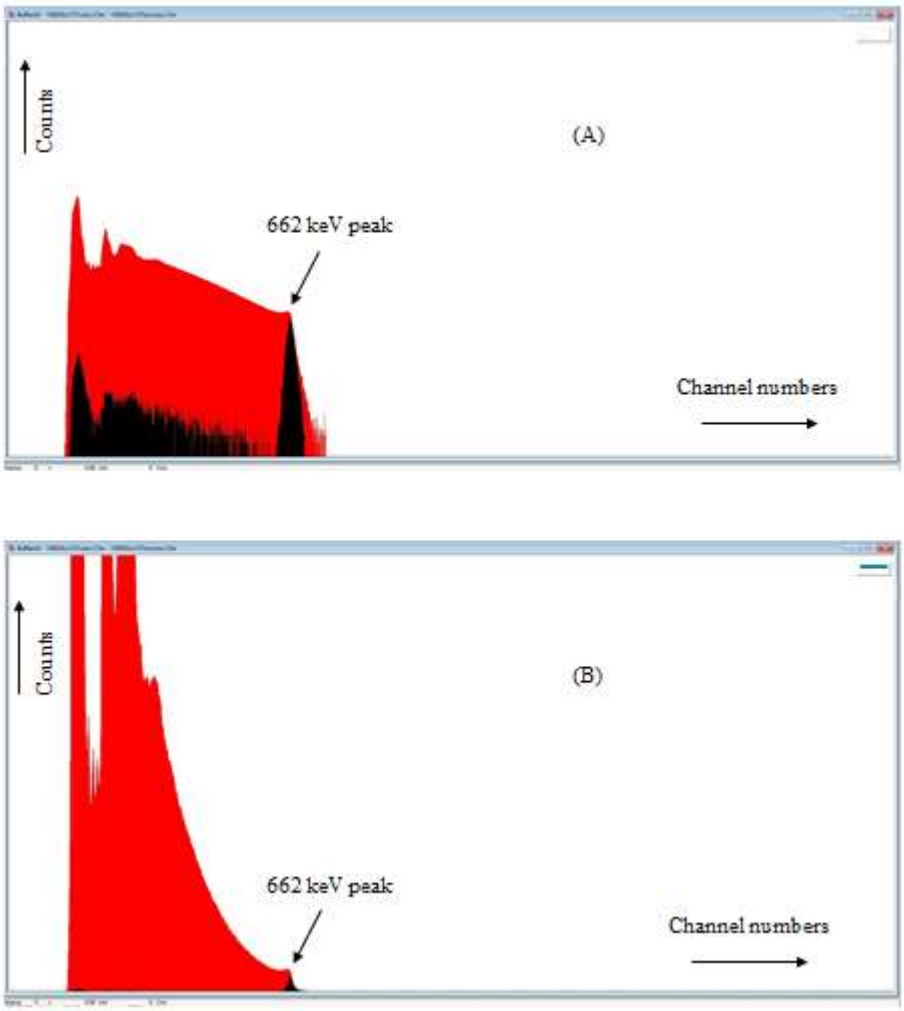

Figure 7. Comparisons of the spectra in Figs. 5 and 6. (A) in log scale, (B) in linear scale (Red: Noisy spectrum in Fig. 5, Black: Noise free spectrum in Fig. 6).

Figs. 4-7 are the direct MCA screen views. In these figures, x axes stand for the channel number, y axes label the counts per channel of the MCA screen.

It is clear from the Fig. 7 that a huge amount of the noise was overlapped the ^{137}Cs gamma spectrum. Moreover, it can be expressed that a large amount of noise signals were eliminated by means of the followed method.

4. GENERAL EVALUATION AND RESULTS

It can be concluded from Figs. 5-7 that the used spectrometer was highly successful in discriminating the noise components due to some effects such as ambient light, medium temperature, background, scattering etc., and in revealing the noise free gamma spectrum by the MPPC. By this way, it is possible to use the MPPC in the detection of any gamma radiation source for obtaining the neat energy spectrum, increasing the energy resolution of the MPPC also. This situation will help to use it in any gamma radiation detection spectrometer by eliminating the noise components in the future research studies as well as the student experiments.

REFERENCES

[1] https://www.hamamatsu.com/eu/en/product/optical-sensors/mppc/index.html (Accessed date: May, 11, 2022).

[2] Zheng-Hua, A., Jun-Guang, L., Feng, S., Tao, H., Xiao, C., Bo-Xiang, Y., Jian, F., Yu-Guang- X., Zhi-Gang W., Zhen, X., Xi-Lei, S., Qi-Wen, L., Ai-Wu, Z., FeiPeng, N., Li, Z., Li-Jun S., Yong- Shuai, G., Ying-Biao, L., Chong, W. (2012). Performance of MPPC at low temperature, Chinese Physics C, 36(7). https://doi.org/10.1088/1674-1137/36/7/012 (Accessed date: May, 11, 2022).

[3] Grodzicka, M., Moszynski, M., Szczesniak, T., Kapusta, M., Szawlowski, M., Wolski, D. (2013). Energy resolution of small scintillation detectors with SiPM light readout, Journal of Instrumentation, 8, P02017. https://doi.org/10.1088/1748-0221/8/02/P02017 (Accessed date: May, 11, 2022).

[4] Nagano, T., Sato, K., Ishida, A., Baba, T., Tsuchiya, R., Yamamoto, K. (2012). Timing resolution improvement of MPPC for Tof-Pet imaging, IEEE Nuclear Science Symposium and Medical Imaging Conference Record, N22-2. https://doi.org/10.1109/NSSMIC.2012.6551376 (Accessed date: May, 11, 2022).

[5] Kataoka, J., Kishimoto, A., Fujita, T., Nishiyama, T., Kurei, Y., Tsujikawa, T., Oshima, T., Taya, T., Iwamoto, Y., Ogata, H., Okochi, H., Ohsuka, S., Ikeda, H., Yamamoto, S. (2015). Recent progress of MPPC-based scintillation detectors in high precision X-ray and gamma-ray imaging, Nuclear Instruments and Methods A, 784. http://dx.doi.org/10.1016/j.nima.2014.11.004 (Accessed date: May, 11, 2022).

[6] Ermis, E.E., Celiktas, C. (2018). Revealing ^{226}Ra alpha peak by a multi-pixel photon counter, Nuclear Science, 3(3). https://doi.org/10.11648/j.ns.20180303.12 (Accessed date: May, 11, 2022).

[7] Grodzicka-Kobylka, M., Moszynski, M., Szczesniak, T. (2019). Silicon photomultipliers in gamma spectroscopy with scintillators, Nuclear Instruments and Methods A, 926. https://doi.org/10.1016/j.nima.2018.10.065 (Accessed date: May, 11, 2022).

[8] Carnesecchi, F., Agrawal, N., Alici, A., Antonioli, P., Arcelli, S., Basile, M., Bellini F., Cavazza, D., Cifarelli, L., Cindolo F., Colocci, M., De Caro, A., De Gruttola, D., De Pasquale, S., Fusco Girard, M., Giacalone, M., Hatzifotiadou, D., Jacazio, N., Liu, Z., Margotti, A., Nania, R., Noferini, F., Pinazza, O., Preghenella, R., Scapparone, E., Scioli, G., Wilkinson, J., Williams, M.C.S., Zampoli, C., Zichicci, A., Zuyeuski, R. (2020). Experimental study of the time resolution of SiPM coupled to scintillator, Nuclear Instruments and Methods A, 982, 164484. https://doi.org/10.1016/j.nima.2020.164484 (Accessed date: May, 11, 2022).

[9] Takahashi, H., Hirade, N., Uchida, N., Hirose, K., Mizuno, T., Fukazawa, Y., Yamaoka K., Tajima, H., Ohno, M. (2021). Silicon photomultiplier (Si-PM) comparisons for low-energy gamma ray readouts with BGO and CsI(Tl) scintillators, Nuclear Instruments and Methods A, 989, 164945. https://doi.org/10.1016/j.nima.2020.164945 (Accessed date: May, 11, 2022).

[10] Szawlowski, M., Meier, D., Maehlum, G., Wagenaar D.J., Patt, B.E. (2007). Spectroscopy and timing with MPPC and LYSO scintillators, IEEE Nuclear Science Symposium Conference Record, MM1-5, 4591-4596. https://doi.org/10.1109/NSSMIC.2007.4437131 (Accessed date: May, 11, 2022).

[11] Swiderski, L., Brylew, K., Drozdowski, W., Kobylka, M.G., Janiak, L., Moszyński, M. (2022). LuAG:Pr, LuAG:Pr,Mo and LuYAG:Pr relative light yield measured at wide temperature range with MPPC readout, Nuclear Instruments and Methods A, 1021, 165924. https://doi.org/10.1016/j.nima.2021.165924 (Accessed date: May, 11, 2022).

[12] Okazaki, K., Tanaka, H., Takata, T., Kawabata, S., AKabori, K., Sakurai, Y. (2020). Evaluation of the energy resolution of a prompt gamma-ray imaging detector using LaBr3(Ce) scintillator and 8 x 8 array MPPC for an animal study of BNC. Applied Radiation and Isotopes, 163, 109214. https://doi.org/10.1016/j.apradiso.2020.109214 (Accessed date: May, 11, 2022).

[13] Bedwell, M.O. and Paulus, T.J. (1979). A constant fraction differential discriminator for use in fast timing coincidence systems. IEEE Transaction on Nuclear Science, NS-26(1). https://doi.org/10.1109/TNS.1979.4329669 (Accessed date: May, 11, 2022).

TECHNO-ECONOMIC ANALYSIS OF FDCA PRODUCTION FROM BIOMASS AND BIOETHANOL AS A CO-PRODUCT

Chemical Engineer, Özge DOYRANLI [1], Assoc. Prof. Dr. Hasan Şıldır[2], Asst. Prof. Dr. Muhammed Enes ORUÇ[3], Dr. Abdullah Bilal ÖZTÜRK[4]

Gebze Technical University, -0000-0002-2937-559X[1]

Gebze Technical University, -0000-0003-1016-9865[2]

American University of the Middle East, -0000-0001-6661-6498[3]

Yıldız Technical University, -0000-0002-8414-4225[4]

Biorenewable polymers is crucial for plastic manufacturing industry because of their advantages on enviromental sustainability and the sustainable production for value-added products. These polymers can be produced from low costly biomass such as plant biomass, food wastes, agricultural wastes and biowastes. Petroleum-based polymers used in the production of food containers, packaging, plastic bottles etc. can be substituted by bio-based polymers. FDCA has attracted considerable attention as a building block for bio-based polymers, as it can substitute conventional petroleum-derived terephthalic acid (TPA) as a monomer for the synthesis of polyethylene terephthalate (PET). Beside that, bioethanol is produced by fermentation of renewable biomass, its usage can significantly reduce fossil fuels use and exhaust greenhouse gas emission. Lignocellulose consists of lignin, cellulose and hemicellulose and low costly therefore they can be used for bioethanol production. Beside that, different feedstocks for bioethanol production and global production of bioethanol is investigated. The aim of the study is to make a techno-economic analysis of the process in which bioethanol is produced as a by-product in addition to the production of 2,5- Furandicarboxylic acid (FDCA) from 5-hydroxymethylfurfural (HMF). To validate the process parameters for an industrial-scale process, it is critical to examine the effects of process parameters using a process simulation tool. To this end, a techno-economic evaluation of the FDCA production from the lignocellulosic biomass via catalytic oxidation was performed using SuperPro Designer. For the scenario under consideration, the total capital investment charged to this project was found 84.056.000 $ and the payback time was 5.19 years.

Keywords: 2,5- Furandicarboxylic acid (FDCA), 5-hydroxymethylfurfural (HMF), bioethanol, biomass, SuperPro Designer

BİR OTOMOBİL MOTOR ALT BRAKET SACININ KABARTMA TİPLERİNE BAĞLI OLARAK DOĞAL FREKANSININ ARTIRILMASI

EMRE YUMURTACI [1], ALTUĞ BAKIRCI [2] , SEVDA TELLİ ÇETİN [3]

[1] Bursa Uludağ Üniversitesi, 0000-0001-5832-2035

[2] Bursa Uludağ Üniversitesi, 0000-0003-0438-6337

[3] Bursa Uludağ Üniversitesi, 0000-0002-3281-9112

ÖZET

Araçların hafifletilmesi günümüzde yakıt verimliliği ve sürdürülebilirlik konularının öne çıkmasıyla önemli bir konu haline gelmiştir. Araçlarda motorlar dış etkilere karşı korunması gereken önemli parçalar arasında bulunur. Titreşerek çalışan motorun bir koruyucu tarafından korunması gerekmektedir. Motordan gelen titreşim sebebiyle motor koruyucu braketin doğal frekansının istenilen değerlerde olması ihtiyacı doğar. Bir sac parçası üzerinde belirli bölgelerde şekil değişiklikleri ile frekansın değiştirilmesi hedeflenebilinir. Aynı zamanda uygun yerlerden boşaltmalar yapılarak hafifletme yapılırken frekans kontrol altında tutulabilinir. Bu çalışmada 6 noktadan motora sabitlenmiş motor altındaki braketin formunda oynamalar yapılarak bu değişikliklerin doğal frekansının yükseltilmesi üzerindeki etkisi incelenmiştir. Topografya optimizasyonu ve modal analizler kullanılmıştır. Topografya analizinde yatay, dikey ve dairesel yönelim kısıtlarının olduğu ve yönelim kısıtının olmadığı optimizasyon çalışmaları yapılmıştır ve dizayn hacminden dolayı kabartmaların yükseklik kısıtı 6 mm olarak belirlenmiştir. Topografya sonuçlarına bağlı olarak farklı kesit görünümlerine sahip formlarda tasarımlar yapılmış ve modal analiziyle bu form değişiklerinin ve yönelimlerin doğal frekans üzerindeki etkisi ölçülmüş ve karşılaştırılmıştır. Çalışma sonucunda yatay ve dikey yönlendirilmiş form tiplerinde frekans değerleri birbirine yakın çıkmıştır. Frekans değeri artışı genel olarak kabartma sayısına bağlı olarak değil topografya kısıtındaki 6 mm yüksekliğine sahip yüzeylerin alanının büyüklüğüne bağlı olarak arttığı gözlemlenmiştir. En yüksek frekans değeri topografya analizinde yönlendirme kısıtı olmadan sadece yükseklik kısıtıyla yapılan analiz sonucunda tespit edilen bölgelerin tümünün yükseltilmesiyle ortaya çıkan sacın formunda elde edilmiştir.

Anahtar Kelimeler : Doğal Frekans, Motor Braketi, Form Şekli, Kabartma Yönelimi

1. GİRİŞ

Enerji tasarrufu ve çevre kirliliği, son yıllarda otomotiv mühendisliği alanında en önemli araştırma alanı haline gelmiştir. Bir aracı hareket ettirmek için gereken enerji çoğunlukla ağırlığı ile

orantılıdır. Hafif tasarım modern otomobil üretiminde önemli bir konu olarak günümüzde ciddi çalışmalara alan açmaktadır [1,2]. Hafifletilen otomobil parçalarında ikincil konulardan biri özellikle motora yakın elemanlarda frekansın istenilen seviyede tutulmasıdır. Motor içinde oluşan titreşim, içten yanmalı motorların ileri geri hareket eden ve dönen parçalarından kaynaklanmaktadır; ayrıca dişli kutusunun dönmesi ve diferansiyel gibi diğer parçalar da iç titreşimin etkilerini arttırmakta, bu da destekleyici yapının farklı modlarda davranış göstermesine neden olmaktadır. Bu tip çalışmalar otomotiv sektöründe genel olarak NVH (gürültü, titreşim ve sertlik) adı altında gerçekleştirilmektedir [3,4,5].

Park ve diğ. yaptıkları çalışmada genel olarak mühendisin tecrübesine bırakılan frekans ve mukavemet iyileştirmek için metal sac üzerine yapılan kabartma desenin doğal frekans üzerindeki etkilerini sistematikleştirmeye yönelik çalışmalardan bahsetmiştir. Bahsi geçen çalışmalarda kabartmaların şekil, boyut, konum ve yönelimlerinin kısıtlara göre sistematik bir şekilde yerleşimi üzerine çalışmalara değinilmiş ve bu çalışmalarda frekans kontrolünün en iyi şekilde nasıl yapılabileceği araştırılmıştır ve bu eklemeleri optimum bir şekilde yapabilmek için birçok yaklaşım geliştirilmeye çalışmıştır. İlgili çalışmada da çevredeki tüm kabartmalı elemanların frekans artış hassasiyetleri analiz edildikten sonra komşu küçük kabartma elemanların birleştirilmesiyle oluk şekli oluşturulmuştur. İlk kanal açma konumu, modal gerinim enerjisi en yüksek olan elemandan başlatılmış ve kanal açma komşu elemanlara doğru genişletilmiştir. Önerilen yöntem kullanılarak, doğal frekans, bir mühendisin deneyimiyle değil, sistematik algoritmayla büyük ölçüde artırıldığı ve hassasiyet kontrol alanı ve komşu kenar yaklaşımlarıyla hesaplama verimliliği önemli ölçüde azaltılabildiği görülmüştür [6].

Bu çalışmada 6 noktadan motora sabitlenmiş braketin saca plastik şekil vermeyle farklı kabartma tiplerinde ve yönelimlerinde saca form verilmesiyle sacın desensiz halinde sahip olduğu doğal frekans değerinin artırılması hedeflenmektedir. Hedefe ulaşabilmek için farklı kabartma şekillerinin ve yönelimlerinin etkisine bakılmıştır. Bu şekillerin ve yönelimlerinin desen belirlenirken karar verici rol oynaması beklenmektedir.

2. MATERYAL ve METOT

İşlemsiz halde 900 mm genişliğinde 730 mm boyunda ve 2 mm kalınlığında dikdörtgen plakadan imal edilen motor alt braket sacı Görsel 1'de verilmiştir. Motor koruma sacı 6 tane bağlantı noktasından gövdeye ve motora sabitlenmiştir. Bu sac üzerinde plastik şekil verme ile eklenen kabartmaların tiplerinin ve yönelimlerinin doğal frekansa etkisi araştırılmaktadır. Analizler Hypermesh Student sürümünde topografya optimizasyonu uygulanmış ve 10 farklı mod olmak üzere doğal frekanslarına bakılmıştır. Topografya optimizasyonunda saca eklenecek kabartmaların yönelimleri optimizsayon kısıtı olarak girilmiştir. Bu yönelim kısıtları dikey, yatay, dairesel yönelime sahip ve bir tane de herhangi bir yönelimi olmayacak şekilde 4 farklı tipte belirlenmiştir. Yapılan optimizasyonda sacın plastik şekil verilmesindeki kesit alanı kısıtları minimum kabartma genişliği 8 mm ve yüksekliği maksimum 6 mm olarak bağlantı noktaları ve dizayn hacmi düşünülerek tespit edilmiştir. Sabitleme noktaları dizayn hacmi dışında bırakılmıştır. Görsel 2'de kullanılan kabartma tiplerinin kesitleri ve kesitteki boyutlandırmaları verilmiştir. Bu kesit tiplerine sahip sac formunda kalıptan çıkma veya şekil verme esnasında olası buruşma ve yırtılmalar göz önünde bulundurularak haddelemeye uygunluğun da sağlanması için kenarlara 3 mm'lik köşe

yuvarlatma işlemi uygulanmıştır. Çıkan topografya sonuçlarına göre motor braketine yatay, dikey ve dairesel yönelimli ve yönelimsiz kabartmalar Catia yüzey modellemesinde eklenmiştir. Farklı şekillerde eklenmiş kabartmaların modelleri oluşturulmuş ve her birine ayrı ayrı Hypermesh'te modal analiz uygulanmıştır.

Görsel 1. Motor alt koruma sacının ham görünümü

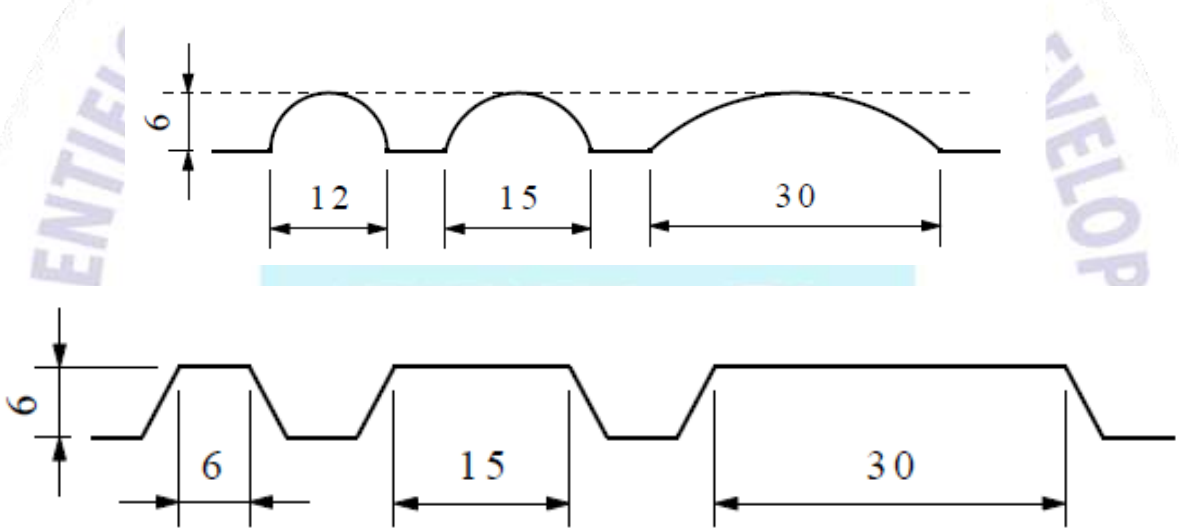

Görsel 2. Analizlerde kullanılan silindir ve yamuk kesite sahip kabartmaların kesit görünüşleri

Her bir modele modal analizi uygulanırken ilk olarak yüzeylerdeki fazla çizgi ve noktalar silinerek tek bir yüzey haline getirilmiştir (Görsel 3). Ardından birbirine yakın iki çizgi arası mesafeye göre mesh ölçülerine karar verilmiş ve tüm yüzey seçilerek mesh uygulaması yapılmıştır. Sonrasında her bir mesh tekrardan gözden geçirilmiştir. Mesh kalitesi sorun oluşturabilecek bölgeler (Görsel 4a) tespit edilerek tekrardan lokal olarak mesh işlemi yapılmıştır. Yapılan lokal mesh düzeltme işlemi Görsel 4b ve Görsel 4c'de verilmiştir. Düzeltme sonucunda mesh kalitesi tekrar kontrol edilerek; kenar, açısal çarpıklık ve çarpılma oranları (aspect ratio, jacobian, skew, warpage) gibi kriterlere göre referans noktasının altında kalan bölgeler hızlı bir şekilde optime edimiştir. Ardından malzeme bilgileri ve özellikleri parçaya tanımlanmıştır. Sabitleme noktaları belirlenmiş ve bu noktalar parçaya tanımlanmıştır. Görsel 5'te sabitleme noktaları mavi renk ile optimizasyon dışında bırakılan bölgeler mor ve dizayn alanı yeşil ile gösterilmiştir. Sonrasında analiz kısmında modal analiz seçilerek mod sayıları program arayüze girilerek analiz koşturulmaya hazır hale getirilmiştir.

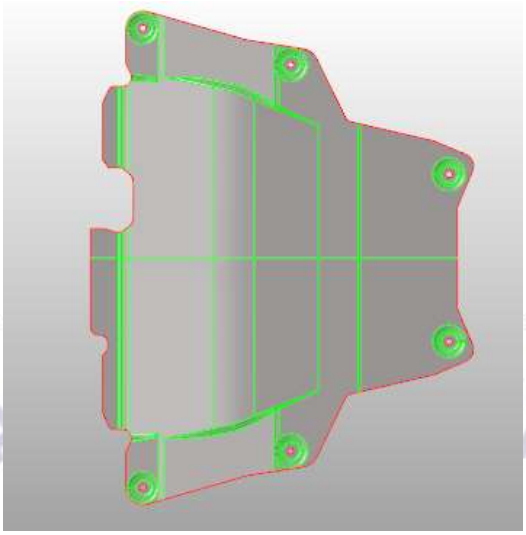

Görsel 3. Fazla çizgilerin hypermeshte yok edilmesi

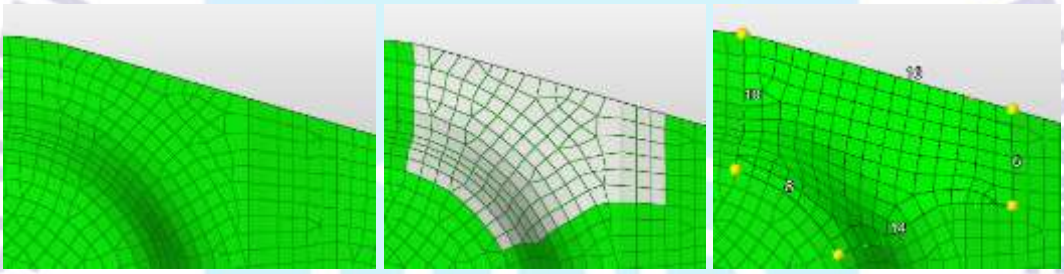

a **b** **c**

Görsel 4. Ağ yapısında oluşan çarpıklıkların giderilmesi

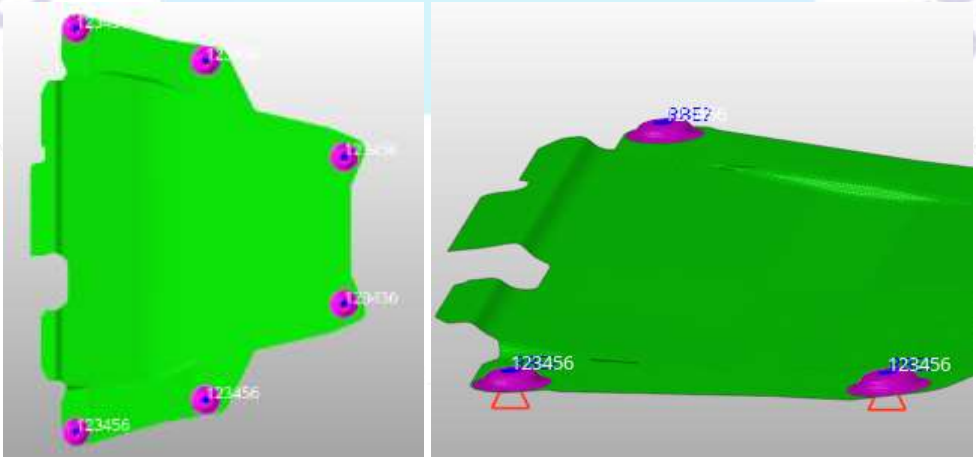

Görsel 5. Motor braketinin sabitlendiği 6 nokta

Çıkan topografya analizleri sonucunda oluşturulan modellere belirli bir model kodu verilmiştir. Numunelerin kodlandırılması: R, referans değeri; YL1, yatayda lineer yamuk kesit; YL2, yatayda

lineer geniş; YL3, yatayda lineer çoklu; YS1, yatayda lineer silindir kesit; YDS, yatayda dikey silindir; D dairesel çoklu; DT, dairesel içi dolu; DLS, dikeyde lineer silindir kesit ve SÇ, serbest çalışmayı ifade edecek şekilde yapılmıştır.

3. SONUÇLAR VE DEĞERLENDİRME

Topografya optimizasyonu sonucunda kırmızı alanlar 6 mm maksimum yükseklikte kabartma eklenmesi gerektiğini ifade ederken mavi bölgeler kabartma eklemenin doğal frekansı değiştirmeyeceğini ifade eden 0 mm yüksekliği göstermektedir. Kırmızı ve mavi bölge arasında yüksekliklerin ölçeklendirmesi sırasıyla kırmızı, turuncu, sarı, yeşil ve mavi renkte gösterilerek 6 mm'den 0 mm ye yaklaşmaktadır. Görsel 6'da topografya analiz sonuçları verilmiştir. Analiz sonuçlarına göre kırmızı bölgelere kısıtlar doğrultusunda kabartmalar eklenmesi kararlaştırılmıştır.

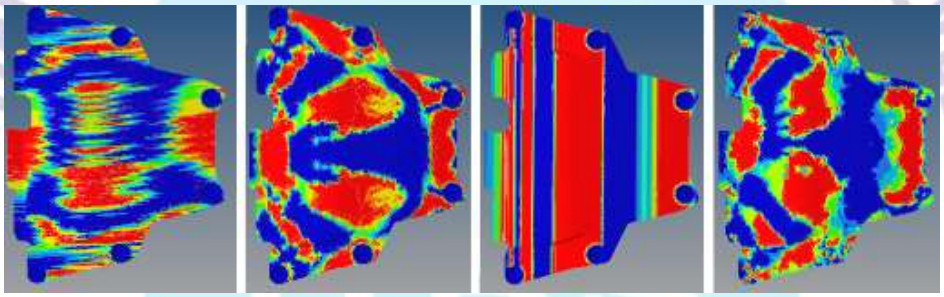

Görsel 6. Topografya analizleri (soldan-sağa) sırasıyla: Dikeyde lineer kabartma; dairesel kabarma; yatayda lineer kabartma; yönelimsiz serbest formda kabartma

Yapılan 4 farklı topografya sonucuna göre dikey (Görsel 7), dairesel (Görsel 8), yatay (Görsel 9), serbest (Görsel 10), kabartmalar modele yamuk ve dairesel kesit görünüme sahip olacak şekilde Görsel 2'de ki gibi eklenmiştir. Her bir topografya sonucuna göre birden fazla farklı kesit görünüşe sahip kabartma tipleri eklenerek birbiri arasındaki frekans değerleri karşılaştırılmış ve hangi kabartma modelinin frekans değeri için daha etkili olduğu tespit edilmiştir.

Görsel 7. Bazı boydan kabartma örnekleri

Görsel 8. Dairesel kabartma şekilleri sırasıyla, iç içe; tek; ve içi dolu

Görsel 9. Yatayda 15 ve 30 mm'lik genişlikteki dairesel ve yamuk kesite sahip kabartma örnekleri

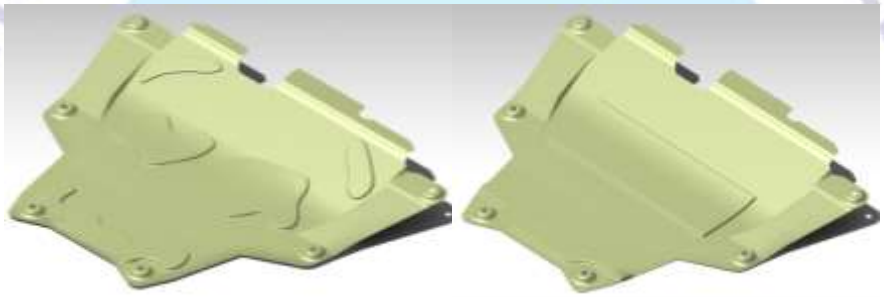

Görsel 10. Serbest form kabartma ve geniş form kabartma

Yapılan analizler sonucunda kabartma eklenmemiş koruma sacı referans değeri olarak kabul edilmiştir. Referans değeri analiz sonucunda 30.18 Hz olarak elde edilmiştir. Diğer numuneler Çizelge 1'de referans değerine göre yüzde artış değişimi olarak verilmiştir.

Çizelge 1. Yapılan eklemelerin braketin ham haline göre yüzde artışı

No	Numune kodları	Hz artışı (%)
Numune R	Referans	0.00
Numune 1	YL1	6.63
Numune 2	YL2	14.84
Numune 3	YL3	5.70

Numune 4	YS1	5.17
Numune 5	YDS	3.58
Numune 6	DÇ	8.55
Numune 7	DT	11.43
Numune 8	DLS	4.54
Numune 9	SÇ	34.76

4. GENEL DEĞERLENDİRME VE SONUÇLAR

Bu çalışmada bir motor alt koruma sacının doğal frekansını artırabilmek için çeşitli yönelim ve geometrik kısıtlar doğrultusunda topografya analizleri gerçekleştirilmiştir. Topografya analizinin sonuçlarına göre farklı tiplerde kabartma desenine sahip modeller tasarlanmış ve bu modellere modal analizler uygulanmıştır. Modal analizlerin sonucunda:

- Topografya analizinde yönlendirme kısıtı olmadan sadece yükseklik kısıtıyla yapılan analiz sonucunda tespit edilen bölgelerin tümünün yükseltilmesiyle ortaya çıkan serbest formda kabartılara sahip sac modeli diğer kabartma modellerine (yamuk-silindir kesit tipli ve yatay-dikey-dairesel yönlenmiş) göre daha etkili olduğu ve doğal frekansı referans modele göre %34.76 attırdığı gözlemlenmiştir.
- Yatay ve dikey yönelimle eklenen yamuk ve silindir kesit tipine sahip olacak şekilde form verilen sacların frekans değerleri birbirine çok yakın çıkmıştır.
- Frekans değeri artışı genel olarak kabartma sayısına bağlı olarak değil topografya kısıtındaki 6 mm yüksekliğe sahip yüzeylerin alanının büyüklüğüne bağlı olarak arttığı gözlemlenmiştir.
- Yamuk, lineer ve dairesel kabarmaların frekans artışı %10-15'lerde iken serbest formda %30 un üzerinde çıkmıştır.

KAYNAKÇA

[1] J. Zhang, G. Shen, Y. Du, and P. Hu, "Modal analysis of a lightweight engine hood design considering stamping effects," Appl. Mech. Mater., vol. 281, pp. 364–369, 2013, doi: 10.4028/www.scientific.net/AMM.281.364.

[2] M. Li, D. Hu, X. Liu, and H. Yuan, "The Topology Optimization Design Research for Aluminum Inner Panel of Automobile Engine Hood," IOP Conf. Ser. Mater. Sci. Eng., vol. 269, no. 1, pp. 0–6, 2017, doi: 10.1088/1757-899X/269/1/012065.

[3] M. Y. Park, Y. Park, and Y. S. Park, "Raising natural frequencies of a structure via surface-grooving technique," Struct. Multidiscip. Optim., vol. 34, no. 6, pp. 491–505, 2007, doi: 10.1007/s00158-007-0103-9.

[4] E. Armentani, V. Giannella, A. Parente, and M. Pirelli, "Design for NVH: Topology optimization of an engine bracket support," Procedia Struct. Integr., vol. 26, no. 2019, pp. 211–218, 2020, doi: 10.1016/j.prostr.2020.06.024.

[5] S. M. Aathif Akmal and G. Bharathiraja, "Analysis of engine mount material for automotive vibration and noise reduction," Mater. Today Proc., 2022, doi: 10.1016/j.matpr.2022.03.462.

[6] S. M. Aathif Akmal and G. Bharathiraja, "Prediction of dynamic characteristics of four cylinder engine chassis using Finite element analysis approach," Mater. Today Proc., 2022, doi: 10.1016/j.matpr.2022.03.370.

KUVARS KUMUNUN AKIŞKAN YATAKLI KURUTUCUDA KURUTULMASININ DENEYSEL İNCELENMESİ

AYSUN ŞENGÜL[1], SONER ÇELEN[2], HERKAİL ÖZEN[3]

[1] ASOS Proses Makina San. ve Tic. A.Ş., 0000-0003-1502-6775

[2] Tekirdağ Namık Kemal Üniversitesi, 0000-0001-5254-4411

[3] ASOS Proses Makina San. ve Tic. A.Ş., 0000-0002-1580-8155

ÖZET

Kurutma veya dehidrasyon, mikrobiyal bozulmaların ve kimyasal reaksiyonların yavaşlatılması veya durdurulması amacıyla katı maddeden su gibi uçucu sıvının uzaklaştırılması işlemidir. Bu çalışmada, kuvars kumunun dikey tip akışkan yataklı kurutucuda kurutulması amaçlanmıştır. Kuvars kumunun kurutulmasının avantajı iyi akış karakteristiği sağlaması ve farklı katkı maddeleri ile daha iyi karışmasıdır. Günümüzde kum kurutma işlemleri çok farklı sistemlerle yapılmaktadır. Kullanılan dikey tip akışkan yataklı kurutucu 108 mm çapında, 151 mm ürün haznesi boyunda ve toplam yüksekliği 853 mm olan paslanmaz çelikten imal edilmiş bir kurutucudur. Kurutma süresince ürünün kaynama hareketini görmek için kurutucunun hazne sonrası camdan imal edilmiştir. Kurutucunun ürün haznesinde ürüne sıcak hava geçişini sağlayan 2 mm çapında delikleri olan perfore paslanmaz bir sac elek mevcuttur. Bu kurutma sisteminde kurutma için kullanılan sıcak hava, bir fan sayesinde hava ısıtıcıdan kurutucuya verilmektedir. Kurutucunun en üst bölümünde kurutma esnasında gerçekleşebilecek ürün kaybını engellemek için bir toz torba filtresi kullanılmıştır. Deneylerde kullanılan kuvars kumunun ilk nem içeriği yaş baza göre %10,56 olarak belirlenmiştir. Denemeler üç test şeklinde gerçekleştirilmiştir. Birinci test sonucunda; kuvarsit numunesinde 140 ºC hava sıcaklığında 1,25 m/s hava hızı ve 24,8 hertz vibrasyon ile kum 3.dakika itibariyle % 0,887 nem değerine, ikinci testte kurutma sıcaklığı 100 ºC'ye düşürülmüş olup hava hızı 1,25 ve 24,8 hertz vibrasyon ile istenilen %2,5 nem miktarına 4 dakika içerisinde ulaşılmıştır. Üçüncü testte kurutma havası sıcaklığı 100 ºC olup hava hızı 2,8 m/s'ye çıkartıldığında 4.dakikada %0,29 neme ulaşılmıştır. Deney sonuçları incelendiğinde hava hızı arttığında ürünün nem kaybının hızlandığı, istenilen değerlere göre en uygun kurutma değerlerinin 100 °C hava sıcaklığı ve 1,25 m/s olduğu görülmüştür.

Anahtar Kelimeler : Kuvars kum, Akışkan yataklı kurutucu, Kurutma

POWER QUALITY IMPROVEMENT FOR NON LINEAR LOAD USING SIX PULSE CONVERTER WITH PASSIVE SHUNT FILTER

AMIT KUMAR [1]

[1] Gautam Buddha University, School of Engineering, ORCID ID- 0000-0001-9379-6244

ABSTRACT

This paper presents the waveform distortion and harmonics reduction of distribution transformer with the help of passive shunt filter. This study examines the effect of harmonic distortion on power transformers when supplying non-sinusoidal load currents. A synchronized 6-Pulse generator is used to fire the six thyristors of a six-pulse converter. The output of the converter is a vector of six pulses individually synchronized on the six thyristor voltages. The pulses are generated alpha degrees after the increasing zero crossings of the thyristor commutation voltages. The line current harmonics cause increase in losses, instability, and also voltage distortion. Shunt filters still dominate the harmonic compensation at medium/high voltage level, whereas active filters have been proclaimed for low/medium voltage ratings. Passive filtering has been preferred for harmonic compensation in distribution systems due to low cost simplicity, reliability, and control less operation. In modern electrical distribution systems there has been a sudden increase of harmonics because of single phase and three-phase non-linear loads. These non- linear loads are cause of harmonics. Passive shunt filter have been used traditionally for mitigating the distortion due to harmonic current in industrial power systems. Simulink model is design through MATLAB Software.

Keywords: Power quality, harmonics, passive filter, transformer, non-linear load.

1. INTRODUCTION

Power quality is a serious concern in electric power system, different type's disturbances like voltage sag, voltage swell, fluctuation, noise, flickers, waveform distortion and harmonics take place. The intensive use of power converters and non-linear loads has contributed for the deterioration of the power quality and this factor affects critical processes, resulting in substantial economic losses [1], [5]. The devices based on power electronics directed to improve power quality are denominated as "Custom-Power" [2]. One Custom-Power device can be obtained from the collective operation of an active filter with a passive filter, which results in a hybrid filter. The hybrid filter used in this work consists of shunt passive filters operating with a series active filter [1] [3]. Nonlinear loads such as saturated coils and transformers are the main cause of producing harmonics in power system. Most of the pollution issues are created due to the nonlinear characteristics [4] and fast switching of Power electronics. Classically, shunt passive filters, mainly consist of tuned LC filters and or high passive filters are used to reduce the harmonics [5] and power capacitors are used to improve the power factor [6]. But they have the limitations of fixed compensation, large size and can also exile resonance conditions [7]. Transformers, motors, cables, interrupters and capacitors are the some equipment which is affected by harmonics converters mainly

produces notches and they basically affect the electronic control devices [8]. There are two routes to the reduction of power quality problems. The first way is known as load conditioning, which assures that the equipment is made less sensitive and effective to power disturbances [9]. The second technique is, to install line-conditioning systems that counteract or suppress the power system disturbances .In distribution systems passive filters have been used to limit of harmonic currents [10].

2. PASSIVE FILTERS

Passive filters were preferred in the earlier time for harmonic reimbursement because they are simple in structure and easy to install different topologies of passive filters. They are mostly categorized into series and shunt passive filters [11]. Series passive filters use high series impedance to block harmonics, and shunt filters divert harmonics by means of a low impedance shunt path. The series filters must be designed to carry full load current [9], [12], whereas shunt filters carry only a fraction of the current that a series filter carries. Also shunt filters, if properly designed, supply reactive power to the load at the fundamental frequency [13]. The shunt passive filter is assembled with passive elements resistance, inductance and capacitance. When the inductive and capacitive reactance of the passive filter become equal at a particular harmonic frequency, shunt passive filter acts as low impedance path for that harmonic component [14].
The selection of these element ratings depends on [14-17]

- Reactive power to be inserted
- Harmonics to be diminished
- Quality factor of the tuned filter circuit
- Tolerance in supply-frequency endorsed
- Tolerance in filter capacitance and inductance value due to ageing and temperature changes.

Shunt passive filters are once more classified as single tuned, double tuned, high pass damped filters [15]. A single tuned filter is a series RLC circuit tuned for particular harmonic frequency, whereas double tuned filter is tuned for two harmonic frequencies [16]. The double-tuned filter is preferred mainly in high-voltage applications, because of the reduction in the number of inductors to be subjected to full line voltages [17]. Triple- and quadruple-tuned filters are rarely used because of the difficulty of adjustment of filter components. Automatically tuned filters use a control system [18], which measures the fundamental frequency reactive power to be compensated by the filter and uses the information to automatically switch the capacitance or to vary the inductance [19]. In order to understand the effectiveness of shunt passive filter in compensating reactive power and harmonics of typical nonlinear load, phase controller for varying power consumed by a series R-L element, is considered [20].

3. DIFFERENT TYPES OF PASSIVE FILTERS

The classification of Passive filter is done on the type of harmonic generation component source present in the system & passive component sys resistor, inductor & capacitor connected in the system & are given as

- Passive Series Filter
- Passive Shunt Filter
- passive Hybrid Filter

A very classical type of passive filter is shown in the figure where filter is connected in the parallel with distribution system through power common coupling point having nonlinear load characteristics.

3.1. Passive Series Filter- The system which come with the voltage source type harmonic which are the product of diode rectifier with R-L connected load it is prefer to use the series type passive filter as considered as potential remedy of harmonic mitigation [21].

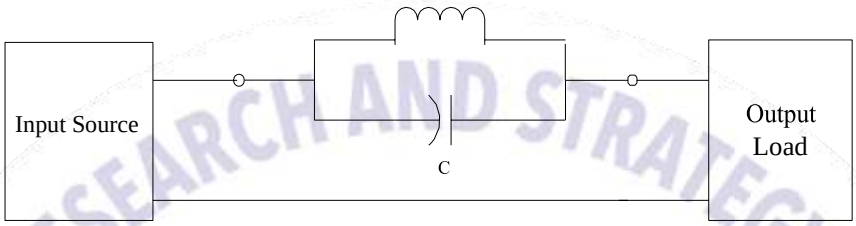

Figure 1 Basic structure of Passive Series Filter

Passive type series filter has property of purely inductive type or LC tuned characteristics. The main component of passive series filter is AC line reactor & DC link filter [2], [19]. Series passive filter is given by these two components connected in series that AC line reactor improves system magnitude of inductance in system that alters the path of current drawn in the rectifier circuit [18].

3.2. Passive Shunt Filter- It is the most common method for the cancellation of harmonic current in the distribution system. Passive harmonic filter are basically designed on principle of either single tuned or band pass filter technology. As the name suggests shunt type filter are connected in system parallel with load [1-6].

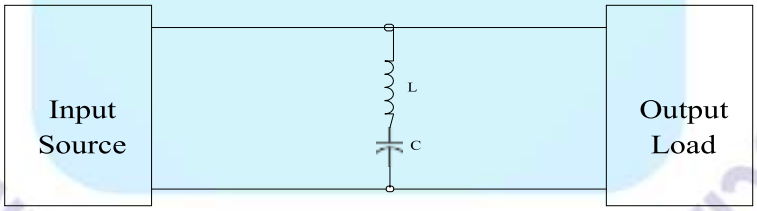

Figure 2 Basic structure of Passive Shunt Filter

Passive filter offer a very low impedance in the network at the tuned frequency to divert all the related current & at given tuned frequency [1]. Because of passive filter always have tendency of offering some reactive power in the circuit so the design of passive shunt filter take place for the two purpose. One is the filtering purpose & another one is to provide reactive compensation purpose of correcting power factor in the circuit at desired level [3-6]. The advantage with the passive shunt type filter is that it only carry fraction of current so the whole system AC power losses are reduced compare to series type filter [13]. The given figure shows the schematic diagram of 6 pulse converter system connected with shunt passive type filter which are simply employed ever connection in distribution system have R-L load in system [7], [11].

3.3. Passive Hybrid Filter- Hybrid filters combine a number of passive and/or active filters and their structure may be of series or parallel topology or a combination of the two [16]. They can be installed in single-phase, three-phase three-wire, and three-phase four-wire distorted systems [21]. The passive circuit performs basic filtering action at the dominant harmonic frequencies (e.g., 5th or 7th) whereas the active elements, through precise control, mitigate higher harmonics [1-3]. This will effectively reduce the overall size and cost of active filtering. The use of passive shunt filter creates the problem of voltage regulation at light loads. It also increases the dc voltage ripple and ac peak current of the rectifier [13], [19]. On the other hand, passive series filter suffers from lagging power factor operation as well as the voltage drop across the filter components both at fundamental frequency as well as harmonic frequencies [21].

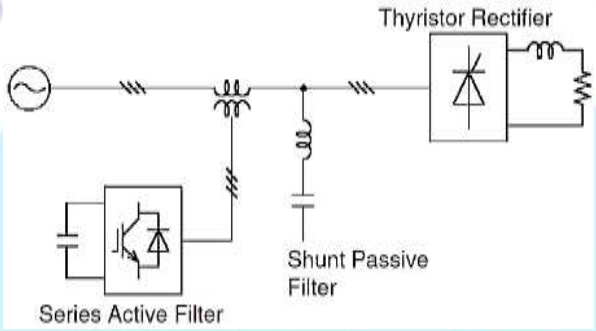

Figure 3 Basic structure of Passive Hybrid Filter

To overcome these drawbacks, a combination of both these configurations is presented as passive hybrid filter [10]. This configuration is able to supplement the shortfalls of both these passive filters and simultaneously it results in improvement in harmonic compensation characteristics for varying load condition even under stiff and distorted ac mains voltage [12], 14].

4. SIMULINK MODEL AND RESULT PERFORMANCE FOR PASSIVE SHUNT FILTER BASED CONVERTER WITH RL LOAD

To demonstrate the performance of these passive filters feeding a three-phase converter with R-L load, these passive filters are modeled in MATLAB environment along with simulink and power system block set toolboxes. Different components of these converters such as low pass filter with R- L load are simulated. Distribution transformer primary winding is connected with source and secondary is connected with the load. The secondary winding of distribution transformer is load connected winding or load side winding.

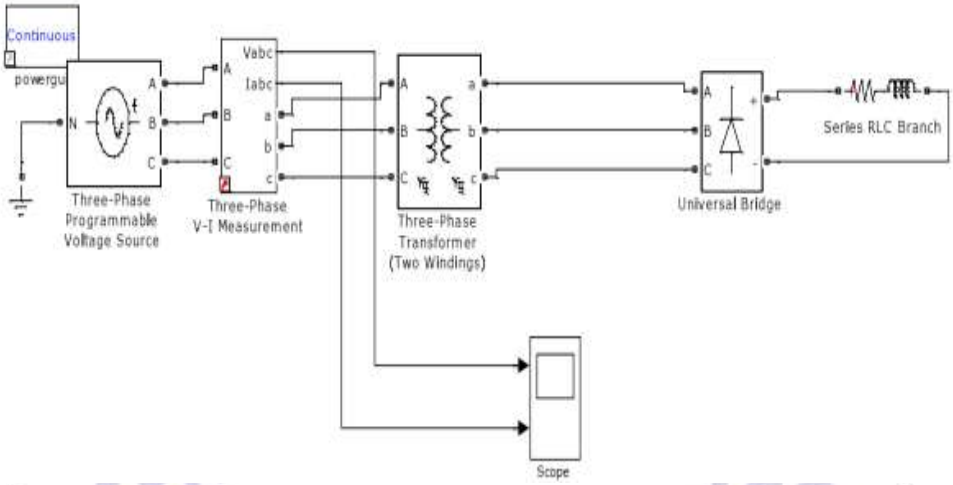

Figure 4 Simulink model for RL load without six-pulse converter and passive shunt filter

5. RESULT AND PERFORMANCE OF SIMULINK MODEL FOR PASSIVE SHUNT FILTER BASED SIX PULSE CONVERTER WITH RL LOAD

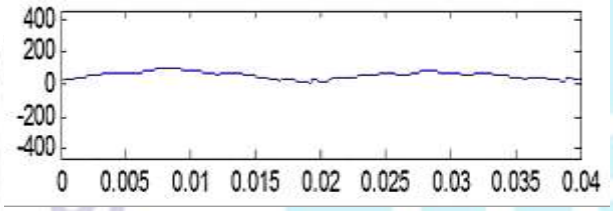

Figure 5 Three Phase voltage source

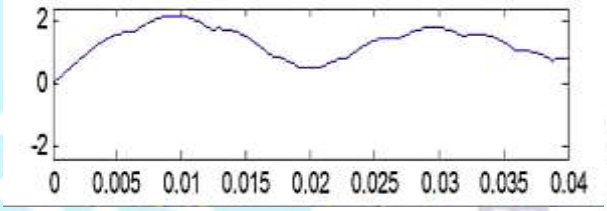

Figure 6 Three Phase current source

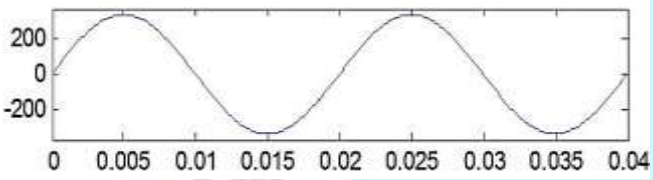

(a)

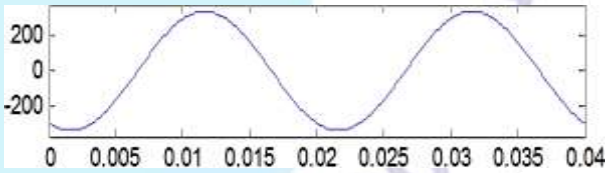

(b)

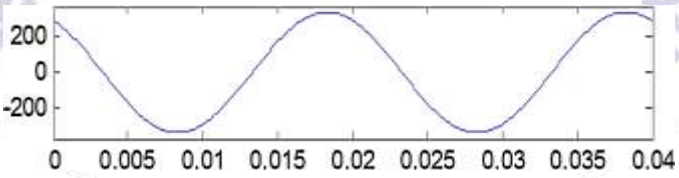

(c)

Figure 7 Three phase transformer- primary winding side Phase A, B and C voltage (a), (b), (c) respectively without passive shunt filter

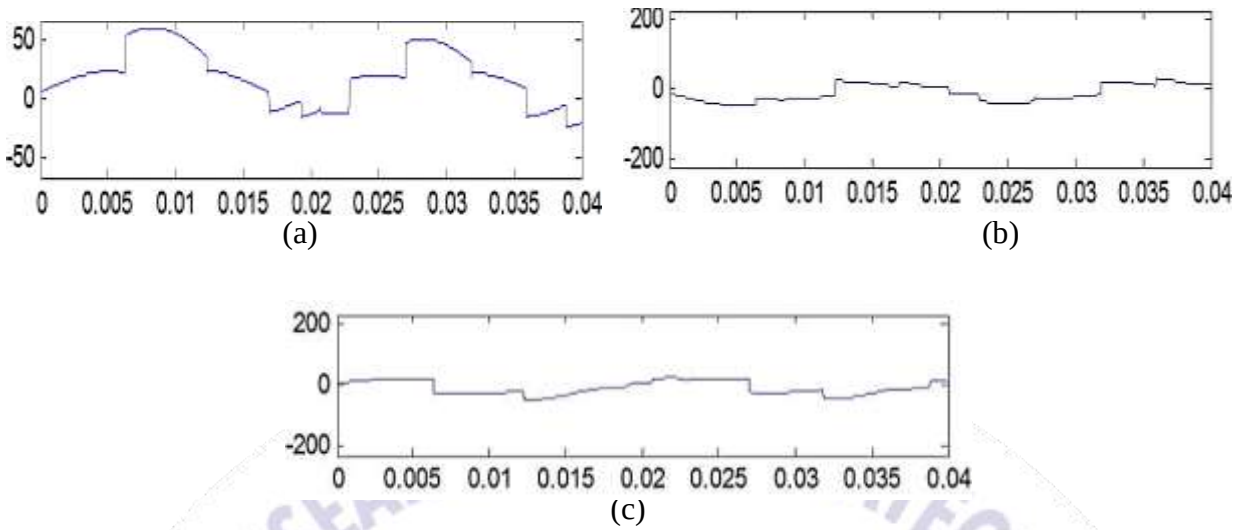

Figure 8 Three phase transformer-secondary winding side Phase A, B and C voltage (a), (b) and (c) respectively without passive shunt filter

6. RESULT AND PERFORMANCE OF SIMULINK MODEL FOR RL LOAD- SIX PULSE CONVERTER WITH PASSIVE SHUNT FILTER

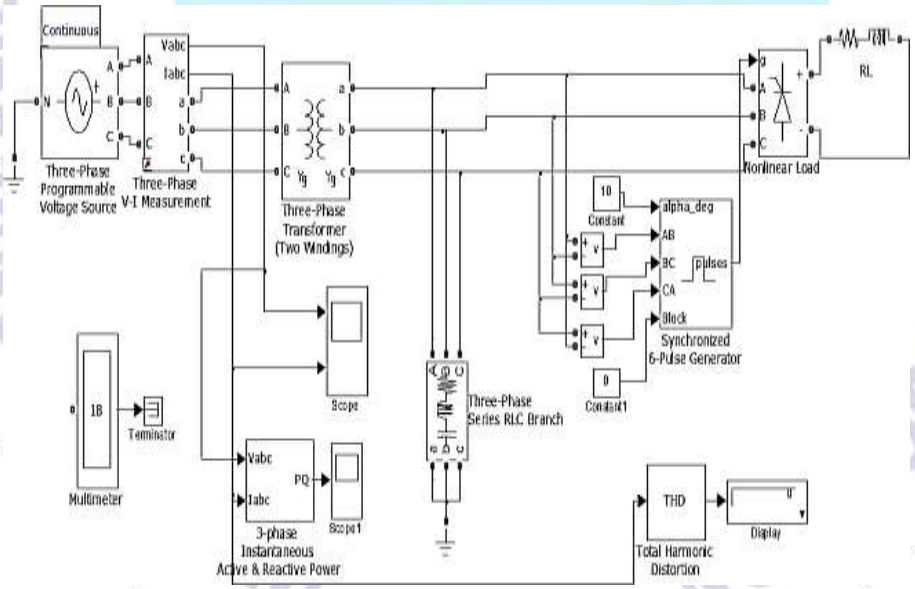

Figure 9 Simulink model for RL connected load with six pulse converter and passive shunt filter

The Simulink model block implements a three-phase zero-impedance voltage source. The common node (neutral) of the three sources is accessible through input N of the block. Time variation for the amplitude, phase and frequency of the fundamental can be pre-programmed. In addition, two harmonics can be superimposed on the fundamental. MATLAB model of a passive series filter based six pulse ac- dc converters with R-L load. Depending on the harmonic spectrum of the supply current, the passive filters designed are low pass filter tuned for 5th order harmonic frequency. The subsystem named shunt filter consists of 5th harmonic frequency. Based on the design carried out the filter component values are L=15e-3, C=25e-6, R=0.80.

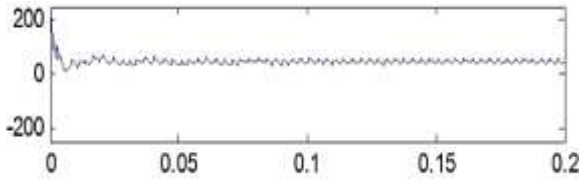

Figure 10 Three phase voltage source

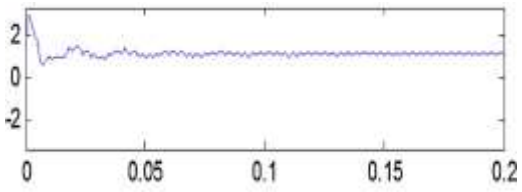

Figure 11 Three phase current source

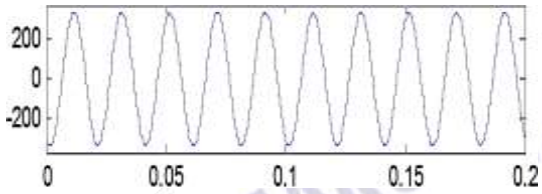

(a)

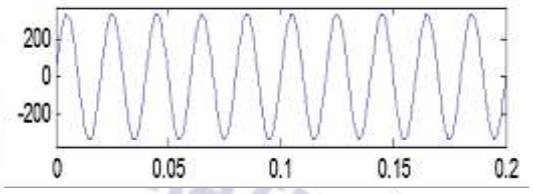

(b)

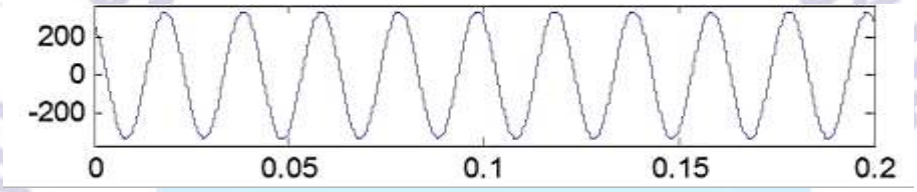

(c)

Figure 12 Three phase transformer- primary winding side Phase A,B and C voltage (a), (b), (c) respectively with passive shunt filter

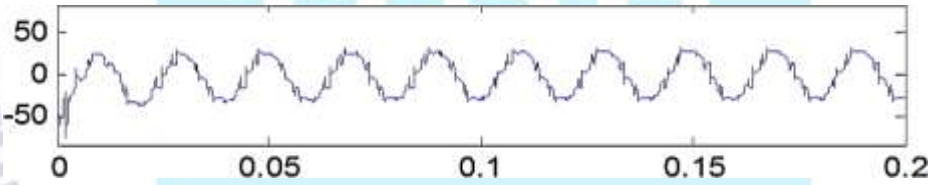

Figure 13 Three phase transformer-secondary winding side Phase A voltage with passive shunt filter

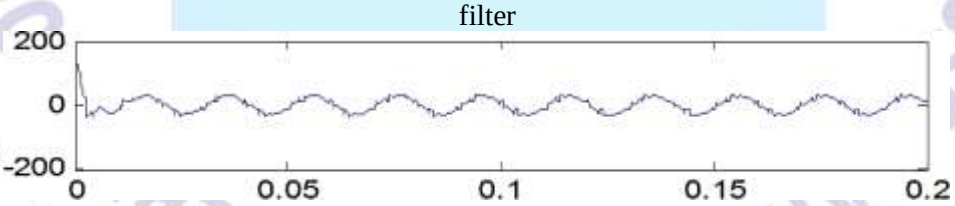

Figure 14 Three phase transformer-secondary winding side Phase B voltage with passive shunt filter

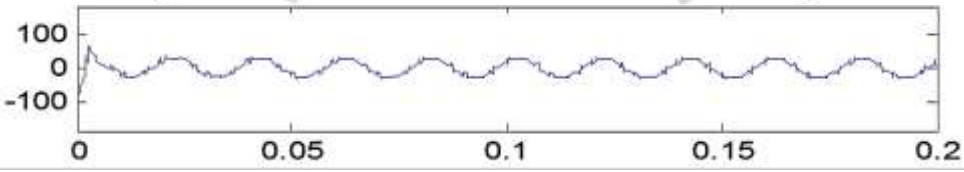

Figure 15 Three phase transformer-secondary winding side Phase C Voltage with passive shunt filter

7. CONCLUSION

The presented single-phase shunt active power filter has demonstrated to be able to improve distorted waveform and compensate the harmonic currents and the power factor produced by loads, making the current at the source side to become almost sinusoidal and in

phase with the system voltage. This current compensation can also prevent voltage harmonics and improvement of waveform distortion for transformer. Simulink model using MATLAB Simulink is proven to be very useful for studying the detailed behavior of the system for harmonic and unbalance compensation, under steady state and transients. The total harmonic distortion of source current is reduced when shunt active power filter is connected to the power system at the point of common coupling. The effect of multiple harmonic sources can be investigated by applying the superposition principle.

REFERENCES

[1] K. V. Kumar, G. Surendar, M. P. Selvan. Performance comparison of shunt active filter and hybrid active filter. NSC, pp. 71-76, Dec. 2008.

[2] IEEE Guide for Application and Specification of Harmonic Filters, IEEE Standard 1531, 2003.

[3] B. Singh and K. Al-Haddad. A review of active filters for power quality improvement. IEEE Transactions on Industrial Electronics, vol. 46, no. 5, pp. 960-971, Oct. 1999

[4] Amit Kumar, Deepak Kumar and Abhay Yadav. Power Quality Improvement of Power Distribution System Under Symmetrical and Unsymmetrical Faults Using D-STATCOM, International Conference on Advancement in Energy, Drive & Control (ICAEDC-2017), pp-111-121, 2017.

[5] Amit Kumar, Nidhi Singh Pal and M.A. Ansari. Mitigation Voltage Sag/Swell, Harmonic Compensation Using Self- Supported DVR. Ist IEEE International Conference on Power Electronics, intelligent Control and Energy Systems (ICPEICES- 2016), pp. 393-399, 2016.

[6] L. Chen, and A. V. Jouanne. A comparison and assessment of hybrid filter topologies and control algorithms. IEEE/PESC Ann. Meeting Conf, vol. 2, pp. 565-570.

[7] H. Fujita, and H. Akagi. Design strategy for the combined system of series active filter and shunt passive. Industry Applications Society Annual Meeting, 1991, pp. 898-903.

[8] F. J. Peng, and H. Akagi. Compensation characteristics of the combined system of shunt passive and series active filters. IEEE Transactions on Industry Applications, vol. 29, no. 1, pp. 144-152, Feb. 1993.

[9] D.M. Said, K.M. Nor. Effects of Harmonics on Distribution Transformers, 2008 Australasian Universities Power Engineering Conference, University of New South Wales, Sydney, Australia 14-17.12.2008.

[10] Dejan Pejovski, Krste Na jdenkoski and Mihail Digalovski. Impact of different harmonic loads on distribution transformers. 4th International Colloquium Transformer Research and Asset Management, Elsevier, vol.202, Pages 76-87, 2017.

[11] Amit Gupta and Ranjana Singh. Computation of Transformer Losses Under The Effects of Non-Sinusoidal Currents. Advanced Computing: An International Journal (ACIJ), Vol. 2, No.6, November 2011.

[12] Kannan Karthik, and J.E.Quaicoe. Voltage compensation and harmonic suppression using series active and shunt passive filters. Electrical and Computer Engineering, Canadian Conference, vol. 1, p. 582-586, 2000.

[13] Balasubramanian, R.; Sankaran, R.; Palani, S. Simulation and performance evaluation of shunt hybrid power filter using fuzzy logic based non-linear control for power quality improvement. Sadhana 2017, 42, 1443–1452.

[14] R.A arison. Fortes, Centro de Ciencias. Optimization of passive filtering system used for mitigating harmonics in distribution networks. IEEE transaction on power quality, 2016.

[15] Kuldeep Kumar Srivastava, Saquib Shakil, Anand Vardhan Pandey. Harmonics & Its Mitigation Technique by Passive Shunt Filter. International Journal of Soft Computing and Engineering (IJSCE) ISSN: 2231-2307, Volume-3, Issue-2, May 2013.

[16] Faiz, J., M. Ghazizadeh and H. Oraee. De-rating of transformers under non-linear load current and non-sinusoidal voltage – an overview. IET Electric Power Applications., vol. 9, iss. 7, pp. 486–495, 2015.

[17] B. P. de Campos, L. A. de Sousa, & P. F. Ribeiro. Mitigation of harmonic distortion with passive filters. Proceedings of the IEEE 17th International Conference on Harmonics and Quality of Power, pp. 646-651, 2016.

[18] Cazacu, E., L. Petrescu and V. Ionita. Derating of power distribution transformers serving nonlinear industrial loads. In: 2017 Inter-national Conference on Optimization of Electrical and Electronic Equipment (OPTIM) & 2017 Intl Aegean Conference on Electrical Machines and Power Electronics (ACEMP). Brasov: IEEE, 2017, pp. 90–95, 2017.

[19] Kendyala Rudradath, N Ramchander and R Muneeshwar. Power quality enhancement in domestic non-linear loads with single phase shunt apf. International Journal of Pure and Applied Mathematics Volume 120 No. 6, pp.7949-7963, 2018.

[20] Balasubramanian, R.; Palani, S. Simulation and performance evaluation of shunt hybrid power filter for power quality improvement using PQ theory. Int. J. Electr. Comput. Engg, vol 6, pp,2603–2609, 2016.

[21] Sang sum Kim & Prasad N. Enjethi. A New Hybrid Active Power Filter Topology. IEEE Transactions on Power Electronics, vol no1, Jan, 2002.

APPENDIX

These constraints are used to design Simulink model:

Components	**Specification**
AC Source	Vs=400v, f=50 Hz
Non-liner Load	Universal bridge R=40, (Ω) L=50e-3 (H)
Passive Filter	R=0.80 L=16e-3,C=25e-6

ENVIRONMENTAL IMPACTS OF USE OF BIODIESEL PRODUCED FROM WASTE COOKING OILS IN DIESEL ENGINES

İlker ÖRS [1], Savaş YELBEY [2], Selçuk SARIKOÇ [3]

[1] Selcuk University, School of Civil Aviation, 0000-0001-8385-9846

[2] Yozgat Bozok University, Yozgat Vocational School, 0000-0003-4942-320X

[3] Amasya University, Tasova Yüksel Akin Vocational School, 0000-0003-1190-5238

ABSTRACT

Air pollution, terrestrial degradation and pollution of clean water resources cause the total environmental pollution to increase day by day. One of the important factors affecting air pollution is exhaust emissions from vehicles used in transportation. Waste cooking oils, on the other hand, cause pollution of both soils and fresh water resources. In this study, the effects of the use of biodiesel as an alternative fuel for diesel engines, which are the power source of land, rail and sea transportation vehicles used for transportation, on engine performance and environmental factors were investigated. Biodiesel used as fuel was produced separately from domestic waste cooking oils and food factory waste oils by transesterification method and the results were compared with diesel fuel. The diesel engine, which is used in experiments, is a 3-cylinder, water-cooled, naturally aspirated compression ignition engine. The experiments were carried out at full throttle opening, at different loads and engine speeds. As a result, it was observed that the torque value of domestic waste oil biodiesel decreased by about 8.5% and that of food factory oil waste biodiesel by 20.5%, but this reduction was up to 10.1% with biodiesel produced by mixing both oils. Biodiesel produced from blended oils reduced the maximum torque value by approximately 15.87% compared to diesel fuel. In addition, with the use of biodiesel produced with mixed waste oils, approximately 10% increase in fuel consumption has been detected. The calorific energy values of fuels are one of the important parameters affecting engine performance parameters. In addition, it was determined that biodiesel produced especially from blended oils decreased CO emission and smoke density values by 16.43% and 34%, respectively, but increased NOx emissions by 16.93%. The oxygen contained in the biodiesel is an important factor in the results obtained for the emission values. As a result, the use of waste cooking oil as diesel engine fuel is an important solution not only for reducing the pollution of air, soil and clean water resources, but also for reducing the dependence on petroleum-based fuels.

Keywords: Biodiesel, Environmental pollution, Exhaust emissions, Engine performance.

1. INTRODUCTION

Waste cooking oils can be collected from homes, food factories, school or private cafeterias, restaurants and hotels. Mixing these wastes into city sewers causes pollution of both clean water resources and soil. The collection of waste cooking oils for use as fuel is also legally supported by many countries. Pure waste cooking oils can be converted into biodiesel, an alternative diesel engine fuel, after some simple processes such as filtering, rest and removal of water content.

Although biodiesel exhibits lower engine performance values compared to petroleum-based diesel fuel, it has much lower emission values. In addition, it is a very important advantage that they can be used in diesel engines without any modification [1]. All vegetable, animal oils and algae can be said as biodiesel feedstock. The most widely used biodiesel production method is the transesterification method. Thanks to this method, glycerin left over from biodiesel production is used in soap making [2-5].

Many studies have been conducted on the use of biodiesel produced from waste frying oil or waste cooking oil in diesel engines. When these studies are examined, it is seen that biodiesel is mostly used by mixing with diesel fuel in certain proportions. According to the results obtained from the studies, it has been observed that biodiesel generally reduces engine power [6-10], but in some cases, especially the addition of up to 20% biodiesel causes an increase in engine power [11]. In many studies, it has been stated that although biodiesel increases the specific fuel consumption [12-15], it improves the thermal efficiency [1, 16, 17]. Studies have shown that although biodiesel increases CO_2 emissions [15, 18-20], it significantly reduces CO and HC emissions [6, 15, 21-23]. When the exhaust gas temperature and NOx emission values, which are significantly affected by the end-combustion temperature, are examined, it has been determined that biodiesel increases both parameters, but in some studies [3, 15, 24-26], although rare, the NOx value is lower than diesel fuel [12, 18, 27-29]. In almost all studies, it has been stated that biodiesel reduces emissions of smoke, soot or particulate matter thanks to the oxygen it contains [3, 19, 30, 31].

In this study, domestic waste cooking oil and food factory waste oil were used as feedstock and converted to biodiesel by transesterification method. In addition, biodiesel was also produced from the mixed waste oil obtained by mixing both waste oils in the same proportions. These three biodiesels were used as fuel in a diesel engine and their fuel properties, engine performance parameters and exhaust emission characteristics were compared. It is aimed to minimize both the damage of waste cooking oil to nature and the environmental pollution of diesel engine emissions by revealing the possibility of using biodiesel obtained from waste cooking oils as pure fuel in diesel engines.

2. MATERIALS AND METHODS

The test fuels used in the experimental study are the biodiesels produced by the transesterification method from the domestic waste cooking oils used in the houses and the waste cooking oil collected from the food factories. Methanol was used for the precipitation of glycerol in the oil and sodium hydroxide was used as a catalyst. Both domestic waste cooking oil and food factory waste cooking oil were mixed volumetrically in the same proportions after water removal and blended biodiesel was produced. Some fuel properties of the obtained biodiesels are given in Table 1. According to Table 1, HB; the biodiesel from domestic waste cooking oil, FB; the biodiesel from food factory waste cooking oil and HFB; the biodiesel from domestic waste cooking oil (50% vol.) and food factory waste cooking oil (50%vol.).

Table 1. Some properties of test fuels

PROPERTIES	UNIT	Diesel	HB	FB	HFB
Density, at 20 C	g/cm^3	836.1	855.6	902.2	865.7
Viscosity, at 40 C	mm^2/s	2.803	4.113	4.775	4.236
Calorific Value	MJ/kg	43.25	37.63	35.88	36.91
Oxygen Content	%	-	8.8	9.3	9.1
Cetane Index	-	48.3	51.2	50.8	50.9

In order to more accurately evaluate the suitability of the results obtained with the use of biodiesel to the actively used diesel engines, the fuels were tested in a 3-cylinder diesel engine, the technical specifications of which are presented in Table 2.

Table 2. Technical specifications of test engine

Model	LDW 1003
Engine type	Four stroke, direct injection (DI)
Number of cylinders	3
Cylinder volume	1028 cm^3
Bore–stroke	75–77.6 mm
Compression ratio	22.8
Maximum Engine Power	26.5 HP

The experiments were carried out at full throttle opening, by measuring the performance (torque and fuel consumption) and exhaust emission values (CO, NOx, smoke opacity and exhaust gas temperature) at different engine speeds. The schematic view of the experimental setup is shown in Figure 1.

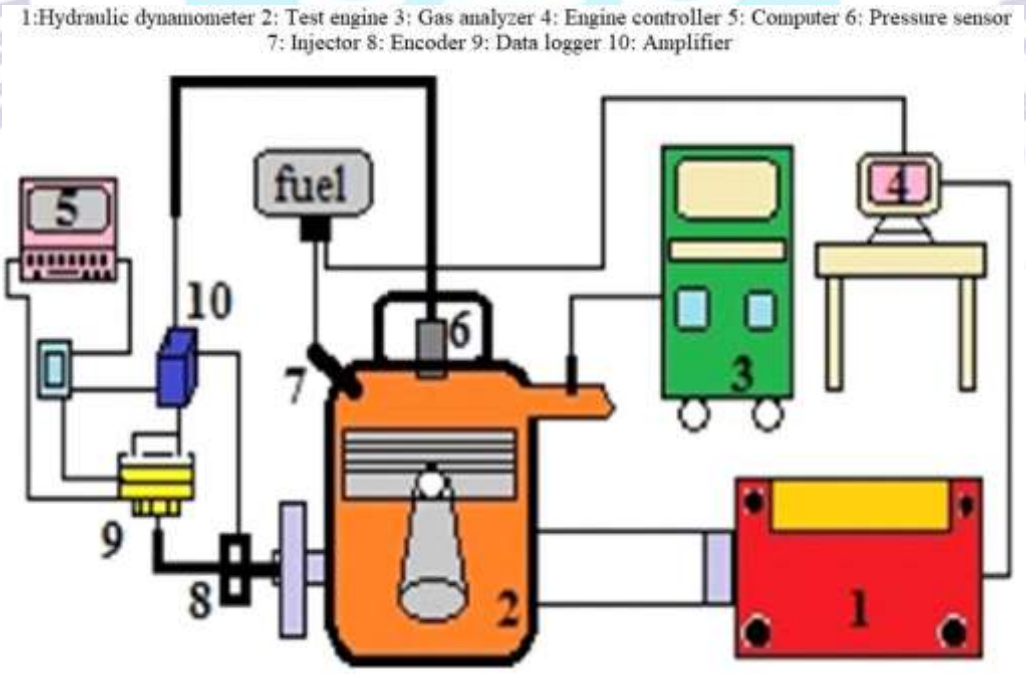

Figure 1. The schematic view of the experimental setup

3. RESULTS AND DISCUSSION

Figure 2 shows the engine torque and specific fuel consumption values of the test fuels. In general, it is seen that the use of biodiesel reduces the torque value and increases the specific fuel consumption value compared to diesel fuel. It can be said that the main reason for this is that biodiesel has a lower calorific value than diesel fuel. Considering the maximum torque values, it was determined that HB, FB and HFB fuels decreased the torque value by 12.7%, 23.81% and 15.87%, respectively, compared to diesel. On average, there is a decrease of approximately 8.51%, 20.75% and 10.11% for test fuels, respectively. With the use of test fuels, an increase of 5.94% for HB, 11.65% for FB and 5.8% for HFB was observed in specific fuel consumption values.

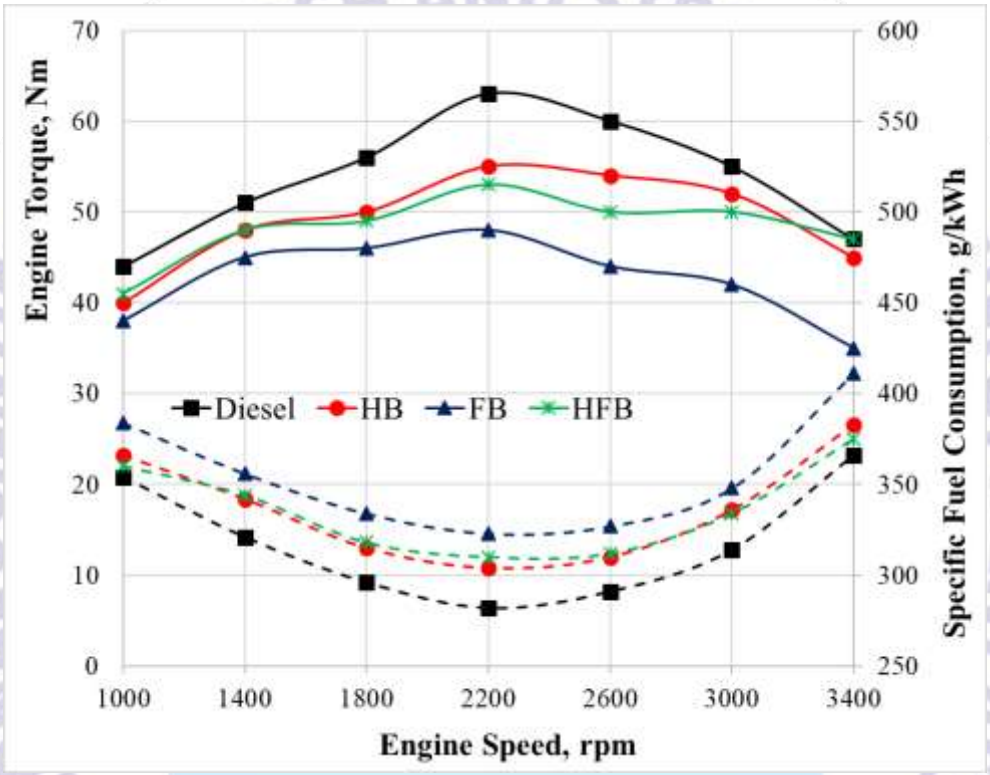

Figure 2. Engine performance parameters of test fuels

The lower calorific value of FB fuel compared to HB caused a further decrease in performance. However, it is seen that the performance values of HFB, which is a blend biodiesel, are much better than FB. This situation enables the use of cooking oil wastes from the food factory more efficiently in terms of engine performance.

The CO emission and smoke opacity values of the test fuels are given in Figure 3. The lack of oxygen during combustion causes the formation of CO and smoke emissions. Thanks to the oxygen content of biodiesel, much lower CO emission and smoke opacity values were revealed compared to diesel fuel. CO emission has been reduced with HB fuel by 23.74%, FB fuel by 12.21%, and HFB fuel by 31.12%. The use of biodiesel significantly reduced the smoke opacity value. While the smoke opacity values of HB and FB fuels are approximately 52.43% and 34.27% less, respectively, compared to diesel fuel, the smoke opacity value of HFB is 51.92% lower than that of diesel fuel.

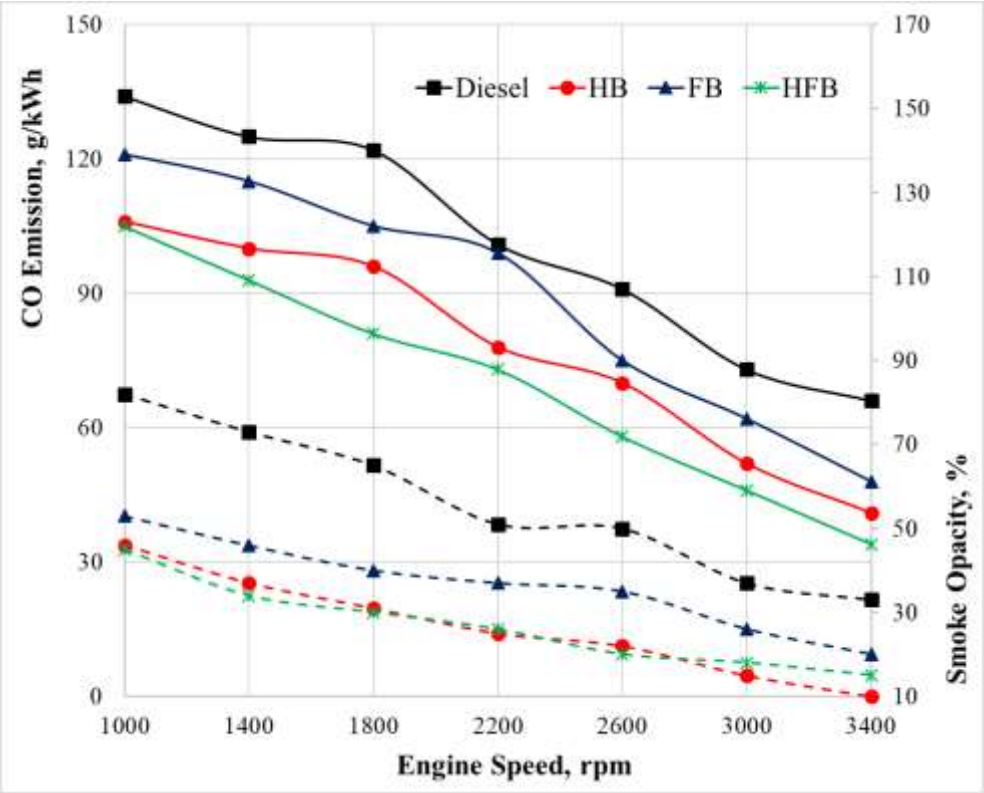

Figure 3. CO emissions and smoke opacity values of test fuels

Since nitrogen and oxygen atoms react at high temperatures, the temperature value after combustion is an important parameter in the formation of NOx. Exhaust gas temperature is also an important indicator of this formation.

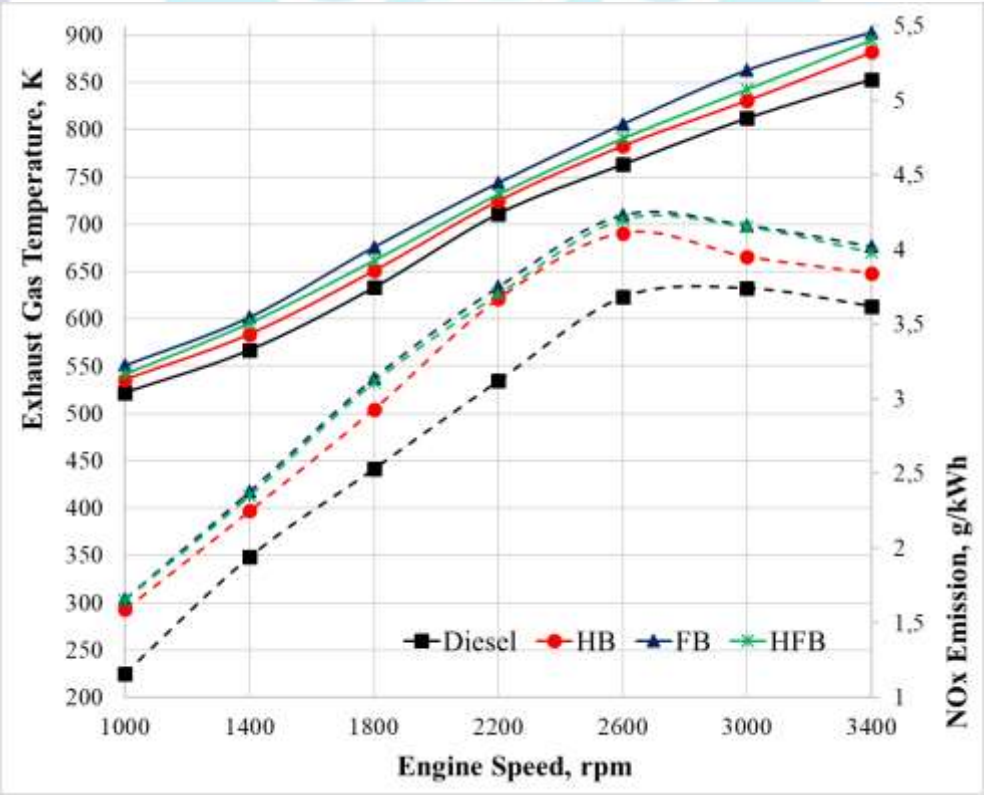

Figure 4. NOx emissions and exhaust gas temperature values of test fuels

The oxygen in the biodiesel causes the combustion to be more efficient, resulting in a higher exhaust gas temperature value. This causes biodiesel to have higher NOx emission values than diesel fuel. Figure 4 shows the NOx and exhaust gas temperature values of the test fuels. With the use of biodiesel, the exhaust gas temperature values increased by approximately 5.84% on average compared to diesel fuel, and this caused an increase in NOx emissions up to 17.94%. The oxygen content of biodiesel increased the NOx formation tendency for the nitrogen atoms reacting during combustion. This is another reason for the increase in NOx emissions.

3. CONCLUSIONS

As a result of the experiments, it is seen that biodiesel has some negative effects on engine performance parameters, but significantly improves exhaust emissions. It has been observed that biodiesels produced from different waste cooking oil sources have very different effects. It has been determined that especially the biodiesel produced from the waste cooking oil of the food factory significantly reduces the engine performance, but this negativity is significantly eliminated with the biodiesel produced by mixing it with the domestic cooking waste oil. In addition, it was determined that the blended waste cooking oil biodiesel caused very significant improvements in exhaust emissions.

Waste cooking oils collected from food factories are exposed to more chemical degradation because they are used for much longer periods and at higher temperatures than domestic waste cooking oils. Therefore, the negative impact of the use of biodiesel produced from the waste cooking oil of the food factory has been greater. With biodiesel produced using the blending technique, this problem has been eliminated to a great extent.

As a result, mixing waste cooking oil from the food factory and other cooking oil with similar properties with domestic waste cooking oil without converting it to biodiesel will result in better engine performance and lower exhaust emission values of the produced biodiesel.

REFERENCES

[1] Can, Ö. (2014). Combustion characteristics, performance and exhaust emissions of a diesel engine fueled with a waste cooking oil biodiesel mixture. Energy Conversion and Management, 87, 676-686.

[2] Sharon, H., Jackson, R. J., Prabha, C. Impact of Diesel-ButanolWaste Cooking Oil Biodiesel Blends on Stationary Diesel Engine Performance and Emission Characteristics (Chapter 9) in Recent Technologies for Enhancing Performance and Reducing Emissions in Diesel Engines, IGI Global Publisher of Timely Knowledge, February 2020.

[3] Calam, A. (2020). Combustion Performance and Emission Characteristics of a Direct Injection Diesel Engine Fueled with Waste Frying Oil Biodiesel. Dokuz Eylul University Faculty of Engineering Journal of Science and Engineering, 22(64), 97-106.

[4] Köse, S. Aylanşık, G., Babagiray, M. and Kocakulak, T. (2020). Biodiesel Production from Waste Sunflower Oil and Engine Performance Tests. International Journal of Automotive Science and Technology, 4(4), 206-212.

[5] Alptekin, E., Canakci, M., Ozsezen, A. N., Turkcan, A. and Sanli, H. (2015). Using waste animal fat based biodiesels–bioethanol–diesel fuel blends in a DI diesel engine. Fuel, 157, 245-254.

[6] Yaqoob, H., Teoh, Y. H., Sher, ., Farooq, M. U., Jamil, M. A., Kausar, Z., Sabah, N. U., Shah, M. F., Rehman, H. Z. U. and Rehman, A. U. (2021). Potential of Waste Cooking Oil Biodiesel as Renewable Fuel in Combustion Engines: A Review. Energies, 14, 2565.

[7] Yesilyurt, M. K. (2019). The effects of the fuel injection pressure on the performance and emission characteristics of a diesel engine fueled with waste cooking oil biodiesel-diesel blends. Renewable Energy, 132, 649–666.

[8] Muralidharan, K. and Vasudevan, D. (2011). Performance, emission and combustion characteristics of a variable compression ratio engine using methyl esters of waste cooking oil and diesel blends. Applied Energy, 88, 3959–3968.

[9] Buyukkaya, E. (2010). Effects of biodiesel on a DI diesel engine performance, emission and combustion characteristics. Fuel, 89, 3099–3105.

[10] Youssef, H. E. H., Fetni, S., Boubahri, C., Said, R. and Lassoued, I. (2019). An Experimental Study of Optimization of Biodiesel Synthesis from Waste Cooking Oil and Effect of the Combustion Duration on Engine Performance. International Journal of Renewable Energy Research, 9(3), 542-550.

[11] Kumar, S. B., Sushma, U. S., Chandrasagar, L., Raju, V. B. and Devi, V. (2017). Use of Waste Frying Oil as C.I. Engine Fuel—A Review. Open Access Library Journal, 4, e3958.

[12] Attia, A. M. and Hassaneen, A. E. (2016). Infuence of diesel fuel blended with biodiesel produced from waste cooking oil on diesel engine performance. Fuel, 167, 316–328.

[13] Nanthagopal, K., Raj, R. T. K., Ashok, B., Elango, T. and Saravanan, S. V. (2019). Influence of Exhaust Gas Recirculation on Combustion and Emission Characteristics of Diesel Engine Fuelled with 100% Waste Cooking Oil Methyl Ester. Waste Biomass Valorization, 10, 2001–2014.

[14] Selim, M. Y. E., Ghannam, M. T., Saleh, M. E., Alameri, M. T. A., Zaghloul, M. G. and Mansour, A. (2020). Behavior of Water-Waste Cooking Oil Biodiesel Emulsion for Diesel Engine Performance, Engine Roughness and Exhaust Emissions. International Journal of Engineering Research & Technology, 9(7), 1282-1288.

[15] Abed, K. A., El Morsi, A. K., Sayed, M. M., El Shaib, A. A. and Gad, M. S. (2018). Effect of waste cooking-oil biodiesel on performance and exhaust emissions of a diesel engine. Egyptian Journal of Petroleum, 27, 985-989.

[16] Ramadhas, A. S., Jayaraj, S. and Muraleedharan, C. (2006). Theoretical modeling and experimental studies on biodiesel-fueled engine. Renewable Energy, 31, 1813–1826.

[17] Devan, P. K. and Mahalakshmi, N. V. (2009).Study of the performance, emission and combustion characteristics of a diesel engine using poon oil–based fuels. Fuel Processing Technology, 90, 513–519.

[18] Teoh, Y. H., Masjuki, H. H., Kalam, M. A., Amalina, M. A. and How, H. G. (2013). Impact of Waste Cooking Oil Biodiesel on Performance, Exhaust Emission and Combustion Characteristics in a Light-Duty Diesel Engine. SAE Paper No: 2013-01-2679.

[19] Aksoy, F., Uyumaz, A., Boz, F. and Yılmaz, E. (2017). Experimental Investigation of Neutralized Waste Cooking Oil Biodiesel/Diesel Mixture and Diesel Fuel in a Diesel Engine at Different Engine Loads. International Journal of Automotive Science and Technology, 1(1), 7-15.

[20] Wei, L., Cheung, C. and Ning, Z. (2017) Influence of waste cooking oil biodiesel on combustion, unregulated gaseous emissions and particulate emissions of a direct-injection diesel engine. Energy, 127, 175–185.

[21] Guo, J., Peltier, E., Carter, R. E., Krejci, A. J., Stagg-Williams, S. M. and Depcik, C. (2012). Waste Cooking Oil Biodiesel Use in Two Off-Road Diesel Engines. ISRN Renewable Energy, 130782.

[22] Min Allah, F. U. and Alexandru, G. (2016). Waste cooking oil as source for renewable fuel in Romania. IOP Conf. Series: Materials Science and Engineering, 147, 012133.

[23] Li, R., Wang, Z., Ni, P. et al. (2014). Effects of cetane number improvers on the performance of diesel engine fuelled with methanol/biodiesel blend. Fuel, 128, 180–187.

[24] Prabu, S. S., Asokan, M., Roy, R. et al. (2017). Performance, combustion and emission characteristics of diesel engine fuelled with waste cooking oil bio-diesel/diesel blends with additives. Energy, 122, 638–648.

[25] Valente, O. S., Pasa, V. M. D., Belchior, C. R. P. et al. (2012). Exhaust emissions from a diesel power generator fuelled by waste cooking oil biodiesel. Sci Total Environmental, 431, 57–61.

[26] Şener, R. (2021). Experimental and Numerical Analysis of a Waste Cooking Oil Biodiesel Blend used in a Compression Ignition Engine. Int. J. Adv. Eng. Pure Sci., 33(2), 299-307.

[27] Tirkey, J. V., Singh, A. K. and Shukla, S. K. (2015). Performance and Emission Characteristics of CI Engine Operated with Waste Cooking oil Methyl-Ester and Diesel Blends, International Journal of Engineering and Advanced Technology, 5(1), 57-61.

[28] Geng, P., Mao, H., Zhang, Y. et al. (2017). Combustion characteristics and NOx emissions of a waste cooking oil biodiesel blend in a marine auxiliary diesel engine. Applied Thermal Engineering, 115, 947–954.

[29] Selvam, D. J. P. and Vadivel, K. (2014). The effects of ethanol addition with waste pork lard methyl ester on performance, emission, and combustion characteristics of a diesel engine. Thermal Science, 18(1), 217–228.

[30] Cheung, C. S., Man, X. J., Fong, K. W. and Tsang, O. K. (2015). Effect of waste cooking oil biodiesel on the emissions of a diesel engine. Energy Procedia, 66, 93-96.

[31] Xue, J. (2013). Combustion characteristics, engine performances and emissions of waste edible oil biodiesel in diesel engine. Renewable Sustainable Energy Review, 23, 350–365.

SPIN-ON TİPİ YAĞ FİLTRESİNİN HESAPLAMALI AKIŞKANLAR DİNAMİĞİ YÖNTEMİYLE ANALİZİ

Arş. Gör. YETKİN KARABULUT [1 2], Doç. Dr. YILDIZ KOÇ[3]

[1]İskenderun Teknik Üniversitesi, Mühendislik Fakültesi,

[2]Gaziantep Üniversitesi, ORCID ID: 0000-0002-7504-5655

[3]İskenderun Teknik Üniversitesi, ORCID ID: 0000-0002-2219-645X

ÖZET

Kuru sürtünme, özellikle içten yanmalı motorlarda ciddi oranda aşınmaya ve enerji kaybına neden olduğundan istenmeyen bir durumdur. Birbirine göre hareketli parçaların temas eden yüzeyleri yağ filmi ile kaplandığında sürtünmeyi ve aşınmayı azalttığı için motor ömrü uzar. Spin-on yağ filtreleri , içten yanmalı motorlarda yağda biriken ; metal parçaları, metal oksitler, asitler, ekzoz gazları , yakıtı ,suyu, kurumu , tozu ve kum parçacıkları gibi zararlı partikülleri süzerek motorların düşük aşınma ile çalışmasını sağlayan bir komponenttir. Akışkan akarken filtredeki ; ani kesit alanı değişimine, akış yönü değişimlerine, tesisat elemanlarına, filtre kağıdının kalınlığına, kağıdın gözenek yapısına ,viskoz sürtünmeye, partikül birikimiyle oluşan tıkanmaya bağlı olarak enerji kayıpları ve dolayısıyla basınç kayıpları oluşur. Bundan dolayı verimliliği arttırılması istenen bir içten yanmalı motorda kayıpların minimuma indirgenmesi, yağ pompasının çalışması için gerekli gücü azaltıp yakıt tüketiminin düşmesini sağlar. Bu çalışmada, Hesaplamalı Akışkanlar Dinamiği (HAD) yazılımı olan FLUENT® kullanılarak, çeşitli giriş hızlarında (0.5, 1, 1.5, 1.75 ve 2 m/s) filtrenin akış analizi yapılmıştır. Programda akış analizini yaparken, Navier-Stokes ve Darcy denklemleri kullanılmıştır. Motor yağı deney standardına uygun olarak ISO VG-100 seçilmiş ve buna bağlı olarak yoğunluk ve dinamik viskozite değerleri bulunmuştur. Gözenekli ortam olan filtre kağıdının simüle edilmesi için; deneysel verilerden elde edilen giriş hızına bağlı basınç kaybı değerleri, kullanılarak Darcy denkleminde kullanılan geçirgenlik ve viskoz direnç değerleri hesaplanmıştır. Akışkanın hızı ve filtrenin içindeki boşlukların kesit alanları dikkate alınarak hesaplanan Reynolds sayıları sonucunda akış türünün Laminar olduğu belirlenmiş ve analizde kullanılmıştır. Analiz sonucunda filtrenin içindeki akış çizgileri, hız ve basınç dağılımları bulunmuştur. Elde edilen analiz sonuçları deneysel veriler ile karşılaştırılmıştır.

Anahtar Kelimeler : Hesaplamalı Akışkanlar Dinamiği, Basınç Kaybı, Filtre, Analiz

1. GİRİŞ

Birbirine temas eden ve göreceli hareket eden nesneler sürtünme kuvveti oluşturur , buna bağlı olarak doğrudan temas eden parçalarda kuru sürtünme oluşur [1]. Kuru sürtünme, özellikle içten yanmalı motorlarda ciddi oranda aşınmaya ve enerji kaybına neden olduğundan istenmeyen bir durumdur. Birbirine göre hareketli parçaların temas eden kısımları yağ filmi ile kaplanırsa sürtünme ve aşınma azaltılmış olur, motor ömrü uzatılır [2]. Modern içten yanmalı motorlar çok düşük aşınmalar gösterirler ve bunun sonucunda mikrometre ve nanometre boyutunda partiküller oluşur [3]. Metal parçaların dışında, metal oksitler, asit oluşumları ,eksoz gazları

,yakıt,su,kurum,toz ve kum parçacıklar yağı kirletir. Bu parçacıklar da yağlamayı engelleyerek motor hasarlarına neden olur [4]. Yağ filtrelerinin görevi de yağın içindeki zararlı parçacıkları yakalayıp yağı temizlemektir. Akışkan akarken ; ani kesit alanı ve akış yönü değiştirmesine, tesisat elemanlarına, gözenek yapısına ,viskoz sürtünmeye, partikül birikimiyle oluşan tıkanmaya bağlı olarak basınç kayıpları oluşur.

(a) **(b)**

Görsel 1.1 Spin-On Yağ Filtresinin CAD görünümü (a) , Çalışma Prensibi (b)

Son zamanlarda, spin-on filtreleri kapsayan farklı uygulama alanları hakkında çeşitli çalışmalar yayınlanmıştır. Kırar [5] spin-on yağ filtre kapak tasarımlarını, Sonlu Elemanlar Metodu (FEM) ile bilgisayarda analiz ederek optimizasyon çalışması yapmıştır ve yüksek basınca dayanıklı kapak tasarımını elde etmiştir. Bahalı [6], spin-on yağ filtre kapağı ve kovan tasarımlarını çeşitli sac kalınlıkları için FEM yöntemi ile analiz ederek karşılaştırmıştır. Mastai [7], spin-on yağ filtresinin Hesaplamalı Akışkanlar Dinamiği (HAD) analizini 3 ayrı giriş çapı için (6,8,10 mm) yapmıştır. Ayrıca analiz modelini 3'e ayırarak çözümü basitleştirmiş ve sonuçlarını birleştirmiştir. HAD analizlerini ve deneyin sonuçlarını karşılaştırmıştır.

Bu çalışmada HAD ile mevcut bir spin-on filtre modelinin bilgisayarda akış analizinin yapılmıştır. Elde edilen basınç kaybı değerleri, deneysel sonuçları ile karşılaştırılmıştır.

2. HAD SİMÜLASYONLARININ OLUŞTURULMASI

Simülasyonlarda SOLİDWORKS® 'te çizilmiş olan 3 boyutlu katı model analiz yapılacak olan ANSYS® Workbench 16.0 paket programına aktarılmıştır. Filtre dönel simetrik olduğu için

1/8 dilimi alınıp içinden akışkan geçmeyen bütün parçaları çıkarılmıştır. Böylece, HAD analizinde kullanılacak olan model oluşturulmuştur. Analiz modeli HAD analizinin yapılacağı FLUENT 16.0 programına aktarılıp gerekli olan parametreler girilmiştir. Akışkanın sıkıştırılamaz, laminer olduğu kabul edilmiştir. İncelenen problem için; Süreklilik, Navier-Stokes ve Darcy Denklemleri kullanılır. Bu denklemler genel olarak,

$$\frac{\partial \rho}{\partial t} + \nabla.(\rho V) = 0 \quad (1)$$

$$\frac{\partial}{\partial t}(\rho V) + \nabla.(\rho VV) = -\nabla P + \nabla.\overline{\tau} + \rho g \quad (2)$$

$$S_i = -\left(\frac{\mu}{\alpha} V_i + C_2 . \frac{1}{2} \rho |V| V_i\right) \quad (3)$$

olup burada yoğunluk ρ ,zaman t , hız V ,basınç P , gerilme tensörü $\overline{\tau}$,yerçekimi g , dinamik viskozite μ ,geçirgenlik α ve atalet direnci C_2 ile gösterilmektedir [8].Basınç kaybı deneyi ,filtrenin girişi ve çıkışı arasındaki basınç farkını ölçmek için yapılır. Deneyde ISO VG-100 standardına uyan yağ kullanılır.

Çizelge 2.1 ISO VG Standartı Yağların Özellikleri [9]

ISO VG		**32**	**46**	**68**	**100**
ρ , 15˚C, (g/ml)	ASTM D 4052	0,874	0,879	0,885	0,889
υ , 40˚C, (mm^2/s)	ASTM D 445	32,0	46,0	68,0	100,0
υ , 100˚C, (mm^2/s)	ASTM D 445	5,5	6,8	8,7	11,1
Viskozite İndeksi	ASTM D 2270	100	100	100	95
Parlama Noktası, (˚C)	ASTM D 92	195	210	220	230
Akma Noktası, (˚C)	ASTM D 97	-27	-24	-24	-21

Burada kinematik viskozite ,υ ile gösterilir ve HAD analizinde yağın 40°C 'deki viskozitesi kullanılmıştır.

Çizelge 2.2 Deneysel Basınç Kaybı Değerleri

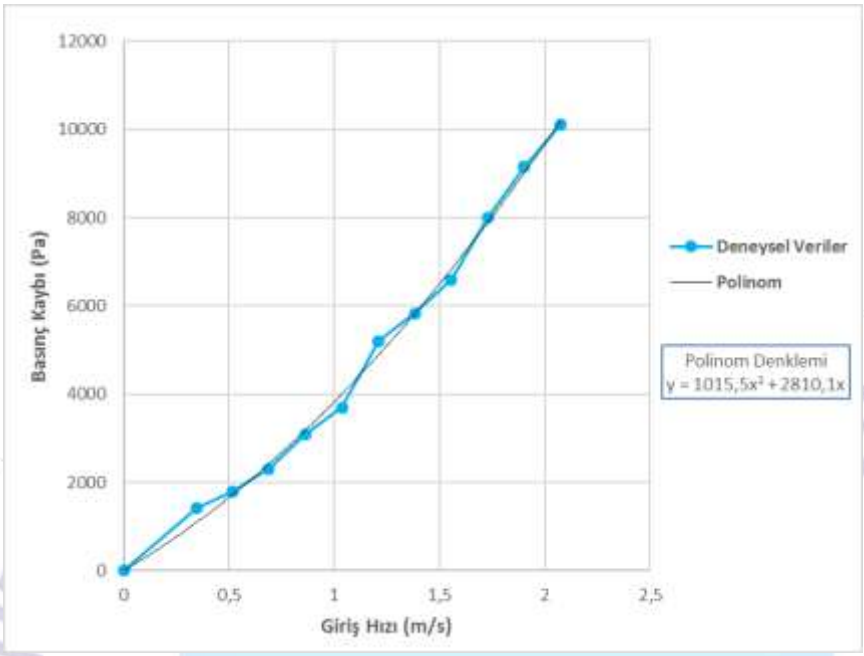

Çizelge 2.2'deki basınç kaybı değerleri kullanılarak 2. dereceden bir polinom oluşturulmuştur. Polinom denkleminin katsayıları kullanılarak da geçirgenlik ve atalet direnci değerleri hesap edilmiştir. Filtre kağıdı yani gözenekli ortam oluşturulurken elde edilen katsayılar kullanılır.

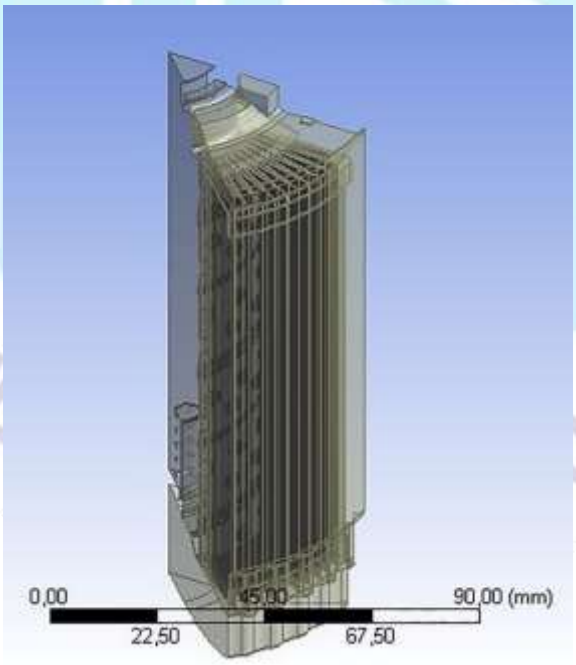

Görsel 2.1 1/8 Analiz Model

HAD simülasyonunda kullanılacak olan mesh yapısı oluşturulurken mesh bağımsızlığına da bakılması gerekmektedir. Bunun için mesh boyutu değiştirilerek 6 ayrı analiz yapılmış ve

sonuçları Çizelge 2.3'te karşılaştırılmıştır. Süreklilik ve x,y,z eksenlerindeki hızlar için yakınsama kriteri 1E-05 olarak seçilmiştir. Çözüm süresi ve analiz sonucundaki yakınsama değerleri dikkate alınarak 4,70E+06 eleman sayılı model seçilmiştir.

Çizelge 2.3 Mesh Sayısı Değişiminin Basınç Kaybına Etkisi

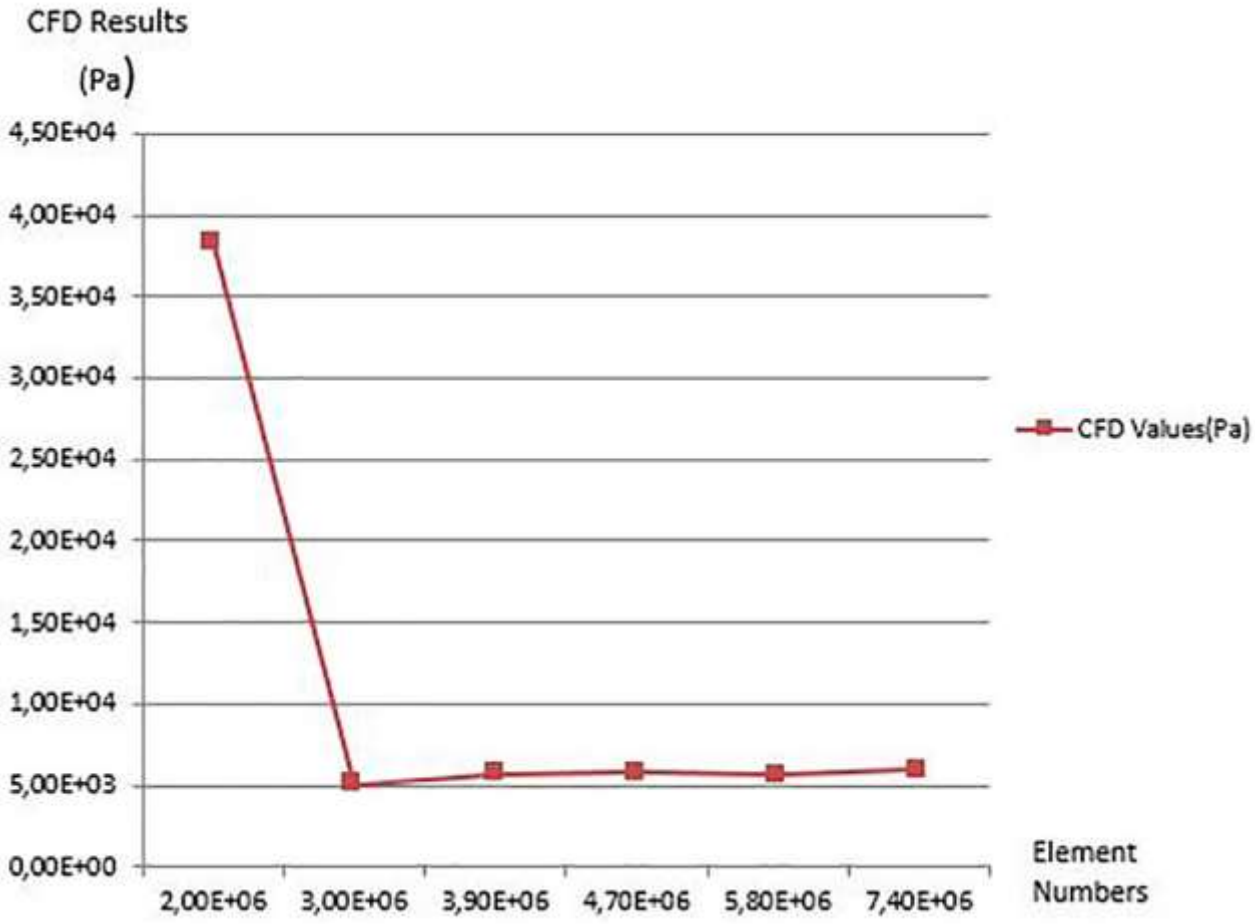

3. BULGULAR VE TARTIŞMA

HAD analizleri Çizelge 2.2 baz alınarak ; 0.5 , 1 , 1.5 , 1.75 , 2 m/s giriş hızlarında toplam 5 adet analiz yapılmıştır. Ortalama analiz süresi 36 saat olarak ölçülmüştür. Elde edilen sonuçlarda hız ve basınç dağılımları bulunmuştur.

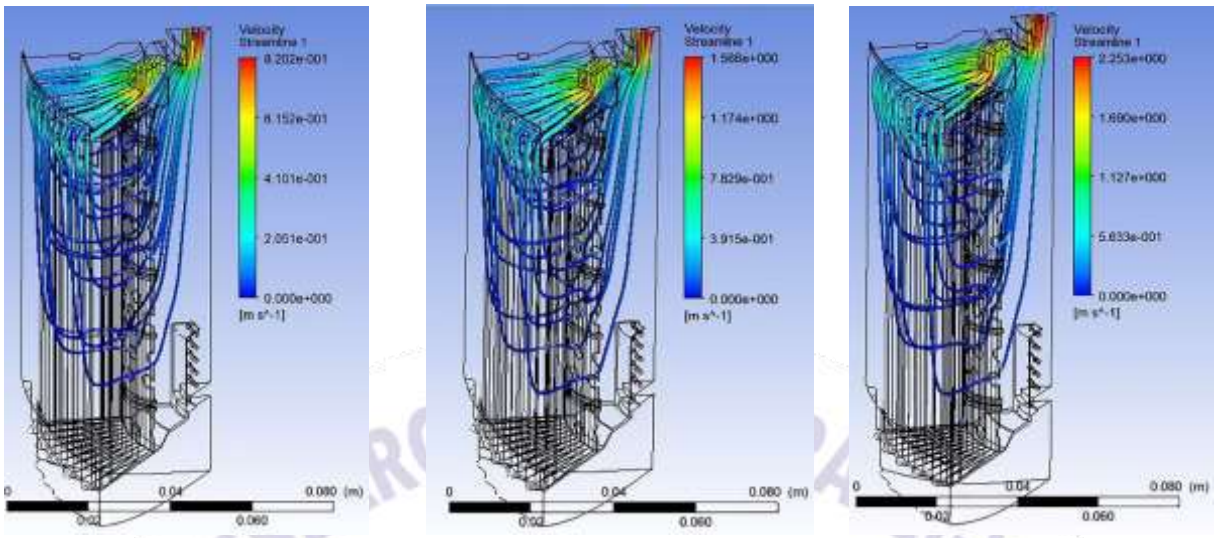

(a) **(b)** **(c)**

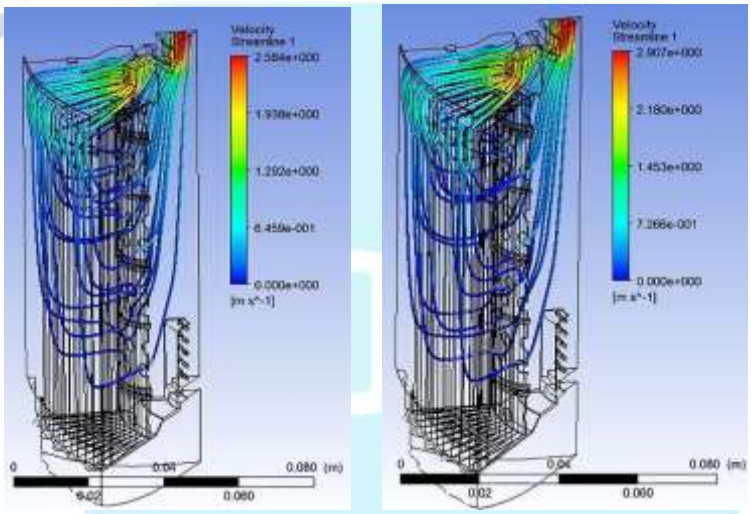

(d) **(e)**

Görsel 3.1 Farklı Giriş Hızlarında Akım Çizgileri
a) 0.5 m/s b) 1 m/s c) 1.5 m/s d) 1.75 m/s e)2 m/s

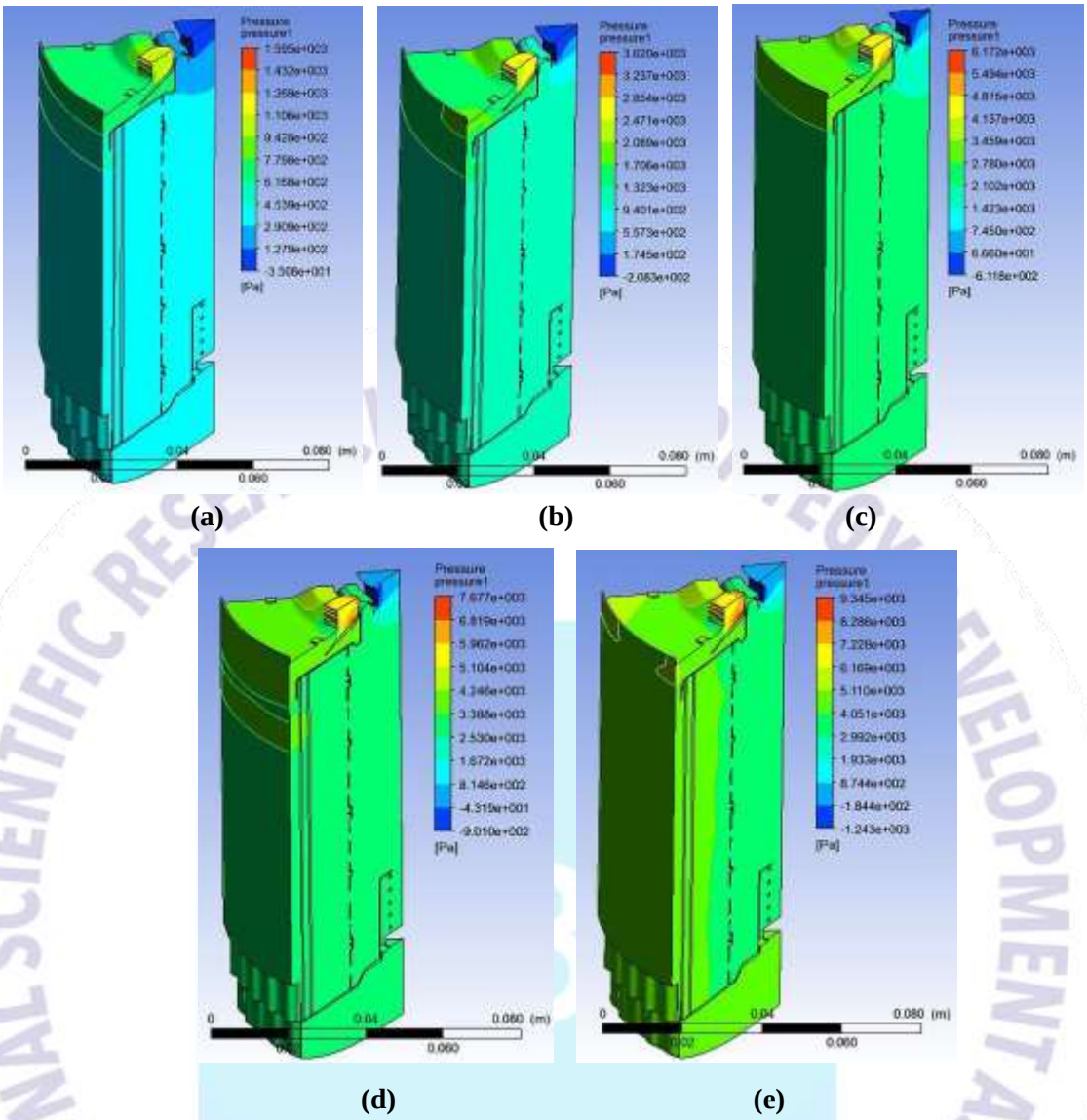

(a) **(b)** **(c)**

(d) **(e)**

Görsel 3.2 Farklı Giriş Hızlarında Modelin Dış Yüzeyindeki Basınç Dağılımı
a) 0.5 m/s b) 1 m/s c) 1.5 m/s d) 1.75 m/s e)2 m/s

Filtredeki basınç dağılımları incelendiğinde, yağın giriş hızı arttıkça , basınç kayıplarının da arttığı bulunmuştur. Bu da Navier-Stokes ve Darcy denklemlerini doğrulamaktadır. Viskoz sürtünme, gözenekli ortam, ani kesit ve yön değişimleri basınç değişimlerinde başlıca etkendir. Akışkanın aktığı kesit alanı ilerledikçe genişlediğinden, akışkanın hızı azalmıştır; ancak çıkış kısmında kesit alanı azaldığından hız artmıştır ve en yüksek hız değerleri burada bulunmuştur.

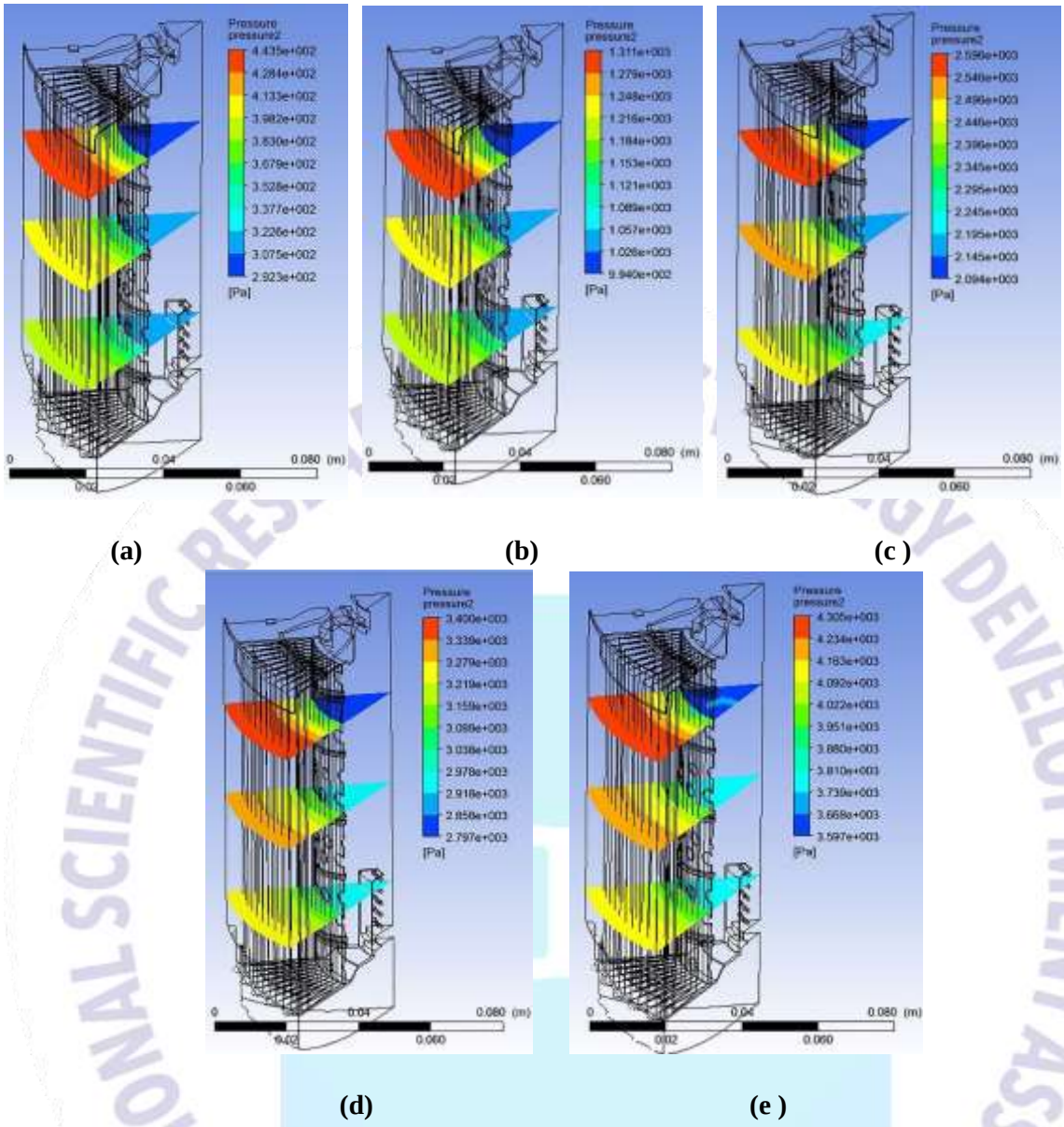

(a) **(b)** **(c)**

(d) **(e)**

Görsel 3.3 Farklı Giriş Hızlarında Modelin Yatay Kesitlerdeki Basınç Dağılımı
a) 0,5 m/s b) 1 m/s c) 1,5 m/s d) 1,75 m/s e) 2 m/s

Daire dilimi şeklindeki yatay kesitte akışkan filtrenin merkezine doğru akmaktadır. Yatay kesitte akışkan zikzak şeklindeki filtre kağıdından ve iç kılıfın deliklerinden geçerken, basınç değerinin düştüğü bulunmuştur. Burada iç kılıfın filtre kağıdına göre basınç kaybına daha fazla etki ettiği gözlenmiştir. Giriş hızı arttığında, basınç kaybı da artmıştır. Modelin alt kısmına gittikçe Görsel 3.1'deki akım çizgilerinin seyrekleştiği ve hızın düştüğü görülmüştür. Buna bağlı olarak da yatay kesitteki basınç farkı azalmıştır.

HAD analizleriyle yapılan çalışmalarda bulunan sonuçların doğrulama çalışmasının yapılması güvenilirliği sağlamaktadır. Bundan dolayı doğrulama için analiz sonuçları, Çizelge 3.1 'de deneysel veriler ile kıyaslanmıştır.

Çizelge 3.1 HAD Analizi Sonuçları ile Deneysel Verilerin Tablo Karşılaştırılması

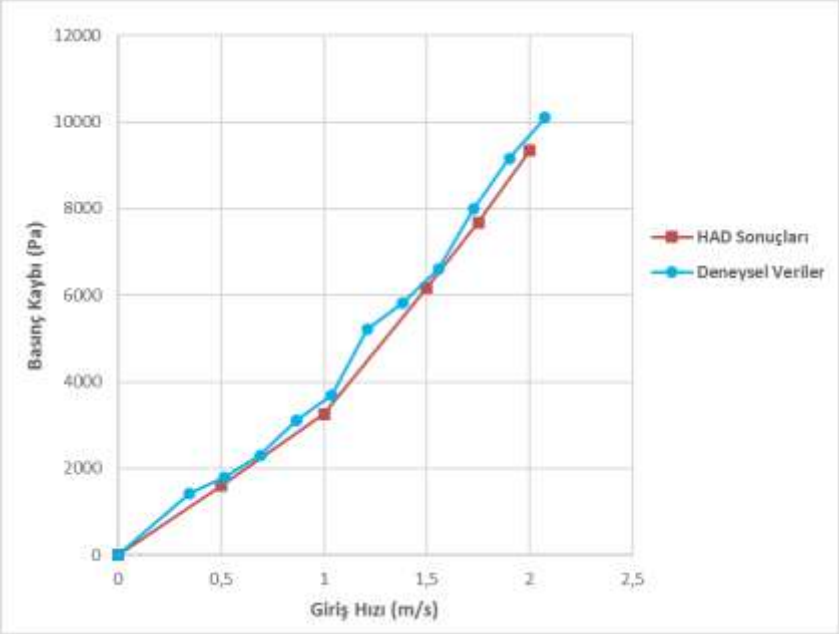

buna göre, HAD analizinde filtrenin girişi ile çıkışı arasındaki basınç kaybı, deneysel verilere göre ortalama %9 fark ile bulunmuştur. Ek olarak 1/8 dilimlik modelin kullanılması ,bütün modele göre daha kısa sürede analizlerin yapılmasını sağlamıştır.

Çizelge 3.2 HAD Analizi Sonuçları ile Deneysel Verilerin Tablo Karşılaştırılması

Akışkanın Giriş Hızı (m/s)	**0,5**	**1**	**1,5**	**1,75**	**2**
Deneysel Verideki Basınç Kaybı (Pa)	1681	3916	6702	8303	10042
HAD Analizindeki Basınç Kaybı (Pa)	1595	3260	6172	7677	9345

4. SONUÇ

Spin-on yağ filtresinde HAD analizlerinin, eşdeğer gözenekli ortam yaklaşımı ile yapılabileceği ispat edilmiştir. Filtrenin dönel simetrik olmasından dolayı, 1/8'lik model oluşturulmuş; analiz süresini ve gerekli olan bilgisayar işlemcisi gücünü düşürmüştür. Basınç kaybı deneyinden elde edilen veriler kullanılarak, gözenekli olan ortamın parametreleri olan geçirgenlik ve atalet direnci bulunmuştur. Akışkanın giriş hızına bağlı olarak yapılan HAD analizlerinin sonucunda, filtre içindeki basınç ve hız dağılımları bulunmuştur. Deneysel ve HAD analizinin basınç kaybı değerleri karşılaştırıldığında, örtüştükleri görülmüştür.

Filtreler üzerinde yapılacak olan optimizasyon çalışmaları, verimliliğinin ve dayanıklılığın artırılması üzerine olabilir. Motor yağının akışı esnasında oluşan basınç kayıplarının azaltılması yağ pompasının daha düşük güç ile çalışmasını sağlayarak içten yanmalı motorların daha verimli çalışmasını sağlayabilir. Ayrıca, filtrenin çalışması esnasında biriken partiküllerin akışa olan etkisi ve filtre parçalarında oluşan gerilmeler incelenerek gerekli tasarım değişiklikleri yapılabilir. Otomotiv endüstrisindeki rekabet göz önünde bulundurulduğunda, bu tür çalışmaların önemi daha iyi anlaşılmaktadır.

KAYNAKÇA

[1] Pasăre, M. & Ianăşı, P. D. C. , Trıbologıcal Propertıes of Composıte Materıals. *Fiability& Durability/Fiabilitate si Durabilitate*, (1),2016.

[2] Plaksin, A., Gritsenko, A., & Glemba, K. ,Modernization of the Turbocharger Lubrication System of An Internal Combustion Engine. *Procedia Engineering*, *129*, 857-862 ,2015.

[3] Haiden, C., Wopelka, T., Jech, M., Keplinger, F., & Vellekoop, M. J. , A Microfluidic Chip and Dark-Field Imaging System for Size Measurement of Metal Wear Particles in Oil. *IEEE Sensors Journal*, *16*(5), 1182-1189, 2015.

[4] Kurre, S. K., Garg, R., & Pandey, S. ,A Review of Biofuel Generated Contamination Engine Oil Degradation and Engine Wear. *Biofuels*, *8*(2), 273-280, 2017.

[5] Kırar E. , *Design of High Pressure Resistant Oil Filter*, Yüksek Lisans Tezi, İskenderun Teknik Üniversitesi/Mühendislik ve Fen Bilimleri Enstitüsü/Makine Mühendisliği Anabilim Dalı, Yöktez, 408933, 2015.

[6] Bahalı D. , *Comparison of Oil Filter Boilers with Finite Elements Method* ,Yüksek Lisans Tezi, İskenderun Teknik Üniversitesi/Mühendislik ve Fen Bilimleri Enstitüsü/Makine Mühendisliği Anabilim Dalı, Yöktez, 557804, 2019.

[7] Mastai, L. , *Modeling and CFD Analysis of An Oil Filter for Automotive Application* Master's Degree Thesis, Politecnico di Torino, 2021.

[8] ANSYS Fluent 15.0 User's Guide, Ansys Inc. , 2013.

[9] https://www.opetfuchs.com.tr/content/pdf/tbf_dura_serisi(1).pdf (Erişim tarihi: 05.05.2022)

FeCrAl/U_3Si_2 YAKITIN STANDART UO_2/Zr YAKITI İLE AYNI YANMA ORANINA ULAŞMASI İÇİN GEREKLİ ZENGİNLİĞİNİN BELİRLENMESİ

Dr. Öğr. Üye. BANU BULUT ACAR

Hacettepe Üniversitesi, https://orcid.org/0000-0002-7498-5151

ÖZET

Günümüzde işletmede olan nükleer reaktörler yaygın olarak UO_2 peletli ve Zirkonyum zarflı (UO_2/Zr) yakıt tasarımını kullanmaktadır. 2011 yılında yaşanan Fukushima Daiichi nükleer santral kazasından sonra, reaktörlerin güvenliğini artırmak amacıyla, standart UO_2/Zr yakıtın kaza koşullarına daha dayanıklı olan yakıt tasarımları ile değiştirilmesi önerilmiştir. Kaza koşullarında Zirkonyum zarf malzemesinin artan korozyon hızı ve bunun sonucundaki hidrojen üretimi malzeme özelliklerini olumsuz etkiler ve mevcut UO_2/Zr yakıt elemanı tasarımının performansını sınırlar. Kazaya toleranslı yakıtların santralin normal işletme koşullarında standart UO_2/Zr yakıt ile aynı enerji üretim performansını göstermesi ancak kaza koşullarında zarf malzemesinin oksidasyona daha dirençli olması hedeflenmiştir. Bu amaçla, standart UO_2/Zr yakıt elemanındaki UO_2 pelet yerine farklı bir yakıt malzemesi kullanılarak, Zirkonyum alaşım zarfı oksidasyona daha az yatkın bir malzeme ile değiştirerek veya zarf üzerine oksidasyona dirençli bir tabaka eklenerek kazaya toleranslı yakıt tasarımları geliştirilmiştir. Önerilen tasarımlar arasında yakıt peletinde UO_2 yerine yüksek yoğunluğa sahip olan U_3Si_2 malzemesinin kullanıldığı ve Zirkonyum alaşım zarfın oksidasyona daha dirençli FeCrAl alaşım ile değiştirildiği kazaya tolaranslı yakıt tasarımı öne çıkmıştır. Bu çalışmada, tipik bir PWR tipi reaktörde standart UO_2/Zr yakıtı yerine aynı yanma oranına ulaşacak U_3Si_2 peletli ve FeCrAl alaşım zarflı kazaya toleranslı yakıt kullanılması durumunda gerekli taze yakıt zenginliği belirlenmiştir. Referans reaktör olarak kurulu gücü 1000 MWe, termal verimi % 32,5 ve kapasite faktörü % 80 olan bir PWR alınmıştır. Bu reaktörde 1000 gün ışınlanma süresi sonrasında 50 GWd/tHM yanma oranına ulaşan kütlece 4,7 % zenginlikteki standart UO_2/Zr yakıt ile aynı yanma oranına ulaşacak FeCrAl zarflı U_3Si_2 peletli kazaya toleranslı yakıtın zenginliği Monteburns yanma ve bozunum kodu kullanılarak belirlenmiştir.

Anahtar Kelimeler: Kazaya toleranslı yakıt, Yanma oranı, FeCrAl, Monteburns, Zenginlik

DETERMINATION OF ENRICHMENT OF FeCrAl/ U_3Si_2 FUEL TO REACH THE SAME BURNUP WITH THE STANDARD UO_2/Zr FUEL

ABSTRACT

Currently, nuclear reactors commonly use the fuel design with UO_2 pellet and Zirconium cladding (UO_2/Zr). After the Fukushima Daiichi nuclear power plant accident in 2011, to increase the safety of the reactors, it has been proposed to replace the standard UO_2/Zr fuel with designs that are more resistant to accident conditions. The accelerated corrosion rate of the Zirconium clad material and the resulting hydrogen production have a negative effect on the material properties and limit the performance of the current UO_2/Zr fuel element design in accident conditions. In the accident tolerant fuel concept, it is aimed that fuel shows the same energy production performance with the standard UO_2/Zr fuel under normal operating conditions of the power plant while the clad material is more resistant to oxidation under accident conditions. For this purpose, accident-tolerant fuel designs have been developed by using a different fuel material instead of the UO_2 pellet in the standard UO_2/Zr fuel element, replacing the Zirconium alloy clad with a less corrosion-prone material, or using an oxidation-resistant coating above the clad surface. Among the proposed designs, accident tolerant fuel in which the high-density U_3Si_2 material is used instead of UO_2 in the fuel pellet and the Zirconium alloy clad is replaced with a more oxidation-resistant FeCrAl alloy has come to the fore. In this study, enrichment of accident tolerant fuel with U_3Si_2 pellet and FeCrAl cladding that reaches the same burnup with the standard UO_2/Zr fuel in a typical PWR type reactor is determined. A PWR with nominal power of 1000 MWe, thermal efficiency of 32.5 %, and a capacity factor of 80 % is taken as reference reactor. Enrichment of the FeCrAl/U_3Si_2 accident-tolerant fuel to reach the same burnup with the standard UO_2/Zr fuel having 4.7 w/o enrichment and attains to 50 GWd/tHM burnup after 1000 days of irradiation in the reference reactor is determined by using the Monteburns burnup and depletion code.

Keywords: Accident tolerant fuel, Burnup, FeCrAl, Monteburns, Enrichment

EVALUATING GEOENGINEERING PROPERTIES OF EVAPORITIC ROCKS FROM THE CITY OF ABU DHABI, UNITED ARAB EMIRATES (UAE): OVERVIEW AND DATA BASE GENERATION

Prof. Dr. HASAN ARMAN [1], Prof. Dr. ALA ALDAHAN [2], Assoc. Prof. Dr. OSMAN ABDELGHANY [3], MSc. SAFWAN PARAMBAN [4]

[1] United Arab Emirates University, 0000-0002-8173-0587

[2] United Arab Emirates University, 0000-0001-5784-574X

[3] United Arab Emirates University, 0000-0001-8492-2253

[4] United Arab Emirates University, 0000-0002-2569-8631

ABSTRACT

Evaporite rocks and soil occur in many parts of the United Arab Emirates (UAE) at the surface or at depth and constitute an important part of the geoengineering foundation column. The high variability of evaporites composition and texture strongly affect the vulnerability of these rocks to chemical and mechanical changes in the environment such as changes in groundwater chemistry and climatic conditions, which can affect the durability of evaporites with time. Data on the geoengineering properties of evaporites of the UAE are meagre and this study present to evaluate the geoengineering properties of evaporites, in the Abu Dhabi city. Geologic units of young and old sediments contain evaporites that make the foundations of many engineering structures such as buildings, highways, bridges, etc. The study includes intensive evaluation of the chemical, textural and mechanical properties of the evaporites from selected sites. The chemical tests will target analyses of the mineralogy, chemical composition and solubility experiments. The textural identification will focus on the macro and micro-textual features and their dependence on the chemical and mineralogical properties. Comprehensive site enquiries, in-situ and laboratory mechanical investigation of the materials will be carried out at the selected sites. All the data will be integrated to identify factors affecting the geoengineering properties of the evaporitic rocks in each site that will contribute to available geoengineering database and thus help minimizing risks and increasing the safety of engineering structures and for further research and development. Ultimately the project outcomes will minimize the cost of the big construction projects in the Abu Dhabi and UAE and benefit the economy.

Keywords : Geoengineering properties, Evaporitic rocks, Tectural and chemical compositions, Database, Safety and risk management, Economy

UTILIZATION OF WASTES AS ALTERNATIVE RAW MATERIAL IN CEMENT INDUSTRY

Nurten Deva

University of Mitrovica "Isa Boletini' Mitrovice., ORCID ID /0000-0003-4883-8024

Muharrem Zabeli, University of Mitrovica "Isa Boletini' Mitrovice

ORCID ID /0000-0001-6712-0005

ABSTRACT

The production of clinker as the main content for cement production required the several materials that are necessary for its obtaining .Nowadays it is very important to take into consideration and the wastes that are generated during the several other processes in different plants in metallurgy industry and to see the possibility to reuse them for clinker obtaining. Based in their chemical suitability of these wastes, these can be used as raw materials and ad they will provide the constituents required for the production of clinker. Therefore is very important to classify them into primary desired chemical elements such are lime, silica, alumina and iron as well as sulfur, alkalis and others , which can be classified into different groups according to their chemical composition. The use of wastes as a raw material during the clinker burning process involves the substitution of sulfur and the oxides contained in the wastes used as raw materials. These include calcium oxide (CaO), silica (SiO2), alumina (Al_2O_3) or iron oxide (Fe_2O_3) for the respective raw material constituents. Also, power station ash (fly ash), blast furnace slag, and other process residues gained as secondary products can be used as partial replacements for the natural raw materials.

Keywords: Waste, Raw material, Clinker, Composition,

KADASTRO PAFTALARININ YENİLEME SONRASI DEĞERLENDİRİLMESİ[1]

Harita Mühendisi GÜRHAN DEMİRTAŞ[1], Prof. Dr. HEDİYE ERDOĞAN[2]
[1]Aksaray Üniversitesi, 0000-0003-4342-0665
[2]Aksaray Üniversitesi, 0000-0002-6470-5857

ÖZET

Ülkemizde kadastro çalışmaları yaklaşık olarak 90 yıldır devam etmektedir. İlk yapılan tesis kadastrosu dönem şartları düşünüldüğünde eski yöntemler ve eski ölçü aletleriyle yapılmış, çoğu herhangi bir koordinat sistemine dayandırılmamış veya mevzi olarak koordinat verilip oluşturulmuştur. Uzun dönemde kadastro çalışmalarında değişimler dünya bazında yaşanmış, gelişmeler ortaya çıkmıştır. İlk kadastro sonucu oluşturulan bu kadastro paftaları gelişen teknoloji karşısında hem teknik olarak hem de hukuki olarak yetersiz kalmıştır. Değişen bu teknolojiye uyum sağlanabilmesi ve teknik sorunların giderilmesi gibi nedenlerden ötürü paftaların güncellenmesi ihtiyacı doğmuştur.

Ülkemizde ilgili birimlerde kadastro çalışmaları %99.48 tamamlanmış, tamamlanamayan birimler ise sorunlu birimlerdir. Bu birimlerde kadastro yapılmaması halkın faydasına olacağı düşünüldüğünden kadastro yapılmamıştır. Kadastro faaliyetleri çağın imkanlarına göre şekillendiğinden farklı metotlar kullanılarak yapılmıştır. Bunları grafik yöntem ve sayısal yöntem olarak sınıflandırmak mümkündür.

Bu çalışmada, eski ve güncelliğini yitirmiş yöntemlerle oluşturulmuş kadastro paftaları ile günümüz teknolojileri ve yöntemleri kullanılarak oluşturulan nispeten eskiye oranla hata oranı minimize edilmiş paftaların karşılaştırılması amaçlanmıştır.

Anahtar Kelimeler: Kadastro, Kadastro paftalarının yenilenmesi, Kadastro oluşturulma yöntemleri,

1.GİRİŞ

Kadastro; en temel tanımıyla taşınmazın geometrik ve hukuki durumunun bilimsel araştırma olanaklarına gereksinim duyduğu biçimde cevap veren bir kamu hizmetidir. Kadastro çalışmaları sonucunda imar planlarına, kamulaştırma projelerine, mühendislik projelerinin alt yapısını oluşturmak ve bu çalışmaların günümüz teknolojisine cevap verebilecek nitelikte olması kaçınılmazdır.

Kadastro; mülkiyet içerikli bilgilerden oluşur, ilişkileri parsel bazında ele alır. Sistemin temel objesi mülkiyettir. Teknik yanını kadastro haritaları oluşturur. Kadastro çalışmaları sonunda taşınmazların teknik ve hukuki durumları tespit edilmektedir [1]. Kadastro yaşayan ve devamlılık gerektiren bir hizmettir [2]. 1990'lı yıllarda ve günümüzde çağdaş teknolojik olanaklarla kadastro çalışmaları sürdürülmekte, daha nitelikli kadastro haritaları üretilmektedir [URL 1].

[1] Bu çalışma, ikinci yazar danışmanlığında birinci yazarın hazırladığı yüksek lisans tezinden üretilmiştir.

Önceki dönemlerde üretilen kadastro paftalarının dönem şartları düşünüldüğünde; yetiştirilmiş elaman eksikliği, alet-teçhizat eksikliği, teknik donanım eksikliği gibi şartlarla üretildiğinden, üretilen kadastro paftalarının dönem ihtiyaçları baz alınarak üretimine ağırlık verilmiştir. Değişen günümüz teknolojisi, hızla büyüyen kentler beraberinde yeni imar planları hazırlanmasını zorunlu hale getirmiş, parsellerin değeri gün be gün artmıştır. Bundan dolayı eski yöntemlerle oluşturulan kadastro paftalarının şimdiki çalışmalara kıyasla daha az hassasiyetle oluşturulduğu bilimsel olarak da kanıtlanmıştır. Değişen günümüz sonrası daha hassas ölçümlerle üretilen kadastro paftalarına ihtiyaç arttığı ve bu gibi sebeplerle kadastro parsellerinin yenilenmesi ihtiyacı doğmuştur.

Bu çalışmada Bitlis ili tüm ilçelerinde yapılan kadastro güncelleme çalışmalarında paftaların yenilenmesi işlem adımları, yeni paftalar ve eski paftaların karşılaştırılması yapılmıştır.

2. MATERYAL VE METOD

Yaklaşık 90 senedir üretilen kadastro paftaları; gelişen teknoloji karşısında teknik olarak yetersiz kalabilmekte ve süreç içerisinde paftalarda silinti, yırtılma, kaybolma, nem alıp deformasyona uğrama gibi nedenlerle, kullanılamaz hale gelebilmektedir. 3402 sayılı Kadastro Kanunu'nun 22-a maddesi gereğince tapulama, kadastro veya değişiklik işlemlerine ilişkin; sınırlandırma, ölçü, çizim ve hesaplamadan kaynaklanan hataları gidermek üzere, teknik nedenlerle yetersiz kalan, uygulama özelliğini kaybeden, eksikliği görülen ve zemindeki sınırları gerçeğe uygun göstermediği tespit edilen paftalarda yenileme yapılır [URL 2].

Yapılan çalışmanın bu bölümünde Bitlis ile ve ilçelerinde yapılan kadastro paftalarının güncellenmesi konusu işlenip güncelleme sonrası paftaların karşılaştırılıp değerlendirme yapılması amaçlanmıştır. Kadastro güncelleme çalışmasında kadastro müdürlüğünce ilk olarak çalışma ekibi oluşturulur. Oluşturulan bu ekipte, sayısallaştırma ekibi, kadastro güncelleme ekibinde yer alan teknisyen ile birimin kontrolünden sorumlu kontrol memuru/mühendis ve kontrol mühendisinden oluşturulur. Yapılan güncelleme çalışması bu ekip tarafından yapılır ve kontrolü sağlanır.

Kadastro güncelleme alanının belirlenmesinde önemli rol oynayan Tapu ve Kadastro Genel Müdürlüğü, Tapu ve Kadastro Bölge Müdürlükleri ve onlara bağlı Kadastro müdürlükleridir. Kadastro Müdürlükleri talebe bağlı işlemleri (Aplikasyon, Yer Gösterme, Cins değişikliği) gerçekleştirirken paftaların uygulama niteliklerinin olmadığını veya zeminde olan yol, dere gibi tesislerin paftada gösterilmediğini, zemindeki sınırlar ile paftadaki sınırların birbirlerini tutmadığını tespit ederler. Böyle durumlarda bahsedilen teknik hatalar giderilmeden taleplerin karşılanması mümkün değildir. Bu ve benzeri hataların ve işlem taleplerinin yoğun olduğu birimler uygulama alanının seçilmesinde belirleyici olurlar. Kadastro Müdürlüklerinin yanı sıra aşağıdaki durumlarla karşılaşan kurum ve kuruluşların talepleri de uygulama alanının belirlenmesinde önemli yer tutmaktadır:

- Yatırımların temelini oluşturan kamulaştırma projelerini yapan bütün kamu kurum ve kuruluşları kadastro haritalarının kusurlarından ötürü projelerinin uygulanamamasında,

- Tapu iptal ve tescil davalarında kadastro haritalarının kusurlarından dolayı karar verememe durumlarında,
- Tescile konu harita ve plan yapan serbest harita mühendislerinin uygulama yapamadığı hallerde ,
- TKGM ile veri paylaşımı sağlayan kurumların parsellerin konum hatalarından ötürü hatalı sonuç ürettikleri durumlarda (Çiftçi Kayıt Sistemi vb.)
- Eski Tapulama Müdürlüğünün yaptığı Tesis kadastro çalışmalarında yapılan fen klasörü hataları ve paftalar üzerindeki tersimat hatalarının düzeltilmesinde.
- Fen klasörüne alanların yanlış yazıldığı gibi durumlarda kadastro müdürlüğüne bildirim yapılır ve işin önemine göre çalışma bölgesi seçilir [3].

Çalışma yapılan Bitlis ili tamamında kadastro paftalarının tamamına yakınının hatalı olduğu gözlenmiş, ihtiyaç taleplerinin karşılanmadığı (aplikasyon, imar uygulamaları, cins değişikliği, vb.) kadastro müdürlüğünce belirlenmiş yenilenme bölgesi olarak seçilmiştir.

Kadastro Güncelleme Çalışması Uygulama Genelgesi'ne göre, yapılacak kadastro güncelleme alanının ilanı, çalışmalara başlamadan en az on beş (15) gün önceden çalışmanın yapılacağı alanlarda, kadastro bölgesi merkezinde ve bölgenin bağlı olduğu il merkezinde alışılmış vasıtalarla duyurulur, varsa yerel gazete ile ilân edilir ve ilana dair tutanak düzenlenir. Çalışmaların başlanacağının bildirimi mahallin mülki amirine, tapu müdürlüğüne, mahalli hukuk ve kadastro mahkemelerine, ilgisi bulunması halinde Çevre ve Şehircilik Bakanlığı Milli Emlak Genel Müdürlüğü, Tarım ve Orman Bakanlığının mahalli birimleri ile diğer ilgili kamu kurum ve kuruluşlarına bildirilir [4].

Güncelleme çalışmasında uygulama bölgesi ve ekibi belirlendikten sonra eski yöntemlerle oluşturulmuş kadastro paftaları sayısallaştırılır. Yapılan ilk ölçü değerleri sayısallaştırılan pafta üzerinde çakıştırılır. Bazı durumlarda paftaların sayısallaştırılması, bazı eksikliklerden dolayı hatalı olacak veya sayısallaştırma mümkün olmayacaktır. Bu gibi durumlar aşağıdaki görsellerde incelenmiştir.

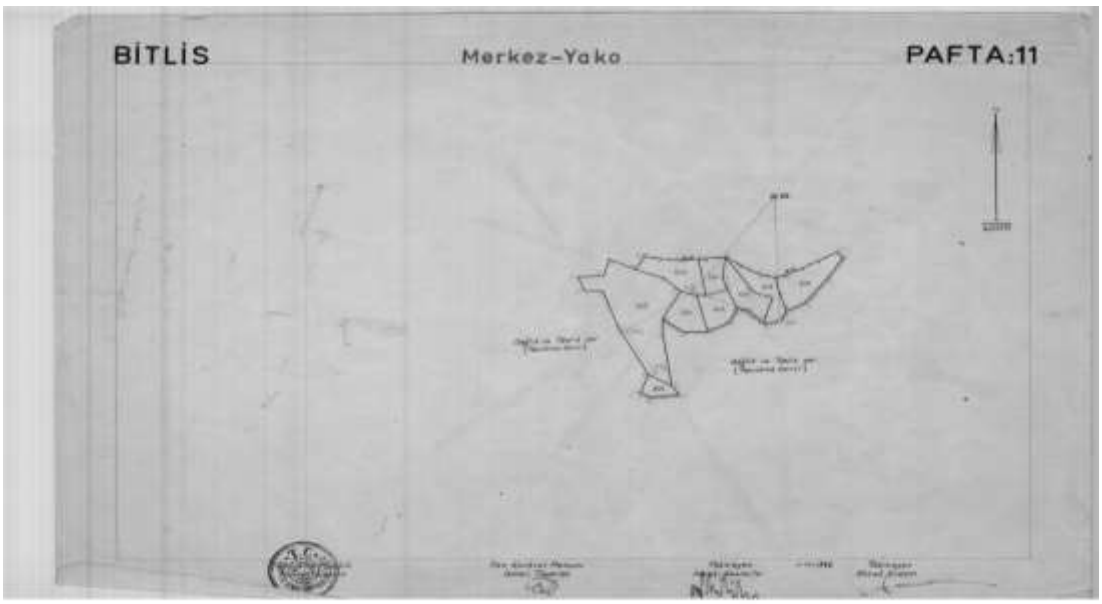

Görsel 1. Teknik nedenlerle yetersiz kalan pafta

Görsel 1'de Bitlis ili Merkez ilçesi Yako köyü sınırları içerisinde bulunan alana ait pafta gösterilmektedir. Pafta üzerinde poligonların isimleri yanlış ve eksik olduğundan paftadan doğru olarak faydalanılamaz. Teknik olarak yetersiz kalan pafta eğer kullanılırsa günümüzün sorunlarına karşı oluşturulacak planlar hatalı olacaktır. Çünkü altlık olarak kullandığımız pafta doğru sayısallaştırılamayacaktır. Altlık olarak kullandığımız pafta hatalı ise oluşturulacak projeler de hatalı olacaktır. Vatandaş aplikasyon talebinde bulunduğunda doğru sonuç alamayacaktır.

Görsel 2'de aynı bölgeye ait sayısallaştırma sonrası pafta ve arazide ölçümü yapılmış bilirkişi ve muhtar beyanları doğrultusunda oluşturulmuş yeni sınırlar görünmektedir.

Görsel 2 Güncelleme sonrası aynı bölgeye ait pafta

Görsel 2'de de Bitlis ili Merkez ilçesi Yako köyü sınırları içerisinde kalan pafta görünmektedir. Kırmızı olarak gösterilen Görsel 1 ile aynı alana ait paftadır.

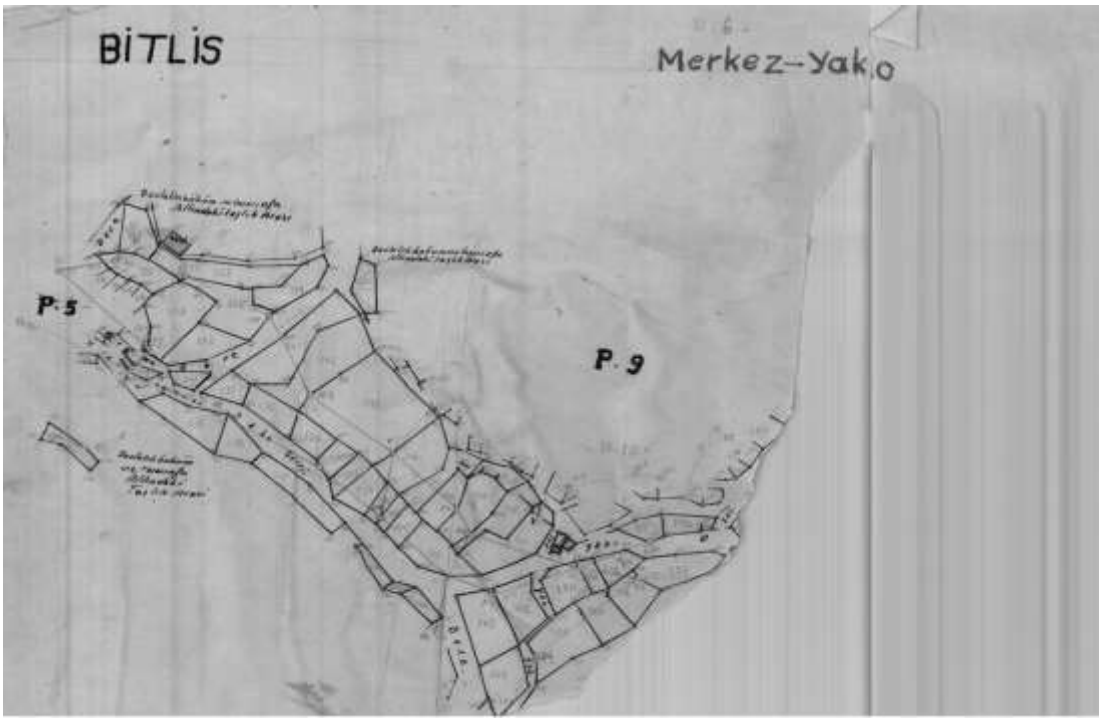

Görsel 3. Uygulama özelliğini kaybeden yırtılmış pafta

Aynı bölgede (Bitlis ili Merkez ilçesi Yako köyü) Görsel 3'te görüleceği üzere pafta zaman içerisinde zarar görmüş, yırtılmış ve kullanılamaz hale gelmiştir. Bu tip problemlerle çok sık

karşılaşılmaktadır. Kadastro paftalarının zarar görmesi kullanılamaz hale gelmesi durumlarında, bölgede yapılacak tüm planlama çalışmalarında, imar çalışmalarında, kişiye özel taleplerde (aplikasyon, cins değişikliği), kamulaştırma projelerinde altlık olmayacağı için çalışmalar yapılamayacaktır.

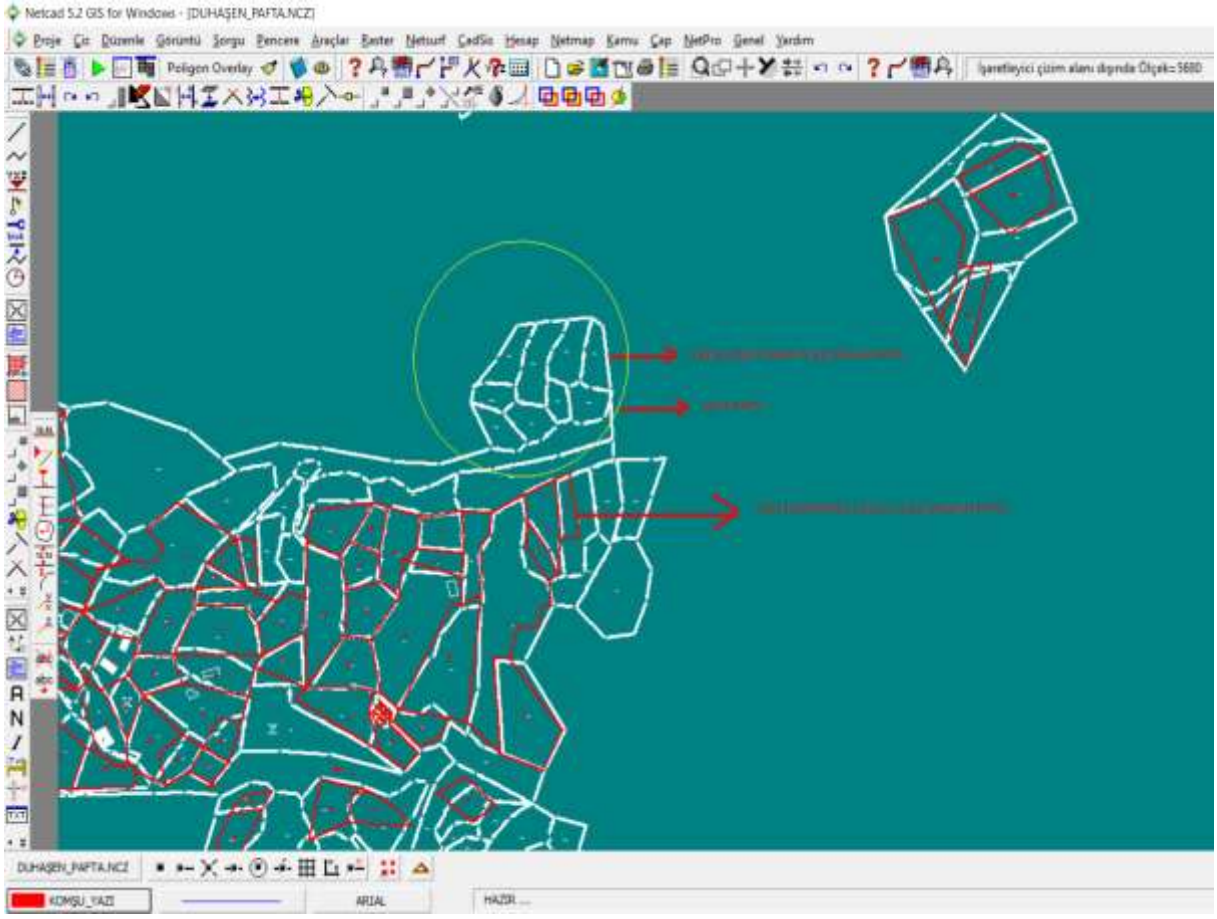

Görsel 4. Eksikliği görülen pafta

Bitlis ili merkez ilçesi Duhanşen köyüne ait Görsel 4'te çember içerisine alınan bölgede kadastro çalışmaları yapılmış, fakat pafta kayıp olduğundan dolayı yenileme çalışması yapılana kadar bu bölgede herhangi bir proje yapılamamıştır. Bu gibi durumlarla karşılaşmak da mümkündür.

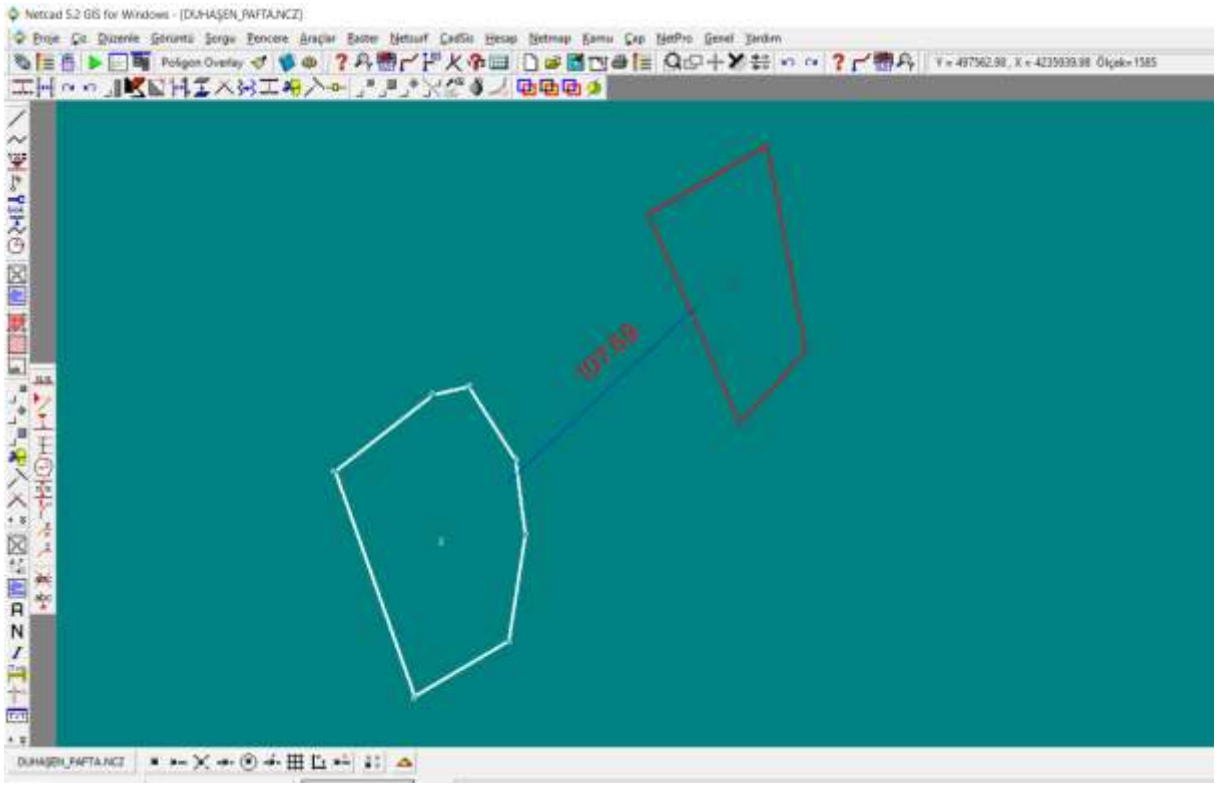

Görsel 5. Zemindeki sınırın gerçeği göstermediği pafta

Aynı il sınırlarında Duhanşen köyüne ait Görsel 5'te yeni oluşturulan parsel sınırı beyaz ile gösterilmekte eski parsel sınırı kırmızı ile gösterilmektedir. Aynı parselin ilk oluşturulan kadastro ve yenileme sonrası oluşturulan kadastral durumu arasında 107.69 metre kayıklık mevcuttur. Tesis kadastrosu 1960 yılında yapılan bu parselin günümüze kadar (2022) kullanımı aynıdır. Bu kanıya bilirkişilerin ve muhtarın beyanları doğrultusunda ulaşılmıştır. Arazide ölçüsü alınan bu parsel sık ölçü noktası alınmadığından dolayı parselin şekli de bozuk olarak görünmektedir. Dolayısıyla eski yapılmış kadastro gerçeği yansıtmamaktadır. Yenileme gerekliliği bu görselde de ortaya çıkmıştır.

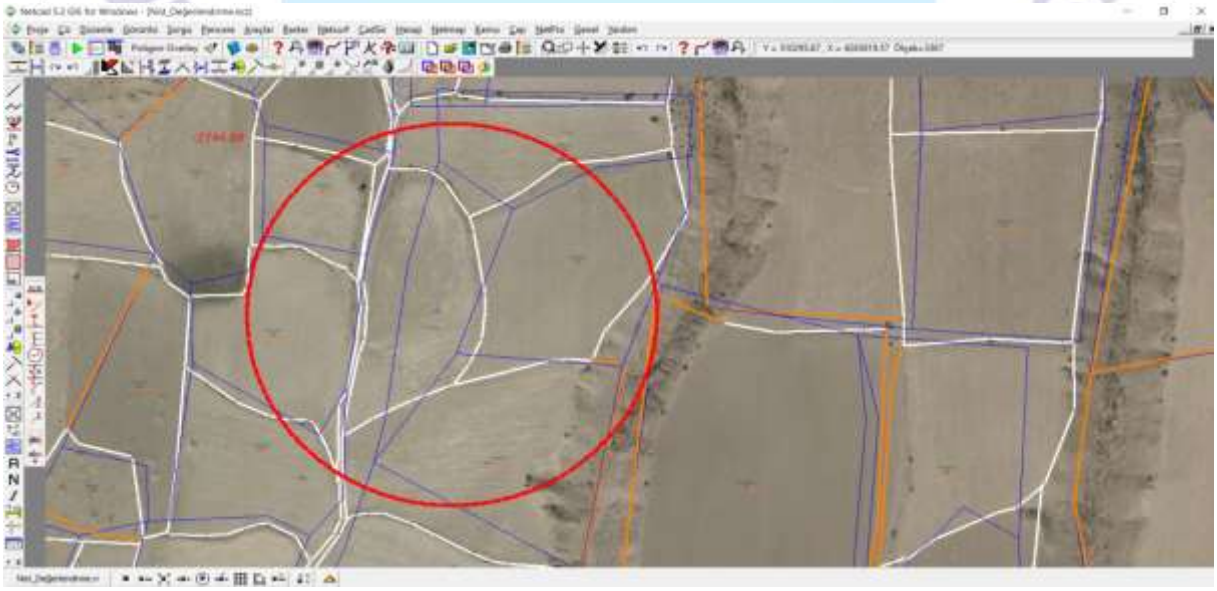

Görsel 6. Tersimat hatası

Bitlis ili Güroymak ilçesi Nist köyüne ait görsel 6'da çember içerisindeki üçgen olan parselin arazide ölçülen sınırlar kroki tutularak çizilir ve bu noktaların yanlış bir noktaya bağlanması sonucu tersimat hatası ortaya çıkar. Yine bu parselde de Görsel 5'te olduğu gibi sık nokta okuması yapılmamış, parselin şekli gerçeğini yansıtmamaktadır. Yenileme gerekliliği bu görselde de ortaya çıkmıştır.

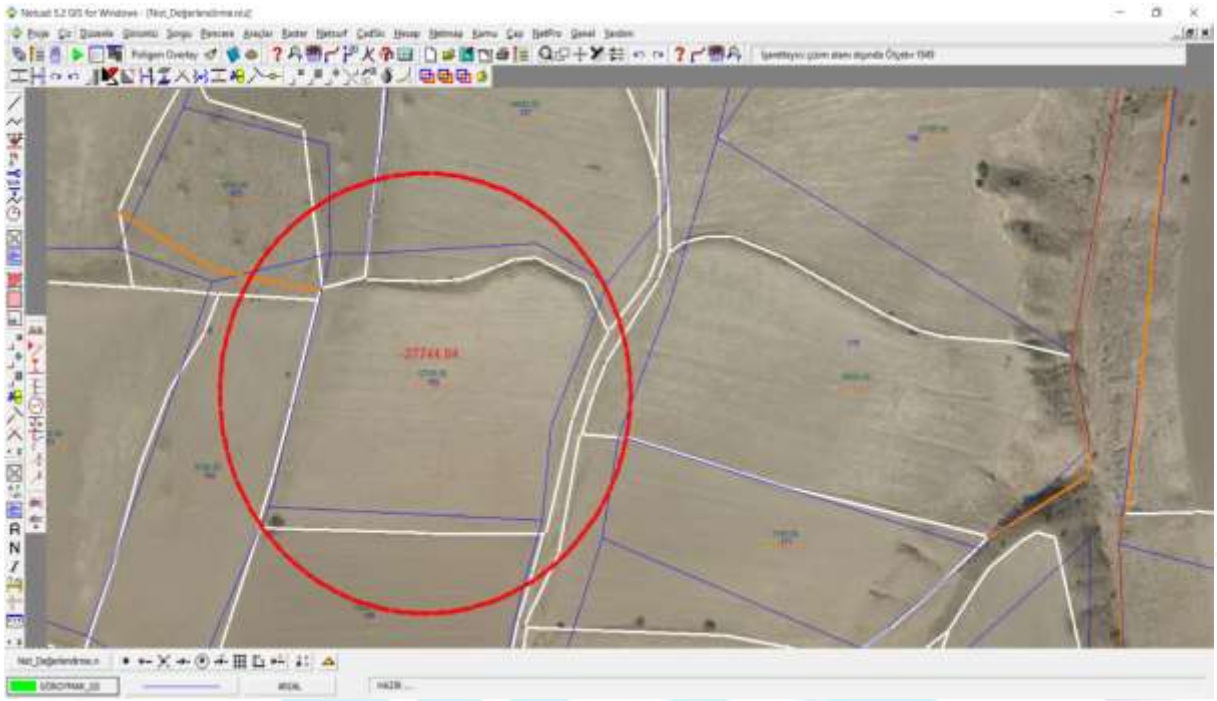

Görsel 7. Alan hesabı hatası

Bitlis ili Güroymak ilçesi Nist köyüne ait görsel 7'de çember içerisindeki parsel; mavi ile gösterilen ilk pafta beyaz sınırlar ise yeni güncelleme sonrası halini göstermektedir. İlk hali ve son halinde çok fazla kayıklık bulunmamasına rağmen alanlar arasında büyük bir fark olduğu tespit edilmiştir. Değerlendirme sonucunda ilk kadastro yapılırken alanın yanlış hesaplandığı saptanmıştır. Yapılan tüm proje çalışmalarında pafta esas olduğu için bu durumun düzeltilmesi yapılacak olan projelerin doğruluğu için fazlası ile önemlidir. Bu gibi durumlarla çok sık karşılaşılmaktadır. Paftaların yenilenmesi gerekmektedir.

Eski paftaların sayısallaştırma işlemlerinden sonra kadastro güncelleme ekibiyle sınırlandırma çalışmalarına başlanır. Kadastro güncelleme ekibi, ilân edilen gün ve saatte, belirtilen adaya gider. Kadastro güncelleme alanına ait kayıt ve belgeler; zeminde mevcut olan sınırlar, kadastro haritaları, ilgililerince ibraz edilecek belgeler, ilgili hak sahipleri ile muhtar ve bilirkişilerin beyanları dikkate alınmak suretiyle mahalline uygulanır ve kadastro teknik mevzuatına göre taşınmazın sınırlandırması yapılır. Sınırlandırma çalışmalarında, temin edilen harita, bilgi ve belgelerden de yararlanılır.

Parsel sınırının yol, dere, ark, vb. genişletilmeye elverişli yerlere isabet ettiği durumlarda öncelikle bu sınırların değişip değişmediği kontrol edilir ve değiştiğinin anlaşılması halinde bu sınırlar

"değişebilir sınır" olarak kabul edilir. Teknik belgeleri ile uyumlu ve/veya zeminde sabit sınır içeren eden bu sınırlar; tanımlarına uygun olarak, sabit sınır veya geçerli sınır tipinde belirlenir. Sınır tiplerine arazide karar verilir [5].

Görsel 8. Tesis kadastrosuyla oluşturulmuş ilk pafta

Bitlis ili Güroymak ilçesi Pav köyü sınırları içerisinde kalan bu bölgeye ait parselin uygulama öncesi hali, değerlendirme aşamaları ve uygulama sonrası değişimi gösterilmektedir. Görsel 8'de parsellerin ilk hali gösterilmektedir. Görsele göre zemin pafta uyumu arasında bariz kayıklıklar mevcuttur.

Görsel 9. Güncelleme çalışması değerlendirme aşaması

Görsel 9'de aynı bölgeye ait görselde kırmızı sınır; ortofoto zemin ölçümünü, mavi sınır; pafta sınırlarını, yeşil sınır; tesis kadastrosu yapılırken ilk ölçü değerlerini, beyaz sınır ise değerlendirme sonucunu göstermektedir.

Değerlendirme çalışması, güncelleme çalışması içerisinde çok önemli bir işlem adımıdır. Görsel 9'de de anlaşılacağı üzere, değerlendirme çalışması tek bir ölçüme veya tek bir parametreye dayandırılmamaktadır. 1960 yılında ilk kadastrosu yapılmış bu bölgeye ait tüm ölçüm değerleri, paftalar, dijital ortama aktarılır. Bölgeye ait varsa eski ortofotolar, fen klasörüne ve ölçü karnelerine girilmiş değerler tümü sayısallaştırılmış tesis kadastrosu paftaları üzerinde incelenir.

Görsel 10. Değerlendirme sonrası sınırlar

Değerlendirme sonrasında Görsel 10'de görüleceği üzere sınırlar arazi kullanımı ve mevcut imar planıyla bire bir örtüştüğü görülmektedir. Kadimden beri kullanımı bu şekilde olduğu anlaşılan eski ortofoto kayıtları ve bilirkişi beyanları bu yönde olduğundan sınırların yeni hali değerlendirme aşamasında bu şekilde belirlenmiştir.

Değerlendirme aşaması tamamlandıktan sonra arazide kontrolleri yapılan sınırlar, yapı tesisler sonucunda ölçü ve sınırlandırma krokisi düzenlenir.

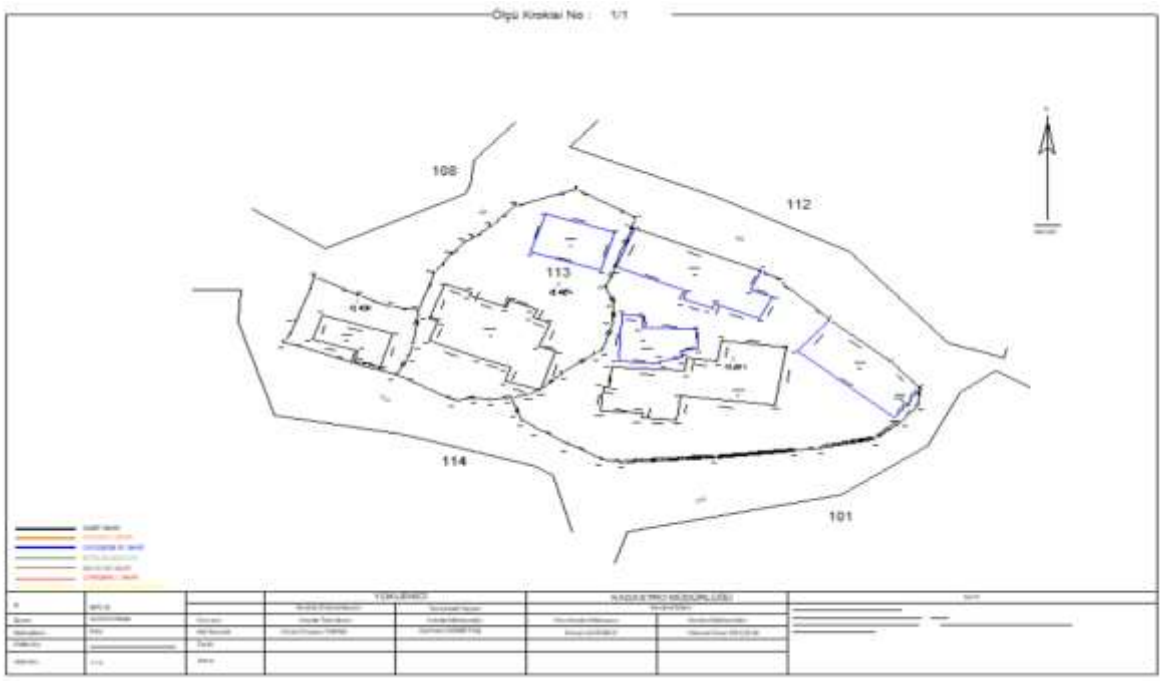

Görsel 11. Ölçü krokisi

Görsel 11'de zeminde ölçümü yapılan tüm detay noktaları ölçü krokisinde gösterilir. Kadastro çalışma alanında işleme ölçü işlerine başlanılmadan önce, bu alan içerisindeki tescile konu parsel sınırlarındaki teknik hatalar var ise öncelikle bu hatalar giderilir. Ölçü krokisinde zeminde bulunan tescile konu ve tescile konu olmayan tüm yapı ve tesisler bulunur, bu yapı ve tesislerin nokta numaraları, cephe ölçüleri yazılır. Parselin nokta numaraları, parselin cephe uzunlukları, yeni ada ve parsel numaraları, eski parsel numaraları, lejant, kuzey oku bulunur.

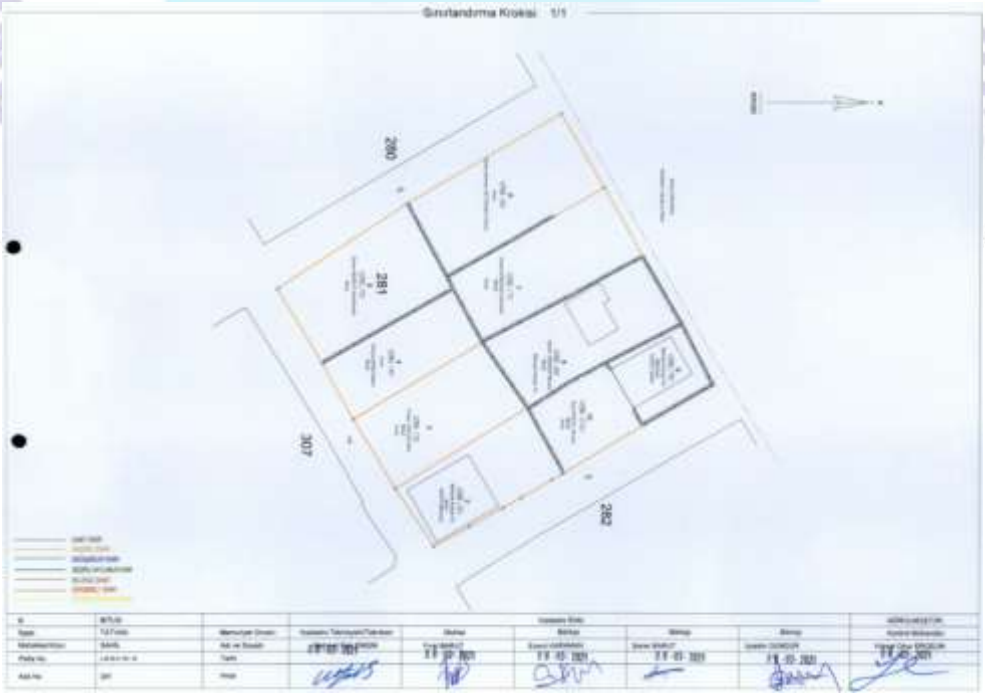

Görsel 12. Sınırlandırma krokisi

Sınır tipleri arazide uygulama ekibince belirlenen sınırlar görsel 12'de olduğu gibi sınırlandırma kroki üzerinde gösterilir. Ölçü krokisinden farklı olarak; malik bilgisi, taşınmaz cinsi, yapı ve tesisler gösterilir.

Hazırlanan sınırlandırma krokileri birleştirilerek kesin paftaları oluşturur. Paftalar hazırlandıktan sonra bir aylık süreyle ilk askı süreci olan bilgilendirme askı sürecine çıkar. İlk askı süreci yerleşim yerlerinde vatandaşların görebileceği yerde olmalıdır (belediyeler, muhtarlıklar, köy camisi, köy lokalleri vb). 15 günlük süreç içerisinde kadastro müdürlüklerine dilekçe yoluyla yapılan çalışma itirazları yapılabilir. Gelebilecek itirazlara karşılık öncesinde komisyon ekibi kadastro müdürlüğünce oluşturulur. Komisyon itirazları karara bağlar. Bu süreç tamamlandıktan sonra 30 günlük süreyle kesin askı süreci başlar burada yapılacak itirazlar kadastro mahkemesine dava olarak açılır.

Uygulama bittikten sonra kesinleşme işlemi gerçekleşen paftalara, "Bu pafta, 3402 sayılı Kadastro Kanununun 22'nci maddesinin (a) bendi gereği .....no'lu paftanın veya paftaların veya bu paftaların işaretli bölümünün yerine geçerli olmak üzere düzenlenmiştir" şeklinde belirtme yapılır . Müdürlük tarafından tarih yazılarak imzalanır ve *onaylanır* [6].

3. SONUÇLAR VE DEĞERLENDİRME

Yapılan kadastro çalışması güncelleme örneğinde Bitlis ili örnek olarak ele alınmıştır. Kadastro çalışmaları dönem şartları gereği zor koşullarda çok uzun bir süreç içerisinde hazırlanmıştır. Gelişen teknoloji ve ölçü aletleri karşısında hassasiyet bakımından bariz farkların olduğu yeni ölçü sistemleri hassas konum belirleme ve birim zamanda hızlı ve doğru konuma ulaşma imkanı sağlamıştır. Paftalarda zamanla yırtılma, okunmama, kaybolma, deformasyona uğrama, pafta zemin uyuşmazlığı, ölçüm hataları gibi nedenlerden ötürü yenileme ihtiyacı doğmuştur.

4. GENEL DEĞERLENDİRME VE SONUÇLAR

Cumhuriyetimizin ilanından sonra kadastro çalışmaları sürekli devam etmiştir. Kadastro hizmeti yaşayan, süreklilik isteyen bir hizmet dalıdır. Kadastro çalışmaları sonucunda üretilen kadastro paftaları günümüz ihtiyaçlarına cevap vermemektedir. Bunun sonucunda ise kadastro paftalarının yenilenmesi gerekliliği ortaya çıkmıştır.

Üretilen eski kadastro paftaları, yetişmiş eleman eksikliği, teknik donanım eksikliği gibi nedenlerden ötürü günümüz ihtiyaçlarına cevap vermemektedir. Hızlı kentleşme, imar uygulamaları, çoğalan nüfus sonucunda üretilen parsel miktarı nüfusa oranla yetersiz kaldığından dolayı parsellerin birim m^2 fiyatları artmıştır. Geçmiş dönemde üretilen kadastro paftalarındaki hata miktarları bu değer artışına maruz kalan paftalar için günümüzde büyük problemlere yol açmaktadır.

Yapılan kadastro çalışmalarının tümünde önceden yapılan hataları minimuma indirmek için seçilecek olan kadastro teknik ekibin daha önceden benzer projelerde çalışmış olması, ülkemiz adına iyi olacaktır. Daha önce çalışmamış olsalar dahi bir eğitim programına dahil olmaları gerekmektedir.

Yeminli bilirkişi seçiminde husumetli olmayacak bilirkişilerin seçilmesi gereklidir. Bilirkişi heyeti içerisinde kendi aralarında sorun olan kişilerin bilirkişi seçilmemeleri gereklidir. Sınırlandırma çalışmalarında bilirkişilerin ve muhtarın beyanı önem arz etmektedir.

KAYNAKÇA

[1] Dikici, M., Kadastro harita ve bilgilerinin güncellenmesi ihtiyacı ve karşılaşılan teknik sorunlar, TMMOB Harita ve Kadastro Mühendisleri Odası 13. Türkiye Harita Bilimsel ve Teknik Kurultayı, 1, Ankara, 2011

[2] Eser, Ö., Kadastral Paftaların Yenilenmesi, Yüksek lisans tezi, 5, İstanbul, 2006

[3]Yıldırım, S., Kadastro paftalarının yenilenmesi üzerine bir inceleme: Erzurum bölge müdürlüğü örneği, Yüksek lisans tezi, 25-26 ,Gümüşhane , 2014

[4] Kadastro Güncelleme Çalışması Uygulama Genelgesi, 5, Ankara, 2018

[5] Kadastro Güncelleme Çalışması Uygulama Genelgesi, 10, Ankara, 2018

[6] Kadastro Güncelleme Çalışması Uygulama Genelgesi, 32, Ankara, 2018

[URL 1] https://www.hkmo.org.tr/resimler/ekler/4c00e610a6465b2_ek.pdf

[URL 2] https://tapu-kadastro.net/index.php/makaleler/yenileme22a-2/259-1367-sayili-genelge-ilkoegretim-ve-egitim-kanununun-tapu-dairelerini-ilgilendiren-maddeleri-hk

Performance of Binary Logistic Regression and Random Forest Model in Creating GIS based Landslides Susceptibility Map at Rangamati Metropolitan Area, Bangladesh

Md. Sharafat Chowdhury[1]

MS Research Student, https://orcid.org/0000-0001-5046-1671

Bibi Hafsa[1]

Assistant Professor

ABSTRACT

The north-eastern hilly areas of Bangladesh seek attention in recent times for increasing landslides leads to huge casualties and economic loss. This study aims to evaluate the performance of GIS-based binary logistic regression (BLR) and Random Forest (RF) techniques in producing landslide susceptibility map (LSM) in the Rangmati Metropolitan Area. Of the 194 landslides in landslide inventory database, 70% (136) landslides were used to prepare the LSMs and 30% (58) landslides were used to validate the maps. The landslide conditioning factors of elevation, slope aspect, slope angle, geology, distance to fault, profile curvature, plan curvature, distance to stream, stream density, stream power index, topographic wetness index, annual rainfall, land use, distance to road, normalized differential vegetation index and bare soil index were used to prepare the LSMs. According to the multicollinearity of the causative factors, lowest tolerance is 0.37, and the highest variance inflation factor is 2.7. The LSMs produced using BLR and FR were classified into five classes of very low, low, medium, high and very high susceptible zones using natural breaks classification method. The ROC values of BLR and RF were 0.870 and 0.821 for training data and 0.838 and 0.807 for testing data, respectively. The ROC values indicate a good accuracy of the models in predicting landslides. But, in such a complex terrain condition, multiple regression model (BLR) showed better performance than machine learning (FR) model. The LSMs can be used to reduce the impact of landslides in the study area.

Keywords : Geographic Information Systems, Binary Logistic Regression, Random Forest, Landslide Susceptibility Map, ROC curve.

[1]Department of Geography and Environment, Jahangirnagar University, Dhaka, Bangladesh

EARTHQUAKE SPATIAL ZONING OF BANGLADESH: A STUDY ON THE SPATIAL AUTOCORRELATION BETWEEN EARTHQUAKE EPICENTERS AND GEO-TECTONIC FAULT LINES

Khandakar Hasan Mahmud[1], Associate Professor, 0000-0003-1222-0791

Raju Ahmed[1], Postgraduate Researcher, 0000-0002-0833-9178

Md. Abu Sayeid[1], Postgraduate Researcher

Jannatun Hussna Tuya[1], Postgraduate Researcher, 0000-0003-1111-9413

ABSTRACT

Bangladesh is susceptible to earthquake risk due to its geographical and geotectonic location. The Himalayan Mountain range and Tibetan plateau which are located just north of the country had formed as a result of the collision between the Indian Plate and Eurasian Plate. At a local scale Two major faultlines are located in the north-east (Dauki fault of Meghalaya) and south-east (Arakan-Yoma of Myanmar) of the country. This research aims to explore the correlation between earthquake epicenters and geotectonic fault lines of the study area. The earthquake data from 1920 to 2020 has been collected from the USGS that is processed with ArcGIS tools. In this research, Spatial Autocorrelation (Global Moran's I) has been conducted for identifying the relationship between the earthquake epicenter and Faultline. Average Nearest Neighbor analysis has also been conducted to identify the spatial pattern of earthquakes. The Geostatistical Spline has been used for predicting the risk zone of surrounding Bangladesh. ArcGIS tools have been used for analyzing and mapping this research. The Global Moran's Index shows a strong positive spatial correlation value of 0.81 with a significance level of 99% ($p < 0.01$) indicating a high magnitude earthquake occurred along the Faultline. A cluster earthquake spatial pattern indicates the spatial arrangement of the earthquake that occurred clustering. The geostatistical interpolation found four risk zones in Bangladesh, where the eastern portion being a high-risk zone, moderate-risk zone, low-risk zone and negligible-risk zone with values of 0.36, 0.24, 0.16, and 0.10 in the western part accordingly.

Keywords: Earthquake, Geotectonic Faultline, Epicenter, Magnitude, Bangladesh.

[1] Department of Geography and Environment, Jahangirnagar University, Savar, Dhaka-1342

Pb AĞIR METALİ İÇEREN BACA GAZI TOZUNUN SOLİDİFİKASYON/STABİLİZASYON PROSESİYLE BERTARAF EDİLEBİLİRLİĞİNİN İNCELENMESİ

Müh. MERVE ÖZGEL [1,2], Doç. Dr., GÜRDAL KANAT [1],Yüksek Müh. BEKİR TOMBUL[1,2]

[1] Yıldız Teknik Üniversitesi, 000-0002-3168-7664

[1] Yıldız Teknik Üniversitesi, 0000-0003-2600-2912

[2]İSTAÇ İstanbul Çevre Yönetimi San.ve Tic. A.Ş., 0000-0001-7673-7146

ÖZET

Kentleşme ve teknolojik gelişmeler tehlikeli ve tehlikesiz atık miktarında sürekli bir artışa neden olmaktadır. Atık yönetimi hiyerarşine göre atıklar; önleme, azaltma, yeniden kullanma, geri dönüşüm, enerji geri kazanımı ve bertaraf prosesiyle yönetilmektedir. Atıkların uygun olmayan şekilde bertaraf edilmesi, insan sağlığı ve çevre için ciddi bir tehdit oluşturmakta bununla birlikte hava, toprak ve yeraltı suyunun kirlenmesine neden olmaktadır. Özellikle zehirlilik, aşındırıcılık, yanıcılık vb. içeren tehlikeli atıklar bulundukları ülkenin atık yönetim mevzuatına uygun olarak yönetilmektedir. Tehlikeli atıkların bertarafında öne çıkan yöntemlerden biri de düzenli depolamadır. Düzenli depolama öncesi ön işlemi olan solidifikasyon/stabilizasyon (S/S) prosesi tehlikeli atıkların arıtılmasında kullanılan başlıca yöntemlerden biridir. S/S prosesi ön arıtma olmadan bertaraf edilmesi yasak olan bileşenleri içeren atıkların bağlayıcılarla fiziksel ve kimyasal özelliklerinin dönüştürülmesini içermektedir. S/S prosesinde zararlı olan inorganik ve/veya organik kirleticiler bağlayıcı malzemeyle oluşturulan bir matrisle stabilize edilmekte ve monolitik bir yapıya dönüştürülmektedir. S/S prosesinin amacı, düzenli depolama alanı kabul kriterlerini sağlamak için atıktaki kirleticilerin çevresel riskini minimize etmektir. Düşük maliyeti, erişilebilir olması ve ağır metallerin stabilizasyonundaki etkinliğinden dolayı çimento yaygın kullanılan bağlayıcı bir malzemedir. Yapılan bu çalışmada, demir çelik üretiminden kaynaklanan ve yüksek konsantrasyonda Pb ağır metali içeren baca gazı tozunun tehlikeli atık düzenli depolama sınırlarına indirgenmesi için farklı %'lerde atık ve çimento içeren toplam 4 adet farklı matris hazırlanmıştır. Çalışmada, Pb konsantrasyonunun depolama sınırlarına indirgenmesi için gerekli optimum çimento miktarının belirlenmesi amaçlanmıştır. Çalışmada kullanılan atığa ve numunelere Toksisite Karakteristiği Süzme Prosedürü (TKSP) ve Atıkların Düzenli Depolanmasına Dair Yönetmelik (ADDDY) Ek-2'sinde belirtilen depolama atık kabul kriterlerini içeren sızıntı testleri uygulanmıştır. 14 günlük kür süresine sahip numunelerine basınç dayanım testi yapılmış ve uluslararası basınç dayanım sınır değerlerine göre karşılaştırmalar yapılmıştır.

Anahtar Kelimeler: tehlikeli atık, kurşun (Pb) ağır metali, solidifikasyon/stabilizasyon, düzenli depolama, baca gazı tozu

INVESTIGATION OF THE DISPOSAL OF FLUE GAS DUST CONTAINING Pb HEAVY METAL WITH SOLIDIFICATION/STABILIZATION PROCESS

BSc. MERVE ÖZGEL [1,2], Assoc. Prof. Dr.,GÜRDAL KANAT [1],MSc. BEKİR TOMBUL[1,2]

[1] Yildiz Technical University, 000-0002-3168-7664

[1] Yildiz Technical University, 0000-0003-2600-2912

[2] ISTAÇ Istanbul Environmental Management Indust.and Trad Inc., 0000-0001-7673-7146

ABSTRACT

Urbanization and technological developments cause a continuous increase in the amount of hazardous and non-hazardous waste. According to the waste management hierarchy; wastes are managed by prevention, reduction, reuse, recycling, energy recovery and disposal processes. Improper disposal of waste poses a serious threat to human health and the environment, and also causes pollution of air, soil and groundwater. Hazardous wastes which Especially for toxicity, corrosiveness, flammability etc. containing are managed in accordance with the waste management legislation of the country in which they are located. One of the prominent methods of disposal of hazardous wastes is landfill. The solidification/stabilization (S/S) process which is the pre-treatment before landfill, is one of the main methods used in the treatment of hazardous wastes. The S/S process involves the conversion of the physical and chemical properties of wastes containing components that are forbidden to be disposed of without pretreatment with binders. In the S/S process, harmful inorganic and/or organic pollutants are stabilized by a matrix formed with binder material and converted into a monolithic structure. The aim of the S/S process is to minimize the environmental risk of pollutants in the waste to meet the landfill acceptance criteria. Cement is a widely used binder material due to its low cost, availability and effectiveness in stabilizing heavy metals. In this study, a total of 4 different matrices containing different percentages of waste and cement were prepared in order to reduce the flue gas dust generating from iron and steel production and containing Pb heavy metal in high concentration to the hazardous waste landfill limits. In the study, it was aimed to determine the optimum amount of cement required to reduce the Pb concentration to the storage limits. Leaching tests including the waste acceptance criteria specified in the Toxicity Characteristics Leaching Procedure (TCLP) and the Regulation on Regular Landfilling of Wastes (RRLW) Annex-2 were applied to the waste and samples used in the study. Compressive strength test was performed on samples with 14-day curing time and comparisons were made according to international pressure strength limit values.

Keywords: hazardous waste, lead (Pb) heavy metal, solidification/stabilization, landfill, flue gas dust

COĞRAFİ BİLGİ SİSTEMİNDE KANALİZASYON VE İÇME SUYU ALTYAPI BİLGİ SİSTEMİ OLUŞTURULMASI[1]

Harita Mühendisi FURKAN KOCAMAN[1], Prof. Dr. HEDİYE ERDOĞAN[2]

[1]Aksaray Üniversitesi, 0000-0002-1821-8628

[2]Aksaray Üniversitesi , 0000-0002-6470-5857

ÖZET

Küçük şehirlerden ve köylerden nüfus, daha gelişmiş ve büyük şehirlere hızla kaymaktadır. Bunun sonucunda altyapı sorunları ortaya çıkmaktadır. Altyapı sorunlarının şehirde oluşturduğu olumsuz etki ile mal ve can kaybı yaşanabilmektedir. Altyapı hatları geçmişten günümüze kadar farklı yollarla ve farklı standartlarla yapılmıştır. Bu hatlar, bütün şehir için göz önüne alındığında çok uzun ve karışık yapılar ortaya çıkmaktadır. Farklı kurum ve kuruluşların altyapı çalışmaları vardır. Çalışma alanlarında can ve mal kaybının olmaması için bu kurum ve kuruluşların birbiriyle koordine olması gerekir. Bu koordine, altyapı bilgi sistemiyle sağlanabilir. Kent bilgi sisteminin yerleşim bölgesinin altyapısına (yağmur suyu, kanalizasyon, içme suyu, doğalgaz şebekeleri vb.) uygulanmasıyla altyapı bilgi sistemi elde edilir. Altyapı Bilgi Sistemi (ABS) Coğrafi Bilgi Sistemi (CBS) tabanlı olan bir bilgi sistemidir. Yapılan çalışmada, coğrafi bilgi sistemi tabanlı ArgGIS programı kullanılarak Tatvan ilçesinde CBS yardımıyla kanalizasyon ve içme suyu konumsal verileri kullanılarak altyapı bilgi sistemi örneği oluşturulmuştur. Oluşturulan altyapı bilgi sistemi yardımıyla, örnek bir uygulama yapılmıştır.

Anahtar Kelimeler: Altyapı, Bilgi Sistemi, CBS, Kanalizasyon, İçme suyu.

1.GİRİŞ

Ülke içinde bulunan bir yapıda ihtiyaç duyulan kanalizasyon, yol, su, elektrik ve doğal gaz gibi tesisatların bütünü altyapı olarak adlandırılmaktadır. Ayrıca kent için gerekli iş ve işlemlerinin yerine getirebilmesi, modernleşmesi ve gelişmesi için gerekli olan temel hizmetler, araç, gereç ve donatılar şeklinde de tanımlanabilir [1].

Altyapı, kentler için önemli yapılarından biridir. Altyapı sorunlarının insan yaşamındaki etkisi çok büyüktür. Altyapı tesislerinin ve yapılarının gelişen teknoloji ile modern ve sisteme uygun şekilde

[1] Bu çalışma, ikinci yazar danışmanlığında birinci yazarın hazırladığı yüksek lisans tezinden üretilmiştir.

yapılması gerekir. İnsanların kent yaşamındaki kaliteyi en üst seviyeye çıkarır. Bu da altyapı hizmetlerinin sayısının artmasını ve çeşitlenmesini sağlar. Kentlere göçün artması ile birlikte altyapı sorunları meydana gelmektedir. Altyapı hizmetlerinin sayısının artması ve çeşitlenmesi, insanların kent yaşamındaki kaliteyi en üst seviyeye çıkarır [2].

Kanalizasyon sisteminde oluşabilecek arızalar, sistemin normal işletme koşullarını bozmakta, bakım-onarım maliyetlerini üst seviyeye çıkarmakta, çevre, hayvan ve insan sağlığı açısından önemli sorunlar ortaya çıkarabilmektedir. Bu sebeple bu tür sistemlerde tesislerdeki arıza ve yapısal kusurların tespit edilmesi, konuma ve zamana bağlı değişimlerin izlenmesi, etki faktörlerin belirlenip analiz edilmesi gerekmektedir[3].Toplum için temiz su temini ihtiyacının önemi, her geçen zamanla birlikte artmaktadır. Bu açıdan altyapı bilgi sistemi son derece önemlidir [4].

Kent bilgi sisteminin yerleşim bölgesinin altyapısına (yağmur suyu, kanalizasyon, içme suyu, doğalgaz şebekeleri vb.) uygulanmasıyla altyapı bilgi sistemi elde edilir. Altyapı bilgi sistemi CBS tabanlı olan bir bilgi sistemidir. Coğrafi Bilgi Sistemleri ise coğrafi veri altlıklarını kullanan çalışmaların hızını, koordineli bir şekilde arttıran sayısal ve sözel verilerin yazılım ve donanım aracılığı ile veri tabanına işlendiği ve bununla sorgulama ve analizin ihtiyaca göre yanıt veren problemlerin doğru sonuca ulaşmasını sağlayan bir sistemdir. CBS'yi bilgi sistemlerinden ayıran özellik ise nesnelerin öznitelik bilgilerinin yanında konumsal (x,y,z) bilgilerinin de saklanıyor olmasıdır [5,6].

Kurum ve kuruluşlar, kendi altyapı çalışmaları sırasında kullandığı veri standartlarının ve CBS uygulamalarının farklı olması, altyapı tesisleri arasındaki veri paylaşımını zorlaştırmaktadır. Altyapı bilgi sistemi, verilerin kurumlar tarafından ortak kullanılmasını sağlamak amacıyla oluşturulan politikalar ve belirli standartlar bütünü kapsamaktadır [7].

Yapılan çalışmada, Bitlis ili Tatvan ilçesindeki kanalizasyon ve içme suyu altyapısında oluşabilecek bir probleme anında en doğru karar verilebilmesi, konumsal sorgulamaların yapılabilmesi için altyapı bilgi sisteminin bir uygulaması yapılmıştır.

2. MATERYAL VE METOD

Kanalizasyon ve içme suyu altyapı bilgi sistemi uygulaması için Bitlis ilinin Tatvan ilçesi seçilmiştir. Bunun sebebi ise Bitlis il merkezi ve bağlı ilçelerinin içinde en fazla nüfusa ve altyapı hatları en yeni olan ilçe olmasıdır.

Tatvan, Doğu Anadolu Bölgesi'nde Van Gölü'nün batı yakasında 38° 29′ 31″ Kuzey enlemleri ile 42° 16′ 57″ Doğu boylamları arasında yer alan Bitlis iline bağlı bir ilçedir. Tatvan ilçesinin Bitlis il haritasındaki yerini gösteren harita, Görsel 1'de verilmiştir.

Görsel 1. Bitlis il haritası

Tatvan ilçesinin kanalizasyon ve içme suyu altyapı bilgi sistemi uygulamasının yapılması için Tatvan Belediyesi Fen İşleri Müdürlüğü tarafından mevcut veriler temin edilmiştir. Yapılan çalışma için kanalizasyon ve içme suyuna ait mevcut veriler, Netcad ortamında ITRF koordinat sisteminde alınmıştır. Bu sayede içme suyu ve kanalizasyon verileri Arcmap uygulamasında görüntülenmiştir. Mevcut verilerle içme suyu ve kanalizasyon hatlarının Arcmap uygulanmasında gösterimi sağlanmıştır. Elde edilen içme suyu hattı (mavi çizgi ile gösterilmiştir) ve kanalizasyon hattı (kırmızı çizgi ile gösterilmiştir) altyapı haritası, Görsel 2'de verilmiştir.

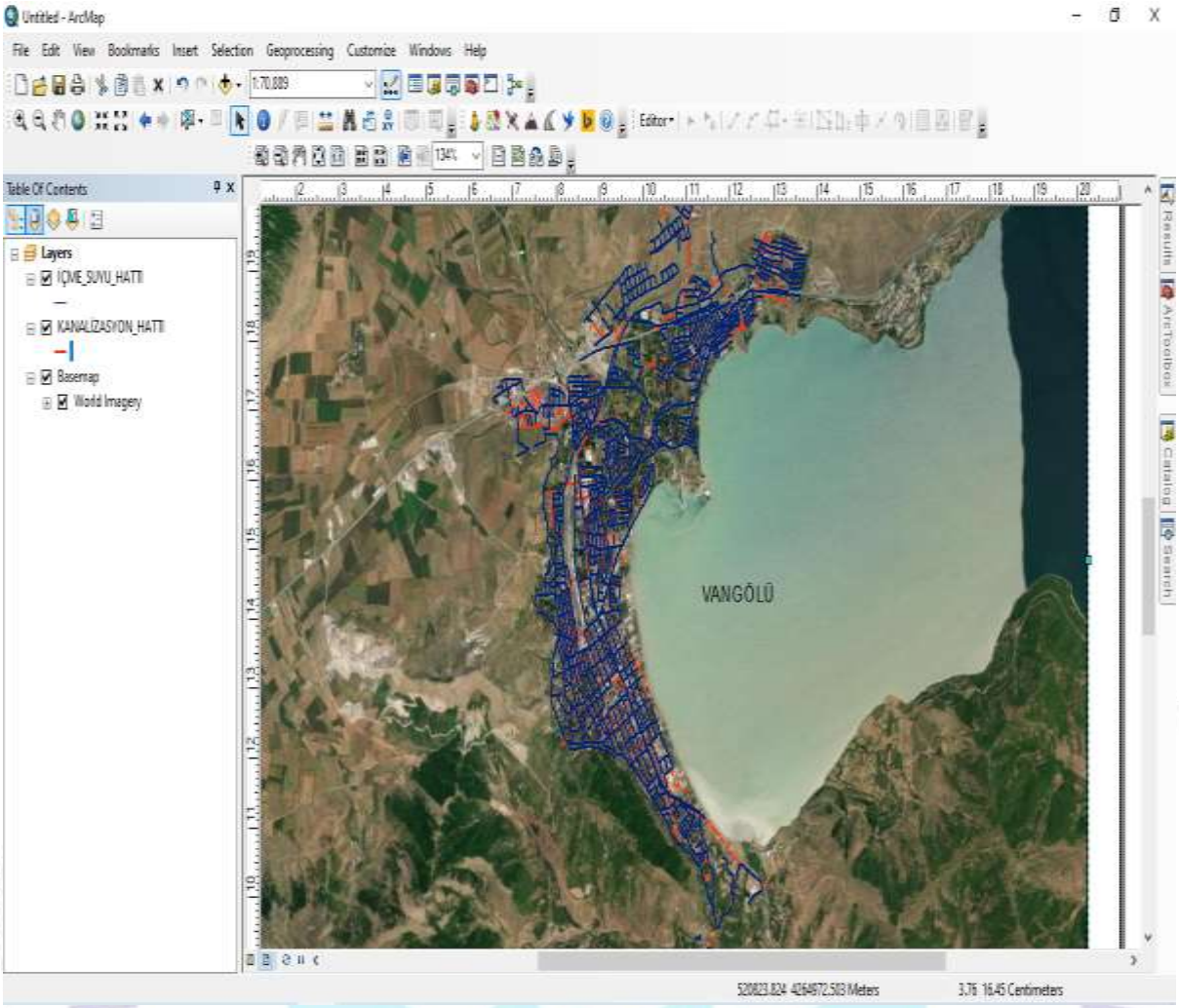

Görsel 2. Tatvan ilçesi içme suyu ve kanalizasyon altyapı haritası

Tatvan ilçesindeki içme suyu ve kanalizasyon yer altı şebeke hatlarının incelenmesi ve işleyişinin takip edilmesi altyapı bilgi sistemiyle mümkün olmaktadır. Netcad verileri, Cad Reader uygulaması ile Arcmap uygulamasında açılması sağlanmıştır. Arcmap bir araya getirilerek kanalizasyon hatları kırmızı, içme suyu hatları mavi renkte gösterilmiştir. Çizgi kalınlıkları 1.5 olarak ayarlanmış ve görsel olarak çözünürlüğü yüksek tutulup daha iyi bir görsel olması sağlanmıştır. ArcGIS basemap online üzerinden istediği haritayı altlık olarak kullanabileceği gibi başka yerden de istediği haritayı indirerek kullanabilmektedir. ArcMap yazılımına ncz uzantılı verilerin nasıl ekleneceğine ilişkin ekran fotoğrafı Görsel 3'te verilmiştir.

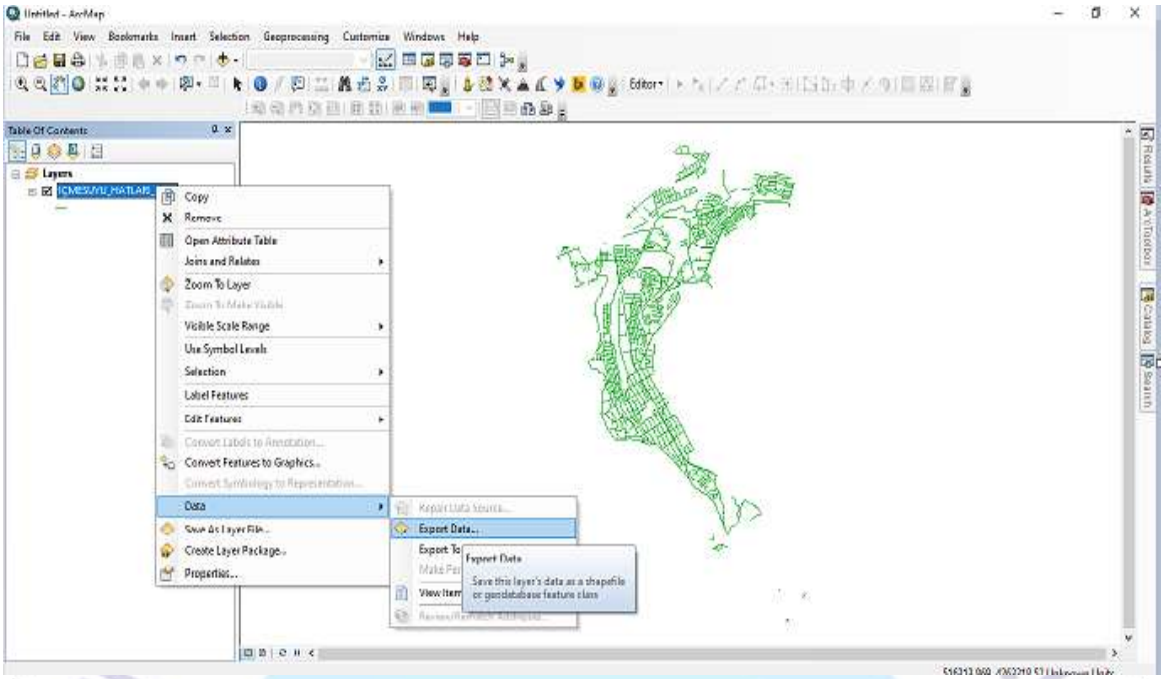

Görsel 3. İçme suyu ana hat verilerinin arcmap arayüzüne aktarılması

İçme suyu ana hat verileri ncz uzantılı olduğundan dolayı Cadreader alt programı yardımıyla arcmap arayüzüne aktarılmıştır. Arcmap arayüzüne aktarılan içme suyu ana hat verileri export data seçeneği yardımıyla verilen tüm özellikleriyle daha sonra kullanmaya imkan sağlanmıştır. ArcMap yazılımına basemap online haritaların nasıl ekleneceğine ilişkin ekran resmi Görsel 4'te verilmiştir.

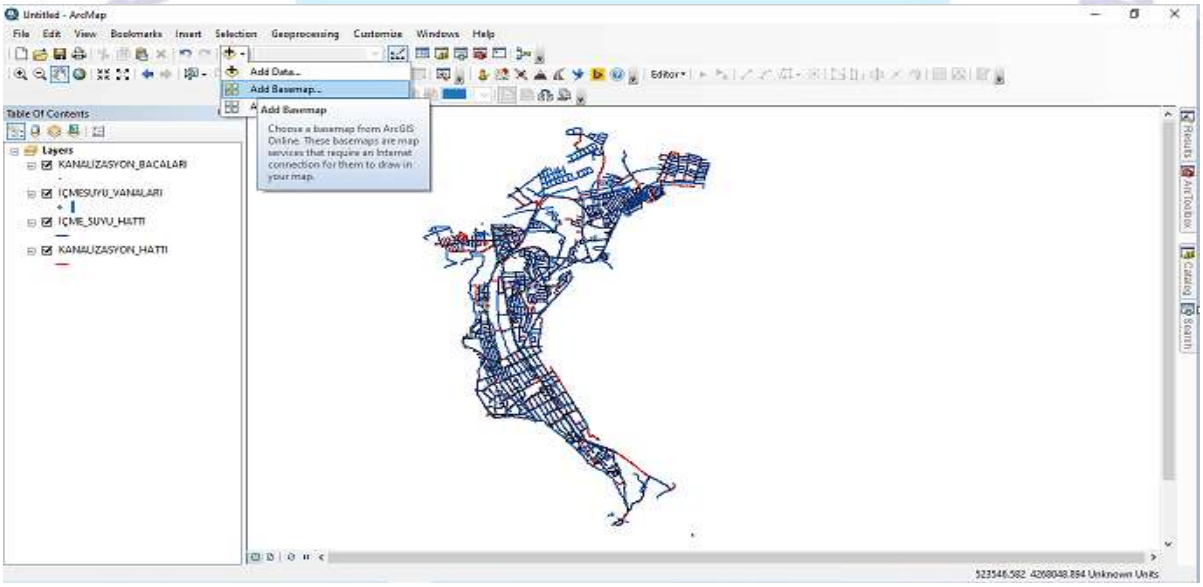

Görsel 4. ArcMap yazılımına basemap online haritaların eklenmesi

Tatvan ilçe sınırları içinde içme suyu ve kanalizasyon hatlarının coğrafi varlıklarının konumlarının olması yanı sıra öznitelik bilgilerinin sorgulanabilmesi için CBS temelli sistemlerinin vazgeçilmez özelliklerindendir. Çalışma yapılan ilçede mevcut olan ve yenilenen içme suyu ve kanalizasyon hatlarının her birinin öznitelik tablosuna (attribute table) görülmesi istenen ve uygulama için yarı olan sütunlar eklenmiştir. Örnek olarak Kanalizasyon hatları için öznitelik tablosuna eklenen sözel bilgiler Görsel 5'te verilmiştir.

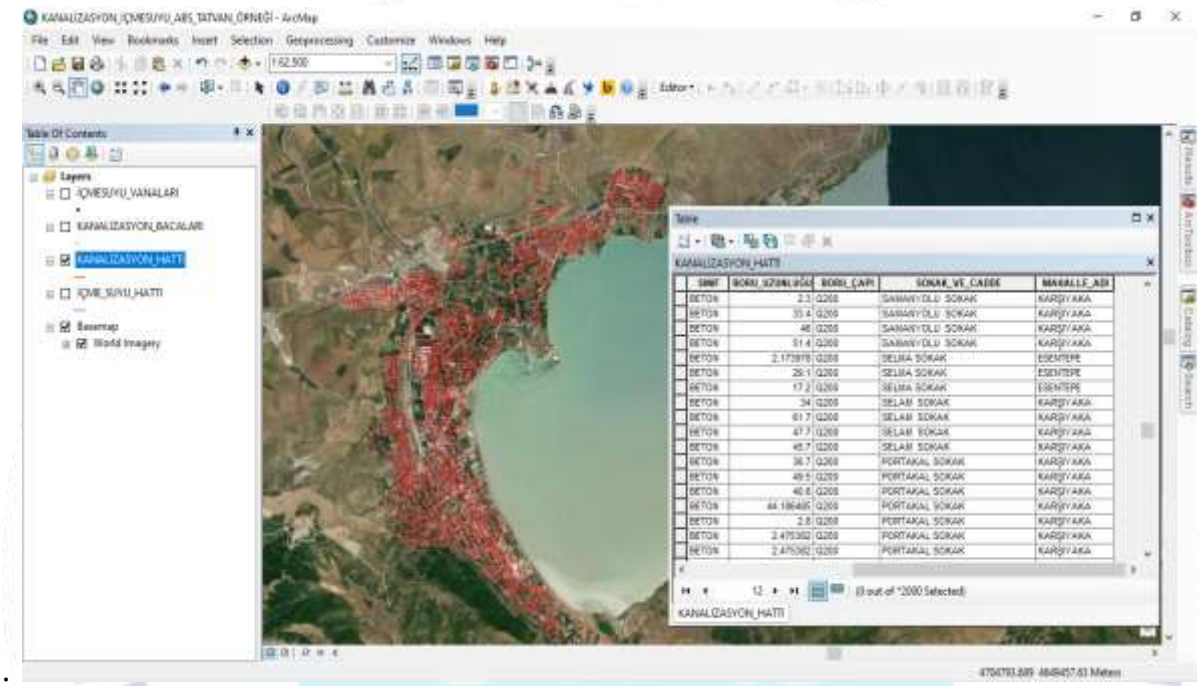

Görsel 5. Tatvan ilçesi kanalizasyon ana hatlarına ait öznitelik tablosu

Kanalizasyon hatları için oluşturulan öznitelik tablosuna borunun cinsi, boru çapı, iki baca arası boru uzunluğu, cadde ve sokak adı ve mahalle adı eklenmiştir. Bu bilgilerin öznitelik tablosunda olması ile hangi mahallede arıza olduğu hangi boru çapının olduğu vb, bilgiler bu sistemle öğrenilip, arızaya giden ekibe bilgi verilecektir. Böylece arıza hızlı çözülecektir. Yapılan uygulamada, kanalizasyon ve içme suyu hatlarının konumsal verilerinde bazı eksiklikler bulunmaktadır. Bu eksikliklerin nedeni, mevcut olan altyapı hatlarının eski olması ve bu hatlara ait konumsal verilerin alınmamasından kaynaklanmaktadır. Eksik bilgilerle sisteme aktarılan verilerden dolayı, bazı hatların iki ucunun boşta ve şebekesinden ayrı olarak görünmesine sebep olmaktadır. Konumsal verilerin eksik olduğu yerlerde, yer altı hatlarının mevcut olmadığı anlamına gelmemektedir. Bu alanlarda içme suyu ve kanalizasyon hatları işlevine uygun çalışmaktadır. Kanalizasyon hatlarındaki konumsal veri eksikliklerinin olduğu alan, Görsel 6'da verilmiştir.

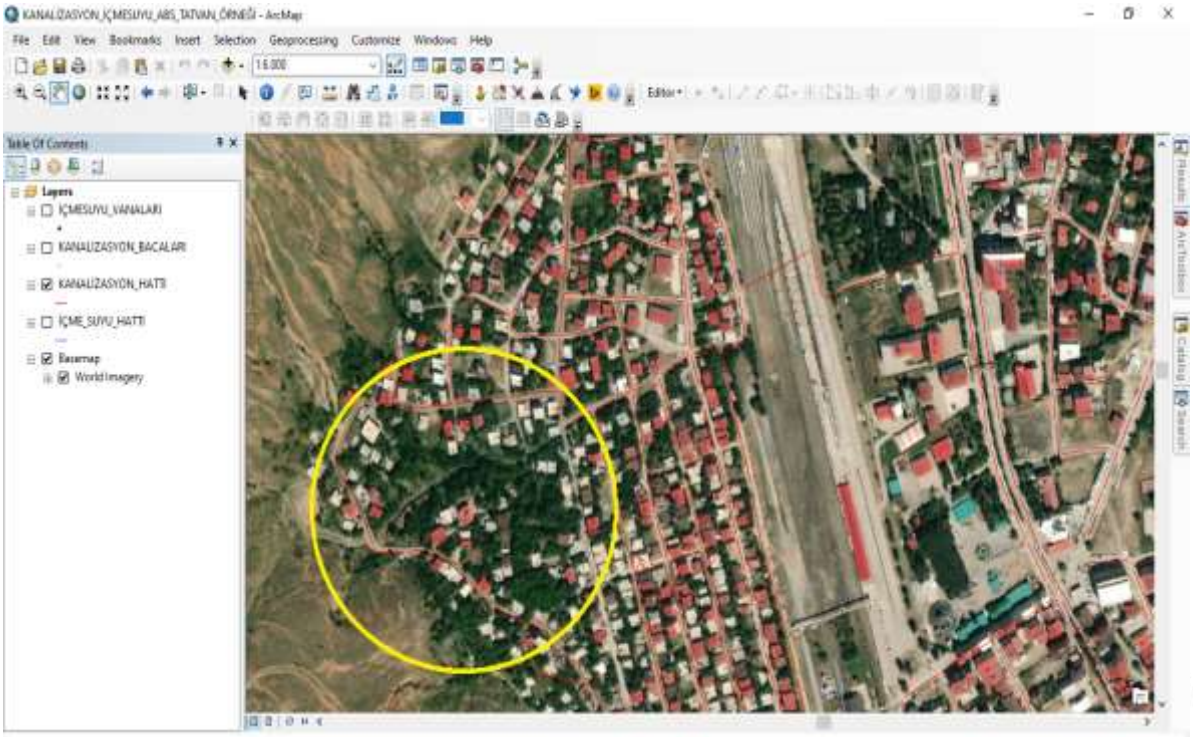

Görsel 6. Kanalizasyon hattına ait eksik verilerin gösterilmesi

Uygulama örneğinde, konumsal verileri bulunan kanalizasyon altyapı hatları kırmızı renkte gösterilmiştir. Görsel 6'da sarı renkteki daire içerisinde gösterilen kısmın çoğunda kanalizasyon hatlarının olmadığı görülmektedir. Ancak bulunan alanda yaşam olması, çevre ve temizlik açısından kanalizasyon hattının olmasının zaruri olduğu bir gerçektir. Burada kanalizasyon altyapısına ait hatların görünmemesinin sebebi ise söz konusu alanda konumsal verilerin alınmamış olmasından kaynaklanmaktadır.

Tatvan ilçesinde yapılan uygulamada, ilçede mevcut yeraltı şebeke ana hatlarının durumunu özetleyen ve ihtiyaç duyulan şebeke hatlarına ait öznitelik bilgilerinin sorgulanabildiği, kanalizasyon bacalarının ve içme suyu vanalarının sorgulandığı bir örnek altyapı bilgi sistemi oluşturulmuştur. Netcad ortamında alınan bilgilerde cadde, sokak ve mahalle adı eksik olan verilerin bilgileri ArcGIS programına işlenerek mevcut verilerle entegresi sağlanmıştır. Bu sayede oluşturulan sistem, çeşitli sorgulamaların yapılabildiği ve aranmak istenen konum adresi bilinen bir ABS haline getirilmiştir. İçme suyu ana hattı sorgulamaların yapılması, Görsel 7'de verilmiştir.

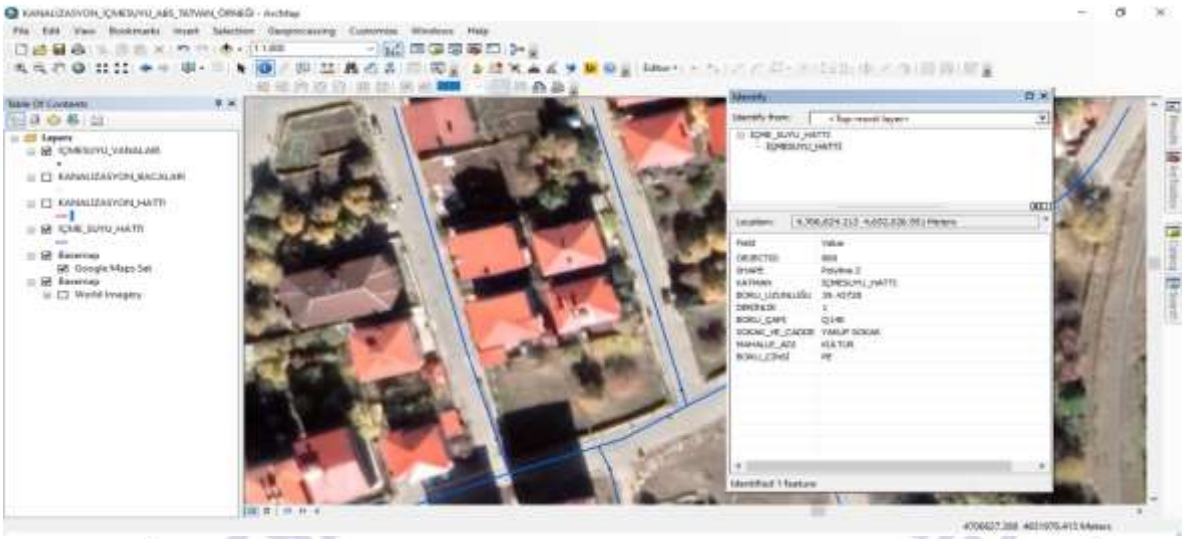

Görsel 7. İçme suyu ana hattı sorgulamaların yapılması

Görsel 7'de ArcGIS programında bulunan identify seçeneği yardımıyla sorgulaması yapılan bir içme suyu ana hat borusunun öznitelik bilgileri yer almaktadır. Örnek olarak, sorgulaması yapılan ana içme suyu borusunun arızası durumunda, hangi sokak içinde kalan yapıların içme suyu hizmeti alamayacağı bilgisi bulunabilir. Oluşturulan ABS'deki bilgilerden faydalanılarak arızaya müdahaleye gidecek ekibin hangi içme suyu hattında çalışma yapacağı ve gerekli olan boru cinsi malzemelerinin temininde kolaylık sağlayacaktır. İçme suyu vana sorgulamasının yapılması, Görsel 8'de verilmiştir.

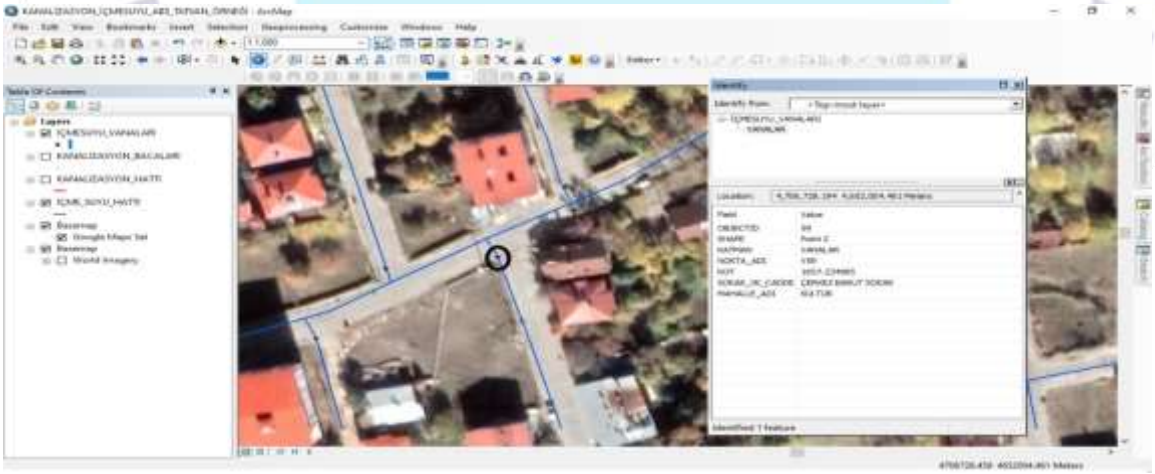

Görsel 8. İçme suyu vana sorgulamasının yapılması

Görsel 8'de içme suyu vana sorgulamasının identify yardımıyla yapılmasıyla öznitelik bilgileri görüntülenmektedir. Bu bilgiler ışığında oluşacak arza veya bir hat yenileme çalışmasında vananın konumunun bilinmesi önemli rol oynamaktadır. Konumu bilinen vananın hangi sokaklarda,

caddede veya mahallede suyu kesik olacak yapılar bilinebilmektedir. Hyperlink menüsü kullanılarak hatlara çeşitli görsel ve linkler eklenmekte ve o konumda arazinin nasıl olduğu rahatlıkla Görsel 9'daki gibi görülmektedir.

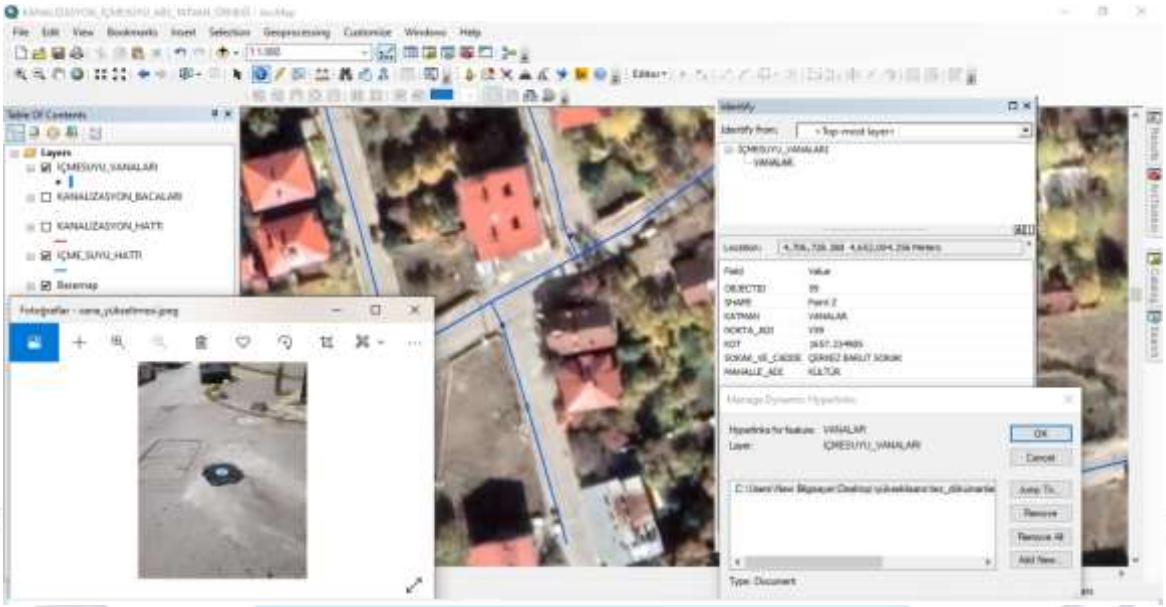

Görsel 9. İçme suyu ana hat vanasına ait sorgulamanın görsel yapılması

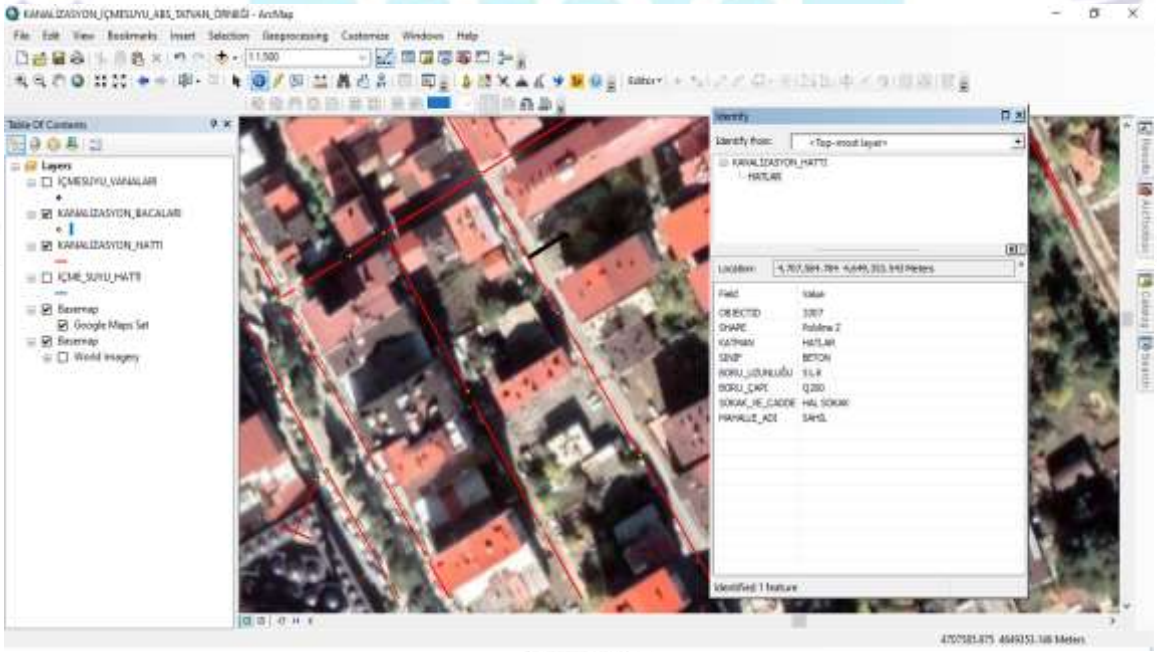

Görsel 10. Kanalizasyon ana hatta ait sorgulamanın yapılması

Görsel 10'da kanalizasyon ana hattında oluşacak arızanın identify yardımıyla sorgulaması yapılarak öznitelik sözel bilgilerine ulaşılabilmektedir. Kanalizasyon bacalarına ait sorgulamanın yapılması, Görsel 11'de verilmiştir.

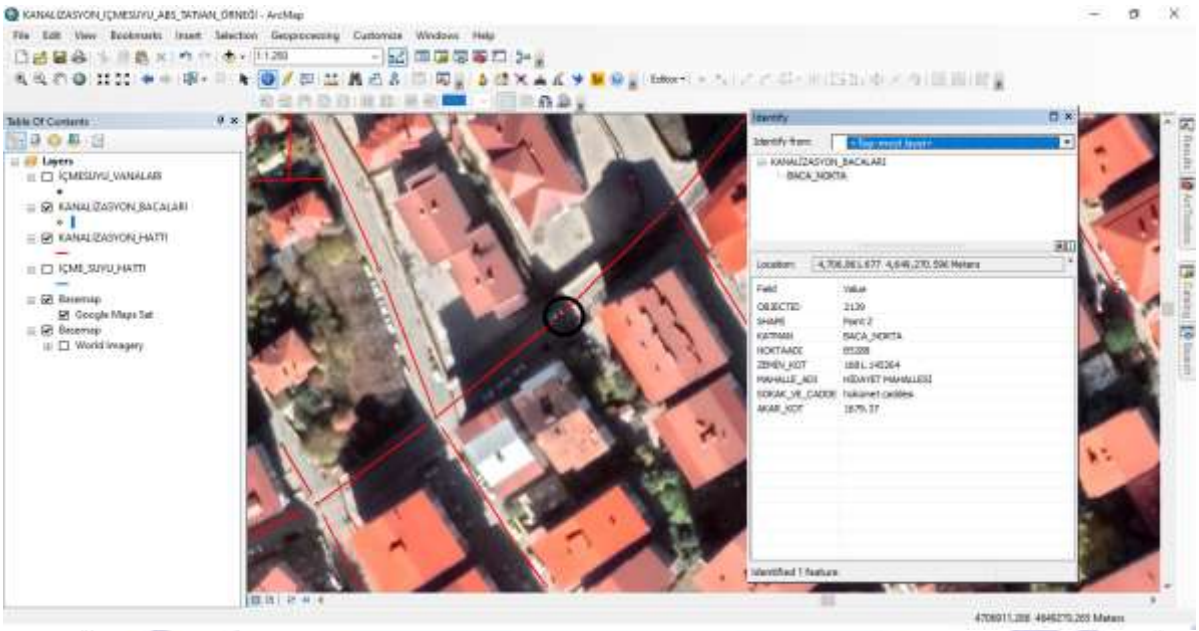

Görsel 11. Kanalizasyon bacalarına ait sorgulamanın yapılması

Görsel 11'de kanalizasyon ana hat bacalarına ait veriler identify yardımıyla sorgulaması yapılarak öznitelik sözel bilgilerine ulaşılabilmektedir. Bu durumda kanalizasyon hattında bacalarda oluşacak arızanın hangi sokakta olduğunun tespitinin yapılması müdahale edilecek yere hangi malzemelerin götürüleceğin tespiti yapılarak zaman maliyetten tasarruf edilmektedir. Ayrıca kanalizasyon bacalarında yenileme çalışması yapılması istendiğinde kanal akar kotları bilindiğinden ona göre plan ve proje yapılabilecektir.

3. SONUÇLAR VE DEĞERLENDİRME

Uygulama yapılan yerleşim yerinde yaşayan insanlara, yaşanabilir güzel bir şehir bırakmak için kanalizasyon ve içme suyu gibi altyapıların düzgün yapılmış olması önemlidir. Yapılan çalışmada; Tatvan ilçesindeki kanalizasyon ve içme suyu altyapısı hatlarına ait verilerinin sisteme girilmesi sağlanmıştır. Sözel bilgi olan sokak ve cadde, mahalle adı, boru cinsi ve boru çapı gibi sözel bilgiler tespit edilerek sisteme dâhil edilmiştir. Daha sonra eldeki verilerin kullanılmasıyla sistemin analizi yapılmıştır. Altyapı verileri ile bilgi sistemi tasarlanmıştır. Bunun sonucunda da analiz işlemleri ile sorgulamalar yapılmıştır.

4. GENEL DEĞERLENDİRME VE SONUÇLAR

Kanalizasyon ve içme suyu hatlarında meydana gelebilecek problemlerin önceden tespitinin yapılıp gerekli tedbirlerin alınabilmesi için kurum veya kuruluşların, kamu ve vatandaşın yararını

sağlaması için altyapı hizmetlerini fayda sağlayacak şekilde yapması için, Altyapı koordinasyon birimi oluşturulması, sistemi kullanacakların uzman kişiler olması, Altyapı verilerinin sürekli güncel tutulması, altyapı verisi olmayan bölgeler için gerekli verilerin alınması gibi bilgilerin dikkate alması son derece önemlidir.

Altyapı tesisleri imar planı göz önünde bulunarak mümkün olduğu sürece sadece yollardan geçirilmeli ve sonradan imar değişikliğine gidilmemelidir.

Teknolojiden faydalanılarak kanalizasyon ve içme suyu altyapı bilgi sisteminin uygulanmasıyla, gelecek nesillere güzel ve temiz bir şehir bırakılacaktır. Son zamanlarda kullanım olarak artan bilgi sistemi her alanda hayatımızı kolaylaştırmaya ve bizlerin geleceğini daha yaşanılır hale getirecektir.

.

KAYNAKÇA

[1] Erkaya, H., *Altyapı mühendislik ölçmeleri, önemi ve gerek*liliği, TMMOB Diyarbakır Kent Sempozyumu, Bildiriler Kitabı, 88-103, Diyarbakır, 2009.

[2] Akıner, M. E. ve Akıner, İ., Altyapı Sorunlarına Yenilikçi Çözüm Önerilerinin Getirilmesi. Avrupa Bilim ve Teknoloji Dergisi, Ejosat 2021 Ek Sayı 1, 755-763, 2021.

[3] Gök, S. ve Fırat, M., *Analysis of Faults in SewageSystemswithGeographical Information Systems*, 4th International Conference of ContemporaryAffairs in Architecture andUrbanism (ICCAUA-2021) 20-21 May 2021, 786-797, Antalya, 2021.

[4] Nahwani, A. ve Husin, A.E.,Water Network Improvement Using InfrastructureLeakage Index andGeographic Information System, CivilEngineeringand Architecture, 9, 3, 909 – 914, 2021.

[5] Kapluhan, E., Coğrafi Bilgi Sistemleri'nin (CBS) Coğrafya Öğretiminde Kullanımının Önemi ve Gerekliliği, Marmara Coğrafya Dergisi, 29, 34-59, 2014.

[6] Yomralıoğlu, T., Coğrafi Bilgi Sistemleri: Temel Kavramlar ve Uygulamalar. 7.Baskı, s.480, ISBN 975-97369-0-X, İber Ofset, İstanbul, 2015.

[7] Bayraktar, Z., *Altyapı Koordinasyon Merkezleri İçin Konumsal Veri Standartlarına Uygun Bilgi Sistemi Tasarımı: Trabzon Örneği*, Yüksek Lisans Tezi, Karadeniz Teknik Üniversitesi, Fen Bilimleri Enstitüsü, Trabzon, 2019.

YAPAY SİNİR AĞLARI İLE RÜZGAR GÜCÜ TAHMİNİ

Ayhan Tokmak
Recep Tayyip Erdoğan Üniversitesi – 0000-0002-9483-406X

Doç. Dr. Övgü Ceyda Yelgel
Recep Tayyip Erdoğan Üniversitesi - 0000-0001-5888-5743

ÖZET

Günümüzde enerji ihtiyacının oldukça büyük bir kısmı fosil yakıtlardan (doğalgaz, petrol, kömür gibi) karşılanmaktadır. Bu yakıtların çevreye verdiği zararlardan, zamanla tükenmeye başlamalarından ve küresel ısınmaya sebep olmalarından dolayı artan enerji ihtiyacımızın temiz ve yenilenebilir enerji kaynaklarından karşılanması oldukça büyük önem kazanmış ve dünya ülkelerinin enerji politikalarının belirleyici unsuru haline gelmiştir. Rüzgar enerjisi teknolojilerinin gelişmesi, rüzgar türbin kurulumunun hızlıca gerçekleştirilebilmesi ve rüzgar türbinlerinden üretilen elektrik enerjisinin birim maliyetinin azalmasıyla beraber diğer yenilenebilir enerji kaynakları ile rekabet edebilir düzeye yaklaşmasından dolayı rüzgar enerjisi kullanımı dünya çapında bir artış göstermektedir. Rüzgar enerjisinin değişken yapısından kaynaklanan sistem belirsizliğinin azaltılması ve rüzgar santrallerinin üretim gelirlerinin arttırılması için daha kararlı rüzgar gücü tahmin modellerine ihtiyaç duyulmaktadır. Bu çalışmada Çanakkale Mahmudiye bölgesinin rüzgar gücü potansiyeli altı farklı rüzgar türbin modeli için (GamesaG97, SuzlonS.88, SiemensSWT2.3, NordexN100, EnerconE82 ve VestasV117) yapay sinir ağları kullanarak çalışılmıştır. Ayrıca bu çalışmamızda rüzgar gücü tahmini yapılırken yapay sinir ağları modeline farklı nöron sayılarının etkisi ve farklı aktivasyon fonksiyonlarının etkisi detaylıca tartışılmıştır.

Anahtar Kelimeler: yapay sinir ağları ; yenilenebilir enerji ; rüzgar enerjisi ; rüzgar hızı ; rüzgar gücü

WIND POWER PREDICTION WITH ARTIFICIAL NEURAL NETWORKS

ABSTRACT

Today, a large part of the energy need is met from fossil fuels (such as natural gas, oil, coal). Due to the damage of these fuels to the environment, their depletion over time and the fact that they cause global warming, meeting our increasing energy needs from clean and renewable energy sources has gained great importance and has become the determining element of the energy policies of the world countries. The use of wind energy is increasing worldwide due to the development of wind energy technologies, the rapid implementation of wind turbine installation and the decrease in the unit cost of electrical energy produced from wind turbines, as well as approaching the level of competition with other renewable energy sources. More stable wind power forecasting models are needed to reduce system uncertainty caused by the variable nature of wind energy and to increase generation revenues of wind power plants. In this study, the wind power potential of Çanakkale Mahmudiye region was studied using artificial neural networks for six different wind turbine models (GamesaG97, SuzlonS.88, SiemensSWT2.3, NordexN100, EnerconE82 and VestasV117). In addition to that, the effect of different neuron numbers on the artificial neural network model and the effect of different activation functions on the wind power estimation are discussed in detail.

Keywords: artificial neural networks ; renewable energy ; wind energy ; wind speed ; wind power

Unsteady 3D Post-Stall Aerodynamics Accounting for Effective Loss in Camber Due to Flow Separation

[1]Aritras Roy, [2]Rinku Mukherjee ,

[1]Indian - Institute of Technology Madras, Chennai, India

[2]Assistant Professor, Applied Mechanics, Indian Institute of Technology Madras, Chennai, India

Abstract:

The current study couples a quasi-steady Vortex Lattice Method and a camber correcting technique, 'Decambering' for unsteady post-stall flow prediction. The wake is force-free and discrete such that the wake lattices move with the free-stream once shed from the wing. It is observed that the time-averaged unsteady coefficient of lift sees a relative drop at post-stall angles of attack in comparison to its steady counterpart for some angles of attack. Multiple solutions occur at post-stall and three different algorithms to choose solutions in these regimes show both unsteadiness and non-convergence of the iterations. The distribution of coefficient of lift on the wing span also shows sawtooth. Distribution of vorticity changes both along span and in the direction of the free-stream as the wake develops over time with distinct roll-up, which increases with time.

Keywords: Post-stall, unsteady, wing, aerodynamics.

HYDROELECTRIC POTENTIALS OF SMALL STREAMS WITHOUT FLOW MEASUREMENT STATIONS IN THE EUPHRATES AND TIGRIS BASINS: A CASE STUDY IN BATMAN BASIN

Ibrahim Yuksel*

ORCID: https://orcid.org/0000-0002-9856-8133

Istanbul Rumeli University, Faculty of Engineering and Natural Sciences, Department of Civil Engineering, Istanbul, Turkey

ABSTRACT

Hydroelectric; It is a long-lasting energy source with low operating and maintenance costs. Although the initial investment cost of hydroelectric energy is high, it is quite economical in the medium and long term since it has low production costs. Turkey has an important hydro energy potential in its river basins. A large part of this potential is in small streams. Since the existing potentials have not been determined exactly, Small Hydroelectric Power Plants (HPPs) are not sufficiently developed in the world. Flow rate is one of the most important parameters for the planning of water resources. However, since there are not Stream Gaging Station (SGS) on small rivers in Turkey, the current values of these rivers and their hydroelectric potential are not known. In this study, flow rates of eight small streams without Stream Gaging Station (ungauged streams) in the Batman sub-basin which is located in the Euphrates-Tigris Basin, were obtained by using fins and pitot tube methods and Batman sub-basin and these eight small streams are selected as study area. The hydro energy potential of the selected streams has been estimated by using the results which are calculated in this study. The end of the study, to achieve the maximum energy capacity in the selected streams some suggestions are presented.

Keywords: Water Resources, Renewable Energy, Small Hydropower Plants, Euphrates-Tigris Basin, Turkey

*Prof. Dr., Istanbul Rumeli University, Faculty of Engineering and Natural Sciences, Department of Civil Engineering, Istanbul Turkey

INTRODUCTION

In the literature, there are different methods proposed for determining the hydro energy potentials of rivers. Some of these are: Hypsometric Curves (HC) Method, Drop-Current Diagrams (DCDs) Method, Discharge-Continuity Curve (DCC) Method and Energy Tree (ET) etc.

Discharge-Continuity Curve (DCC) is a key element for Small Hydropower (SHP) planning and design. DCC is defined as a graph corresponding to the percentage of time a given flow rate is greater than or equal to that flow.

Environmental issues and climate change are the most important problems in the last decade. The source and type of energy produced in the world has a significant impact on these problems. Hydropower is the most important type of energy in minimizing these problems.

Therefore, it is necessary to turn the renewable, sustainable and clean energy sources. Hydro energy, solar energy and wind energy are the forefront of the renewable, sustainable and clean energy sources.

Hydropower and biomass have the largest share in renewable energy in Turkey [3-10]. But, the environmental issues in energy production cause the use of biomass energy to decrease gradually. In this reason, renewable energy production decline due to the decrease in biomass production in Turkey. As a result, the way of renewable energy production has changed and the market share of wind energy has increased.

On the other hand, the market share of bio-energy is gradually decreasing due to the spread of other renewable energy sources as a result of increasing air pollution and deforestation [2,6,9,10].

Depending on the social and economic development in Turkey, the demand for energy and electricity is also increasing rapidly. The main energy sources are hydropower, coal and natural ga in the country.

Oil and gas reserves, which play an important role in meeting the energy needs, are not sufficient in Turkey. In addition to a large part of these materials are imported. This situation makes the country dependent on foreign energy [11].

as in many other countries, since oil has the largest share in total energy consumption in Turkey, in the last decade the rate of use of natural gas is gradually increasing in the country.

On the other hand, wives point of geographical location, Turkey has great advantages using of renewable energy resources. Hydro energy is one of the renewable energy sources. This is followed by wind, geothermal and solar energy, respectively.

Turkey has 26 main river basins and there are a lot of rivers in these basins. Therefore, Turkey's hydropower potential is also quite high. For this reason, the use of this potential, which is a natural resource, will contribute to the solution of both employment and economic problems of the country.

For the reasons as it is mentioned in the above, in this study, the installed power and gross hydro energy potentials for the selected small streams were determined by using the flow values obtained from in a study [12].

It is well known from the literature that there are a lot of formulas to determine installed power and hydro energy potential. The installed power and hydro energy potential for the eight selected small streams were determined by using some of these formulas.

As it is known, the basis of energy calculations is the determination of the gross energy amount. The basic equation for gross energy is as follows [13].

$$E_g=m*g*H \quad (1)$$

Where:

E_g,: Gross energy measured in Joules (J) or (watts/hour),

M: Water mass (kg),

g: Gravitational acceleration (m/s^2),

H: Difference of water levels (m).

When the gross energy is calculated for any stream or basin, the hydro energy potential of these were calculated also.

Therefore, the aim of this study is to estimate the hydro energy potentials of the selected small streams by using the measured values and to bring them into the system.

As a result, this energy, which is brought to the system, will make significant contributions to the country's economy.

In order to accurately calculate the hydro energy potentials of the selected small streams; it is necessary to know both the correlation coefficients of the stations in the basin, where these small streams are located and some characteristics of the selected small streams, such the peak flow values and peak discharge period.

The calculated correlation coefficients of the stations in the basin and, the peak discharge values and peak period of the selected small streams are given in the Table 1and Table 2 respectively [12].

Table 1. The calculated correlation coefficients for the selected stations in the study area

Name of the Station	**Observation Values**	**Model Results**	**Total Period**
	Period 1985-1989 ve 2014-2017	**Period 1990-2013**	**Period 1985-2017**
	R^2	**R^2**	**R^2**
Batman-Beşiri	0.853	0.884	0.871
Batman-Kozluk	0.745	0.825	0.796
Batman-Sason	0.652	0.678	0.668

Table 2. The peak discharge values and peak period of the selected small streams

Name of The Small Stream	Peak Discharge (m^3/s)	Peak Period
Han Stream	55.3	27 Dec. 2005
Sevek Stream	2.2	4 Feb. 2005
Sevay Stream	7.0	27 Dec. 2005
Merga Stream	10.8	27 Dec. 2005
Zugut Stream	6.9	10 May 2011
Kulluk Stream	7.9	11 April 2011
Asagıyanikli Stream	8.5	4 Feb. 2005
Rapka Stream	10.3	10 May 2011

1. DATA USED FOR SELECTED STREAMS

Flow rates used in this study for selected small streams are taken from a previous study [12]. In the aforementioned study, fins and pitot tube methods were used to measure flow velocities.

Consistency, control and completion of missing data of these measured flow rates; The data of other rivers with Flow Observation Stations and whose flow rates were measured in the studied basin were made using different methods such as hydrological models, ANN, Regression and Correlation analysis. Obtained results;

In the aforementioned study, the results obtained using the fins and pitot methods were compared with the values measured at the flow observation stations. As a result, it was concluded that the values obtained in this study were usable, since the differences were seen to be very small.

In the aforementioned study, the values obtained by the fins and pitot tube methods are given in Table 3 and Table 4 respectively [12].

Table 3. Water discharges by using fins method in the selected small streams

No	Name of The Small Stream	Water Discharge (Q (m^3/s)			
		Jan.-March 2019	April-June 2019	July-Sept. 2019	Oct.-Dec. 2019
1	Han Stream	14.946	32.618	4.306	10.273
2	Sevek Stream	1.041	1.013	0.088	0.547
3	Sevay Stream	12.040	16.960	1.556	6.289
4	Merga Stream	7.760	8.964	0.841	1.470
5	Zugut Stream	3.489	2.396	0.024	1.678
6	Kulluk Stream	1.974	0.988	0.037	0.119
7	Asagıyanikli Stream	0.324	0.353	0.016	0.091
8	Rapka Stream	3.016	2.310	0.050	0.645

Table 4. Water discharges by using pitot method in the selected small streams.

No	Name of The Small Stream	Water Discharge (Q (m^3/s)			
		Jan.-March 2019	April-June 2019	July-Sept. 2019	Oct.-Dec. 2019
1	Han Stream	13.195	27.795	6.849	10.104
2	Sevek Stream	0.585	1.251	0.055	0.453
3	Sevay Stream	9.438	11.506	1.442	6.630
4	Merga Stream	6.084	11.648	3.550	4.688
5	Zugut Stream	4.019	4.761	0.601	3.313
6	Kulluk Stream	2.589	3.899	1.570	1.228
7	Asagıyanikli Stream	0.439	0.569	0.019	0.222
8	Rapka Stream	2.894	7.641	0.206	1.202

2. METHODS AND APPLICATIONS

Considering the flow rates calculated in Tables 3 and Table 4 for the selected rivers, the Flow Continuity Curve (DSE) method, which is the most widely used in the scientific world, was used in the calculation of the installed power and gross hydroelectricity for these rivers.

Flow Continuity Curve Method:

The Flow Continuity Curve (DSE) shows the percentage of time that the flow rates are exceeded for a daily, monthly or selected time period in a river basin [14-16].

DSE is a method that is frequently used in water supply, irrigation, dam planning and especially in the planning of small hydroelectric power plants [15].

When making hydropower capacity calculations by using DSE, the probabilities of exceeding the flow can be accepted as 20%-30% and 10%-20% for small hydroelectric power plants and dams respectively [17].

Since there is no water storage in small hydroelectric power plants, the selection of the project flow rate is the most important factor. Generally, flow rates that are less likely to be exceeded (between 1% and 10%) in the flow continuity curve are not taken into account in SHP planning.

Similarly, flow rates that are likely to be exceeded (between 90% and 99%) generally represent base currents and these flow rates are very important in generating firm energy in HEPPs.

On the other hand, flow rates between 10% and 90% which are likely to be exceeded, are usually considered in the design [18].

Flow continuity curve is obtained by plotting the water discharge values on the vertical axis and the percentages on the horizontal axis when the water discharges are equal to or greater than a certain value (Figure 1). From this curve, the amount of flow corresponding to a certain ratio of any time period can be read [19].

Flow continuity curve is obtained by marking the flow rate values on the vertical axis and the percentages when the flow rates are equal to or greater than a certain value on the horizontal axis (Figure 1). From this curve, the flow rate corresponding to a certain percentage of any time period can be read [19].

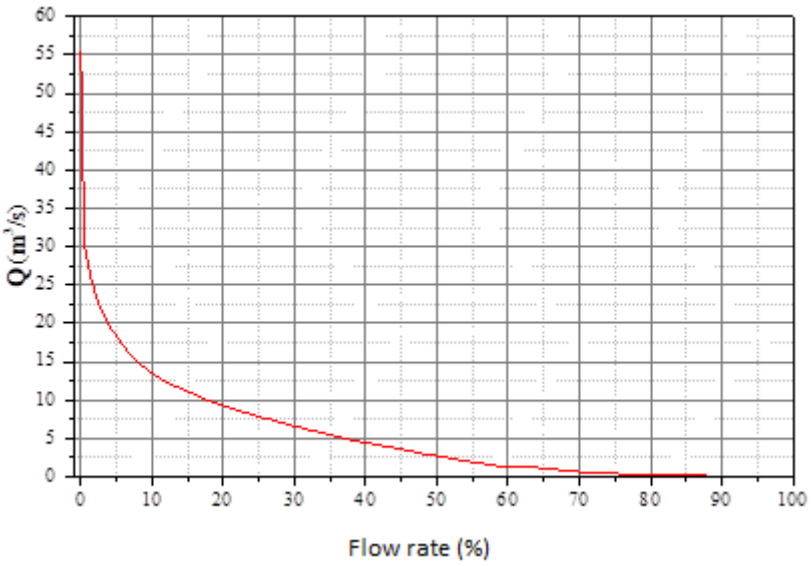

Figure 1. Flow continuity curve (FCC)

After the flow continuity curve has been established, the flow rate corresponding to a certain percentage of time on this curve is selected.

Using this flow rate in the FCC, the hydraulic capacity and water altitude of the water power are determined for the hydropower plant which is planned. Then the amount of the hydropower energy is calculated by using some equations in the energy formulae.

These equations as follows [20,21]:

$$\eta = \eta_T * \eta_J * \eta_{TR} \quad (2)$$

Here:

η_T= Efficiency (This is 0.85-0.90, 0.91-0.96 and 0.97-0.985 for turbine, generator and transformer respectively).

When the average efficiency is written down in the water power equation:

$$P_{brüt} = \gamma * Q_{ort} * H * \eta \quad (3)$$

The equation is obtained and by using it, the equation used to calculate the annual net gross potential is obtained as follows.

$$E_{brüt} = \gamma * Q_{ort} * H * \eta * 24 * 365 \quad (4)$$

Using the values calculated from these equations, the power-time percentage graph (power continuity curve) of a hydroelectric power plant (Figure 2) is obtained as follows.

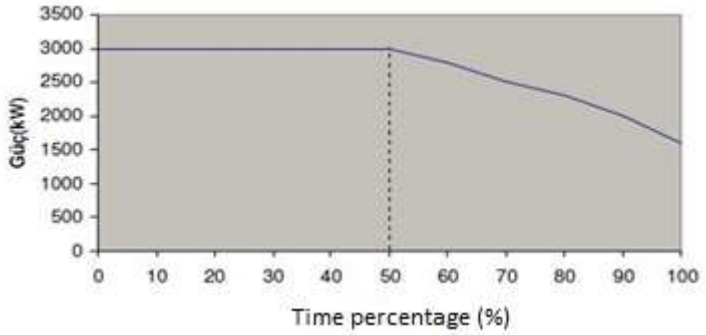

Figure 2. Power continuity curve

Since the hydraulic capacity of a hydroelectric power station is calculated based on the flow available 50% of the time:

When Figure 2 is analysed, the power value will remain constant up to 50% of the time. But after this point, the power value will gradually decrease as lower flow rates will come.

3. CALCULATING HYDROELECTRIC POTENTIAL IN THE SELECTED STREAMS

In the selected small streams, the installed power and hydroelectric potential are calculated by using in the flow-continuity curves method and the equations 2,3 and 4.

The calculated installed power and hydroelectric potential are given in the Table 5 and Table 6 for the fins and pitot methods respectively.

Table 5. Installed power and hydroelectric potential for the fins method

Name of The Small Stream	Installed Power (P), (kW)	Hydroelectric Potential (E), (MWh)
Han Stream	149121.7	1306306.8
Sevek Stream	4491	39341.3
Sevay Stream	98785.9	865365.1
Merga Stream	37305.7	326798.6
Zugut Stream	12540.8	109858.1
Kulluk Stream	3513.4	30777.4
Asagıyanikli Stream	261.4	2290.6
Rapka Stream	6832.0	59848.8
Baskoy Stream	2814.5	24655.3
Celebiyan Stream	64209.2	562472.6
Total	**379876.1**	**3327715.1**

Table 6. Installed power and hydroelectric potential for the pitot method

Name of The Small Stream	**Installed Power (P), (kW)**	Hydroelectric Potential **(E), (MWh)**
Han Stream	139047.5	1218056.5
Sevek Stream	3914.6	34291.9
Sevay Stream	77797.5	681506.7
Merga Stream	50907.3	445948.2
Zugut Stream	20989.1	183864.7
Kulluk Stream	10469.1	91710
Asagıyanikli Stream	417.2	3655.1
Rapka Stream	13554	118733.4
Baskoy Stream	4296.7	37639.1
Celebiyan Stream	81064.5	710125.1
Total	402457.8	3525530

4. CONCLUSIONS

When the energy amounts obtained as a result of the measurements made for the small rivers selected in this study are compared with the others measured before in the same basin; Although it is simple and can be applied in basins without measurement values, it gives more mediocre results than the DA method since it does not take into account the morphological changes of the basin.

On the other hand, although the amount of energy calculated by the DSE method is technically sufficient to estimate the hydroelectric potential, the efficiency of the DSE should be analysed by considering the parameters such as turbine type and decreasing of the flows.

The most important conclusion that can be found out from this study; as in the study area, the small hydroelectric energy potential in Turkey has a very high value and this potential should be evaluated to the country's economy.

To evaluate this potential the simplified method which is proposed in this study can be applied to determine the hydroelectric potential for a lot of basins in Turkey.

At the end of these determinations, a significant contribution will be made to the country's economy, employment, cultural and social activities.

REFERENCES

[1] O. Yuksek, M. I. Komurcu, I. Yuksel, ve K. Kaygusuz, "The role of hydropower in meeting Turkey ' s electric energy demand", *Energy Policy*, c. 34, ss. 3093–3103, 2006, doi: 10.1016/j.enpol.2005.06.005.

[2] MENR, "Energy report of Turkey in 2008", 2008.

[3] DPT, "Ninth development plan 2007–2013", Ankara, Türkiye, 2006.

[4] MEF, "First national communication of Turkey on climate change", Ankara, Türkiye, 2007.

[5] TEIAS, "Short history of electrical energy development in Turkey", 2009. Available at: http://www.teias.gov.tr.

[6] EIE, "Renewable energy activities of the EIE", 2009. [Çevrimiçi]. Available at: http://www.eie.gov.tr.

[7] K. Kaygusuz ve A. Kaygusuz, "Renewable energy and sustainable development in Turkey", *Renew. Energy*, c. 25, ss. 431–453, 2002.

[8] K. Kaygusuz, "Bioenergy as a clean and sustainable fuel", *Energy Sources, Part A Recover. Util. Environ. Eff.*, sayı October 2014, ss. 37–41, 2009, doi: 10.1080/15567030801909839.

[9] I. Yuksel ve K. Kaygusuz, "Renewable energy sources for clean and sustainable energy policies in Turkey", *Renew. Sustain. Energy Rev.*, c. 15, sayı 8, ss. 4132–4144, 2011, doi: 10.1016/j.rser.2011.07.007.

[10] M. S. Celiktas ve G. Kocar, "A quadratic helix approach to evaluate the Turkish renewable energies", *Energy Policy*, c. 37, sayı 11, ss. 4959–4965, 2009, doi: 10.1016/j.enpol.2009.06.061.

[11] IEA, "Energy policies of IEA countries", Paris, 2009.

[12] I.H. Demirel, "Investigation of the Most Appropriate Model for Determination of Hydro Energy Potential in Small River Basins", Thesis (Ph.D.), Yildiz Technical University, Graduate School of Natural and Applied Sciences, Istanbul, Turkey, 2021 (in Turkish). (*Advisor: Prof. Dr. Ibrahim Yuksel*)

[13] http://nser.nbed.nb.ca/sites/nser.nbed.nb.ca/files/noteattach//y2011/Dec/

[14] A. Castellarin, G. Galeati, L. Brandimarte, A. Montanari, ve A. Brath, "Regional flow-duration curves: Reliability for ungauged basins", *Adv. Water Resour.*, c. 27, sayı 10, ss. 953–965, 2004, doi: 10.1016/j.advwatres.2004.08.005.

[15] E. S. Han ve A. goleman, daniel; boyatzis, Richard; Mckee, "Flow-duration curves i: new interpretation and confidence intervals", *J. Water Resour. Plan. Manag.*, c. 120, sayı 4, ss. 485–504, 1994.

[16] J. K. SEARCY, "Flow duration curve", 1959. doi: 10.1201/b19113-16

[17] F. Heitz, L., "Hydrologic evaluation methods for hydropower studies", University of Idaho Graduate School, 1981.

[18] B. Yanık, "Regional analysis in determining the natural flow hydroelectric potential Approach", Thesis (Ph.D.), Istanbul Technical University, Institute of Science and Technology, Istanbul, Turkey, 2004 (in Turkish).

[19] M. Beyazıt, Hydrology (Book), Birsen Publishing House, Istanbul, Turkey, 2013 (in Turkish).

[20] V. Ozkok, "Hydroelectric potential determination methods and applications", Thesis (M.Sc.), Istanbul Technical University, Institute of Science and Technology, Istanbul, Turkey, 2006 (in Turkish).

[21] U. ACE, "Hydropower engineering and design", Washington, D.C., 1985.

INVESTIGATION OF HEAT AFFECTED ZONE OF STEEL P92 USING THE THERMAL CYCLE SIMULATOR

Petr Mohyla, Ivo Hlavatý, Jiří Hrubý, Lucie Krejčí
P. Mohyla is with VSB – Technical University of Ostrava, Faculty of Mechanical Engineering, Czech Republic.
I. Hlavaty, J. Hruby, and L. Krejci are with VSB – Technical University of Ostrava, Faculty of Mechanical Engineering, Czech Republic.

Abstract:
This work is focused on mechanical properties and microstructure of heat affected zone (HAZ) of steel P92. The thermal cycle simulator was used for modeling a fine grained zone of HAZ. Hardness and impact toughness were measured on simulated samples. Microstructural analysis using optical microscopy was performed on selected samples. Achieved results were compared with the values of a real welded joint. The thermal cycle simulator allows transferring the properties of very small HAZ to the sufficiently large sample where the tests of the mechanical properties can be performed. A satisfactory accordance was found when comparing the microstructure and mechanical properties of real welds and simulated samples.

Keywords: Heat affected zone, impact test, thermal cycle simulator and time of tempering.

DESIGN AND IMPLEMENTATION OF A LOW-COST LASER DIODE DRIVER FOR WIRELESS POWER TRANSMISSION

Hayri YIGIT [1], Ali Rifat BOYNUEGRI [2]

[1] Yildiz Technical University, Faculty of Electrical and Electronics Engineering, 0000-0003-3936-8649

[2] Yildiz Technical University, Faculty of Electrical and Electronics Engineering, 0000-0003-4734-3126

ABSTRACT

Laser Wireless Power Transmission (LWPT) is one of the leading technologies in long distance and high power Wireless Power Transmission (WPT). One of the most important parts of this technology is the transmitter part, which includes the laser and the driving circuit. In this study, a low cost transmitter is proposed by using pulse mode Laser Diodes (LDs). 5 LDs were operated by keeping them at 85 µs of cut-off at 15 µs of transmission, and a 100 µs operating period was obtained by leaving 5 µs of dead time between each LDs to provide cooling as they are using common cooling plate. The proposed system has been designed and experimentally verified in this paper.

Keywords: Wireless power transmission, laser diode, laser driver.

1. INTRODUCTION

The use of Unmanned Aerial Vehicles (UAVs), smart devices, robots and similar mobile devices has been significantly increased in the past years [13-14]. Especially in battery-powered UAVs, the process of charging or replacing the battery when the battery is depleted negatively affects the operating time of this type of vehicle [13] . This has enhanced the interest in Wireless Power Transmission (WPT), which enables power to be transferred without any physical and electrical connection between source and load.

WPT can be examined in four groups as magnetic resonant WPT, capacitive WPT, microwave WPT and optical (laser) WPT [1]. While the efficiency and power levels of magnetic and capacitive WPT are higher than microwave and optical WPT, power transmission cannot be made in long distances due to the weakening of the magnetic field as the distance increases with these methods [2]. In the microwave WPT, power can be transferred easily by passing through the atmosphere at long distance, but the efficiency is low due to the difficulty of focusing the microwaves on the receiving antenna [3]. It is also difficult to implement as a lot of equipment such as transmitting antenna, receiving antenna etc. must be used to direct the microwaves [4].

Laser systems can transmit light energy over long distances with relatively little loss with high intensity. With these systems, power can be transmitted to distant vehicles such as UAVs or land vehicles [5], robots [6], mobile devices [7] and satellites [8]. While the most important advantages of Laser Wireless Power Transmission (LWPT) are its ability to transmit power over long distances, its suitability for mobile applications and its ability to transmit power in the kilowatts range, the most important disadvantages are its low efficiency like microwave WPT and the difficulty in aligning the laser to the receiver [5].

The efficiency is mostly affected by the losses in the receiver and transmitter part. Studies are aimed to increase the efficiency in these parts. In the transmitter part, besides the studies on increasing the efficiency of the laser, there are also studies on the driving of the lasers. Although there are many types of lasers, Laser Diodes (LDs) come to the fore with their high efficiency in the LWPT [9]. LDs can be operated in Continuous Wave (CW) mode or pulse mode [10]. While CW lasers are generally used, there are studies examining the effect of working in pulse mode on laser performance [11].

In this paper, a new operation method is proposed because of the high cost of the CW lasers. 5 lasers operating in pulse mode were used at a certain duty cycle, respectively. The recommended system has been tested experimentally. By this way, a low cost laser system is proposed.

The paper is structured as follows: In the following section the system overview of the proposed system is explained. In section 3, experimental results are presented and the final section closes with a conclusion.

2. SYSTEM OVERVIEW

The LWPT system scheme has been presented in figure 1. The system consists of two parts, the receiver and the transmitter. In the transmitter part, electric is converted to beam via laser diode. The beam emitted from the laser is collimated with the aid of a collimator lens. In the receiver, specific PV cells convert the laser light back into electricity. Then, it is transferred to the load for purposes such as charging a battery etc.

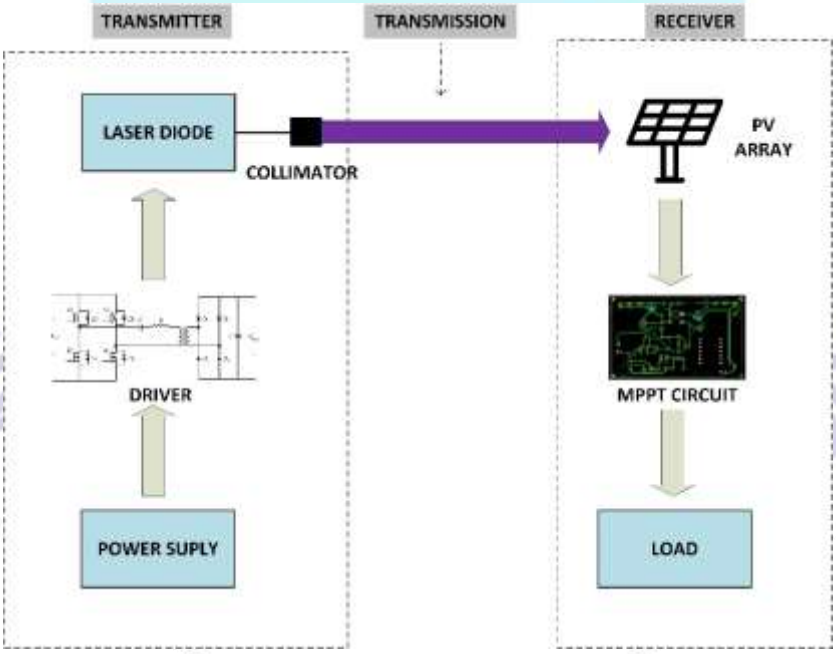

Figure 1. Schematic diagram of a LWPT system

LD is a basis part of the system. Since LDs are current driven devices, its output power depends on the current flowing through it. The relationship between the input current i and the output optical power p_o is given by the following equation [11]:

$$p_o = \eta_d(i - I_{th}) \quad (1)$$

where η_d is the differential slope efficiency and I_{th} is the threshold current of the LD. The conversion efficiency η can be characterized in the (2):

$$\eta = \frac{p_o}{p_i} = \frac{\eta_d (i - I_{th})}{v_{LD}.i} \quad (2)$$

Here, p_i is the input power and v_{LD} is the voltage across the LD's terminals. As can be seen from the equations, optical power rises linearly as the current increases above the threshold current.

In the LWPT application, LDs can be run in CW or pulse mode. As can be seen in the figure 2. , CW lasers emit light continuously at a constant power. There is no interruption in this types of laser. Unlike CW lasers, pulse mode lasers work intermittently.

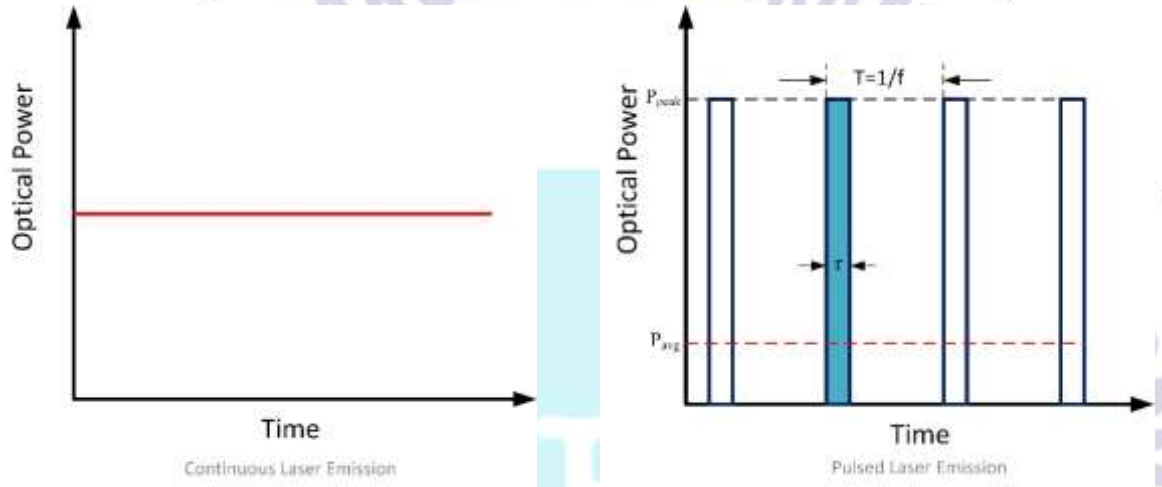

Figure 2. Modelled laser emission

While the average power is also the maximum power in CW laser emission, the average power (P_{avg}) and peak power (P_{peak}) are different from each other in pulsed laser emission. For this reason, it is necessary to compare both types of emission in terms of energy or to express the average power of the pulse laser emission. In the (3), T is the period and f is the frequency or repetition rate, the two are inverses of each other:

$$T = \frac{1}{f} \; and \; f = \frac{1}{T} \quad (3)$$

The energy (E) in a period can be expressed as the product of the peak power and the pulse width (τ) by the (4):

$$E = P_{peak} * \tau \quad (4)$$

Average power can be calculated from pulse energy by using (5):

$$P_{avg} = \frac{E}{T} = E * f \quad (5)$$

The relationship between peak power and average power can be given as in the (6):

$$P_{avg} = P_{peak} * f * \tau = \frac{P_{peak} * \tau}{T} = P_{peak} * duty\ cyle \quad (6)$$

Duty cycle is the ratio of the laser emission time to the period.

The proposed system consists of 5 LDs connected in parallel, which is shown in figure 3. MOSFETs are connected in series to each LD. LDs are activated by switching relevant MOSFET. The synchronous buck converter is connected between the power supply and the lasers to provide the necessary current and voltage for the LDs.

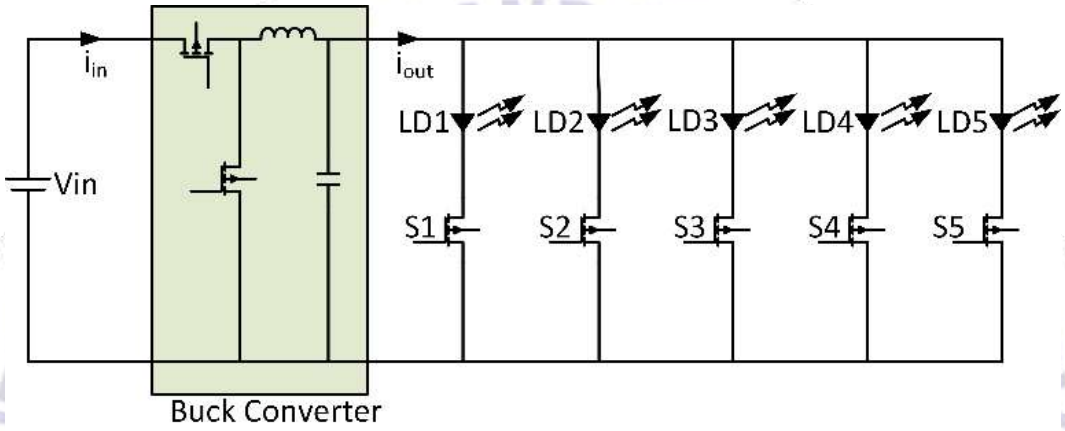

Figure 3. Main circuit

Synchronous buck converter has been used to drive the LDs. The reason for using this converter as a driving circuit is that it provides a good filter thanks to the inductance and capacitance at the output. Power losses are diminished by replacing the commutating diode in the classic buck converter with a power MOSFET [12]. This driving circuit steps down 40 V input voltage to 5.5 V. The output is set to 5.5 V for the LDs to operate in the safe zone. As a result of the tests, it has been seen that if the LDs are driven with a higher voltage, the passing over it increases and this situation causes heating and damages the LDs. In this high frequency switching circuit, 13 µH inductance and 3 parallel capacitances of 4.7 µF each are used to filter current and voltage.

Table-1: LD specifications

Wavelength	905 nm
Peak Optical Power	125 W
Nominal Operating Voltage	11 V
Maximum Forward Current	40 A
Maximum Pulse Width	100 ns
Maximum Duty Cycle	0.1%
Threshold Current	0.6 A

The parameters of LD used during experiment are shown in Table-1. According to the information given in the table, the average power of the laser was calculated as 0.44 W with the help of the above equations. It is aimed to increase the pulse width by reducing the operating current and voltage of this LD, in other words the peak power. With the help of the cooling system applied, an

effective operation was achieved by increasing the average power to 2.25 W at a LD 15% duty cycle at 10 kHz switching frequency. Therefore, the total operating period of the each LD is set to 100 µs. Every LD is ON in 15 µs and OFF in 85 µs. 15 µs dead time is left between each laser for a better cooling performance as they are all mounted in one cooling plate.

3. EXPERIMENTAL RESULTS

Experimental verification of the proposed LWPT system is explained in this section and the results are presented. At first, MOSFET driver circuit has been created and then the circuit including the connections of the lasers with the MOSFET has been made. After this circuit is coupled to the synchronous buck converter, it is connected to the power supply. Finally, in order to get a result from the output, a PV cell was placed 50 cm away from the lasers and an MPPT (Maximum Power Point Tracking) circuit was created to obtain maximum power from this cell.

In figure 4. the gate signals generated for MOSFETs are viewed. As stated in the Section 2, each LD is ON in 15 µs and a gap of 5 µs is left between the LDs. These signals are applied to the MOSFETs and the LDs are switched sequentially.

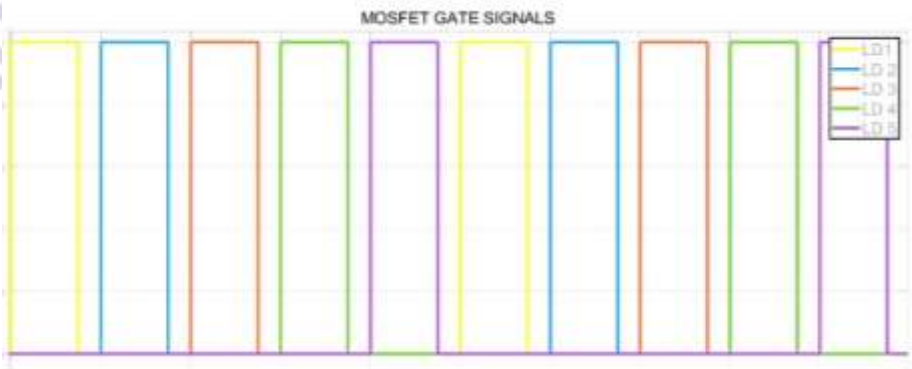

Figure 4. Gate signals of the MOSFETs

The waveform of the output voltage of the synchronous buck converter is shown in the figure 5. when 40 V is supplied from the power supply. DC bus voltage is about 5.43 V. It is seen that there is not much fluctuation except during the cutting of LDs.

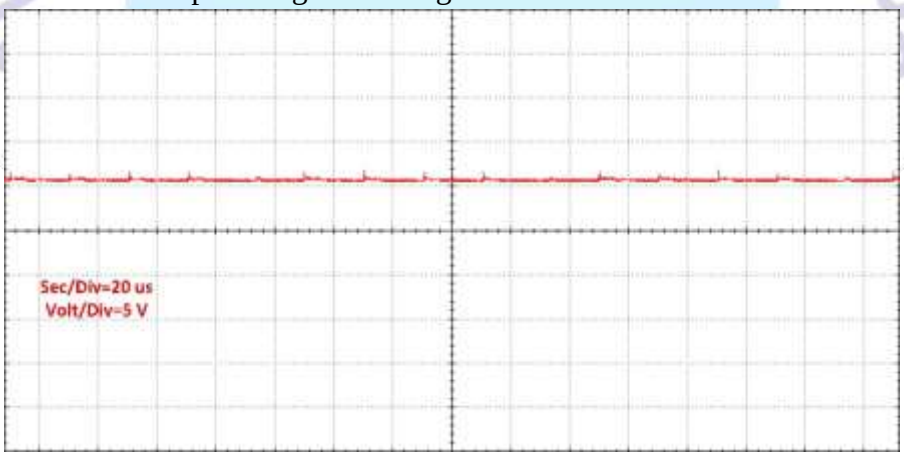

Figure 5. DC bus voltage

Figure 6. illustrates the current drawn by the LDs. It is seen that LDs draw a current of at most 3.8 A and at least 3.2 A during transmission. When the current waveform is zoomed in, it is seen that the maximum fluctuation is 80 mA, except for the spikes during the cut-off of the LDs.

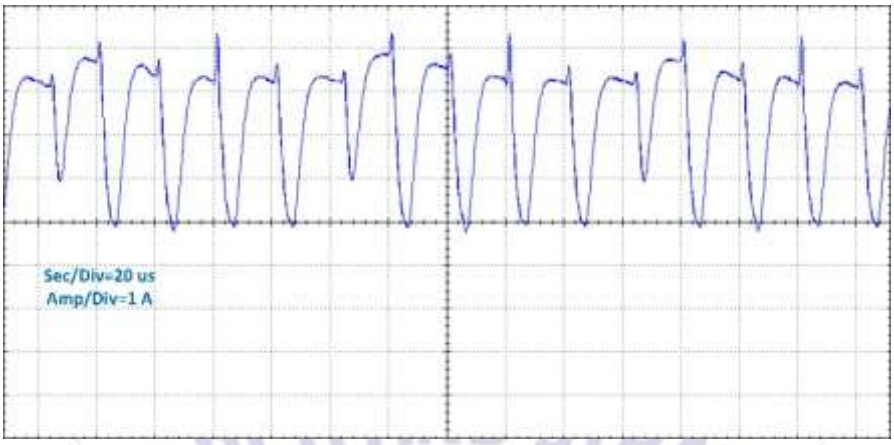

Figure 6. DC bus current

In figure.7, the current and voltage at the maximum power point (MPP) of the PV cell placed 50 cm away from the LDs are given. While the average value of the voltage at the cell output is 424 mV, the average current value is 1.6 A. Therefore, 0.678 W power is taken from the PV output.

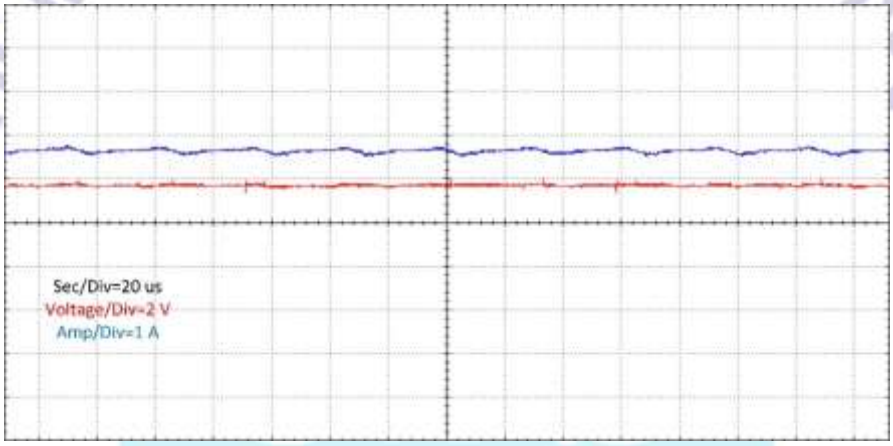

Figure 7. PV voltage and current

4. CONCLUSIONS

In this study, a low-cost design in the transmitter part is proposed for LWPT. The proposed system is verified in a laboratory environment. LWPT is achieved for 0.678 W output power successfully. The price of CW lasers with similar wavelength and power is minimum 300 USD. However, the total cost of the proposed 5 LDs system with the cost of auxiliary devices included is approximately 105.19 USD. Thus the proposed system brings a great advantage at least %65. However, pulsed LDs has a limited lifetime under operating on reverse voltage so to protect LDs an extra reverse diode is used. In future studies, the aging characteristic of the proposed system will also be investigated.

ACKNOWLEDGMENT

Scientific Research Project Coordination Unit of Yildiz Technical University supported this research study with the project number FYL-2021-4443. The authors would like to thank the Yildiz Technical University for financial support.

REFERENCES

[1] Triviño, A., González-González, J. M., & Aguado, J. A. (2021). Wireless power transfer technologies applied to electric vehicles: A review. Energies, 14(6), 1547.

[2] Rajakaruna, S., Shahnia, F., & Ghosh, A. (Eds.). (2015). Plug In Electric Vehicles in Smart Grids: Integration Techniques. Springer.

[3] Park, J. H., Kim, D. I., & Choi, K. W. (2020, November). Experiments and Modeling of 5.8 GHz Microwave Wireless Power Transfer with Multiple Antennas. In 2020 IEEE Wireless Power Transfer Conference (WPTC) (pp. 115-118). IEEE.

[4] Shidujaman, M., Samani, H., & Arif, M. (2014, May). Wireless power transmission trends. In 2014 International Conference on Informatics, Electronics & Vision (ICIEV) (pp. 1-6). IEEE.

[5] Jin, K., & Zhou, W. (2018). Wireless laser power transmission: A review of recent progress. IEEE transactions on power electronics, 34(4), 3842-3859.

[6] Kawashima, N., & Takeda, K. (2008). Laser energy transmission for a wireless energy supply to robots. Robotics and Automation in Construction, 10, 373-380.

[7] Fang, W., Deng, H., Liu, Q., Liu, M., Jiang, Q., Yang, L., & Giannakis, G. B. (2021). Safety analysis of long-range and high-power wireless power transfer using resonant beam. IEEE Transactions on Signal Processing, 69, 2833-2843.

[8] Shi, D., Zhang, L., Ma, H., Wang, Z., Wang, Y., & Cui, Z. (2016, May). Research on wireless power transmission system between satellites. In 2016 IEEE wireless power transfer conference (WPTC) (pp. 1-4). IEEE.

[9] Rathod, Y., & Hughes, L. (2019). Simulating the charging of electric vehicles by laser. Procedia Computer Science, 155, 527-534.

[10] Sharma, A., Panwar, C. B., & Arya, R. (2016, December). High power pulsed current laser diode driver. In 2016 International Conference on Electrical Power and Energy Systems (ICEPES) (pp. 120-126). IEEE.

[11] Zhou, W., & Jin, K. (2015). Efficiency evaluation of laser diode in different driving modes for wireless power transmission. IEEE Transactions on Power Electronics, 30(11), 6237-6244.

[12] Nowakowski, R., & Tang, N. (2009). Efficiency of synchronous versus nonsynchronous buck converters. Texas Instruments, 14.

[13] Boukoberine, M. N., Zhou, Z., & Benbouzid, M. (2019). A critical review on unmanned aerial vehicles power supply and energy management: Solutions, strategies, and prospects. Applied Energy, 255, 113823.

[14] Alladi, T., Chamola, V., Sahu, N., & Guizani, M. (2020). Applications of blockchain in unmanned aerial vehicles: A review. Vehicular Communications, 23, 100249.

A REVIEW ON ARTIFICIAL NEURAL NETWORKS

Dr. Öğr. Üyesi, İsmail AKGÜL[1], Dr. Öğr. Üyesi, Volkan KAYA[2]

[1] Erzincan Binali Yıldırım Univesity, 0000-0003-2689-8675

[2] Erzincan Binali Yıldırım Univesity, 0000-0001-6940-3260

ABSTRACT

The concept of artificial intelligence has become one of the important research topics with the increase in technological activities in recent years. In particular, the widespread use of computers in every field from day to day accelerates artificial intelligence work. Artificial neural networks, which emerged within the scope of artificial intelligence studies, providing support to the field of artificial intelligence inspired by the basic functions of the human brain, and a sub-field of artificial intelligence, offer many advantages to the computer system. Artificial neural networks are frequently used in solving complex problems that cannot be solved by traditional computational methods and provide superior success in many different fields.

In this study, information about the development, structure, usage areas, and classification of artificial neural networks is given. In addition, preliminary information is provided to researchers for studies to be carried out in this field.

Keywords: Artificial intelligence, artificial neural networks, artificial learning

1. INTRODUCTION

Artificial neural networks (ANN) are computer systems developed to realize skills such as generating, deriving, and developing new information by utilizing the information processing technique of the human brain [1]. The first application of ANN studies in computer systems started with the modeling of neurons. Neurons are interconnected by links that have a numerical weight. By adjusting these weights, learning takes place in the neural network [2,3].

Artificial neural networks can also be defined as a system designed to model a function that takes place in the human brain. Artificial neural networks are formed by connecting nerve cells in layers [4]. Artificial neural networks can be used to perform basic operations such as classification, clustering, data aggregation, conceptualization, and prediction.

Artificial neural networks are used in fields such as engineering, military, industrial, finance, entertainment, medicine, and health applications [5].

2. ARTIFICIAL NEURAL NETWORKS

2.1. Historical Development

Artificial neural networks are a sub-field of artificial intelligence developed to imitate human behavior in parallel with the technological developments in recent years. Artificial neural networks start with people's interest in neurobiology and their application to computer science. Studies on artificial neural networks are divided into two as before and after 1970 [1,6].

In 1943, Warren McCulloch and Walter Pitts developed the first artificial neural network model [7]. In 1949, Donald Hebb developed the Hebbian learning rule, which is the basis of many learning rules today. In 1958, Rosenblatt developed the perceptron, which is the basic unit of a single-layer artificial neural network. In 1969, it was seen that single-layer perceptrons were limited in solving problems, and in 1982, the problems were solved by developing multi-layer perceptrons. In the same years, studies on Hopfield networks were published by Hopfield. As a result of Hopfield's work, Hinton and his friends developed the Boltzmann machine in 1984 [1].

Back Propagation Algorithm was developed by David Rumelhart and James McClelland in 1986 and is used effectively in the financial field today [8].

2.2. Biological Structure

To understand artificial neural networks, it is necessary to understand how the human brain structure works [6]. Artificial neural networks are a complex network that imitates the functioning of the human brain [9]. Artificial neural networks consist of neurons with information processing capability. Figure 1 shows a biological neuron structure with dendrite, soma, axon, and synapse [10].

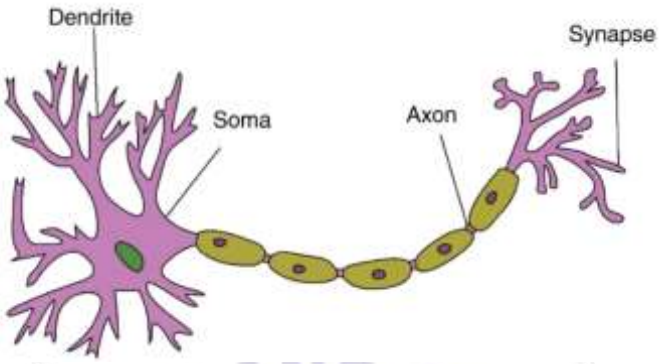

Figure 1. Biological neural network [11].

2.3. General Structure

Artificial neural networks are a structure formed by connecting artificial nerve cells, similar to the structure of biological nerve cells. Artificial neural networks are formed in layers or layers by the combination of neurons. The neurons used in this structure are in contact with each other to receive inputs and transmit outputs.

In general, the artificial neural network consists of the input layer that transmits the inputs to the next layer, the hidden layer that transmits the information from the input layer to the output layer bypassing certain processes, and the output layer that produces output to the information coming in the input layer [1]. Figure 2 shows the relationships between these three layers.

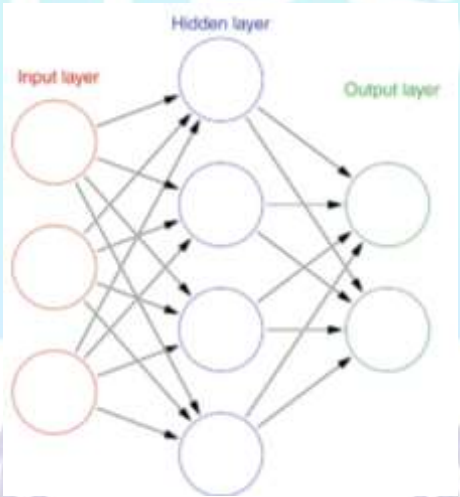

Figure 2. General structure of artificial neural network [11].

In the input layer, there are as many neurons as the number of features of the samples that need to be taught to the network. In the neural network, the hidden layer is determined according to the solution of the problem. That is, there is no specific rule for the number of hidden layers, and it changes from problem to problem. In the output layer, calculations are made that classify or label the information coming from the input layer.

2.4. Activation Functions

Activation functions in artificial neural networks are part of the neural network and are widely used [12]. The activation function is used to decide whether a neuron will be active or not. Generally, in artificial neural networks, Step, Linear, Sigmoid, Hyperbolic Tangent, Rectified Linear Unit (ReLU), Leaky ReLU, A Self-Gated - Swish, and Softmax activation functions are used. Graphs of commonly used activation functions are shown in Figure 3.

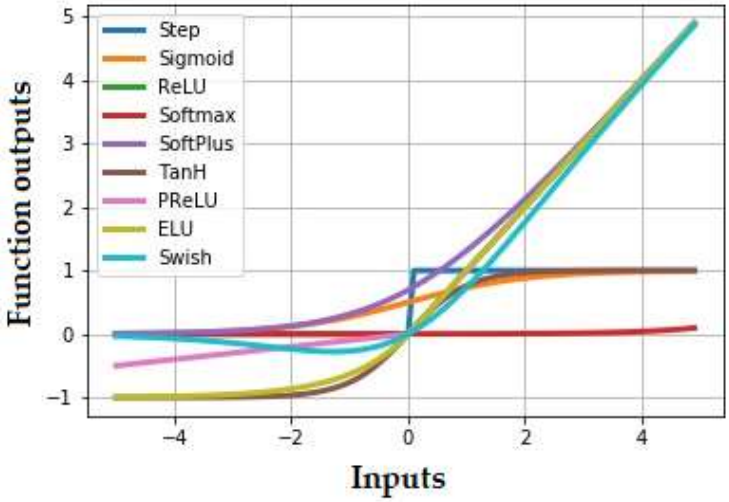

Figure 3. Activation functions [13].

2.5. Usage Areas

In recent years, artificial neural networks have gained a wide range of applications by showing superior results in real-life problems that are difficult and complex to solve [1,14]. Artificial neural networks are used in areas such as image and sound recognition, classification, association, clustering, prediction and estimation, defense, healthcare, and verification. [15,16].

Since artificial neural networks are used in applications for a specific purpose, they need special environments, special software, and special hardware to process faster. [14].

2.6. Classification of Artificial Neural Networks

Since artificial neural networks consist of interconnected neurons, they are classified according to three basic criteria [6]. The first of the classification criteria is the network connection structure used in the architecture of the artificial neural network. Networks in this structure are made in the form of feedforward, and feedback [6,17].

In feedforward neural networks, the information flow is made in one direction from the input layer to the output layer, and an output value that responds quickly to the input data is obtained. This structure is used in cases where all the information about the problem is given as

input and the output value is determined based on the input value [18]. The model of this structure is shown in Figure 4.

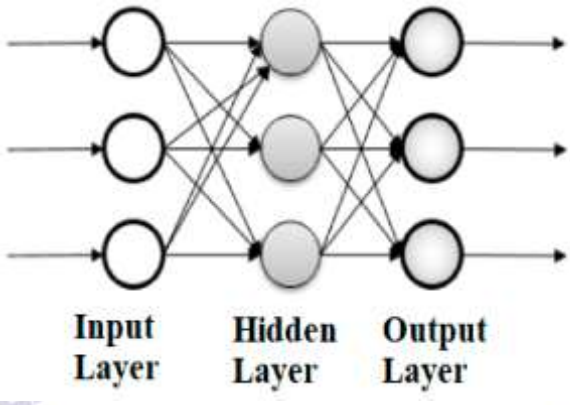

Figure 4. Feedforward network structure [19].

In Figure 4, the data coming to the input layer is transmitted to the neurons in the hidden layers without any changes and then processed here to form the network output [14].

In feedback networks, input data can be transmitted both forward and back. That is, loops are used in these networks and new data is obtained during each loop. Therefore, since the output reflects both the current inputs and the previous inputs, the training process of such networks is longer than the feedforward network. These neural networks are generally used in prediction applications [6,17]. Figure 5 shows the feedback network structure.

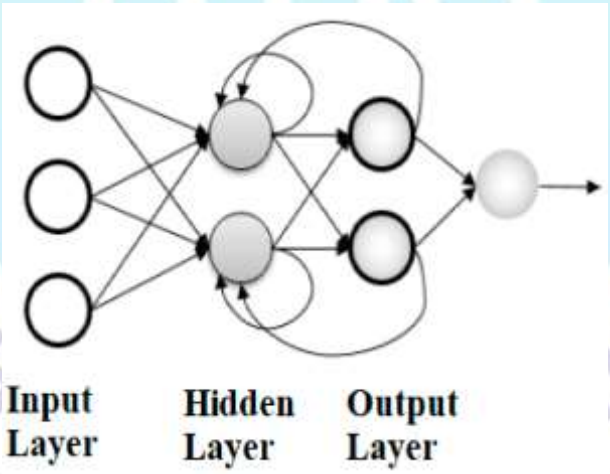

Figure 5. Feedback network structure [19].

The second classification criterion is the learning method of the network. In this network structure, three learning methods are used as supervised, unsupervised, and reinforcement [1].

Supervised learning is the process of giving the values that must be obtained at the output to the network in response to the sample data given to the input during the training of the neural network. That is, in supervised learning, a match is made between the input data given to the neural

network and the output values obtained from these data, and the relationships between the inputs and outputs of the problem are learned.

In supervised learning, it is tried to reduce the difference between the results obtained from the neural network and the targeted results. This difference is accepted as the error rate. This error rate is continuously tested until the desired accuracy value is obtained. Figure 6 shows the supervised learning structure.

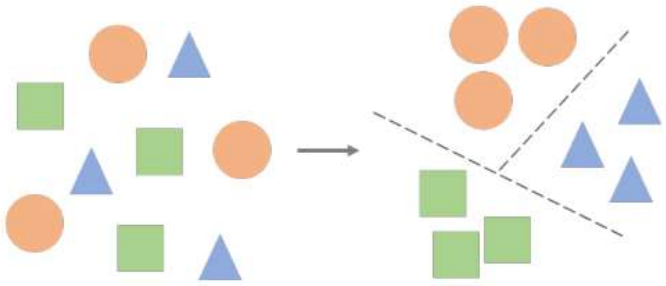

Figure 6. Supervised learning structure [20].

To solve the problem in unsupervised learning, only input examples are given to the neural network and the network is asked to learn. That is, the network learns the data samples given to the input of the network by itself and obtains the output value. For this reason, in this learning algorithm, classification is made according to certain features by using uncertain data [21]. Figure 7 shows the unsupervised learning structure.

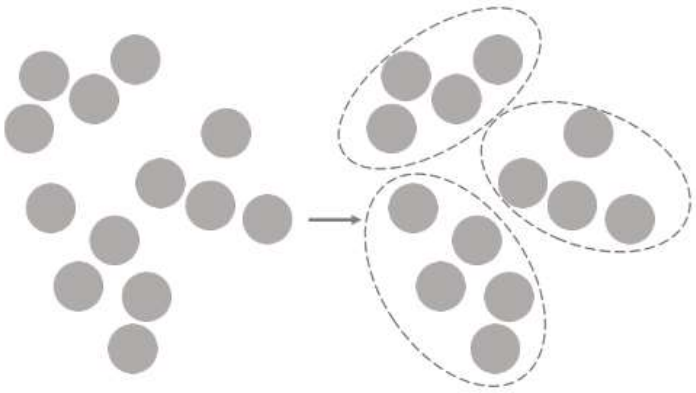

Figure 7. Unsupervised learning structure [20].

In reinforcement learning, learning is carried out using a different structure from supervised and unsupervised learning. In this learning, the output values corresponding to the input values given to the network are not directly given to the network, but learning takes place after they are evaluated according to a certain criterion. In this learning, a learning structure framework called an agent is used. In reinforcement learning, learning takes place by trial and error by using the feedback received from an agent's experiences and actions [21]. Figure 8 shows the reinforcement learning structure.

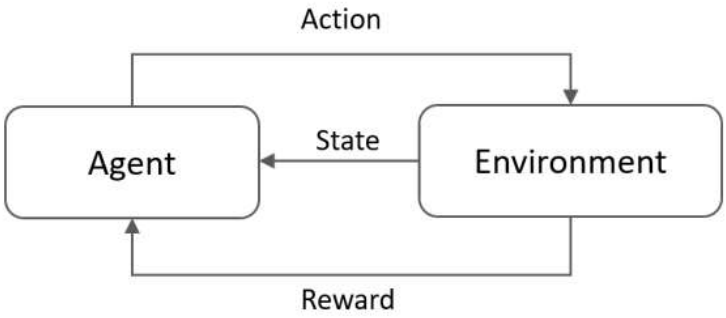

Figure 8. Reinforcement learning structure [20].

The third classification criterion is the single-layer and multi-layer classification made according to the number of layers.

Single-layer neural networks consist of one or more input and output layers. There are signals in the input layer and neurons in the output layer. The neurons in the output layer are connected to all input signals, and each connection has a separate weight value for each output neuron. Figure 9 shows the single-layer neural network structure.

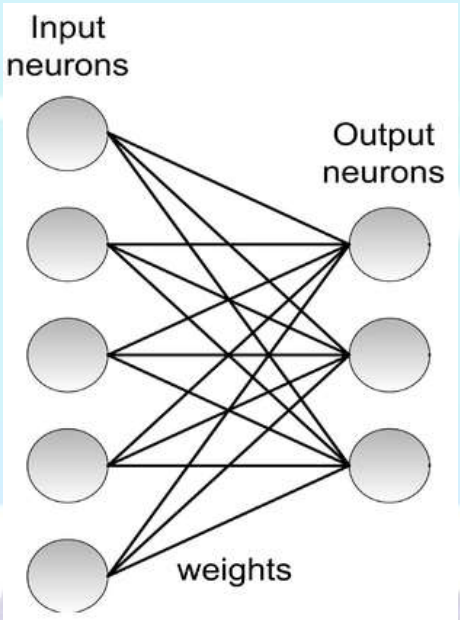

Figure 9. Single-layer neural network [22].

Multi-layered neural networks, on the other hand, are a structure consisting of more than one layer, which is formed by connecting more than one neuron. This structure includes the input layer, output layer, and hidden layer. The hidden layer in the structure of multi-layer neural networks is used both in predictions and in solving complex problems [23]. Figure 10 shows the multi-layer artificial neural network structure.

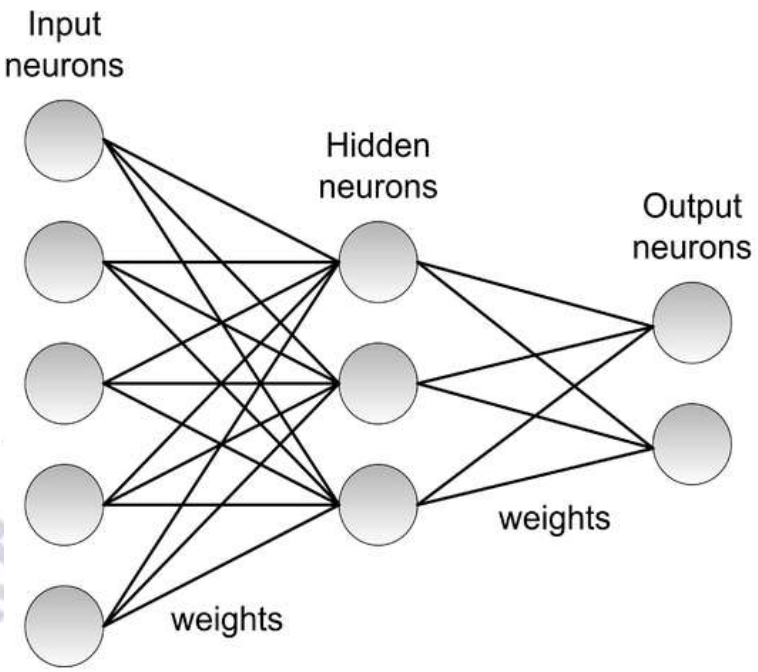

Figure 10. Multi-layer neural network [22].

In this neural network structure, there are one or more hidden layers between the input and output layers. The neurons in this hidden layer provide input to the next neurons using a nonlinear transfer function [24].

3. CONCLUSIONS

In this study, information about the historical development, biological and general structures, activation functions, usage areas, and classifications of artificial neural networks that support artificial intelligence studies are given. It has been seen in the study that artificial neural networks have gained a wide application area in solving difficult and complex problems encountered in real life.

In addition, the application of multiple hidden layer structures of artificial neural networks has led to very successful results in areas such as image and sound recognition, classification, association, clustering, prediction and estimation, defense, health services, and verification.

REFERENCES

[1] Öztemel, E., *Yapay sinir ağları,* Papatya Yayıncılık, İstanbul, 2003.

[2] Arı, A., Berberler, M.E. (2017). Yapay Sinir Ağları ile Tahmin ve Sınıflandırma Problemlerinin Çözümü İçin Ara yüz Tasarımı, *Acta Infologica, 1*(2), 55-73.

[3] Negnevitsky, M., Artificial Intelligence: A Guide to Intelligent Systems, Pearson Education, 2005.

[4] Ataseven, B. (2013). Yapay sinir ağları ile öngörü modellemesi. Öneri Dergisi, 10(39), 101-115.

[5] Uğur, A., Kınacı, A. C. (2006). Yapay zeka teknikleri ve yapay sinir ağları kullanılarak web sayfalarının sınıflandırılması. XI. Türkiye'de İnternet Konferansı (inet-tr'06), Ankara, 1(4).

[6] Özdemir, R., *Elektrodepolama Yöntemi İle Elde Edilen Znfe İnce Filmlerinin Elektriksel Özdirenç Özelliklerinin Sezgisel Yöntemler Yardımıyla İncelenmesi*, Yüksek Lisans Tezi, Fen Bilimleri Enstitüsü, Kilis, 2010.

[7] Muller, B., Reinhardt, J., and Strickland, M. T., *Neural Networks: An Introduction,* Springer-Verlag, New York, 1995.

[8] Rumelhart, D. E., McClelland, J. L., PDP Research Group, *Parallel distributed processing* New York, 1988.

[9] Walczak, S. Cerpa, N., *Artificial Neural Networks*, Encyclopedia of Physical Science and Technology (Third Edition), 631-645, 2003.

[10] Anderson, D., McNeill, G. (1992). Artificial neural networks technology. *Kaman Sciences Corporation*, *258*(6), 1-83.

[11] Zhang, Q., Yu, H., Barbiero, M., Wang, B., Gu, M. (2019). Artificial neural networks enabled by nanophotonics. *Light: Science & Applications*, *8*(1), 1-14.

[12] İnik, Ö., Ülker, E. (2017). Derin öğrenme ve görüntü analizinde kullanılan derin öğrenme modelleri, *Gaziosmanpasa Journal of Scientific Research*, *ISSN*, 85–104

[13] http://buyukveri.firat.edu.tr/2018/04/17/derin-sinir-aglari-icin-aktivasyon-fonksiyonlari/ (Erişim tarihi: 01.04.2022)

[14] Yurtoğlu, H., *Yapay Sinir Ağları Metodolojisi İle Öngörü Modellemesi: Bazı Makroekonomik Değişkenler İçin Türkiye Örneği*, Uzmanlık Tezi, 2005.

[15] Larose, D. T., Larose, C. D. *Discovering knowledge in data: an introduction to data mining*, John Wiley & Sons, 2014.

[16] Alpaydın, E., *Machine Learning,* Massachusetts Institute of Technology, USA. 2004.

[17] Nabiyev, V.V., *Yapay Zeka*, Seçkin Yayıncılık, Ankara, 2010.

[18] Zhang, G. P. (2004). Business forecasting with artificial neural networks: An overview, *Neural networks in business forecasting*, 1-22.

[19] Al-Bakri, A. Y., Sazid, M. (2021). Application of Artificial Neural Network (ANN) for Prediction and Optimization of Blast-Induced Impacts, *Mining*, *1*(3), 315-334.

[20] Sah, S. (2020). Machine Learning: A Review of Learning Types, *Preprints*, (doi: 10.20944/preprints202007.0230.v1

[21] Elmas, Ç., *Yapay Sinir Ağları*, Seçkin Yayıncılık, Ankara, 2003.

[22] Camuñas-Mesa, L. A., Linares-Barranco, B., Serrano-Gotarredona, T. (2019). Neuromorphic spiking neural networks and their memristor-CMOS hardware implementations. *Materials*, *12*(17), 2745.

[23] Zhang, G., Patuwo, B. E., Hu, M. Y. (1998). Forecasting with artificial neural networks:: The state of the art. *International journal of forecasting*, *14*(1), 35-62.

[24] Smith, K. A., 2002. Neural Networks for Business: An Introduction, *Neural Networks in Business: Techniques and Applications*, 1-24.

EVALUATION OF TECHNOLOGICAL DEVELOPMENT WITHIN THE CONTEX OF ENVIRONMENTAL SUSTAINABILITY APPROACH

Dr. Öğr. Üyesi TUBA ÖZTÜRK

Tekirdağ Namık Kemal University, ORCID ID:0000-0003-1851-6120

ABSTRACT

Always evaluated as an integral part of the life rhythm, the change progresses at such a high speed as to give rise to the deterioration of the harmony with the natural balances today. As well as bringing forward some properties such as transience, the reality of this fast change paves the way for certain approaches, which are actually not so new, to find even more meaning. Particularly in this process where technology dominates all spheres of life, other realities of life such as balance, capacity, and adaptation also confront societies overtly together with change and development. This, in turn, shows most tangibly that either economic or technological development can be achieved solely with environmental sustainability. Generally, the environmental sustainability approach is based on planning all sorts of today's activities by taking into consideration also the future generations in terms of natural resources and ecological balance. This situation was addressed at the global scale in the recent period especially owing to raw materials needed increasingly by advanced technology. This was most fundamentally due to the fact that, despite rapidly growing needs and increasing consumption levels, accessing these materials gets harder with each passing day for reasons such as the scarcity and dispersion of natural resources, production cost, failure in waste management, and administrative policies and geopolitical limits of origin countries. As a consequence of this situation, the raw materials that are of vital importance for several strategic sectors such as renewable energy, e-mobility, defense, aviation, metallurgy, and electronics are defined as critical raw materials. One of the most critical raw material groups that are evaluated under this category is the rare earth elements. It is known that the currently available critical material resources including the rare earth elements as well will fail to meet the demand that will rise along with the further sophistication and miniaturization of technology. At this point, it is a big necessity to speed up the studies about the recycling from waste, the reduction of their usage, and the development of substitutes for them by addressing the issue with sustainability approach for the future of technology.

Keywords: Critical Raw Material, Environmental Sustainability, Rare Earth Elements, Metals

1.INTRODUCTION

It is an undeniable fact that today's people depend on many products, which are the output of an industrial production process, at the point of need or habit, and the cost of this situation to nature, of which it is a part. At this point, various multidisciplinary approaches are used in order to identify, reduce and manage the problems arising from this production-consumption cycle, which is accelerating day by day. However, the solution of the problem requires a joint action that will

ensure a certain harmony and balance between the society, economy and natural environment in the global sense. Thus, the concept of sustainability is shaped by changing and developing over time as a complex and multidimensional approach. In general, the main objective of the sustainability approach, which is based on the planning of all activities of today, taking into account the needs of future generations, constitutes the understanding of intergenerational responsibility, sharing and balance in the view of the natural environment and resources [1-4]. It began to be accepted among both developed and developing countries that sustainable development can only be achieved by adopting this understanding. This approach is also supported by studies on population growth and distribution for the future, and broad perspective analyzes. According to the evaluations, it is predicted that the world population will reach 9.7 billion by 2050, and the rate of life in cities, which increased from 14% to 55% between 1900 and 2018, will reach 68%. It is known that this situation will cause the current pressure on natural resources to increase and become larger and more severe. However, it is obvious that the life models, economy, technology, dynamics, understanding and requirements of the current century changed and will continue to change all supply-demand patterns [4-6].

Sustainability of advanced technology is of great importance for sectors such as medicine, defense, metallurgy and electronics, etc. which will ensure their parallel development by supporting clean production and clean energy approach, especially in the transition to a low carbon economy all over the world. For this reason, raw materials, which are increasingly needed by modern technology, recently started to be handled on a global scale. The creation of advanced technology and the necessary infrastructure is too sensitive and a priority to not be put at risk in terms of modern society life as well as national security of countries [6-10]. However, the prerequisite for achieving technological sustainability is the achievement of sustainable resource usage all over the world. Studies on natural resource reserves reveal the fact that these resources are not infinite for everyone. However, due to the rapid usage and consumption of existing resources, there are serious concerns that there will be problems with resource insufficiency, supply-demand imbalance, development and diffusion of new technologies in the not too distant future [5,7,8,11,12]. In fact, on the basis of these concerns, there are various uncertainties and obstacles related to access to raw materials such as the rapidly increasing need and consumption, the scarcity of natural resources, as well as their dispersion, production cost and difficulty, fluctuations, unsuccessful waste management, management policies of the source countries and geopolitical limits. This situation causes countries to identify and define the raw materials that are vital for strategic sectors that produce and use high technology, and develop approach strategies related to their procurement [10,11,13,14]. Ensuring uninterrupted and stable access to this raw material class, which is mostly made up of various metals, is a must for sustainable technology and development. Strategies developed for this purpose include the rational management of natural resources all over the world, as well as the promotion and development of various alternatives, which became imperative for sustainability, such as recycling these substances from secondary sources, reducing their usage, and developing substitutes [7,8,11,12].

2. THE CONCEPT OF CRITICALITY AND CRITICAL RAW MATERIALS

Critical raw materials are generally defined as substances with a high probability of experiencing supply problems in the future, as well as their economic value and importance. The basic steps of sustainable development are to determine these substances and to make more rational evaluations about their current and future situations, to develop mining activities, and to take effective measures to reduce or completely eliminate possible risks. For this reason, countries and researchers working on this subject are developing various approaches and methodologies that will meet the concept of criticality in the most accurate and complete way. The main criticality

parameters considered in this context are roughly listed as economic importance, supply security and environmental impacts. However, the mentioned parameters allow for long-term assessments by opening and elaborating including the effects of raw materials on the national economy and security, their contribution to clean energy and clean production, their place in the advanced technology and industrial production chain, their costs, foreign dependence, reserve concentrations and their distribution according to regions, the political and economic characteristics of the source countries, environmental effects of mining activities, recycling potentials, primary and secondary supply ratios [9,12,14].

In recent years, many countries, especially European Union, USA, Canada and China, created their own critical raw material lists in line with their national development strategies, depending on their economic programs, priorities and needs. These lists are regularly updated and developed to reflect the changes that will occur over time. It is seen that the critical mineral list, which was published in the USA in 2018 and consists of 35 materials, includes 50 items in the draft version, which was updated and published in 2021 [14,15]. Similarly, the EU published its first list of substances of high importance in 2011, including the main producer countries, their substitutability, foreign dependency and recycling rates. Thus, with this list, a total of 14 items, including rare earth elements, platinum group metals and 12 more, were declared as critical raw materials for the EU. The second of the lists, which was reported to be regularly updated at least every three years, was published in 2014 with 20 critical items. In the 2014 list, it was observed that 13 of the 14 materials in the previous list, except tantalum, remained the same, and six more new substances were added. In this new list, in which tantalum was removed due to its low supply risk, rare earth elements (REE) were also included as two different substance groups as heavy rare earth elements (HREE) and light rare earth elements (LREE). In the third list, which was updated and published in 2017, 27 items were defined as critical by the EU. In the report of the commission, it was stated that nine new materials were added to the list, while chromium and magnesite were removed from the list. The fourth EU critical raw material list published in 2020 and included 30 items. In the report, it was stated that helium was removed from this last list, which was further expanded with the addition of four new substances, due to the decrease in its economic value, but it will be closely monitored [14,16-20]. In Figure 1, EU critical raw material lists are given schematically.

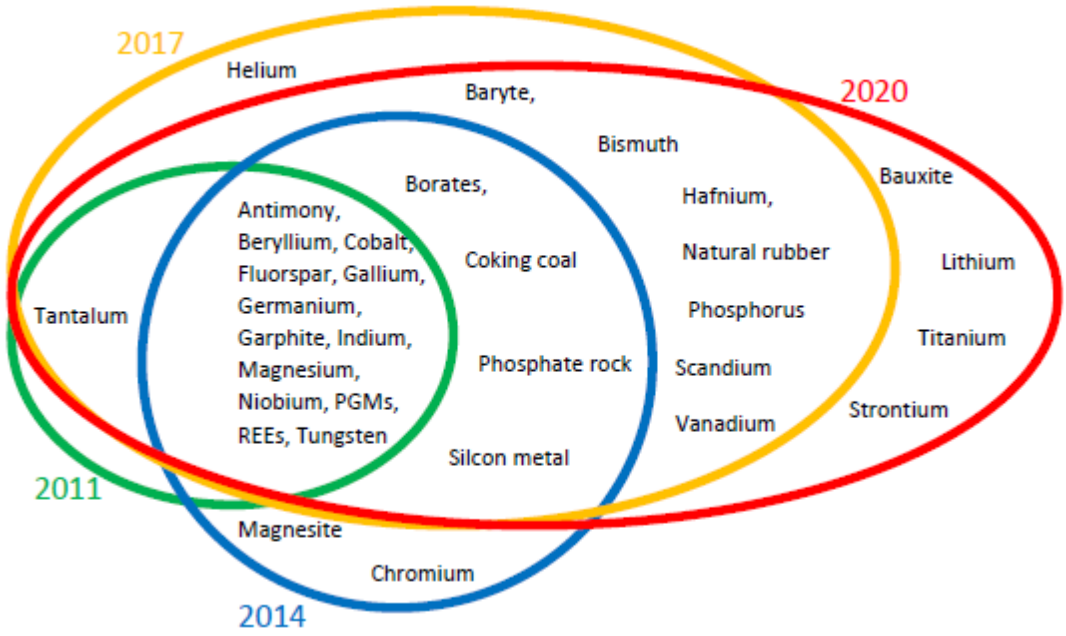

Figure 1. Critical raw materials for EU [17-20].

3.TECHNOLOGICAL DEVELOPMENT AND ENVIRONMENTAL SUSTAINABILITY

From past to present, it is known that people use metal or metal-containing materials for many activities in their daily lives. Metals, which accompanied the development of humanity since ancient times, are at the center of economic and social development, especially after industrial production. At this point, metals are indispensable materials for the sustainable supply of all kinds of goods and products that people need, and accordingly for the sustainable development of the global production economy. This situation, especially in the current century, causes a rapid increase in the demand for metal all over the world and serious concerns about the future of natural metal resources. However, it is clear that such intensive usage of metals, which are already finite natural resources, cannot be sustainable for metals that are not one of the basic components of the earth's crust. However, researchers draw attention to the fact that most of the elements in the periodic table will be used increasingly in order to meet the expectations for increasing the functionality and efficiency of the products and to reach the low carbon economy and climate policy targets. For this reason, as a prerequisite for sustainable development for most countries, it is of great importance to identify critical substances and control their sources [6,10-14,21,22]. In Figure 2, the main usage areas of critical raw materials are given.

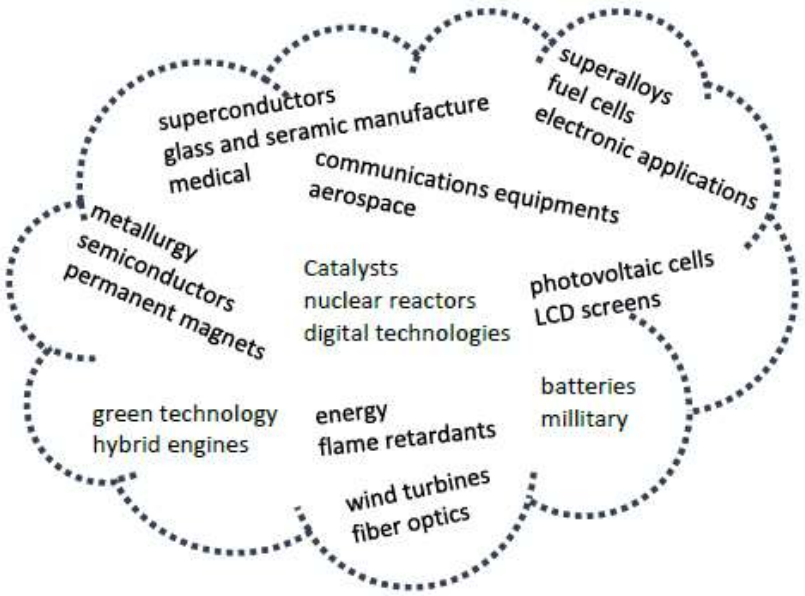

Figure 2. Usage areas of critical raw materials [7,11,20,23].

Depending on their structure, critical substances are substances that make emerging technologies such as green and advanced technology in the axis of clean energy, clean production more complex and miniaturization, and that make them preferred with their increasing properties and abilities. Rare earth elements constitute one of the most important groups among these critical items. REEs refer to the group of elements including lanthanides with atomic numbers between 57-71 and yttrium (Y) and scandium (Sc), which are chemically similar to lanthanides. REEs are mostly grouped under two sub-headings, where lanthanum (La), cerium (Ce), praseodymium (Pr), neodymium (Nd), promethium (Pm), samarium (Sm) and europium (Eu) are classified as light rare earth elements (57-63), gadolinium (Gd), terbium (Tb), dysprosium (Dy), holmium (Ho), erbium (Er), thulium (Tm), ytterbium (Yb), lutetium (Lu) and yttrium (Y) as heavy rare earth elements (64-71,Y). However, in some geochemistry sources, elements between Nd-Tb are evaluated under a separate heading as medium REEs. Rare earth elements, a very important geochemically consistent element group for various geological studies, are a strategic raw material whose commercial value is increasing day by day. REEs are generally found in different amounts and dispersed in geological environments [7,8,21-23]. In the research conducted by the USA in 2020, it was stated that the REE reserves in the whole world are 120 million tons and are concentrated in Brazil, Vietnam, Russia and India, especially in China [22]. However, it is stated that other countries other than China are mainly the source of light REE, and more than 70% of the total medium and heavy REEs in the world are located in China. Today, REEs are defined as key components with a wide range of usages due to their electronic, optical and magnetic properties [7,8,11,23]. Another group of substances among the critical raw materials is platinum group metals (PGMs). PGMs refer to an element group consisting of six transition metals: ruthenium (Ru), platinum (Pt), palladium (Pd), rhodium (Rh), osmium (Os) and iridium (Ir). Metals in this group are considered as precious metals with similar physical and chemical properties and which can replace each other. It is stated that the use of PGMs in products, along with gold and silver, began to decrease in recent years, but their supply is still at serious risk [11,14]. It seems that the properties that allow the critical identification of materials, together with these metal groups, are in fact properties related many metal. At the point of supply of metals, whether developed or developing, many countries meet their needs through imports to a large extent. The United States is heavily dependent on imports for 31 metals, which are among the raw materials that it defines as critical [10]. The main source for metal elements is natural metal sources, which we call primary

sources. However, at the point we arrived at, it is seen that primary sources alone cannot be sufficient and that they are supported by secondary sources is a great necessity. In general, all kinds of metal-containing waste and out of use forms of products released during mining activities and an industrial production process are considered as secondary sources [6,9,22]. The efficient recycling of critical metals from secondary sources is of great importance for the protection of natural resources, reducing the environmental impact of mining activities and successful waste management. This also means that technological development and environmental sustainability, of which green technology is a part, are linked to complement each other and can only be achieved together.

4. CONCLUSION

Technology and industrial production, which shape the needs, expectations and goals of modern society life, are limited by the ecological balance and natural resources at the point of the current production-consumption relationship, technology and its continuity. Today, it is clearly demonstrated by the researches that technological and economic development can be achieved depending on the creation of a certain harmony and balance between the society, economy and natural environment in the global sense. This situation requires the development of an environmentalist perspective on natural resources, raw materials, energy and waste management on a global scale. Recently, this point of view gained even more importance due to the raw materials needed by modern technology in increasing numbers and amounts and the potential problems related to access to them. Global sustainable resource usage, which became a prerequisite for technological sustainability, includes the rational usage of primary resources as well as the use of secondary resources in the most efficient way that will minimize the loss of raw materials.

5. REFERENCES

[1] Lapkin, A., *Sustainability Performance Indicators,* Renewables-Based Technology:Sustainability Assessment, J. Dewulf, H. Van Langenhove, Ed. John Wiley&Sons, 2006.

[2] Apetrei, C.I., Caniglia, G., Von Wehrden, H., Lang, D.J., Just Another Buzzword? A Systematic Literature Review of Knowledge-Related Concepts in Sustainability Science, Glob. Environ. Change, 68, 102222, 2021.

[3] Gunnarsdottir, I., Davidsdottir, B., Worrell, E., Sigurgeirsdottir, S., Sustainable Energy Development:History of the Concept and Emerging Themes, Renew. Sust. Energ. Rev., 141, 110770, 2021.

[4] Superti, V., Merino-Saum, A., Baur, I., Binder, C.R., Unraveling How the Concept of Circularity Relates to Sustainability: An Indicator-Based Meta-Analysis Applied at the Urban Scale, J. Clean. Prod., 315, 128070, 2021.

[5] Graedel, T.E., Reck, B.K., Six Years of Criticality Assessments What Have We Learned So Far?, Forum, 20, 4, pp. 692-699, 2015.

[6] Van Der Ent, A., Parbhakar-Fox, A., Erskine, P.D., Treasure from Trash: Mining Critical Metals from Waste and Unconventional Sources, Sci. Total Environ., 758, 143673, 2021.

[7] Atwood, D.A., *Sustainability of Rare Earth Resources*, The Rare Earth Elements: Fundamentals and Applications, D. A. Atwood, Ed. Wiley, 2012.

[8] McLennan, S.M., Taylor, S.R., *Geology, Geochemistry, and Natural Abundances of the Rare Earth Elements*, The Rare Earth Elements: Fundamentals and Applications, D. A. Atwood, Ed. Wiley, 2012.

[9] Vollprecht, D., Krois, L.M., Sedlazeck, K.P., Müller, P., Mischitz, R., Olbrich, T., Pomberger, R., Removal of Critical Metals from Waste Water by Zero-Valent Iron, J. Clean. Prod., 208, 1409-1420, 2019.

[10] Panda, S., Akcil, A., Securing Supplies of Technology Critical Metals: Resource Recycling and Waste Management Waste Manag., 123, 48-51, 2021.

[11] Zhang, S., Ding, Y., Liu, B., Chang, C-C., Supply and Demand of Some Critical Metals and Present Status of Their Recycling in WEEE**,** Waste Manag., 65, 113-127, 2017.

[12] Watari, T., Nansai, K., Nakajima, K., Review of Critical Metal Dynamics to 2050 for 48 Elements, Resour Conserv Recycl., 155, 104669, 2020.

[13] Morf, L.S., Gloor, R., Haag, O., Haupt, M., Skutan, S., Di Lorenzo, F., Böni, D., Precious Metals and Rare Earth Elements in Municipal Solid Waste–Sources and Fate in a Swiss Incineration Plant**,** Waste Manag., 33, 634-644, 2013.

[14] Yan, W., Wang, Z., Cao, H., Zhang, Y., Sun, Z., Criticality Assessment of Metal Resources in China, iScience, 24, 102524, 2021.

[15] U.S. Geological Survey, "021 Draft List of Critical Minerals, USGS, Department of the Interior, Federal Register, 86, 214, 2021.

[16] Klimpel, F., Bau, M., Graupner, T., Potential of Garnet Sand as An Unconventional Resource of the Critical High-Technology Metals Scandium and Rare Earth Elements, Sci. Rep., 11, 5306, 2021.

[17] European Commission, Tacklıng The Challenges in Commodity Markets and on Raw Materıals/on the 2011 List of Critical Raw Materials for the EU", EU Commission Report-Final/25, Brussels, 2011.

[18] European Commission, On the Review of the List of Critical Raw Materials for the EU and the IImplementation of the Raw Materials Initiative/on the 2014 List of Critical Raw Materials for the EU, EU Commission Report-Final/171, Brussels, 2014.

[19] European Commission, on the 2017 List of Critical Raw Materials for the EU, EU Commission Report-Final/490, Brussels, 2017.

[20] European Commission, Critical Raw Materials Resilience: Charting a Path Towards Greater Security and Sustainability/on the 2020 List of Critical Raw Materials for the EU, EU Commission Report-Final/474, Brussels, 2020.

[21] Tepe, N., Romero, M., Bau, M., High-Technology Metals as Emerging Contaminants: Strong Increase of Anthropogenic Gadolinium Levels in Tap Water of Berlin, Germany, from 2009 to 2012, App. Geochemistry, 45, 191-197, 2014.

[22] Liu, T., Chen, J., Extraction and Separation of Heavy Rare Earth Elements: A Review, Sep. Purif. Technol., 276, 119263, 2021.

[23] Rim, K-T., *Trends in Occupational Toxicology of Rare Earth Elements,* Rare Earth Elements in Human and Environmental Health: At the Crossroads Between Toxiciy and Safety, G. Pagano, Ed. Pan Stanford Publishing, 2017.

BLOK ZİNCİR UYGULAMALARI İLE KAPALI DÖNGÜ TEDARİK ZİNCİRİNDE BİLGİ YÖNETİMİNİN DEĞERİ

Arş. Gör., Belkız TORĞUL[1], Prof. Dr., Turan PAKSOY [2]

[1] Konya Teknik Üniversitesi, 0000-0002-7341-9334

[2] Necmettin Erbakan Üniversitesi, 0000-0001-8051-8560

ÖZET

Günümüzde hızla gelişen bilişim teknolojileri birçok alanda olduğu gibi tedarik zincirlerinde de doğru, yeterli ve güvenli bilgi paylaşımını sağlayarak çok daha verimli yapılar elde etme beklentilerini artırmaktadır. İzlenebilirlik, tedarik zinciri yönetiminde, özellikle gıda, ilaç vb. gibi güvenliğe duyarlı sektörlerde kritik bir unsurdur. Blok zincir teknolojisi, izlenebilirlik, şeffaflık ve güvenlik sağlayan merkezi olmayan bir kayıt platformudur ve geleneksel tedarik zinciri yönetimi sorunlarını hafifletme konusunda umut vaat etmektedir. Blok zincir teknolojisi dikkat çekerken, tedarik zincirine entegrasyonuna odaklanan çok az uygulama çalışması bulunmaktadır. Bu çalışma, etkili ve verimli tedarik zinciri yönetimi için ileri ve tersine akış faaliyetleri koordinasyonunda blok zincir teknolojisinin uygulama olanaklarını ve açıklayıcı senaryolar aracılığıyla uygun modeller geliştirerek elde edilen kazanımları göstermektedir. Blok zincir teknolojisi ile tedarik zincirine güvenilir, sürdürülebilir ve daha az maliyetli bir yapı kazandırılabileceği düşünülmektedir. Bu kapsamda öncelikle geleneksel bir kapalı döngü tedarik zinciri ağı tasarlanmış ve modellenmiştir. Ardından mevcut durumun yanında blok zincir teknolojisinin mevcut modele kısmi, tam, ileri ve tersine akışta uygulaması olmak üzere farklı durumlar için dört senaryo daha oluşturularak ana model geliştirilmiş ve uygulama sonuçları analiz edilmiştir. Senaryo analizi sonucu elde edilen sonuçlar, blok zinciri teknolojisinin tedarik zinciri maliyetlerini önemli ölçüde düşürme yeteneğinin olduğunu göstermektedir. Bu doğrultuda, böylesine önemli bir teknolojiyi uygulayacak firmaların kârlarını arttırma konusunda büyük bir avantaj elde edeceği beklenmektedir. Bu çalışma, blok zincirin tedarik zincirine entegre edilebilirliğini, blok zincir teknolojisi uygulamalarının mevcut tedarik zincirinde ne tür kazanımlar sağladığını ve bunun maliyetleri nasıl etkilediğini göstermektedir. Bu makalenin amacı, blok zincir

[1] Sorumlu Yazar

teknolojisinin tedarik zinciri yönetimi üzerindeki etki düzeyini ortaya koyarak ilgili literatüre katkıda bulunmaktır.

Anahtar Kelimeler: Blok zincir teknolojisi, Kapalı döngü tedarik zinciri optimizasyonu, Bilgi Yönetimi, Karma tamsayılı doğrusal programlama, Geri dönen ürün yönetimi.

DNS BASED SCANNING APPROACH FOR TRICKBOT BANKING TROJAN DETECTION

UMUT BABAYİĞİT [1], Assoc. Prof. ALİ GEZER [2]

[1]KAYSERİ University, 0000-0002-6053-6961

[2] KAYSERİ University, 0000-0001-8265-1736

ABSTRACT

Trickbot banking malware, one of the most dangerous types of botnet family, constantly changes its attack behavior by updating itself. Developing a defense mechanism according to this changing attack behavior is extremely important for the banking sector. At the same time, the security problem, which is the biggest problem in IoT devices, offers an attractive environment for the botnet family. Signature-based approaches do not always detect malware when they do not receive the necessary updates. That's why DNS-based approaches or both should be used. On the other hand, when the security layers are increased, the system should be configured to operate optimally, since the speed parameter of the system will decrease. In this study, it is aimed to reveal the behavior of Trickbot malware updated with a DNS-based approach and to increase the cyber resilience of the network within the framework of this instant data.

Keywords: Trickbot, DNS-based scanning, Signature-based approach, Cyber resilience

1. INTRODUCTION

The rapid development of communication technologies has made people's lives much easier, and at the same time, the easy communication of devices with each other has been a revolutionary change that paves the way for people to do their work remotely. As a result of this situation, not only do people communicate but also objects communicate among themselves and devices can access the Internet [9].

Developments in the field of communication have also affected computer and information technologies, causing the emergence of new fields while these positive developments have also brought negative situations. Internet of Things (IoT), smart cities, etc. systems such as these can adversely affect communication channels; It has created problems such as too many devices sending data in the cloud environment (BIG DATA) and insufficient bandwidth. The bandwidth

problem has been solved with the help of 5G technology and fiber optic cables. However, increasing object internet traffic seems to be among the communication problems of the future.

On the other hand, these developments also created an important security problem. Information security consists of three main laws, these are; Confidentiality, Integrity, and Accessibility, the negative situation brought by this developing technology has created danger in the Confidentiality law [10].

We use Internet and network technologies (WAN and LAN) in our daily life, as well as in advanced factories and workplaces. With the concept of Industry 4.0, the use of the internet and network technologies for automation systems and robots in the factory environment has included these technologies in the internet environment. These technologies, which are included in the internet environment, offered the opportunity to be easily controlled remotely. However, devices that are included on the internet have become vulnerable to cyber attacks. If cyber resilience is not increased and these devices are used in the default mode, an attack may become inevitable for them. In this case, it shows us that cyber security has become the most important structure of our lives in this digital world.

After the developments experienced, the rapid increase in the use of the Internet of Things (IoT) makes itself felt in every aspect of our lives; such as smart homes, agriculture, transportation, health, industry, and environmental control. According to the statistics report, it is predicted that there will be 75.44 billion IoT devices by 2025. This exponential growth brings with it several challenges; security, communication, data processing, integration, interoperability, and privacy [1].

Security is one of the biggest challenges because most devices are manufactured with a minimal cost approach which causes devices to have poor security considerations. Although almost most of the devices have detected the security vulnerability, they do not get enough support from their manufacturers on time. In addition, due to the IoT development stage and its limited structure, advanced security solution methods are not available. Because users of IoT devices usually use the device in its default option, as it does not change the default security settings. There is a situation that can easily be hunted by a malicious person. Due to such vulnerabilities, IoT devices are vulnerable and open the door for attackers to use them for their nefarious activities [2].

Another reason why IoT botnet attacks have become more dangerous today is that they are published on the internet as open-source code. This problem causes botnets to become more

dangerous. The abundance of botnets that are effective in the IoT, the botnet organization working in coordination with each other, and the effective attack began to take place. If this case is presented the investigation as a report; Before the release of the Mirai source code, its victims were approximately 213,000. Shortly after the code was released, many new Mirai variants began appearing, with the number of Mirai bots increasing to approximately 493,000 [3]. With a little change in the existing codes, botnet developers can easily bypass the security levels [4].

One of the victims most affected by this negative situation is undoubtedly the banking sector. All banks want to serve their customers in the easiest, fastest, and most reliable way. To solve the security problem, cyber security experts are employed in the institutions of the banks, the experts need to analyze the malware to close the security gaps, and defense methods are developed according to the behavior of this malicious software. In this study, a detailed dynamic analysis of Trickbot malware was made and contributed to the literature. The aggressive behavior of the Trickbot banking virus in the network and the file download methods were analyzed in detail by the open-source tools we used, and its behavior was examined.

Besides, botnets that have infected devices create bot traffic by sending many packets to infect other devices on the network, thus both infecting other devices in the network and creating bot traffic, reducing the communication speed of other users who want to communicate on the network, or making them unable to communicate at all. Malware that takes advantage of these vulnerabilities can target end-users and steal their data, important files, or money.

3. CYBER RESILIENCE

The ability to restore a system after cyberattacks are important for systems with different structures. Cyberattacks against critical infrastructure, including water resources, energy and communication networks, and healthcare facilities, have enormous consequences [6]. Health institutions, which were exposed to attacks such as ransomware attacks, have reduced their important work to manual data processing methods instead of doing it digitally [7]. Such attacks can harm the economic well-being of an organization and a large part of society, and even endanger people's lives. For example, the notorious Trickbot and another ransomware attacking botnet demonstrated fast and effective recovery even after authoritative malware-fighting organizations attempted to remove them [8]. When adverse events occur against the system and the system is affected by it; The functionality of the system begins to deteriorate, after which the system engages in various mechanisms and processes (which may or may not include human actions), recovering from adverse effects, and

then restoring the functionality of the system shown in Figure 1. The cyber security structure tries to strengthen the system to prevent such attacks and disruption of the structure of the system [5].

The cyber resilience system focuses on recovery. Recovery may be full or partial, depending on the damage done by the attack, and in some cases may include adaptations to increase functionality or resilience to future adverse events. Failure of a system, cyber resilience before the adverse event, system design, controls, preparation, foresight, training, etc.

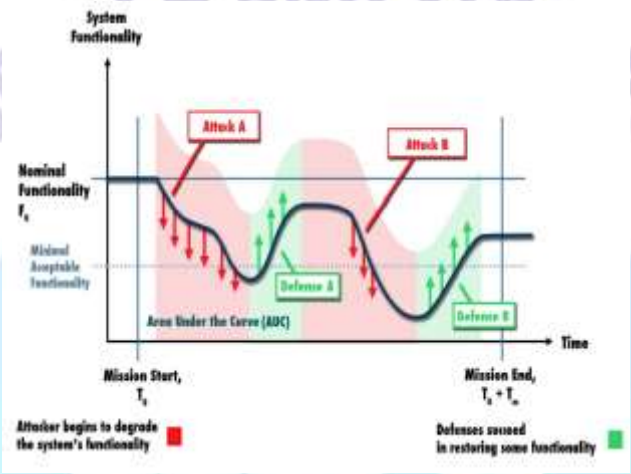

Figure 1. Stages of cyber resilience [5].

depends on its directions. However, the final assessment of cyber resilience begins with the recognition of the inevitability of adverse events: when the system is affected, the functionality deteriorates, then the focus of the system is the rate of recovery. Starting from Figure 1, a more robust system will exhibit a larger Area Under the Curve (AUC) - the integral of the protected system functionality F(t) over the total duty time Tm. If so, we can define the amount of elasticity [5].

$$R = (AUC)/(F(0)*T_m) \quad (1)$$

It is emphasized that it is extremely important to defend quickly in the event of a cyber-attack and to keep the system working between "Nominal Functionality (F(0))" and "Minimal Acceptable Functionality". Unless this defense can fully realize, it is obvious that the system will not be able to serve. Cyber defense is extremely important for the system.

4. RELATED WORKS

Another study found that actively monitoring the banking Trojan threat landscape, helps defenders learn more as threats evolve. Changes have been noticed in the distribution of the Trickbot Trojan. At that time, the observed change only applied to infection attempts on Windows 10 64-bit operating systems (OSs). In these cases, Trickbot ran the malware but did not save its typical modules and configurations to disk. Trickbot is the best-known malware and bot variant that performs attacks in an organized manner. This software appeared in August 2016 and has entered the testing period whether it is self-development or not. It is a modern, sophisticated and modular Trojan, thanks to its structure similar to the behavior of the Dyre Trojan. The infected operating system is prone to active account theft or infecting other computers within the network. For the malware to do these operations, the executable file tries to pull extra modules from the command and control (C&C) server to give its operators better control and access to the infected device. Trickbot's modules contain malicious functions that it uses to trick users into revealing their online banking credentials, and information that allows them to leak and retrieve information. Over the years, its developers have made frequent improvements in a quest to keep it private, difficult to investigate and bypass basic security checks on user devices, so TrickBot has continually evolved. Although the structure of Trickbot has been constantly changing since then, one of the latest improvements to TrickBot's code is designed to help it stay more private on devices running Windows 10 [11].

4.1. Mirai-Botnet Behavior

Mirai is one of the malware with the highest rate of infected IoT devices. Bots can launch attacks on some smart production technologies, especially IoT such as shown in Figure 2 Typical IoT devices combine a relatively low-power processor with wireless networking capabilities. The wireless network is not a very secure communication area because it works like a hub. Therefore, it can be directly attacked by people within the radio range. When the firewall is used, the cyber-attack can be prevented. Furthermore, the rules created in the firewall prevent unauthorized access. However, since giving traffic to each IoT device through the firewall will create both cost and speed problems, a more optimal solution must

be found. Instead, each device should be responsible for its security. In this case, it is a difficult task due to the reduced capabilities of IoT devices [12].

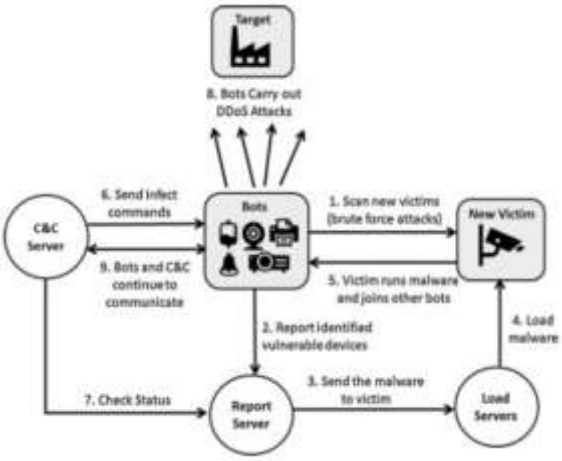

Figure 2. Mirai botnet operations [12].

4.2. Botnet Life-cycle

Botnets carry out group zombie attacks on infected computers, causing serious damage to online banks, e-commerce websites, and industries. Such attacks become more effective with the unconscious use of computers by users, causing people to be unable to transact on the internet. Therefore, behavioral analysis is extremely important. One of the serious cybercriminals is botnets, called software robots or bots, which operate automatically and systematically. Zombie computers are controlled remotely by attackers. Thus, attackers can carry out mass attacks on a vulnerable target without revealing their identity shown in Figure 3 [13].

Terrorist acts taking place today, the war between states has now created another battlefield, this area is also called cyber warfare. Pirate hacker groups, including states, carry out cyber attacks on the audience, institutions, or states they define as the target, obtaining data about them or damaging them. They can perform these actions with their tools or bots. They can easily access their codes on the internet, revise them according to their interests and attack again. It is extremely important for the life cycle of the bot not to be caught by security and protection programs during the attack. Consequently, malware analysis and cyber defense, which is a new field, have become increasingly important in today's digital world.

Consequently, malware analysis and cyber defense, which is a new field, have become increasingly important in today's digital world.

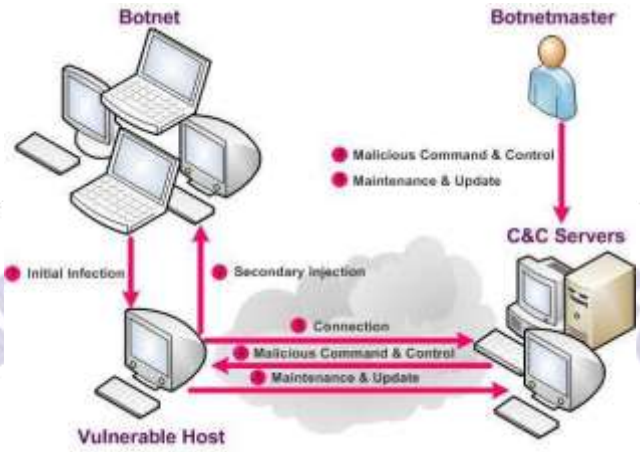

Figure 3. A typical Botnet Life-cycle [14].

5. TRICKBOT

Trickbot is one of the most dangerous banking viruses of the botnet family, created by malicious people who have developed themselves in the software field and trying to steal money and data from people's bank accounts. When a search is made on the internet, different names may appear. These; TheTrick, Trickster, and TrickLoader. The Dyre trojan displays the same behavior after infecting the computer, too. This indicates that the code structures may be the same. Due to what is written in the Trickbot binary, it can download the modules it needs from the control and command (C&C) servers to launch attacks on targeted banks and infect other computers on the local network. Using these modules, Trickbot can trick people by redirecting them to infected websites and stealing the private data of the person on the infected computer. When the malware connects live to the interface of the bank's original web page, the computer user, redirects to a decoy page, which is a web page where malicious code is injected by the attacker to steal the victim's money. Displays the correct URL of the bank in the address bar with the bank's original SSL certificate. Also, this Bot adds itself as a task in Windows Task Scheduler and unless it is deleted or stopped; It is automatically restarted by the Trickbot Task Scheduler Engine. Trickbot is not limited to only these features, but also that it can infect other computers and devices via e-mail. As well, it can also infect computers using fake Adobe Flash Player updates. In 2017, it updated itself by adding a component to its structure to inject itself into other computers, and it became more dangerous. Another behavior of Trickbot in the operating system it is running is to turn off the antivirus program belonging to that operating system, thus increasing its privacy. therefore, as Trickbot is developed, it becomes

more difficult to detect. Although antivirus programs have updated themselves and gained new features, Trickbot developers have bypassed security measures by injecting different attack methods or code structures into this bot, and they continue their attacks by developing a new attack strategy [15].

The Federal Bureau of Investigation, the Cybersecurity, and Infrastructure Security Agency tweeted an important warning of a ransomware attack on its healthcare providers. The agency said that malicious hackers used Ryuk ransomware, the malicious software used to encrypt and lock information, and the infected computer Trickbot to steal information, disrupt healthcare services, and steal money from healthcare facilities [16].

From these studies, it is clear that the Trickbot malware is not only collaborating with its own family of Trickbots but also with other malware. shows that it has improved over time by properly updating its code structure.

Trickbot is a banking trojan used in cyberattacks targeting businesses and individuals in the UK and overseas. These botnet attacks are used to obtain unauthorized personal data, access online bank accounts, and spoof identity. Trickbot is sometimes used to sneak into a network. Once inside the network, it can be used to infect other machines within the network by downloading ransomware and other account-stealing programs. Trickbot targets its victims via email, pretending to be from trusted companies or government-based brands that people use all the time. These malicious emails sent often contain an attachment or link that instructs victims to open it, then infects their machine with malware. Trickbot is a trojan horse for Microsoft Windows and other operating systems [17].

6. METHODOLOGY

Trickbot is one of the most dangerous banking viruses of the botnet family, created by malicious people who have developed themselves in the software field and trying to steal money and data from people's bank accounts. When a search is made on the internet, different names may appear When Trickbot malware's first release and its latest developed version are analyzed carefully, it is seen that the modules it has downloaded to our computer are different. By using these modules, it can organize attacks on targeted banks. During this attack, it can exchange packets from target IP addresses. In our dynamic analysis method, when we work on about 250 Trickbot samples that we run in the virtual machine, apart from sending extra packets, it downloads attack modules to the infected machine and by using them, it can perform bot zombie attacks both by infecting other

computers in the local network and globally on the internet. A literature review showed a signature-based analysis of Trickbot malware, nevertheless no detailed analysis with DNS scanners. Signature-based approaches Because viruses update themselves by the botmaster, the previous signature version is changed to avoid being caught by security programs, so signature-based analysis may not always give accurate results for virus detection. For this reason, it is extremely important to support virus analyzes with DNS-based approaches rather than signature-based ones. In our research, the analysis of the traffic was studied in detail by using Wireshark packet catcher, an open-source tool in traffic analysis, and the IP addresses with which it exchanged packets, the traffic of the clean machine, and the infected machine were compared. Finally, new modules downloaded by this bot have been observed in detail. Bots exchange high packets, creating heavy traffic on the internet or local network, which can be a big problem for other users on that network. It occupies the communication structure of the system and renders the communication channels unusable. Similarly, Mirai targets industrial IoT devices, causing them to become inoperable. If bots propagating within the network cannot be blocked, it may cause a temporary system crash. Since these botnets are open source, their code structure can be easily updated so that they can bypass security programs. Signature-based security approaches may not be very effective against the nature of developing bots. Therefore, supporting it with a DNS-based approach increases security.

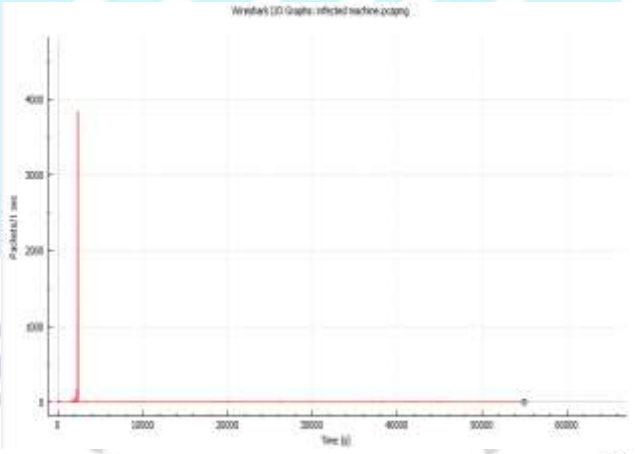

Figure 4. infected machine I/O packets graph

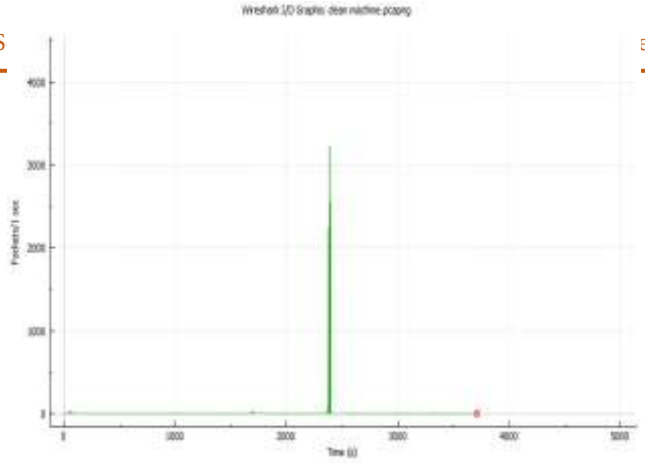

Figure 5. clean machine I/O packets graph

Figure 4 and Figure 5 are the Wireshark Input/Output (I/O) graph analyzed in the virtual machine in 1 second. Upon careful examination of the graphs, ınstantaneous traffic of over 3500 packets per second was observed, during this time the Trickbot trojan downloaded the attack modules. The clean machine downloaded approximately 3250 packages in the same period. If the package change amount is calculated from the formula at (2).

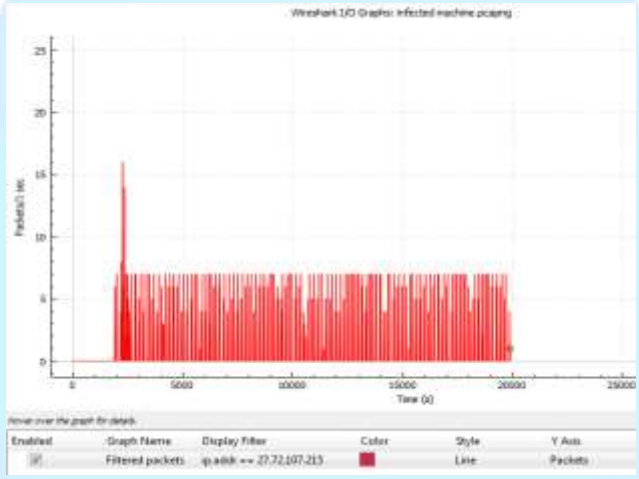

Figure 6. infected machine of IP address 27.72.107.215 I/O packets graph

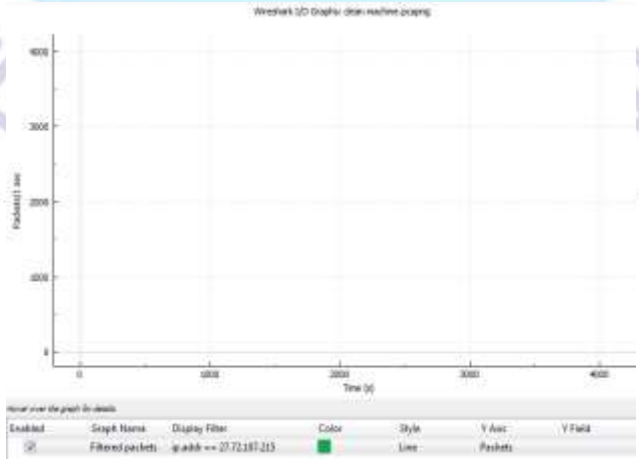

Figure 7. clean machine of IP address 27.72.107.215 I/O packets graph

$$\Delta P = P_{inf} - P_{cle} \qquad (2)$$

ΔP is the packet change amount, P_{inf} is the packet amount downloaded by the infected machine, and P_{cle} is the packet amount downloaded by the clean machine. Based on this formula, if ΔP = 3500 – 3250 => ΔP = 250, This equation is files and modular downloaded by the Trickbot, which has about 250 more packages.

Figure 8. Files and launcher downloaded by Trickbot malware

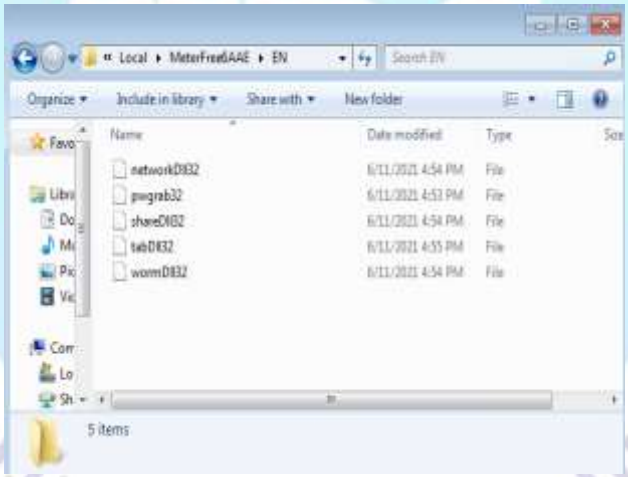

Figure 9. Modules downloaded by Trickbot malware

Networkdll32: Trickbot, which is secretly infected by malicious people, uses this encrypted module to scan the network and steal network information (personal credentials).

Pwgrab32 module: It is a new module of Trickbot and steals credentials from these applications which are used by many people such as PasswordGrabber, Filezilla, Microsoft Outlook, and

WinSCP which contain users' personal data. With this module, Trickbot can access usernames and passwords, cookies, search history, auto-fills, and HTTP posts.

ShareDll32 module: The most important purpose of Tirickbot is to protect its privacy in the infected network and to infect other users secretly. Therefore, it uses this module to spread within the network and infect other computers. In addition, there are services that start this botnet every time the machine is turned on to make itself permanent on the infected machine. These; Service Technology can be seen in names such as Service-Techno2, Techniques-Service2, Technoservices Advanced-Technic-Service, and ServiceTechno5.

TabDll32 module: enables WDigest Authentication by changing the UseLogonCredential value in the registry. This change saves the credentials to lsass.exe memory (Local Security Authority Subsystem Service). The TabDll32 module then injects the built-in screen-lock module in explorer.exe and locks it with the lock screen, forcing the user to log in again. It then waits for the next user to log in and steals the user's credentials from the LSASS memory. In the next step, it downloads the necessary loads from the URL registered in it and uses this module to set the persistence of the downloaded loads. This module also contains the main code of the shareDll32 module and uses it to propagate it over the network. Using the payloads in it, it copies it to the C:\WINDOWS\SYSTEM32\ and C:\WINDOWS\SYSTEM32\TASKS folders and executes the payload. Finally, it copies the Payload to C:\Users\<User Profile>\AppData\Roaming\ and protects them by creating shortcuts in the profile's Startup folder and creating a 'Run' key in the profile's registry.

WormDll32 module: This module propagates Trickbot by leveraging EternalBlue. Enumerates the infected machine using Active Directory Service. It injects the shell code into process memory and executes it according to the system's operating structure's wishes. The injected shellcode downloads and launches Trickbot from a fixed URL whose IP address does not change [18,19].

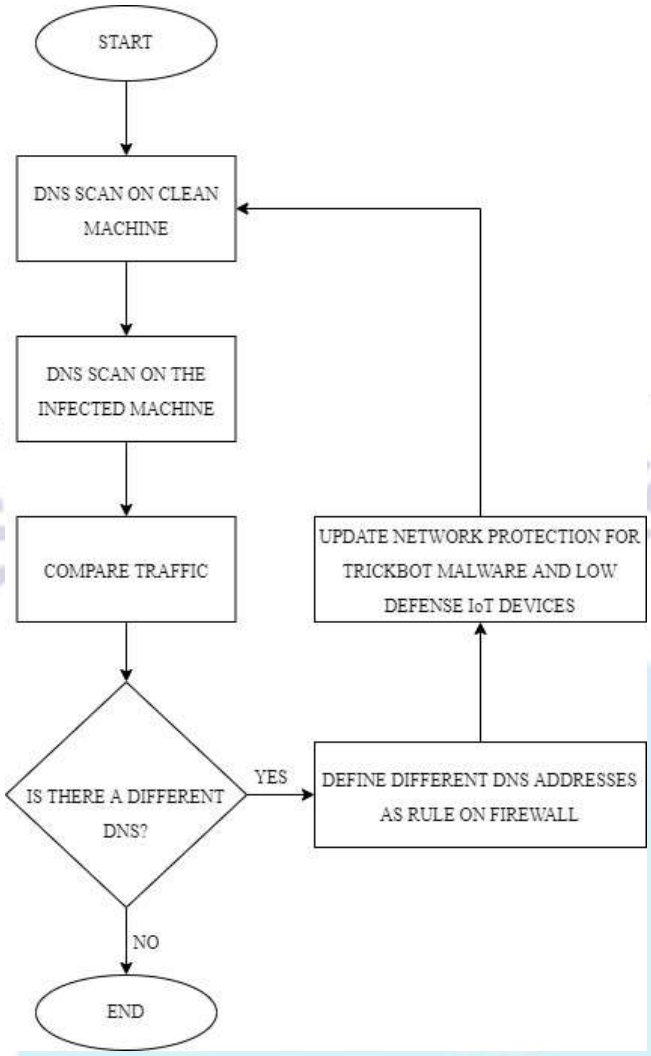

Figure 10. DNS protected approach algorithm

7. CONCLUSION

In this research with Trickbot, it has been shown that the existing behavior analysis and security layers of Trickbot should be constantly analyzed to ensure complete information security. Likewise, in terms of security measures, using only signature-based antivirus may not provide full protection. Therefore, system security needs to develop DNS-based detections and define them in antivirus or firewall device rules. In this study, many variants of Trickbot malware were analyzed. A study was made on the detection methods of its behavior and its behavior in the network was observed. This data we obtain is based on the processing of the system's protection program or reporting it as Firewall feedback. An algorithm has been created for this purpose. Thus, it is suggested that System Functionality can be kept between "Nominal Functionality (F(0))" and "Minimal Acceptable Functionality". In this method; It is recommended that the security layers of IoT devices and networks are constantly analyzed according to the structure of the updated malware and send

feedback to the protection programs. We observed that when Trickbot provides the necessary connections, it sends and receives packets to certain IP addresses and downloads different modules from its previous versions. This change in behavior means that it has received an update and now it has changed. Additionally, malware has shown that sometimes encrypted communication protocols can be used to send packets. Our future research; will be aimed to detect viruses and decipher the structure of encrypted communication protocols by processing the packets with the help of artificial intelligence.

REFERENCES

[1] https://www.statista.com/statistics/471264/iot-number-of-connected-devices-worldwide/ (Access date: 30.04.2022)

[2] Hassan, W. H. (2019). Current research on the Internet of Things (IoT) security: A survey. Computer networks, 148, 283-294.

[3] Kolias, C., Kambourakis, G., Stavrou, A., & Voas, J. (2017). DDoS in the IoT: Mirai and other botnets. Computer, 50(7), 80-84.

[4] Kambourakis, G., Kolias, C., & Stavrou, A. (2017, October). The Mirai botnet and the IoT zombie armies. In MILCOM 2017-2017 IEEE Military Communications Conference (MILCOM) (pp. 267-272). IEEE.

[5] Abbas, S. G., Hashmat, F., Shah, G. A., & Zafar, K. (2021). Generic signature development for IoT Botnet families. Forensic Science International: Digital Investigation, 38, 301224.

[6] Linkov, I., Eisenberg, D. A., Plourde, K., Seager, T. P., Allen, J., & Kott, A. (2013). Resilience metrics for cyber systems. Environment Systems and Decisions, 33(4), 471-476.

[7] https://www.fiercehealthcare.com/tech/uhs-breach-shows-dangers-facing-hospitals-growing-cyber-threats (Access date: 06.03.2022)

[8] https://www.techtarget.com/searchsecurity/news/252490814/After-a-brief-pause-Trickbot-rebounds-from-takedown-efforts (Access date: 06.03.2022)

[9] D. Kim, and M. G. Solomon, "Fundamentals of information systems security," Jones & Bartlett Publishers, 2013.

[10] F. Kausar, "Security and Privacy Challenges for the IoT Based Smart Homes with Limited Resources and Adoption Immaturity," vol. 1, Innovative Computing Review, 2021, pp. 43-59.

[11] https://securityintelligence.com/posts/the-curious-case-of-a-fileless-trickbot-infection/ (Access date: 30.04.2022)

[12] N. Tuptuk, and S. Hailes, "Security of smart manufacturing systems," vol. 47, Journalof manufacturing systems, 2018, pp. 93-106.

[13] J. M. Ceron, K. Steding-Jessen, C. Hoepers, L. Z. Granville, and C. B. Margi, vol. 727, "Improving iot botnet investigation using an adaptive network layer," Sensors, 2019.

[14] M. Feily, A. Shahrestani, and S. Ramadass, "A survey of botnet and botnet detection," In 2009 Third International Conference on Emerging Security Information, Systems and Technologies, pp. 268-273, June 2009.

[15] A. Gezer, G. Warner, C. Wilson, and P. Shrestha, "A flow-based approach for trickbot banking trojan detection," vol. 84, Computers & Security, 2019, pp. 179-192.

[16] ELGawish, R., Hashem, M., ElGohary, R. A. E., & Abu-Rizka, M. (2022). A Threshold-based Technique to Cluster Ransomware Infected Medical Records on the Internet of Medical Things. International Journal of Intelligent Computing and Information Sciences, 22(1), 16-31.

[17] https://www.ncsc.gov.uk/news/trickbot-advisory (Access date: 30.04.2022)

[18] https://securelist.com/trickbot-module-descriptions/104603/ (Access date: 30.04.2022)

[19] https://www.webroot.com/blog/2018/03/21/trickbot-banking-trojan-adapts-new-module/ (Access date: 30.04.2022)

Laser Beam Micro-Drilling Effect on Ti-6Al-4V Titanium Alloy Sheet Properties

Petr Homola, Roman Růžek

Czech Aerospace Research Centre, Beranovych ,Czech Republic

Czech Aerospace Research Centre, Czech Republic

Abstract:

Laser beam micro-drilling (LBMD) is one of the most important non-contact machining processes of materials that are difficult to machine by means oeqf conventional machining methods used in various industries. The paper is focused on LBMD knock-down effect on Ti-6Al-4V (Grade 5) titanium alloy sheets properties. Two various process configurations were verified with a focus on laser damages in back-structure parts affected by the process. The effects of the LBMD on the material properties were assessed by means of tensile and fatigue tests and fracture surface analyses. Fatigue limit of LBMD configurations reached a significantly lower value between 15% and 30% of the static strength as compared to the reference raw material with 58% value. The farther back-structure configuration gives a two-fold fatigue life as compared to the closer LBMD configuration at a given stress applied.

Keywords: Fatigue, fracture surface, laser beam micro-drilling, titanium alloy.

The Effect of Nylon and Kevlar Stitching on the Mode I Fracture of Carbon/Epoxy Composites

Nisrin R. Abdelal, Steven L. Donaldson

Assistant Professor in the Aeronautical Engineering Department at Jordan University of Science and Technology

Associate Professor in the Civil and Environmental Engineering and Engineering Mechanics Department at University of Dayton–Dayton-Ohio- USA

Abstract:

Composite materials are widely used in aviation industry due to their superior properties; however, they are susceptible to delamination. Through-thickness stitching is one of the techniques to alleviate delamination. Kevlar is one of the most common stitching materials; in contrast, it is expensive and presents stitching fabrication challenges. Therefore, this study compares the performance of Kevlar with an inexpensive and easy-to-use nylon fiber in stitching to alleviate delamination. Three laminates of unidirectional carbon fiber-epoxy composites were manufactured using vacuum assisted resin transfer molding process. One panel was stitched with Kevlar, one with nylon, and one unstitched. Mode I interlaminar fracture tests were carried out on specimens from the three composite laminates, and the results were compared. Fractographic analysis using optical and scanning electron microscope were conducted to reveal the differences between stitching with Kevlar and nylon on the internal microstructure of the composite with respect to the interlaminar fracture toughness values.

Keywords: Carbon, delamination, Kevlar, mode I, nylon, stitching.

Two-Stage Launch Vehicle Trajectory Modeling for Low Earth Orbit Applications

Assem M. F. Sallam, Ah. El-S. Makled

Space Technology Center, Cairo, Egypt
Military Technical College, Cairo, Egypt.

Abstract:

This paper presents a study on the trajectory of a two stage launch vehicle. The study includes dynamic responses of motion parameters as well as the variation of angles affecting the orientation of the launch vehicle (LV). LV dynamic characteristics including state vector variation with corresponding altitude and velocity for the different LV stages separation, as well as the angle of attack and flight path angles are also discussed. A flight trajectory study for the drop zone of first stage and the jettisoning of fairing are introduced in the mathematical modeling to study their effect. To increase the accuracy of the LV model, atmospheric model is used taking into consideration geographical location and the values of solar flux related to the date and time of launch, accurate atmospheric model leads to enhancement of the calculation of Mach number, which affects the drag force over the LV. The mathematical model is implemented on MATLAB based software (Simulink). The real available experimental data are compared with results obtained from the theoretical computation model. The comparison shows good agreement, which proves the validity of the developed simulation model; the maximum error noticed was generally less than 10%, which is a result that can lead to future works and enhancement to decrease this level of error.

Keywords: Launch vehicle modeling, launch vehicle trajectory, mathematical modeling, MATLAB-Simulink.

DETERMINATION OF AGRICULTURAL CHARACTERISTICS OF SMOOTH BROMEGRASS (BROMUS INERMIS LEYSS) LINES UNDER KONYA REGIONAL CONDITIONS

Abdullah Özköse, Ahmet Tamkoç

Selçuk University

Abstract:

The present study was conducted to determine the yield and yield components of smooth bromegrass lines under the environmental conditions of the Konya region during the growing seasons between 2011 and 2013. The experiment was performed in the randomized complete block design (RCBD) with four replications. It was found that the selected lines had a statistically significant effect on all the investigated traits, except for the main stem length and the number of nodes in the main stem. According to the two-year average calculated for various parameters checked in the smooth bromegrass lines, the main stem length ranged from 71.6 cm to 79.1 cm, the main stem diameter from 2.12 mm from 2.70 mm, the number of nodes in the main stem from 3.2 to 3.7, the internode length from 11.6 cm to 18.9 cm, flag leaf length from 9.7 cm to 12.7 cm, flag leaf width from 3.58 cm to 6.04 mm, herbage yield from 221.3 kg da^{-1} to 354.7 kg da^{-1} and hay yield from 100.4 kg da^{-1} to 190.1 kg da^{-1}. The study concluded that the smooth bromegrass lines differ in terms of yield and yield components. Therefore, it is very crucial to select suitable varieties of smooth bromegrass to obtain optimum yield.

Keywords: Semiarid region, smooth bromegrass, yield, yield components.

MATHEMATICAL MODELING ON CAPTURING OF MAGNETIC NANOPARTICLES IN AN IMPLANT ASSISTED CHANNEL FOR MAGNETIC DRUG TARGETING

Shashi Sharma, V. K. Katiyar, Uaday Singh

Indian Institutes of Technology

Abstract:

In IA-MDT, the magnetic implants are placed strategically at the target site to greatly and locally increase the magnetic force on MDCPs and help to attract and retain the MDCPs at the targeted region. In the present work, we develop a mathematical model to study the capturing of magnetic nanoparticles flowing within a fluid in an implant assisted cylindrical channel under magnetic field. A coil of ferromagnetic SS-430 has been implanted inside the cylindrical channel to enhance the capturing of magnetic nanoparticles under magnetic field. The dominant magnetic and drag forces, which significantly affect the capturing of nanoparticles, are incorporated in the model. It is observed through model results that capture efficiency increases as we increase the magnetic field from 0.1 to 0.5 T, respectively. The increase in capture efficiency by increase in magnetic field is because as the magnetic field increases, the magnetization force, which is attractive in nature and responsible to attract or capture the magnetic particles, increases and results the capturing of large number of magnetic particles due to high strength of attractive magnetic force.

Keywords: Capture efficiency, Implant assisted-Magnetic drug targeting (IA-MDT), Magnetic nanoparticles (MNPs).

IMPROVING THE EXPLOITATION OF FLUID IN ELASTOMERIC POLYMERIC ISOLATOR

[1]Haithem Elderrat, [2]Huw Davies, [3]Emmanuel Brousseau

[1] PhD candidate in Cardiff School of Engineering, Cardiff University
[2,3] Cardiff School of Engineering, Cardiff University - UK

Abstract:

Elastomeric polymer foam has been used widely in the automotive industry, especially for isolating unwanted vibrations. Such material is able to absorb unwanted vibration due to its combination of elastic and viscous properties. However, the 'creep effect', poor stress distribution and susceptibility to high temperatures are the main disadvantages of such a system. In this study, improvements in the performance of elastomeric foam as a vibration isolator were investigated using the concept of Foam Filled Fluid (FFFluid). In FFFluid devices, the foam takes the form of capsule shapes, and is mixed with viscous fluid, while the mixture is contained in a closed vessel. When the FFFluid isolator is affected by vibrations, energy is absorbed, due to the elastic strain of the foam. As the foam is compressed, there is also movement of the fluid, which contributes to further energy absorption as the fluid shears. Also, and dependent on the design adopted, the packaging could also attenuate vibration through energy absorption via friction and/or elastic strain. The present study focuses on the advantages of the FFFluid concept over the dry polymeric foam in the role of vibration isolation. This comparative study between the performance of dry foam and the FFFluid was made according to experimental procedures. The paper concludes by evaluating the performance of the FFFluid isolator in the suspension system of a light vehicle. One outcome of this research is that the FFFluid may preferable over elastomer isolators in certain applications, as it enables a reduction in the effects of high temperatures and of 'creep effects', thereby increasing the reliability and load distribution. The stiffness coefficient of the system has increased about 60% by using an FFFluid sample. The technology represented by the FFFluid is therefore considered by this research suitable for application in the suspension system of a light vehicle.

Keywords: Anti-vibration devices, dry foam, FFFluid

GENERALIZED MAXIMUM ENTROPY METHOD FOR COSMIC SOURCE LOCALIZATION

[1]Youssef Khmou, [2]Said Safi, [3]Miloud Frikel

[1,2] Department of Mathematics and Informatics, Polydisciplinary Faculty, Sultan Moulay Slimane University, Beni Mellal, Morroco

[3]GREYC Lab UMR 6072 CNRS, Equipe Automatique,

Abstract:

The Maximum entropy principle in spectral analysis was used as an estimator of Direction of Arrival (DoA) of electromagnetic or acoustic sources impinging on an array of sensors, indeed the maximum entropy operator is very efficient when the signals of the radiating sources are ergodic and complex zero mean random processes which is the case for cosmic sources. In this paper, we present basic review of the maximum entropy method (MEM) which consists of rank one operator but not a projector, and we elaborate a new operator which is full rank and sum of all possible projectors. Two dimensional Simulation results based on Monte Carlo trials prove the resolution power of the new operator where the MEM presents some erroneous fluctuations.

Keywords: Maximum entropy, Cosmic source, Localization, operator, projector, azimuth, elevation, DoA, circular array.

MHD UNSTEADY FREE CONVECTION OF HEAT AND MASS TRANSFER FLOW THROUGH POROUS MEDIUM WITH TIME DEPENDENT SUCTION AND CONSTANT HEAT SOURCE/SINK

Praveen Saraswat, Rudraman Singh

Faculty of Mathematics, Department of Mathematics, SRM University NCR Campus Modinagar India

Abstract:

In this paper, we have investigated the free convection MHD flow due to heat and mass transfer through porous medium bounded by an infinite vertical non-conducting porous plate with time dependent suction under the influence of uniform transverse magnetic field of strength H_0. When Temperature (T) and Concentration (C) at the plate is oscillatory with time about a constant non-zero mean. The velocity distribution, the temperature distribution, co-efficient of skin friction and role of heat transfer is investigated. Here the partial differential equations are involved. Exact solution is not possible so approximate solution is obtained and various graphs are plotted.

Keywords: Time Dependent Suction, Convection, MHD, Porous.

EVOLUTION OF CORD ABSORBED DOSE DURING OF LARYNX CANCER RADIOTHERAPY, WITH 3D TREATMENT PLANNING AND TISSUE EQUIVALENT PHANTOM

Mohammad Hassan Heidari, Amir Hossein Goodarzi, Majid Azarniush

Departement of Radiation Oncology, Hafte teir Hospital, Shahre ray, Iran

Departement of Radiation Oncology, Hafte teir Hospital, Shahre ray, Iran

Islamic Azad University, VARAMIN Branch,Tehran, Iran

Abstract:

Radiation doses to tissues and organs were measured using the anthropomorphic phantom as an equivalent to the human body. When high-energy X-rays are externally applied to treat laryngeal cancer, the absorbed dose at the laryngeal lumen is lower than given dose because of air space, which it should pass through, before reaching the lesion. Specially, in case of high-energy X-rays, the loss of dose is considerable. Three-dimensional absorbed dose distributions have been computed for high-energy photon radiation therapy of laryngeal and hypopharyngeal cancers, using a coaxial pair of opposing lateral beams in fixed positions. Treatment plans obtained under various conditions of irradiation.

Keywords: 3D Treatment Planning, anthropomorphic phantom, larynx cancer, radiotherapy.

Synthesis and Application of Tamarind Hydroxypropane Sulphonic Acid Resin for Removal of Heavy Metal Ions from Industrial Wastewater

Aresh Vikram Singh, Sarika Nagar

Professor with Department of Chemistry, Jai Narain Vyas University, Jodhpur-342001, India
Research Scholar at Department of Chemistry, Jai Narain Vyas University

Abstract:

The tamarind based resin containing hydroxypropane sulphonic acid groups has been synthesized and their adsorption behavior for heavy metal ions has been investigated using batch and column experiments. The hydroxypropane sulphonic acid group has been incorporated onto tamarind by a modified Porath's method of functionalisation of polysaccharides. The tamarind hydroxypropane sulphonic acid (THPSA) resin can selectively remove of heavy metal ions, which are contained in industrial wastewater. The THPSA resin was characterized by FTIR and thermogravimetric analysis. The effects of various adsorption conditions, such as pH, treatment time and adsorbent dose were also investigated. The optimum adsorption condition was found at pH 6, 120 minutes of equilibrium time and 0.1 gram of resin dose. The orders of distribution coefficient values were determined.

Keywords: Distribution coefficient, industrial wastewater, polysaccharides, tamarind hydroxypropane sulphonic acid resin, thermogravimetric analysis.

A TISM MODEL FOR STRUCTURING THE PRODUCTIVITY ELEMENTS OF FLEXIBLE MANUFACTURING SYSTEM

Sandhya Dixit, Tilak Raj

Department of Mechanical Engineering, YMCA University of Science and Technology, Faridabad, Haryana India

Abstract

Flexible Manufacturing System (FMS) is seen as an option for industries which want to boost productivity as well as respond quickly to an increasingly changing marketplace. FMS produces in mid variety, mid volume range and can meet the changing market demands very quickly. But still the impact of adoption of FMS on the productivity of any industry is not very clear. In this paper an attempt has been made to model the various factors affecting the productivity of FMS installation using Total Interpretive Structural Modelling (TISM) Technique.

Keywords: Flexible manufacturing system, productivity, total interpretive structural modelling.

A GRAPH THEORETIC APPROACH FOR QUANTITATIVE EVALUATION OF NAAC ACCREDITATION CRITERIA FOR THE INDIAN UNIVERSITY

Nameesh Miglani, Rajeev Saha, R. S. Parihar
PhD Research Scholar at Sunrise University, Alwar, India.
faculty member in the Department ofMechanical Engg., YMCA University of Science and Technology, Faridabad, India
Registrar at Sunrise University, Alwar, India

Abstract:

Estimation of the quality regarding higher education within a university is practically long drawn process besides being difficult to measure primarily due to lack of a standard scale. National Assessment and Accreditation Council (NAAC) evolved a methodology of assessment which involves self-appraisal by each university/college and an assessment of performance by an expert committee. The attributes involved in assessing a university may not be totally independent from each other thereby necessitating the consideration of interdependencies. The present study focuses on evaluation of assessment criteria using graph theoretic approach and fuzzy treatment of data collected from the students. The technique will provide a suitable platform to university management team to cross check assessment of education quality by considering interdependencies of the attributes using graph theory.

Keywords: Graph theory, NAAC accreditation criteria, Indian University accreditation process.

SELECTION OF STRATEGIC SUPPLIERS FOR PARTNERSHIP: A MODEL WITH TWO STAGES APPROACH

Safak Isik, Ozalp Vayvay

Marmara university

Abstract:

Strategic partnerships with suppliers play a vital role for the long-term value-based supply chain. This strategic collaboration keeps still being one of the top priority of many business organizations in order to create more additional value; benefiting mainly from supplier's specialization, capacity and innovative power, securing supply and better managing costs and quality. However, many organizations encounter difficulties in initiating, developing and managing those partnerships and many attempts result in failures. One of the reasons for such failure is the incompatibility of members of this partnership or in other words wrong supplier selection which emphasize the significance of the selection process since it is the beginning stage. An effective selection process of strategic suppliers is critical to the success of the partnership. Although there are several research studies to select the suppliers in literature, only a few of them is related to strategic supplier selection for long-term partnership. The purpose of this study is to propose a conceptual model for the selection of strategic partnership suppliers. A two-stage approach has been used in proposed model incorporating first segmentation and second selection. In the first stage; considering the fact that not all suppliers are strategically equal and instead of a long list of potential suppliers, Kraljic's purchasing portfolio matrix can be used for segmentation. This supplier segmentation is the process of categorizing suppliers based on a defined set of criteria in order to identify types of suppliers and determine potential suppliers for strategic partnership. In the second stage, from a pool of potential suppliers defined at first phase, a comprehensive evaluation and selection can be performed to finally define strategic suppliers considering various tangible and intangible criteria. Since a long-term relationship with strategic suppliers is anticipated, criteria should consider both current and future status of the supplier. Based on an extensive literature review; strategical, operational and organizational criteria have been determined and elaborated. The result of the selection can also be used to determine suppliers who are not ready for a partnership but to be developed for strategic partnership. Since the model is based on multiple criteria for both stages, it provides a framework for further utilization of Multi-Criteria Decision Making (MCDM) techniques. The model may also be applied to a wide range of industries and involve managerial features in business organizations.

Keywords: Kraljic's matrix, purchasing portfolio, strategic supplier selection, supplier collaboration, supplier partnership, supplier segmentation.

Identifying and Ranking Critical Success Factors for Implementing Leagile Manufacturing Industries Using Modified TOPSIS

Naveen Virmani, Rajeev Saha, Rajeshwar Sahai

PhD from YMCA University of Science and Technology, Faridabad.
Assistant Professor at Department of Mechanical Engineering, YMCAUST, Faridabad
Director at Rattan College, Faridabad, India

Abstract:

Leagile is combination of both lean and agile system. Lean is concerned with less of everything i.e. less material, less time, less space, less manpower to produce a product, while agile is concerned with quick respond to customer demand and to reconfigure the system as soon as possible to meet the customer expectations well on time. The market is excessively competitive, so there is a dire need for the companies to adopt new and modern technologies with latest equipments. It has been seen that implementation of leagile system become tedious so the purpose of the paper is to find critical success factors (CSF) affecting leagile manufacturing system using literature review and rank them by using modified TOPSIS (Technique of order preference by similarity to ideal solution) technique.

Keywords: Agile manufacturing, lean manufacturing, leagile manufacturing, modified TOPSIS.

NON-SINGULAR GRAVITATIONAL COLLAPSE OF A HOMOGENEOUS SCALAR FIELD IN DEFORMED PHASE SPACE

Amir Hadi Ziaie

Department of Physics, Shahid Bahonar University, Kerman, Iran

Abstract

In the present work, we revisit the collapse process of a spherically symmetric homogeneous scalar field (in FRW background) minimally coupled to gravity, when the phase-space deformations are taken into account. Such a deformation is mathematically introduced as a particular type of noncommutativity between the canonical momenta of the scale factor and of the scalar field. In the absence of such deformation, the collapse culminates in a spacetime singularity. However, when the phase-space is deformed, we find that the singularity is removed by a non-singular bounce, beyond which the collapsing cloud re-expands to infinity. More precisely, for negative values of the deformation parameter, we identify the appearance of a negative pressure, which decelerates the collapse to finally avoid the singularity formation. While in the un-deformed case, the horizon curve monotonically decreases to finally cover the singularity, in the deformed case the horizon has a minimum value that this value depends on deformation parameter and initial configuration of the collapse. Such a setting predicts a threshold mass for black hole formation in stellar collapse and manifests the role of non-commutative geometry in physics and especially in stellar collapse and supernova explosion.

Keywords: Gravitational collapse, non-commutative geometry, spacetime singularity, black hole physics.

SOLAR-POWERED ADSORPTION COOLING SYSTEM: A CASE STUDY ON THE CLIMATIC CONDITIONS OF AL MINYA

El-Sadek H. Nour El-deen, K. Harby

Department of Mechanical Power Engineering and Energy, Faculty of Engineering, Minia University, Egypt

Abstract:

Energy saving and environment friendly applications are turning out to be one of the most important topics nowadays. In this work, a simulation analysis using TRNSYS software has been carried out to study the benefit of employing a solar adsorption cooling system under the climatic conditions of Al-Minya city, Egypt. A theoretical model was carried out on a two bed adsorption cooling system employing granular activated carbon-HFC-404A as working pair. Temporal and averaged history of solar collector, adsorbent beds, evaporator and condenser has been shown. System performance in terms of daily average cooling capacity and average coefficient of performance around the year has been investigated. The results showed that maximum yearly average coefficient of performance (COP) and cooling capacity are about 0.26 and 8 kW respectively. The maximum value of the both average cooling capacity and COP cyclic is directly proportional to the maximum solar radiation. The system performance was found to be increased with the average ambient temperature. Finally, the proposed solar powered adsorption cooling systems can be used effectively under Al-Minya climatic conditions.

Keywords: Adsorption, solar energy, environment, cooling, Egypt.

CLUSTER ANALYSIS OF CUSTOMER CHURN IN TELECOM INDUSTRY

Abbas Al-Refaie

Department of Industrial Engineering in the University of Jordan, Amman, 11942

Abstract:

The research examines the factors that affect customer churn (CC) in the Jordanian telecom industry. A total of 700 surveys were distributed. Cluster analysis revealed three main clusters. Results showed that CC and customer satisfaction (CS) were the key determinants in forming the three clusters. In two clusters, the center values of CC were high, indicating that the customers were loyal and SC was expensive and time- and energy-consuming. Still, the mobile service provider (MSP) should enhance its communication (COM), and value added services (VASs), as well as customer complaint management systems (CCMS). Finally, for the third cluster the center of the CC indicates a poor level of loyalty, which facilitates customers churn to another MSP. The results of this study provide valuable feedback for MSP decision makers regarding approaches to improving their performance and reducing CC.

Keywords: Cluster analysis, telecom industry, switching cost, customer churn.

APPLICATION OF MOM-GEC METHOD FOR ELECTROMAGNETIC STUDY OF PLANAR MICROWAVE STRUCTURES: SHIELDING APPLICATION

Ahmed Nouainia, Mohamed Hajji, Taoufik Aguili

SysCom Laboratory, National Engineering School of Tunis and Department of Physics, Faculty of Sciences of Tunis, Tunis El Manar University, Tunisia

Abstract

In this paper, an electromagnetic analysis is presented for describing the influence of shielding in a rectangular waveguide. A hybridization based on the method of moments combined to the generalized equivalent circuit MoM-GEC is used to model the problem. This is validated by applying the MoM-GEC hybridization to investigate a diffraction structure. It consists of electromagnetic diffraction by an iris in a rectangular waveguide. Numerical results are shown and discussed and a comparison with FEM and Marcuvitz methods is achieved.

Keywords: Inductive irises, MoM-GEC, waveguide, shielding.

MODELLING A HOSPITAL AS A QUEUEING NETWORK: ANALYSIS FOR IMPROVING PERFORMANCE

Emad Alenany, M. Adel El-Baz

Industrial Engineering Department at Zagazig University, Egypt

Abstract

In this paper, the flow of different classes of patients into a hospital is modelled and analyzed by using the queueing network analyzer (QNA) algorithm and discrete event simulation. Input data for QNA are the rate and variability parameters of the arrival and service times in addition to the number of servers in each facility. Patient flows mostly match real flow for a hospital in Egypt. Based on the analysis of the waiting times, two approaches are suggested for improving performance: Separating patients into service groups, and adopting different service policies for sequencing patients through hospital units. The separation of a specific group of patients, with higher performance target, to be served separately from the rest of patients requiring lower performance target, requires the same capacity while improves performance for the selected group of patients with higher target. Besides, it is shown that adopting the shortest processing time and shortest remaining processing time service policies among other tested policies would results in, respectively, 11.47% and 13.75% reduction in average waiting time relative to first come first served policy.

Keywords: Queueing network, discrete-event simulation, health applications, SPT.

DOMINANT CORRELATION EFFECTS IN ATOMIC SPECTRA

Hubert Klar

Duale Hochschule BW, Department of Mechanical Engineering, Hangstrasse Germany

Abstract:

High double excitation of two-electron atoms has been investigated using hyperpherical coordinates within a modified adiabatic expansion technique. This modification creates a novel fictitious force leading to a spontaneous exchange symmetry breaking at high double excitation. The Pauli principle must therefore be regarded as approximation valid only at low excitation energy. Threshold electron scattering from high Rydberg states shows an unexpected time reversal symmetry breaking. At threshold for double escape we discover a broad (few eV) Cooper pair.

Keywords: Correlation, resonances, threshold ionization, Cooper pair.

MODELING DRYING AND PYROLYSIS OF MOIST WOOD PARTICLES AT SLOW HEATING RATES

Avdhesh K. Sharma

University of Science and technology - India

Abstract:

Formulation for drying and pyrolysis process in packed beds at slow heating rates is presented. Drying of biomass particles bed is described by mass diffusion equation and local moisture-vapour-equilibrium relations. In gasifiers, volatilization rate during pyrolysis of biomass is modeled by using apparent kinetic rate expression, while product compositions at slow heating rates is modeled using empirical fitted mass ratios (i.e., CO/CO_2, ME/CO_2, H_2O/CO_2) in terms of pyrolysis temperature. The drying module is validated fairly with available chemical kinetics scheme and found that the testing zone in gasifier bed constituted of relatively smaller particles having high airflow with high isothermal temperature expedite the drying process. Further, volatile releases more quickly within the shorter zone height at high temperatures (isothermal). Both, moisture loss and volatile release profiles are found to be sensitive to temperature, although the influence of initial moisture content on volatile release profile is not so sensitive.

Keywords: Modeling downdraft gasifier, drying, pyrolysis, moist woody biomass.

REAL TIME PLATE RECOGNITION WITH RASPBERRY PI AND PHYTON

Prof. Dr. Ergün Erçelebi1, İbrahim Halil Polat2

1Head of Electrical & Electronics Engineering Department at Gaziantep University, Gaziantep, Turkey

2MSc Student at Electrical & Electronics Engineering Department at Gaziantep University, Gaziantep, Turkey

Abstract:

Nowadays, with the increasing traffic density, the need for a system to detect dangerous situations arises for reliable transportation. For these cases, a remote control system with a camera is required. With the increasing number of cameras in cities

video traffic analysis system can provide useful information for the transportation segment. One such analysis is Automatic.

License Plate Recognition (ALPR). This analysis system consists of vehicle location, license plate detection, character segmentation and optical character recognition sections. In order to obtain a stable result at the exit of these sections, a technical infrastructure should be established. In the technical part, there are two parts; hardware and software. After processing the plate we read from the camera with the deep learning process by integrating the application we wrote with the "Pyhton" programming language into the "Raspberry Pi" operating system, which is called a mini computer in the hardware part, a notification is made by sending an e-mail to the desired e-mail address of the plate value and that value. The created process filters in order to detect the frame and scales the frame to make Tesseract optical character recognition (TesseractOCR). After recognition, it completes the detection process of the correct license plate, which is formed by making comparisons with the characters defined in the deep learning infrastructure. In order to receive the notification of the detected data, SMTP mail sending method was used. With this designed system, the data of the plate that it sees at any time will be taken from a fixed camera. As a result of this situation, high security will be achieved with low cost.

Keywords: Plate Recognition, Camera, Raspberry Pi, TesseractOCR, Phyton

APPLICATION OF RADIAL BASIS FUNCTIONS METHOD TO ADVECTION-DIFFUSION PROBLEM

Yusuf Tunçay, Cenk Güngör[2]

[1] Istanbul Altınbaş University, 0002-6147-2162
[2] T.C. Istanbul Rumeli University, 0002-5044-1651

ABSTRACT

The objective of this paper is to demonstrate an application of radial basis functions method to linear and nonlinear advection-diffusion problems. To this extend, the radial basis functions method is considered, multiquadrics and thin-plate splines types of functions are used in the study. Firstly, the study is handling the linear advection-diffusion type of equation in one dimensional cases with specific examples in order to compare with the analytical solutions existing in the literature. Then, nonlinear advection-diffusion equation is solved to demonstrate the efficiency of the method. Especially, for multiquadric radial basis functions solutions, the shape parameter effect is investigated and shape parameter optimization is carried out with the known exact solutions. It can be claimed from all implementations that this meshless radial basis functions collocation method is very easy to code, flexible with respect to high-dimensional geometries and efficient in comparison with the other methods.

Keywords: Radial Basis Functions, Multiquadric, Thin-plate splines, Shape parameter, Meshfree, Shape parameter

1. INTRODUCTION

Many problems in science and engineering are reduced to a set of differential equations through a process of mathematical modeling. It is not easy to obtain their exact solutions, so numerical methods must be resorted to. There are a lot of techniques available such as the Finite Difference Method (FDM) and the Finite Element Method (FEM). These methods require the definition of a mesh (domain discretization) where the functions are approximated locally. The construction of a mesh in two or more dimensions is a nontrivial problem. Only low-order approximations are employed resulting in a continuous approximation of the function across the mesh. The discontinuity of the approximation of the derivative can adversely affect the stability of the solution. Even though, significant advances have been made in the area of grid generation over the last decades, it still remains a complex and time consuming process, particularly for complex geometries. This problem has motivated the development of so-called meshfree or meshless methods that try to circumvent the cumbersome issue of grid generation [1].

In the last decade, there has been great interest in using meshless methods to find the numerical solution of partial differential equations (PDE) [2]. Various types of meshless methods have been developed in last recent decades.

One of the meshless methods is due to the pioneering effort of Kansa, who solved PDEs by collocation employing radial basis functions. His work was motivated by advances in the field of function approximation. This method is known as the unsymmetric Radial Basis Function Collocation Method where the unknown function is expanded in terms of radial basis functions (RBFs). The unsymmetric RBF collocation method generates full, unsymmetric coefficient matrices. Theoretical proofs for the invertibility of the resultant coefficient matrices exist in the

literature for the symmetric collocation method [3]; however, for Kansa's unsymmetric method, the proofs are still elusive.

Many studies have shown that the RBFs method can be numerically more accurate than FDM and FEM. Additionally, RBFs have an advantage of being easily applicable to high dimensional problems. This method has been successfully applied to a number of areas including tissue engineering problems [4], heat transfer [5], convection-diffusion problems [6], nonlinear problems [7, 8, 9] and free boundary problems [10].

2. LITERATURE REVIEW

The solution of the advection-diffusion equation is a long standing problem and many numerical methods have been introduced to model accurately the interaction between advective and diffusive processes. This modelling is the most challenging task in the numerical approximation of the partial differential equations and the available numerical solutions are very sophisticated in order to avoid two undesirable features: oscillatory behavior and numerical diffusion, which are mainly due to the advection term when it dominates [11].

The numerical solution of this equation is a difficult task because of two reasons; Firstly, the nature of the governing equation, which includes first-order and second-order partial derivatives in space. According to the value of κ (diffusion coefficient) and ν (advection coefficient), the equation becomes parabolic for diffusion dominated processes or hyperbolic for advection dominated processes.

The advection-diffusion equation is the basis of many physical and chemical phenomena [12]. A large number of problems in physics, chemistry and other branches of science can be modeled by the advection-diffusion equation. Especially, advection–diffusion processes occur in many evolutionary problems, such as fluid dynamics, transport of pollutants, heat and mass transfer,… etc [13].

In Li and Chen's paper [14], the time independent advection-diffusion problem is considered. They investigate the unsymmetric radial basis function collocation method for solving advection-diffusion problem with high Peclet numbers. They found that this method can still solve high Peclet number problems reasonably well by using more nodes and domain decompositon techniques. Apart from this study, in most cases the time dependent advection-diffusion problems are more commom in the literature.

Boztosun *et. al.* [6] have carried out a numerical solution of advection-diffusion equation based on thin plate spline radial basis function. The efficiency of the method in terms of computational processing time, accuracy and stability is discussed and they obtained excellent results compared to the results of the FDM.

Another paper of Boztosun and Charafi [15] compares the results with the findings from the dual reciprocity boundary element and FDM as well as with the analytical solution. There, 2-D advection-diffusion problem is also investigated with given exact solution.

Zerroukat *et.al.* [16], the linear advection-diffusion problem is developed and validated. Unlike the above-mentioned paper of Charafi, this time the scheme uses well distributed quasi-random points and approximates the solution using global radial basis functions. This allows the computation of problems with complex-shaped boundaries in higher dimensions with no need for complex mesh/grid structure and with no extra implementation difficulties. Solutions of the equation for 1-D and 2-D cases are approximated with an additional polynomial. The augmented form is used in this solution to reduce the error of numerical approximation.

In the literature, there are many approaches to the solution of advection-diffusion type of problems. Thiffeault [17] shows that the advection-diffusion equation in Lagrangian coordinates can be reduced to the one dimensional diffusion equation along the stable manifold of the flow. Chantasiriwan [18] suggests that the solution of the advection-diffusion equation with the cartesian grid method by collocation using radial basis functions combines the global radial basis functions and fundamental solutions and yields more accurate solutions that are less sensitive to the shape parameter of multiquadrics and node arrangement. Hernandez [19] uses a high-order finite volume method (FVM) based on piecewise interpolant polynomials to discretize spatially the one-dimensional and two-dimensional advection-diffusion equation. The mathematical difficulty of the advection-diffusion equation arises when the diffusion is very small. Many grid points are necessary to obtain reliable solutions to avoid this limitation and high-order methods must be considered to solve this equation. Advection-diffusion problem is solved using the domain decompositon method by Lesnic [20]. Hon and Chen [21] solve the advection-diffusion equation is solved using Boundary Knot Method (BKM) under complicated geometry. The Radial Point Collocation Method (RPCM or PIM) is simply implemented to advection-diffusion equation as well as in the papers by Xin [22].

As seen from the literature survey, numerous kinds of approximation techniques and numerical studies have been carried out to solve the advection-diffusion problem. There are considerably more studies done on the numerical solution of advection-diffusion problem using this technique. All the papers above were reviewed to see what has been done for the solution of advection-diffusion type of problems. We can easily observe that the application of radial basis function collocation method is presently gaining attention. Due to its simple implementation and its advantage of being independent of dimension it has become very popular as a numerical method.

3. METHOD AND DEFINITION OF THE PROBLEMS

The mathematical difficulty of the advection–diffusion equation arises when the diffusion is very small. Solutions may present boundary layers together with long diffusive lengths that make difficult to approximate them. When the diffusion is very small and classical second-order methods are considered, many grid points are necessary to obtain reliable solutions [23]. It is well known that FDM and FEM solutions of the advection-diffusion equation present numerical problems of oscillations and damping [12]. In order to avoid such limitations, the radial basis functions method application has demonstrated that this meshless method has great advantages in approximating over traditional methods.

In the solution procedure of the Meshless Methods (MLM), the RBF must be constructed after the nodes are generated. Without relying on elements, the construction of the RBF in MLM is solely based on the relationship among nodes. The methods for constructing basis functions are very important in the sense that they have direct effects on the efficiency and accuracy of the solution. Radial Basis Functions Method has been under intensive research as a technique for multivariate data and function interpolation in the past decades. Since its easy implementation on linear and non-linear partial differential equations for numerical solution and also in multi-dimensional applications, this method has currently become more applicable in various areas in science and engineering. The function u is approximated with global radial basis functions as;

$$u_i^b = \phi_{ij} \lambda_j^b \tag{1}$$

$$u_i^b(\mathbf{x},t) = \sum_{j=1}^{N} \phi(r_{ij}) \lambda_j^b = \sum_{j=1}^{N} \phi(\|x_i - x_j\|) \lambda_j^b \quad (2)$$

where *i* denotes the node / point on the domain, and *b* is the time step, *N* refers to number of nodes defined on the domain, x_j are the centres of the radial basis function interpolant, $\emptyset_{ij}$ chosen radial basis function, *r* is the distances between the nodes on the domain, and λ_j are the unknown coefficients to be calculated. RBFs can be globally supported, infinitely differentiable, and contain a free parameter, c, called the shape parameter [8]. In all the interpolation methods for scattered data sets, RBFs outperforms all the other methods regarding accuracy, stability, efficiency, memory requirement, simplicity of the implementation.

The first trial of such exploration was made by Kansa [24] using radial basis functions as a meshless method to solve partial differential equations possesses the following advantages; First of all, it is a truly mesh-free method, and is independent of spatial dimension. Furthermore, in the context of scattered data interpolation, it is known that some RBFs have spectral convergence. This shows the applicability of the RBFs for solving high-dimension problems [7]. The choice of basis function is another flexible feature of radial basis function methods [8]. There exists several RBFs to choose. The most common RBFs can be categorized into three main groups according to their differentiability and supported features. Some of the functions include free-parameter and some of them are parameter-free. The choice of suitable radial basis functions can vary in terms of the problem types. The present study also explores the effectiveness of the most common radial basis functions while implementing these functions to advection-diffusion problem. Common choices of $\emptyset_r$ are [13, 25, 26]; Piecewise smooth RBFs which are parameter-free i.e. Piecewise Polynomials, Thin Plate Splines (TPS) (3); Infinitely smooth RBFs with a free parameter i.e. Multiquadrics (MQs) (4), Inverse Multiquadrics, Inverse Quadratics, Gaussian; and Compacty supported piecewise polynomials with free parameter.

$$r^{\beta} \ln r \qquad \beta > 0\,,\ \beta \in 2N \quad (3)$$

$$\left(r^2 + c^2\right)^{\beta/2} \qquad \beta > 0\,,\ \beta \in 2N+1 \quad (4)$$

Where c is the shape parameter. As far as the shape parameter is considered, the value of the shape parameter for the MQ directly affects the approximation. Although a number studies have been conducted to determine the optimum value of the shape parameter, there is still no conclusive answer. There are however some expressions that provide starting values for a trial and error procedure to find a good c value. For example, a suggestion due to Hardy [27] is $0.815r_{average}$. Hon et al [21] state that satisfactory results were obtained for *c* between $5r_{average}$ and 8 $r_{average}$. Another suggestion for *c* given by Wu and Hon in 2003 is $4r_{min}$ [26]

As a time integration method, fourth order Runge-Kutta method is used in this study because it is known to work well for smooth problems. Moreover, it is a self starting method so that the initial input will be sufficient to proceed in time. It involves four evaluations per time step and the local truncation error is fourth order. Also, since the expected results are smooth, adaptive step size control is not deemed necessary.

Many problems were solved for different coefficient of advection and diffusion in the literature. You may review the papers to observe how the differences occur when either advection or diffusion coefficients are dominated [11, 8, 12, 28].

3.1. The Linear Advection-Diffusion Problem

The linear advection-diffusion problem with a constant advection and diffusion coefficient in 1-D will be handled. From [29], we have a linear advection-diffusion problem in one dimension. In this case, we consider a column initially free of solute and subjected to a continuous source u_0 at the inlet. The following is the governing equation for advection-diffusion reduced to one-dimensional case,

$$\frac{\partial u}{\partial t} = \kappa_x \frac{\partial^2 u}{\partial x^2} + v_x \frac{\partial u}{\partial x} \tag{5}$$

The domain of the problem is in 1-D, the independent space variable x interval is $0 \leq x \leq 100$ and N is the total number of nodes on the defined domain. The initial condition, the boundary conditions and the exact solution are respectively given in the equations (6,7, and 8). The constants are u_0=1, κx=0.5, vx=-1 ,and Pe = -2 for uniformly distributed nodes on domain. A total of N= 401 time steps were used with Δt=0.1 given in the tables.

$$u(x,t) = u(x,0) = 0, \qquad x > 0,\ t = 0 \tag{6}$$

$$u(x_1,t) = u_0 \ \ u(x_N,t) = 0 \ \ t > 0 \tag{7}$$

$$u(x,t) = \frac{u_0}{2}\left[erfc\left(\frac{x + v_x t}{2\sqrt{\kappa_x t}}\right) + \exp\left(\frac{-v_x x}{\kappa_x}\right) erfc\left(\frac{x - v_x t}{2\sqrt{\kappa_x t}}\right)\right] \tag{8}$$

3.2. The Nonlinear Advection-Diffusion Problem

The governing nonlinear advection-diffusion equation in 1-D can be written as

$$\frac{\partial u}{\partial t} = \left(\frac{\partial u}{\partial x}\right)^2 + u\frac{\partial^2 u}{\partial x^2} - \frac{\partial u}{\partial x} \tag{9}$$

A line source problem will be solved. The evolution will be for three different source strengths at a given location. This one dimensional version of the equation retains the symmetry-breaking effects of advection, but ignores transverse spreading. The domain of the problem in 1-D and the time interval are given as , $-10 \leq x \leq 130$, $1 \leq t \leq 101$. The time interval starts with the initial condition at t = 1. s and provides the conditions $u(0,t)=t^{\beta}$ where β can be 0, 1/10, or -1/4. for the left and the right extreme points. Numerical solutions are obtained at times t = 21, 41, 61, 81 and 101 for different source strengths.

4. RESULTS AND DISCUSSION OF THE PROBLEMS

4.1. The Linear Advection-Diffusion Problem

In the study, the linear advection-diffusion problem is solved using radial basis functions meshless collocation method directly comparing the numerical solutions between multiquadrics, thin-plate splines and the given exact solution. The governing Equation 5 is discretized using mutliquadratic and thin-plate spline functions. The first and the second derivative of the dependent function are also discretized using radial basis functions. With the given boundary and the initial values, system matrix is constructed in order to evaluate the numerical solution.

The following figures 1,2,3 and 4 are obtained using multiquadric solutions with different number of nodes on the domain. Time step size effects are also investigated with error analysis. Error norm can be interpreted observing RMS errors which are inserted on the related tables. In multiquadric

solutions, shape parameter optimization is carried out and optimum shape parameter is determined. Focusing on the final time of the time interval has provided to determine optimum shape parameter. The final time can be assumed the time at which solution of the problem becomes stable. RMS versus "c" shape parameter curves are plotted in order to verify how the shape parameter is determined. The minumum RMS error is observed to specify the optimum shape parameter.

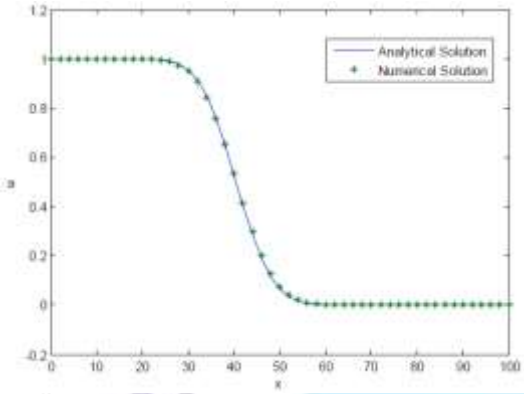

Figure 1 MQ-RBF Solution, c = 14.56, N = 51, dt = 0.1 , t = 40 s, RMS = 8.41e-04

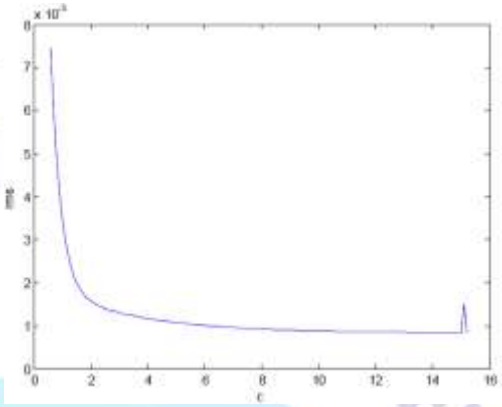

Figure 2 RMS and "c" vary, N = 51, dt = 0.1, t= 40 s

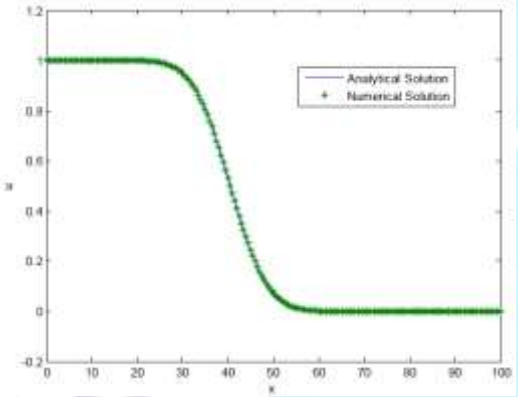

Figure 3 MQ-RBF Solution, c = 0.8, N = 201, dt = 0.1, t = 40 s, RMS = 3.87e-04

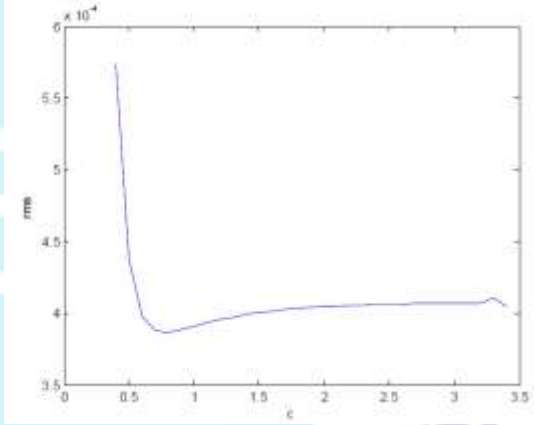

Figure 4 RMS and "c" vary, N = 201, dt = 0.1, t = 40 s

Table 1- MQ-TPS-RBF Solution of The Linear Advection-Diffusion Problem, RMS Errors

RBF	Optimum "c" or Order of the TPS	Number of Nodes	Time Step	Time (s)	RMS error (10^{-4})
MQ	19,1	41	0,1 0,01	40	9,52 1,79
	14,6 14 14	51	0,1 0,01 0,001	40	8,41 1,45 0,86
	9 8,8 8,5	81	0,1 0,01 0,001	40	6,07 0,78 0,63
	7	101	0,1	40	5,75

			0,01		5,68
	0,8 3,1	201	0,1 0,01	40	3,87 0,44
TPS	2 4 6 8	41	0,1 0,1 0,1 0,1	40	25 10 8,15 -
	2 4 6	51	0,1 0,1 0,1	40	16 8,45 7,7
	2 4 4 4	81	0,1 0,1 0,01 0,001	40	6,64 6,43 0,84 0,44
	2 4 4 4	101	0,1 0,1 0,01 0,001	40	4,61 5,74 0,65 0,23
	2 4	201	0,1 0,05	40	2,27 2,05

For the thin-plate splines, the spline functions from first order to fourth order were used. Only the unaugmented form of thin-plate spline functions are investigated. Due to the sensitivity of this type of function to number of nodes, for some situations we can not obtain any results because of the ill-conditioning of the coefficient matrix. This can be explained as the coefficient matrix becoming singular or solution instability occurs. It may be overcome with the addition of polynomials to the approximation function. RMS error decreases when the time step size has been lowered in the convergence range. It is deduced from the thin-plate splines approximation functions, the RMS error decreases as the number of nodes increases in a certain ranges. Figure 6 has been provided to demonstrate the decrease in error with increasing number of nodes.

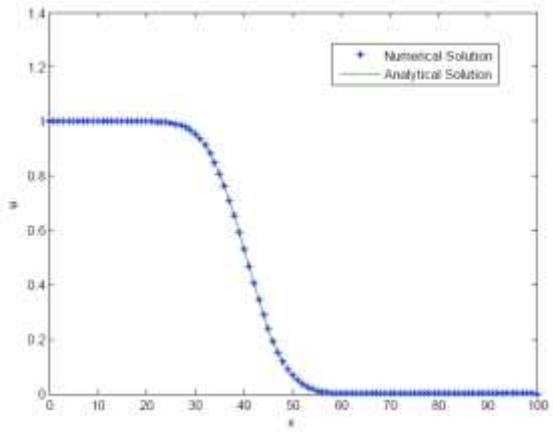

Figure 5 TPS-RBF solution, m = 4, dt = 0.01, t = 40 s, RMS = 6.51e-05

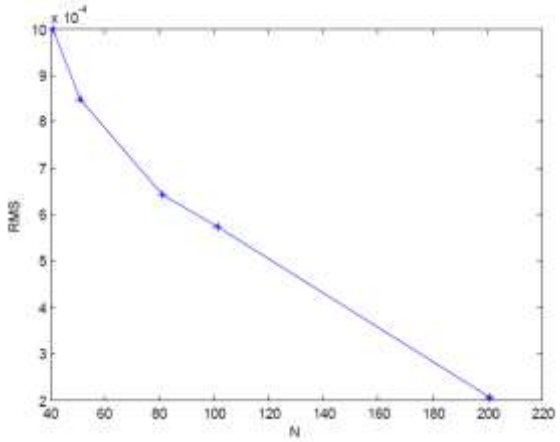

Figure 6 TPS-RBF solution, RMS vs. N, m = 4, dt = 0.1, t = 40 s

4.2. The Nonlinear Advection-Diffusion Problem

The nonlinear advection-diffusion problem is solved using radial basis functions collocation method as an example of a highly nonlinear advection-diffusion case. The governing equation 9 is

again discretized using radial basis functions. The system matrix of the problem is carefully constructed considering the nonlinear terms. As the problem is nonlinear, the solution is iterative. The initial condition shows sharp variation in the vicinity of coordinate x = 0. The boundary conditions are determined according to this condition. Different source strengths which are applied at this location lead to different solutions. The shape parameter is accepted as c = 1, and time step is taken as dt = 0.04. This is not the optimum shape parameter, but satisfies the solutions given in [30]. Using these, results which are in good agreement are obtained when compared with the results given in [30]. Providing those minumum conditions, great computational time decrease and efficiency has been found. But when β = 1/10, N = 656, time difference dt = 0.005 are considered. To eliminate the stability problem and to obtain more smooth curve, the number of nodes can be increased and time step can be decreased.

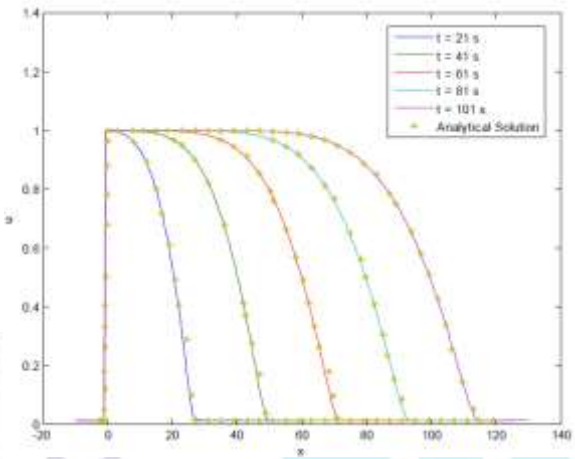

Figure 7 MQ-RBF solution, for β = 0, N = 264, dt = 0.04, c = 1

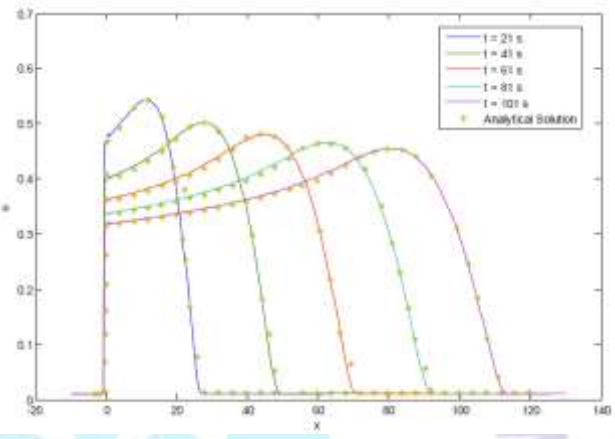

Figure 8 MQ-RBF solution, for β = -1/4, N = 264, dt = 0.04, c = 1

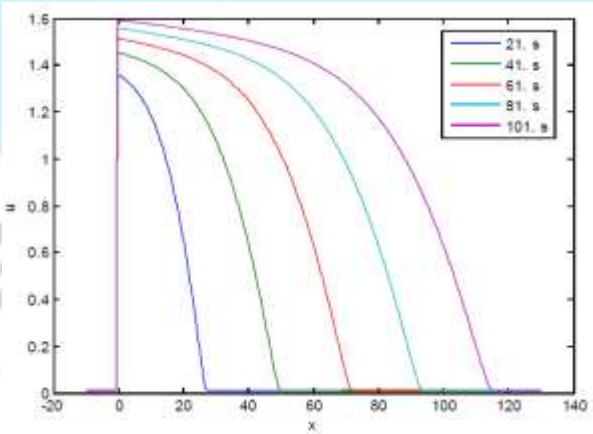

Figure 9 MQ-RBF solution, for β = 1/10, N = 656, dt = 0.005, c = 0.2

5. CONCLUSIONS AND RECOMMENDATIONS

In this study, an application of the meshless radial basis functions method to the advection-diffusion is demonstrated. Numerical experiments show that this meshless method has many advantages over traditional methods. Nodes are assigned to the related domain and radial basis functions are defined radially between the nodes. Radial basis functions method is based on the collocation scheme. The approximation function is the product of radial basis functions with

unknown coefficients. Coding is easy, only assigning the boundary conditions is a delicate work. Inversion of the coefficient matrix is important to consider. Mostly the singularity of the so-called matrix may be overcome with an addition of a polynomial term, adaptive node method or by applying symmetric version of the method called the symmetric collocation method.

Multiquadrics and thin-plate spline radial basis functions were used. Multiquadrics have a free-parameter and thin-plate spline has parameter-free feature. The accuracy of the multiquadric approximation is adjusted with the parameter called shape parameter. The MQ-RBF is purely geometric. But from the Table 1, the optimum shape parameter varies according to number of nodes and time step. For the linear advection-diffusion problem we obtain shape parameter optimization curves for specific time steps. The optimum shape parameter is determined for minumum RMS error. The shape parameter variations for different number of nodes and time differences are also tabulated. It can be observed that the RMS error and the solution accuracy of the problem are affected by those parameters. RMS error decreases when the number of nodes increase. But it does not mean there is less or more error difference in comparison with the thin-plate spline approximation, because it differs from one problem to another [31].

For the Multiquadric-RBF (MQ-RBF), the shape parameter effect is investigated and shape parameter optimization is shown using a curve for each problem. The optimum shape parameter "*c*" is determined considering the minumum Root Mean Square (RMS) error, and specified in the tables for the solution with different number of nodes and time step sizes. First to fourth order Thin-Plate Splines (TPS-RBF) are used. It is observed when number of nodes are increased, the RMS error decreases. Thin-Plate Splines are much more sensitive to collocation points or number of nodes on the domain.

It is observed that the thin-plate spline functions are more sensitive to the number of nodes. It does not include a free parameter like multiquadrics. But it shows stability in small time step sizes. The order of thin-plate splines are investigated from first order to fourth. When multiquadrics and thin-plate spline function approximations are compared, we can not attain an accurate judgement. For some solution of problems, MQ-RBF gives less error in comparison with the TPS-RBF solutions. To sum up, all observations and investigations done throughout the study, it can be infered that the meshless radial basis functions collocation method is quite easy to code and very convenient to implement both linear and nonlinear type of partial differential equations. In addition to all advantages of radial basis functions collocation method, the most important side is that this method is entirely information based method. With this method, you can easily find value of a function that you haven't assign an coefficient to be determined using interpolation property of approximation function. The advantage of being dimension independent and only being in conjuction with regular or irregular node distrubition may render the method possible to apply everywhere in science and engineering problems. The efficiency increases when the method is applied to high dimension of problems. I hope the method will become more widespread and popular in the following years with more possible investigations.

REFERENCES

[1] Jianyu, L., L. Siwei, Q. Yingjian and H. Yaping, "Numerical Solution of Elliptic Partial Differential Equation by Growing Radial Basis Function Neural Networks", Proceedings of the International Joint Conference on Neural Networks 2003, Vol.1, pp. 85-90, Northern Jiatong University, China, 2003

[2] Gomez, J.A.M., P.G. Casanova and G.G. Rodriguez ,"Domain Decomposition by Radial Basis Functions for Time Dependent Partial Differential Equations", Proceedings of the IASTED International Conference on Advances in Computer Science and Technology, pp.105-109, 2006

[3] CLi, J., C.S. Chen and D. Pepper, "Meshfree method for groundwater modeling", University of Nevada, USA

[4] Lui, Y., Z. Xin and M. Lu, "A meshless method based on least-squares approach for steady- and unsteady-state heat conduction problems", An International Journal of Computation and Methodology - Numerical Heat Transfer, Part B, Fundamentals, Vol. 47:3, pp. 257-275, Tsinghua University, 2005

[5] Chantasiriwan, S., "Multiquadric Collocation Method for Time-Dependent Heat Conduction Problems with Temperature-Dependent Thermal Properties", Journal of Heat Transfer, Vol. 129, No. 2, pp. 109-113, February 2007

[6] Boztosun, I., A. Charafi, M. Zerroukat and K. Djidjeli, "Thin-Plate Spline Radial Basis Function Scheme for Advection-Diffusion Problems", Electronic Journals of Boundary Elements ,Vol. Beteq , No.2, pp. 267-282, 2002

[7] Shu, C., H. Ding and K.S. Yeo, "Solution of partial differential equations by a global radial basis function-based differential quadrature method", Engineering Analysis with Boundary Elements, Vol. 28, No. 10, pp. 1217-26, Singapore, 2004

[8] Sarra, S.A., "Adaptive radial basis function methods for time dependent partial differential equations", Applied Numerical Mathematics, Vol. 54, No.1, pp. 79-94, June 2005, Marshall University, Huntington, 2004

[9] Williams, H.A. and E. Jensen, "Two-Dimensional Nonlinear Advection-Diffusion in a Model of Surfactant Spreading on a Thin Liquid Film", Journal of Applied Mathematics, Vol. 66, pp. 55-82, University of Cambridge, 2000

[10] Soroushian, A. and J. Farjoodi, "A unified starting procedure for the Houbolt method", Communications in Numerical Methods in Engineering, Vol.23, pp. 1-13, Iran, 2006

[11] Fasshauer, G.E., "Solving Partial Differential Equations by Collocation with Radial Basis Functions", Northwestern University, Evanston, 1996

[12] E.J. Kansa, "Multiquadrics - A Scattered Data Approximation Scheme with Applications to Computational Fluid-Dynamics - Solutions to Parabolic, Hyperbolic and Elliptic Partial Differential Equations", *Computers Math. Applic.*, Vol. 19, No. 8/9, pp. 147-161, 1990

[13] Heryudono, A. and T. Driscoll, "Adaptive Radial Basis Function Methods with Residual Subsampling Technique for Interpolation and Collocation Problems", Computers and Mathematics with Applications, Vol. 53, No. 6, pp. 927-939, March 2007

[14] Li, J. and C.S. Chen, "Some Observations on Unsymmetric Radial Basis Function Collocation Methods for Convection-Diffusion Problems", Vol. 57, pp. 1085-1094, University of Nevada, Las Vegas, USA, 2002

[15] Boztosun, I. and A. Charafi, "An Analysis of the Linear Advection-Diffusion Equation Using Mesh-Free and Mesh-Dependent Methods", Engineering Analysis with Boundary Elements, Vol.26, pp. 889-895, 2002

[16] Zerroukat, M., K. Djidjeli and A.Charafi, "Explicit and Implicit Meshless Methods for Linear Advection-Diffusion Type Partial Differential Equations", International Journal For Numerical Methods in Engineering, Vol. 48, pp. 19-35, U.K., 2000

[17] Thiffeault, J.L. ,"Advection–Diffusion in Lagrangian Coordinates", Physics Letters A, Vol. 309, No. 5-6, pp. 415-22, New York , 31 March 2003

[18] Chantasiriwan, S. , "Cartesian grid methods using radial basis functions for solving Poisson, Helmholtz, and diffusion–convection equations", Engineering Analysis with Boundary Elements, Vol. 28, No. 12, pp. 1417-1425, Thailand, 2004

[19] Hernandez, J.A., "High-order Finite Volume Schemes For the Advection-Diffusion Equations", International Journal For Numerical Methods in Engineering, Vol. 53, pp. 1211-1234, Madrid, Spain, 2001

[20] Lesnic, D., "The Decomposition Method for Cauchy Advection-Diffusion Problems", An International Journal of Computers and Mathematics with Applicaions, Vol. 49, pp. 525-537, University of Leeds, U.K., 2005

[21] Hon, Y.C. and W. Chen, "Boundary knot method for 2D and 3D Helmholtz and convection-diffusion problems under complicated geometry", City University of Hong Kong, China

[22] Xin, L., "Radial point collocation method (RPCM) for solving convection-diffusion problems", *Journal of Zhejiang University Science A*, Vol. 6, pp. 1061-1067, Zhejiang University, China, 2006

[23] Heryudono, A. and T. Driscoll, "Adaptive Radial Basis Function Methods with Residual Subsampling Technique for Interpolation and Collocation Problems", Computers and Mathematics with Applications, Vol. 53, No. 6, pp. 927-939, March 2007

[24] E.J. Kansa, "Multiquadrics - A Scattered Data Approximation Scheme with Applications to Computational Fluid-Dynamics - Solutions to Parabolic, Hyperbolic and Elliptic Partial Differential Equations", *Computers Math. Applic.*, Vol. 19, No. 8/9, pp. 147-161, 1990

[25] Larsson, E. and Fornberg, B., "A Numerical Study of some Radial Basis Function based Solution Methods for Elliptic PDEs", Uppsala University, Sweeden, 2003

[26] Börekçi ,O., The Radial Basis Function Collocation Method: A Meshless Method for the Solution of Boundary Value Problems, Department of Civil Engineering, Lecture notes, Boğaziçi University, 2005

[27] R.L. Hardy, "Multiquadric equations of topography and other irregular surfaces", *Journal of Geophys. Res.*, Vol. 76, pp. 1905-1915, 1971

[28] Hornberger and Wiberg, "Numerical Methods for Solving First-Order Ordinary Differential Equations", notes, Numerical Methods in the Hydrological Sciences, 2005

[29] Li,C., Y.Chen and D. Pepper, "Radial Basis Function Method for 1-D and 2-D Groundwater Contaminant Transport Modelling", Computational Mechanics, Vol. 32, pp. 10-15, Las Vegas, USA, 2003

[30] Doa, C. and F.T. Pinho, "Fully-Developed Pipe and Planar Flows of Multimode Viscoelastic Fluids", *J. Non-Newtonian Fluid Mech.*, Vol. 141, pp. 85–98, 2006

[31] Tuncay, Y., "Application of Radial Basis Functions Method to Advection-Diffusion and Viscoelastic Flow Problems", M.Sc. Thesis, Boğaziçi University, 2009

INVESTIGATION OF BIOMIMICRY APPROACHES ON DESIGN OF ENERGY HARVESTING DEVICES FROM WATER MOTION

Arş. Gör. Dr. ERMAN ÇELİK [1]

[1] Fırat Üniversitesi, Teknoloji Fakültesi, 0000-0002-4254-9611

ABSTRACT

Due to the negative effects of fossil fuels on the environment, the interest in energy conversion methods without carbon emission and the number of studies on increasing their efficiency have increased considerably. The method of obtaining energy from liquid fluid movements and potential is one of the energy conversion methods with high capacity and reliability without carbon emission. Biomimicry is used to make energy harvesting methods from liquid motion and potential, the most widely known of which is water turbines, more efficient. In its most general form, biomimicry can be defined as the process of applying the technical advantages of the limbs and structures found in biological structures in nature to systems by imitating their forms in engineering applications. In this study, improvements made by biomimicry method are discussed in order to increase the performance of systems that convert energy from liquid fluid motions. The improvements made are classified according to parameters such as the basis of the applied biomimicry approach, the type of conversion system applied and the final output of the biomimicry on the system. As a result of the study, it was seen that the source of biomimicry applied to systems that convert fluid motion and potential into energy, contrary to expectations, is based not only on creatures living in water, but also on creatures living on land. It has been found that airborne plant seeds are also used as a source of biomimicry.

Keywords: Biomimicry, Hydraulic Turbines, Wave Energy,

INTRODUCTION

The industrialization rate of the world has been increased excessively with developed technology and growth of the population. For this reason, the need for energy, which is the most important building block needed for the development and industrialization of civilizations, has increased in an extraordinary way. The consumption of fossil fuel fuels of which the most widely used ones like coal, oil and natural gas increased producing harmful impacts on nature [1], [2]. Carbon Dioxide, 77% of which is produced as product of fossil fuel combustion and 23% of which arises from deforestation, is seen to be increased its existence in atmosphere almost 30%. This means mean temperature of earth got higher by 1 to 5 ℃ causing climate change and affecting negatively living species and populations[3] . From this point of view, the need for renewable energy sources has increased due to both the limited available resources and the increasing need for cleaner energy sources.

Renewable energy sources come in a wide variety of types like hydropower, modern biomass, geothermal, solar, direct solar, wind, wave and tidal energy[4]. Although renewable energy resources are clean, reliable and they are found widely distributed in nature, it is still necessary to be developed new devices to harvest energy comes from nature in such a way with less investment costs, long lasting operability and higher capability of energy capturing specification. Biomimicry or bioinspiration is one of the emerging approaches to develop energy harvesting devices. Although these two words have slightly different scope like biomimicry stands for directly mimicking nature to systems on the other hand biosimilarity considers function and evaluation of reference object while mimicking, they are widely used almost same meaning. Although bioinspiration based designs are not exact solutions for technical challenges even having new disadvantageous specifications, they promise significant gains after some optimization and improvement studies [5] [6]. Thus the interest on bioinspired designs taking great interest in present [7].

In this study biomimicry approaches applied on energy harvesting devices from water motion will be evaluated in terms of biomimicry approach, type of energy conversion system and final output of biomimicry. Methods of energy harvesting from water potential and motion are grouped under three titles as Hydroelectric turbines, wave energy converters and tidal stream power capturers in the study.

BIOMIMICRY ON HYDROELECTRIC TURBINES

Humpback whale fins have become an important bioreference in hydrodynamic performance improvement studies. It is thought that the fin structures of whales are specialized to provide the maneuvering abilities they need for hunting styles. Examined as 2.5 cm thick sections from 71 points, the whale fin was found to have a bluntly rounded leading edge and a highly conical trailing edge which offers the whale high lift and provides fast maneuverability [8]. Thanks to the tubercles located on the fin leading edge, more stable turbulence parameters and balanced force distributions are obtained, and it has been reported that more balanced structures with lift and drag forces can be obtained by such a bioinspiration approach. Structure of a whale fin with tubercles is given in Figure 1a. Lately the performance of a novel hydrofoil with wavy leading edge protuberances has been investigated numerically by Li et. al. As a result of the numerical analysis, a hydrofoil with protrusions similar to tubercles in whale fins offsets the separation surface, reducing cavitation and balancing the force distributions on the hydrofoil. It is understood that Streamwise vorticities generated by protrusions on leading edge are the most effective actor in the suppressed cavitation and transmission of force to the hydrofoil surface [9].

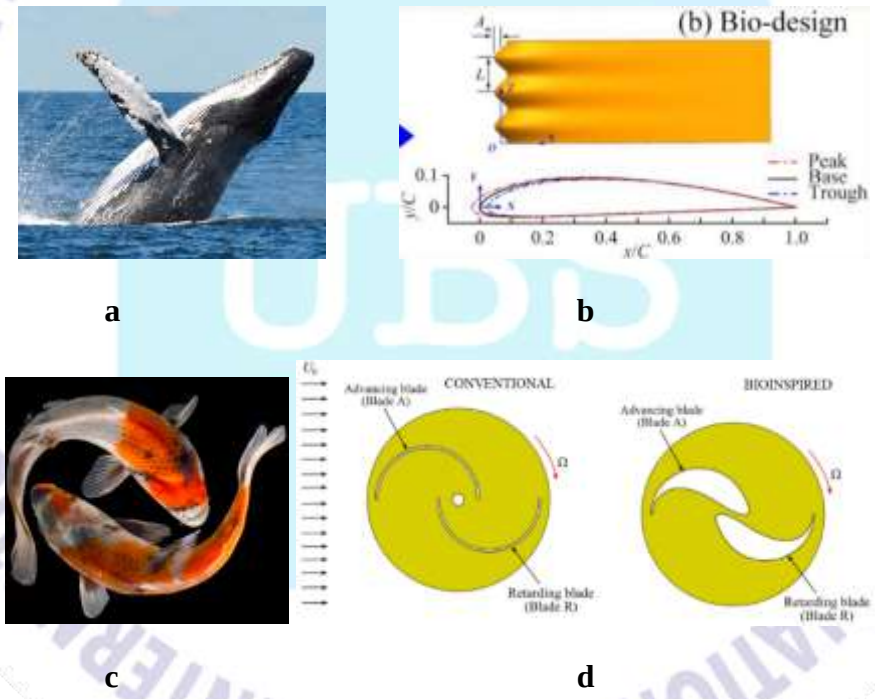

Figure 1. Whale fin tubercles (a)(National Geographics Society), hydrofoil with protrusions similar to tubercles in whale fins by Li et. al. (b) couple of swimming Koi Fish (c) and biomimic Savonius Type hydrokinetic turbine by Hashem et.al. (d).

Savonius turbines are designed to be operated in streaming water in nature which has low speeds of flow. Torque has been generated based on drag. Savonius turbines have resistant and plain design architecture however, their efficiencies below average and under effect of highly fluctuant static torque make them needed to be much more developed. Hashem et. al. intended to develop a

novel biomimic Savonius hydrokinetic turbine inspiring from a couple of Koi fish swimming synchronic. The distance between two blades is defined using overlap and gap ratios as design parameters. After optimizations performed in the study the highest power coefficient is reported to be achieved at overlap ratio of 0.2085 and gap ratio of 0.0057. The biomimic design is reported to be operated 0.2521 power coefficient at maximum. This value means overall performance is 17.6% higher than conventional Savonius turbines. As result of the study the biomimic design would be an appropriate candidate for performance enhancement[10].

WAVE ENERGY CONVERTERS

Present WEC devices are needed to be developed to recess their high costs, increase energy conversion efficiency and heal their lifetime and reliability. At this point, the importance of biosimilarity approaches emerges.

The smoot sway motion of kelp plant under sea water attracted the attention of many scientists to devise a wave energy converter. Wang et. al. designed a Triboelectric Nanogenerator (TENG) wave energy converter mimicking kelp plant as shown in Figure 2a. A fundamental TENG consists of kelp leaf like triboelectric electrode layers as arrays and a shell around them. A power unit consists of each pair of a plurality of strips. Each strips are connected to a vertical base from its one end standing vertically and the other end of the strip is free thus they can vibrate freely like swaying kelp plant. The design in the form of a kelp plant gives the device the ability to oscillate with smooth movements even at very small frequencies. Numerous biomimic TENG units are possible to be connected each other to generate energy in larger amounts as seen in Figure 2a covering a larger energy harvesting area [11]. Kelp plant has also been a source of inspiration for Bio Power company in the development of O-Drive wave energy capture module. Main operating principal of the device is capturing wave motion by sway motion to compress gas with pistons thus generating high energy potential. The design is eligible to be positioned parallel to sea ground during harsh air conditions for safety. As seen from Figure 2 b the device is fixed to ground of sea. Upper part of the device is connected to ground part to swing with wave motion [12].

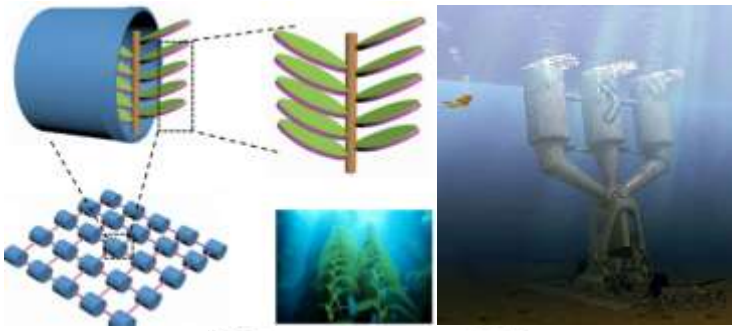

a b

c

Figure 2. Kelp inspired TENG unit and network diagram with a kelp plant under sea ground (a) O-Drive converter by BPS company (b) Oyster type energy harvesting device.

Oyster type wave energy converters are designed mimicking motion of oysters living in the ocean for a nearshore energy solution. The device pierces water free surface to harvest energy as a flap type device as shown in Figure 2 c. This device pressurizes the water to move it to a higher location, increasing the hydroelectric potential of the water[13].

TIDAL STREAM POWER CAPTURERS

The morphology of seeds, which have the ability to fly long distances in nature and provide a wide breeding and scattering area for the plant, has attracted the attention of scientists. Dryobalanops Aromatica seed is one of the biological structures which has attracted the attention of researchers as a source of bio similarity. Its convenience to marine current turbine has been evaluated in terms of hydrodynamic performance and wake properties via CFD tools by Chu et.al. [14]. As result of the study, Dryobalanops Aromatica seed based biomimetic turbine is capable of generating 1110% higher torque than a standard turbine investigated by Bahaj et al. and has 10,6% shorter recovery length respect to conventional IFREMER-LOMC turbine. Considering Dryobalanops Aromatica seed based biomimetic turbine is determined to be more environment friendly having high power

coefficient while operating at lower tip speed ratios thus reducing collision deformation risks on blades. The biomimicry modelled turbine is defined to produced 13.24% higher thrust at its optimum Tip Speed Ratio (TSR) 1.5 than the turbine proposes by Bahaj et. al. which has optimum TSR=6.

CONCLUSION

In the field of renewable energy, energy production based on water movements is important. Especially when designing wave energy converter devices, the biomimicry approach is more common. Although biological structures on land are also encountered as a source of biomimicry, it has been observed that biomimicry is made mostly by being inspired by sea creatures. While performing biomimicry, only the hydrodynamic designs of the biostructures that were referenced were not focused on. The natural movements of living things have also been a source of biomimicry. As in many areas, it has been seen that biomimicry is promising in the field of energy harvesting from water movements.

REFERENCES

[1] W. Li, X. Yu, N. Hu, F. Huang, J. Wang, and Q. Peng, "Study on the relationship between fossil energy consumption and carbon emission in Sichuan Province," *Energy Reports*, vol. 8, pp. 53–62, 2022, doi: 10.1016/j.egyr.2022.01.112.

[2] W. Lu, C. Chen, M. Su, B. Chen, Y. Cai, and T. Xing, "Urban energy consumption and related carbon emission estimation: a study at the sector scale," *Front. Earth Sci.*, vol. 7, no. 4, pp. 480–486, 2013, doi: 10.1007/s11707-013-0363-1.

[3] N. K. M. A. Alrikabi, "Renewable Energy Types," *J. Clean Energy Technol.*, vol. 2, no. 1, pp. 61–64, 2014, doi: 10.7763/jocet.2014.v2.92.

[4] N. L. Panwar, S. C. Kaushik, and S. Kothari, "Role of renewable energy sources in environmental protection: A review," *Renew. Sustain. Energy Rev.*, vol. 15, no. 3, pp. 1513–1524, 2011, doi: 10.1016/j.rser.2010.11.037.

[5] N. K. Katiyar, G. Goel, S. Hawi, and S. Goel, "Nature-inspired materials: Emerging trends and prospects," *NPG Asia Mater.*, vol. 13, no. 1, 2021, doi: 10.1038/s41427-021-00322-y.

[6] A. du Plessis *et al.*, "Beautiful and Functional: A Review of Biomimetic Design in Additive Manufacturing," *Addit. Manuf.*, vol. 27, no. March, pp. 408–427, 2019, doi: 10.1016/j.addma.2019.03.033.

[7] H. Zhang and G. A. Aggidis, "Nature rules hidden in the biomimetic wave energy converters," *Renew. Sustain. Energy Rev.*, vol. 97, no. August, pp. 28–37, 2018, doi: 10.1016/j.rser.2018.08.018.

[8] F. E. Fish and J. M. Battle, "Hydrodynamic design of the humpback whale flipper," *J. Morphol.*, vol. 225, no. 1, pp. 51–60, 1995.

[9] J. Li, C. Liu, and X. Li, "Effects of wavy leading-edge protuberance on hydrofoil performance and its flow mechanism," *J. Mar. Sci. Eng.*, vol. 9, no. 10, 2021, doi: 10.3390/jmse9101138.

[10] I. Hashem and B. Zhu, "Metamodeling-based parametric optimization of a bio-inspired Savonius-type hydrokinetic turbine," *Renew. Energy*, vol. 180, pp. 560–576, 2021, doi: 10.1016/j.renene.2021.08.087.

[11] N. Wang *et al.*, "Kelp-inspired biomimetic triboelectric nanogenerator boosts wave energy harvesting," *Nano Energy*, vol. 55, no. October 2018, pp. 541–547, 2019, doi: 10.1016/j.nanoen.2018.11.006.

[12] Y. Zhang, Y. Zhao, W. Sun, and J. Li, "Ocean wave energy converters: Technical principle, device realization, and performance evaluation," *Renew. Sustain. Energy Rev.*, vol. 141, no. September 2020, p. 110764, 2021, doi: 10.1016/j.rser.2021.110764.

[13] E. Renzi, K. Doherty, A. Henry, and F. Dias, "How does Oyster work? the simple interpretation of Oyster mathematics," *Eur. J. Mech. B/Fluids*, vol. 47, no. April, pp. 124–131, 2014, doi: 10.1016/j.euromechflu.2014.03.007.

[14] Y. J. Chu, "A new biomimicry marine current turbine: Study of hydrodynamic performance and wake using software OpenFOAM," *J. Hydrodyn.*, vol. 28, no. 1, pp. 125–141, 2016, doi: 10.1016/S1001-6058(16)60614-5.

Challenge of Matrix-Light Technology on Automotive Exterior Lighting

Orhan Uras KURTULUŞ [1]

[1] RENAULT GROUP, ORCID 0000-0001-8183-6376

1. ABSTRACT

Recently, Matrix-light technology which involve many single micro (µLED) or mini LEDs which could be run independently from each other in order illuminate particular regions on the road as well dimming specification according to determination and behaviour of objects around enviroment the vehicle. This technology needs to be considered within some functions such as environment signalling, enviroment communication, curve illumination and sensor intellegence. Matrix-LED illumination technology is used headlight which indicate high beam and low beam distribution as well taillight for reflect any kind of warning patterns on scope of the road communication. Matrix-LED system and its development will become more challenging in hardware and software. Modern LEDs enable to be hold out longer than the operating time of the vehicle. Furthermore, their have long lifetime and high-quality production capability assure long service life. In this paper, it is examined most recent micro and mini LEDs which are convenient to integrate both headlight and taillight of the vehicle for ensure matrix-light purpose within application instances which comprise any kind of luxury class models of OEM.

Keywords: Automotive Lighting, Matrix LED, Adaptive Driving Beam

2. INTRODUCTION

Matrix-LED comprise majority of micro or mini LEDs collected in a joint module. Each of LEDs has particular running algorithm which indicate driving circuit for variable control of illumination intensity and on/off switching. Usage of lenses and reflectors enables the LED based module to ensure a huge number of illumination variations in optical distribution without the need for any pivoting mechanism. Thus, Matrix-LED technology splits up the previously one-spot high beam into multiple sub-beams that can be independently controlled. High power LEDs deliver high efficiency and high flux density that enable tight beam control as well as exceptional high luminance, making these individually produced beams equally as powerful as the one-spot halogen beam [1].

3.AUTOMOTIVE LATEST LED TECHNOLOGY

In fact, LED based lighting systems are starting to be a remarkable key role regarding their design in the vehicles. To make full use of distinctive characteristics such as small size and digital controllable device, LEDs are developing new designs of lamps or lighting systems, which have been unrealized by conventional technology [2]. Regarding Matrix-LED systems, arrays of top or side emitting LEDs with LED size down to 0.3 mm, providing monochrome, white or even multicolor (RGB) light with high luminance. Micro-LEDs with size less than 0.3mm, either produced by monolithic fabrication remaning on their original waver or transferred to a receive

substrate, e.g. via laser lift-off or another mass transfer process [3]. Beside, white LEDs are being adopted for wide applications such as general lightings, displays, mobile phones, etc. Comparing much higher efficiency and energy saving compared to traditional technology like incandescent lamps or halogen lamps [2]. Most recent micro and mini LEDs from LED manufacturers;

The TOPLED E1608 which is illustrated in Fig. 1, expands ams OSRAMs low power portfolio by offering one of the smallest LED industry standard footprints in a highly reliable and well proved package concept. Its outstanding performance is suitable for a huge variety of applications especially automotive interior where a small package design with excellent reliability is needed. The TOPLED E1608 is available in a broad variety of colors and brightness versions. Its features are specified below [4].

- White pre-mold top looker package with reflector
- Low profile 0.6mm
- Dimension 1.6mm x 0.8mm
- Availability of full color spectrum and brightness range
- 3 different colors

Fig. 1: TOPLED E1608

This kind of LED component for headlights, taillights, turn indicators and center-mounted stop lights enable to design most convenient illumination system which also illustrated as a instance in Fig. 2 and Fig. 3, as well communication patterns with other vehicle, pedestrian and cyclists. The future of the automotive exterior goes way beyond simple illumination. To fulfil the require-ments of higher levels of autonomous driving innovative solutions are needed that significantly enhance safety in road traffic. »Car-2-X«-communication is one of the crucial cornerstones to meet this ambition. Via visual codes on displays (e.g. rear combination lights, RCL) messages and symbols can be personalized and transmitted more clearly, thus enabling efficient communication between road participants and vehicles [4,5].

Fig. 2: Dynamic rear functions for a variety of styles [5]

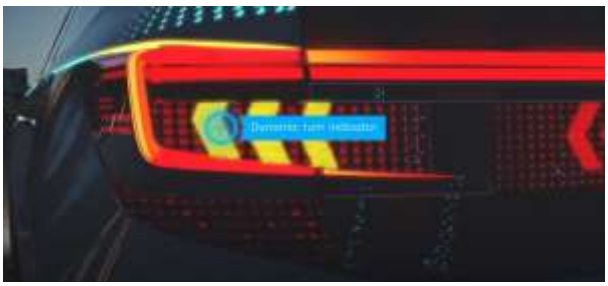

Fig. 3: Dynamic turn indicators for various styles [5]

Samsung is also other LED manufacturer, has PixCell LED and mini LED which are meet requirements of automotive regulation and homologation obligatory. The PixCell LED uses sharp precision to deliver enhanced visibility for safer driving at night and in poor weather conditions. sing leading semiconductor technology, PixCell LED sets silicon walls between each of its pixels to create a superior contrast ratio that minimizes glare from oncoming and preceding traffic. Headlamps with PixCell LED can selectively distinguish areas on the road that need to be lit or kept dim, helping drivers navigate tough road conditions which is illustrated as a instance in Fig. 4. PixCell LED's LES is 1/16 the size of a traditional LES, significantly reducing optic system volume, is illlustred in Fig. 5. Its compact size creates slimmer, lighter, and energy-efficient lamps for modern and stylish vehicles. With 100 individually addressable pixels, PixCell LED complies with diverse global regulations and can be applied to headlamps in various countries at lower cost, using minimal software adjustments for desired beam patterns.

The PixCell LED module can be used in low-beam, high-beam, and ADB lighting for different headlamps [6]. Of course, the price is flexible depending on the both of demanding design. Finally, this technology can be appliedd to the entire external lighting as well single LED solution will be a unique and representative solution to the vehicle's next generation lighting field [7].

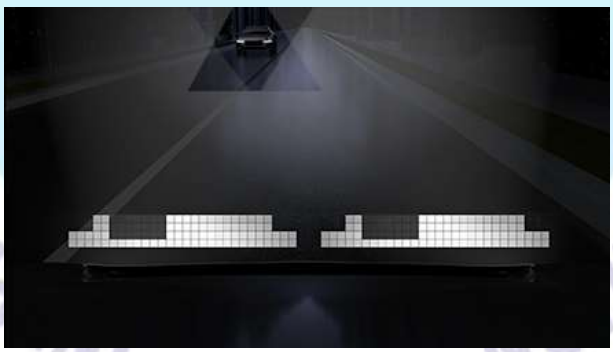

Fig. 4: Various illumination functions according to road conditionals [6]

Fig. 5: Compact PixCell LED module [6]

4. MATRIX LIGHT OVERVIEW

In front lighting regulation world the Matrix technology is usually defined together with Adaptive Driving Beam (ADB) applications. ADB mostly means the mechanical movement of a vertical cut off in a high beam projector module [8]. Furthermore, ADB system comprises independently programmable and switchable LEDs which works with an electronic control unit (ECU) simultaneously which also collect datas from sensors according to traffic actions and enables to ensure communication between sensors and ADB system in order to determine working behavior and function of illumination. Matrix based ADB system is used most generally on driving visibility at night circumstances. It is also most significant point that light does not need to blind eyes of driver of oncoming vehicle as well front vehicle.

How Matrix Systems Work

Conventional ADB headlights react only to vehicle's driving status such as the wheel rotation speed, yaw (motion along the vehicle's vertical axis), and movement of steering wheel. Matrix LED systems take a leap forward with its ability to interact with driving environment via the car's onboard camera system in which an imaging sensor monitors the road environment in front of the vehicle. It is illustrated as instance Fig. 6 and Fig.7 [1].

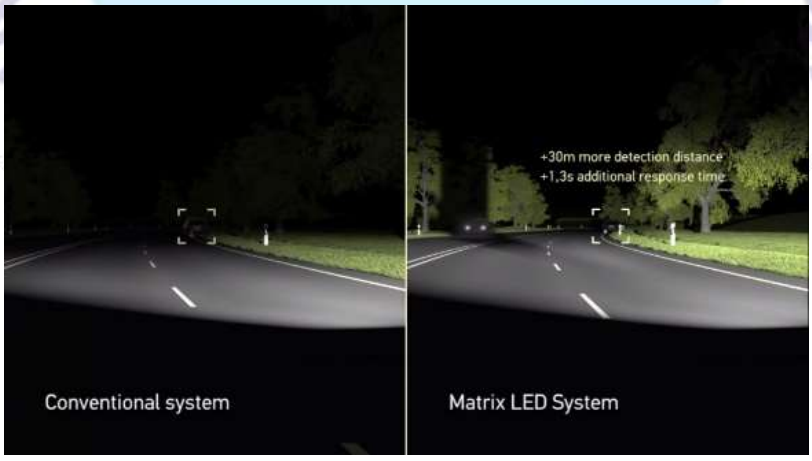

Fig. 6: Comparation of Conventional and Matrix LED for any object on the road [1]

Fig. 7: Comparation of Conventional and Matrix LED for oncoming vehicle [1]

Camera which is sensitive to visible and near infrared light is equipped front bumper of vehice or behind interior rear view mirror structure which is connected within front window in order to detect behaviour of objects on the traffic and road. Except of the camera, some of OEM prefer to integrate other kind of detection systems such as lidar, radar or ultrasonic sensors. Data collected by the camera are interpreted by the ECU which then sends directions to the control circuitry regulating the light output of each LED engine. Upon detection of an object in front of the vehicle, the adaptive lighting system will mask out the oncoming vehicle by dimming or switching off LED engines that produce distracting glare while other LED engines of the high beam light (which is illustrated in Fig. 8 and Fig. 9) continue to illuminate everywhere else on the road. When driving in curves, the high beam LEDs of the matrix headlight will shift the focal point of the light along the curve and illuminate the side of the road more than the road itself. Computer vision can extract the road lane information, which can help improve the precision of adaptive lighting. Additionally, integration with GPS makes it possible to perform predictive headlight control [1].

Fig. 8: Individually controllable and dimmable LED engines [12]

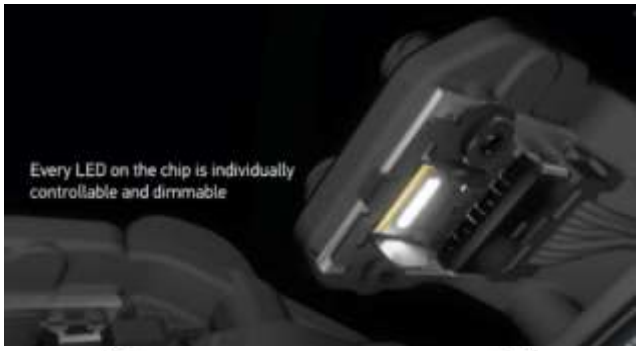

Fig. 9: LED engine [12]

While keeping its overall look intact, the 2022 Renault Samsung SM6 has upgraded safety and convenience features such as LED matrix vision headlamps in all of its trims. The LED matrix vision headlamps are smart headlamps that can automatically adjust their brightness using 18 LEDs on each side depending on traffic conditions, preventing glare for oncoming drivers [9]. Also new depending on the equipment, are Renault Espace of the adaptive LED matrix headlights (is illustrated in Fig. 10), which automatically adjust the illumination of the road to the traffic situation (is illustrated in Fig. 11). The light output is said to have increased by 50 percent. The maximum headlight range increases from 175 to 220 meters [10].

Fig. 10: Renault Espace of the adaptive LED matrix headlights [11]

Fig. 11: Automatically adjust the illumination of the road to the traffic situation [11]

5. SUMMARY

Matrix applications will offer better sustainability for future digitalization, situation dependent system reactions and dynamic effects. With headlight and taillight, also applied to interior lighting will allow more OEM oriented functionalities and performance where needed by driving situation and visibility tasks. Digitalization in lighting is sponsored by Matrix functions. In future applications, also segmentation will give the chance to either generate different patterns or combination of segments, or to attract the following driver's attention to the activated function, in fact taillighting. Beside, In interior lighting World the idea of Matrix technology was completely unknown. The individual switching of segments in interior lighting was not linked to a visual performance improvement in interior illumination. With the implementation of an interior lighting Matrix, the luminance area can be shifted according to the needs of the passenger. Dynamic glare avoidance for headlight, dynamic sequencing for taillight and dynamic adaption to the visual taks for interior lighting are only possible with Matrix systems. Driving force is to improve lighting and comfort for the user. Matrix systems are the enabler of Dynamics and thus the enabler of Digitalization. Future applications that improve the lighting functionality, visibility and communication by the help of lighting functions can now be invented with the quasi unlimited possibilities of Matrix systems [8].

6. REFERENCES

[1] https://www.manufacturer.lighting/info/1162/
[2] K. Bando: New Generation LEDs and LD for Automotive Lighting, ISAL, 2017
[3] M. Kleinkes, W. Pohlmann, C. Wilks, all HELLA GmbH & Co. KGaA: Boost Safety & Styling – New HD LED Systems for front and rear, ISAL, 2019
[4] https://www.osram.com/os/applications/automotive-applications/interior_functional_illumination.jsp
[5] https://www.osram.com/os/applications/automotive-applications/automotive_extrior_applications.jsp
[6] https://www.samsung.com/led/automotive-modules/pixcell-led/
[7] Jonghun Lee, G. Ko, Junho. Lee, Samsung Electronics, Republic of Korea: Implementation of Pixel Technology for Automotive Lighting System based on Wafer-Level Process, ISAL, 2019
[8] M. Hamm: Matrix is Everywhere: Front, Rear and Interior Lighting goes Digital, ISAL, 2017
[9] Kim So-hyun: Renault Samsung SM6 upgrades safety, convenience features, The Korea Herhald, Feb 23, 2022
[10] https://topgear-autoguide.com/category/Van/Renault-espace-facelift-led-matrix-light-and-new-assistans1607833203
[11] https://www.netcarshow.com/renault/2020-espace/
[12] https://www.youtube.com/watch?v=xYSiX5r38qY

DELIVERY OPERATIONS IN WAREHOUSES BY ULTRACAPACITOR POWERED DRONES

Furkan YANIK [1], Dr. Ali Rıfat BOYNUEĞRİ [2], Dr. Yavuz EREN [3]

[1] Yıldız Teknik Üniversitesi, 0000-0001-8473-4578

[2] Yıldız Teknik Üniversitesi, 0000-0003-4734-3126

[3] Yıldız Teknik Üniversitesi, 0000-0001-9128-2856

Abstract- In recent years, it has become an important target for companies to reduce the fixed costs (number of workers, number of vehicles, etc.) on each level of the production process as well as storing the products. In this manner, the autonomous drones operating in closed warehouses have been often addressed. They provide an alternative solution to the storage problem in terms of effort, time spent, and occupational safety thanks to their good throughput and ease of access in confined locations. In this study, a practical delivery algorithm in a closed warehouse has been presented to achieve assigned duties to carry the payload to the storage positions by utilizing the autonomous operated drones. The drone fleets have been respectively equipped with lithium-ion battery and ultracapacitors (UCs) and each case have been simulated to reveal the merits of the procedure. For the test, we have randomly assigned 7200 payload items subjected to the delivery process and the matching among the drones and payloads have been realized by the proposed procedure. The simulation studies have been realized in Matlab® and the results are examined. The results show that the drone fleet powered by the UCs reveals excellent performance than the fleet powered by batteries in terms of delivery time and long-term operational costs.

Keyword: Drone, ultracapacitor, delivery by drones.

1. INTRODUCTION

In the last few decades, unmanned aerial vehicles (UAVs) have been recently referenced in many practical applications [1][2][3]. The main reasons for this trend are based on the special abilities of the UAVs such as hovering, passing through narrow places, endurance in rough terrains and the speed for the product delivery. Those features allow the widespread use of drones, especially in commercial and military fields [4].

Although UAVs are used in many applications, they have some problems in the power management system [5]. The basis of these problems is the Lithium-ion battery systems of the drones [6]. Lithium-ion batteries are frequently used as power units of UAVs due to their high energy density and relatively lower costs in recent years [7]. However, they have some disadvantages such as requiring long charging times, relatively limited charging capacity, and safety problems due to overheating [8]. For those reasons, ultracapacitors (UCs) become prominent alternatives for the UAVs operating in medium and long-distance missions. Hence, UCs are proposed for the energy supplier system for the drones operated in a closed warehouse [9][10][11].

With the recent developments, UCs have become more suitable for the mentioned missions because they have shorter charging times and they have over one million charge-discharge cycles compared to the batteries. However, UCs have relatively lower energy density compared to the batteries [12], which limits the operation range of the drones. For compensation the inadequate energy density of UCs, some efficient algorithmic procedures may be carried out for the short-term mission flights of the drones. In this study, it is aimed to match best pair among the drone set and flight missions. Therefore, it is planned to get maximum efficiency from the drone by avoiding the longer charging time which reduces the period of utilization. The proposed method has been tested in the simulation environment and the performance has been revealed.

The rest of the manuscript is given as follows. Chapter 2 includes the system description. Chapter 3 gives the simulation studies. Chapter 4 provides results and comments.

2. DYNAMICS OF THE DRONES

In this section, it is presented mathematical models of drones. The basic forces acting on a drone is given by Figure 1. Figure 1.a (Figure 1.b) illustrates the forces induced on the drone when it moves vertically (horizontality) with a constant velocity of $V_v(V_v)$ .F_w is the force by the gravity, and F_{DH}, and F_{DV} are the forces arising by the disruption of airflow in horizontal and vertical directions, respectively. Besides, F_t is the generated force by the propellers of the drone which is the input force of the system to control the direction and velocity of the drone. The mathematical formulation of the forces F_w, F_{DH}, and F_{DV} are stated in (1), (2), and (3), respectively.

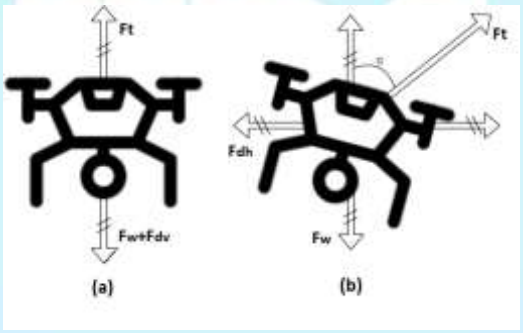

Figure 1. The forces acting on the drone

$$F_w = (m_d + m_p)g \quad (1)$$

$$F_{DV} = \frac{1}{2}\rho A_t C_d v_v^2 \quad (2)$$

$$F_{DH} = \frac{1}{2}\rho A_f C_d v_h^2 \quad (3)$$

where, m_d and m_p are the mass and payload of the drone, respectively. The gravity acceleration is denoted by g. A_f and A_t are the horizontal and vertical cross-sectional areas, C_d is the drag

coefficient, and ρ is the air density. Besides, the force providing the vertical movement ($F_{T,v}$) of the drone is calculated by (4). On the other hand, the calculation of the force required for horizontal movement ($F_{T,h}$) is given in (5).

$$F_{T,v} = F_w + F_{DV} = (m_d + m_p)g + \frac{1}{2}\rho A_t C_d v_v^2 \quad (4)$$

$$F_{T,h} = \sqrt{{F_w}^2 + {F_{DH}}^2} = \sqrt{((m_d + m_p)g)^2 + (\frac{1}{2}\rho A_t C_d v_v^2)^2} \quad (5)$$

The thrust force (F_T) formulated by (6) is generated by the induced air going through the revolving propeller.

$$F_T = 2\rho A_p v_i^2 \quad (6)$$

where, A_p is the disk area of the propellers and v_i is the induced airflow rate. In addition, the relationship between power consumption and control force is expressed by (7).

$$P_T = F_T vi = \sqrt{\frac{(mg)^3}{2\pi\rho r^2}} \quad (7)$$

Considering the hovering mode of the drone flight, the parameters are specified to run the dynamic equations of the drone. The weight of the drone (m) is 865g and the weight of the UC is 510g. Besides, ρ, r and g are 1.225 kg/m^3, 230 mm and 9.796 ms^{-2}, respectively. Note that, the gravitational force and air density do not change at the altitude considered as they are taken as constant. Those parameters specify the energy consumption of the drone as well as the flight records of the drone.

Besides, due to the efficiencies of motor angular velocity and torque, the power consumed by actual motors differs from the power obtained by the dynamics. In this context, it is possible to estimate more accurate power by measuring the angular velocity of the motor. The higher the angular velocity, the greater the amount of air passing through the propellers. In this way, F_T can be formulated in terms of the motor angular velocity given in (8).

$$F_T = \frac{1}{2}N\rho A_p C_t (wr)^2 \quad (8)$$

where N is the number of rotors, ω is the angular velocity of the rotors, C_t is the thrust coefficient, and r is the radius of the propellers. Typically, the thrust coefficient (C_t) is set between 0.01 and 0.05 [9]. Hence, the required thrust for a certain flight route is calculated by (1) - (5). Also, the

angular speed which defines the upper and lower limits of the maximum load capacity and horizontal speed is generated by (7).

Energy dissipated by the drone can be calculated by considering the flight modes [13]. Those modes are described as idle, armed-idle, take-off, hover, payload carrier, vertically flying up, horizontally flying, and vertically down flying. Energy equations for those modes are given in Table 1. t_1 and t_2 are the consumed time in idle loaded mode and armed mode, respectively. t_3 and t_4 are the corresponding time expanded in the air and the period of the horizontal flight. V is the speed of the drone. The flight altitude of the aircraft and the altitude of the landing slot are represented by H_1 and H_2, respectively. The payload carried by the drone is L. Finally, D is the distance the drone travels on the horizontal route.

Operation Mode	Energy Equation
Idle mode	$E_{IM} = 8.195 * t_1 - 0.087$
Armed mode	$E_{AM} = 29.027 * t_2 - 0.087$
Taking-off	$E_{TOM} = 0.432 * V^2 + 3.786 * V - 1.224$
Hovering	$E_{HM} = (4.917 * H_1 + 275.204) * t_3$
Flying horizontally	$E_{FHM} = 308.709 * t_4 - 0.852$
Flying vertically upward	$E_{FVUM} = 315 * D - 211.261$
Flying vertically downward	$E_{FVDM} = 68.956 * H_2 - 65.183$
Payload	$E_{PM} = 0.311 * \mathrm{L} + 1.735$

Tablo 1. Energy consumption equations for operation modes of the drone [14].

In this study, we assume that the drones do not operate at the idle mode. Hence, the total energy for any drone is calculated by the sum of the other mode-based functions given in (9).

$$E(t_2, t_3, t_4, D, L, H_1, H_2, V) = E_{AM}(t_2) + E_{TOM}(V) + E_{HM}(t_3, H_1) + E_{FHM}(t_4) + E_{FVUM}(D) + E_{FVDM}(H_2) + E_{PM}(L)$$

3. PROPOSED PROCEDURE AND SIMULATION STUDIES

In this section, the corresponding matchings between the payload and the drones have been simulated by the proposed technique. The two-dimensional diagram of the warehouse is shown in Figure 2. The warehouse is a closed environment, and the drone fleet includes two drones. The distances between shelves, distribution points and strips are also detailed in Figure 2. The payload

delivery process is realized from the storage area on the shelves to the delivery points. In this manner, the proper tasks are assigned to the drones by the proposed procedure.

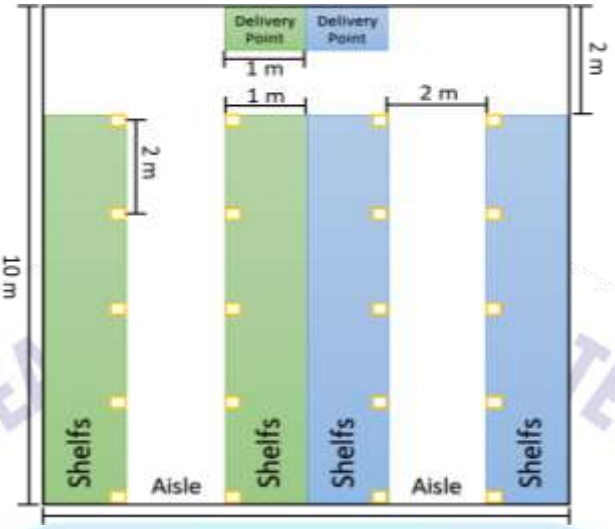

Figure 2. Warehouse Scheme

Indoor drones are gaining increasing popularity due to their delivery time and high manoeuvrability. Besides, the biggest problems of those drones are the long charging times. The charging time of standard Lithium-ion batteries used in the drones requires at least nearly threefold time of charging than the flight time. In order to solve this problem, many studies on fast charging and wireless charging applications are carried out [17][18]. However, those methods either involve very complex processes or require relatively higher cost. In this study, an alternative configuration is proposed for the operation of indoor unmanned aerial vehicles. We introduce a structural change to increase the flight/charge time ratio of drones by preferring ultracapacitors instead of lithium-ion batteries as energy storage unit. Hence, the charging times of drones have become incomparably shorter than standard lithium-ion batteries. Moreover, ultracapacitors have over a million charge-discharge cycles due to the advantage of their physical structures [19].

In this paper, we presented a feasible drone operating algorithm for delivering the payloads in a closed warehouse. In the warehouse environment, two autonomous drones are planned to carry random delivery requests. During the operation, it is guaranteed that the drones do not exceed the capacity as well as they do not collide each other by assigning different flight attitudes for each drone. In this algorithm, drones are assigned to the fixed storage areas. Each drone is only responsible for its own operation area, and the delivery request was made on the drone matching area. The cargo items in the warehouse are assigned among the drones. Each drone is paired with a delivery point and the drones deliver the items only to the designated point. The matches between the drone and the delivery points are shown by different colours in Figure 2. As seen from the figure, the destination points of the drones correspond to the closest regions. Therefore, the colour codes in the regions refer to the closest points in the delivery area. Hence, each drone is only responsible for a specific route. The corresponding algorithm is given in Figure 3.

To simulate the proposed method, we have preferred to use Inter/Aero drone [14]. This model provides the required flexibility and easy load-carrier structure for delivery operations. The

technical specifications of the drone are given in Table 2. Besides, Maxwell/BCAP3000 UCs have been preferred as they have higher energy density, and they are prevailed in the market. The specific characteristics for the UCs are presented in Table 3.

Characteristic feature	Value
Weight (without battery)	865g
Width	360mm
Height	222mm
Propeller diameter	230mm

Table 2 Specifications of Intel aero [15]

Characteristic Feature	Value
Capacity	3000F
Voltage	2,7V
Weight	510g
Dimensions (Length x height)	138 x 60,4 mm

Table 3 Specifications of Maxwell BCAP3000 [16]

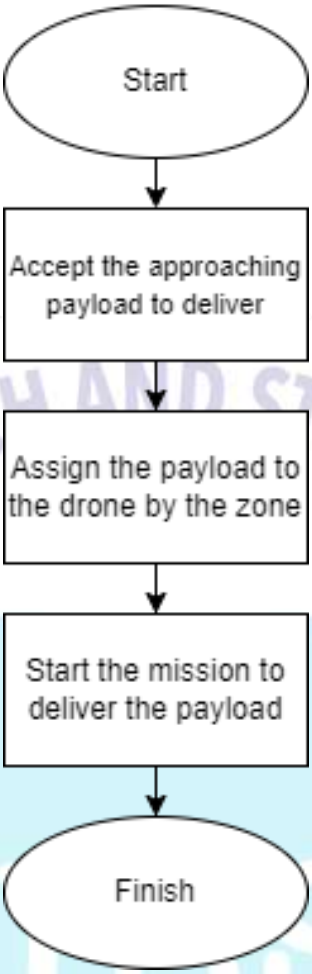

Figure 3. Flow Chart of the proposed procedure

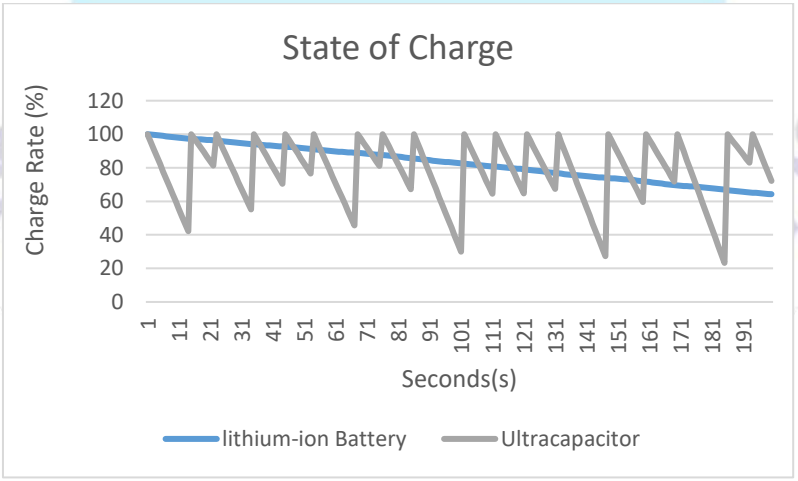

Figure 4. Short-term State of charge of the battery and ultracapacitor

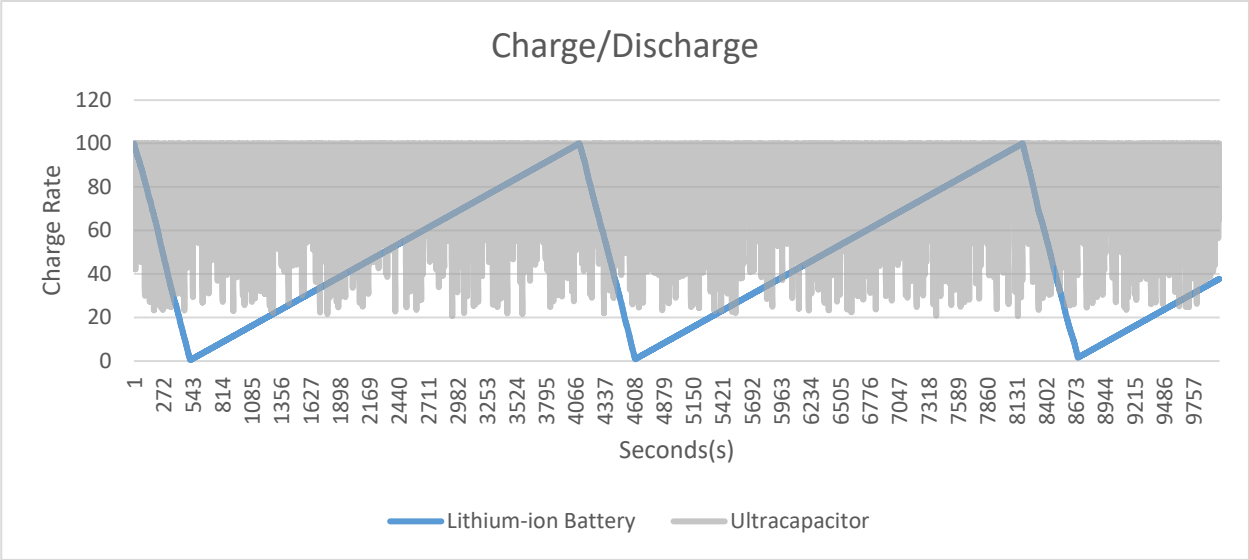

Figure 5 Long-term Energy Status of Battery and Ultracapacitor

Figure 4 presents state of charge levels of UC and battery for first 20 duties assigned to a drone. As the energy density of the UC is lower than the battery, UC requires to be recharged before each flight. Besides, UC needs relatively very short time to be recharged, hence this delay periods do not significantly affect the operation.

On the other hand, Figure 5 illustrates the charge-discharge trends of UC and lithium-ion battery to meet the delivery requests for the first 10000 seconds. This figure clearly shows that batteries cause delay in cargo operation as they need relatively higher periods than the UCs to be recharged. Moreover, lithium-ion batteries have the charge/discharge cycles between 500 and 1000. Hence, they often need to be replaced and this case adds extra cost for industrial delivery operations.

Total Energy Consumption	36357369,19J
Number of Delivery Items	7200

Table 4 Simulation Results

	Number of Tasks	Total Energy Consumption
Drone 1	3593	18217873,7J
Drone 2	3607	18139495,48J

Table 5. The number of tasks and energy consumption for each drone

For simulation studies, a random list of 7200 delivery items is generated. The weight of each item is randomly assigned. Then, the total amount of energy consumed by the drones is given in Table 4. Besides, Table 5 shows the total number of missions and the total amount of energy consumed by each drone. From this table, it is seen that there is a difference between the task assignments of drones. Therefore, it can be interpreted that the aging factor on the drones will be dominant factor on the operational lifetime of the drones. Hence, considering the relatively higher charge-discharge cycles capacity of UCs, they are suitable option to be used as energy storage systems for the drones which operated in a limited closed space.

Figure 6 presents the main result of the paper. Total delivery time is compared for the drones equipped with UC and battery. As seen from the figure, the drone fleet with UC nearly requires 20% of the time needed for the drone fleet powered by battery. By the merit of the structural modification on energy storage systems, the operational time for drone-based delivery procedure of randomly chosen 7200 items has been significantly decreased.

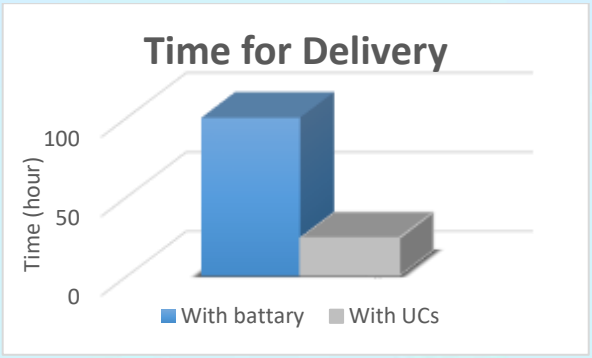

Figure 6. Comparison of total delivery times for the fleets equipped with UC and battery

4. CONCLUSION

In this study, a feasible method is presented to perform delivery service in a closed warehouse using autonomous drones. Since it is desired to emphasize the flight/charge cycle time of the drones, the matching procedure between the drones and payloads is specified to operate in a limited area. Simulation results show that UCs are more suitable than standard lithium-ion batteries by considering the operation time and the number of charge/discharge cycles. For future studies, the algorithm which provides more feasible solution for the matching of larger fleet of the drones and the payloads will be examined.

5. REFERENCES

[1] F. B. Sorbelli, F. Corò, S. K. Das and C. M. Pinotti, "Energy-Constrained Delivery of Goods With Drones Under Varying Wind Conditions," in *IEEE Transactions on Intelligent Transportation Systems*, vol. 22, no. 9, pp. 6048-6060, Sept. 2021, doi: 10.1109/TITS.2020.3044420.

[2] H. Shakhatreh et al., "Unmanned aerial vehicles (UAVs): A survey on civil applications and key research challenges", *IEEE Access*, vol. 7, pp. 48572-48634, 2019.

[3] F. Betti Sorbelli, C. M. Pinotti and V. Ravelomanana, "Range-free localization algorithm using a customary drone: Towards a realistic scenario", *Pervas. Mobile Comput.*, vol. 54, pp. 1-15, Mar. 2019.

[4] F. Betti Sorbelli, S. K. Das, C. M. Pinotti and S. Silvestri, "Range based algorithms for precise localization of terrestrial objects using a drone", *Pervas. Mobile Comput.*, vol. 48, pp. 20-42, Aug. 2018.

[5] S. Obayashi, Y. Kanekiyo and T. Shijo, "UAV/Drone Fast Wireless Charging FRP Frustum Port for 85-kHz 50-V 10-A Inductive Power Transfer," *2020 IEEE Wireless Power Transfer Conference (WPTC)*, 2020, pp. 219-222, doi: 10.1109/WPTC48563.2020.9295562.

[6] M. Shi, J. Hu, H. Han and X. Yuan, "Design of Battery Energy Storage System based on Ragone Curve," *2020 4th International Conference on HVDC (HVDC)*, 2020, pp. 37-40, doi: 10.1109/HVDC50696.2020.9292767.

[7] J. Kim, Y. Choi, S. Jeon, J. Kang and H. Cha, "Optrone: Maximizing Performance and Energy Resources of Drone Batteries," in *IEEE Transactions on Computer-Aided Design of Integrated Circuits and Systems*, vol. 39, no. 11, pp. 3931-3943, Nov. 2020, doi: 10.1109/TCAD.2020.3012790.

[8] A. Garg and M. Das, "High Efficiency Three Phase Interleaved Buck Converter for Fast Charging of EV," *2021 1st International Conference on Power Electronics and Energy (ICPEE)*, 2021, pp. 1-5, doi: 10.1109/ICPEE50452.2021.9358486.

[9] M. K. Andreev, "An Overview of Supercapacitors as New Power Sources in Hybrid Energy Storage Systems for Electric Vehicles," *2020 XI National Conference with International Participation (ELECTRONICA)*, 2020, pp. 1-4, doi: 10.1109/ELECTRONICA50406.2020.9305104.

[10] M. N. Boukoberine, Z. Zhou, M. Benbouzid and T. Donateo, "A Frequency Separation Rule-based Power Management Strategy for a Hybrid Fuel Cell-Powered Drone," *IECON 2020 The 46th Annual Conference of the IEEE Industrial Electronics Society*, 2020, pp. 4975-4980, doi: 10.1109/IECON43393.2020.9255118.

[11] E. Kim, Y. Lee, L. He, K. G. Shin and J. Lee, "Power Guarantee for Electric Systems Using Real-Time Scheduling," in *IEEE Transactions on Parallel and Distributed Systems*, vol. 31, no. 8, pp. 1783-1798, 1 Aug. 2020, doi: 10.1109/TPDS.2020.2977041.

[12] M. K. Andreev, "An Overview of Supercapacitors as New Power Sources in Hybrid Energy Storage Systems for Electric Vehicles," *2020 XI National Conference with International Participation (ELECTRONICA)*, 2020, pp. 1-4, doi: 10.1109/ELECTRONICA50406.2020.9305104.

[13] H. V. Abeywickrama, B. A. Jayawickrama, Y. He and E. Dutkiewicz, "Comprehensive Energy Consumption Model for Unmanned Aerial Vehicles, Based on Empirical Studies of Battery Performance," in IEEE Access, vol. 6, pp. 58383-58394, 2018, doi: 10.1109/ACCESS.2018.2875040.

[14] H. V. Abeywickrama, B. A. Jayawickrama, Y. He and E. Dutkiewicz, "Comprehensive Energy Consumption Model for Unmanned Aerial Vehicles, Based on Empirical Studies of Battery Performance," in IEEE Access, vol. 6, pp. 58383-58394, 2018, doi: 10.1109/ACCESS.2018.2875040.

[15] Intel Australia. (2017). *Speci_cations for the Intel Aero Ready to Fly Drone*. [Online]. Available:https://www.intel.com.au/content/www/au/en/support/articles/000023272/drones/development-drones.html (Accessed: 15.04.2022)

[16]https://pdf1.alldatasheet.com/datasheet-pdf/view/558210/MAXWELL/BCAP3000.html (Accessed: 15.04.2022)

[17] C. Rong *et al*., "Optimization Design of Resonance Coils With High Misalignment Tolerance for Drone Wireless Charging Based on Genetic Algorithm," in *IEEE Transactions on Industry Applications*, vol. 58, no. 1, pp. 1242-1253, Jan.-Feb. 2022, doi: 10.1109/TIA.2021.3057574.

[18] S. Obayashi, Y. Kanekiyo and T. Shijo, "UAV/Drone Fast Wireless Charging FRP Frustum Port for 85-kHz 50-V 10-A Inductive Power Transfer," *2020 IEEE Wireless Power Transfer Conference (WPTC)*, 2020, pp. 219-222, doi: 10.1109/WPTC48563.2020.9295562.

[19] F. Balsamo, C. Capasso, M. Fantauzzi, D. Lauria and O. Veneri, "Ultra-Capacitor Models for All Electric and Hybrid Ship Power Systems," *2019 International Conference on Clean Electrical Power (ICCEP)*, 2019, pp. 527-533, doi: 10.1109/ICCEP.2019.8890139.

A REVIEW STUDY ON THE EFFECTS OF DIMETHYL ETHER ON NOx EMISSIONS IN DIESEL ENGINES

İsmet Sezer
Gümüşhane University, ORCID ID: 0000-0001-7342-9172

ABSTRACT

This review study was created from the various studies which were completed on the use of dimethyl ether in diesel engines as a fuel or fuel additive. The several methods are available for the decreasing of the harmful emissions in diesel engines. The first method for the reduction of harmful emissions is improved the combustion by modification of engine design and fuel injection system, but this process is expensive and time consuming. The second method is the using various exhaust gas devices like catalytic converter and diesel particulate filter. However, the use of such devices affects negatively diesel engine performance. The last method to reduce emissions and also improve diesel engine performance is the use of various alternative fuels or fuel additives. The major pollutants of diesel engines are oxides of nitrogen (NOx) and particulate matter (PM). It is very difficult to reduce NOx and PM simultaneously in practice. The most researches declare that the best way to reduce these emissions is the use of various alternative fuels i.e. natural gas, biogas, biodiesel or using some additives with the alternative fuels or conventional diesel fuel. Therefore, it is very important that the results of various studies on alternative fuels or fuel additives are evaluated together to practice applications. Especially, this study focuses on the usage of dimethyl ether in diesel engines as fuel or fuel additive. This review study investigates the effects of using dimethyl ether on NOx emissions.

Keywords: Diesel engine performance, Dimethyl ether, Fuel additives, NOx emissions

1. INTRODUCTION

Diesel engines are prime power sources among the automobile engines because of their better performance, higher fuel economy and lower exhaust emissions of hydrocarbons (HCs), carbon monoxide (CO) and carbon dioxide (CO_2) than gasoline engines [1]. However, current diesel engines emit higher levels of particulate matter (PM) and nitrogen oxides (NOx) than those of gasoline engines. Therefore, many researchers have researched to develop low-pollution diesel engines and progressive studies have been conducted on alternative fuels which may produce clean diesel engine emissions [2]. Among the various alternatives, DME is the most promising alternative for automotive fuel from the standpoint of energy security, because it can be industrially produced from coal, natural gas and many kinds of biomass fuels [3]. However, physical properties of DME such as lower viscosity, lubricity, combustion enthalpy and boiling point need the modifications to diesel engine internal structures and components. The technology with pure DME as an alternative fuel for CI engine and vehicle is still under development stage. However, DME can be used as an additive fuel with diesel and other alternative fuel [4]. It is very important that the results of various studies on DME are evaluated together to practice applications. This review study investigates the effects of using dimethyl ether on NOx emissions.

2. CHARACTERISTICS OF DIMETHYL ETHER

DME is the simple ether with the chemical formula of CH3–O–CH3 as seen in Fig. 1. In general, the physical properties of DME are similar to those of LPG. Therefore, the storage, fuel handling, and transportation requirements for DME are similar to those for LPG [3]. DME can be produced using indirect or direct synthetic methods as seen in Fig. 2. Indirect synthetic methods generate DME through a dehydration reaction after synthetic reaction of methanol, while direct synthetic methods make DME directly from natural gas [5]. DME production costs less than diesel fuel or gasoline on an energy equivalent basis. DME economics are similar to CNG or LNG, when large scale plants are considered [6]. DME is gaseous and almost non-toxic at atmospheric pressure and room temperature. Therefore, DME needs to be pressurized to over 0.5 MPa to keep it in a liquid state under ambient temperature and pressure conditions. The fuel delivery pressure should be increased to 1.7-2.0 MPa under engine operating conditions to prevent vapor lock in the fuel injection system [7, 8].

Fig. 1. Chemical structure of DME [5]

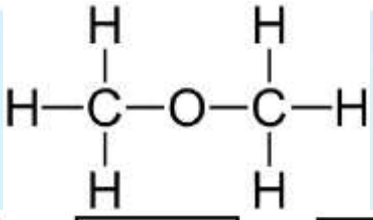

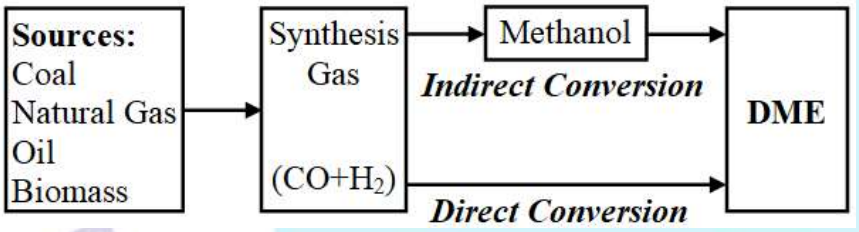

Fig. 2. Production methods of DME [9]

The properties of DME and diesel fuel are shown in Table 1. It can be seen that the properties of DME are quite different from those of diesel fuel. DME has high vapor pressure and low boiling temperature, which is a gas fuel at room temperature and atmospheric pressure. The heating value of DME is significantly lower than conventional diesel fuel. Therefore, the fuel supply and injection system, and the combustion system of the engine should be redesigned or modified [10]. The cetane number of DME is higher than that of diesel fuel, which demonstrates good ignition capability. The latent heat of evaporation of DME is much higher than that of diesel fuel, which is beneficial for reducing the mixture temperature.

Table 1. The properties of DME and diesel fuel

Property	**DME**	**Diesel**
Chemical formula	CH_3-O-CH_3	C_xH_y
Molecular weight, g	46.07	170
Boiling point, °C	-24.9	180-360
Liquid density, kg/lt	668	840
Liquid viscosity, cP	0.15	4.4-5.4

Lower heating value, kJ/kg	28430	42500
Ignition temperature, °C	235	250
Cetane number	55-60	40-55
Stoichiometric air/fuel ratio	9	14.6
Modulus of elasticity, N/m^2	$6.37x10^8$	$1.486x10^9$
Mass fraction of carbon	52.2	86
Mass fraction of hydrogen	13	14
Mass fraction of oxygen	34.8	0

DME has only C–H and C–O bonds, without C–C bonds, and contains about 34.8% oxygen. Because of these properties, DME combustion produces almost zero PM emissions, low noise level and can tolerate a higher exhaust gas recirculation (EGR) rate to reduce NOx emissions to a greater extent than with conventional diesel fuel [6]. The low viscosity of DME causes leakage in the fuel supply system, which relies on small clearances for sealing. Its lower lubricity characteristics result in intensified surface wear on the moving parts within the fuel injection system. Therefore, addition of proper additives to prevent leakage and surface wear is essential for DME. The compressibility of DME is generally higher than that of diesel, so DME also requires more compression pump work compared to the diesel. In general, DME deteriorates the rubber seals, mainly due to its corrosive nature. For that reason, all existing rubber seals in injection systems should be replaced with non-corrosive materials [1]. Another advantage of DME is that it is non-corrosive to the fuel system structure and metal surfaces [5].

3. STUDIES ON DIMETHYL ETHER

There are a number of studies in the literature on dimethyl ether such as the production technologies [9, 11, 12], fuel characteristics [5, 13-15], spray and injection characteristics [16-23], combustion characteristics [13, 24-36], performance characteristics [37-58] and exhaust emissions [59-80].

4. EFFECTS OF DIMETHYL ETHER ON NOx EMISSIONS

Fig. 3(a) shows the comparison of the NOx emissions characteristics for DME and diesel fuels. The formation of NOx emissions is highly dependent on the temperature of the combustion gas, the oxygen content, and the residence time for the reaction. The advance of the injection timing caused the increase of the NOx emission in both fuels. This is the reason why the ignition of fuel occur the high combustion temperature and pressure near TDC, and it affects the increase of the NOx formation. As shown in Fig. 3(a), the NOx emission of DME fuel shows slightly high compared to that of diesel at the same engine load and speed condition. It can be explained because the rapidly ignition of DME mixture leads to an increased combustion temperature compared to diesel. As a result, the elevated temperature (NOx formation rate is high) produces

more NOx emissions during the combustion of DME fuel than that of diesel fuel [2]. NOx emission is shown in Fig. 3(b). NOx emission was higher with DME when engine was operated at retarded injection timing. Possible reason for high NOx emission with DME is the early start of combustion and more after compression of combustion products leads to a higher temperature. However, advancing the injection timing reduced NOx well below the diesel operation [3].

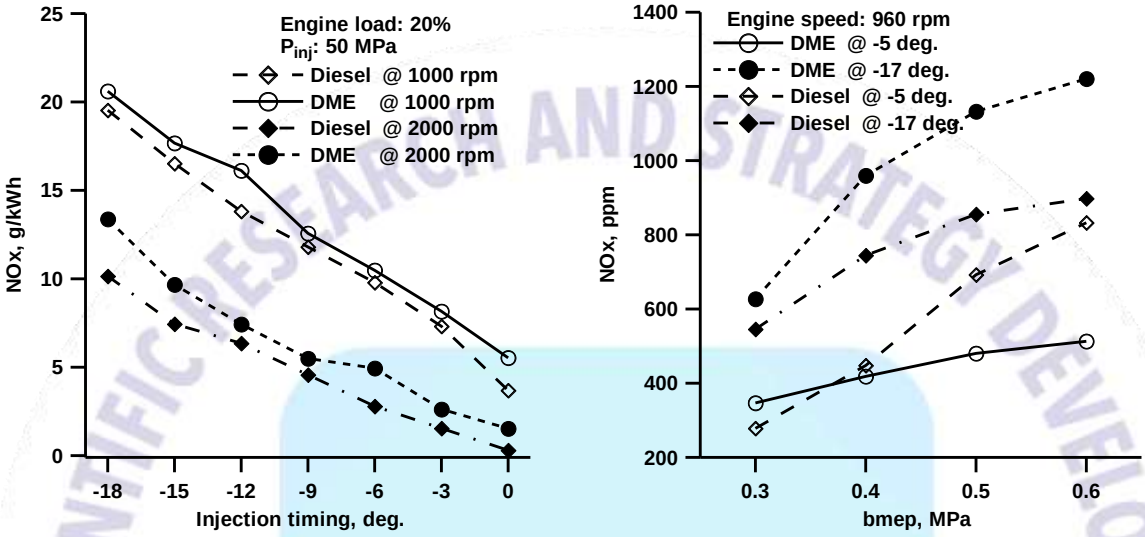

(a) (b)

Fig. 3. The variation of NOx emissions for a) injection timing [2] b) bmep [3]

Fig. 4(a) is shown the NOx emissions under different loads. Under various conditions, the composite combustion has lower NOx emissions than the pure diesel combustion. It is mainly due to the higher latent heat of DME vaporization in the composite combustion mode, which reduces the cylinder temperature at the early combustion stage. And owing to the lower calorific value of DME combustion, the cylinder temperature of DME combustion is lower than that of pure diesel combustion. When the DME air premixed volume maintaining at 1.89 kg/h, as the load increases, the NOx emission is largely reduced. This may be because the exhaust gas recirculation under a large load has large impact on the homogeneous DME charge compression combustion [7]. Fig. 4(b) shows the comparison of NOx emission between DME and diesel fuel under different engine loads and at engine speeds of 1400 rpm. It is illustrated that the DME engine exhibits substantial reduction in NOx emission at all test range of loads. At the BMEP of 1.52 MPa and engine speed of 1400 r/min, NOx emission of the DME engine is reduced by 28.1%, in comparison with that of the diesel engine. Reduction of NOx is mainly attributed to the physicochemical properties of DME. For the DME engine, retardation of ignition timing due to longer fuel injection delay, shorter ignition delay due to high cetane number and larger latent heat of DME lead to a decrease in cylinder pressure and local temperature which result in a reduction of NOx emission [10].

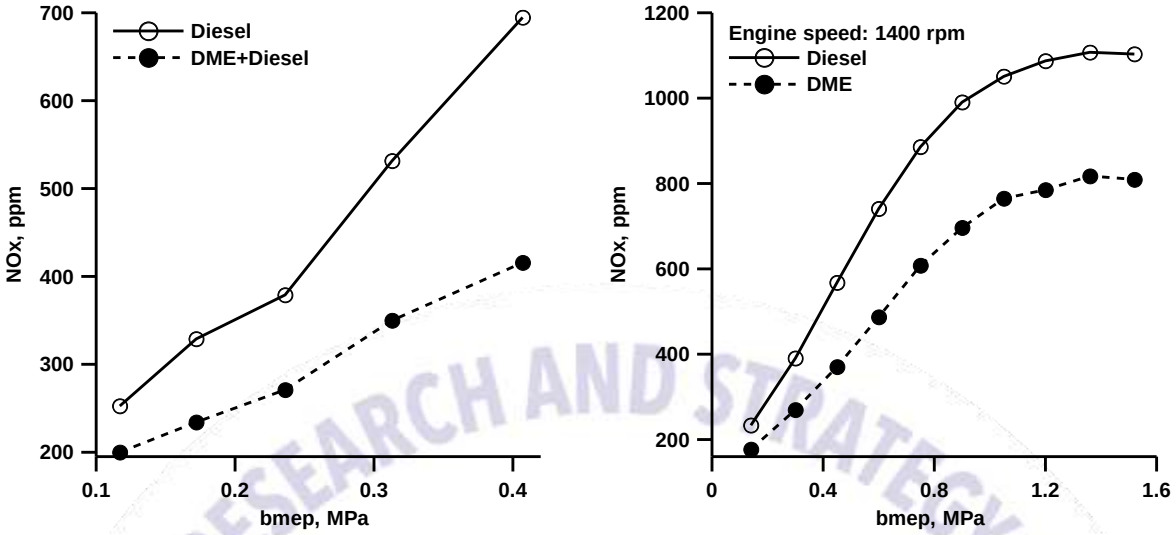

(a) (b)

Fig. 4. The variation of NOx emissions for a) bmep [7] b) bmep [10]

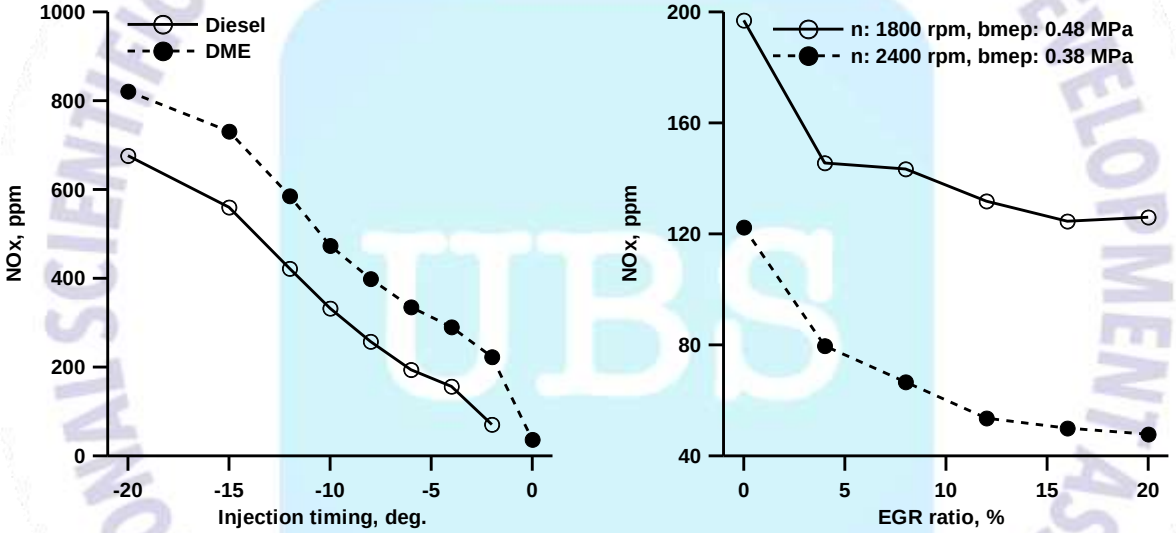

(a) (b)

Fig. 5. The variation of NOx emissions for a) injection timing [13] b) EGR ratio [13]

Fig. 5(a) shows the NOx emission characteristics for both fueled engines. Since the faster ignition of the DME fuel mixture increased the charge temperature in the cylinder, NOx formation was higher during the combustion process for DME fuel than for diesel fuel. When a constant input energy was supplied to the engine, the DME fuel showed faster ignition and reduced late combustion compared with diesel fuel. The formation of NOx emission is highly dependent on combustion temperature, oxygen content, and combustion duration. The rapid ignition of the DME-air mixture occurs at an increased combustion temperature compared to the diesel engine. Therefore, in order to reduce the NOx emissions, the lower initial heat release rate is expected to contribute to the lower NOx emission [13]. Fig. 5(b) shows the effect of EGR rate on NOx emissions in a DMEfueled engine. The NOx emission from the engine is considerably reduced with the increase in EGR rate, and the decrease in oxygen concentration of the intake air results in an decrease in NOx emissions. As shown in Fig. 5(b), NOx emission is reduced about 40% at 20% of the EGR rate. After decreasing the intake charge temperature

due to low EGR, the combustion temperature in the engine cylinder is suppressed by decreasing the oxygen content in the suction air [13]. Wang et al. (2008) have carried out in their study performance and emission of three kinds of DME-diesel blends and diesel fuel are evaluated in a four-cylinder test engine. In the experiments were used the blends of DME10, DME15 and DME20. As seen in Fig. 6(a), with the addition of DME into diesel fuel, NOx emissions decrease a little. But, it is concluded that the fuel supply advance angle is retarded appropriately, the power output would be improved somewhat and NOx emission could be reduced further [17]. Fig. 6(b) represents the effect of injection angle on NOx emissions according to the injection timing. The NOx emissions at the injection timing of 20 °BTDC had higher values, compared to those of the other injection timing. The NOx emissions distribution with narrow injection angles centered on the projecting point of the right bowl wall, and that with wide injection angles appeared from the bottom of bowl wall. The cylinder peak temperature with the injection timing of 20 °BTDC had a high temperature above 2000 K during the combustion process. The nitrogen oxides, including nitrogen monoxide and dioxide, were rapidly formed by an increasing reaction rate between nitrogen and oxygen at high temperature. On the other hand, the combustion with injection timing of 40 °BTDC occurred at a peak temperature below 2000 K because it is thought that the homogenous combustion occurred by the spread of air-fuel mixture in the piston bowl [18].

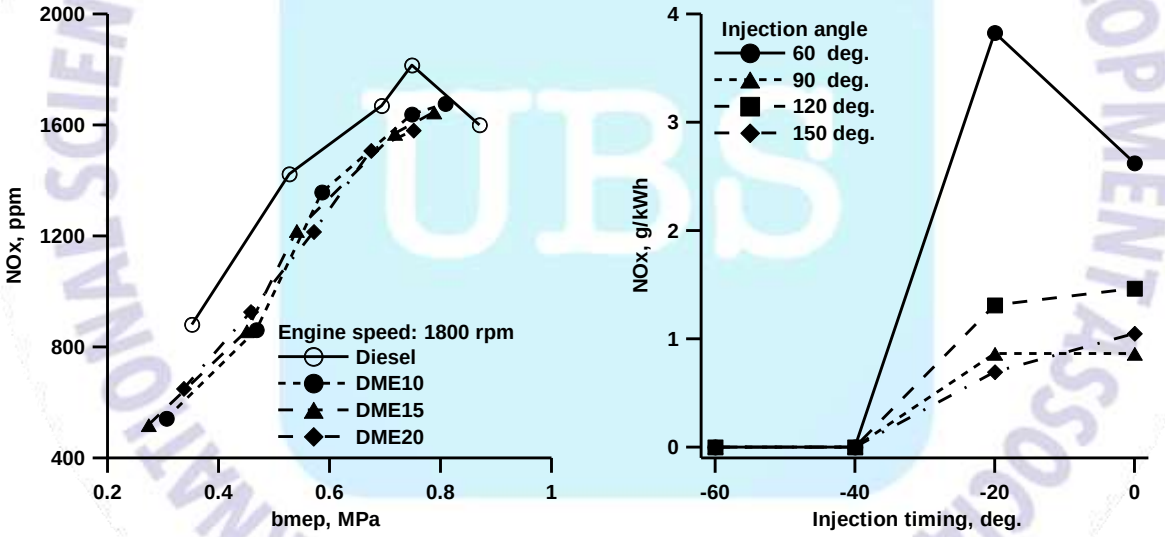

(a) (b)

Fig. 6. The variation of NOx emissions for a) bmep [17] b) injection timing [18]

Fig. 7(a) shows the NOx emissions for various injection timings. The NOx emissions for the DME fuel were higher than those for the diesel fuel. This is because the combustion temperature is increased by the higher IMEP and power than for the diesel fuel. The NOx emissions for the fuel blends increased with increasing DME fuel mass fraction [20]. NOx in the cylinder depends on the cylinder temperature or the combustion rate. An observation of Fig. 7(b) shows that the NOx emissions from LPG/DEE and LPG/DME operations are lower by about 65% at full load as compared to diesel operation. The lesser concentration of NOx may be attributed to lower in-cylinder temperature [24]. NOx emissions for a DME-diesel dual-fuel operation at the speed of 1700 rpm and the load of 0.36 MPa are exhibited in Fig. 8(a). NOx emission of diesel-DME dual fuel operation is slightly lower compared with that of diesel DICI operation, and shows a

decrease with a rise of quantity of DME initially but this decreasing trend discontinues with a higher DME quantity [25].

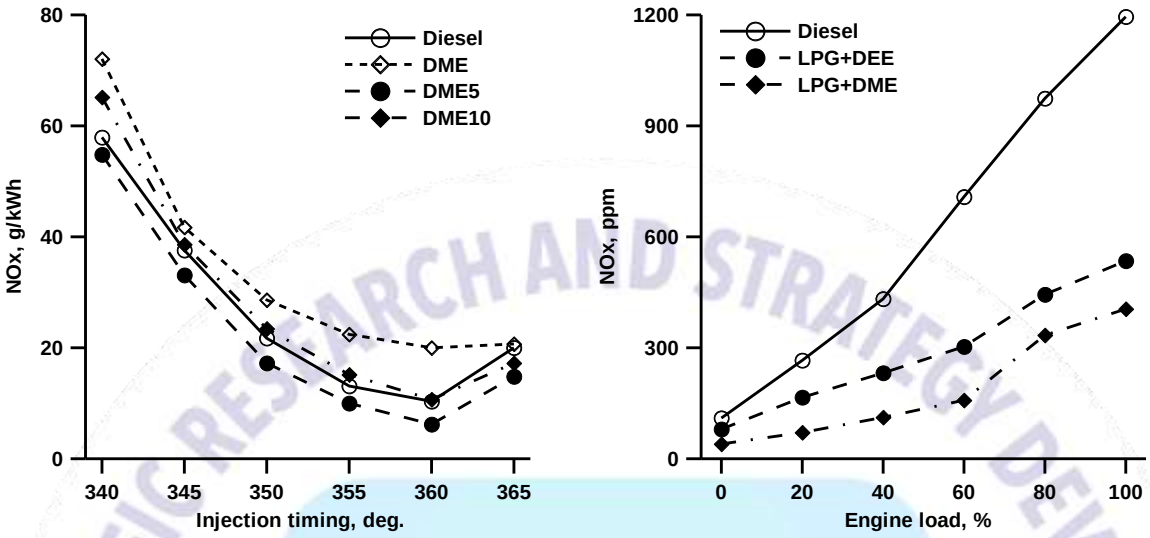

(a) (b)

Fig. 7. The variation of NOx emissions for a) injection timing [20] b) engine load [24]

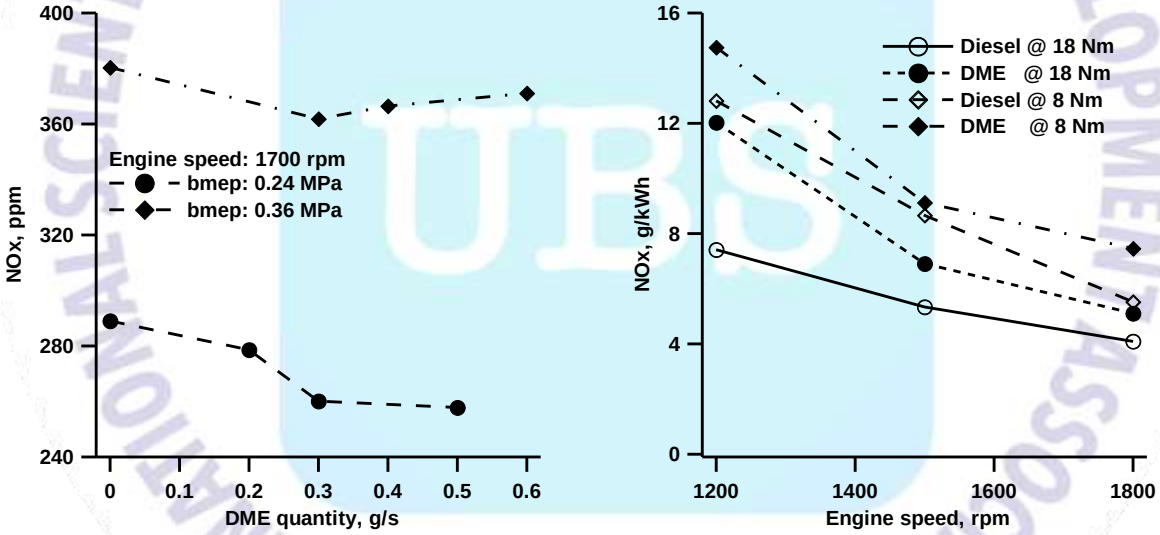

(a) (b)

Fig. 8. The variation of NOx emissions for a) quantity of DME [25] b) engine speed [26]

As seen in Fig. 8(b), combustion with the DME fuel produced a higher level of NOx emissions than diesel fuel at the same engine load conditions. Due to the higher cetane number, active combustion and oxygen content characteristics of the DME fuel, the exhausted NOx emissions per unit power were higher than that of the diesel fuel. The NOx formation is strongly correlated with the combustion temperature and the equivalence ratio. The characteristics of DME fuel, short ignition delay and superior evaporation, led to rapid combustion in a short time. Moreover, due to the fact that the oxygen content of approximately 38.4% in DME fuel was supplied as an additional oxidizer, a highly increased temperature was induced, and nitrogen oxides were instantly produced at elevated temperatures. When the engine speed was accelerated, a decrease in the amount of NOx emissions was observed in Fig. 8(b). For low engine speeds, the ignition

of both fuels started near TDC under high-temperature/high-pressure ambient conditions. On the other hand, at the higher engine speed, the combustion took place in the expansion stroke (lowtemperature/low-pressure ambient conditions). These various initial conditions resulted in the differences in the combustion temperature and the NOx formation rate. In addition, the superior evaporation property of the DME fuel allowed the injected fuel to mix well with the compressed air. As a result, a low equivalence ratio was formed before the start of combustion, and the combustion temperature increased relatively, generating more nitrogen oxides than diesel combustion [26]. The variation of NOx emissions depending on air excess ratio is shown in Fig. 9(a). The level of NOx emissions from DME is equivalent to or slightly higher than that from gas oil. However, it may be possible to reduce the emission of NOx from DME fuel because DME burns without any smoke. Although EGR is not applicable to a gas oil diesel engine due to the resulting increase in smoke emissions, a large amount of EGR can be applied to a DME diesel engine, even at a high load range [30]. Nitrogen oxides are toxic emissions produced from diesel combustion and consist of nitric oxide (NO) and nitrogen dioxide (NO_2). The engine operates with DME and LPG injection found the higher NOx emission than of the diesel operation as shown in Fig. 9(b). The increase of oxides of nitrogen formation for all loads is associated with oxygen content, which influences higher adiabatic flame temperatures and hence produces more NOx [32].

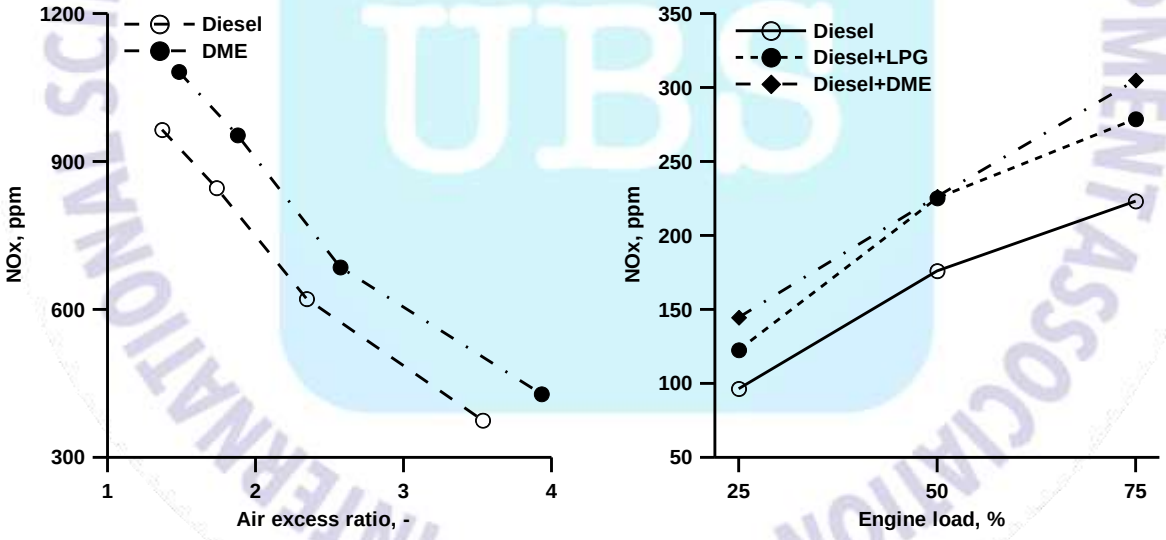

Fig. 9. The variation of NOx emissions for a) air excess ratio [30] b) engine load [32]

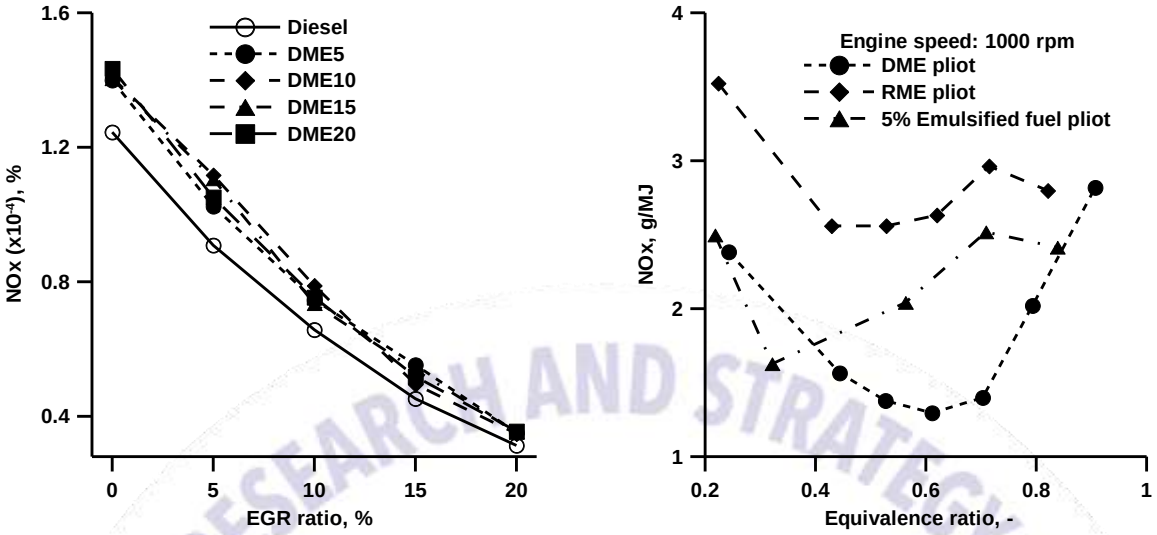

(a) (b)

Fig. 10. The variation of NOx emissions for a) EGR ratio [33] b) equivalence ratio [39]

The key parameters to NOx formation are local temperature, residence time, and concentration of oxygen in higher flame temperature zone. Fig. 10(a) shows the well-established advantage of EGR in decreasing NOx emissions from diesel engine. For all DME-diesel blends (0–20%) and EGR rates (0–20%), NOx formation is marginally higher than neat diesel due to higher in-cylinder temperature. More cetane number and fuelbounded oxygen of DME compared to diesel results in higher NOx formation. Less NOx formation is observed for EGR20 for all DME-diesel blends compared to without EGR case. It has been noticed that there is a significant drop in NOx formation approximately by 60% (overall) due to EGR [33]. Fig. 10(b) shows specific NOx emissions plotted against equivalence ratio for all tested pilot fuels at 1000 rpm. It was seen that the emulsified pilot fuels produce lower amounts of NOx than neat RME, especially at lower equivalence ratios. It is also noted that both emulsions have similar trends. After an equivalence ratio of 0.55 however, NOx emissions of the emulsified fuel increase to approach that of neat RME. This is contrary to the expected constant reduction throughout the equivalence ratio range resulting from water vapourising during combustion. One possible explanation is that the microexplosion phenomenon has a much greater effect at these high equivalence ratios, resulting in improved distribution of fuel droplets. Therefore, it can be said that the microexplosions offset the cooling efect brought on during water vapourisation within the fuel droplet. This would improve ignition as well as flame propagation through the natural gas and air mixture. It is seen that DME produces significantly lower specific NOx than the liquid pilot fuels. This reduction stems from the lower combustion temperatures at the lower loads, as shown by the lower combustion pressures achieved. The comparatively slow flame propagation coupled with the cooling effect upon injection can be the cause. In addition, the significantly longer ignition delay of the DME pilot fuel would result in slower combustion and thus slower NOx formation rates. At higher equivalence ratios however (>0.6, where combustion temperatures are highest), NOx levels rise to a similar level as the neat pilot fuel [39].

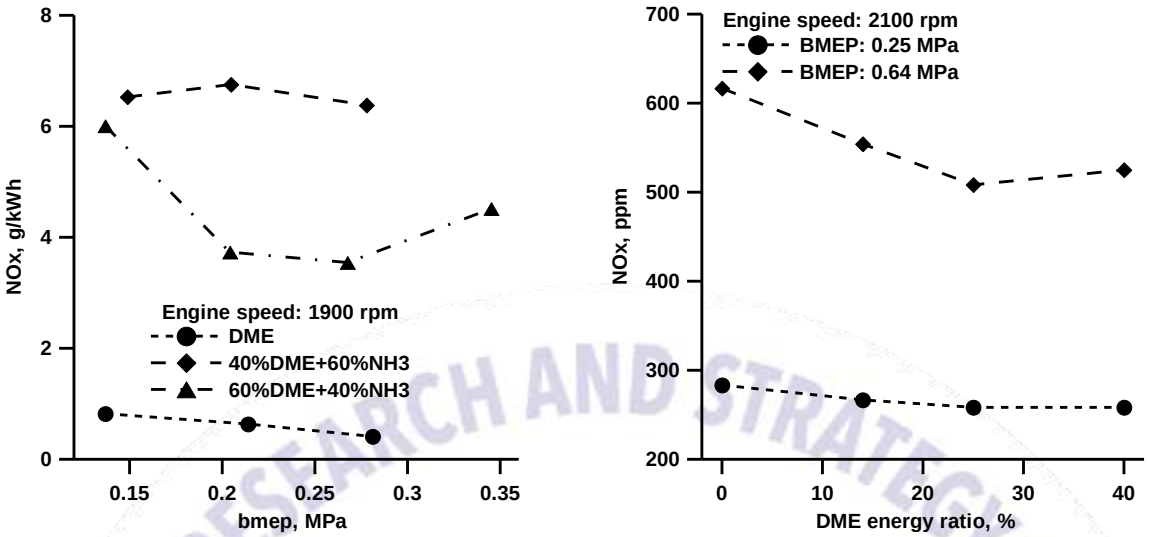

(a) (b)

Fig. 11. The variation of NOx emissions for a) bmep [41] b) DME energy ratio [45]

Fig. 11(a) shows NOx emissions for different fuel mixtures versus BMEP. It is found that NOx emissions for ammonia mixtures increase considerably relative to DME, but still do not exceed EPA emission regulations (7.5 g/kWh) for small output engines. The level of NOx emissions is approximately 6.5 g/kWh for 40%DME–60%NH3 at 1900 rpm. It is believed that the increase in NOx emissions is primarily due to fuel NOx formation generated from ammonia combustion [41]. The variations of NOx concentration as a function of DME energy ratio were exhibited in Fig. 11(b). As widely accepted, NOx almost has no strong correlation to the fuel structure but greatly depends on how the combustion was organized. Generally, the formation of nitrogen oxides is favored by high charge temperature and oxygen concentration. NOx mainly forms outside sprays of directly injected fuel, where the temperature is higher than that of inside sprays and where there are less hydrocarbons competing with nitrogen for oxygen. In our experiment, although the in-cylinder mass-averaged temperature went up with a rise of DME energy ratio, NOx emission was not expected to be higher for DME-diesel dual fuel combustion. In fact, NOx concentration under the dual fuel operation was a little lower compared to the one under normal diesel operation, and NOx emission showed a descent tendency with a rise of DME energy ratio at first, and then the descent tendency was inhibited. In the case of the dual fuel combustion, the reason for this first NOx reduction was the ignition delay of injected diesel fuel shortened slightly via the intake DME induction. In the mean time, the gas after premixed homogeneous charge combustion could function as internal EGR and reduce the charge oxygen concentration by dilution, and therefore, suppressed NOx formation [45]. Fig. 12(a) gives the effects of various DME pilot quantities on NOx emission of PCCI-DI engine and NOx reduction rate under the different loads at 1400 rpm. At 0.23 MPa (low load), the greatest NOx reduction rate achieved is 84% at 1400 rpm for PCCI-DI operation with 30.4 mg/cyc DME pilot quantity; the greatest NOx reduction rate achieved is 48% at 1400 rpm with 22.8 mg/cyc DME pilot quantity. While, at 0.67 MPa (medium and high load), the greatest NOx reduction rate achieved is only 29.2% at 1400 pm with 30.4 mg/cyc DME pilot quantity; the greatest NOx reduction rate achieved is 43.5% at 1400 rpm with 22.8 mg/cyc DME pilot quantity. Obviously, NOx emission for PCCI-DI combustion shows a descending tendency with an increase in DME pilot

quantity at low loads. However, when the speed and load increases to a certain degree, NOx emission for PCCI-DI emission shows a mildly elevating tendency with an increase in DME pilot quantity. This is owing to the trade-off relationship between the reduction of NOx during the premixed homogeneous charge combustion and the increase of NOx during CIDI diffusive combustion. On one hand, DME undergoing premixed homogeneous charge combustion produces little NOx so that an increase in DME pilot quantity would decrease the NOx. On the other hand, the heat release of premixed gas raises the in-cylinder temperature and pressure so that NOx increases with an increase in pilot quantity. Therefore, an optimal solution of DME pilot quantity for all operation loads should be determined by plenty of experiments and studies [46]. NOx and PM emissions are the main focus of today's diesel emission. NOx emission mainly occurred under the high temperature combustion and the high local oxygen concentration. DME premixing operation at 25% and 50% of maximum load was a lower NOx emission than the conventional diesel operating conditions as seen in Fig. 12(b). In order to the low-temperature DME pre-mixing combustion is reduce in-cylinder combustion temperature. The resulting in a substantial reduction in NOx emission compare with neat diesel fuel. However, the higher NOx had been found during the high-temperature combustion with increasing DME injection (>50%) when engine exhaust gas from engine operation on mid (50%) and high (75%) engine load conditions was used. The highest NOx produced by around 810 ppm has been found on 75% (high load) engine load with increased high DME pre-mixing. In additions, DME addition enhanced in-cylinder combustion zone, lead to thermal NOx are occurred [52].

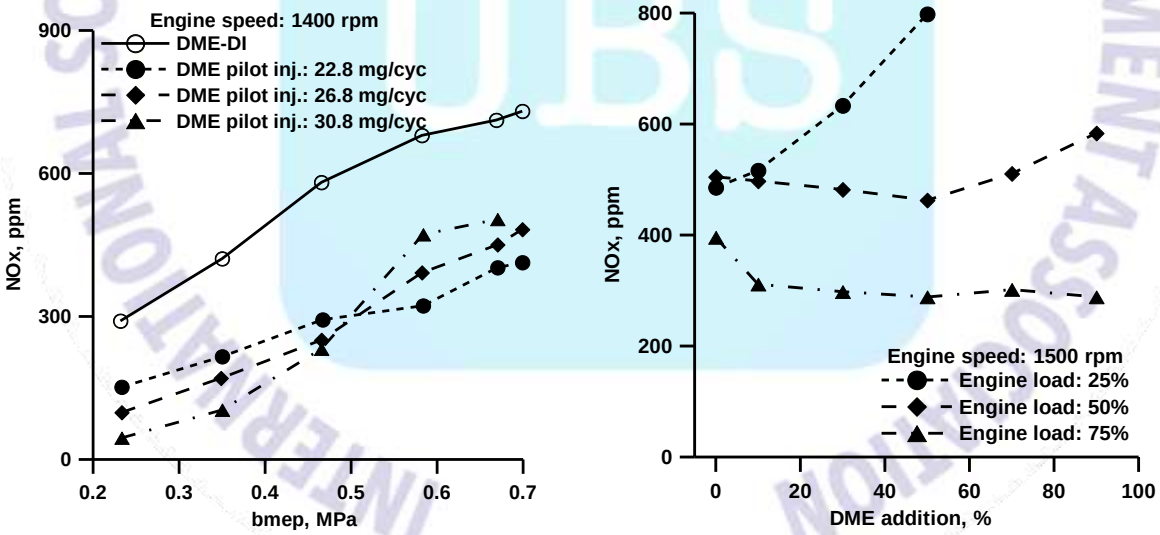

(a) (b)

Fig. 12. The variation of NOx emissions for a) bmep [46] b) DME addition [52]

From Fig. 13(a) the nitrous oxide increases as DME percentage is increased to diesel. This is due to increases the temperature of combustion. DME increases the combustion gas temperature and when temperature increases the NOx increases. This is due to incomplete combustion [56]. As can be confirmed from the Fig. 13(b), NOx emissions were decreased with increasing biogas ratio. The reason for the reduction of NOx with increasing mixing ratio of biogas is due to CO_2 in the biogas, which makes achieving high in-cylinder temperature difficult. Further, the effect of biogas mixing on NOx emissions became clear as the SOI advanced. Moreover, it can be

found that the biogas-DME dual fuel combustion with a mixing ratio biogas of 0.2-0.6 emitted lower NOx than pure DME combustion [58].

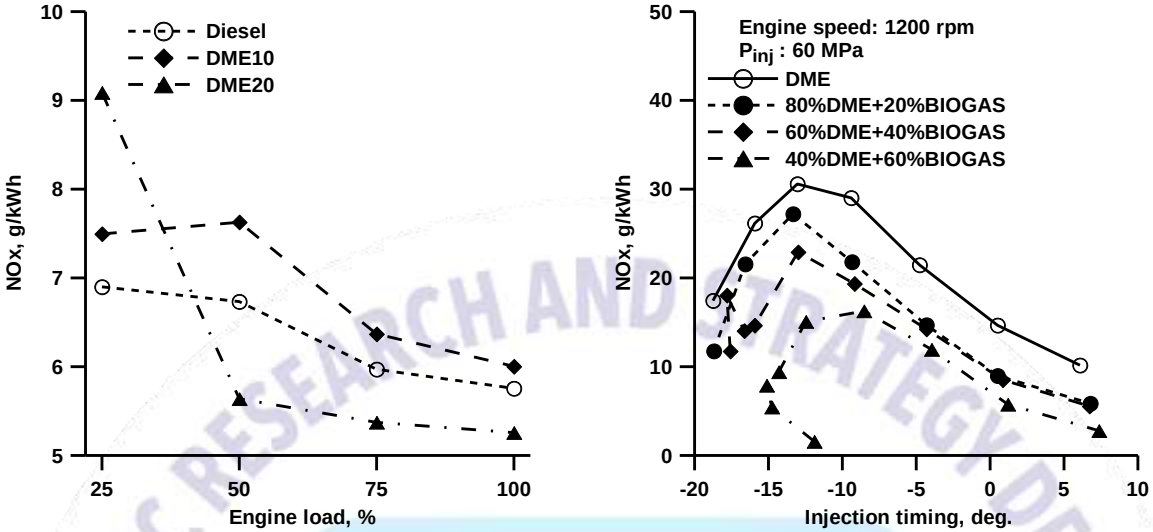

(a) (b)

Fig. 13. The variation of NOx emissions for a) engine load [56] b) injection timing [58]

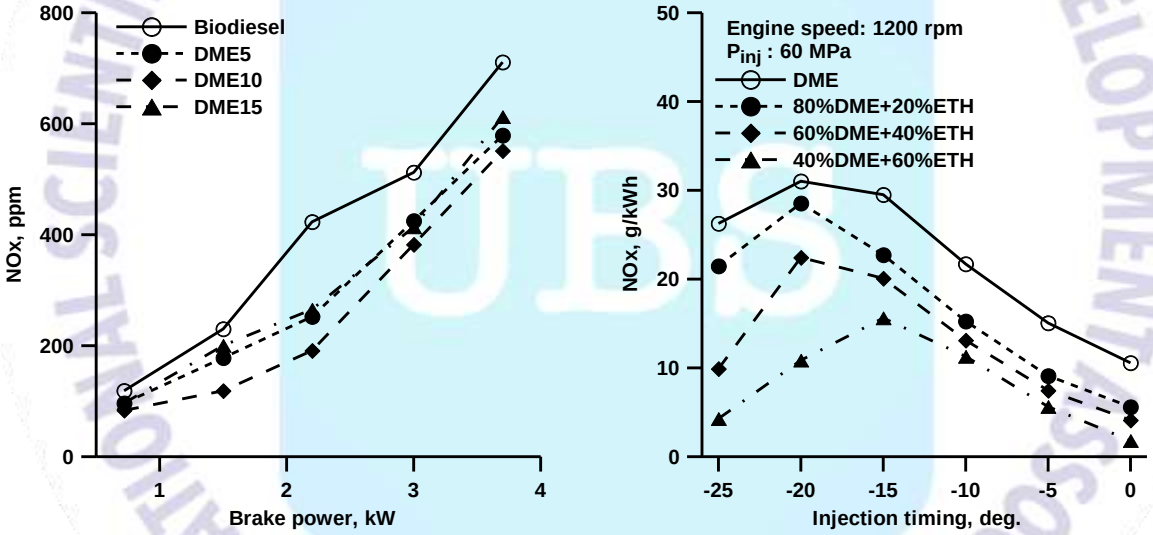

(a) (b)

Fig. 14. The variation of NOx emissions for a) brake power [59] b) injection timing [61]

The NOx emissions are shown in Fig. 14(a). The NOx emissions increase with increase in the engine load. Compared with the neat biodiesel, the NOx emissions for DME15 decreased by 15% at full load. In addition, with increase of dimethyl ether quantity in biodiesel, the NOx emission also decreases. The thermal mechanism dominates the formation of NOx in biodiesel combustion. Thus the major factors affecting NOx formation are combustion temperature, local oxygen concentration and residence time in the high temperature zone. For the DME blends, the cooling effect of dimethyl ether associated with its lower calorific value and higher latent heat of evaporation could reduce the combustion temperature and hence reduce the NOx emissions. For the DME fuels, the cooling effect of ethanol seems to be the dominating effect leading to the overall reduction of NOx emission. The percentage of reduction of NOx for DME5, DME10 and DME15 is 14%, 10%, and 7% at full load compare to neat biodiesel [59].

Fig. 14(b) shows the NOx emission characteristics for the ethanol fraction, DME in-cylinder injection timing, and premixed combustion duration for dual-fuel combustion. As the in-cylinder injection timing was advanced, NOx first increased and then decreased, as shown in Fig. 14(b). The increase of NOx was due to an active combustion reaction and an increase of the combustion temperature, and the subsequent decrease was due to the geometric characteristics of the combustion chamber. In addition, increasing ethanol fraction caused a decrease of NOx emissions. Thus, the increased ethanol fraction induced a decrease in in-cylinder combustion temperature due to the high evaporative latent heat of ethanol. A decrease in DME as the ignition source also contributed to the decrease in NOx [61]. The NOx emissions are shown in Fig. 15(a). The NOx emissions increase with increase in the engine load. NOx emissions for DME15 decreased by 15% at full load compared with the biodiesel. In addition, with increase of dimethyl ether quantity with biodiesel, the NOx emission also decreases. The thermal mechanism dominates the formation of NOx in biodiesel combustion. Thus the major factors affecting NOx formation are combustion temperature, local oxygen concentration and residence time in the high temperature zone. For the DME blends, the cooling effect of dimethyl ether associated with its lower calorific value and higher latent heat of evaporation could reduce the combustion temperature and hence reduce the NOx emissions. The percentage of reduction of NOx for DME5, DME10 and DME15 is 17%, 28%, and 35 % at full load compare to biodiesel [63].

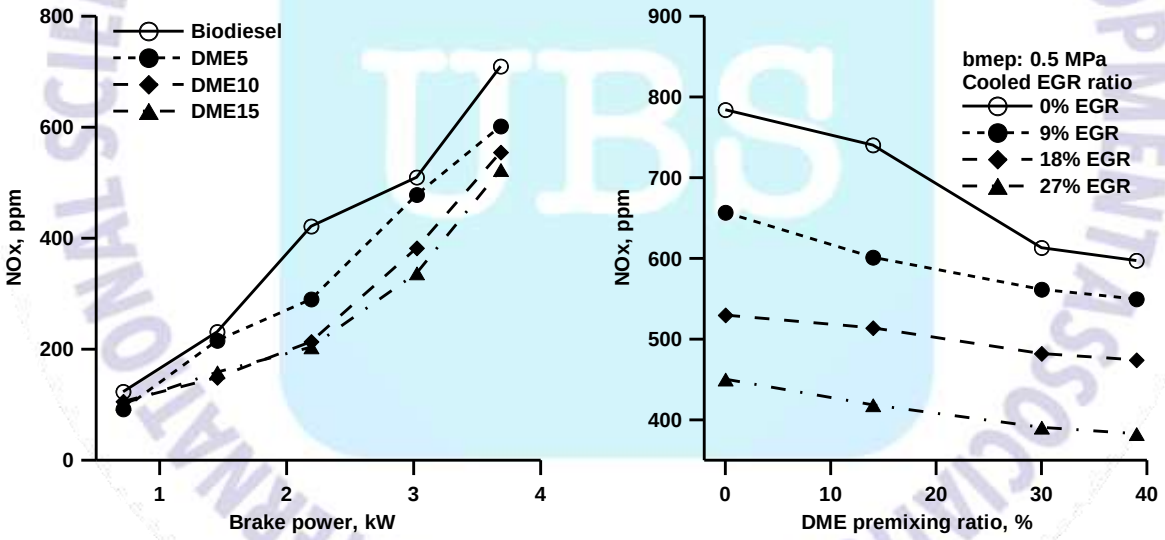

(a) (b)

Fig. 15. The variation of NOx emissions for a) brake power [63] b) DME premixing ratio [64]

The variations of NOx emission and smoke opacity versus the different pre-mixing ratios and EGR rates were demonstrated in Fig. 15(b). It is well known that main factors affecting NOx formation include the local temperature, the local oxygen concentration, and the residence time in the high-temperature zone. A high oxygen concentration and a high in-cylinder temperature result in a high level of NOx emission. As shown in Fig. 15(b), NOx emission under the dual fuel operation was a little lower than the one under the conventional diesel operation and showed a descent tendency with an increase in DME pre-mixing ratio. In the case of dual fuel combustion, the ignition delay of the diesel fuel became shorter due to a higher in-cylinder temperature and pressure. The diesel burned faster in the diffusion combustion stage and the

local hightemperature regions shortened. Thus, NOx formation was suppressed. Furthermore, with an increase in DME pre-mixing ratio, more homogeneous mixture was introduced into the cylinder and then the oxygen-rich and high-temperature regions were reduced, which also effectively prevented the formation of NOx. NOx emission with EGR exhibited a decreasing trend as expected. It was caused by a reduced oxygen concentration and a decreased flame temperature in the combustible mixture. Furthermore, it could be observed that the decreasing level in NOx emission gradually weakened with an increase in DME pre-mixing ratio. This was because that the DME HCCI combustion reduced the inhibition of EGR on NOx formation. Consequently, at a high premixing ratio, a high level of EGR could be used to decrease NOx [64]. Fig. 16(a) shows NOx emissions of DME-biodiesel blends. The results show that, by increasing the load, the NOx emissions of four fuels all increase due to the higher mean temperature in the cylinder. With the increase of DME proportion, the NOx emissions of biodiesel, DME50, DME70 and DME100 decrease gradually. For example, at 1.52 MPa BMEP, the NOx emissions of biodiesel, DME50, DME70 and DME100 are 1266 ppm, 723 ppm, 649 ppm and 413 ppm, respectively. Compared with biodiesel, NOx emissions decrease by 43%, 49% and 67%, respectively. The atomization performance of biodiesel spray is inferior to that of DME spray under the same injection and ambient conditions. By increasing DME mass fraction in the fuel, the fuel is distributed uniformly in the combustion chamber and the in-cylinder temperature distributes irregular. The latent heat value of DME is larger than that of biodiesel, and a large amount of heat is absorbed during the vaporization process. Therefore, with the increase of DME, in-cylinder temperature decrease and NOx emissions decrease [65]. In the case of NOx emissions shown in Fig. 16(b), the NOx emissions of DME10 and DME20 are reduced somewhat in comparison with the engine fueled with neat diesel fuel. DME has a higher cetane number value and an excellent auto-ignition characteristic, so the ignition delay is shorter and the amount of premixed combustion is smaller than diesel fuel, which makes the maximum in-cylinder pressure and temperature lower and prohibits the formation of NOx. On the other hand, the real injection timing of diesel-DME blends is delayed due to their lower modulus of elasticity than that of diesel, which can reduce the NOx emissions effectively. It is believed that through further modification of injection timing, NOx emissions can be effectively reduced. For DME30, NOx emission is reduced somewhat in comparison with the neat diesel fuel at low and medium load. However, NOx emission, measured in terms of g/kWh, is higher than that of diesel due to its very low power output [66].

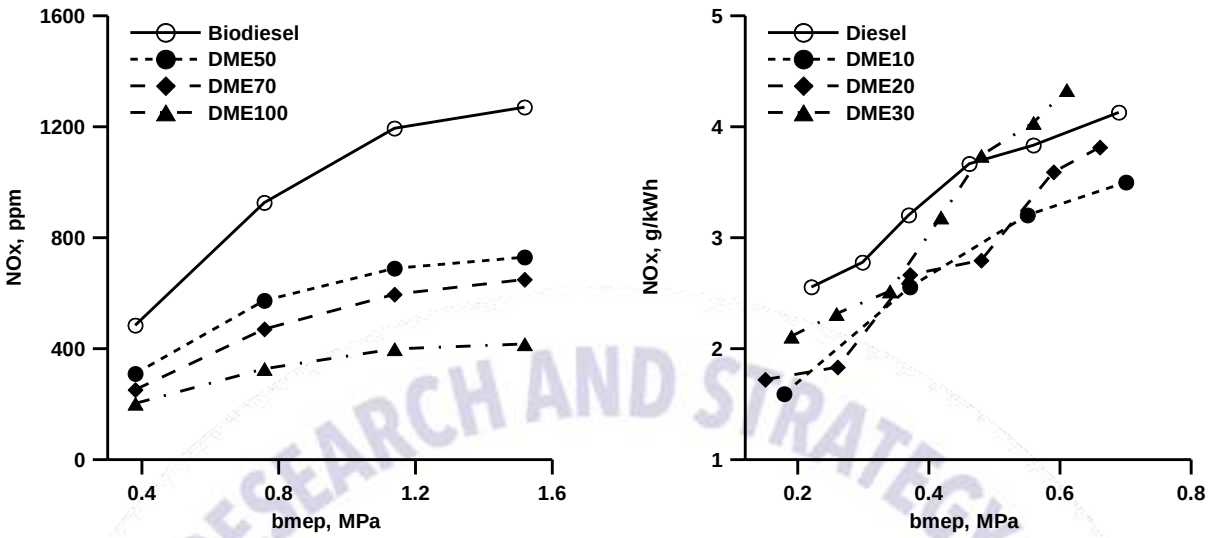

(a) (b)

Fig. 16. The variation of NOx emissions for a) bmep [65] b) bmep [66]

The variations of NOx emissions for diesel, GTL and DME at engine loads are shown in Fig. 17(a). NOx emissions for all of the fuels increase significantly when the engine load increases. Both of GTL and DME show greater NOx emission reductions in comparison to diesel, especially at high load. GTL and DME fuels averagely reduce NOx emissions by 15.6% and 48.2%, respectively, in comparison to diesel. The decreases in NOx with the use of GTL and DME are attained through their lower combustion temperatures, which may be caused by the shorter ignition delay for GTL and DME in comparison to diesel. Furthermore, aromatic content and density exhibit a good correlation with NOx emissions, so lower NOx emissions are also owing to lower aromatics content and lower density for GTL and DME fuels [67]. Fig. 17(b) showed NOx variation under the different port DME quantity and injection timing. At the fixed injection timing, NOx emission of PCCI operation was slightly lower compared with the one of diesel DICI operation, and presented a decreasing trend with a rise of DME at first but this decreasing trend ceased at a higher DME quantity. Two main factors led to the NOx initial reduction. Firstly, the diesel ignition delay shortened owing to the increased in-cylinder pressure and temperature from port premixing DME HCCI. Secondly, the gases after HCCI combustion as internal EGR could reduce the oxygen content in the mixture charge through dilution. As a result, NOx formation could be prohibited to a certain extent. The cease of NOx decreasing trend hereafter was that a large quantity of DME made a rapid high-temperature reaction, which increased the charge temperature. At the situation of a fixed DME quantity, when diesel injection timing retarded, a reduction in NOx emissions could be observed in Fig. 17(b) late injection decreased the in-cylinder maximum pressure as more fuel burned after TDC, which resulted in lower in-cylinder temperatures [69].

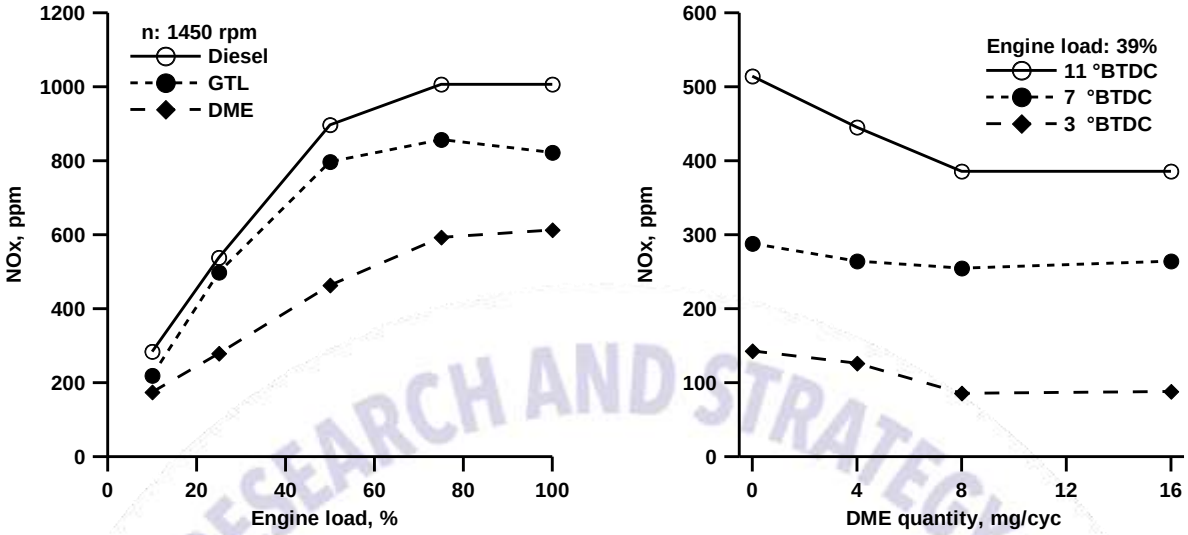

(a) (b)

Fig. 17. The variation of NOx emissions for a) engine load [67] b) DME quantity [69]

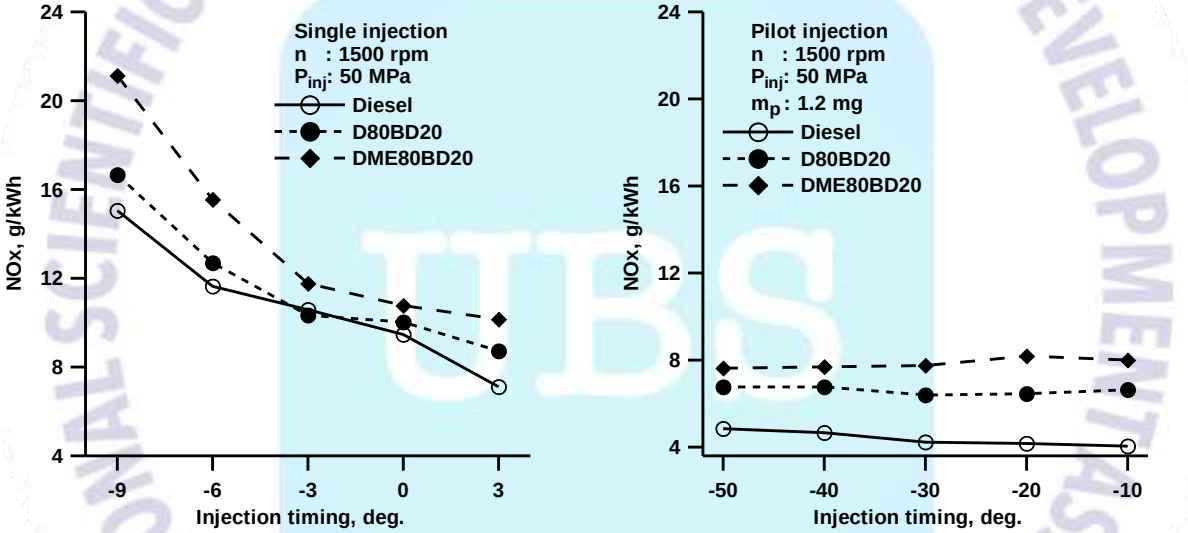

(a) (b)

Fig. 18. The variation of NOx emissions for a) single injection b) pilot injection [73]

In general, NOx emissions are strongly dependent on combustion temperature. In pilot injection mode, as shown in Fig. 18(a) and (b), the NOx emissions of DME fuel are higher than those of diesel and biodiesel-diesel blend (BD80D20) regardless of injection timings. It can be observed that the NOx emissions significantly decreased when compared to the single injection case. DME80BD20 fuel showed higher concentrations for all test ranges in pilot injection operation, while conventional diesel and BD80D20 fuel exhibited low concentrations of NOx emission. In the case of pilot injection case, the NOx concentration indicated the similar values at whole pilot injection timings [73]. For a specific engine speed characteristics, the temperature becomes the key factor that determines NOx formation and emission level. As the engine load increasing, more fuel needs to be burned, resulting in a higher cylinder temperature and a higher NOx emission level. As seen in Fig. 19(a) and (b), NOx emission increases with the increase of engine load for both DME and diesel fuel, however, DME engine has a smaller step. Besides, NOx emission of both DME and diesel engines decreases as engine speed elevated. A higher

engine speed means larger friction loss power, more fuel should be burned to give more power, leading to a higher cylinder temperature. While, the residence time of the temperature is decreased simultaneously. And in this case, the residence time becomes the key factor that determines the NOx formation, the decrease of the time causes the reduction of NOx emission. The most attractive phenomenon is that, compared to diesel engine, NOx emission is decreased more than 50% when the engine ran on DME at the same fuel injection timing. The lower NOx emission characteristic of DME engine lies in its fuel feature: high cetane number and high latent heat. In comparison with diesel fuel, there is less quantity of the flammable mixture prepared during the ignition delay for DME fuel due to its higher cetane number, though it evaporates easily. As a result, the maximum combustion temperature is decreased. The high latent heat of DME also contributes to the decrease of the temperature. They together result in the reduction of the NOx emission of DME engine. The NOx emission can be further significantly reduced by retarding the injection timing. Compared with the condition of injection timing of 25 CA BTDC, NOx emission is reduced about 20% and 35% with the delay of injection timing of 3 and 6 CA BTDC respectively. As DME delivery delayed, the fuel injection timing closes to the TDC. The initial temperature and pressure of the in-cylinder gas is elevated, resulting in a shorter ignition delay. Less fuel will be burned during the premixed combustion. Thus, the maximum combustion temperature and NOx emission for DME operation are remarkably reduced [74].

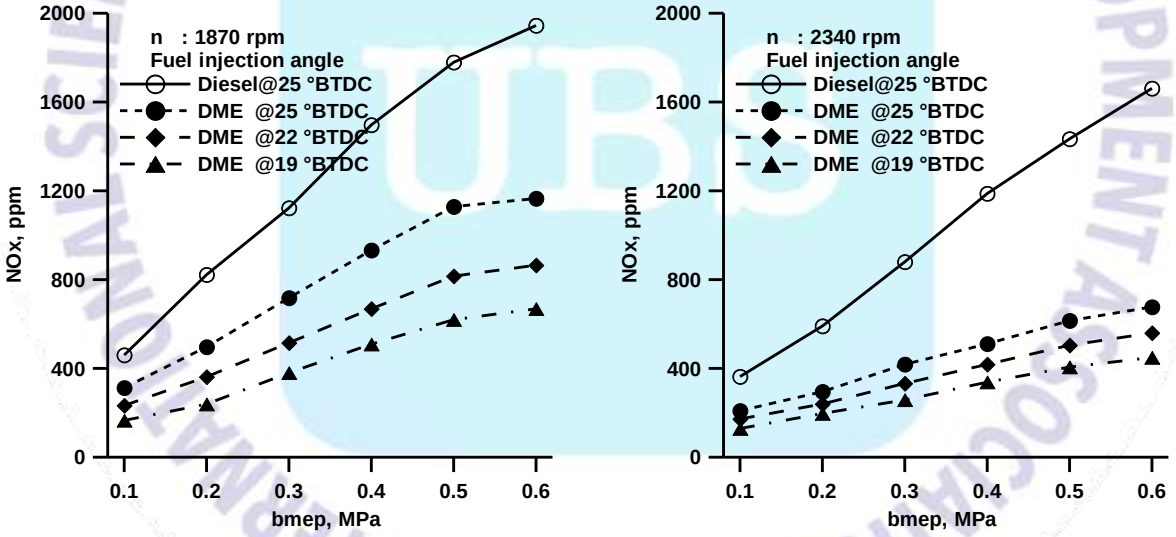

Fig. 19. The variation of NOx emissions for a) 1870 rpm b) 2340 rpm [74]

Fig. 20(a) shows the NOx emission characteristics for SOI at a 60 MPa injection pressure and a 1200 rpm engine speed. A decrease in NOx seems with the retardation of SOI at the right side of the figure. The decrease of NOx occurs with the advance of SOI at the left side of the figure. SOI between 10-15 °BTDC where most of the injected DME flowed into the piston bowl after targeting an area beneath the piston lip, resulting in total mixing with mixed biogas-air. Hence, a more uniform mixture of air and fuel can be formed and then a more active combustion process can take place. Consequently, these parameters have influenced NOx emissions, which are mainly affected by the combustion temperature. On the other hand, the NOx emissions tended to decrease in all SOI ranges with increasing biogas premixing ratio. A decrease in peak

combustion temperature occurs due to the slower flame speed of biogas relative to pure DME. Hence, NOx emissions were decreased. Another reason for the reduction of NOx with increasing mixing ratio of biogas is due to CO_2 in the biogas, which makes achieving high in-cylinder temperature difficult. Further, the effect of biogas mixing on NOx emissions became clear as the SOI advanced. Moreover, it can be found that the biogas-DME dual fuel combustion with a mixing ratio of biogas of 0.2-0.6 emitted lower NOx than pure DME combustion in all SOI ranges [75]. Fig. 20(b) shows there is increase in NOx emission as the load increases. This is due to higher oxygen content in exhaust gas which further increases the NO emissions. This can be reduced by using Exhaust Gas Recirculation (EGR) system. DME allows higher rates of EGR mixing rates due to its higher cetane number [79].

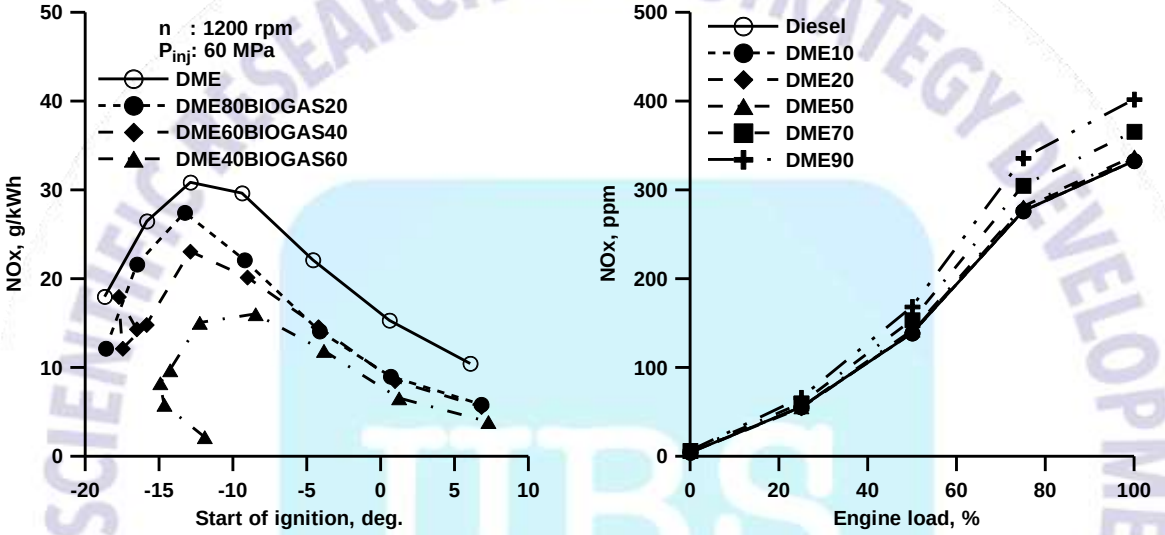

(a) (b)

Fig. 20. The variation of NOx emissions for a) start of ignition [75] b) engine load [79]

5. CONCLUSIONS

The effects of using DME in diesel engines are investigated on NOx emissions characteristics in this review study. The following conclusions can be summarized as results of the study.

- Some researches reported that DME combustion results in lower NOx emissions than diesel combustion due to the lower heating value, the higher heat of vaporization, the shorter ignition delay, the smaller amount of fuel injected during the ignition delay period and the smaller amount of fuel burned during the premixed burning phase which results in the lower peak combustion temperature.
- It is possible that higher amount of NOx can be produced from DME than diesel fuel for an early start of injection since the duration of the peak temperature would be longer in the initial combustion period due to shorter ignition delay of DME. When injection retardation is optimized for each fuel, NOx from DME is lower than from diesel fuel.
- NOx emissions decreases when the addition of DME into diesel fuel. But, it is concluded that the fuel supply advance angle is retarded appropriately, the power output would be improved somewhat and NOx emission could be reduced further.
- Compared with neat biodiesel, NOx emissions for biodiesel-DME blends decreased. NOx emissions also decrease with increase of DME quantity into biodiesel. The thermal

mechanism dominates the formation of NOx in biodiesel combustion. Thus, the major factors affecting NOx formation are combustion temperature, local oxygen concentration and residence time in the high temperature zone. For the biodiesel-DME blends, the cooling effect of DME associated with its lower calorific value and higher latent heat of evaporation could reduce the combustion temperature and hence reduce the NOx emissions.

REFERENCES

1. Yoon, S.H., Cha, J.P. and Lee, C.S. An investigation of the effects of spray angle and injection strategy on dimethyl ether (DME) combustion and exhaust emission characteristics in a common-rail diesel engine. *Fuel Processing Technology*, 91, 1364-1372, 2010.
2. Youn, I.M., Park, S.H., Roh, H.G. and Lee, C.S. Investigation on the fuel spray and emission reduction characteristics for dimethyl ether (DME) fueled multi-cylinder diesel engine with common-rail injection system. *Fuel Processing Technology*, 92, 1280-1287, 2011.
3. Alam, M. and Kajitani, S. *DME as an alternative fuel for direct injection diesel engine*. 4th International Conference on Mechanical Engineering, Dhaka, 2001.
4. Maji, S., Ahmed, S., Siddiqui, W.A. and Kumar, A. Impact of di-methyl ether (DME) as an additive fuel for compression ignition engine in reduction of urban air pollution. *International Journal of Innovative Research in Science, Engineering and Technology*, 3(11), 17221-17228, 2014.
5. Park, S.H. and Lee, C.S. Applicability of dimethyl ether (DME) in a compression ignition engine as an alternative fuel. *Energy Conversion and Management*, 86, 848-863, 2014.
6. Wattanavichien, K. Implementation of DME in a small direct injection diesel engine. *International Journal of Renewable Energy*, 4(2), 1-12, 2009.
7. Duan, J., Sun, Y., Yang, Z. and Sun, Z. *Combustion and emissions characteristics of diesel engine operating on composite combustion mode of DME and diesel*. Proceedings of International Conference on Mechanical Engineering and Material Science, Shanghai, China, 2012.
8. Kowalewicz, A. and Wojtyniak, M. Alternative fuels and their application to combustion engines. *Journal of Automobile Engineering*, 219, 103-125, 2005.
9. Azizi, Z., Rezaeimanesh, M., Tohidian, T. and Rahimpour, M.R. Dimethyl ether: A review of technologies and production challenges. *Chemical Engineering and Processing*, 82, 150-172, 2014.
10. Huang, Z., Qiao, X., Zhang, W., Wu, J. and Zhang, J. Dimethyl ether as alternative fuel for CI engine and vehicle. *Frontiers of Energy and Power Engineering in China*, 3(1), 99-108, 2009.
11. Lecksiwilai, N., Gheewala, S.H., Sagisaka, M. and Yamaguchi, K. Net energy ratio and life cycle greenhouse gases (GHG) assessment of bio-dimethyl ether (DME) produced from various agricultural residues in Thailand. *Journal of Cleaner Production*, 134, 523-531, 2016.
12. Inayat, A., Ghenai, C., Naqvi, M., Ammar, M., Ayoub, M. and Hussin, M.N.B. Parametric study for production of dimethyl ether (DME) as a fuel from palm wastes. *Energy Procedia*, 105, 1242-1249, 2017.
13. Park, S.H. and Lee, C.S. Combustion performance and emission reduction characteristics of automotive DME engine system. *Progress in Energy and Combustion Science*, 39, 147-168, 2013.

14. Teng, H., McCandless, J. C. and Scheneyer Jeffrey, B. Thermochemical characteristics of dimethyl ether alternative fuel for compression-ignition. *Society of Automotive Engineers*, Paper no 2001-01-0154, 2001.
15. Maji, S., Ahmed, S., Siddiqui, W.A., Aggarwal, S. and Kumar, A. Impact of di-methyl ether (DME) as an additive fuel for compression ignition engine in reduction of urban air pollution. *American Journal of Environmental Protection*, 3(2), 48-52, 2015.
16. Guangxin, G., Zhulin, Y., Apeng, Z., Shenghua, L. and Yanju, W. Effects of fuel temperature on injection process and combustion of dimethyl ether engine. *Journal of Energy Resources Technology*, 135, 1-5, 2013.
17. Jalanapurkar, M., Patel, K., Patel, T., Rathod, G. and Granipa, H. A literature review on combine effect of di-methyl ether (DME) as an additive & the injection pressure on the performance & emission of 4 stroke C.I engine. *International Journal of Advance Engineering and Research Development*, 2(1), 262-266, 2015.
18. Kim, H.J., Park, S.H., Lee, K. S. and Lee, C.S. A study of spray strategies on improvement of engine performance and emissions reduction characteristics in a DME fueled diesel engine. *Energy*, 36, 1802-1813, 2011.
19. Xu, S., Wang, Y., Zhang, X., Zhen, X. and Tao, C. Development of a novel common-rail type dimethyl ether (DME) injector. *Applied Energy*, 94, 1-12, 2012.
20. Lim, O.T. and Iida, N. A study on the spray and engine combustion characteristics of diesel-dimethyl ether fuel blends. J Automobile Engineering, 229(6), 782-792, 2015.
21. Suh, H.K. and Lee, C.S. Experimental and analytical study on the spray characteristics of dimethyl ether (DME) and diesel fuels within a common-rail injection system in a diesel engine. *Fuel*, 87, 925-932, 2008.
22. Genbao, L., Jianming, C., Minglong, L., Yuhua, Q. and Zhaoyang, C. Experimental study on the size distribution characteristics of spray droplets of DME/diesel blended fuels. *Fuel Processing Technology*, 104, 352-355, 2012.
23. Mohan, B., Yang, W., Yu, W. and Tay, K.L. Numerical analysis of spray characteristics of dimethyl ether and diethyl ether fuel. *Applied Energy*, 185, 1403-1410, 2017.
24. El-Hagar, M.M.E-G. Effect of diethyl ether and dimethyl ether with liquefied petroleum gas on combustion and emissions characteristics of diesel engine. International Journal of Computer Science and Engineering, 2(3), 193-198, 2014.
25. Wang, Y., Xiao, F., Zhao, Y., Li, D. and Lei, X. Study on cycle-by-cycle variations in a diesel engine with dimethyl ether as port premixing fuel. *Applied Energy*, 143, 58-70, 2015.
26. Jeon, J., Kwon, S., Park, Y.H., Oh, Y. and Park, S. Visualizations of combustion and fuel/air mixture formation processes in a single cylinder engine fueled with DME. Applied Energy, 113, 294-301, 2014.
27. Baskaran, R. Analysis on synthesis, storage & combustion characteristics of DME as fuel in CI engines. *International Journal for Research in Applied Science & Engineering Technology*, 3(1), 133-140, 2015.
28. Park, S. Optimization of combustion chamber geometry and engine operating conditions for compression ignition engines fueled with dimethyl ether. *Fuel*, 97, 61-71, 2012.

29. Benajes, J., Novella, R., Pastor, J.M., Hernández-López, A. and Kokjohn, S.L. Computational optimization of the combustion system of a heavy duty direct injection diesel engine operating with dimethyl-ether. *Fuel*, 218,127-139, 2018.
30. Oda, Y., Osafune, Y., Ueda, H. and Fujimura, K. Clean combustion technology in diesel engines operated with dimethyl ether. *Mitsubishi Heavy Industries Ltd. Technical Review*, 40(6), 1-5, 2004.
31. Song, J., Huang, Z., Qiao, X. and Wang, W. Performance of a controllable premixed combustion engine fueled with dimethyl ether. *Energy Conversion and Management*, 45, 2223-2232, 2004.
32. Khunaphan, S., Hartley, U.W. and Theinnoi, K. Characterization and potential of dimethyl ether (DME) as dual fuel combustion in a compression ignition engine. *International Journal of Engineering Science and Innovative Technology*, 2(3), 79-85, 2013.
33. Lamani, V.T., Yadav, A.K. and Narayanappa, K.G. Influence of low-temperature combustion and dimethyl ether-diesel blends on performance, combustion, and emission characteristics of common rail diesel engine: a CFD study. *Environmental Science and Pollution Research*, 24, 15500-15509, 2017.
34. Chapman, E.M. and Boehman, A.L. Pilot ignited premixed combustion of dimethyl ether in a turbodiesel engine. *Fuel Processing Technology*, 89, 1262-1271, 2008.
35. Ying, W., Longbao, Z., Zhongji, Y. and Hongyi, D. Study on combustion and emission characteristics of a vehicle engine fuelled dimethyl ether. *Journal of Automotive Engineering*, 219, 263-269, 2005.
36. Benajes, J., Novella, R., Pastor, J.M., Hernández-López, A. and Kokjohn, S.L. Computational optimization of a combustion system for a stoichiometric DME fueled compression ignition engine. *Fuel*, 223, 20-31, 2018.
37. Kropiwnicki, J., Dominiczak, P. and Kneba, Z. Analysis of the possibilities of using of DME fuel in motor boat drive systems. *Combustion Engines*, 171(4), 74-80, 2017.
38. Smolec, R., Idzior, M., Karpiuk, W. and Kozak, M. Assessment of the potential of dimethyl ether as an alternative fuel for compression ignition engines. *Combustion Engines*, 169(2), 181-186, 2017.
39. Namasivayam, A.M., Korakianitis, T., Crookes, R.J., Bob-Manuel, K.D.H. and Olsen, J. Biodiesel, emulsified biodiesel and dimethyl ether as pilot fuels for natural gas fuelled engines. *Applied Energy*, 87, 769-778, 2010.
40. Jang, J. and Bae, C. Effects of valve events on the engine efficiency in a homogeneous charge compression ignition engine fueled by dimethyl ether. *Fuel*, 88, 1228-1234, 2009.
41. Ryu, K., Zacharakis-Jutz, G.E. and Kong, S.-C. Performance characteristics of compression- ignition engine using high concentration of ammonia mixed with dimethyl ether. *Applied Energy*, 113, 488-499, 2014.
42. Semelsberger, T.A., Borup, R.L. and Grene, H.L. Dimethyl ether (DME) as an alternative fuel. *Journal of Power Sources*, 156, 497-511, 2006.

43. Li, G. Dimethyl ether (DME): a new alternative fuel for diesel vehicle. *Advanced Materials Research*, 156-157, 1014-1018, 2011.
44. Sezer, I. Thermodynamic, performance and emission investigation of a diesel engine running on dimethyl ether and diethyl ether. *International Journal of Thermal Sciences*, 50, 1594-1603, 2011.
45. Wang, Y., Zhao, Y. and Yang, Z. Dimethyl ether energy ratio effects in a dimethyl ether-diesel dual fuel premixed charge compression ignition engine. *Applied Thermal Engineering*, 54, 481-487, 2013.
46. Ying, W., Li, H., Longbao, Z. and Wei, L. Effects of DME pilot quantity on the performance of a DME PCCI-DI engine. *Energy Conversion and Management*, 51, 648-654, 2010.
47. Chen, Z., Konno, M. and Kajitani, S. Performance and emissions of DI compression ignition engines fueled with dimethyl ether. *JSME International Journal*, 43(1), 82-88, 2000.
48. Arcoumanis, C., Bae, C., Crookes, R. and Kinoshita, E. The potential of di-methyl ether (DME) as an alternative fuel for compression-ignition engines: A review. Fuel, 87(7), 1014-1030, 2008.
49. Taghavifar, H., Khalilarya, S., Mirhasani, S. and Jafarmadar, S. Numerical energetic and exergetic analysis of CI diesel engine performance for different fuels of hydrogen, dimethyl ether, and diesel under various engine speeds. *International Journal of Hydrogen Energy*, 39, 9515-9526, 2014.
50. Patil, K.R. and Thipse, S.S. The potential of DME-diesel blends as an alternative fuel for CI engines. *International Journal of Emerging Technology and Advanced Engineering* 2(10), 35-41, 2012.
51. Vispute, K.M. and Pawar, T.J. Study and prospects of di-methyl ether as an alternative fuel in C.I. engine: review. *International Journal of Trend in Research and Development*, 3(4), 134-138, 2016.
52. Theinnoi, K., Suksompong, P. and Temwutthikun, W. Engine performance of dual fuel operation with in-cylinder injected diesel fuels and in-port injected DME. *Energy Procedia*, 142, 461-467, 2017.
53. Deepak, K.M., Karthick, M., Dineshbabu, D., Srikanth, P. and Ramachandran, M.G. Investigation on the effect of dimethyl ether in compression ignition engine. *International Journal of Innovative Research in Science, Engineering and Technology*, 4(2), 401-407, 2015.
54. Kajitani, S. A study of low compression ratio diesel engines operated with neat dimethyl ether (DME). *JSME TED Newsletter*, 42, 1-14, 2004.
55. Hewu, W. and Longbao, Z. Performance of a direct injection diesel engine fuelled with a dimethyl ether/diesel blend. *Journal of Automobile Engineering*, 819-824, 2017.
56. Prabhakaran, B., Thennarasu, P. and Karthick, S. Performance and characteristics of a CI engine using DME (Dimethyl Ether). *International Journal of Innovative Research in Science, Engineering and Technology*, 4(2), 31-34, 2015.

57. Kajitani, S. and Chen, Z. Fundamental research on next generation fuel (dimethyl ether) engines. *Journal of Scientific & Industrial Research*, 62, 133-144, 2003.
58. Abhishek, Rahul, K., Santosh, K. and Martha, O. Blending impacts of biogas and dimethyl ether (DME) on compressed ignition engine. *International Research Journal of Engineering and Technology*, 4(4), 2174-2177, 2017.
59. Loganathan, M., Anbarasu, A. and Velmurugan, A. Emission characteristics of jatropha-ethanol and jatropha-dimethyl ether fuel blends on a DI diesel engine. *Journal of Mechanical Engineering*, 42(1), 38-46, 2012.
60. Kim, H.J. and Park, S.H. Optimization study on exhaust emissions and fuel consumption in a dimethyl ether (DME) fueled diesel engine. *Fuel*, 182, 541-549, 2016.
61. Park, S.H., Shin, D. and Park, J. Effect of ethanol fraction on the combustion and emission characteristics of a dimethyl ether-ethanol dual-fuel reactivity controlled compression ignition engine. *Applied Energy*, 182, 243-252, 2016.
62. Geng, P., Cao, E., Tan, Q. and Wie, L. Effects of alternative fuels on the combustion characteristics and emission products from diesel engines: A review. *Renewable and Sustainable Energy Reviews*, 71, 523-534, 2017.
63. Loganathan, M., Anbarasu, A. and Velmurugan, A. Emission characteristics of jatropha-dimethyl ether fuel blends on a DI diesel engine. *International Journal of Scientific & Technology Research*, 1(8), 28-32, 2012.
64. Zhao, Y., Wang, Y., Li, D., Lei, X. and Liu, S. Combustion and emission characteristics of a DME (dimethyl ether)-diesel dual fuel premixed charge compression ignition engine with EGR (exhaust gas recirculation). *Energy*, 72, 608-617, 2014.
65. Hou, J., Wen, Z., Jiang, Z. and Qiao, X. Study on combustion and emissions of a turbocharged compression ignition engine fueled with dimethyl ether and biodiesel blends. *Journal of the Energy Institute*, 87, 102–113, 2014.
66. Ying, W., Longbao, Z. and Hewu, W. Diesel emission improvements by the use of oxygenated DME/diesel blend fuels. *Atmospheric Environment*, 40, 2313-2320, 2006.
67. Xinling, L. and Zhen, H. Emission reduction potential of using gas-to-liquid and dimethyl ether fuels on a turbocharged diesel engine. *Science of the Total Environment*, 407, 2234-2244, 2009.
68. Yanju, W., Kun, W., Wenrui, W., Shenghua, L., Xiao, C., Yajing, Y. and Shanwen, B. Comparison study on the emission characteristics of diesel- and dimethyl ether-originated particulate matters. *Applied Energy*, 130, 357-369, 2014.
69. Wang, Y., Zhao, Y., Xiao, F. and Li, D. Combustion and emission characteristics of a diesel engine with DME as port premixing fuel under different injection timing. *Energy Conversion and Management*, 77, 52-60, 2014.
70. Park, S.H., Kim, H.J. and Lee, C.S. Effects of dimethyl-ether (DME) spray behavior in the cylinder on the combustion and exhaust emissions characteristics of a high speed diesel engine. *Fuel Processing Technology*, 91, 504-513, 2010.
71. Thomas, G., Feng, B., Veeraragavan, A., Cleary, M.J. and Drinnan, N. Emissions from DME combustion in diesel engines and their implications on meeting future emission norms: A review. *Fuel Processing Technology*, 119, 286-304, 2014.

72. Yoon, S.H., Han, S.C. and Lee, C.S. Effects of high EGR rate on dimethyl ether (DME) combustion and pollutant emission characteristics in a direct injection diesel engine. *Energies*, 6, 5157-5167, 2013.
73. Roh, H.G., Lee, D. and Lee, C.S. Impact of DME-biodiesel, diesel-biodiesel and diesel fuels on the combustion and emission reduction characteristics of a CI engine according to pilot and single injection strategies. *Journal of the Energy Institute*, 88, 376-385, 2015.
74. Zhu, Z., Li, D.K., Liu, J., Wei, Y.J. and Liu, S.H. Investigation on the regulated and unregulated emissions of a DME engine under different injection timing. *Applied Thermal Engineering*, 35, 9-14, 2012.
75. Park, S.H., Yoon, S.H., Cha, J. and Lee, C.S. Mixing effects of biogas and dimethyl ether (DME) on combustion and emission characteristics of DME fueled high-speed diesel engine. *Energy*, 66, 413-422, 2014.
76. Bogdan, J., Nicolae, B., Călin, I. and Vlad, B.N. Study of emissions for a compression ignition engine fueled with a mix of DME and diesel. *Materials Science and Engineering*, 252, 1-9, 2017.
77. Kim, H.J., Park, S.W. and Lee, C.S. Numerical and experimental study on the combustion and emission characteristics of a dimethyl ether (DME) fueled compression ignition engine. *Oil & Gas Science and Technology*, 67(3), 479-489, 2012.
78. Wang, H.W., Zhou, L.B., Jiang, D.M. and Huang, Z.H. Study on the performance and emissions of a compression ignition engine fuelled with dimethyl ether. *Journal of Automotive Engineering*, 214, 101-106, 2000.
79. Ambekar, Y. and Hole, J. A. Preliminary optimization of duel fuel engine using dimethyl ether premixed combustion. *International Research Journal of Engineering and Technology*, 5(10), 274-278, 2018.
80. Longbao, Z., Hewu, W. and Ying, W. *Experimental study on Performances and combustion characteristics of DME powered vehicle*. Conference on Better Air Quality in Asian and Pacific Rim Cities (BAQ 2002), 16-18 December 2002, Hong Kong, p. 1-6, 2002.

A REVIEW STUDY ON THE EFFECTS OF DIMETHYL ETHER ON PM EMISSIONS IN DIESEL ENGINES

İsmet Sezer
Gümüşhane University, ORCID ID: 0000-0001-7342-9172

ABSTRACT
This review study was created from the various studies which were completed on the use of dimethyl ether in diesel engines as a fuel or fuel additive. The several methods are available for the decreasing of the harmful emissions in diesel engines. The first method for the reduction of harmful emissions is improved the combustion by modification of engine design and fuel injection system, but this process is expensive and time consuming. The second method is the using various exhaust gas devices like catalytic converter and diesel particulate filter. However, the use of such devices affects negatively diesel engine performance. The last method to reduce emissions and also improve diesel engine performance is the use of various alternative fuels or fuel additives. The major pollutants of diesel engines are oxides of nitrogen (NOx) and particulate matter (PM). It is very difficult to reduce NOx and PM simultaneously in practice. The most researches declare that the best way to reduce these emissions is the use of various alternative fuels i.e. natural gas, biogas, biodiesel or using some additives with the alternative fuels or conventional diesel fuel. Therefore, it is very important that the results of various studies on alternative fuels or fuel additives are evaluated together to practice applications. Especially, this study focuses on the usage of dimethyl ether in diesel engines as fuel or fuel additive. This review study investigates the effects of using dimethyl ether on PM emissions.

Keywords: Diesel engine performance, Dimethyl ether, Fuel additives, PM emissions

1. INTRODUCTION
Diesel engines are prime power sources among the automobile engines because of their better performance, higher fuel economy and lower exhaust emissions of hydrocarbons (HCs), carbon monoxide (CO) and carbon dioxide (CO_2) than gasoline engines [1]. However, current diesel engines emit higher levels of particulate matter (PM) and nitrogen oxides (NOx) than those of gasoline engines. Therefore, many researchers have researched to develop low-pollution diesel engines and progressive studies have been conducted on alternative fuels which may produce clean diesel engine emissions [2]. Among the various alternatives, DME is the most promising alternative for automotive fuel from the standpoint of energy security, because it can be industrially produced from coal, natural gas and many kinds of biomass fuels [3]. However, physical properties of DME such as lower viscosity, lubricity, combustion enthalpy and boiling point need the modifications to diesel engine internal structures and components. The technology with pure DME as an alternative fuel for CI engine and vehicle is still under development stage. However, DME can be used as an additive fuel with diesel and other alternative fuel [4]. It is very important that the results of various studies on DME are evaluated together to practice applications. This review study investigates the effects of using dimethyl ether on PM emissions.

2. CHARACTERISTICS OF DIMETHYL ETHER
DME is the simple ether with the chemical formula of CH3–O–CH3 as seen in Fig. 1. In general, the physical properties of DME are similar to those of LPG. Therefore, the storage, fuel handling, and transportation requirements for DME are similar to those for LPG [3]. DME can be produced using indirect or direct synthetic methods as seen in Fig. 2. Indirect synthetic

methods generate DME through a dehydration reaction after synthetic reaction of methanol, while direct synthetic methods make DME directly from natural gas [5]. DME production costs less than diesel fuel or gasoline on an energy equivalent basis. DME economics are similar to CNG or LNG, when large scale plants are considered [6]. DME is gaseous and almost non-toxic at atmospheric pressure and room temperature. Therefore, DME needs to be pressurized to over 0.5 MPa to keep it in a liquid state under ambient temperature and pressure conditions. The fuel delivery pressure should be increased to 1.7-2.0 MPa under engine operating conditions to prevent vapor lock in the fuel injection system [7, 8].

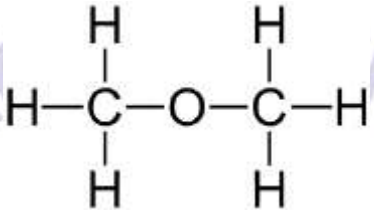

Fig. 1. Chemical structure of DME [5]

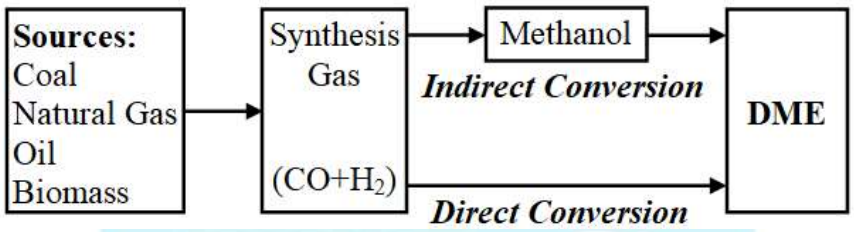

Fig. 2. Production methods of DME [9]

The properties of DME and diesel fuel are shown in Table 1. It can be seen that the properties of DME are quite different from those of diesel fuel. DME has high vapor pressure and low boiling temperature, which is a gas fuel at room temperature and atmospheric pressure. The heating value of DME is significantly lower than conventional diesel fuel. Therefore, the fuel supply and injection system, and the combustion system of the engine should be redesigned or modified [10]. The cetane number of DME is higher than that of diesel fuel, which demonstrates good ignition capability. The latent heat of evaporation of DME is much higher than that of diesel fuel, which is beneficial for reducing the mixture temperature.

Table 1. The properties of DME and diesel fuel

Property	**DME**	**Diesel**
Chemical formula	CH_3-O-CH_3	C_xH_y
Molecular weight, g	46.07	170
Boiling point, °C	-24.9	180-360
Liquid density, kg/lt	668	840
Liquid viscosity, cP	0.15	4.4-5.4
Lower heating value, kJ/kg	28430	42500
Ignition temperature, °C	235	250
Cetane number	55-60	40-55
Stoichiometric air/fuel ratio	9	14.6
Modulus of elasticity, N/m^2	$6.37x10^8$	$1.486x10^9$
Mass fraction of carbon	52.2	86
Mass fraction of hydrogen	13	14
Mass fraction of oxygen	34.8	0

DME has only C–H and C–O bonds, without C–C bonds, and contains about 34.8% oxygen. Because of these properties, DME combustion produces almost zero PM emissions, low noise level and can tolerate a higher exhaust gas recirculation (EGR) rate to reduce NOx emissions to a greater extent than with conventional diesel fuel [6]. The low viscosity of DME causes leakage in the fuel supply system, which relies on small clearances for sealing. Its lower lubricity characteristics result in intensified surface wear on the moving parts within the fuel injection system. Therefore, addition of proper additives to prevent leakage and surface wear is essential for DME. The compressibility of DME is generally higher than that of diesel, so DME also requires more compression pump work compared to the diesel. In general, DME deteriorates the rubber seals, mainly due to its corrosive nature. For that reason, all existing rubber seals in injection systems should be replaced with non-corrosive materials [1]. Another advantage of DME is that it is non-corrosive to the fuel system structure and metal surfaces [5].

3. STUDIES ON DIMETHYL ETHER

There are a number of studies in the literature on dimethyl ether such as the production technologies [9, 11, 12], fuel characteristics [5, 13-15], spray and injection characteristics [16-23], combustion characteristics [13, 24-36], performance characteristics [37-58] and exhaust emissions [59-80].

4. EFFECTS OF DIMETHYL ETHER ON PM EMISSIONS

Fig. 3(a) shows the soot emissions characteristics of Diesel and DME fuels. As can be seen in figure, the soot emission for DME fuel is nearly zero due to the chemical structure characteristics. The DME fuel has no carbon-to-carbon bond, and it has about 34.8% oxygen content in fuel. These chemical structures have originally influenced on the restraint of the soot formation. Also, the fast diffusion combustion of DME fuel and the suppression of the soot generation cause nearly zero soot emission of DME fuel. On the other hand, the increased engine speed the increase of the soot emission. The increase of the engine speed resulted in the lack of oxidation time for the soot emission. Consequently, the soot emission increased [2]. One of the main advantages of DME is the soot free combustion when burned in a DI diesel engine Fig. 3(b) and this soot-less combustion of DME might be due to the lean fuel-air mixture formation at the engine cylinder [3].

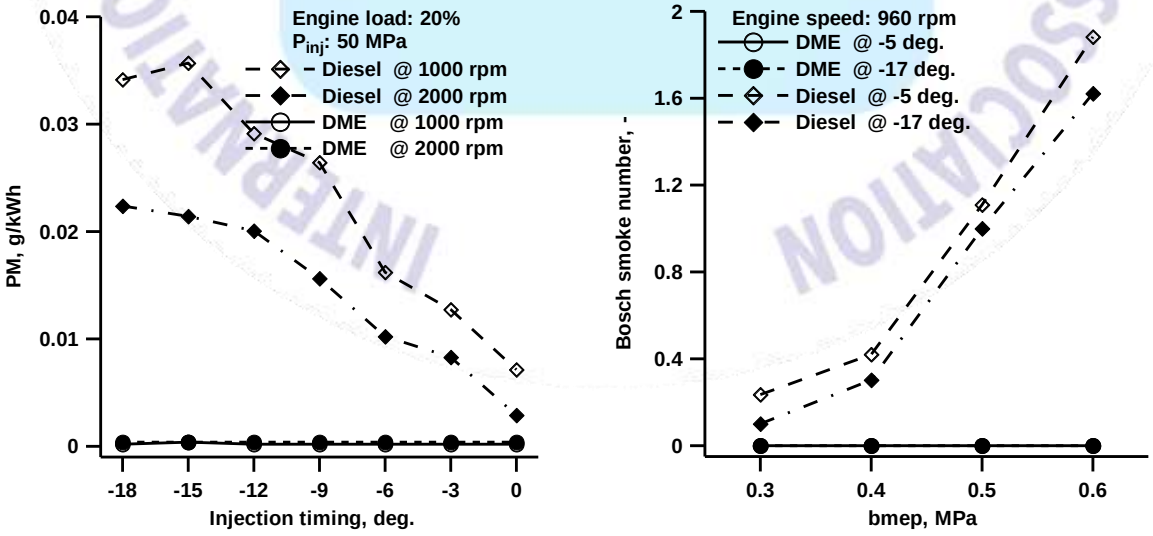

(a) (b)

Fig. 3. The variation of PM emissions for a) injection timing [2] b) bmep [3]

Fig. 4(a) is the smoke emission curves with load variation in the two combustion modes. The figure shows that the emissions in the composite combustion mode are only about 50% of the emissions in the diesel DI mode. It is because DME, lacking C-C bond in its molecular structure, breaks down easily for oxidation reaction of combustion. As a result it is not easy to form carbon smoke nuclei. And it is easy for DME, with higher oxygen content, to complete oxidation of C. Under heavy load conditions, the DME HCCI facilitates the diffusion and combustion of diesel. In this way the smoke emissions in composite combustion mode are much lower than that in the diesel DI mode [7]. The comparison of smoke emission between the DME engine and the diesel engine under different loads at an engine speed of 1400 rpm and 2200 rpm is indicated in Fig. 4(b). DME presents almost zero emission of smoke at all test engine loads and speeds. High oxygen content and absence of C–C bonds in the molecular structure of DME promises a smoke-free combustion [10].

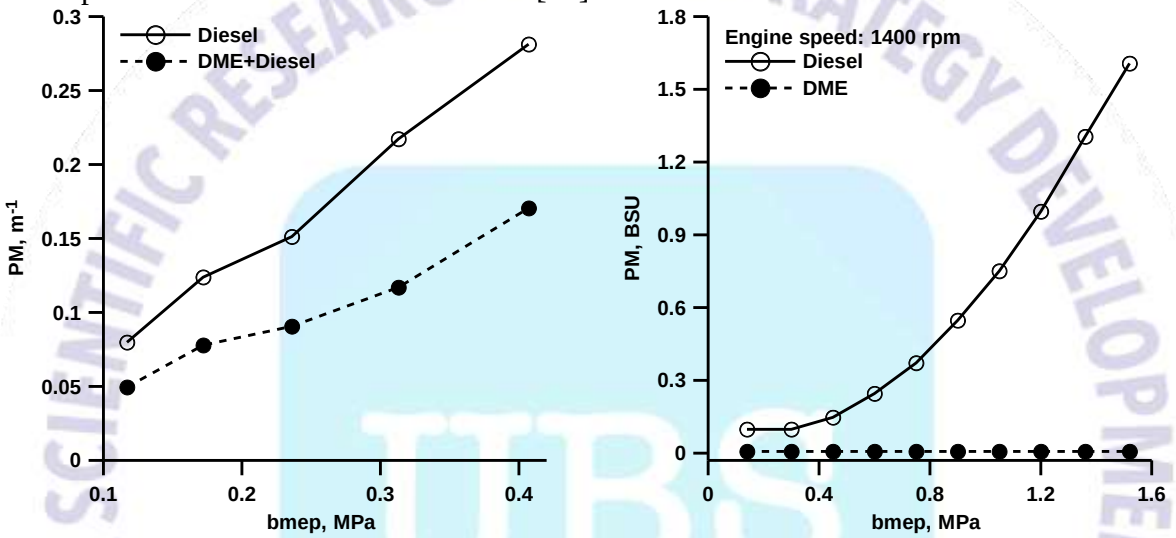

Fig. 4. The variation of PM emissions for a) bmep [7] and b) bmep [10]

Fig. 5(a) shows the smoke production, which was higher for the DME fuel at all the injection timings because the DME fuel has a high oxygen content, which leads to high oxidation rates of particulates. Therefore, with increasing DME fuel addition, smoke production decreased. The smoke emissions for the fuel blends DME5 and DME10 were reduced by 20% compared with those for the diesel fuel [20]. Fig. 5(b) show the smoke and particulate emission behavior of the engine operated with LPG-DEE and LPG-DME compared to the standard diesel operation. It can be observed that the engine operated with LPG exhibits a significant reduction in smoke and particulate emission at all loads. This is mainly because LPG has a lower carbon/hydrogen ratio, which makes the engine clean and free from the formation of any smoke. Moreover LPG contains low molecular weight as well as lesser number of carbon-to-carbon bonds typical of petroleum based hydrocarbon fuels. In addition LPG and DEE mixture also LPG and DME mixture is available inside the cylinder as a homogeneous charge. Hence there is an absolutely free from liquid fraction of fuel pockets (gaseous state) unlike heterogeneous combustion that takes place in a conventional direct injection diesel engine. The maximum reduction in smoke and particulate emission is observed to be about 85% and 89% respectively, at full load compared to that of diesel operation [24].

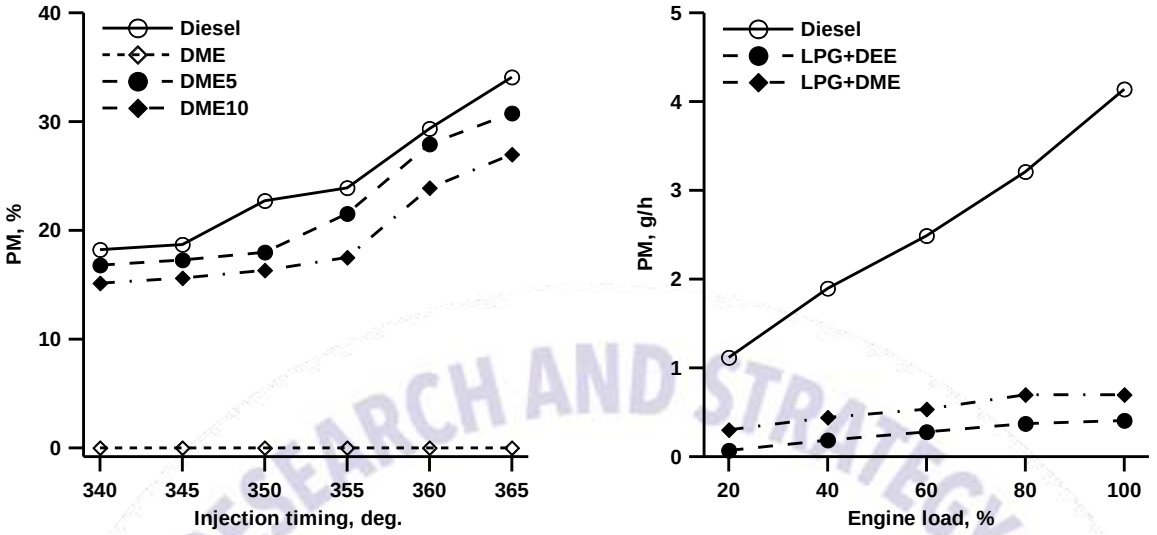

(a) (b)

Fig. 5. The variation of PM emissions for a) injection timing [20] and b) engine load [24]

PM emissions for a DME-diesel dual-fuel operation at the speed of 1700 rpm and the load of 0.36 MPa are exhibited in Fig. 6(a). Due to a decrease in the diffusion phase for DME-diesel PCCI combustion and the smokeless nature of DME, smoke emission is observed to be reduced with a rise of DME quantity in Fig. 6(a) [25]. The DME-fueled engine exhausted no soot emissions regardless of the engine speed and load due to the chemical structure characteristics. The precursors of soot, acetylene and polycyclic aromatic hydrocarbons (PAH), play a key role in soot formation. The formation of the precursors depends largely on radicals with carbon–carbon bonds in the fuel chemical structure. The chemical structure for DME fuel, CH3-O-CH3, contains no carbon-carbon bonds and has a high oxygen content, which significantly suppresses soot generation. The absence of carbon bonds in the fuel also restrained the formation of the soot precursors, and the oxygen content caused high particulate oxidation. Therefore, the soot emissions under DME operation were nearly zero. In contrast, the diesel-fueled engine exhausted a heightened amount of PM emissions in Fig. 6(b). Since the short ignition delay period for the low engine speed reduced the time during which the fuel-air mixture was formed, the soot emissions increased under locally rich mixture conditions [26].

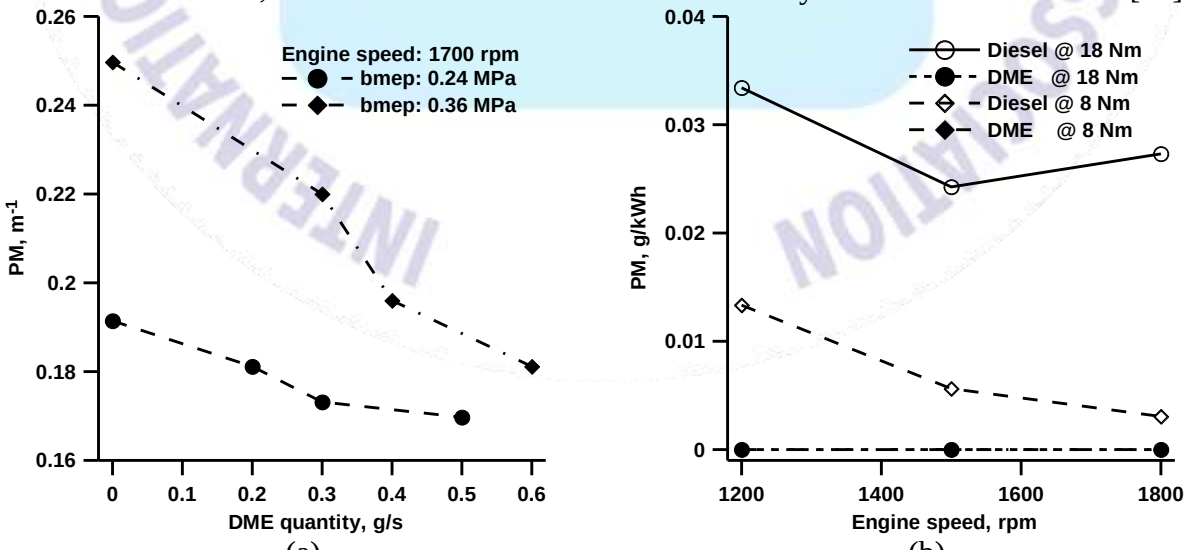

(a) (b)

Fig. 6. The variation of PM emissions for a) DME quantity [25] and b) engine speed [26]

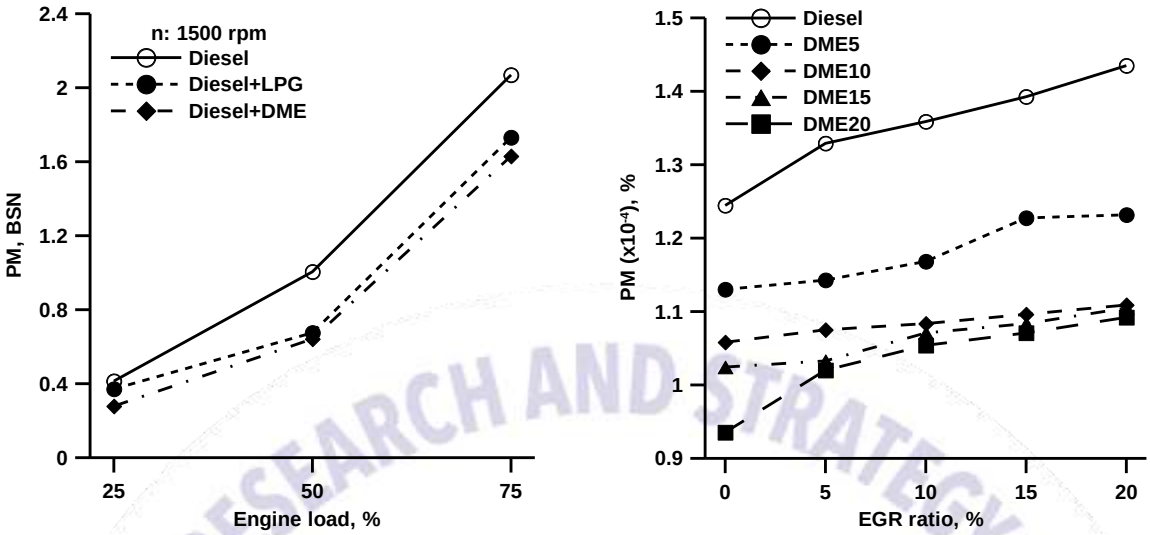

Fig. 7. The variation of PM emissions for a) engine load [32] and b) EGR ratio [33]

Fig. 7(a) shows the variation of smoke emissions under different engine load at 1500 rpm. It can be seen that the smoke emission from DME or LPG operated dual fuel engine reduces significantly than that of diesel operation. At 75% engine load in the DME-operated engine smoke is observed to be 1.6 BSN (Bosch Smoke Number) compared to LPG mode of 1.7 BSN and diesel mode of 2.1 BSN. The high oxygen content of DME fuel and low carbon to hydrogen ratio leads to high flame temperature and diffusive combustion in the combustion chamber. DME fuel combustion tends to improve engine smoke [32]. Fig. 7(b) shows the effect of DME-diesel blend and EGR rate on soot formation. The DME-fuelled engine exhausts very less soot emissions due to its chemical compositions. Formation of soot occurs in rich fuel and medium temperature zone. The precursors of soot, i.e., acetylene and polycyclic aromatic hydrocarbons (PAH), play a key role in soot formation. The formation of the precursors depends largely on radicals with carbon-carbon bonds in the fuel chemical structure. The chemical structure for DME fuel contains no C-C bonds and has more oxygen content which causes high particulate oxidation and suppresses soot formation. EGR decreases the oxygen concentration inside the combustion chamber which leads to a partial combustion and the high soot formation. It has been observed that with more EGR rate, in-cylinder soot formation increases. Results are compared for DME0 without EGR rate with various blends (DME5, DME10, DME15, and DME20) and different EGR rates (5, 10, 15, and 20%). Less soot formation is observed for DME20 blend (25%) compared to DME0 for without EGR case. As EGR increases, the effect of blends on PM is not significant. In the present range of study, it is noticed that the effect of blends (10, 15, and 20%) on reduction in soot formation at 20% EGR is almost constant. Soot formation takes place due to the combined effect of in-cylinder temperature as well as oxygen content in the charge. Increase in oxygen content enhances the soot oxidation, whereas decrease in temperature increases the soot formation. In-cylinder temperature decreases due to increase in blend and EGR rates, whereas oxygen contents increase with blends and decreases with EGR. Finally, the overall effect of these parameters on soot formation is marginal at higher blend and EGR rates [33].

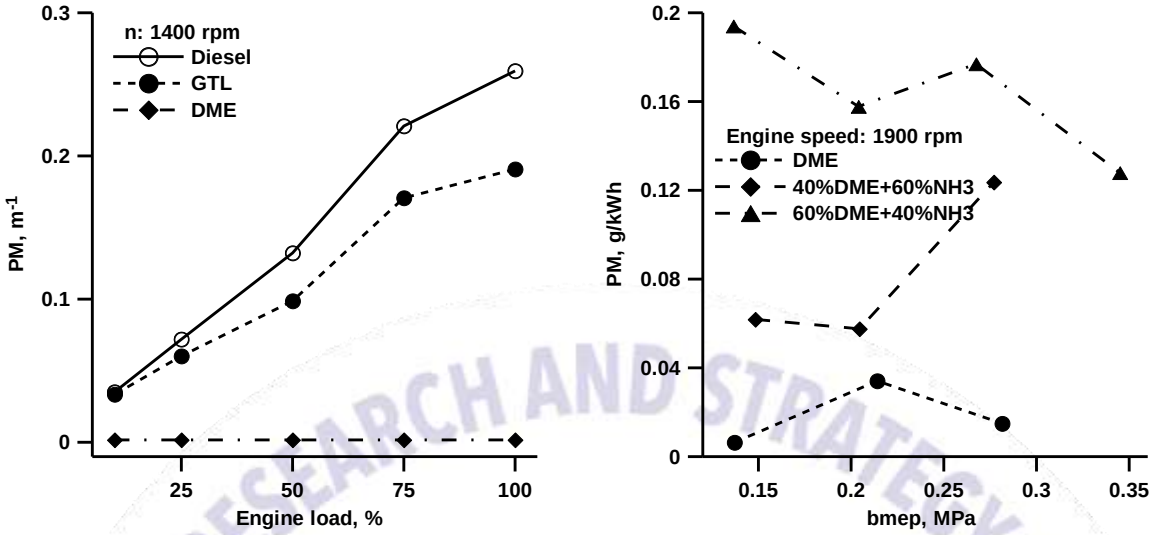

(a) (b)

Fig. 8. The variation of PM emissions for a) engine load [38] and b) bmep [41]

Majority of published research results on exhaust emissions from diesel engines fueled with DME indicates a significantly better emission performance compared to diesel fuel. Scarce emission of PM observed during DME combustion is most likely the result of combustion of the lubricating oil or the fuel lubricants. The reduced emission of particulate matter is mainly a result of the low boiling temperature that causes better evaporation of the fuel and its better mixing with air, simple composition of the molecule, presence of oxygen in the molecule and no direct bonds between the atoms of carbon. The comparison of smoke opacity tests performed on an engine fueled with different fuels has been shown in Fig. 8(a) presents the results of particulate matter tests performed on a diesel engine fueled with diesel fuel and DME. It is noteworthy that, in terms of mass, the engine fueled with DME generates much less particulate matter compared with diesel fuel [38]. Fig. 8(b) shows soot emissions for the three fuel mixtures. It is found that soot emissions for 60%DME+40%NH3 and 40%DME+60%NH3 are slightly greater than those for 100%DME; however, all three fuel mixture exhibit very low soot levels of which do not exceed 0.002 g/kW h. It should be noted that both fuel mixtures containing ammonia produce higher levels of soot than 100%DME even though the mixtures containing ammonia have fewer carbon. This can be attributed to the higher levels of incomplete combustion present in the 60%DME+40%NH3 and 40%DME+60%NH3 [41].

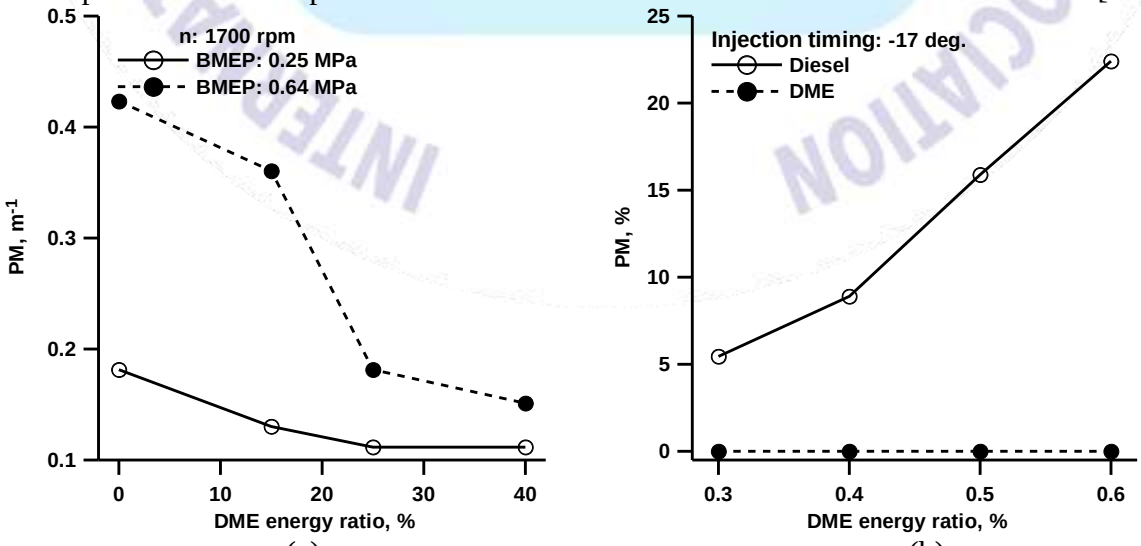

(a) (b)

Fig. 9. The variation of PM emissions for a) DME energy ratio [45] and b) bmep [47]

From Fig. 9(a), it was clear that smoke emissions under dual fuel combustion operation are lower compared to the ones under normal diesel operation for all cases examined. In a diesel engine, smoke was formed in the center of the fuel spray where the air/fuel ratio was low during the phase of diffusive combustion. On a basis of heat release analysis, the peak of diffusive combustion dropped with a rise of DME energy ratio due to the reduction of diesel injection mass change rate. In addition, less smoke may be related to a shorter diesel injection event and the avoidance of the later injection stages. As a result, the peak of diffusive combustion dropped and smoke opacity reduced with a rise of DME energy ratio. Taking account into these factors, it was discovered that DME-diesel dual fuel combustion operation was a feasible method to reduce smoke concentration at almost all test conditions. Practically, DME, being a lower member in the ester family, has very small tendency to produce smoke. Gaseous fuel also produced almost no smoke, while it contributed to the oxidation of the smoke formed from the combustion of the liquid fuel [45]. The emission of PM with DME operation was virtually zero over the whole range of engine load in Fig. 9(b). The reason for the low soot emission may be considered that DME molecules contain oxygen and are without direct C-C bonds [47].

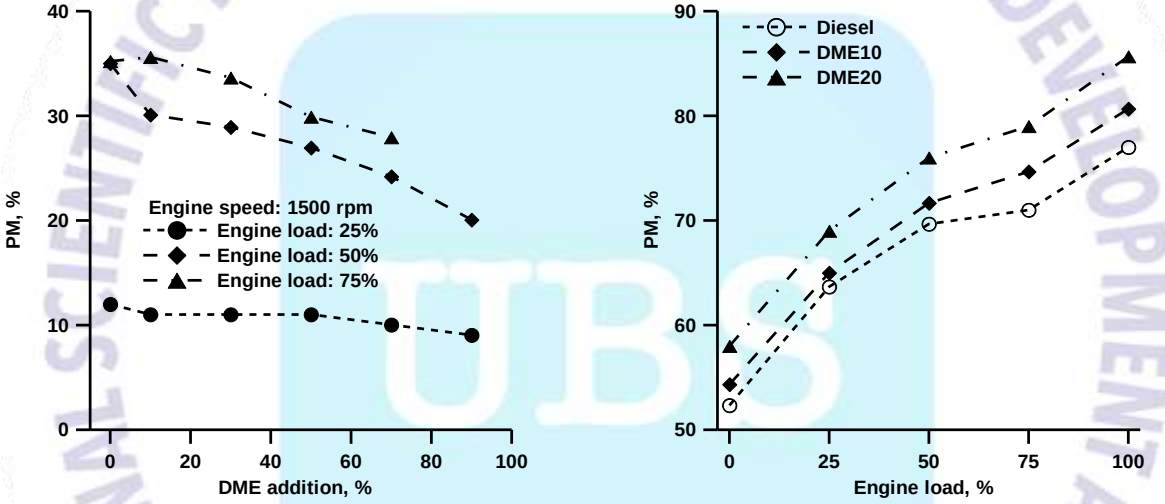

(a) (b)

Fig. 10. The variation of PM emissions for a) DME addition [52] and b) engine load [56]

The effect of DME injection on black smoke as showed in Fig. 10(a). DME pre-mixing combustion has the lower black smoke in order to the DME and fresh air are well mixed before entrain to combustion chamber. The high DME injection (90% of total fuel) can be reduce black smoke about 43.2% compare to diesel fuel combustion under low (25%) engine load. The low temperature combustion zone was found with DME injection, hence, soot was unable to further oxidized. In additions, the DME has molecular structure which C–C bonds are the effect of the black smoke decreasing [52]. From Fig. 10(b) the percentage of smoke increases as DME is added to diesel. This is due to incomplete combustion of the combustion product. When DME is added to diesel fuel, the combustion becomes incomplete. So, the smoke emission is more as percentage of DME increases [56].

Smoke emission is primarily produced at a high-temperature and fuel-rich region. In Fig. 11(a), smoke emission showed a clear descent tendency with an increase in DME pre-mixing ratio. The reason for this smoke reduction was that almost no smoke produced in the HCCI combustion stage due to an absence of C-C bonds in the molecular structure of DME. Secondly, an increase in the DME HCCI combustion and a decrease in the diffusion combustion resulted in an elevated in-cylinder temperature and an accelerated gas-flow, which improved the evaporation of diesel and led to a more complete combustion. Conversely, smoke emission

increased obviously with an increase in EGR rate. EGR resulted in a reduction in oxygen concentration and an increase in the number of anoxic zones in the cylinder, finally leading to a relatively incomplete combustion and the resultantly high smoke emissions [64]. Fig. 11(b) shows smoke emissions, of DME-biodiesel blends. By increasing the load, the smoke emissions of four fuels all increase. With increase of DME proportion, the smoke emission of biodiesel, DME70 and DME100 decrease gradually. Because high oxygen content and absence of carbon-carbon bonds in the molecular structure, low auto-ignition temperature and almost instantaneous vaporization in the cylinder, DME presents almost smoke-free combustion. It is noteworthy that the smoke emissions of DME50 are higher than those of biodiesel. However, the atomization performance of the DME50 spray is inferior to that of the DME100 and DME70 spray due to 50% biodiesel blended [65].

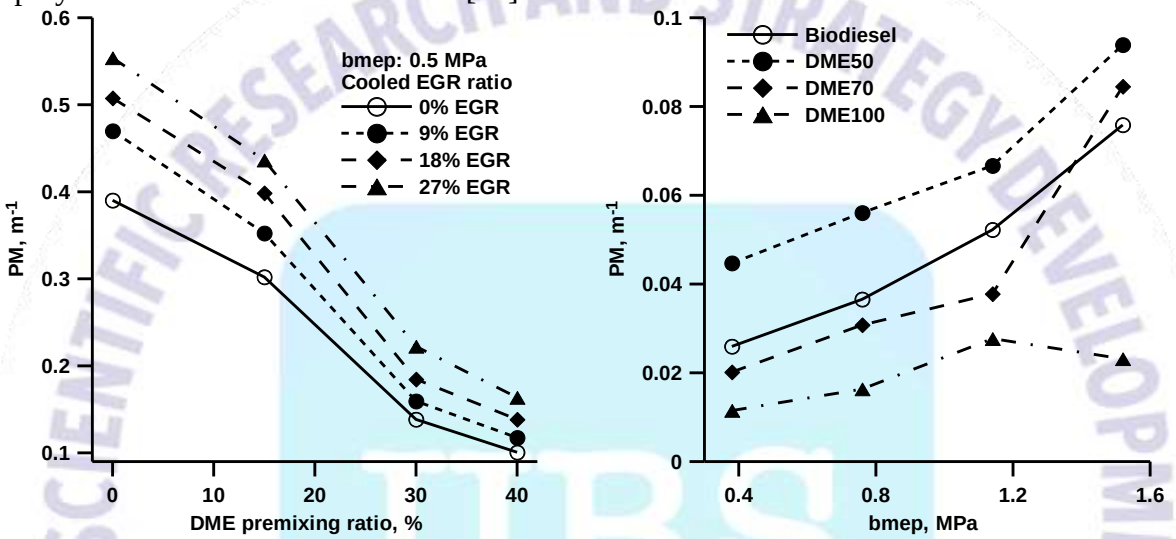

(a) (b)

Fig. 11. The variation of PM emissions for a) DME premixing ratio [64] and b) bmep [65]

Fig. 12(a) shows the comparisons of smoke emission under different BMEPs at an engine speed of 2000 rpm. It can be seen that DME blends can reduce the smoke density significantly, especially at higher loads. It is that an oxygenate additive DME is effectively introduced to the fuel regions and suppress soot formation in combustion chamber. High oxygen content of the blends combined with low C-H ratio and aromatics fractions are also assumed to contribute the reduction of smoke [66]. In Fig. 12(b) smoke emission reduced with a rise of DME quantity at the fixed injection timing. Based on heat release rate (HRR) analysis, the peak value of diffusion phase decreased with a rise of DME quantity. In addition, more DME quantity led to higher mixture homogeneity thus less smoke. These factors possibly resulted in the reduction of smoke. Moreover, smokeless nature of DME fuel also had a positive effect on smoke reduction. Like DICI combustion, smoke emission of PCCI combustion decreased with an earlier injection. The possible reason was a better air/fuel mixing owing to more time available for oxidation of smoke with an earlier injection [69].

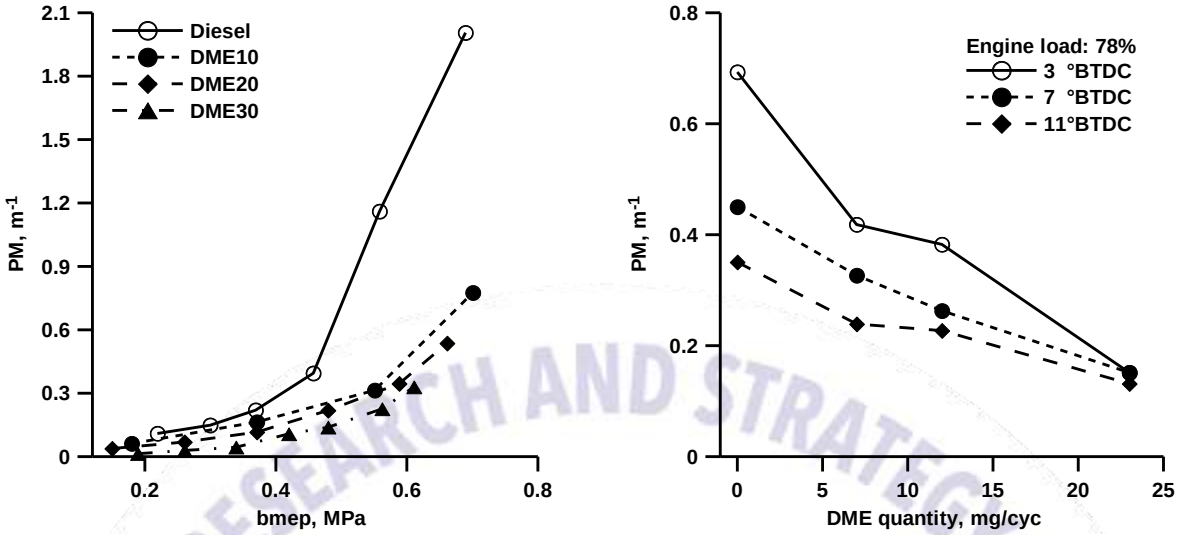

(a) (b)

Fig. 12. The variation of PM emissions for a) bmep [66] and b) DME quantity [69]

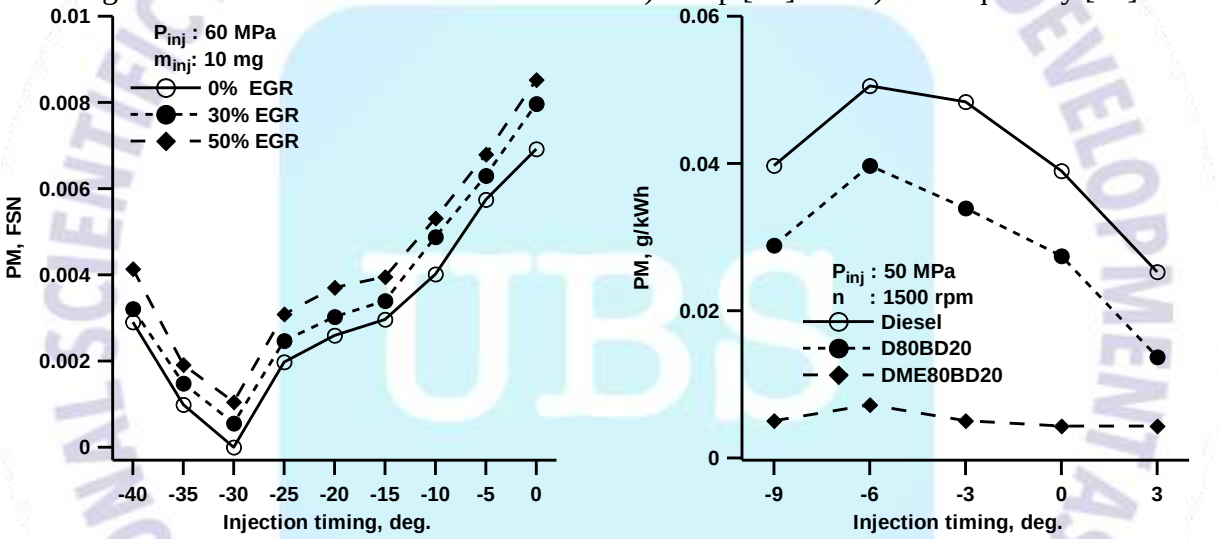

(a) (b)

Fig. 13. The variation of PM emissions for a) injection timing [72] and b) injection timing [73]

Fig. 13(a) shows the soot emission variation with EGR rate. In general, both soot formation and soot oxidation mechanisms are a function of combustion temperature and net soot release is maximized when the two mechanisms equally compete with each other. A decrease in combustion temperature due to higher EGR rate resulted in a significant reduction of soot formation in the engine than soot oxidation in the cylinder because insufficient oxygen concentration by higher amount of exhaust gas recirculation. However, if combustion temperature is higher than the location of maximum net soot release, the soot formation decreases more slowly than soot oxidation. In comparison with conventional diesel fuel, DME contains the fuel-borne oxygen content in fuel, which can be about 35% by mass, may promote a more complete combustion and thus effectively reduce engine-out emissions of particulate matter [72].

Fig. 13(b) shows that the soot emission for the DME-biodiesel blend (DME80BD20) was nearly zero for both the single and pilot injection modes, while diesel and D80BD20 fuel in pilot injection show a higher distribution of soot emission. Results of diesel and D80BD20 showed the higher concentration of soot emissions than that of DME80BD20 blend because the

insufficient fuel and air mixing time before the initiation of combustion in the pilot injected fuel [73].

5. CONCLUSIONS

The effects of using dimethyl ether in diesel engines are investigated on the PM emissions characteristics in this review study. The following conclusions can be summarized as results of the study.

- DME presents almost smoke-free combustion because high oxygen content and absence of carbon-carbon bonds in the molecular structure, low auto-ignition temperature and almost instantaneous vaporization in the cylinder.
- The increased engine speed and load increase the soot (smoke, PM) emissions. The increase of the engine speed resulted in the lack of oxidation time for the soot emission. Consequently, the soot emission increased.
- DME addition into diesel fuel provides decreased smoke production. The chemical structure of DME fuel contains no C-C bonds and has more oxygen content which causes high particulate oxidation and suppresses soot formation.
- Soot formation takes place due to the combined effect of in-cylinder temperature as well as oxygen content in the charge. Increase in oxygen content enhances the soot oxidation, whereas decrease in temperature increases the soot formation. In-cylinder temperature decreases due to increase in blend and EGR rates, whereas oxygen contents increase with blends and decreases with EGR. Finally, the overall effect of these parameters on soot formation is marginal at higher blend and EGR rates.
- The smoke emissions increase by increasing the load. The smoke emissions of the biodiesel-DME blends decrease gradually with increase of DME proportion. Because high oxygen content and absence of carbon-carbon bonds in the molecular structure, low auto-ignition temperature and almost instantaneous vaporization in the cylinder, DME presents almost smoke-free combustion.

REFERENCES

81. Yoon, S.H., Cha, J.P. and Lee, C.S. An investigation of the effects of spray angle and injection strategy on dimethyl ether (DME) combustion and exhaust emission characteristics in a common-rail diesel engine. *Fuel Processing Technology*, 91, 1364-1372, 2010.
82. Youn, I.M., Park, S.H., Roh, H.G. and Lee, C.S. Investigation on the fuel spray and emission reduction characteristics for dimethyl ether (DME) fueled multi-cylinder diesel engine with common-rail injection system. *Fuel Processing Technology*, 92, 1280-1287, 2011.
83. Alam, M. and Kajitani, S. *DME as an alternative fuel for direct injection diesel engine*. 4th International Conference on Mechanical Engineering, Dhaka, 2001.
84. Maji, S., Ahmed, S., Siddiqui, W.A. and Kumar, A. Impact of di-methyl ether (DME) as an additive fuel for compression ignition engine in reduction of urban air pollution. *International Journal of Innovative Research in Science, Engineering and Technology*, 3(11), 17221-17228, 2014.
85. Park, S.H. and Lee, C.S. Applicability of dimethyl ether (DME) in a compression ignition engine as an alternative fuel. *Energy Conversion and Management*, 86, 848-863, 2014.
86. Wattanavichien, K. Implementation of DME in a small direct injection diesel engine. *International Journal of Renewable Energy*, 4(2), 1-12, 2009.
87. Duan, J., Sun, Y., Yang, Z. and Sun, Z. *Combustion and emissions characteristics of diesel engine operating on composite combustion mode of DME and diesel*. Proceedings of

International Conference on Mechanical Engineering and Material Science, Shanghai, China, 2012.
88. Kowalewicz, A. and Wojtyniak, M. Alternative fuels and their application to combustion engines. *Journal of Automobile Engineering*, 219, 103-125, 2005.
89. Azizi, Z., Rezaeimanesh, M., Tohidian, T. and Rahimpour, M.R. Dimethyl ether: A review of technologies and production challenges. *Chemical Engineering and Processing*, 82, 150-172, 2014.
90. Huang, Z., Qiao, X., Zhang, W., Wu, J. and Zhang, J. Dimethyl ether as alternative fuel for CI engine and vehicle. *Frontiers of Energy and Power Engineering in China*, 3(1), 99-108, 2009.
91. Lecksiwilai, N., Gheewala, S.H., Sagisaka, M. and Yamaguchi, K. Net energy ratio and life cycle greenhouse gases (GHG) assessment of bio-dimethyl ether (DME) produced from various agricultural residues in Thailand. *Journal of Cleaner Production*, 134, 523-531, 2016.
92. Inayat, A., Ghenai, C., Naqvi, M., Ammar, M., Ayoub, M. and Hussin, M.N.B. Parametric study for production of dimethyl ether (DME) as a fuel from palm wastes. *Energy Procedia*, 105, 1242-1249, 2017.
93. Park, S.H. and Lee, C.S. Combustion performance and emission reduction characteristics of automotive DME engine system. *Progress in Energy and Combustion Science*, 39, 147-168, 2013.
94. Teng, H., McCandless, J. C. and Scheneyer Jeffrey, B. Thermochemical characteristics of dimethyl ether alternative fuel for compression-ignition. *Society of Automotive Engineers*, Paper no 2001-01-0154, 2001.
95. Maji, S., Ahmed, S., Siddiqui, W.A., Aggarwal, S. and Kumar, A. Impact of di-methyl ether (DME) as an additive fuel for compression ignition engine in reduction of urban air pollution. *American Journal of Environmental Protection*, 3(2), 48-52, 2015.
96. Guangxin, G., Zhulin, Y., Apeng, Z., Shenghua, L. and Yanju, W. Effects of fuel temperature on injection process and combustion of dimethyl ether engine. *Journal of Energy Resources Technology*, 135, 1-5, 2013.
97. Jalanapurkar, M., Patel, K., Patel, T., Rathod, G. and Granipa, H. A literature review on combine effect of di-methyl ether (DME) as an additive & the injection pressure on the performance & emission of 4 stroke C.I engine. *International Journal of Advance Engineering and Research Development*, 2(1), 262-266, 2015.
98. Kim, H.J., Park, S.H., Lee, K. S. and Lee, C.S. A study of spray strategies on improvement of engine performance and emissions reduction characteristics in a DME fueled diesel engine. *Energy*, 36, 1802-1813, 2011.
99. Xu, S., Wang, Y., Zhang, X., Zhen, X. and Tao, C. Development of a novel common-rail type dimethyl ether (DME) injector. *Applied Energy*, 94, 1-12, 2012.
100. Lim, O.T. and Iida, N. A study on the spray and engine combustion characteristics of diesel-dimethyl ether fuel blends. J Automobile Engineering, 229(6), 782-792, 2015.
101. Suh, H.K. and Lee, C.S. Experimental and analytical study on the spray characteristics of dimethyl ether (DME) and diesel fuels within a common-rail injection system in a diesel engine. *Fuel*, 87, 925-932, 2008.
102. Genbao, L., Jianming, C., Minglong, L., Yuhua, Q. and Zhaoyang, C. Experimental study on the size distribution characteristics of spray droplets of DME/diesel blended fuels. *Fuel Processing Technology*, 104, 352-355, 2012.
103. Mohan, B., Yang, W., Yu, W. and Tay, K.L. Numerical analysis of spray characteristics of dimethyl ether and diethyl ether fuel. *Applied Energy*, 185, 1403-1410, 2017.

104. El-Hagar, M.M.E-G. Effect of diethyl ether and dimethyl ether with liquefied petroleum gas on combustion and emissions characteristics of diesel engine. International Journal of Computer Science and Engineering, 2(3), 193-198, 2014.
105. Wang, Y., Xiao, F., Zhao, Y., Li, D. and Lei, X. Study on cycle-by-cycle variations in a diesel engine with dimethyl ether as port premixing fuel. *Applied Energy*, 143, 58-70, 2015.
106. Jeon, J., Kwon, S., Park, Y.H., Oh, Y. and Park, S. Visualizations of combustion and fuel/air mixture formation processes in a single cylinder engine fueled with DME. Applied Energy, 113, 294-301, 2014.
107. Baskaran, R. Analysis on synthesis, storage & combustion characteristics of DME as fuel in CI engines. *International Journal for Research in Applied Science & Engineering Technology*, 3(1), 133-140, 2015.
108. Park, S. Optimization of combustion chamber geometry and engine operating conditions for compression ignition engines fueled with dimethyl ether. *Fuel*, 97, 61-71, 2012.
109. Benajes, J., Novella, R., Pastor, J.M., Hernández-López, A. and Kokjohn, S.L. Computational optimization of the combustion system of a heavy duty direct injection diesel engine operating with dimethyl-ether. *Fuel*, 218,127-139, 2018.
110. Oda, Y., Osafune, Y., Ueda, H. and Fujimura, K. Clean combustion technology in diesel engines operated with dimethyl ether. *Mitsubishi Heavy Industries Ltd. Technical Review*, 40(6), 1-5, 2004.
111. Song, J., Huang, Z., Qiao, X. and Wang, W. Performance of a controllable premixed combustion engine fueled with dimethyl ether. *Energy Conversion and Management*, 45, 2223-2232, 2004.
112. Khunaphan, S., Hartley, U.W. and Theinnoi, K. Characterization and potential of dimethyl ether (DME) as dual fuel combustion in a compression ignition engine. *International Journal of Engineering Science and Innovative Technology*, 2(3), 79-85, 2013.
113. Lamani, V.T., Yadav, A.K. and Narayanappa, K.G. Influence of low-temperature combustion and dimethyl ether-diesel blends on performance, combustion, and emission characteristics of common rail diesel engine: a CFD study. *Environmental Science and Pollution Research*, 24, 15500-15509, 2017.
114. Chapman, E.M. and Boehman, A.L. Pilot ignited premixed combustion of dimethyl ether in a turbodiesel engine. *Fuel Processing Technology*, 89, 1262-1271, 2008.
115. Ying, W., Longbao, Z., Zhongji, Y. and Hongyi, D. Study on combustion and emission characteristics of a vehicle engine fuelled dimethyl ether. *Journal of Automotive Engineering*, 219, 263-269, 2005.
116. Benajes, J., Novella, R., Pastor, J.M., Hernández-López, A. and Kokjohn, S.L. Computational optimization of a combustion system for a stoichiometric DME fueled compression ignition engine. *Fuel*, 223, 20-31, 2018.
117. Kropiwnicki, J., Dominiczak, P. and Kneba, Z. Analysis of the possibilities of using of DME fuel in motor boat drive systems. *Combustion Engines*, 171(4), 74-80, 2017.
118. Smolec, R., Idzior, M., Karpiuk, W. and Kozak, M. Assessment of the potential of dimethyl ether as an alternative fuel for compression ignition engines. *Combustion Engines*, 169(2), 181-186, 2017.
119. Namasivayam, A.M., Korakianitis, T., Crookes, R.J., Bob-Manuel, K.D.H. and Olsen, J. Biodiesel, emulsified biodiesel and dimethyl ether as pilot fuels for natural gas fuelled engines. *Applied Energy*, 87, 769-778, 2010.
120. Jang, J. and Bae, C. Effects of valve events on the engine efficiency in a homogeneous charge compression ignition engine fueled by dimethyl ether. *Fuel*, 88, 1228-1234, 2009.

121. Ryu, K., Zacharakis-Jutz, G.E. and Kong, S.-C. Performance characteristics of compression- ignition engine using high concentration of ammonia mixed with dimethyl ether. *Applied Energy*, 113, 488-499, 2014.
122. Semelsberger, T.A., Borup, R.L. and Grene, H.L. Dimethyl ether (DME) as an alternative fuel. *Journal of Power Sources*, 156, 497-511, 2006.
123. Li, G. Dimethyl ether (DME): a new alternative fuel for diesel vehicle. *Advanced Materials Research*, 156-157, 1014-1018, 2011.
124. Sezer, I. Thermodynamic, performance and emission investigation of a diesel engine running on dimethyl ether and diethyl ether. *International Journal of Thermal Sciences*, 50, 1594-1603, 2011.
125. Wang, Y., Zhao, Y. and Yang, Z. Dimethyl ether energy ratio effects in a dimethyl ether-diesel dual fuel premixed charge compression ignition engine. *Applied Thermal Engineering*, 54, 481-487, 2013.
126. Ying, W., Li, H., Longbao, Z. and Wei, L. Effects of DME pilot quantity on the performance of a DME PCCI-DI engine. *Energy Conversion and Management*, 51, 648-654, 2010.
127. Chen, Z., Konno, M. and Kajitani, S. Performance and emissions of DI compression ignition engines fueled with dimethyl ether. *JSME International Journal*, 43(1), 82-88, 2000.
128. Arcoumanis, C., Bae, C., Crookes, R. and Kinoshita, E. The potential of di-methyl ether (DME) as an alternative fuel for compression-ignition engines: A review. Fuel, 87(7), 1014-1030, 2008.
129. Taghavifar, H., Khalilarya, S., Mirhasani, S. and Jafarmadar, S. Numerical energetic and exergetic analysis of CI diesel engine performance for different fuels of hydrogen, dimethyl ether, and diesel under various engine speeds. *International Journal of Hydrogen Energy*, 39, 9515-9526, 2014.
130. Patil, K.R. and Thipse, S.S. The potential of DME-diesel blends as an alternative fuel for CI engines. *International Journal of Emerging Technology and Advanced Engineering* 2(10), 35-41, 2012.
131. Vispute, K.M. and Pawar, T.J. Study and prospects of di-methyl ether as an alternative fuel in C.I. engine: review. *International Journal of Trend in Research and Development*, 3(4), 134-138, 2016.
132. Theinnoi, K., Suksompong, P. and Temwutthikun, W. Engine performance of dual fuel operation with in-cylinder injected diesel fuels and in-port injected DME. *Energy Procedia*, 142, 461-467, 2017.
133. Deepak, K.M., Karthick, M., Dineshbabu, D., Srikanth, P. and Ramachandran, M.G. Investigation on the effect of dimethyl ether in compression ignition engine. *International Journal of Innovative Research in Science, Engineering and Technology*, 4(2), 401-407, 2015.
134. Kajitani, S. A study of low compression ratio diesel engines operated with neat dimethyl ether (DME). *JSME TED Newsletter*, 42, 1-14, 2004.
135. Hewu, W. and Longbao, Z. Performance of a direct injection diesel engine fuelled with a dimethyl ether/diesel blend. *Journal of Automobile Engineering*, 819-824, 2017.
136. Prabhakaran, B., Thennarasu, P. and Karthick, S. Performance and characteristics of a CI engine using DME (Dimethyl Ether). *International Journal of Innovative Research in Science, Engineering and Technology*, 4(2), 31-34, 2015.
137. Kajitani, S. and Chen, Z. Fundamental research on next generation fuel (dimethyl ether) engines. *Journal of Scientific & Industrial Research*, 62, 133-144, 2003.

138. Abhishek, Rahul, K., Santosh, K. and Martha, O. Blending impacts of biogas and dimethyl ether (DME) on compressed ignition engine. *International Research Journal of Engineering and Technology*, 4(4), 2174-2177, 2017.
139. Loganathan, M., Anbarasu, A. and Velmurugan, A. Emission characteristics of jatropha-ethanol and jatropha-dimethyl ether fuel blends on a DI diesel engine. *Journal of Mechanical Engineering*, 42(1), 38-46, 2012.
140. Kim, H.J. and Park, S.H. Optimization study on exhaust emissions and fuel consumption in a dimethyl ether (DME) fueled diesel engine. *Fuel*, 182, 541-549, 2016.
141. Park, S.H., Shin, D. and Park, J. Effect of ethanol fraction on the combustion and emission characteristics of a dimethyl ether-ethanol dual-fuel reactivity controlled compression ignition engine. *Applied Energy*, 182, 243-252, 2016.
142. Geng, P., Cao, E., Tan, Q. and Wie, L. Effects of alternative fuels on the combustion characteristics and emission products from diesel engines: A review. *Renewable and Sustainable Energy Reviews*, 71, 523-534, 2017.
143. Loganathan, M., Anbarasu, A. and Velmurugan, A. Emission characteristics of jatropha-dimethyl ether fuel blends on a DI diesel engine. *International Journal of Scientific & Technology Research*, 1(8), 28-32, 2012.
144. Zhao, Y., Wang, Y., Li, D., Lei, X. and Liu, S. Combustion and emission characteristics of a DME (dimethyl ether)-diesel dual fuel premixed charge compression ignition engine with EGR (exhaust gas recirculation). *Energy*, 72, 608-617, 2014.
145. Hou, J., Wen, Z., Jiang, Z. and Qiao, X. Study on combustion and emissions of a turbocharged compression ignition engine fueled with dimethyl ether and biodiesel blends. *Journal of the Energy Institute*, 87, 102–113, 2014.
146. Ying, W., Longbao, Z. and Hewu, W. Diesel emission improvements by the use of oxygenated DME/diesel blend fuels. *Atmospheric Environment*, 40, 2313-2320, 2006.
147. Xinling, L. and Zhen, H. Emission reduction potential of using gas-to-liquid and dimethyl ether fuels on a turbocharged diesel engine. *Science of the Total Environment*, 407, 2234-2244, 2009.
148. Yanju, W., Kun, W., Wenrui, W., Shenghua, L., Xiao, C., Yajing, Y. and Shanwen, B. Comparison study on the emission characteristics of diesel- and dimethyl ether-originated particulate matters. *Applied Energy*, 130, 357-369, 2014.
149. Wang, Y., Zhao, Y., Xiao, F. and Li, D. Combustion and emission characteristics of a diesel engine with DME as port premixing fuel under different injection timing. *Energy Conversion and Management*, 77, 52-60, 2014.
150. Park, S.H., Kim, H.J. and Lee, C.S. Effects of dimethyl-ether (DME) spray behavior in the cylinder on the combustion and exhaust emissions characteristics of a high speed diesel engine. *Fuel Processing Technology*, 91, 504-513, 2010.
151. Thomas, G., Feng, B., Veeraragavan, A., Cleary, M.J. and Drinnan, N. Emissions from DME combustion in diesel engines and their implications on meeting future emission norms: A review. *Fuel Processing Technology*, 119, 286-304, 2014.
152. Yoon, S.H., Han, S.C. and Lee, C.S. Effects of high EGR rate on dimethyl ether (DME) combustion and pollutant emission characteristics in a direct injection diesel engine. *Energies*, 6, 5157-5167, 2013.
153. Roh, H.G., Lee, D. and Lee, C.S. Impact of DME-biodiesel, diesel-biodiesel and diesel fuels on the combustion and emission reduction characteristics of a CI engine according to pilot and single injection strategies. *Journal of the Energy Institute*, 88, 376-385, 2015.
154. Zhu, Z., Li, D.K., Liu, J., Wei, Y.J. and Liu, S.H. Investigation on the regulated and unregulated emissions of a DME engine under different injection timing. *Applied Thermal Engineering*, 35, 9-14, 2012.

155. Park, S.H., Yoon, S.H., Cha, J. and Lee, C.S. Mixing effects of biogas and dimethyl ether (DME) on combustion and emission characteristics of DME fueled high-speed diesel engine. *Energy*, 66, 413-422, 2014.
156. Bogdan, J., Nicolae, B., Călin, I. and Vlad, B.N. Study of emissions for a compression ignition engine fueled with a mix of DME and diesel. *Materials Science and Engineering*, 252, 1-9, 2017.
157. Kim, H.J., Park, S.W. and Lee, C.S. Numerical and experimental study on the combustion and emission characteristics of a dimethyl ether (DME) fueled compression ignition engine. *Oil & Gas Science and Technology*, 67(3), 479-489, 2012.
158. Wang, H.W., Zhou, L.B., Jiang, D.M. and Huang, Z.H. Study on the performance and emissions of a compression ignition engine fuelled with dimethyl ether. *Journal of Automotive Engineering*, 214, 101-106, 2000.
159. Ambekar, Y. and Hole, J. A. Preliminary optimization of duel fuel engine using dimethyl ether premixed combustion. *International Research Journal of Engineering and Technology*, 5(10), 274-278, 2018.
160. Longbao, Z., Hewu, W. and Ying, W. *Experimental study on Performances and combustion characteristics of DME powered vehicle*. Conference on Better Air Quality in Asian and Pacific Rim Cities (BAQ 2002), 16-18 December 2002, Hong Kong, p. 1-6, 2002.

APPLICATION OF GRASSHOPPER OPTIMIZATION ALGORITHM IN DESIGN PROCESS OF LEAD RUBBER BEARING SEISMIC ISOLATOR

Fatemeh Mehri[1], Arman Atasoy[2], Somayeh Mollaei[3], Mehdi Babaei[4], Fakhraddin Ghahramani[5]

[1] University of Bonab, Faculty of Civil Engineering

[2] Istanbul Rumeli University, Faculty of Civil Engineering, https://orcid.org/0000-0001-7748-8380

[3] University of Bonab, Faculty of Civil Engineering, https://orcid.org/0000-0001-6592-179X

[4] University of Bonab, Faculty of Civil Engineering, https://orcid.org/0000-0002-9080-1893

[5] Urmia University, Faculty of Civil Engineering

ABSTRACT

In this study, sensitivity analysis of the seismic behavior of the isolated building structures in relation to the mechanical parameters of the lead rubber bearing seismic isolation (LRB) system was evaluated. The nonlinear behavior of the LRB isolator was simulated by a bilinear hysteresis model. Also, the nonlinear time history dynamic analysis method was used to analyze the isolated structures. The design optimization problem of the LRB isolator was solved using the grasshopper optimization algorithm (GOA). The results of sensitivity analysis on the seismic behavior of isolated structures with LRB show that the parameter of base shear yield ratio is the most effective and the mass irregularity is the least effective parameter on the seismic behavior of isolated structures.

Keywords: lead rubber bearing (LRB) Isolator, optimization, mass irregularity, near-fault earthquake.

1. INTRODUCTION

During ground motions, structures vibrate, and if the structures have a weak in dissipating of input energy, they will be damaged, and in more severe cases, the structures will be collapsed. In recent decades, extensive studies have been conducted on the development of structural control systems for the robust design of structures under seismic excitations [1]. In structural control systems, the mechanism of control devices has a major role in the energy dissipating caused by earthquakes. A seismic isolation system with suitable force-displacement hysteresis properties can have the desired characteristics such as optimum flexibility, high damping, and

reduction of horizontal earthquake forces [2]. The main purpose of the seismic isolation method is to prevent the transfer of horizontal ground motions and seismic force to the superstructure. The reduction of transmitted seismic force to the superstructure is done by increasing the natural period of the structure and energy dissipation at the isolation level [3]. One of the most common types of isolation systems is the lead rubber bearing (LRB).

The seismic behavior of isolated structures is affected by different parameters. Various studies have been conducted to evaluate the isolation system behavior. In Some studies, the effect of the isolators type and the effect of isolator mechanical parameters [4, 5] have been evaluated. Also, the effect of soil interaction on the isolation system [6], isolation in tall buildings [7], evaluation of fragility curves in systems Isolation [8], reliability analysis [9] and reliability-based design [10] in isolated systems, semi-active isolation systems [11] and the cost benefits of isolations in the seismic design of structures [12] have been studied.

Also, some studies show that the performance of the isolation systems can be affected by factors such as geometric conditions, irregularity of the structure, and seismic excitation characteristics. The damage caused by earthquakes depends on many factors such as failure mechanism, the site location, soil type, and earthquake record characteristics including frequency content, duration, and amplitude [13]. Some researchers have studied the effect of ground motion [14], the effect of horizontal and vertical components [15], and the effect of earthquake frequency content [16] on the performance of isolated systems. The effect of near-fault and far-fault earthquakes have also been considered in some other studies [17-19]. It should be noted that buildings that have irregularity criteria in terms such as geometrical shape, mass, and stiffness distribution the plan or height, are considered as irregular structures. In a number of studies, the effect of asymmetricity in structure [20], the presence of soft stories [21], and eccentricity [22] on the isolated structures have been studied.

Determining the mechanical parameters of isolator devices to achieve efficient performance for the isolation system is a complex process. However, studies have shown that the behavior of these systems can be influenced by various conditions. Therefore, the design of isolation systems is defined in the framework of design optimization problems. One of the efficient methods in solving engineering optimization problems is meta-heuristic algorithms [23]. So far, several metaheuristic algorithms have been introduced such as charged system search (CSS), colliding bodies optimization (CBO), vibrating particle system (VPS) [23], ant colony optimization (ACO) [24], grasshopper optimization algorithm (GOA) [25], and so on. In this study, the optimum design of seismic isolation system with LRB isolators is solved using the GOA and considering the mass irregularity and near-fault earthquake effects.

2. SEISMIC ISOLATION SYSTEMS

Rubber supports can provide the flexibility and deformation required for vibration isolation. If these supports are combined with a lead core to dissipate input energy, the necessary damping is also provided for this system. The steel plates are used in this system to shear deformation of the lead core. The Lead core deforms against shear forces and causes a bilinear hysteresis behavior in the device [26]. Also, the rubber part of this isolation system is responsible for providing the restoration force (figure 1). The LRB system has sufficient stiffness in the vertical direction to restrain of structure and provide horizontal flexibility with the restoring force and providing the required hysteresis damping.

In practice, all LRB isolations systems are simulated with a bilinear hysteresis model based on the three parameters of elastic stiffness (K_1), post-yield stiffness (K_2), and specified yield strength (Q_y), as shown in Figure 1. The post-yield stiffness is obtained from the desired period

of the structural system. For Lead Rubber Bearing (LRB) and frictional pendulum systems (FPS), elastic stiffness is a coefficient of post-yield stiffness [18].

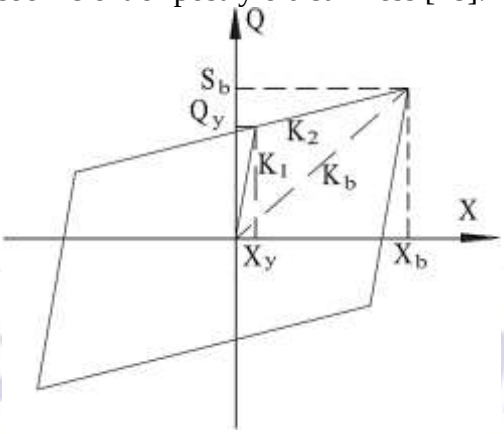

Figure1- Bilinear hystersis model of Lead Rubber Bearing system [18]

Initially, a time period is selected for the isolated structure (T_2) at the design displacement level, which is usually between 2 and 3 seconds. Then the post-yield stiffness of the isolated system for the selected period can be calculated using Equation (1):

$$K_2 = M \times \left(\frac{2\pi}{T_2}\right)^2 \quad (1)$$

In this relation, M is the total mass of the whole structure isolated at the base. Also, the yield shear strength at the isolation level (Q_y) can be defined using Equation (2):

$$Q_y = \alpha M g \quad (2)$$

In this relation, α is the yield shear coefficient. Assuming a value between 0 and 1, the effective shear force on the structure can be determined. In the bilinear behavioral model, the value of the elastic stiffness of the system (K_1) can be determined by selecting the yield deformation component (X_y) as the elastic behavior limit.

$$K_1 = \frac{Q_y}{X_y} \quad (3)$$

Therefore, the ratio of initial stiffness to post-yield stiffness is defined as the parameter α_k in relation (4):

$$\alpha_k = \frac{K_1}{K_2} \quad (4)$$

Also, the damping of the isolation system (c_b) in terms of the effective damping ratio (ξ_b), which represents the dissipated energy, is equal to Equation (5):

$$c_b = 2\xi_b\sqrt{K_2 \times M} \quad (5)$$

3. NONLINEAR DYNAMIC ANALYSIS

The dynamic response of a structural system beyond its linear elastic range can usually not be calculated by analytical solution. Even if the excitation temporal changes are described by a simple function. Therefore, the use of numerical methods in the analysis of nonlinear systems is necessary. Newmark method with modified Newton-Raphson iteration method is generally used for the solution of nonlinear dynamic equations [27].

The dynamic equation of a structure with nonlinear behavior is written as Eq (6):

$$M\ddot{U}(t) + C\dot{U}(t) + F_S(t) = P(t) \quad (6)$$

where *t* is the time; *U*, $\dot{U}$ and $\ddot{U}$ are displacements, velocity and acceleration vectors relative to the ground, respectively; M is mass matrix; C is damping matrix; F_S is the vector of resisting

forces, which is a function of displacement and P(t) is applied force that for seismic case it is given by ground acceleration time history. Also, the initial condition is $U(0) = U_0$ and $\dot{U}(0) = \dot{U}_0$. According to the equilibrium in each time interval, the equation of motion during the time step t_{i+1} can be written as follows:

$$M\ddot{U}_{i+1} + C\dot{U}_{i+1} + F_{s_{i+1}} = P_{i+1} \quad (7)$$

In 1959, N.M. Newmark developed time-stepping methods based on the variation of acceleration over a time step. In this paper, the constant average acceleration method with Newton–Raphson iteration has been used to analyze nonlinear MDOF structures. At first, the initial state of the structural system is determined (K_{T0} and F_{s0}). Then, also, the initial acceleration is calculated:

$$\ddot{U}_0 = M^{-1}\left(P_0 - C\dot{U}_0 - F_{s0}\right) \quad (8)$$

then for each time step:

$$\bar{P}_{i+1} = P_{i+1} + a_1 U_i + a_2 \dot{U}_i + a_3 \ddot{U}_i \quad , \quad i = 0.1.2. \ldots \quad (9)$$

where:

$$a_1 = \left(\frac{1}{\beta(\Delta t)^2}\right) M + \left(\frac{\gamma}{\beta \Delta t}\right) C \quad (10)$$

$$a_2 = \left(\frac{1}{\beta \Delta t}\right) M + \left(\frac{\gamma}{\beta} - 1\right) C \quad (11)$$

$$a_3 = \left(\frac{1}{2\beta} - 1\right) M + \Delta t \left(\frac{\gamma}{2\beta} - 1\right) C \quad (12)$$

If the resisting forces are not equal to the applied force, a residual force vector is defined as:

$$\bar{R}_{i+1} = \bar{P}_{i+1} - (F_s)_{i+1} - a_1 U_{i+1} \quad (13)$$

By using the Newton–Raphson iteration method, the additional displacement due to this residual force is determined by solving:

$$\Delta U = (\bar{K}_T)_{i+1}^{-1} \times \bar{R}_{i+1} \quad (14)$$

where $\bar{K}_T$ is the tangent stiffness that can be considered as follows:

$$(\bar{K}_T)_{i+1} = (K_T)_{i+1} + a_1 \quad (15)$$

The responses of a nonlinear structure can be obtained as follow:

$$U_{i+1} = U_i + \Delta U \quad (16)$$

$$\dot{U}_{i+1} = \left(\frac{\gamma}{\beta \Delta t}\right) \Delta U + \left(1 - \frac{\gamma}{\beta}\right) \dot{U}_i - \Delta t \left(1 - \frac{\gamma}{2\beta}\right) \ddot{U}_i \quad (17)$$

$$\ddot{U}_{i+1} = \left(\frac{1}{\beta(\Delta t)^2}\right) \Delta U - \left(\frac{1}{\beta \Delta t}\right) \dot{U}_i + \left(1 - \frac{1}{2\beta}\right) \ddot{U}_i \quad (18)$$

where γ and δ are Newmark parameters, in this study, $\gamma = 0.5$ and $\delta = 0.25$ have been used for nonlinear analysis of the structure.

4. GRASSHOPPER OPTIMIZATION ALGORITHM

Optimization methods in the classical form use the derivation information of the objective function to find the optimal solution. These methods fall into the locale optimum point for complex problems and cannot be used for underivable functions. Another type of optimization method that reduces these two challenges are stochastic methods such as meta-heuristic algorithms. These methods are generally population-based algorithms inspired by nature. One of the evolutionary algorithms is the grasshopper optimization algorithm (GOA) which is inspired by the grasshopper lifecycle [25]. Nature-inspired algorithms logically divide the search process into exploration and exploitation. In exploration, search agents are driven by random movements, while, in the exploitation phase, they tend to move locally around their place. These two actions in search of the target are performed naturally by grasshoppers.

The mathematical model used to simulate the behavior of grasshoppers was initially in the form of Equation (19):

$$X_i = S_i + G_i + A_i \quad (19)$$

where X_i indicates the position of the grasshopper i, S_i is the social interaction, G_i is the force of gravity applied to the grasshopper i, and A_i represents the direction of the wind. The value of S_i, that is, the social interaction for grasshopper i, is calculated by Equation (20):

$$S_i = \sum_{j=1}^{N} S(d_{ij})\widehat{d_{ij}} \quad (20)$$

where d_{ij} indicates the distance between grasshoppers i and j and is calculated as Equation (21):

$$d_{ij} = |x_i - x_j| \quad (21)$$

as shown in Equation (20), $\widehat{d_{ij}}$ is a unit vector from the ith to the jth grasshopper. S is also a function for defining social force pressure. The function S, which defines a social force, is calculated as in Equation (22):

$$S(r) = fe^{\frac{-r}{l}} - e^{-r} \quad (22)$$

where f represents the intensity of gravity and I represents the length of the gravity scale. Parameters I and f significantly change the comfort zone, attraction, and repulsion.

Research has shown that the initial grasshopper motion relationship can not be used in swarm simulation and optimization algorithms. Because this relationship prevents exploration and exploitation in the search space around a solution. In fact, the model is used for outdoor crowding. Therefore, Equation (23) has been used and can simulate the interaction between the grasshopper in the swarm.

$$x_i^d = c\left(\sum_{j=1}^{N} c\frac{ub_d - lb_d}{2} s(|x_j^d - x_i^d|)\frac{x_j - x_i}{d_{ij}}\right) + \widehat{T_d} \quad (23)$$

where ub_d is the upper bound in the d-th dimension and lb_d is the lower bound in the d-th dimension and $\widehat{T_d}$ is the value of the d-th dimension in the target (the best solution ever seen) and c is a decreasing constant to reduce the area of comfort, repulsion, and attraction.

In the equation (23), S is obtained from Equation (19) and the parameters of gravity (G) and wind direction (A) are not considered. This equation shows that the next position of a grasshopper is defined based on its current position, the target position, and the position of all other grasshoppers. In order to maintain a balance between exploration and exploitation, parameter c needs to decrease with increasing repetition times during the algorithm. The coefficient c reduces the comfort zone in proportion to the number of repetitions and is calculated as Equation (24):

$$c = c_{max} - i\frac{c_{max} - c_{min}}{l} \quad (24)$$

where C_{max} is the maximum value, C_{min} is the minimum value, i represents the current iteration number, and l is the maximum number of iterations of the algorithm. In the simulations, the value of C_{max} is 1 and the value of C_{min} is 0.00001.

5. DESIGN FORMULATION

Design variables are a set of parameters that affect design details and design results. Different parameters affect the design of base isolation systems in building structures. Parameters that are independently involved in the behavior mechanism of Lead Rubber Bearing are selected as design variables. The behavioral model of any Lead Rubber Bearing is influenced by independent factors such as yield displacement (X_y), secondary time period (T_2), base shear yield coefficient (α), damping ratio (ξ_b), etc that parameters such as initial hardness (K_1), Secondary stiffness (K_2), yield shear strength (Q_y) and damping coefficient (c_b) are functions of these changes. In the optimum design of a Lead Rubber Bearing, these parameters are

selected as the designed variables. Constraints on the optimum design of isolations, apply to the design variables due to the physical limitations and acceptable results of the problem. According to the above, the optimum design of Lead Rubber Bearing for building structures is formulated as Equation (18):

$$\begin{aligned} &Find: Design\ Variables\ X = \begin{Bmatrix} X_y \\ T_2 \\ \alpha \\ \xi_b \end{Bmatrix} \\ &which\ minimizes\ Objective\ Function: f(X) \\ &Subject\ to: \begin{cases} X_{y_{min}} \le X_y \le X_{y_{max}} \\ T_{2_{min}} \le T_2 \le T_{2_{max}} \\ \alpha_{min} \le \alpha \le \alpha_{max} \\ \xi_{b_{min}} \le \xi_b \le \xi_{b_{max}} \end{cases} \end{aligned} \quad (25)$$

In this paper, the objective function for the optimization problem is defined based on performance indexes of inter-story drift. This index shows the effect of control devices on system performance and is expressed based on the ratio of controlled maximum drift response to uncontrolled maximum response:

$$Objective\ Function = f(\mathrm{X}) = \left| \frac{Max(drift_{i,Controlled})}{Max(drift_{i,Uncontrolled})} \right| \quad (26)$$

where, $drift_i$ is the inter-story drift of the *i*-th story.

6. NUMERICAL CASE STUDY

In this article, the numerical studies include three cases:

Case 1: In the first case, the seismic behavior of the base-isolated building structure with LRB is analyzed for sensitivity to evaluate the effect of LRB mechanical parameters and the mass irregularity of the structure.

Case 2: In the second case, the LRB isolation system is designed using the GOA meta-heuristic optimization method for building structures.

Case 3: Finally, in the third case, the seismic behavior of isolated building structures with optimized LRB isolators is evaluated under near-fault earthquakes and mass irregularities, and the performance of LRB isolators is compared in different conditions.

For numerical studies, benchmark structural model was used; a 5-story building structures. These structures have a two-dimensional lumped mass shear building system. The mechanical properties of these structures, such as mass, stiffness, and damping of stories, are assumed to be the same for all stories. Table 1 presents the dynamic properties of these structural models. For these models, the damping ratio (ξ_s) is assumed to be 0.02 and the damping coefficient (c) for each story can be calculated using the Riley method.

Table 1 - Mechanical properties of structural models [18]

Story	5- Story Model	
	Mass (ton)	Stiffness (MN/m)
1	445	448
2	445	448
3	445	448
4	445	448
5	445	448

In order to calculate the seismic responses to optimize the design of the LRB isolator, the generated Gaussian random white noise with a duration of 40 seconds and a maximum acceleration of 0.35 g is used as ground motion acceleration (Figure 2). Also, in order to study the seismic behavior and responses of isolated building structures with the optimal LRB system, in regular and irregular conditions, the ground acceleration of near-fault earthquakes is used. For this purpose, the horizontal component of the Imperial Valley, Northridge, and Chichi earthquakes is used [18]. The details of these earthquakes are presented in Table 2. Irregular conditions for building models are defined based on mass irregularities in the height of the structure. Irregularity for this building model is defined as a 50% variation in the mass of successive stories.

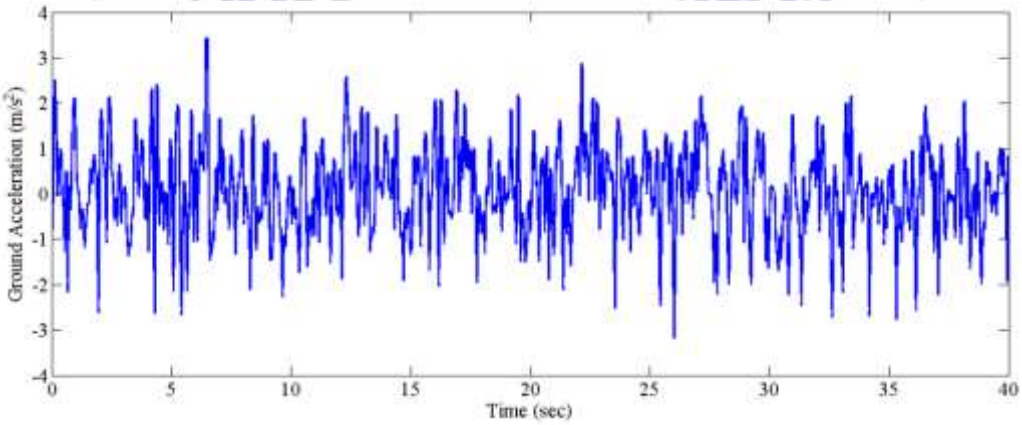

Figure 2. Time history of ground acceleration in random white noise (W(t))

Table 2 - Details of earthquakes used in this study [18]

Event	Station	Magnitude	Distance (km)	PGA ($\frac{m}{s^2}$)	$\frac{PGV}{PGA}$
Imperial Valley	El Centro	6.5	1.35	4.40	0.26
Northridge	NWH-360	6.7	6.8	5.79	0.17
Chichi	TCU-052	7.6	1.84	3.56	0.52

7. RESULTS AND DISCUSSION

To show the effect of each parameter of isolator on system performance the sensitivity analysis is used. To this aim, the sensitivity of the seismic responses of isolated structures with LRB is evaluated to changes in the values of yield base shear coefficient, secondary period, yield displacement, damping coefficient, and mass irregularity. Every parameter changes incrementally in the range [35% + 35% -] relative to the initial design value. The changes of maximum inter-story drift responses per each component are shown in Figure 3. As shown in this figure, the structural drift response has a high sensitivity to the yield base shear ratio.

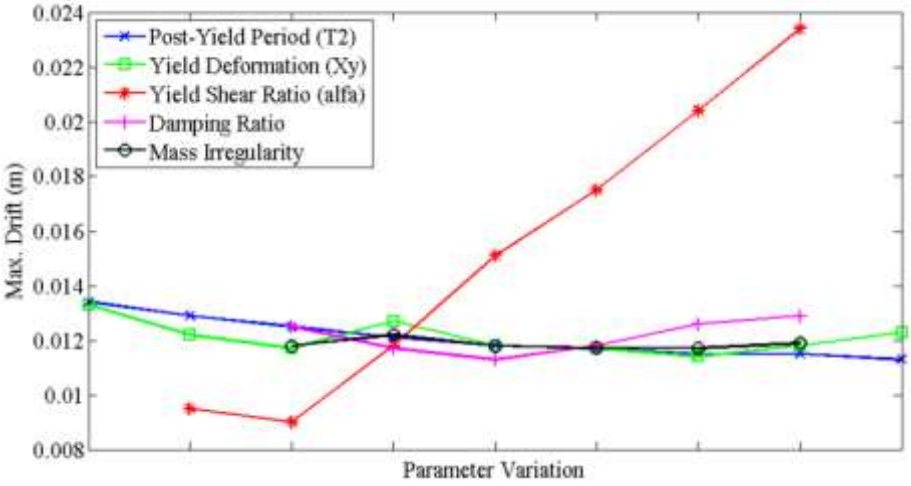

Figure 3- The variation of maximum drift response in a 5-story isolated building structure relative to system parameters

In the second part, the results obtained from solving the optimization problem in the design of isolation systems with LRB isolators are presented. The outputs of this problem include the convergence history of the objective function, the minimum value calculated for the objective function, and the optimal values of design variables. Figure 4 shows the convergence history diagram for the defined objective function based on controlled seismic responses in the isolated building with LRB isolators for the GOA. According to this method, the minimum value for the ratio of maximum controlled responses to uncontrolled responses for the 5-story structural models is 0.19995. Table 3 shows the results obtained from the optimal design of LRB isolators, including design variables and constraints for the 5-story structural models.

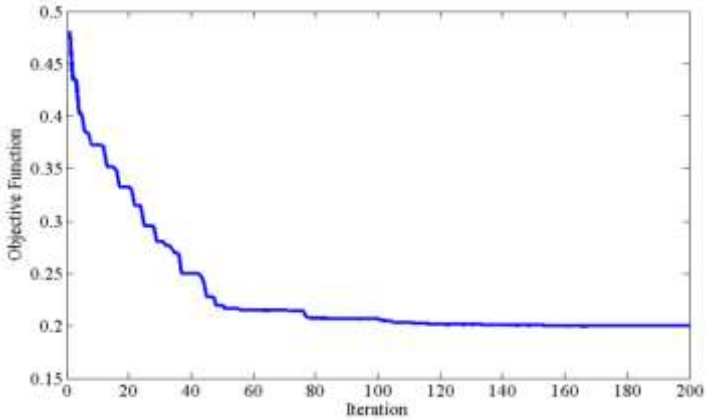

Figure 4 - Convergence history of the objective function for the design of LRB with the GOA

Table 3- Optimal design results for LRB isolator with GOA algorithm

Set	Parameter	Dimension	Value
			5- Story
Objective Function	Controlled Responses	-	0.19995
Design Variables	Yield Base Shear Ratio (α)	-	0.055024
	Yield Deformation (X_y)	cm	0.019219
	Secondary Period (T_2)	s	2.9937
	Damping Ratio (ζ_b)	%	0.20751
Constraints	Stiffness Ratio (α_k)	-	0.1569

	Isolator Deformation	cm	0.20127

Finally, the seismic behavior of isolated building structures using optimized LRB isolators is evaluated in both regular and mass irregularity cases under near-fault earthquakes. In this regard, the time history of seismic inter-story drift response at the maximum level is compared for the near-fault records of the Imperial Valley, Northridge, and Chichi. Figures 5 to 7 show the drift time history of the structure for each earthquake. Under the Imperial Valley earthquake, the maximum drift is 0.95 cm for the regular structural model and 0.99 cm for the irregular structural model. For the Northridge earthquake, the maximum drift is 0.72 cm for the regular structural model and 0.70 cm for the irregular structural model. Also, under the Chichi earthquake, the maximum drift value is 1.10 cm for the regular structural model and 1.05 cm for the irregular structural model.

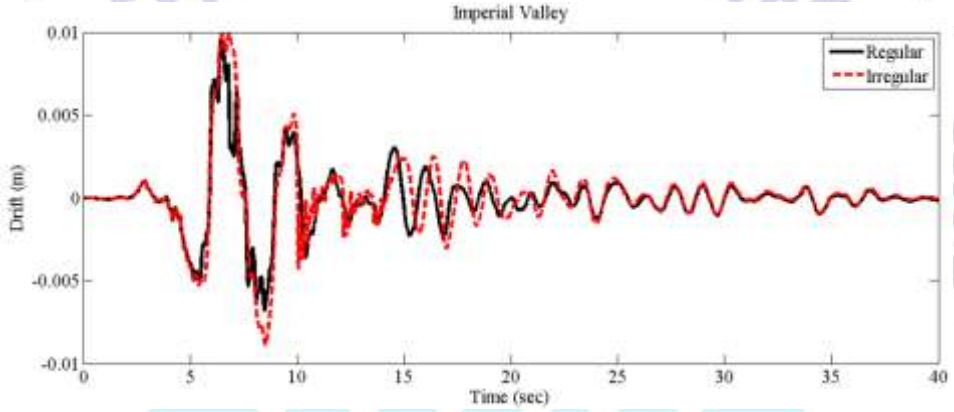

Figure 5 - Time history of maximum drift for the model under Imperial Valley

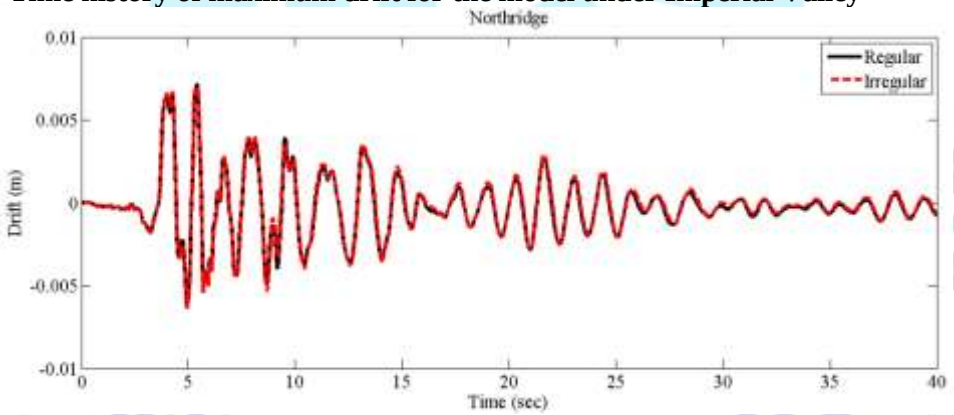

Figure 6 - Time history of maximum drift for the model under Northridge

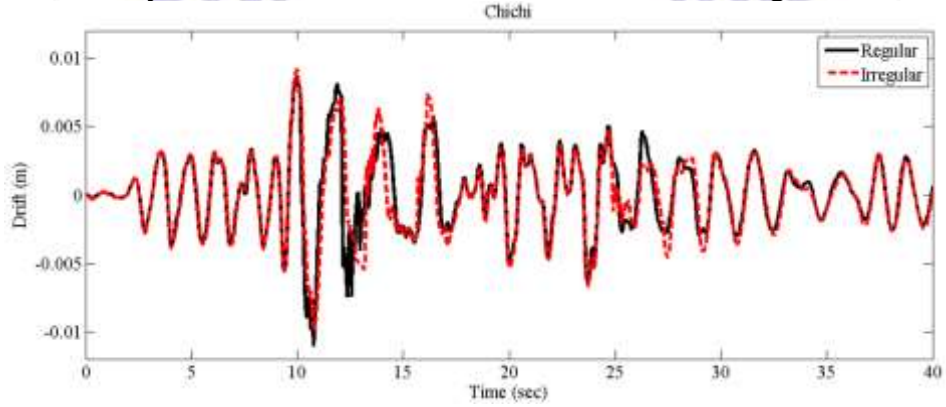

Figure 7 - Time history of maximum drift for the model under Chi-chi

8. CONCLUSIONS

The main purpose of this study was to optimum design a lead rubber bearing seismic isolation system, and evaluate the effects of mass irregularity and near-fault seismic excitation on seismic responses of building. Also, the sensitivity analysis of the isolated structures to the mechanical parameters of the lead-rubber bearing system and the mass irregularity was conducted and the seismic responses of the isolated structures were investigated. The results of sensitivity analysis on the seismic behavior of isolated structures with LRB isolators show that the yield base shear ratio is the most effective parameter on the performance of isolators. Also, the mass irregularity of the structure shows the least effect on the seismic behavior of the isolated structures. The GOA has a good ability to solve the optimization problem of the isolation systems design for building structures. The seismic performance of LRB isolation systems where optimally designed for regular structures is not affected by the mass irregularities in the structure. In other words, the behavior of isolated structures with optimized LRB isolators is not affected by the mass irregularities. Also, the LRB isolation system has same performance in controlling the seismic responses of structures in the presence of mass irregularity under near faults earthquakes for the 5-story structural models.

REFERENCES

[1] Spencer, B.F., Soong, T.T., New application and development of active, semi-active and hybrid control techniques for seismic and non-seismic vibration in the USA, Proceedings of International Post-SMIRT Conference Seminar on Seismic Isolation, Passive Energy Dissipation and Active Control of Vibration of Structures Cheju, Korea, 1999.

[2] Soong, T.T., Spencer, B.F. Supplemental energy dissipation: state of the art and state of the practice, Engineering Structures, 24, pp. 243-259, 2002.

[3] Cheng, F.Y., Jiang, H., Lou, K., Smart Structures, Innovative Systems for Seismic Response Control, CRC Press, Boca Raton, FL, USA, 2008.

[4] Matsagar, V.A., Jangid, R.S., Influence of isolator characteristics on the response of base-isolated structures, Engineering Structures, 26, pp. 1735-1749, 2004.

[5] Tanwer, M.T., Kazi, T.A., Desai, M., A Study on Different Types of Base Isolation System Over Fixed Based, Information and Communication Technology for Intelligent Systems, Smart Innovation, Systems and Technologies, 106, pp. 724-734, 2018.

[6] Spyrakos, C.C., Koutromanos, I.A., Maniatakis, C.A., Seismic response of base-isolated buildings including soil–structure interaction, Soil Dynamics and Earthquake Engineering, 29, pp. 658-668, 2009.

[7] Ei-Bayoumi, K., Naguib, M., Salem, F.A., Dynamic Analysis of High-Rise Seismiccally Isolated Buildings, Amercan Journal of Civil Engineering, SciencePG, 20150302.13, 2015.

[8] Flora, A., Perrone, G., Cardone, D., Evaluating Collapse Fragility Curves for Existing Buildings Retrofitted Using Seismic Isolation, Applied Sciences, 10, 2844, 2020.

[9] Castaldo, P., Palazzo, B., Vecchia, P.D., Seismic Reliability of Base-Isolated Structures with Friction Pendulum Bearings, Engineering Structures, 95, pp. 80-93, 2015.

[10] Peng, Y., Ma, Y., Huang, T., Domenico, D., Reliability-Based Design Optimization of Adaptive Sliding Base Isolation System for Improving Seismic Performance of Structures, Reliability Engineering and System Safety, 2020.

[11] Vargas, C.A.B., Diaz, I.M., Soria, J.M., Palacios, J.H.G., Enhancing Friction Pendulum Isolation Systems Using Passive and Semi-Active Dampers, Applied Sciences, 10, 562, 2020.

[12] Yurdakul, M., Yıldız, M.B., A study on seismic isolation of building used LRB, Challenge Journal of Structural Mechanics, 6(2), pp. 52-60, 2020.

[13] Hayden, C.P., Bray, J.D., Abrahamson, N.A., Selection of Near-Fault Pulse Motions, Journal of Geotechnical and Geoenvironmental Engineering, 140(7), ID. 04014030, 2014.

[14] Mavronicola, E.A., Polycarpou, P.C., Komodromos, P., Effect of ground motion directionality on the seismic response of base isolated buildings pounding against adjacent structures, Engineering Structures, 207, 110202, 2020.

[15] Jamalzadeh, A., Barghian, M., Dynamic Response of a Pendulum Isolator System Under Vertical and Horizantal Earthquake Excitation, Periodica Polytechnica Civil Engineering, 2015.

[16] Cancellara, D., Angelis F.D., A base isolation system for structures subject to extreme seismic events characterized by anomalous values of intensity and frequency content, Composite Structures, 157, pp. 285-302, 2016.

[17] Providakis, C.P., Effect of supplemental damping on LRB and FPS seismic isolators under near-fault ground motions, Soil Dynamic sand Earthquake Engineering, 29, pp. 80-90, 2009.

[18] Rong, Q., Optimum parameters of a five-story building supported by lead-rubber bearings under near-fault ground motions, Journal of Low Frequency Noise, Vibration and Active Control, pp. 1-16, 2019.

[19] Anajafi, H.R., Poursadr, K., Roohi, M., Bell, E.S., Effectiveness of Seismic Isolation for Long-Period Structures Subject to Far-Field and Near-Field Excitations, Frontiers in Built Environment, 6(24), 2020.

[20] Kilar, V., Koren, D., Seismic behaviour of asymmetric base isolated structures with various distributions of isolators, Engineering Structures, 31, pp. 910-921, 2009.

[21] Choudhury, S.S., Patro, S.K., Seismic Control of Soft Storey Buildings Using LRB Isolation System, Recent Developments in Sustainable Infrastructure. Lecture Notes in Civil Engineering, 75. Springer, Singapore, 2020.

[22] Colungaa, A.T., Rojas, C.Z., Dynamic torsional amplifications of base-isolated structures with an eccentric isolation system, Engineering Structures, 28. pp. 72-83, 2006.

[23] Kaveh, A., Advances in Metaheuristic Algorithms for Optimal Design of Structures, Springer Verlag, Wien, 2014.

[24] Dorigo, M., Caro, G.D., Ant colony optimization: a new meta-heuristic, Proceedings of the 1999 Congress on Evolutionary Computation-CEC99, Washington, DC, USA, 2, pp. 1470-1477, 1999.

[25] Saremi, S., Mirjalili, S., Lewis, A., Grasshopper Optimisation Algorithm: Theory and application, Advances in Engineering Software, 105, pp. 30-47, 2017.

[26] Naeim, F. and Kelly, J.M. Design of Seismic Isolated Structures: From Theory to Practice, John Wiley & Sons, Inc., 1999.

[27] Newmark, N.M., A method of computation for structural dynamics, Journal of the engineering mechanics division, 85(3), pp. 67-94, 1959.

THE DETECTION OF DETERIORATED PV MODULES IN TURKEY

Hale Bakır [1]

[1] Sivas Cumhuriyet University, ORCID ID: 000-0001-5580-0505

ABSTRACT

This study includes the field measurement results of the photovoltaic (PV) solar energy system installed in Turkey. Fault detection of 1 MW solar power plant belonging to Malatya province in Turkey was carried out by using real-time thermal drone. As a result of the examinations, 2 connection fault, 4 bypass diode fault, 2 hotspot and 4 shading faults were detected, affecting a total of 16 panels in the entire field. A sustainable renewable energy source is important as developing countries like Turkey will need more energy over the years. Therefore, this article provides better performance enhancements and improvements in power generation from photovoltaic power plants by providing rapid detection by thermal imaging.

Keywords: thermal imaging, solar energy system, fault detection, real-time

1. INTRODUCTION

The use of known renewable energy sources in electrical energy production is becoming more and more important day by day. Among the renewable energy sources, the developments in the technologies of obtaining electrical energy, especially from the sun's rays, have been an area of interest in our country as well as in the whole world. Solar panels are electronic systems with a semiconductor structure that are formed by the combination of photovoltaic cells, have no moving parts and convert solar energy into electrical energy. In such structures, it is important to ensure continuous electricity generation and efficiency. Although the lifetime of the solar panels is long, the efficiency of the panel decreases due to various problems both during panel production and during the establishment of the power plant, thus reducing the amount of energy production [1].

There are a number of malfunctions such as broken connection, corrosion, broken glass, broken cell, coating failure, which are very common in solar panels. Hot spots that occur on the panels due to reasons such as cracks, scratches, bird droppings and broken cells, including manufacturing defects, are called hotspots [2]. These heats can cause a decrease in their production capacity, as well as affect the side cells and prevent them from producing energy.

It is possible to detect these faults with portable thermal cameras, but in areas where the land structure is not suitable, in areas with roof application or in very large production areas, these determinations either take a lot of time or it may not be possible to measure.

In such cases, thermal fault detection in these panels can be made in a very short time, with aircraft equipped with high-resolution cameras.

In this study, fault detection was made with a thermal drone in the solar power plant of 1 MW Malatya/Turkey and images of the faults were given. The number of panels affected by the faults is 16.

2. EXPERIMENTAL RESEARCH (or METHODS)

In general, faults in PV arrays can be grouped according to their time characteristic as permanent, incipient, and intermittent [3]. Connection fault as typical failure types in PV panels is the condition that causes more than one panel connected to each other to not work. Possible causes; Defective inverters, Fuse or junction box problems, cable errors.

Soiling fault results from accumulating snow, dust, dirt or any other particles on the front surface of PV module. While hard shading fault occurs when PV panels are shaded by nearby objects or buildings [4]. The bypass diode faults are integrated in parallel with a certain number of solar cells in the PV module. These bypass diodes prevent reverse bias heating phenomena of solar cells during shading conditions [3]. Open circuit type of fault occurs when a disconnection problems appear in a PV string or more. Most of the disconnection problems are due to poor soldering in strings interconnections [5].

This study focuses on the thermal imaging of 1 MW solar power plants in Malatya/Turkey, the types of failures that occur in solar power plants in Turkey, and the rapid detection of these failures with an experimental thermal drone. The Image of the power plant taken by the drone is given in Figure 1. The thermal drone model used in this study is shown in Figure 2. This drone gives satisfactory results compared to other drone models thanks to its obstacle recognition speed. The thermal drone, which can fly up to 72 km/h, provides a flight time of up to 31 minutes in low cold conditions of -10°C. It supports digital zoom with high resolution thermal and visual cameras and has centimeter level positioning accuracy with RTK module. It helps to make informed decisions by detecting objects instantly using its high resolution thermal sensor.

Figure 1. Image taken by drone of solar power plant in Turkey

Figure 2. DJI mavic enterprise model thermal drone

3. RESULTS AND DISCUSSION

According to the tests performed, the images obtained with the thermal drone are given in Figures 3 and 4. The type of fault detected in Figure 3(a) is bypass diode fault with a Sp1 value of 59.1 degrees and a Sp2 value of 54.3 degrees. Typically 1/3 of the panel is affected, activated bypass diode fault. They are short-circuit faults that occur at the factory outlets or by-pass diodes of the cells. It is recommended to measure losses by performing IV measurements and Electroluminescence test and replace the panel if necessary. The type of fault detected in Figure 3(b) is the hotspot with a Sp1 value of 75,6 degrees and a Sp2 value of 61,5 degrees., that is, the point heating error, which occurs with the square geometry in a single cell. The fault detected in Figure 3(c) is the connection fault. It is the condition that causes more than one panel connected to each other to not work. Possible causes; Defective inverters, Fuse or junction box problems, cable errors. It is recommended to check the inverter, fuse, ports and cable. In Figure 4, it is seen that the plants coming out from under the panel are getting longer and causing shading faults on the panel. As a result of the examinations, 2 connection faults, 4 bypass diode faults, 2 point heating faults and 4 shading faults were detected, affecting a total of 16 panels in the entire field. The measurement values used during the test are given in Table 1. The distribution of faults detected in a 1 MW solar power plant is given in Figure 5.

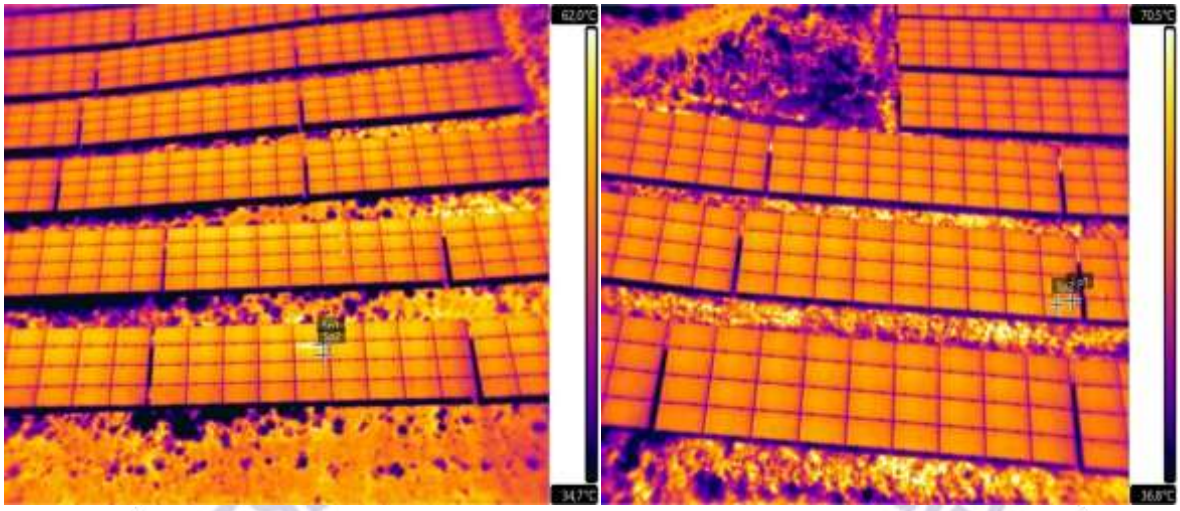

(a) (b)

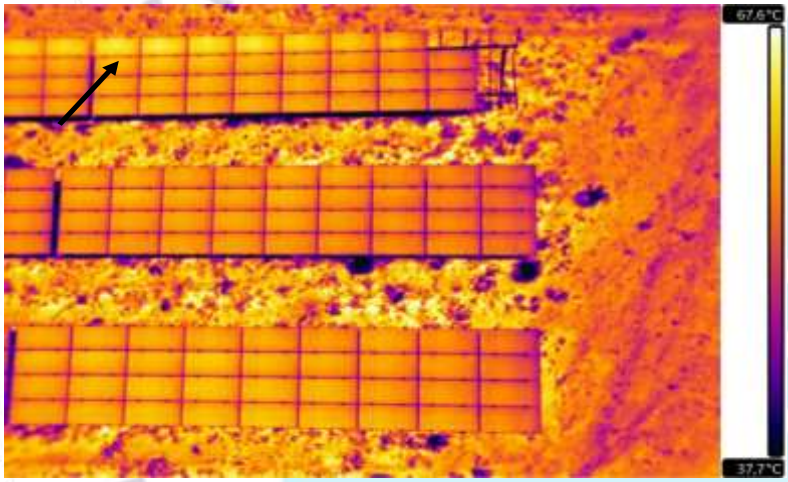

(c)

Figure 3. Faults detected on the panels (a) bypass diode fault (b) hotspot fault (c)connection fault

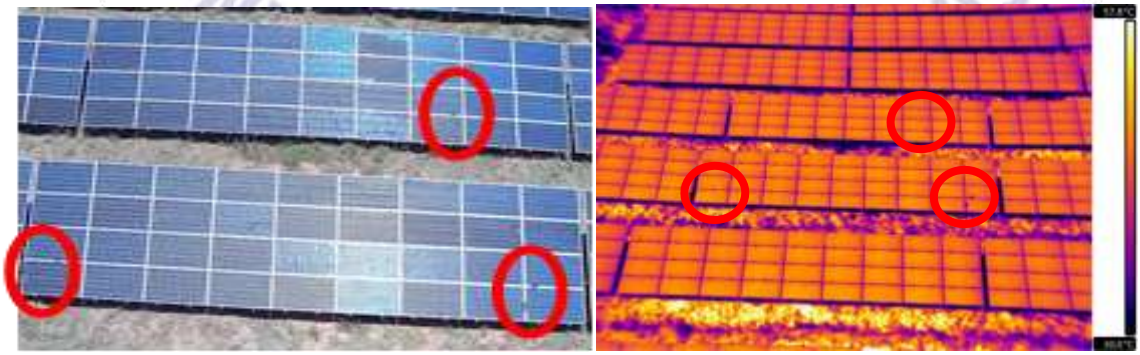

Figure 4. Shading faults detected on the panels

Table 1. Measurement Parameters

Parameters	
Emissivity	0,70
Reflected temperature	12,0°C
Distance	20,0 m
Atmospheric temperature	40,0 °C
Relative humidity	%23
External optics temperature	40,0 °C
External optics transmission	1,00

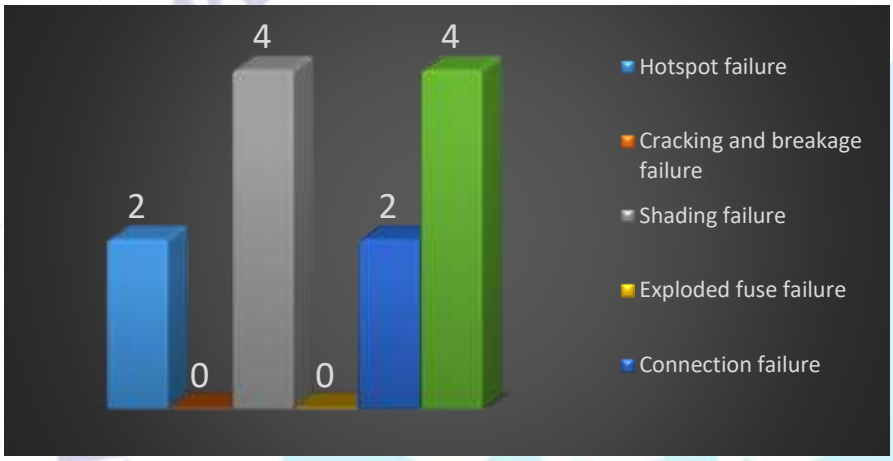

Figure 5. Distribution of faults detected in solar power plant

4. CONCLUSION

As a result of the inspections, a total of 16 faults were detected in the field. The thermal photographs obtained in the study are included, and some of the faults are shown in the panel thermal images. The reason for these faults should be determined by the controls to be made in the field. 4 shading fault, 4 bypass diode fault, 2 hotspot fault, 2 connection fault were detected in the field. No Multi-hotspot fault was detected in the field. No visible Cracking / Breakage fault was detected in the field. And finally, all faults were detected affecting 16 panels in total in the whole field. Sustainable renewable energy source and energy production are important in developing countries such as Turkey. Fault detection with thermal imaging gains speed in the studies.

REFERENCES

[1] Dağlı A, Karaköse E, Durmus A, Solar Panellerde Arıza Analizi , ISAS2019, Ankara, Turkey, 2019.

[2] T.C. Enerji ve Tabii Kaynaklar Bakanlığı website. [Online]. Available: http://www.yegm.gov.tr/MyCalculator/, 2019.

[3] K. AbdulMawjood, S. S. Refaat, W. G. Morsi, Detection and Prediction of Faults in Photovoltaic Arrays: A Review, IEEE Explorer.(2018) doi: 10.1109/CPE.2018.8372609.

[4] Maghami, M. R., Hizam, H., Gomesa, G., Radzia, M. A., Rezadad, M. I., Hajighorbani, S., 2016, "Power loss due to soiling on solar panel: A review", in Renew. Sustain. Energy Rev. 59, pp. 1307-1316.

[5] Gokmen, N., Karatepe, E., Celik, B., Silvestre, S., 2012, "Simple diagnostic approach for determining of faulted PV modules in string based PV arrays", Solar Energy, 86(11), pp. 3364-3377.

FV PANELLERDE ARIZA TESPİTİ VE ANALİZİ

Dr. Hale BAKIR [1]

[1] Sivas Cumhuriyet Üniversitesi, ORCID ID: 000-0001-5580-0505

ÖZET

Bu çalışma Türkiye'de kurulu fotovoltaik (FV) güneş enerjisi sisteminin saha ölçüm sonuçlarını içermektedir. Türkiye'deki Adıyaman iline ait 1 MW'lık güneş enerji santralinin gerçek zamanlı termal drone kullanılarak arıza tespiti gerçekleştirilmiştir. Yapılan tetkikler sonucunda tüm sahada toplam 20 paneli etkileyen 3 adet bağlantı hatası, 2 adet bypass diyot hatası, 2 adet noktasal ısınma hatası tespit edilmiştir. Türkiye gibi gelişmekte olan ülkeler yıllar içinde daha fazla enerjiye ihtiyaç duyacakları için sürdürülebilir bir yenilenebilir enerji kaynağı önemlidir. Dolayısıyla bu makale, termal görüntüleme ile hızlı tespit sağlayarak fotovoltaik enerji santrallerinden güç üretiminde daha iyi performans geliştirme ve iyileştirmeler sağlamaktadır.

Anahtar Kelimeler: FV system, Arıza teşhisi, termal drone, arıza türleri

1. GİRİŞ

Dünya enerji tüketimindeki artış ve fosil yakıtların çevreye verdiği zararlar nedeniyle yenilenebilir enerji kaynaklarına (örneğin güneş, rüzgar, jeotermal) artan bir ihtiyaç vardır. Yenilenebilir enerji, daha iyi verimlilik, güç kalitesi ve daha düşük hava kirliliği gibi birçok fayda sunar [1]. Temiz ve çevre dostu yenilenebilir enerji kaynakları arasında fotovoltaik (PV) enerji, güneş enerjisinin bulunabilirliği ve bolluğu nedeniyle büyük ilgi görmektedir [2]. En önemli sorunlardan biri fotovoltaik (PV) enerjinin konvansiyonel güç kaynaklarından kullanım sırasında akım ve gerilimde tespit edilemeyen arızaların olmasıdır. PV santrallerdeki arızalar, santralin performansını ve hizmetlerini etkileyen kritik ve zararlı durumlara neden olur [3].
Büyük ölçekli PV sistemlerinin görsel denetimi yüksek hata oranı içerdiğinden, uzun işlem süresi nedeniyle gerçek zamanlı koşullarda uygulanması mümkün değildir [4]. I-V ölçümlerine dayalı performans değerlendirmesi Güç üretim verimliliğini analiz etmek için kullanılır. PV modüllerini analiz etmek için en yaygın açık devre voltajı, kısa devre akımı, doldurma faktörü ve maksimum güç noktası ölçümleri kullanılır. Açık devre gerilimi, kısa devre akımı ve maksimum güç ölçümleri gibi ölçümler, Pv modüllerinin çıkarılmasını ve iyi hava koşullarını gerektirirken, IV eğrisi ölçümü, yeterli ölçüm için PV modülleri için performans bilgisi sağlar. Diğer ölçümlerde, pv modüllerinin çıkarılması sistemin kesintiye uğramasına ve güç üretiminin azalmasına neden olur [5]. Görsel inceleme ve IV ölçümleriyle karşılaştırıldığında, termal görüntüleme bir güneş enerjisi santralindeki arızaları tespit etmek için zaman açısından en verimli yöntemdir.

Termal görüntüleme ile bulunan arızalar genellikle kirlenme ve sıcak noktalar gibi çeşitli görsel kusurlardır ve bağlantı hatası, baypas diyot hatası gibi sonuçlar elde edilir. Ana fotovoltaik arızalar (sıcak nokta, arıza hücresi, açık devre, baypas) gerçek fotovoltaik panellerde incelenir.

Bu çalışmada 1 MW Adıyaman ili güneş enerji santralinde termal drone ile arıza tespiti yapılmıştır ve bulunan arızalara ait görüntüler verilmiştir. Arızalardan etkilenen panel sayısı 20 adettir.

2. MATERYAL VE YÖNTEMLER

2.1. PV Sistemlerinde Tipik Arızalar

2.1.1. Hotspot Arızası

Güneş panelinin seri bağlanmış hücrelerinden birinin ürettiği akım diğer hücrelere göre daha düşük ise gerilim tersine döner ve panel yük durumuna geçer. Bu durumda panel yük olarak çalıştığı için akım ve sıcaklık yükselmeye başlar, buna sıcak nokta etkisi denir. Hotspot Arızalarına kuş pisliği, kırık paneller, mikro çatlaklar neden olur.

2.1.2. Bypass Diyot Arızası

Kısa devre arızasına neden olan fabrika üretimi veya by-pass diyotlardan kaynaklanan hücrelerin arızalanmasıdır. Elektrolüminesans testi ve akım-voltaj eğrisi ölçümleri yapılarak kayıplar hesaplanır ve dizi arızası varsa panel sökülüp değiştirilmelidir.

2.1.3. Bağlantı hatası

Sigorta, arızalı inverterler, buat sorunları birden fazla panonun arızalanmasına neden olur. Enerji üretiminde bağlantı arızası önemlidir, bu nedenle kablo arızası, bağlantı portları, invertör, sigorta gibi malzemeler kontrol edilmelidir.

2.1.4. Kirlenme ve Gölgeleme Hatası

Kontaminasyon arızası, PV modülü üzerinde biriken kir, kar, toz ve diğer partiküllerden oluşur. PV panellerin yakınındaki ağaçların, binaların ve direklerin gölgesi PV panelin üzerine düşerse arızaya neden olur. Kirlenme veya gölgeleme hatası, çıkış voltajını düşürür, elektrik üretiminde %10 ila %70'lik bir azalmaya neden olur ve böylece verimliliği düşürür [6].

2.1.5. PV Dizi Bozulması

Cam ile hücreler arasındaki malzemenin renginin beyazdan sarıya veya kahverengiye doğru olması güneş pillerinin daha az ışık almasına neden olur ve verimi düşürür. Ayrıca PV modül katmanları arasındaki yapışma kaybı, ışık yansımasına ve su penetrasyonuna neden olur, yapışma kaybının oluşturduğu boşluklara delaminasyon denir. %50'ye kadar güç çıkışı kaybı bu arızadan kaynaklanır [6].

2.2. DJI Mavic Enterprise Gelişmiş Termal Drone

Bu çalışmada kullanılan termal drone modeli Görsel 1'de gösterilmektedir. Bu drone, engel tanıma hızı sayesinde diğer drone modellerine göre tatmin edici sonuçlar veriyor.
Kendiliğinden ısınan pilleri sayesinde, 72 km/s'ye kadar uçabilen termal drone, -10°C'ye (14°F) kadar düşük soğuk koşullarda 31 dakikaya kadar uçuş süresi sağlıyor. Yüksek çözünürlüklü termal ve görsel kameralara sahiptir, M2EA 32×'e kadar dijital yakınlaştırmayı destekler ve

RTK modülü ile santimetre seviyesinde konumlandırma hassasiyetine sahiptir. Yüksek çözünürlüklü termal sensörünü kullanarak nesneleri anında tespit ederek bilinçli kararlar alınmasına yardımcı olur. 640 × 512 Termal Çözünürlük ve 16× Yakınlaştırma, ±2 °C Sıcaklık Ölçüm Doğruluğu sunar.

Görsel 1. DJI Enterprise Gelişmiş Termal Drone

Bu çalışma, Türkiye'de Adıyaman ili 1 MW lık güneş enerjisi santrallerinin termal görüntülemesine, Türkiye'deki güneş santrallerinde meydana gelen arıza türlerine ve deneysel bir termal drone ile bu arızaların hızlı tespitine odaklanmaktadır. Drone tarafından çekilen santralin fotoğrafı Görsel 2'de verilmiştir. Panelin sıcaklık koşulları Çizelge 1'de gösterilmiştir. Panel sıcaklığı 1 °C'nin altında iken panel normaldir. Panel sıcaklığı 1 °C ile 4 °C arasında iken panel muayene edilmelidir. Pano sıcaklığı 4,0 °C ile 15 °C arasında iken pano tamir edilmelidir. Pano sıcaklığı 15.0 °C'nin üzerinde iken pano acil müdahaleye alınmalıdır.

(b)

Görsel 2. Drone ile çekilmiş Adıyaman güneş enerji santralinin havadan görüntüsü

Çizelge 1. PV panelindeki sıcaklık farklılıkları

Normal	Panel incelenmeli	Panel tamir edilmeli
<1.0 °C	1.0 to 4.0 °C	4.0 to 15.0 °C

3. DENEYSEL ÇALIŞMALAR (veya UYGULAMALAR)

Yapılan testlere göre termal drone ile elde edilen görüntüler Görsel 3'de verilmiştir. Görsel 3(a)'da tespit edilen hata türü tek hücrede kare geometrisi ile oluşan sıcak nokta yani noktasal ısınma hatasıdır. Görsel 3(b)'de tespit edilen hata bağlantı hatasıdır. Birbirine bağlı birden çok panelin çalışmamasına neden olan durumudur. Olası nedenler; Arızalı invertörler, Sigorta ya da bağlantı kutusu problemleri, Kablolama hatalarıdır. İnvertör, sigorta, bağlantı noktaları ve kablolamanın kontrol edilmesi önerilir. Görsel 3(c)'de tespit edilen hata türü dizi hatasıdır. Tipik olarak panelin 1/3'ünün etkilendiği, aktive edilmiş bypass diyot hatasıdır. Hücrelerin

fabrika çıkışlarında ya da by-pass diode'larında oluşan kısa devre hatalarıdır. IV ölçümleri ve Elektrolumınesans testi yapılarak kayıpların ölçülmesi ve gerekirse panelin değiştirilmesi önerilir. Yapılan tetkikler sonucunda tüm sahada toplam 20 paneli etkileyen 3 adet bağlantı hatası, 2 adet bypass diyot hatası, 2 adet noktasal ısınma hatası tespit edilmiştir. 1 MW güneş enerji santralinde tespit edilen hataların dağılımı Görsel 6'da verilmiştir.

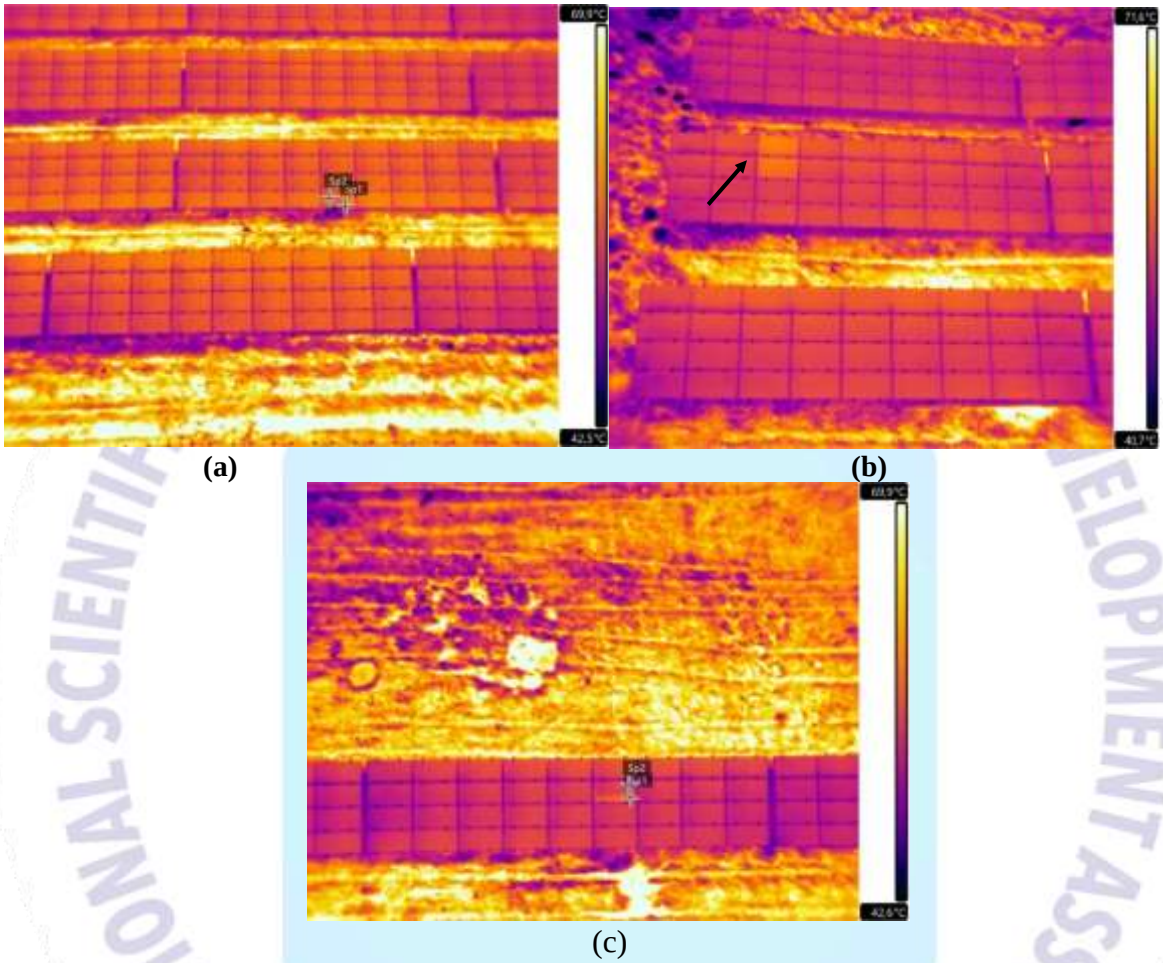

Görsel 5. FV sistemde tespit edilen bypass diyot hatası

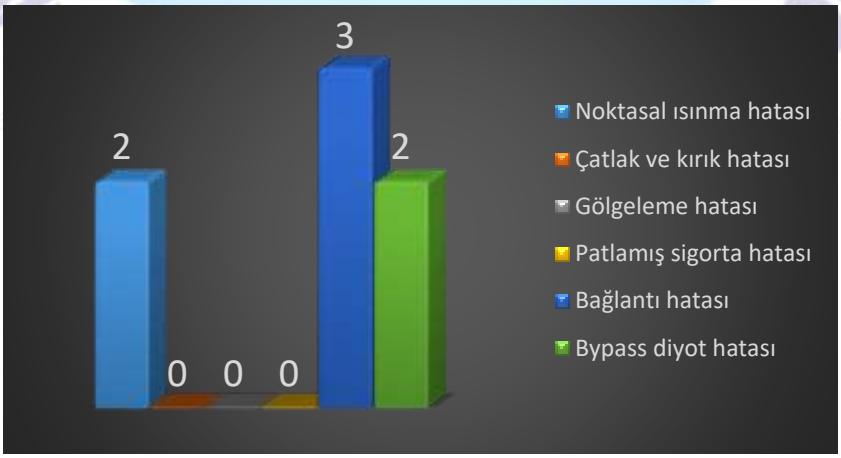

Görsel 6. 1 MW güneş enerji santralinde tespit edilen hataların dağılımı

4. GENEL DEĞERLENDİRME VE SONUÇLAR

Yapılan tetkikler sonucunda sahada toplam 2 adet Noktasal Isınma Hatası tespit edilmiştir. Çalışmada elde edilen termal fotoğraflara yer verilmiş olup, hataların bazıları panel yerleşim haritalarında gösterilmiştir. Bu hataların neden kaynaklandığının sahada yapılacak kontroller ile tespit edilmesi gerekmektedir. Sahada herhangi bir Çoklu Noktasal Isınma Hatası tespit edilmemiştir. Sahada gözle görülebilen herhangi bir Çatlama / Kırılma tespit edilmemiştir. 2 adet Dizi Hatası tespit edilmiştir. Hatanın termal fotoğrafına yer verilmiş olup, panel üzerinde gösterilmiştir. Sahada herhangi bir Gölgelenme problemi tespit edilmemiştir. Ancak sehpaların en altında uzayan otlar olduğu gözlemlenmiştir. Yakın zamanda tedbir alınmazsa en sıralarda yer alan panellere gölge düşme olasılığı bulunmaktadır. Ve son olarak tüm sahada toplam 20 paneli etkileyen 3 adet Bağlantı Hatası tespit edilmiştir. Türkiye gibi gelişmekte olan ülkelerde sürdürülebilir yenilenebilir enerji kaynağı ve enerji üretimi önemlidir. Termal görüntüleme ile hata tespitleri hız kazanmaktadır.

KAYNAKÇA

[1]. Panigrahi, B.K, Bhuyan A, Shukla J, Ray P. K, Pati S, A comprehensive review on intelligent islanding detection techniques for renewable energy integrated power system, Int. Journal of Energy Research. 2012;45:14085-14116. doi:10.1002/er.6641

[2]. Lin X, Wang Y, Zhu D, Chang N, Pedram M, Online failuredetection and tolerance for photovoltaic energy harvesting systems, in: Proceedings of the International Conference on Computer-Aided Design, ACM, 2012; 1-6.doi:

[3]. Bonsignorea L, Davarifarb M, Rabhib A, Tinaa G. M, Elhajjajib, A, Neuro-Fuzzy failuredetection method for photovoltaic systems. Energy Procedia. 2014;62:431 – 441.doi: 10.1016/j.egypro.2014.12.405

[4]. Tsanakas J, Ha L, Buerhop C, Faults and infrared thermographic diagnosis in operating c-Si photovoltaic modules: a review of research and future challenges, Renew. Sustain. Energy Rev. 2016; 62:695-709.

[5]. Gasparin F, Bühler A, Alexandre G, Statistical analysis of IeV curve parameters from photovoltaic modules. Sol. Energy. 2016;131: 30-38.

[6]. Maghami M. R, Hizam H, Gomesa G, Radzia M. A, Rezadad M. I, Hajighorbani S, Power loss due to soiling on solar panel: A Review. in Renew. Sustain. Energy Rev. 2016;59: 1307-1316.

A STUDY OF AN IMPROVEMENT MEDIAN FILTER FOR IMPULSE NOISE

Yunus Sevim

Gazi Üniversitesi, ORCID ID: 0000-0002-6841-9110

Median Filter and Hybrid Median Filters are accepted as the most efficient filters used to remove impulse noises in the literature. Median Filter converts matrices with mask size such as 3x3, 5x5, 7x7 to 1x9, 1x25, 1x49 vectors for all pixels and defines the medium value as the new pixel value. Since the basic Median Filter gives results by applying the same algorithm to all pixels, its effectiveness decreases in some transition regions and edges. Finding a value close to the original pixel is very important, as the pixels have the potential to be used later for image processing. In this study, a decision-making algorithm is used for the new pixel value and the Median Filter is allowed for the threshold value determined to eliminate this disadvantage, while the values that the Median Filter does not take into account in the critical regions are added to the average and a new pixel value is produced. First of all, the average of the first close neighborhood and the average of the second closest neighborhood of the m

edian value are taken. If the raw pixel value is within this range, median filtering is allowed, if not, average-weighted filtering is applied. After deciding to calculate it with the median or the weighted average, it is aimed to further denoise the new pixel value. The performance comparison of the filters was made according to MSE, SSIM and PSNR criteria and it was observed that the new filter gave successful results compared to the Median Filter in many experimental studies. Results can also be compared visually.

Keywords: Denoising, image processing, Median Filter

SAYISAL HAVA TAHMİN VERİLERİ ve MAKİNE ÖĞRENMESİ ALGORİTMALARININ TÜRKİYE'DE GÜN ÖNCESİ GÜNEŞ ENERJİ TAHMİNİ İÇİN KULLANILMASI: ESKİŞEHİR İLİNDE ŞEBEKEYE BAĞLI BİR GÜNEŞ ENERJİSİ SANTRALİNDE ÖRNEK UYGULAMA

Melike Koca[1], Ceyhun Yıldız[2], Ö. Fatih Keçecioğlu[3]
[1]K.Maraş Sütçü İmam Üni., 0000-0001-7850-3554
[2]K.Maraş İstiklal Üni., 0000-0002-5498-4127
[3]K.Maraş Sütçü İmam Üni., 0000-0001-7004-49

ÖZET

Türkiye coğrafi konumu nedeniyle oldukça yüksek bir güneş enerjisi potansiyeline sahiptir ve ülkedeki Güneş Enerjisi Santrali (GES) kurulu gücü hızla artmaktadır. Fakat GES enerji üretimi değişken bir karaktere sahiptir ve üretilen değişken enerji elektrik şebekelerindeki arz-talep dengesini bozucu bir etki oluşturmaktadır. Bu konuda yapılan çalışmalar bozucu etkinin ortadan kaldırılabilmesi için GES üretim tahminlerine ihtiyaç olduğunu ortaya koymuştur. Bu çalışmada GES üretimlerinin gün öncesinden tahmini için modeller geliştirilmiştir. Modelin girişleri Sayısal Hava Tahminleri (SHT) ve uygulama yapılan santralden alınan geçmiş güç değerleridir. Çalışmada kullanılan SHT verileri Meteoroloji Genel Müdürlüğünden (MGM) alınmıştır. Geçmiş güç değerleri ise çalışmada incelenen şebekeye bağlı, 1 MW kurulu gücünde ve Eskişehir ilinde tesis edilmiş bir GES'ten temin edilmiştir. Model girişleri ve dört farklı makine öğrenmesi algoritması kullanılarak gün öncesi üretim tahminleri elde edilmiştir. Çalışmada kullanılan makine öğrenmesi algoritmaları; Doğrusal Regresyon (DR), Regresyon Ağacı (RA), Destek Vektör Makinesi (DVM) ve Gauss Süreç Regresyonu (GSR)'dur. Tahminlerin doğruluğu Ortalama Hata Kareleri Karekökü (RMSE), Ortalama Mutlak Hata (MAE) ve Determinasyon Katsayısı (R) performans değerlendirme kriterleri kullanılarak ölçülmüştür. Çalışma sonunda en iyi performans sergilediği tespit edilen GSR algoritması tahminleri için RMSE, MAE ve R değerleri sırasıyla 129.78, 70.80 ve 0.91 olarak hesaplanmıştır.

Anahtar sözcükler: Yenilebilir Enerji Kaynakları, Güneş Enerjisi Santrali, Gün Öncesi Güç Tahmini, Makine Öğrenmesi

1. GİRİŞ

Tüm dünyada enerji güncel bir sorundur. Teknolojinin gelişmesi ve beraberinde getirdiği enerji tüketim ihtiyacı mevcut fosil yakıt rezervlerinin azalmasına, bu enerji kaynaklarının daha fazla kullanımı ise çevre kirliliğine ve doğal dengenin bozulmasına neden olmaktadır. Bu durum birçok araştırmacıyı yenilenebilir ve temiz enerji kaynakları arayışına yöneltmiştir.

Yenilebilir enerji kaynakları diğer enerji kaynaklarına kıyasla daha ekonomik ve temizdir. Bu sebeple enerji tüketimi içerisindeki payı her geçen yıl artmaktadır. Günümüzde yenilebilir enerji kaynakları içerisinde güneş enerjisi önemli bir yere sahiptir. Fakat GES enerji üretimi değişkendir ve elektrik şebekelerindeki arz-talep dengesini etkilemektedir. Bu nedenle santralin üreteceği güç tahminlerine ihtiyaç duyulmaktadır.

Konu ile ilgili literatürde birçok çalışmanın olduğu görülmektedir. Bazı önemli çalışmalar incelenerek özetlenmiştir. [1] çalışmasında, Orta Anadolu bölgesinde geniş bir alana dağılmış binden fazla güneş enerjisi santralinin saatlik toplam üretim değerlerinin gün öncesinde tahmin edilmesi için çeşitli derin öğrenme teknikleri kullanılmıştır. Literatürde bulunan dört farklı derin öğrenme mimarisi, bu çalışmada önerilen paralel yerel bağlantılı uzun-kısa süreli bellek ağı ile birlikte SHT uzay-zamansal yapısına uyarlanmıştır. Bu çalışmada küresel bir meteorolojik modelden (Global Forecasting System, GFS) alınan tahminlerin kullanıldığı görülmektedir. GFS değerlerinin düşük çözünürlükte doğrulukta olduğu bilinmektedir. [2] çalışmasında, güneş enerjisi tahminlerinde son yıllarda sıkça kullanılan Yapay Sinir Ağları (YSA) ile klasik yöntemlerin karşılaştırması yapılmıştır. Farklı girdiler, veri miktarı ve hesap hedefleri için yapılan karşılaştırmalarda YSA'nın klasik yöntemlerle benzerlik gösterdiği saptanmıştır. Sonuç olarak iki yöntem arasındaki küçük miktarda bulunan doğruluk farkının küçük limitler arasında kaldığı sonucuna varılmıştır. [3] çalışmasında, Konya'da kısa dönem GES üretim tahmini için çeşitli yöntemler kıyaslanarak değerlendirilmiştir. YSA kullanılarak, hava durumu şartlarına göre GES üretimlerinin yüksek hassasiyetle tahmin edilebileceği gösterilmiştir. [4] çalışmasında, Güneydoğu Anadolu Bölgesindeki 5 ilin MGM'den alınan meteorolojik parametre verileri kullanılarak güneş ışınımı ve güneşlenme süreleri için istatistiksel tahmin modelleri geliştirilmeye çalışılmıştır. Tahmin modellerinde, Üstel Ağırlıklı Hareketli Ortalama (ÜAHO) ve Gaussian Dağılım (GD) birlikte kullanılmıştır. [5] çalışmasında, Akdeniz Bölgesi'nden seçilmiş 14 yerleşim yeri için yatay yüzeye gelen aylık ortalama toplam güneş ışınımını tahmin etmek bir model geliştirilmiştir. Modelde YSA ve bazı meteorolojik parametreler kullanılmıştır. Yedi meteorolojik (ortalama hava sıcaklığı, minimum toprak üstü sıcaklığı, 5cm'deki toprak altı sıcaklığı, bağıl nem, bulutluluk, hava basıncı, güneşlenme süresi) ve beş zamansal- konumsal parametre (istasyon, ay, enlem, boylam, yükseklik) bulunan veriler 1993-2010 yılları için MGM'den alınmıştır. Çalışma sonucunda toplam güneş ışınımının tahmin edilen ve ölçülen değerlerinin oldukça yakın olduğu gösterilmiştir.[6] çalışmasında, Fotovoltaik (FV) sistem güç üretimlerinin kısa ve orta dönem tahminleri için bir YSA temelli model geliştirilmeye çalışılmıştır. Sahadaki bir meteoroloji istasyonundan, geçmiş meteorolojik parametre verileri alınmıştır. FV sistem çıkış gücünü

tahmin etmek için bir Doğrusal Olmayan Özbağlanımlı Dış Girdili Ağ Modeli kullanılmıştır. [7] çalışmasında, günlük güneş ışınım tahmin problemi için Uzun Kısa Süreli Bellek (Long Short-Term Memory, LSTM) ağı önerilmiştir. Önerilen yöntemin etkinliği Karar Ağaçları Regresyonu, Rastgele Orman Regresyonu, Gradyan Güçlendirme ve K-En Yakın Komşu gibi makine öğrenmesi algoritmalar ile karşılaştırılmıştır. LSTM modelinin etkinliğini doğrulamak için Çorum- Türkiye'de Temmuz-1983 ve Aralık-2018 tarihleri arasında küresel güneş ışınımı verileri kullanılmıştır. Hesaplama sonuçları, LSTM yönteminin diğer makine öğrenmesi algoritmalarından daha iyi performansa sahip olduğunu göstermiştir.[8] çalışmasında, Türkiye'de şebekeye bağlı 1 MW kurulu gücünde bir GES tesisi için üretim tahmin modeli geliştirilmiştir. Modelde Ampirik Mod Ayrıştırma ve derin Evrişimsel Sinir Ağı kullanılmıştır. Tahmin modeli girdileri olarak, sahadan ölçülmüş meteorolojik parametreler ve GES tesisinden alınmış geçmiş güç verileri kullanılmıştır.[9] çalışmasında, Türkiye'de faaliyet gösteren bir GES tesis için Aşırı Öğrenme Makinesi temelli bir tahmin modeli geliştirilmiştir. Model girişleri olarak sahadan ölçülen meteorolojik parametreler ve santralden alınan geçmiş güç verileri kullanılmıştır.[10] çalışmasında gün öncesi GES üretim tahmini için YSA temelli bir model geliştirilmiştir. Modelde GFS verileri ve geçmiş güç değerleri kullanılmıştır.

Literatürde değerlendirildiğinde Türkiye'de faaliyet gösteren GES'lerin üretim tahmini konusunda kısıtlı sayıda çalışma olduğu görülmektedir. Yukarıda özetlenen çalışmaların çoğunda sadece geçmiş güç ve meteorolojik parametre verileri kullanıldığı görülmüştür [1]–[6], [8], [9]. Fakat konu ile ilgili literatür özeti [11] 'de meteorolojik tahmin verilerinin 4 saatten uzun tahmin ufuklarında iyileştirme yapacağı belirtilmiştir. Ayrıca Türkiye'de yapılmış iki çalışmada küresel ölçekte meteorolojik tahmin verileri elde edilebilen GFS modeli çıktıları kullanıldığı görülmüştür [1], [10] .GFS tahminleri düşük çözünürlükte ve doğrulukta olduklarından GES üretim tahminlerini belirli seviyede iyileştirebilmektedir.

Bu çalışmada güneş enerjisinden üretilen enerjinin şebekede oluşturacağı dengesizliği önlemek amacıyla geçmiş güç ve yüksek kalitedeki SHT tahmin değerleri kullanılarak tahmin modelleri geliştirilmiştir. Kısa dönemlik (24-48-72 saatlik) zaman diliminde MGM'den resim formatında alınan SHT verisindeki sıcaklık, bulutluluk, yağış ve rüzgâr hızı değerleri sayısal verilere dönüştürülmüştür. Elde edilen sayısal değerler ile santralin geçmiş güç değerleri, tahmin modellerinde girdi olarak kullanılıp 24 saatlik zaman ufkunda santralin ne kadar güç üreteceği tahmin edilmiştir. Elde edilen tahminler bazı performans değerlendirme kriterleri kullanılarak değerlendirilmiştir. Çalışmanın literatüre katkısı iki yönlü olmuştur:

1- Kısa dönem güç tahmin modeli oluşturmak için yüksek kaliteli bir meteorolojik ölçüm istasyonu kullanan MGM'den alınan meteorolojik tahmin verileri kullanılmıştır. Bu sayede daha güvenilir ve doğru tahminler için gerekli veri setleri elde edilmiştir.

2- Tahmin modeli oluşturmak için kullanılan dört farklı makine öğrenmesi algoritması; Doğrusal Regresyon (DR), Regresyon Ağacı (RA), Destek Vektör Makinesi (DVM) ve Gauss Süreç Regresyonu (GSR) kıyaslanarak değerlendirilmiştir.

Bu bildiri beş bölümden oluşmaktadır. İlk bölümde konu ile ilgili genel bilgiler, kısa bir literatür özeti ve çalışmanın literatüre katkısı verilmiştir. İkinci bölümde çalışmada kullanılan veriler tanıtılmıştır. Üçüncü bölümde çalışmada kullanılan yöntem detayları anlatılmıştır. Çalışma sonunda elde edilen bulgular dördüncü bölümde verilmiştir. Bulgular ışığında varılan sonuçlar son bölümde bulunmaktadır.

2. MATERYAL

Çalışmada kullanılan veriler, MGM'den alınan meteorolojik tahmin verisi ve ilgili santralden üretilen geçmiş güç değerleridir. Veriler ve çalışmanın gerçekleştirildiği santral ile ilgili detaylı bilgiler bu bölümde verilmiştir. Çalışma Eskişehir'de bulunan KM GES santralinde gerçekleştirilmiştir. Santral ile ilgili teknik bilgiler Çizelge 1'de verilmiştir. Santralin genel görünümü Görsel 1'de olduğu gibidir.

Çizelge 1. Santral teknik bilgileri

Santral Özelliği	Değer
Panel Gücü	265(W)
Kurulu Güç	1(MW)
Üretim Başlangıç Yılı	2014
Konum	Eskişehir, Odunpazarı, Harlak Üstü
Bağlı Olduğu Dağıtım Şirketi	Zorlu Enerji Dağıtım Şirketi

Görsel 1. KM Güneş Enerji Santrali

Çalışmada tahmin modelinin girdisi olarak kullanılan geçmiş güç değerlerinin örnekleme zamanı bir saattir. Her değer bir saat boyunca üretilen toplam kWh biriminde enerji miktarıdır. Çalışmadaki veriler 22.03.21-13.06.21 tarihleri arasını kapsamaktadır. Bu

verilerden seçilen 1 haftalık üretim Görsel 2'de verildiği gibidir. Ayrıca güç verilerine ilişkin bazı istatistiksel bilgiler Çizelge 2'de özetlenmiştir.

Çizelge 2. Güç değerlerinin bazı istatistiksel özellikleri

İstatistiksel Özellik	Elektriksel Güç (kWh)
μ	222.016
M	25.875
σ	303.106
σ^2	91873

μ: Ortalama; M: Medyan ; σ: Standart Sapma; σ^2: Varyans.

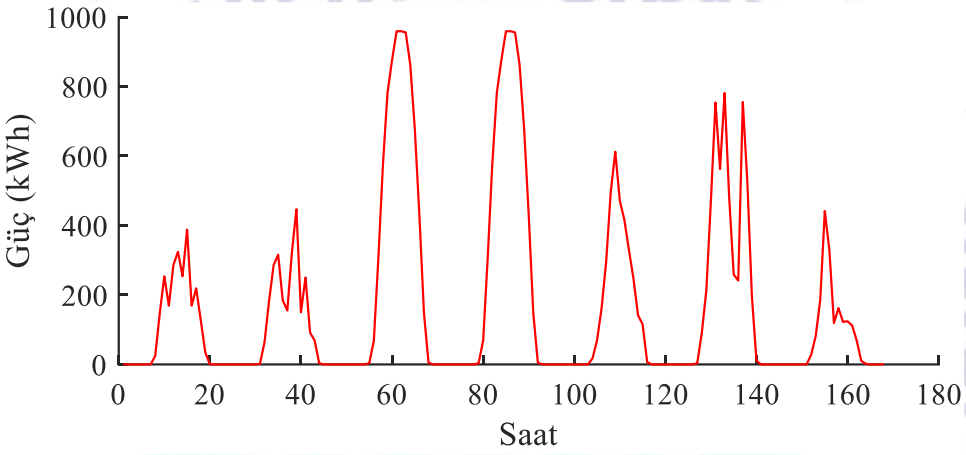

Görsel 2. KM Güneş Enerji Santrali Saatlik Güç Değerleri

Bu çalışmada geliştirilen güç tahmin modellerinin diğer girdisi meteorolojik tahminlerdir. Meteorolojik tahmin; belirli bir ülke, bölge veya merkezde, bir zaman dilimi içinde görülebilecek meteorolojik değerlerin gözlem ve analizler ile elde edilmesidir. Meteorolojik tahmin süreci genel olarak gözlem, analiz ve tahmin aşamalarından oluşmaktadır. Çalışmada kullanılan meteorolojik tahmin değerleri MGM'den alınmıştır. MGM'de birçok tahmin metodu kullanılmaktadır. Bu çalışmada Weather Research and Forecasting (WRF) - Meteogram modeli ile elde edilen meteorolojik tahmin verileri kullanılmıştır. Bu veriler kullanıma açık olup MGM tarafından günlük olarak resim formatında açıklanmaktadır. MGM, santralin bulunduğu Eskişehir ilinin 3 ayrı bölgesi için tahmin hesaplamaktadır. Bu bölgeler; Eskişehir-Merkez, Seyitgazi ve Sivrihisar'dır. Görsel 3'te bu bölgelerin ve incelenen GES'in Google Earth görünümü verilmiştir.

Görsel 3. Meteorolojik tahmin verisi alınan bölgeler ve GES.

Her bir bölgenin 24-48-72 saatlik meteorolojik tahmin verileri günlük olarak erişime açılmaktadır. Bu çalışmada; bulutluluk, sıcaklık, yağış, rüzgâr parametrelerinin gün öncesi tahminleri kullanılmıştır. Tahmin modeli için kullanılan meteorolojik veri seti parametrelerine ilişkin bazı istatistiksel bilgiler Çizelge 3'te verilmiştir. 22.03.21-13.06.21 tarihleri arasını kapsayan SHT veri seti Görsel 4'te verilmiştir.

Çizelge 3. Meteorolojik veri setinin bazı istatistiksel özellikleri

İstatistiksel Özellik	Sıcaklık (ºC)	Bulutluluk (%)	Rüzgâr Hızı (km/s)	Yağış (mm)
μ	12.569	36.809	14.557	0.049
M	13.2	23.4	12.6	0
σ	7.177	36.688	9.208	0.311
σ^2	51.517	13460	84.790	0.097

μ: Ortalama; M: Medyan ; σ: Standart Sapma; σ^2: Varyans

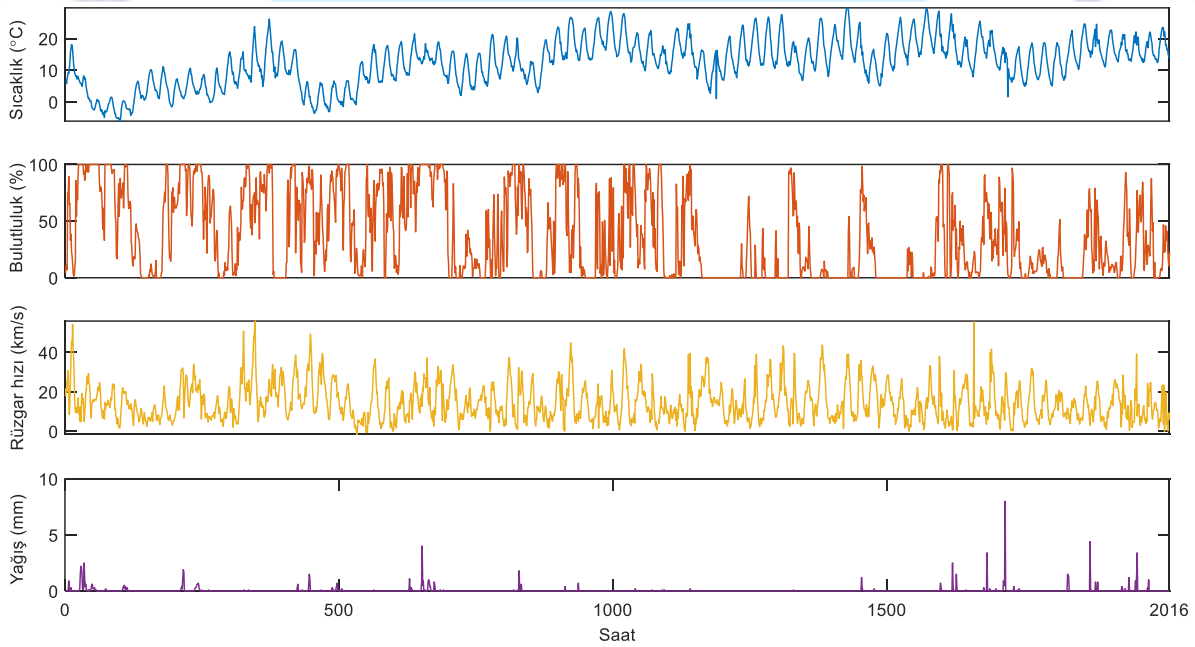

Görsel 4. SHT veri seti.

3. YÖNTEM

Bu çalışmada GES üretimlerinin gün öncesi tahmini için modeller geliştirilmiştir. Modelleme çalışmaları Matlab yazılım dilinde gerçekleştirilmiştir. Makine öğrenmesi algoritmaları Matlab kütüphaneleri kullanılarak modele dâhil edilmiştir. Çalışmada dört farklı makine öğrenmesi algoritması kullanılmıştır. Bunlar; DR, RA, GSR ve DVM'dir. Geliştirilen tahmin modelinin genel yapısı Görsel 5'te verilmiştir. Ayrıca, elde edilen kısa dönemlik güç tahminleri ve santralin ürettiği gerçek güç değerleri bazı performans değerlendirme kriterleri kullanılarak karşılaştırılmıştır.

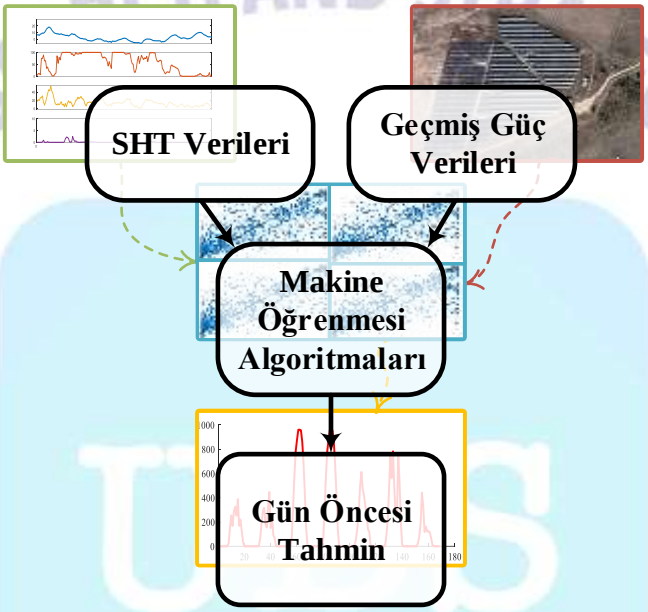

Görsel 5. Tahmin modeli genel yapısı.

Model gün öncesi GES üretim tahmini çıktısı vermektedir. Tahmin ufku 24 saattir. Model girdisi olarak kullanılan SHT verileri 24 saat öncesinden tahmin edilmiş meteorolojik parametrelerdir. Diğer girdi olan geçmiş güç verileri, GES tesisinin tahmin edilecek günden 24 saat önce ürettiği güç değerleridir. Bu iki tip model girdisine ilaveten tahmin edilecek saat bilgisi (1-24)'de model girdisi olarak kullanılmıştır. Toplam 2016 örnek bulunan veri seti eğitim ve test süreçlerini gerçekleştirmek amacıyla iki parçaya bölünmüştür. Bu parçalar eğitim ve test için sırasıyla veri setinin %75 ve %25'lik kısımlarından oluşmaktadır. Ayrıca eğitim sürecinde tahmin modelinin güvenilirliğini irdelemek amacıyla 10 katlamalı çapraz doğrulama kullanılmıştır.

Bu çalışmada, tahmin sistemlerinin etkinliğini değerlendirmek için üç performans değerlendirme kriteri kullanılmıştır. Bunlar RMSE, MAE, R'dır. Kullanılan performans değerlendirme kriterlerini hesaplamak için 1,2 ve 3 denklemler kullanılmıştır. P^t ve P tahmin edilen ve gerçek güçtür, $\bar{P}$ ve $\bar{P}^f$ sırasıyla gerçek ve tahmin edilen n adet güç örneğinin ortalamasıdır.

$$RMSE = \sqrt{\frac{1}{n}\sum_{i=1}^{n}(Pi - P^t i)^2} \quad (1)$$

$$MAE = \frac{1}{n}\sum_{i=1}^{n}|P^t i - Pi| \quad (2)$$

$$R = \frac{\sum_{i=1}^{n}[(P^t i - \bar{P}^t)(Pi - \bar{P})]}{\sqrt{\sum_{i=1}^{n}(P^t i - \bar{P}^t)^2 \sum_{i=1}^{n}(Pi - \bar{P})^2}} \quad (3)$$

4. BULGULAR

Çalışmada, üç bölgeden alınan gün öncesi SHT verileri kullanılarak oluşturulan üç ayrı veri seti ile güç tahmin modelleri geliştirilmiştir. Meteorolojik tahmin verilerinin yanı sıra uygulama yapılan santralden alınmış gün öncesi gerçek güç değerleri ve tahmin edilecek saatin zaman bilgisi de model girdisi olarak kullanılmıştır. Geliştirilen güç tahmin modellerinde 4 farklı makine öğrenmesi algoritması kullanılmıştır. Böylece çalışma kapsamında toplam 12 adet tahmin modeli geliştirilmiş ve performansları değerlendirilmiştir. Değerlendirmeler sonucunda elde edilen RMSE, MAE ve R performans kriterleri Çizelge 4'te verilmiştir.

Çizelge 4.Tahmin modellerinin performans değerleri

Meteorolojik Tahmin Bölgesi	Değerlendirme Kriterleri	Makine Öğrenmesi Algoritması			
		DR	RA	DVM	GSR
Eskişehir Merkez	RMSE	173.49	147.47	152.07	**142.52**
	MAE	117.67	**77.15**	95.24	77.47
	R	0.841	0.887	0.869	**0.895**
Eskişehir Seyitgazi	RMSE	161.79	136.01	149.44	**129.78**
	MAE	109.35	71.74	94.17	**70.80**
	R	0.862	0.902	0.875	**0.91**
Eskişehir Sivrihisar	RMSE	218.93	**140.75**	159.76	149.20
	MAE	123.5	**70.45**	95.16	76.84
	R	0.750	**0.893**	0.861	0.881

RMSE ve MAE değerlerinin 0'a yakın olması iyi bir performansa sahip olunduğunu göstermektedir. Bu durum göz önüne alındığında, Eskişehir Merkez ve Eskişehir Seyitgazi bölgelerinden alınan veriler ile GSR algoritmasının en düşük RMSE değerlerine sahip olduğu görülmüştür**.** Eskişehir Sivrihisar bölgesinden alınan veriler için ise RA algoritması en düşük RMSE değerini yakalamıştır. MAE kriteri incelendiğinde en düşük değerlerin Eskişehir Merkez, Seyitgazi ve Sivrihisar bölgeleri için sırasıyla RA, GSR ve RA algoritmaları tarafından yakalandığı görülmüştür. Çalışmada kullanılan R kriterinin 1'e yakın olması iyi bir performansa sahip olunduğunu göstermektedir. Elde edilen R kriteri değerleri irdelendiğinde,

Eskişehir Merkez ve Seyitgazi verileri için GSR, Eskişehir Sivrihisar verileri için RA algoritmasının 1'e en yakın R değerlerine sahip olduğu görülmüştür. Üç farklı veri seti için genel bir değerlendirme yapıldığında GSR algoritmasının Merkez ve Seyitgazi veri setlerinde daha başarılı olduğu görülmektedir. Sivrihisar bölgesi veri seti için ise RA algoritması en iyi performansı yakalamıştır. Bu durum GSR algoritmasının farklı veri setlerinde iyi bir performansa sahip olduğunu göstermektedir. 3 farklı veri seti ve 4 farklı makine öğrenmesi algoritması ile elde edilen 12 sonuç genel olarak değerlendiğinden ise GSR algoritmasının 0'a en yakın RMSE ve MAE değerlerine ve 1'e en yakın R değerine sahip olduğu görülmüştür.

GSR algoritmasının farklı bölgelerden alınan veriler için sergilediği performansı görsel olarak değerlendirmek amacıyla Görsel 6'de verilen grafikler oluşturulmuştur. Grafikler, test sürecinde gerçekleşen üretimleri ve yapılan tahminleri göstermektedir. Test süreci toplamda üç haftalık zaman aralığındaki veriler kullanılarak gerçekleştirilmiştir. Şeklin en üstündeki, ortasındaki ve en altındaki grafikler sırasıyla test sürecinin ilk, ikinci ve üçüncü haftaları için oluşturulmuştur.

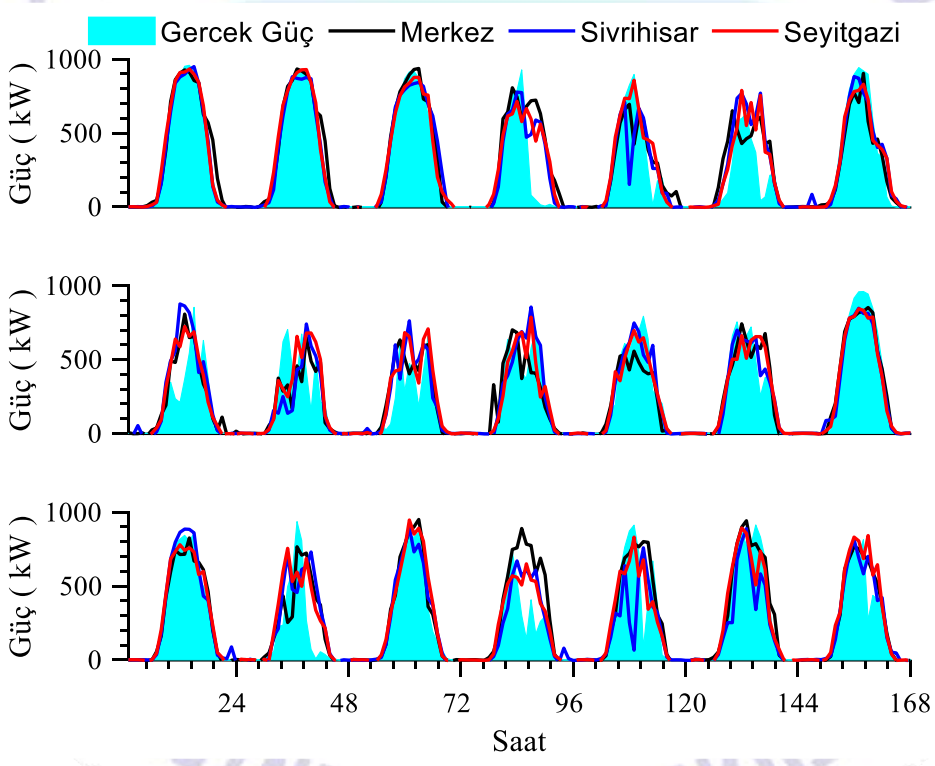

Görsel 6. Test sürecinde gerçekleşen üretimler ve GSR algoritması tahminleri.

Görselde verilen grafikler incelendiğinde GES tesisinin test sürecindeki bazı günlerde kararlı üretim gerçekleştirdiği görülmektedir. 1. Haftanın 1-3. günlerinde, 2. haftanın 7. gününde ve 3. haftanın 1. ve 3. gününde gerçekleşen bu kararlı üretimlerde her üç veri seti ile geliştirilen modeller iyi performans sergilemiş ve tahmin değerleri üretim değerlerine oldukça yaklaşmıştır. GES tesisi test sürecindeki bazı günlerde ise beklenenden düşük üretim gerçekleştirmiştir. 1. haftanın 5 ve 7. günlerinde, 2. haftanın 3-6. günlerinde ve 3. Haftanın 6. günlerinde gerçekleşen bu düşük üretimlerde tahmin modeli performansları üretim karasızlığının artması sebebiyle kabul edilebilir seviyede düşmüştür. Test sürecindeki 1.

haftanın 4 ve 6. günlerinde, 2. haftanın 1. gününde ve 3. haftanın 2, 4 ve 7. günlerinde santral üretimlerinde ani düşüşler olmuştur. Ani üretim düşüşü yaşanan günlerde tahmin modelleri iyi bir performans yakalayamamıştır. Bu durumun santralin bazı tahmin edilemeyen meteorolojik olaylara verdiği tepkiden kaynaklandığı düşünülmektedir.

5. SONUÇ

Yenilebilir enerji kaynakları temiz ve tükenmez olduklarından giderek artan bir hızla elektrik şebeke sistemlerine aktarılmaktadır. Fakat yenilenebilir enerji üretim tesisleri, değişken ve kararsız üretim karakteristiği sergilemekte ve elektrik şebeke işletiminde ek maliyetler oluşturmaktadırlar. Ek maliyetleri ortadan kaldırmak için özellikle gün öncesi planlama sürecinde hesaplamalara dâhil edilecek kaliteli üretim tahminlerine ihtiyaç duyulmaktadır. Bu çalışmada MGM tarafından sağlanan meteorolojik tahminler ve geçmiş GES üretimleri ile makine öğrenmesi algoritmaları kullanılarak gün öncesi tahmin modelleri geliştirilmiştir. Eskişehir ilinde faaliyet gösteren bir GES tesisinde yapılan uygulamalar ışığında aşağıdaki sonuçlara varılmıştır.

1) Çalışmada incelenen Eskişehir ili Odunpazarı ilçesindeki GES tesisi için Seyitgazi, Sivrihisar ve Eskişehir Merkez ilçelerinin meteorolojik tahminleri kullanılarak gün öncesi enerji üretim tahmini yapılmıştır. Gerçekleştirilen test çalışmaları en iyi performansın Seyitgazi verileri ile yakalanabildiği görülmüştür.

2) Geliştirilen tahmin modellerinde DR, RA, DVM ve GSR algoritmaları kullanılmıştır. Elde edilen bulgular GSR algoritmasının diğer üç algoritmaya kıyasla daha başarılı olduğunu göstermiştir.

3) Test sürecindeki model performansları incelendiğinde en yüksek tahmin hatalarının ani üretim düşüşlerinin yaşandığı günlerde gerçekleştiği görülmüştür.

Bu çalışmada bazı meteorolojik tahmin verileri ve makine öğrenmesi algoritmalarının GES üretim tahminindeki performansları ortaya koyulmuştur. Meteorolojik tahminlerin bölgesel olarak farklı doğruluk seviyelerine sahip oldukları bilindiğinden değişik bölgelerde yapılacak çalışmaların literatüre katkı sağlayacağı düşünülmektedir. Ayrıca literatürde bulunan farklı makine öğrenmesi algoritmalarının performanslarının değerlendirilmesi de tahmin kalitesi konusunda katkı sağlayabilecektir.

KAYNAKÇA

[1] Yumru, İ.T., *Spatiotemporal forecasting of solar power generation with deep learning*, Yüksek Lisans Tezi, Fen Bilimleri Enstitüsü, Boğaziçi Üniversitesi, İstanbul, 2020.

[2] Akbaba, E. C., *Using artificial neural network (ANN) techniques for solar irradiation predictions,* Master Of Scıence, Physics Department, Middle East Technical University, Ankara, 2019.

[3] Yavuz, C., *Konya'da Kisa Dönemli Güneş Enerjisi Üretim Tahmini*, Yüksek Lisans Tezi, Fen Bilimleri Enstitüsü, Necmettin Erbakan Universitesi, Konya, 2018.

[4] Kılıç, H., Gümüş, B. ve Yılmaz, M. Güneydoğu Anadolu bölgesi için global güneş ışımasının ve güneşlenme süresinin istatiksel metodlar ile tahmin edilmesi ve karşılaştırılması. Dicle Üniversitesi Mühendislik Fakültesi Mühendislik Derg., 7, 1, 2016.

[5] Okur, Y., Akdeniz bölgesine ait meteorolojik veriler kullanılarak yapay sinir ağları yardımıyla güneş enerjisinin tahmini. Yüksek Lisans Tezi, Fen Bilimleri Enstitüsü, Osmaniye Korkut Ata Üniversitesi, Osmaniye, 2016.

[6] Nkuriyingoma, O. and Selçuklu, S.B., Solar power plant generation forecasting using NARX neural network model: A case study, Int. J. Energy Appl. Technol., 8, 3, 2021.

[7] Ahmet, K., Uzun-Kısa Süreli Bellek Ağı Kullanarak Global Güneş Işınımı Zaman Serileri Tahmini. Gazi Üniversitesi Fen Bilim. Derg. Part C Tasarım ve Teknol., 7, 4, 2019.

[8] Korkmaz, D., Acikgoz, H. and Yildiz, C., A novel short-term photovoltaic power forecasting approach based on deep convolutional neural network. Int. J. Green Energy, 18, 5, 2021.

[9] Yildiz, C. and Acikgoz, H., A kernel extreme learning machine-based neural network to forecast very short-term power output of an on-grid photovoltaic power plant. Energy Sources, Part A Recover. Util. Environ. Eff., 43, 4, 2021.

[10] Gök, A.O., Yıldız, C. and Şekkeli, M., Yapay Sinir Ağları Kullanarak Kısa Dönem Güneş Enerjisi Santrali Üretim Tahmini: Kahramanmaraş Örnek Çalışması. Uluslararası Doğu Anadolu Fen Mühendislik ve Tasarım Derg.,1, 2, 2019.

[11] Ahmed, R., Sreeram, V., Mishra, Y. and Arif, M.D., A review and evaluation of the state-of-the-art in PV solar power forecasting: Techniques and optimization. Renew. Sustain. Energy Rev., 124, 2020.

EKSENEL YÜK ETKİSİNDEKİ ARAMİD FİBER TAKVİYELİ EPOKSİ MATRİS KOMPOZİT PLAKLARIN FARKLI FİBER AÇILARININ DEFORMASYON DEĞİŞİMİNE ETKİLERİNİN İNCELENMESİ

Öğr. Gör. EMRE YILMAZ [1]

[1] İstanbul Aydın Üniversitesi, ABMYO, 0000-0001-5209-0368

ÖZET

Bir ürün tasarımının somut hale dönüştürülmesinde, ilgili tasarımın uygulanması sırasında ihtiyaç ilkelerini karşılayacak bir malzeme seçilmesi gerekmektedir. Bu malzeme seçiminin istenilen kapasiteyi optimum düzeyde karşılayacak şekilde yapılması hem güvenilirliğin sağlanması hem de maliyet analizi açısından önemlidir. Son yıllarda gelişen teknoloji ile birlikte tekil malzemelerin yerini kompozit malzemeler olarak adlandırılan en az iki çeşit malzemeden oluşan yeni bir malzeme türü almıştır. Kompozit malzemeler başta otomotiv ve uçak sanayi olmak üzere tüm sektörlerde ihtiyaçlar doğrultusunda kullanılmaktadır. Tekil yapı malzemelerine kıyasla yüksek özgül mukavemet, yüksek korozyon direnci, yüksek yorulma direnci, yüksek aşınma direnci özellikleri sağlamaktadır. İdeal matris-fiber çiftinin seçimi, üretim tekniği ve optimizasyon da tüm bu özelliklerin oluşmasında önemlidir. Bu ideal unsurlara ulaşmak için deneysel uygulamalar analitik çözümlerle birlikte yürütülür. Elde edilen sonuçlar birbirleriyle karşılaştırılarak optimum matris-fiber çifti ve üretim tekniğine ulaşılabilir. Yük altındaki bir tasarımda deformasyon istenmeyen bir durumdur. Malzeme türü seçimi ile eş zamanlı olarak uygulanacak malzeme boyutlarının doğru belirlenmesi deformasyon güvenliği açısından önemlidir. Aramid lifi ısıya, organik çözücülere dayanıklı ve yüksek mukavemetli bir sentetik lif türüdür. Askeri alanda kurşun geçirmez yelek üretiminde, fren sistemlerinde, tekerlek yapımında, halat-kablo üretiminde, fiber optik kablolarda, bateri yüzeylerinde ve hoparlör diyaframlarında kullanılmaktadır. Bu çalışmada, sonlu elemanlar yöntemine dayalı bilgisayar programı simülasyonu ile yükleme ve plak boyutları sabit alınarak aramid fiber epoksi matris kompozit malzeme plakların düzlem içi yük etkisi altında farklı fiber açıları için deformasyon analizleri yapılmıştır. Farklı fiber açıları için sabit yük altında kompozit plak'ın deformasyon değişimleri tablo ve grafiklerde incelenmiş ve fiber açı derecelerinin aramid fiber epoksi matis kompozit plak'ın deformasyonu üzerindeki etkileri belirlenmiştir.

Anahtar Kelimeler: Eksenel yük, Deformasyon analizi, Kompozit plak, Fiber açısı, Aramid fiber kompozit malzeme.

THE INDIRECT IMPACT OF MINING ON SOCIAL-WELLBEING - CASE OF KOSOVO'S SURFACE COAL MINES

Kemajl ZEQIRI [1]

[1] Mining Engineering Department, https://orcid.org/0000-0001-9362-2156

ABSTRACT

Historically mining industry has supported economic development and social well-being worldwide. While economic impact can be measured by different examples, the indirect impact of the mining industry on social well-being is more complex and consequently hard to track and promoted as well.

This paper shall provide a case study, of Kosovo's coal mining's indirect impact on social wellbeing.

The coal exploration in Kosovo was conducted during the century XX whereby it is found that there are a lot of coal resources in Kosovo. Underground coal exploitation began in 1922, next to existing Kosovo's towns: Obiliq and Lipjan. Systematic research of the Kosovo coal basin started between 1952 and 1957. During this period, preparatory works were conducted for the economic utilization of the Kosovo basin coal, with the transformation from underground mining to surface mining, considering the possibilities for massive utilization of the available resources for coal-powered thermal power plants and industrial coal processing purposes (GoK, 2012). Between the years 1962-1983, in Kosovo were constructed a facilities coal-based electricity generation, with a capacity of about 1500 MW.

Thus, with the purpose of supplying Power Plant (PP) "Kosovo A" with water was constructed the "Batllava" lake, whereas later on, was constructed the lake "Ujmani" to supply PP "Kosovo B". These lakes, beyond a primary purpose, have had a huge positive impact in economy and social wellbeing. This indirect social impact somehow is forgotten that it derives from the mining industry i.e. coal mining.

Keywords: energy, mining, social wellbeing, water, coal, impact.

1. INTRODUCTION

Kosovo is situated in the central part of the Balkan. In the Southwest, it is bordered by Albania, in the West by Montenegro, in the North by Serbia and in the East and Southeast by Macedonia,

with a territory of about 10,900 km2. In Kosovo lives approximately 1,790,133 inhabitants (Bank, 2022).

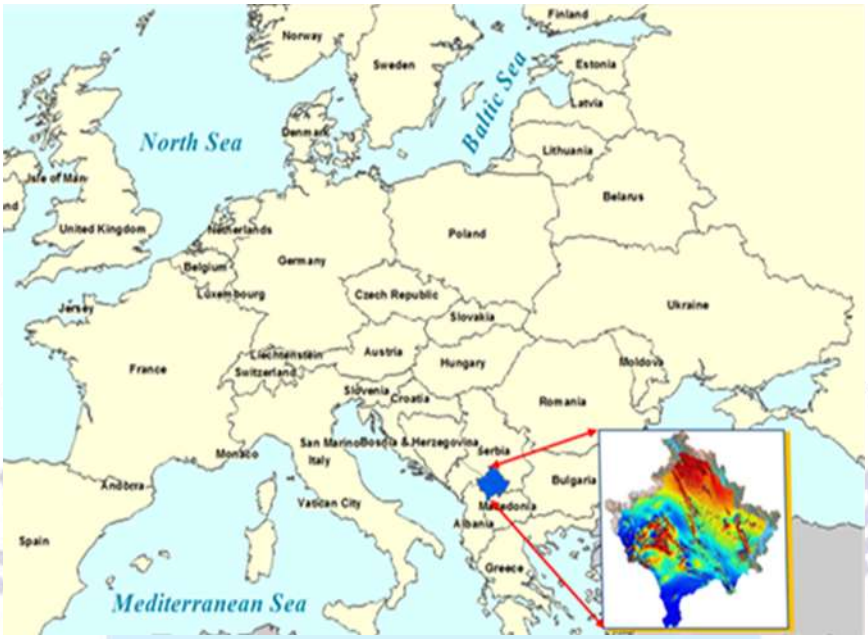

Figure 1. Kosovo's geographic position

Kosovo's climate is influenced by continental air masses resulting in relatively cold winters with heavy snowfall and hot, dry summers and autumns, the territory of Kosovo is characterized by high seismic activity, namely Alpine-Himalaya zone, in the past, 82 earthquakes exceeding 5 degrees of Mercalli-Cancani-Sieberg scale (MSC).

According to the World Bank in 2020, the GDP of Kosovo was $7.72 billion. The GDP growth comes mostly from the private sector, while Kosovo's economy is supported by the majority of industries as are: Energy, Mining and Agriculture. Kosovo's main mineral resources are Lignite with about 12, 50 billion tons of reserves, Lead and Zinc with 60 million tons as well as nickel, silver, magnesium, kaolin, chrome, bauxite, etc. (GoK, 2012). Up to 1988, industry and mining contributed to 47, 40% of the gross domestic production (GDP) of the country, but by 1994, this percentage dropped to 21,1%. Between the years 1990-and 1999, the mining industry has experienced drastic drops associated with exploitation outside any mining standards, the consequences of which are still evident.

Table 1. Kosovo's main mineral reserves

Resources	Reserves	
Lignite	12.50	Billion ton
Lead & Zinc	60.00	Million ton
Nickel	13.00	Million ton
Bauxite	3.00	Million ton
Magnesium	4.00	Million ton

1.1 Mining impact in social development

The mining industry is an inseparable part of the development of human society. Today's economic development and improvement of living conditions cannot even be imagined without the participation of the mining industry.

Table 2. Use minerals from society throughout history

Need	Objective	Period of time
Kitchen utensils	Food, accommodation	prehistoric
Weapons	Hunting, defense , battles	prehistoric
Decorations and ornaments	Jewelry, cosmetics, color	Antique
Currency	Exchange	Early
Structures and equipment	Accommodation and transport	Early
Energy	Heating and travelling	Middle ages
Machinery	Industry	Modern
Electronic	Communication , computers	Modern
Fission nuclear	Energy, wars	Modern

There is no doubt that the mining industry is the key factor in the development of modern society. In other words, the history of the mining industry is fascinating, in parallel with the history of civilization, many stages of different cultures are linked to the identification of any minerals or derivatives as are: "Stone Age" (4000 B.C), "Bronze Minerals" (4000 to 5000 B.C), "Iron Time" (1500 B.C to 1780 C.T), "Steel Time" (1780-1945), and finally the "Nuclear Period" (1945 onwards), this shows that the mining industry was an inseparable part of the development and social modernization (Pruchnicka. J, Zeqiri. K, 2017).

The only question nowadays is how to measure mining's impact on the economy and social well-being as well.

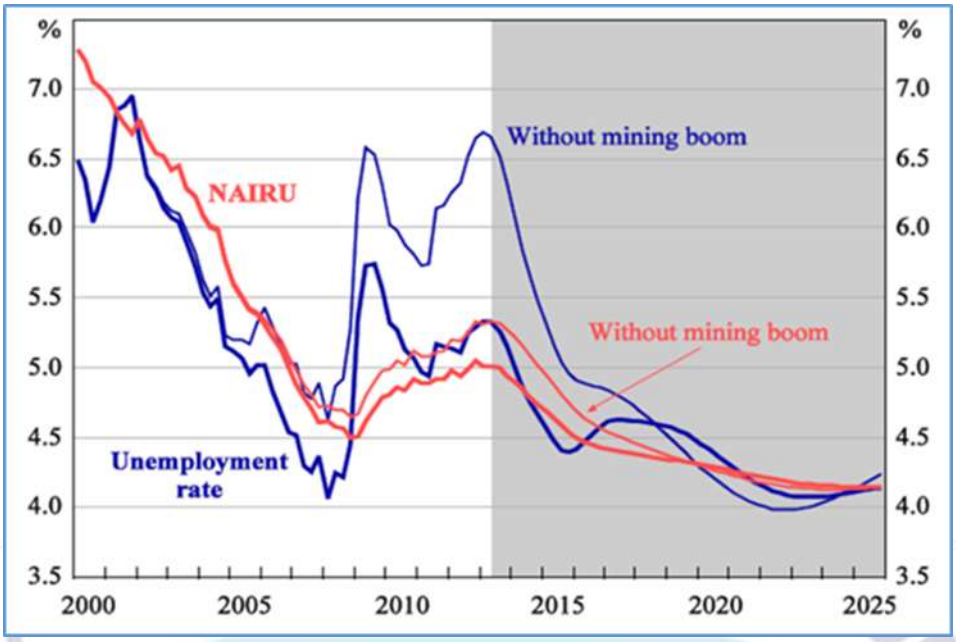

Figure 1. Effect of "mining boom" on unemployment rate in Australia

Fig. 2 shows an example of the mining boom in Australia's unemployment and development over the last two decades and forecast for the next decade. On other hand, one employee in the mining industry indirectly generates 3 to 5 other jobs, and this can be said also, to other chain-impacts on the economy and the social wellbeing.

2. MATERIALS AND METHODS

The based methodology used in this research work was based review of literature, related to mining's impact on the economy, or actually mining's an indirect impact on social wellbeing. As a case study was used Kosovo's mining operation, consequently mining of coal, with aim of electricity production. Thus, the research shall analyse the purpose of the construction of two artificial lakes and their impact on social wellbeing, i.e "Ujmani Lake" and "Batllava" lake.

Figure 3. Ujmani lake (Wikipedia®, 2022)

Ujmani Lake is an artificial lake located in the North West part of Kosovo, and it is the largest lake in Kosova. The lake is formed by the damming of Iber River which flows into the lake, and it has an average depth of 105 meters (Guide, 2022). "Ujmani" lake has been constructed 1979, with the primary aim of supplying the cooling facility of the Power Plant "Kosovo B", but from this canal is supplied also "Ferronickel" mine for industrial purposes. The PP Kosovo was constructed in two units. The first unit (B1) with a power of 339 MW, whereas, the second unit (B2) of this power plant has a power of 339 MW.

Currently, both units are functional and have an annual availability of 85%. Each of these units in recent years operates with more than 7200 working hours within a year (KEK, 2022).

In this regard have been constructed more than 40 km of water canal that is an almost open channel so-called "Iber-Lepenc". At the same time, the lake supports a hydro power plant station which is located at its base and it has an installed capacity of 35 MW.

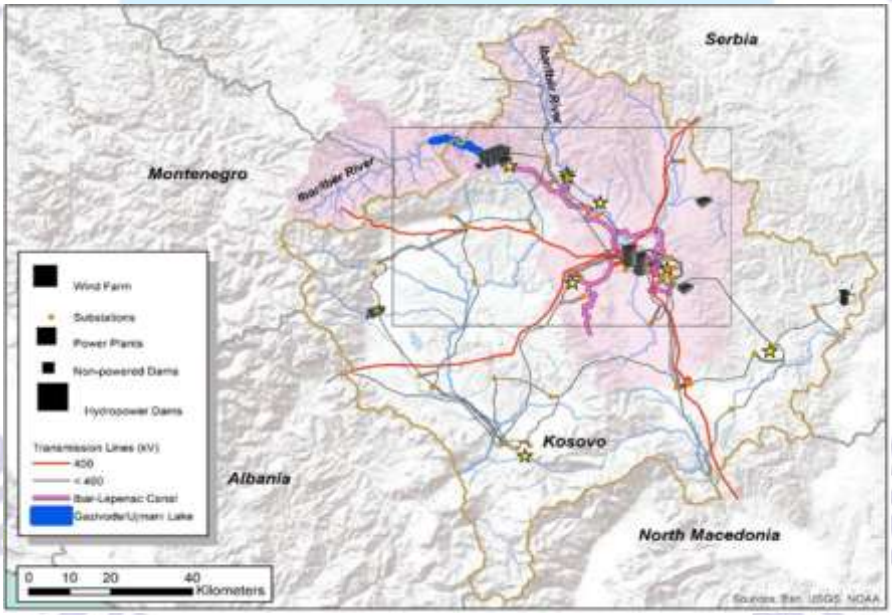

Figure 4. Kosovo water and electricity infrastructure (Voisin N. et.al, 2021)

Fig. 4 represents the Ujmani hydro system that supplies the cities of Mitrovica, Vushtrri, Obiliq, Gllogovc, and Pristina with freshwater through the Ibër-Lepenc canal. Thus, the Ujmani lake i.e. water canal facility, from the north part of Kosovo, beyond the primary aim (water supply of PP Kosova B /industrial purpose) has been used and continues to be used in agricultural, energy as well as is drinking water supply and supports socio-economic development.

Batallava lake, was constructed during the '70th years. The main purpose of the construction of this lake was to supply with water the facilities for the electricity i.e. electricity generation based on coal - the power plant "Kosova A". The "Kosova A" power plant consists of five working units: A1, A2, A3, A4

and A5. The total power of the power plant is: A1+A2+A3+A4+A5 = 65+125+200+200+210 = 800 MW. Nevertheless, only units A3, A4 and A5 are under operation.

Figure 5. Image of Batallava lake

The Batllava lake (Fig.5) is the main water supplier of Kosovo's capital city Prishtina, and its region. "Lake Batllava has an area of 3.29 square kilometres and today is used for summer holidays, picnics, fishing, relaxation in various restaurants, etc. Lake Batllava is undoubtedly one of the most frequented tourist attractions in Kosovo" (Shqip, 2022).

Thus, as shown in the previous text the impact of mining is fascinating and multidimensional, whether in the economy (agronomy, energy, tourism etc.) or social wellbeing (infrastructure development, rural development etc.)

3. RESULTS AND DISCUSSION

Each human era development is associated with a certain mineral use. Technology innovation (medicine, construction, electronic devices, transport, renewable energy etc.) cannot be imagined without mining.

The current energy crisis will increase efforts toward finding a new solution, to coal utilization in line with environmentally friendly principles.

The real impact of the mining industry on socio-economic development is hard to be tracked, two cases mentioned in this research show the multidimensional impact of the mining industry on socio-economic development.

REFERENCES

[1] Pruchnicka. J, Zeqiri. K. (2017). Mining Impact in Social Well-Being - Poland and Kosovo Case. Krakow: MARG.

[2] Voisin N. et.al. (2021). Water Resource Opportunities at Lake Gazivode/Ujmani. U.S. Department of Energy.

[3] KEK. (2022). http://kek-energy.com/kek/termocentrali-kosova-b/. Retrieved from http://kek-energy.com/kek/.

[4] Bank, W. (2022). https://data.worldbank.org/country/kosovo?view=chart. Retrieved from https://www.worldbank.org/en/home.

[5] GoK. (2012). Mining Strategy of the Republic of Kosovo. Prishtina: Government of Kosovo.

[6] Guide, M. (2022). https://mitrovicaguide.com/place/ujmani-lake/. Retrieved from https://mitrovicaguide.com/.

[7] Shqip, V. (2022). https://vizitoshqip.com/turizmi/details/liqeni-i-batllaves. Retrieved from https://vizitoshqip.com/lokacione.

[8] Wikipedia®. (2022). https://en.wikipedia.org/wiki/Gazivoda_Dam.

THE IMPACTS OF CLIMATE CHANGE AND SOCIO-ECONOMIC FACTORS ON FOOD SECURITY: A CASE STUDY OF UNITED ARAB EMIRATES.

Aydın Başarır
United Arab Emirates University

Hasan Arman
United Arab Emirates University

ABSTRACT

The main causes of climate changes in different regions of the world is global warming which changes weather via increasing in floods, regional droughts, earthquakes, hurricanes, tsunamis and etc. The warming may also have some unexpected economic effects mainly on agriculture. The effects on agriculture are expected to be via rainfall, temperature, and humidity. In addition to such climatic factors, socio-economic factors such as population growth rate, income and prices levels, trade, and etc. are affecting the agriculture as well. The previous studies have focused on the effects of climate changes and social/economics factors on agriculture separately. This study combines both in a comprehensive framework by utilizing multivariate econometric analyzes. The main objective of this study is to analyze the impacts of climate change and socio-economic factors on the food security of UAE. The annual agricultural production of UAE was taken as food security indicator. Time series data related to agricultural production (dependent variable) climate change and socio-economic factors (independent variables) were analyzed by using econometric tools such as Augmented Dickey Fuller (ADF) test, Co-integration test, and Vector Error Correction (VEC) estimates. According to the results, the factors seem to have significant effects on food security of UAE.

UAE has high socio-economic standard of living. High temperature, lower humidity and insufficient rainfall cause harsh climate conditions and difficulties in agricultural production. Even though the unit cost of production will be higher, adaptation of production to such climate can contribute to the food security of UAE in the future.

Keywords : Climate Change, Socio-Economic Factors, Food Security, Adaptation.

FACTORS AFFECTING SUSTAINABLE FOOD INNOVATIONS OF MANUFACTURERS: A CASE STUDY OF UNITED ARAB EMIRATES FOOD INDUSTRY

Aydın Başarır
United Arab Emirates University

Mumin Dayan
United Arab Emirates University

ABSTRACT

Food Industry is strategically important in global economy and encompasses many issues such as shorter lifecycle of products, higher quality standards, food safety, and competitiveness which encourage firms to develop innovative foods. As a result of increasing importance of environmental and social concerns in the innovation processes; the innovations should be sustainable for firms considering long term successes. Sustainable innovation can be broadly defined as the innovation that takes into consideration environmental and social issues as well as the needs of future generations. Determining the factors affecting such innovations can enhance decision makers' awareness and actions to be taken accordingly. The main objective of this study is to analyze the factors affecting sustainable food innovations in UAE Food Industry. A survey was developed and conducted on 65 randomly selected food manufacturers in UAE. The survey included questions related to government support, academic-industry collaborations, market dynamics, collaborations with competitors, and sustainable food innovations in a Likert scale structure. By using structural equation models via SmartPLS software, the causal relationship between the variables were analyzed. According to the results, in addition to direct effect of government support on the innovations; the support through the mediators such as academic-industry collaborations, market dynamics, and collaborations with competitors were highly significant.

Even though UAE Food Industry is mainly dependent on the import of raw agricultural products, adding value to them via processing, manufacturing, and partially re-exporting the final products have been developed significantly in recent years. Direct support to the manufacturers and/or mediators mentioned above can further enhance the process of sustainable innovations in UAE Food Industry.

Keywords: Sustainable Food Innovations, Government Support, Academic-Industry Collaborations, Market Dynamics, Collaborations with Competitors

DEGRADATION OF TOXIC POLLUTANT CATALYZED BY SILVER NANOPARTICLES SUPPORTED ON *ALOE VERA* LEAVES

Dr. Şakir YILMAZ[1,2]

[1]Van Yuzuncu Yil University, 0000-0001-9797-0959

[2]Van Yuzuncu Yil University, 0000-0001-9797-0959

ABSTRACT

Today, with the rapid development of the textile and dyeing industry, colored wastes have been produced and a number of environmental problems arise. The countless synthetic dyestuffs emerged in the effluents from different industries including textiles, leather, dyestuff, and paper. Wastewater treatments are of great importance to eliminate these toxic contaminants. Several procedures such as coagulation, ozonation, membrane filtration, adsorption, precipitation, and decolarization, are applied to the removal of various dyes from water resources. These methods may not degrade dyestuffs due to their complex structure and high stability to temperature, and light. The degradation process, which converts toxic organic contaminants into less harmful ones, is a promising technique. Therefore, the aim of this study was to investigate the degradation of an acidic xanthene dye Eosin Yellow (EY) by silver nanoparticles supported with *Aloe vera* leaves (Ag/AV). Furthermore, the effects of dye concentration, amount of catalyst, and reaction time on EY degradation process were evaluated and optimized using response surface methodology (RSM). The analysis of variance (ANOVA) results displayed that the EY degradation process was statistically desirable owing to the model regression factor (R^2 = 0.97) and *p*-value of the suggested model ($p < 0.0001$). On the other hand, the optimization results indicated that 10.96 mg/L, 0.78 mg/mL, and 73.50 s were optimum conditions, and approximately 85% degradation efficiency of EY was achieved. Moreover, the kinetics studies showed that EY degradation process on Ag/AV was best expressed by pseudo-second order model. Finally, this study showed that the produced catalyst is the remarkable performance for the degradation of EY.

Keywords: Degradation pathway, dye, response surface methodology, silver nanoparticles, wastewater treatment.

TÜRKİYE DEPREM VE KURTARMA ÇALIŞMALARI

Dr.Öğr.Üyesi GAMZE BİLGEN[1], MURAT DUYSAK

[1]Zonguldak Bülent Ecevit Üniversitesi, ORCID ID: https://orcid.org/0000-0002-2840-7369

[2]Zonguldak Bülent Ecevit Üniversitesi, ORCID ID: https://orcid.org/0000-0001-9315-9448

ÖZET

Yapılan çalışmada, deprem kavramı, Türkiye'de yaşanan depremler, deprem sonrası arama kurtarma çalışmaları, Afet ve Acil Durum Yönetim Başkanlığı (AFAD), 2018 tarihinde hazırlanmış olan "Türkiye Bina ve Deprem Yönetmeliği (TBDY-2018)" ve "Türkiye Deprem Tehlike Haritası (TDTH)" konuları üzerinde durulmuş başka bir deyişle Türkiye'deki deprem ve kurtarma çalışmaları ele alınmıştır. Türkiye coğrafi olarak pek çok fay hattının geçtiği bir konumda bulunduğundan deprem tehlikesinin yüksek olduğu bir bölgedir. Tarih boyunca büyük maddi kayıpların ve can kaybının gerçekleştiği pek çok deprem yaşanmıştır. Günümüz teknolojisi ile her ne kadar depremin oldurulması veya durdurulması mümkün olmasa da can ve mal kaybının en aza indirilmesi ve deprem sonrası arama, kurtarma konularında yapabilecek mümkünatı olan konular bulunmaktadır. Ülkemizde deprem konusundaki ilk resmi çalışmalar 1939 Erzincan depremine dayanmaktadır. O günden bu yana gelişen teknoloji, yapılarda gözlenen yetersizliklerin belirlenmesi, bilimsel çalışmaların artması, yapı tipleri ve yapı malzemelerin gelişmesi gibi etmenler ile depremde yapılacak yapılar ile ilgili yönetmelikler zaman zaman güncellenmektedir. Ancak, 2018 yılında AFAD tarafından hazırlanmış olan TBDY-2018 yönetmeliği, daha önceki yapı yönetmeliklerin güncellenmesinden öte bir çalışma olarak değerlendirilmektedir. Zira, bu yönetmelikte daha önceki yönetmeliklerde kabul gören ve hatta tüm yönetmeliğin üzerine kurgulanmış olduğu deprem bölgesi, güvenlik sayıları gibi kavram ve parametreler tamamen kaldırılmış yerine yeni tanım ve kavramlar getirilmiştir. Yine bu yönetmelikte, binalardaki statik ve betonarme hesaplama detaylarının yanında, geoteknik konusu da çok daha kapsamlı bir şekilde hesaplara katılmış, aynı yıl güncellenmiş olan TDTH ile interaktif bir şekilde kullanılması üzerine tasarlanmıştır. Daha dayanıklı, can ve mal güvenli açısından daha iyi tasarlanmış yapılar için yer bilimleri konusundaki mühendisler ve inşaat mühendisleri gerek betonarme gerek geoteknik gerekse malzeme konularında çalışmalarına devam etmektedir.

Anahtar kelimeler: Deprem, AFAD, Bina Deprem Yönetmeliği

ABSTRACT

In the study, the following concepts were discussed: the concept of earthquake, earthquakes in Turkey, search and rescue affairs after the earthquake, Disaster and Emergency Management Presidency (AFAD), which has been the only official authority and responsibility for disasters

since 2018, "Turkey Building and Earthquake Code (TBDY-2018)" and "Turkey Earthquake Hazard Map (TDTH)". In other words, earthquake and rescue affairs in Turkey are discussed. Since Turkey is geographically located in a location where many fault lines pass, it is a region with a high earthquake risk. Throughout history, there have been many earthquakes in which great property losses and many deaths occurred. Although it is not possible to do or to stop an earthquake with today's technology, there are possible issues that can be done in terms of minimizing the loss of life and property, and post-earthquake search, rescue and assistance to disaster victims. The first official studies on earthquakes in our country are based on the 1939 Erzincan earthquake. Since then, the regulations related to the structures to be built in an earthquake have been updated from time to time due to factors such as the developing technology, the determination of the deficiencies observed in the buildings, the increase in scientific studies, the development of building types and building materials. However, the TBDY-2018 regulation, which was prepared by AFAD in 2018, is considered by the authors as a study beyond updating the previous building regulations. Because, in this regulation, concepts and parameters such as earthquake zone and safety numbers, which were accepted in previous regulations and even on which the entire regulation was built, were completely removed, and new definitions and concepts were introduced instead. Again, in this regulation, besides the static and reinforced concrete calculation details in the buildings, the geotechnical issue was also included in the calculations in a much more comprehensive way and it was designed to be used interactively with the TDTH, which was updated in the same year. Engineers in earth sciences and civil engineers continue to work on reinforced concrete, geotechnical and material issues for more durable and better designed structures in terms of life and property safety.

Keywords: Earthquake, AFAD, Building Earthquake Regulation

1. GİRİŞ

Yerkabuğu tektonik plakalara bölünmüştür. Bu plakalar milyonlarca yıldır Dünya yüzeyinde çok yavaş ve kesintisiz bir şekilde hareket ederler. Bu kesintisiz hareket, Dünya'nın kabuğunda gerilmeler meydana getirir. Gerilmeler çok büyüdüğünde, fay adı verilen kırıkların (çatlakların) hareketine sebep olur. Tektonik hareketlerin fay hattında meydana getirdiği ani hareketlere "Deprem" adı verilmektedir (URL-1).

Şekil 1. NASA verilerine göre dünya fay hatları (URL-1)

Şekil 1'de NASA tarafından verilen dünyadaki fay hatlarının genel pozisyonu görülmektedir. Bir tektonik plaka ayrımının bulunduğu bölgeler deprem açısından tehlikeli olarak adlandırılırken, Türkiye Afrika Plakası, Avrupa Plakası, Arap plakası ve Anadolu plakasının etkisi altında bulunduğundan, oldukça büyük tehlike potansiyeli taşımaktadır (Meng vd., 2021). Şekil 2'de son olarak 2018'de güncellenmiş olan Türkiye Deprem Tehlike Haritası görülmektedir (URL-2)

Türkiye'deki fay hattı sayısının fazla olmasının yanında, coğrafyanın topoğrafik ve iklimsel yapısı da doğal afetlerle sıklıkla karşılaşılmasına sebep olmaktadır. Ülkemizde, su baskını, sel, çığ, heyelan ve deprem gibi farklı doğal afetler sıklıkla meydana gelmektedir. Afet Yönetim ve Karar Destek Sistem (AYDES) veri tabanından alınan istatistiklere ve AFAD istatistikleri 2020 raporuna göre Türkiye'de sadece 2020 yılında meydana gelen doğa kaynaklı afet sayısı Tablo 1'de görüldüğü üzere 905 adettir. Aynı raporda 1950–2019 yılları arasında meydana gelen heyelan olayları Şekil 3 de görüldüğü şekilde sunulmaktadır. Şekil 3'te açık renkli bölgelerdeki heyelan olayları 6 adet iken renk koyulaştıkça bu sayı 1673'e kadar atmaktadır (AFAD, 2021).

Şekil 2. AFAD, 2018 Türkiye Deprem Tehlike Haritası (URL-2)

Bu çalışma kapsamında, bu kadar yoğun şekilde doğal afetlerin yaşanmakta olduğu ülkemizde meydana gelen afet istatistiklerine, afetler ile ilgili kurum, kuruluş ve organizasyonlara ve bunların gelişim aşamalarına yer verilmiştir. Ayrıca, 2018 itibarı ile afetler konusunda tek yetkili resmi organ olan AFAD'ın hazırlamış olduğu Türkiye Deprem Tehlike Haritası ve Türkiye Bina ve Deprem Yönetmeliği irdelenmiştir.

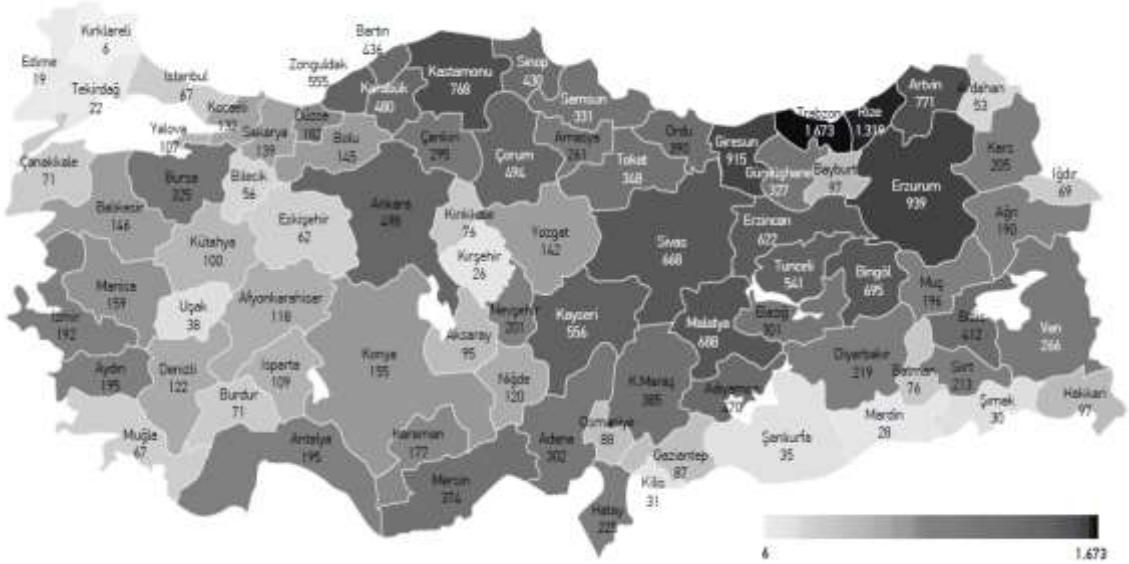

Şekil 3. 1950–2019 Türkiye'de meydana gelen heyelan/kaya düşmesi olayları (AFAD, 2021)

2. ARAŞTIRMA VE BULGULAR

Türkiye'de afetler konusundaki ilk resmi adımların atılması 1939 Erzincan depremine dayanmaktadır. 1959 yılında, 7269 sayılı "Umumi Hayata Müessir Afetler Dolaysıyla Alınacak

Tedbirlerle Yapılacak Yardımlara Dair Kanun" çıkarılmış, Çalışmalar 1988 yılında, afet bölgesine en hızlı şekilde ulaşması ve afetzedelere etkili biçimde müdahalenin yapılması amacıyla "Afetlere İlişkin Acil Yardım Teşkilatı ve Planlama Esaslarına Dair Yönetmelik ile devam etmiştir. 1996 yılında, birkaç gönüllü dağcı tarafından kurulan "Arama Kurtarma Derneği (AKUT)" afetzedelere yardım amacı ile kurulmuş olan ilk organize kurumdur (URL-3). Bunun dışında, "Toprak Ana Arama Kurtarma Ekibi GEA" gibi gönüllülerden oluşan farklı arama kurtarma ekipleri de kurulmuştur (Günaydın vd., 2017). Afet yönetimi ve koordinasyonu açısından resmi olarak en önemli çalışmalar 17 Ağustos 1999 Marmara depremi sonrasında gerçekleşmiştir. Süreç içerisinde devletin farklı bakanlıkları altında afet ile ilgili birimler oluşturulmuştur. Bu birimler, İçişleri Bakanlığı'na bağlı Sivil Savunma Genel Müdürlüğü, Bayındırlık ve İskan Bakanlığına bağlı Afet İşleri Genel Müdürlüğü ve Başbakanlığa bağlı Türkiye Acil Durum Yönetimi Genel Müdürlüğü olarak sıralanabilir (URL-4). Bakanlıklarda kurulan birimlerin dışında, Genelkurmay Başkanlığı tarafından, "TSK Doğal Afetler Arama Kurtarma Tabur Komutanlığı (DAK)", Jandarma Komutanlığı tarafından "Jandarma Arama Kurtarma Timi (JAK)" kurulmuştur (URL-5; URL-6). 1999 depremi sonrası, Ulusal Medikal Kurtarma Ekipleri (UMKE), Sivil toplum afet platformunu (SİTAP), Arama Kurtarma Araştırma Derneği (AKA) gibi pek çok sivil platform oluşturulmuştur (URL-7).

Tablo 1. 2020 Yılı Doğa Kaynaklı Olay İstatistikleri (AFAD, 2021)

Afet Türü	Adedi
Çığ	11
Deprem	321
Diğer	270
Heyelan	107
Kaya Düşmesi	17
Obruk	2
Sel/Su Baskını	117
Genel	**905**

2000'li yıllara gelindiğinde, afet öncesi ve sonrası eş zamanlı ve koordineli bir çalışma sağlaması gereken kurumların afetlerle ilgili yetki ve sorumluluklarının yeniden tanımlanması, ek olarak afet ve acil durumlarda yetki ve koordinasyonun tek elde toplanması uygulaması benimsenmiştir. Bu doğrultuda afetlerle ilgili görev yapan tüm birimler 2009 yılında çıkarılan 5902 sayılı yasa ile Başbakanlığa bağlı Afet ve Acil Durum Yönetimi Başkanlığı çatısı altında toplanmıştır. Son olarak, 15 Temmuz 2018 tarihinde yayınlanan 4 nolu Cumhurbaşkanlığı kararnamesi ile Afet ve Acil Durum Yönetim Başkanlığı (AFAD) İçişleri Bakanlığına

bağlanmıştır (URL-4). AFAD, Bilgi Sistemleri ve Haberleşme Dairesi, Planlama ve Risk Azaltma Dairesi, Sivil Savunma Dairesi, Gönüllü ve Bağışçı İlişkileri Daireleri gibi idari müdürlüklerin yanında, 81 ilde Afet ve Acil Durum Müdürlüğü, 11 Arama ve Kurtarma Birlik Müdürlüğü gibi organları bulunan, afet konusunda tek yetkili kurum olarak görevine devam etmektedir. T.C. İçişleri Bakanlığı 2021 Yılı AFAD Performans Programı raporuna göre AFAD bünyesinde 7780 kadrolu personel bulunmaktadır. AFAD'ın başlıca projeleri aşağıdaki gibidir (URL-8):

*Deprem Gözlem Ağları

*Derin Kuyu Sismometre Ağı Projesi

*EPOS – Avrupa Yer Gözlemleri Sistemi

*Türkiye Bina Deprem Yönetmeliği

*Türkiye Deprem Tehlike Haritası

*Ulusal Deprem Araştırma Programı (UDAP)

*Deprem Mobil Uygulaması

*Risk Yönetim Oluşturma Projesi

*Afet Risk Azaltma Projesi (ARAS)

*Afete Hazır Türkiye Projesi

*Ön Hasar ve Kayıp Tahmin Sistemi

*Afet Sonrası Anlık Görüntü Aktarımı

2.1 2018 Türkiye Deprem Tehlike Haritası ve Türkiye Bina ve Deprem Yönetmeliği

AFAD projeleri arasında, güvenli yapılar ve inşaat mühendisliği adına en önemli uygulama 2018 yılında çıkarılan ve 2019 yılı Ocak ayı itibari ile yürürlüğe konulmuş olan Türkiye Bina ve Deprem Yönetmeliği (TBDY-2018) dir. Bu yönetmelik Türkiye Deprem Tehlike Haritası (TDTH) ile aynı zamanda hazırlanmıştır. TDTH ilk olarak 1947 yılında hazırlanmış, gelişen teknoloji ve bilimsel çalışmalar doğrultusunda farklı tarihlerde 8 kez güncellenmiştir. 2018 yılında yapılan bu son güncelleme daha önceki çalışmaları önemli derecede ileriye taşımıştır. AFAD başkanlığınca hazırlanan 2018 TDTH, Ulusal Deprem Araştırma Programı (UDAP) ve Doğal Afet Sigortaları Kurumu (DASK) tarafından desteklenerek hazırlanmıştır (URL-8). Yapılan çalışmalar sonucu deprem bilgileri interaktif haritaya taşınmıştır. Deprem interaktif bilgilerine https://tdth.afad.gov.tr/ adresinden 7/24 ulaşılabilmektedir (URL-9). Ayrıca, e-

devlet internet sitesi üzerinden istenilen enlem ve boylamdaki (adresteki) deprem tehlike verilerine ulaşılabilmektedir.

Şekil 4. 13 Mart 1992 Erzincan Depremi (URL-12)

Şekil 4, Şekil 5, Şekil 6 ve Şekil 7'de farklı yıllarda Türkiye'nin farklı bölgelerinde meydana gelmiş olan depremler sonrası çekilmiş fotoğraflar görülmektedir. Şekil 4'de, 1992 yılında

meydana gelen Erzincan depreminden bir görüntü bulunmaktadır. İlgili tarihte 1972 yılında hazırlanmış olan TDTH ve 1975 yılında hazırlanmış olan deprem yönetmeliği yürürlükte idi. Şekil 4'den anlaşıldığı kadarı ile iki farklı bina bitişik olarak yapılmıştır. Binalardan birinde sıva dökülmesi ve çatlaklar oluşması gibi hasarlar oluşmakla birlikte ayakta durmakta olduğu, diğerinde ise çökme meydana geldiği görülmektedir. Başka bir deyişle, yan yana olan iki binadan biri ayakta kalırken, bir diğeri çökmüştür.

Şekil 5'de 1999 yılında meydana gelmiş olan Marmara Depremi veya Düzce Depremi olarak anılan deprem sonrası yıkılmış bir bina görülmektedir. İlgili tarihte, 1996 yılında hazırlanmış olan TDTH ve 1998 yılında hazırlanmış olan deprem yönetmeli yürürlükte idi. Fotoğraftan görüldüğü kadarı ile bina sağ tarafa doğru yıkılmış ve sadece yere temas eden kısımda bulunan kolon ve kirişler kırılmıştır. Yere temas etmeyen bölgedeki kolon ve kirişlerin az hasarlı olduğu ve binanın temelinin yerden ayrıldığı görülmektedir.

Şekil 5. 12 Kasım 1999 Düzce Depremi (URL-13)

Şekil 6'da 2020 yılında Elazığ'da meydana gelen depremden bir fotoğraf görülmektedir.Fotoğraftan görüldüğü kadarı ile, etrafta bulunan yapılarda herhangi bir hasar görülmez iken, ortada bulunan iki bina tamamen çökmüştür. Şekil 7'de gine 2020 yılında İzmir'de meydana gelen depremde tamamen çökmüş olan bir bina görülmektedir. İzmir depreminde birinci yazar tarafından yerinde yapılan gözlemlerde, yıkılan bu binanın hemen yanında bulunan binalarda küçük hasarlar görülmüş ama hiç birinin yıkılmadığı belirlenmiştir.

TBDY-2018, en son 2007 yılında hazırlanmış olan "Deprem Bölgelerinde Yapılacak Binalar Hakkında Yönetmelik" (DBYBHY - 2007) yönetmeliğine göre büyük farklılıklar taşımaktadır. İlk olarak 1947 yılında hazırlanmış olan ve 7 kez güncellenen deprem bölgelerindeki binaların yapımı ile ilgili olan yönetmelikte kullanılan kavram ve kabuller 2018 yönetmeliğinde değiştirilmiştir. Örneğin, ilk defa bina yapımında geoteknik özellikler önemli şekilde dikkate alınmıştır. Ayrıca, 2007 yılına kadarki süreçte, deprem bölgeleri tanımlaması bulunmakta iken 2018 yönetmeliğinde

Şekil 6. 24 Ocak 2020 Elazığ Depremi (URL-14)

bu tanım kaldırılmıştır. Böylece, yapı ile ilgili tüm hesaplar, bu hesaplarda kullanılan katsayılar ve ilgili parametreler baştan aşağı değişmek durumunda kalmıştır. TBDY-2018'de deprem bölgesi yerine interaktif olarak kullanılmakta olan TDTH'den alınan veriler üzerine kurgulanmıştır. Başka bir deyiş ile, yapının yapılacağı paftanın verileri girilmek sureti ile, her koordinat için farklı bir katsayı ve parametre alınmaktadır. Böylece, güncel teknoloji ve bilgi birikimleri ile hazırlanmış olan daha güvenilir yapıların tasarlanması mümkün kılınmıştır

(URL-8).

Şekil 7. 30 Ekim 2020 İzmir Depremi (URL-15)

3. SONUÇ

Türkiye, fay hatlarının bulunduğu, deprem ve diğer doğal afetlerin yaşanma olasılığının yüksek olduğu bir coğrafyada konumlanmaktadır. Bu sebeple, her yıl küçüklü büyüklü çok fazla afet yaşanmaktadır. Bu çalışmada, Türkiye'de yaşanan deprem olayları, depremler konusunda ülkemizde bulunan kurum, kuruluş ve organizasyonlara yer verilmiş ve süreçler üzerinde durulmuştur. Yapılan araştırmada, Türkiye depremle ilgili gerek kamusal gerek örgütsel ve sosyal çalışmalar yapma konusunda oldukça yavaş ilerlediği ve bunun bedelini yüksek sayılardaki can kaybı ve yüksek miktarlardaki maddi hasar olarak ödediği görülmüştür. Ancak, 2018 yılında, AFAD tarafından hazırlanan deprem tehlike haritası ve bina deprem yönetmeliği, konu ile ilgili çok olumlu ve büyük adımların atılmasına vesile olmuştur. TBDY-2018 incelendiğinde, teknolojideki gelişmeler ve daha önceki depremlerin, yapılardaki hasarların incelenmesi sonucu elde edilen bilgilerin kullanıldığı ve uzman mühendisler tarafından hazırlanmış olduğu anlaşılmaktadır. Yönetmelik, getirdiği yeni kriterler ile ve özellikle geoteknik konusunda yaptığı değişiklikler ile bina yapımı konusunda çok olumlu adımlar atılmasına aracı olmuştur. Yönetmeliğin kullanılmasında TDTH' nın doğrudan kullanıma alınması bu önemli adımlardan bir tanesidir. İşin doğası gereği, ilerleyen yıllarda, biriken yeni veriler ışığında, konusunda uzman yer bilimciler ve inşaat mühendisleri tarafından bu yönetmeliğin de güncellenmesi daha güvenli yapıların yapılmasına katkı sunacaktır.

KAYNAKÇA

1. URL-1. What Is an Earthquake? NASA Science Space Place. Explore Space and Earth. https://spaceplace.nasa.gov/earthquakes/en/ Ziyaret Tarihi: 18.02.2022
2. Meng, J., Sinoplu, O., Zhou, Z., Tokay, B., Kusky, T., Bozkurt, E., & Wang, L. (2021). Greece and Turkey Shaken by African tectonic retreat. Scientific Reports, 11(1), 1-10.
3. URL-2. AFAD Deprem Tehlike Haritası. https://deprem.afad.gov.tr/deprem-tehlike-haritasi Ziyaret Tarihi: 18.02.2022
4. AFAD. (2021). 2020 Yılı Doğa Kaynaklı Olay İstatistikleri. https://www.afad.gov.tr/kurumlar/afad.gov.tr/e_Kutuphane/Istatistikler/2020yilidogakaynakliolayistatistikleri.pdf Ziyaret Tarihi: 18.02.2022
5. URL-3. Türkiye'nin İlk Gönüllü Arama Kurtarma Derneği. https://www.akut.org.tr/tarihce Ziyaret Tarihi: 18.02.2022
6. Günaydın M. Tatlı Ö. ve Genç E. E. (2017), Arama Kurtarma Örgütleri ve Ulusal Medikal Kurtarma Ekipleri (UMKE), Doğal Afetler ve Çevre Dergisi, Cilt: 3, Sayı 1: 58-60
7. URL-4. AFAD Tarihçe. https://www.afad.gov.tr/afad-hakkinda Ziyaret Tarihi: 18.02.2022
8. URL-5. Türk Silahlı Kuvvetleri Doğal Afetler Arama Kurtarma Tabur Komutanlığı https:// www.tsk.tr/Sayfalar?viewName=DogalAfetAramaKurtarmaTimleri Ziyaret Tarihi: 18.02.2022

9. URL-6. Jandarma Arama Kurtarma Timi. https://erzurum.jandarma.gov.tr/jandarma-arama-kurtarma-timi-jak Ziyaret Tarihi: 18.02.2022
10. URL-7. Afetlerle İlgilenen Ulusal Kuruluşlar https://cdn-acikogretim.istanbul.edu.tr/auzefcontent/20_21_Bahar/sivil_savunma_ve_afet_kuruluslari/12/index.html Ziyaret Tarihi: 18.02.2022
11. URL-8. AFAD Projeleri. https://www.afad.gov.tr/projelerimiz Ziyaret Tarihi: 18.02.2022
12. URL-9. Türkiye Bina Deprem Yönetmeliği. T.C. İçişleri Bakanlığı Afet ve Acil Durum Yönetimi Başkanlığı (AFAD). https://www.afad.gov.tr/turkiye-bina-deprem-yonetmeligi# Ziyaret Tarihi: 18.02.2022
13. URL-10. İnteraktif Deprem Haritası. https://tdth.afad.gov.tr/ Ziyaret Tarihi: 18.02.2022
14. URL-11 < https://deprem.afad.gov.tr/galeri/236369 > Ziyaret Tarihi: 18.02.2022
15. URL-12 1992 Erzincan Depremi https://deprem.afad.gov.tr/galeri/236369 Ziyaret Tarihi: 18.02.2022
16. URL-13 1999 Düzce Depremi https://deprem.afad.gov.tr/galeri/246572 > Ziyaret Tarihi: 18.02.2022
17. URL-14 Elazığ Depremi https://www.haberturk.com/son-dakika-elazig-depremi-afad-dan-cok-onemli-aciklamalar-2562660 Ziyaret Tarihi: 18.02.2022
18. URL-15 2020 İzmir Depremi https://www.takvim.com.tr/guncel/2020/10/31/izmir-deprem-olu-yarali-sayisi-afad-son-dakika-izmir-deprem-olu-yarali-kurtulan-sayisi-kac/3 > Ziyaret Tarihi: 18.02.2022

TÜRKİYE SEL FELAKETLERİ: GİRESUN ÖRNEĞİ

MURAT DUYSAK[1], Dr. Öğr. Üyesi GAMZE BİLGEN[2],

[1]Zonguldak Bülent Ecevit Üniversitesi, ORCID ID: https://orcid.org/0000-0001-9315-9448

[2]Zonguldak Bülent Ecevit Üniversitesi, ORCID ID: https://orcid.org/0000-0002-2840-7369

ÖZET

Yapılan çalışmada, sel ve taşkın kavramları, Doğu Karadeniz Bölgesindeki sel oluşum nedenleri, bu bölgede 22 Ağustos 2020 tarihinde Giresun'da meydana gelen sel felaketi örneği ile tartışılmıştır. Çalışmada, afet sonrasında yapılan incelemeler, hasar tespiti ve alınabilecek önlem çalışmaları ele alınmıştır. Sel, yüksek miktarda yağış sonrası yeryüzünde biriken yüzey sularının, akarsu yataklarını doldurması ve taşarak kuru bölgeleri de kaplaması olayıdır. Taşkın, bir bölgede bulunan akarsuyun yağmur ve kar suyu etkisiyle yıllık ortalama seviyesinin üzerine çıkarak yatağından taşması sonucunda oluşan su baskınlarıdır. Doğu Karadeniz Bölgesi'nde yer alan Giresun ilinin eğimli bir arazi yapısına sahip olması, aşınabilir zemin özellikleri, yıllık yağış miktarının yüksek olması, çok sayıda akarsuyun bulunmasından dolayı sel felaketine sıklıkla maruz kalabilmektedir. Bölgedeki en önemli iki akarsu Aksu Çayı ve Batlama deresidir. İlgili tarihteki yüksek miktarda yağış sonrası oluşan sel felaketinden en çok; Dereli, Yağlıdere ve Doğankent ilçeleri etkilenmiştir. Yörede meydana gelen sel felaketi, köprülere, binalara, işyerlerine, yollara zarar vermiş, ulaşımda aksamalara meydana olmuş, can ve mal kayıpları yaşanmıştır. Yerleşim yerlerinin akarsu yataklarına yakın olması, akarsu yataklarının daraltılması, bölgenin coğrafi yapısı başka bir deyişle arazi yapısının eğimli olmasından dolayı sel felaketi etkisini arttırmıştır. Sel olayında en önemli etmenlerden biri de yöredeki zemin yapısıdır. Bölgede bulunan zeminin kısa sürede doygunluk seviyesine ulaşmasının, sel oluşumu üzerindeki etkisi büyük olmuştur. Sel felaketi sonrası, bölgeye birçok ekip sevk edilmiş, kriz merkezi kurularak, kurtarma ve hasar tespit çalışmaları yapılmıştır. Yörede yapılan incelemeler sonrasında, akarsu yataklarındaki taşkın olabilecek noktalara set yapılması, yolların selden tekrar etkilenmemesi için istinat duvarlarının tahkim edilmesi, akarsuların ıslah edilmesi önlemler arasında sayılabilir.

Anahtar Kelimeler: Afet, sel, taşkın, Giresun

ABSTRACT

In the study, the concepts of flood and deluge, the causes of flooding in the Eastern Black Sea Region, were discussed with the example of the flood disaster that occurred in Giresun on

August 22, 2020, in this region. In the study, post-disaster investigations, damage assessment and preventive measures are discussed. Flood is the event that the surface waters accumulating on the earth after a high amount of precipitation fill the riverbeds and overflow and cover the dry regions. Deluge is the floods that occur as a result of the overflow of the river in a region above the annual average level due to the effect of rain and snow water. Giresun province, located in the Eastern Black Sea Region, can be frequently exposed to flood disasters due to its sloping land structure, eroded soil characteristics, high annual precipitation, and the presence of many streams. The two most important streams in the region are Aksu Stream and Batlama Stream. Of the flood disaster that occurred after the high amount of precipitation in the relevant date; Dereli, Yaglidere and Doğankent districts were affected. Due to the flood disaster in the region, bridges, buildings, workplaces, roads were damaged, transportation was disrupted, and life and property were lost. The fact that the settlements are close to the riverbeds, the narrowing of the riverbeds, the geographical structure of the region, in other words, the slope of the land structure increased the flood disaster effect. One of the most crucial factors in the flood event is the soil structure in the region. The effect of the soil in the region reaching the saturation level in a short time has been great on the flood formation. After the flood disaster, many teams were sent to the region, a crisis centre was established, and rescue and damage assessment studies were carried out. After the examinations made in the region, some measures can be taken to construct barriers at the points that may overflow in the riverbeds, to fortify the retaining walls to prevent the roads from being affected by the flood again, and to rehabilitate the rivers.

Keywords: Disaster, flood, deluge, Giresun

1. GİRİŞ

Sel, bir bölgede yağmur ve kar suyu gibi yüzey sularının akarsu yataklarını doldurması ve akarsuların yatağından taşarak kuru yüzeyleri kaplaması olayıdır. Seller, bünyesindeki suyun hızına göre yavaş , hızlı ve ani seller olmak üzere üçe ayrılmaktadır. Birkaç hafta gibi uzun bir süre zarfında oluşan sellere yavaş sel rejimi, birkaç gün içerisinde oluşan sellere hızlı sel rejimi, bir saat gibi kısa sürede meydana gelen sellere ani sel rejimi denir. Olumları bakımından; kıyı seli, nehir seli, şehir seli, baraj seli, gölet seli gibi selleri gruplandırmak mümkündür. Taşkın, bir bölgedeki akarsuyun çeşitli nedenlerle su kütlesindeki miktarının arttığı ve su seviyesinin yıllık ortalama seviyesinin çok üzerine çıktığı durumlardır. Taşkın sonucunda tarım arazileri, yerleşim yerleri ve altyapı sistemleri etkilenmektedir (URL-1).

Bu çalışma kapsamında, Doğu Karadeniz bölgesinde bulunan Giresun ilinde 22 Ağustos 2020 tarihinde meydana gelen sel felaketi örneği üzerinden, yağışlar sonucunda meydana gelen sel-su taşkınlarının oluşum nedenleri, meydana getirdiği hasarlar tartışılmış ve sel-su taşkınlarına karşı alınması gereken önlemler sunulmuştur.

1. ARAŞTIRMA VE BULGULAR

Giresun, Doğu Karadeniz Bölümünde, iki tarafında koyların bulunduğu, denize doğru çıkıntı oluşturan bir yarımada biçimindedir. Doğu Karadeniz Bölgesi ülkemizin en fazla yağış alan yerlerindendir. Şehir, yağış miktarının fazla olmasından dolayı sıklıkla oluşan; sel, taşkın ve heyelan gibi afetlere maruz kalmaktadır. Ayrıca, doğusunda bulunan Aksu Çayı ve Batıda Batlama Deresi, yağış rejiminin fazla olduğu dönemlerde sel felaketi ve taşkınlara sebep olmaktadır. Şekil 1'de Aksu Çayı ve Batlama Deresinin konumu görülmektedir (Avcı ve Sunkar 2015).

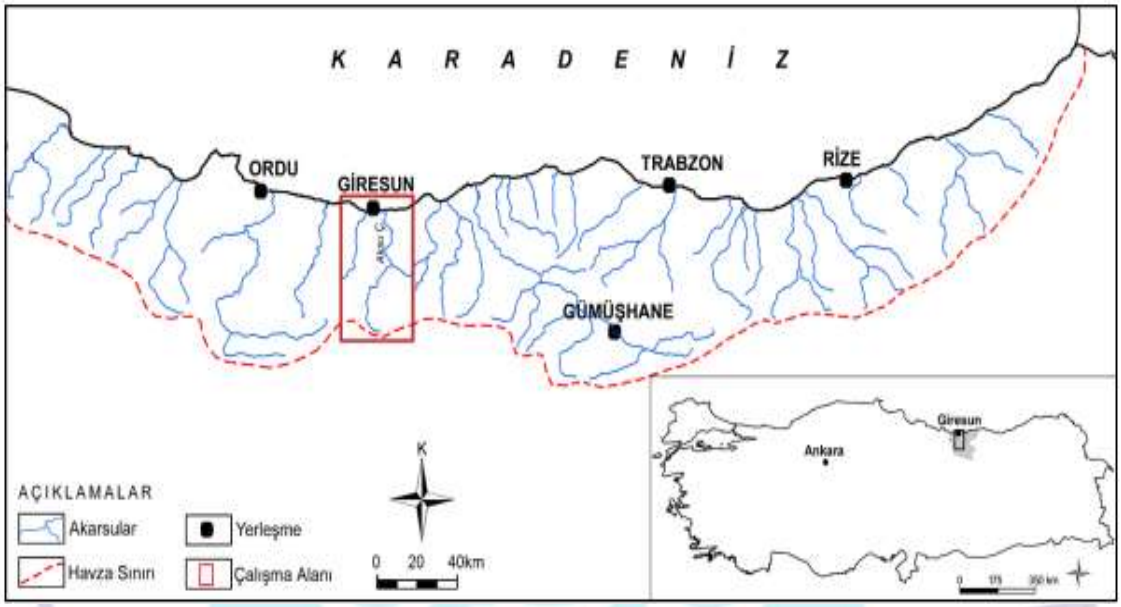

Şekil 2. Aksu Çayı ve Batlama Deresinin Lokasyon Haritası (Avcı ve Sunkar 2015).

Giresun'da 1991-2021 yılları arasında can ve mal kaybına neden olan on tane taşkın meydana gelmiştir. Bu veri, Giresun'da ortalama olarak her üç yılda bir taşkın olayı meydana geldiğini göstermektedir. Yörede meydana gelen su baskınları ve taşkınlar sonucu can kayıplarına, binaların, köprülerin, yolların ve altyapı sistemlerinin ciddi boyutta hasar görmesine sebep olmaktadır. Nitekim, bölgede 22 Ağustos 2020 tarihinde yıllık ortalamanın üzerinde şiddetli yağış gerçekleşmiş ve Dereli, Yağlıdere ve Doğankent ilçelerinde taşkınlar oluşmuştur. Bu yerleşim yerleri taşkın tehlikesi yönüyle benzerlik gösteren akarsu vadileri (Aksu Çayı, Yağlı Dere ve Harşıt Çayı) içinde bulunmaktadırlar. Çevre ve Şehircilik Bakanlığının (CSB) yaptığı açıklamada taşkından dolayı Dereli ilçesinde 3 askeri personel olmak üzere 16 vatandaşımız hayatını kaybetmiştir. Bölgedeki aşırı yağışlar sonucunda, birkaç saat içerisinde, bazı binalara zarar veren, düşük kot seviyesinde bulunan dükkanları, depoları moloz ve çamur yığını ile dolduran, caddeleri kullanılamaz hale getiren bir taşkın afeti olmuştur. (Apaydın 2021).

Giresun'da 12 saat boyunca yağan yağmur ve taşan derelerin tomruk, çamur ve taş parçalarını taşıması selin etkisini arttırmıştır. Yağışlar bu 12 saatlik zaman zarfında kademeli bir şekilde artarak dere yatağı ve çevresindeki zemin doygun hale gelmiştir. 22 Ağustos akşam saatlerinde metrekare başına 35-45 mm'lik yağış dere yataklarında hızlı bir şekilde akışa neden olarak 118 köy yolunun ulaşıma kapanmasına, çevredeki tarım arazilerinin ve fındık bahçelerinin zarar görmesine sebep olmuştur. Ek olarak, taşkından ötürü, 17 bina yıkılmış, 361 bina hasar görmüştür. Ayrıca Aksu ve Yağlı derelerinin, çeşitli noktalardan taşması sonucunda ilçelere ve Giresun-Sivas karayoluna ulaşıma kapatmıştır. (Kömüşçü vd. 2021).

Şekil 2. 22 Ağustos 2020 Giresun/Dereli Sel Felaketi (URL-2)

Şekil 3. 22 Ağustos 2020 Giresun/Dereli Sel Felaketi (URL-3)

Şekil 2' ve Şekil 3'te Giresun'da taşkın sonrası çekilmiş bir fotoğraf bulunmaktadır. Fotoğraflarda, akarsu yatağı kenarına yapılan binaların ve yolların hasar aldığı, sel sularının geçtiği yerlere verdiği zararlar görülmektedir. Şekil 4'te Giresun'daki Dereli ilçesinde meydana gelen selde dere yatağına yakın yapılan binaların zarar gördüğü, çeşitli araçların sel sularından etkilendiği, bazı noktalarda ise zeminlerde kaymalar meydana geldiği görülmektedir.

Şekil 4. 22 Ağustos 2020 Giresun/Dereli Sel Felaketi (URL-4)

Şekil 5. 22 Ağustos 2020 Giresun/Dereli Sel Felaketi (URL-5)

Şekil 5'te sunulan fotoğrafta, yerleşim yerinin sel felaketinden aldığı hasarın boyutu görülmektedir. Sel sularının yol seviyesindeki işyerlerini, bodrum ve zemin katlarını, yolları

moloz ve çamur ile doldurduğu açıkça görülebilmektedir. Araçlar, sel suları arasında sürüklenip savrulmuş yollar, kaldırımlar ve çevre düzenleme çalışmaları yer ile yeksan olmuştur. Şekil 6'da taşkın sularından etkilenen ve yıkılan bir yapı görülmektedir.

Şekil 6. 22 Ağustos 2020 Giresun/Dereli Sel Felaketi (URL-6)

SONUÇ

22 Ağustos 2020 tarihinde meydana gelen sel sonrasında CSB verilerine göre ;Giresun'daki sel felaketinde, Doğankent'te 4 tane yıkık, 200 az hasarlı bina, Dereli'de 3 adet yıkık bina,152 az hasarlı bina ve Yağlıdere'de 10 yıkık, 9 az hasarlı bina tespit edilmiştir (URL-7). Sel sonucu bölgede, toplamda 361 binanın az hasar gördüğü, 17 binanın ise yıkılmış olduğu açıklanmıştır. Sel felaketinin yaşandığı bölgede birçok işyeri, dükkan, depo, apartman dairesi vb kullanılamaz hale geldiği bildirilmiştir. Sel sonrasında yapılan çalışmalarda, 86 köy yolunda 172 adet istinat duvarı ve 32 adet kutu menfez imalatı, 143 konut için 121 önleyici istinat duvarı, 12 adet köprü yapımı ve TOKİ tarafından 369 konut yapımı, 152 adet dükkan yapımına başlanmıştır. Hasar gören 2120 km'lik karayolunun, 826 km'si kullanılır hale getirilmiştir (URL-8)

Karadeniz Bölgesinde, engebeli arazi yapısı, arazinin eğimli olması, akarsu yataklarının sayısının fazla olması ve toprak örtüsünün kolay aşınabilmesi nedeniyle sel felaketinin meydana gelmesindeki etmenlerdir. Yörede meydana gelebilecek sel ve su taşkınlarına karşı çeşitli önlemler alınarak etkileri en aza indirilebilir. Şehir merkezlerinden geçen dere, kanal vb yapıların temizliği düzenli yapılmalı ve buraların üstü kapatılmamalıdır. Menfez ve kanalların genişlikleri, maksimum yağış dolayısı ile oluşan yüzey sularını sorunsuz tahliye edecek ölçülerde inşa edilmelidir. Köy yollarının yapım çalışmalarında, şev açıları çok dik yapılmamalıdır. Su toplama kapasitesi yüksek olan akarsuların çeşitli noktalarına erken uyarı

sistemleri kurulabilir. Yol Yapım çalışmalarında eğimli arazilerde istinat duvarları yapılmalı ve bu duvar arkasındaki zemin içerisinde bulunan suların tahliyesi için borular konulmalıdır. Yollarda bulunan şev açılarına dikkat edilmeli menfezlerin temizliği yapılmalıdır. Akarsu yataklarının sel ve taşkın oluşturabilecek bölgelerine setler yapılmalıdır. Akarsu yatakları daraltılarak bu alanlara yol ve binalar yapılmamalıdır. Su basman kotu yüksek yapılmalı, yapı ve imar denetimleri arttırılmalıdır. Taşkın ve sel riski olan alanlar yerleşime açılmamalıdır.

KAYNAKÇA

1. URL-1. Sel Öncesi ve Sonrası Tedbirli Olun, Güvende Kalın. https://www.afad.gov.tr/sel-oncesi-ani-ve-sonrasi-tedbirli-olun-guvende-kalin Ziyaret Tarihi: 23.02.2022

2. Avcı V. ve Sunkar M. (2015), Giresun'da Sel Ve Taşkın Oluşumuna Neden Olan Aksu Çayı Ve Batlama Deresi Havzalarının Morfometrik Analizleri, İstanbul Üniversitesi Coğrafya Dergisi, Basılı Nüsha ISSN No: 1302-7212, Sayı 30: 92-93

3. Apaydın A. (2021). 22 Ağustos 2020 Tarihli Taşkına Neden Olan Dereli Deresi (Giresun) Havza Analizleri, Taşkının Nedenleri ve Sonuçları, Karadeniz Fen Bilimleri Dergisi, Cilt 11, Sayı 2: 393-395

4. Kömüşçü A.Ü., Aksoy M., Çelik S., Ciba Ö.F., Uğurlu A., Turgu E., Ünal E. (2021). 22 Ağustos 2020 Tarihinde Giresun ve İlçelerinde Meydana Gelen Yağış ve Sel Olayının Meteorolojik ve Hidrometeorolojik Analizi, Su Kaynakları Dergisi 6. (1), 1-12

4. URL-2. 22 Ağustos 2020 Giresun/Dereli Sel Felaketi, https://www.hurriyet.com.tr/gundem/dereli-felaketi-41593901 Ziyaret Tarihi: 23.02.2022

5. URL-3. 22 Ağustos 2020 Giresun/Dereli Sel Felaketi https://tr.euronews.com/2020/08/23/giresun-da-sel-felaketi-en-az-3-kisi-hayat-n-kaybetti-arama-kurtarma-cal-smalar-suruyor Ziyaret Tarihi: 23.02.2022

6. URL-4. 22 Ağustos 2020 Giresun/Dereli Sel Felaketi https://www.dw.com/tr/giresunda-sel-felaketi/a-54664018 Ziyaret Tarihi: 23.02.2022

7. URL-5. 22 Ağustos 2020 Giresun/Dereli Sel Felaketi https://www.egehaber.com/giresundaki-sel-felaketinden-kahreden-haber-geldi-345883/ Ziyaret Tarihi: 23.02.2022

8. URL-6. 22 Ağustos 2020 Giresun/Dereli Sel Felaketi https://www.ensonhaber.com/ic-haber/giresunda-sel-felaketinin-fotograflari Ziyaret Tarihi: 23.02.2022

9, URL-7 Çevre ve Şehircilik Bakanlığının Yapılan Açıklama https://csb.gov.tr/bakan-kurum-sel-felaketinin-yasandigi-giresun-da-incelemelerde-bulundu-bakanlik-faaliyetleri-29811 Ziyaret Tarihi: 23.02.2022

11. URL-8. Giresun Afet ve Acil Durum Müdürlüğü Kriz Merkezinde Yapılan Toplantı ve Hasar Tespit Çalışmaları, http://giresun.gov.tr/giresun-afet-ve-acil-durum-yonetim-merkezinde-degerlendirme-toplantisi-yapildi Ziyaret Tarihi: 23.02.2022

BUDAK (TORUL / GÜMÜŞHANE) VE ÇEVRESİNDEKİ GEÇ KRETASE YAŞLI VOLKANİK KAYAÇLARIN PETROGRAFİK VE JEOKİMYASAL ÖZELLİKLERİ

Prof.Dr. Abdullah KAYGUSUZ [1], Doç.Dr. Alaaddin VURAL [2]

[1] Gümüşhane Üniversitesi, orcid id: 0000-0002-6277-6969

[2] Gümüşhane Üniversitesi, orcid id: 0000-0002-0446-828X

ÖZET

Doğu Pontidlerin Kuzey Zonunda Budak (Torul / Gümüşhane) ve çevresinde yüzeylenen Geç Kretase yaşlı asidik volkanik kayaçlar mineralojik, petrografik ve jeokimyasal olarak incelenmiştir. Budak volkanitleri dasit ve riyolit bileşiminde olup, başlıca plajiyoklas, kuvars, alkali feldispat, amfibol, biyotit ve opak minerallerinden oluşurlar. Volkanitler kalk-alkali karakterli olup, yüksek-K içeriğine sahiptirler. Büyük iyon yarıçaplı litofil elementler ve hafif nadir toprak elementlerce zenginleşmiş, yüksek çekim alanlı elementler bakımından tüketilmişlerdir. Kondrite normalize edilmiş nadir toprak element dağılımları, düşük-orta derecede zenginleşmeyle konkav şekilli olup, volkanitleri oluşturan kayaçların benzer kaynaktan itibaren oluştuklarını gösterirler. Ana oksit ve iz element değişimleri, volkanitlerin gelişiminde başlıca fraksiyonel kristallenmenin rol oynadığını gösterir. Düşük Nb/U ile yüksek La/Nb ve Th/Nb oranları, kayaçların kıtasal kabuk kirlenmesinden de etkilendiğini belirtmektedir. Sonuç olarak, incelenen volkanik kayaçların yay ortamında, yitim ilişkili metasomatize olmuş bir litosferik manto kaynağından türemiş oldukları düşünülmektedir.

Anahtar Kelimeler : Doğu Pontidler, Geç Kretase, Petrografi, Jeokimya, Volkanik kayaçlar, Torul (Gümüşhane).

PETROGRAPHICAL AND GEOCHEMICAL FEATURES OF LATE CRETACEOUS AGED VOLCANIC ROCKS IN THE BUDAK (TORUL / GÜMÜŞHANE) AND SURROUNDING AREA

ABSTRACT

Late Cretaceous aged volcanic rocks of the Budak (Torul/Gümüşhane) and surrounding area in the northern part of the Eastern Pontides are investigated as mineralogical, petrographical and geochemical. Budak volcanic rocks are dacite and rhyolite in composition. The volcanic rocks consists of mainly plagioclase, quartz, alkali feldspar, amphibole, biotite and opaque minerals. They show calc-alkaline affinities and have high-K contents. They are enriched in large ion lithophile and light rare earth elements, with pronounced depleted of high field strength

elements. The chondrite-normalized REE patterns show low to medium enrichment, indicating similar sources for the rock suite. Major oxide and trace element changes indicate that fractional crystallization plays a major role in the development of volcanic rocks. Low Nb/U and high La/Nb and Th/Nb ratios indicate that tha rocks are affected by continental crust contamination. As a result, it is thought that the studied volcanic rocks are derived from a metasomatized lithospheric mantle source related to subduction in the arc setting.

Keywords: Eastern Pontides, Late Cretaceous, Petrography, Geochemistry, Volcanic rocks, Torul (Gümüşhane)

1. GİRİŞ

Alpin-Himalaya orojenik kuşağında yer alan Doğu Pontidler (KD Türkiye), volkanik ve plütonik kayaçların yaygın olarak gözlendiği önemli alanlardan biridir. Doğu Pontid'lerde, Liyas, Kretase ve Erken Eosen (ve sonrasında) olmak üzere üç ana volkanik devre ayırt edilmiştir [1,2].

Doğu Pontidlerde Geç Kretase yaşlı plütonik kayaçların tüm-kayaç jeokimyası, izotop jeokimyası ve jeokronolojileri üzerine yapılmış pek çok çalışma [3–15] olmasına rağmen, volkanik eşdeğerleri ile ilgili yapılmış çalışmalar sınırlıdır [16–21].

Bu çalışmada Budak (Torul/Gümüşhane) ve civarındaki Geç Kretase yaşlı volkanik kayaçların petrografik ve jeokimyasal özellikleri ortaya konularak, Doğu Pontid Geç Kretase magmatizmasının gelişimine açıklık getirilmeye çalışılmıştır.

2. BÖLGESEL JEOLOJİ VE STRATİGRAFİ

Doğu Pontidlerde Geç Kretase önsesi birimler başlıca Geç Karbonifer yaşlı plütonik kayaçlar ile Geç Karbonifer-Erken Permiyen yaşlı metasedimanter kayaçlar [22–28], Erken-Orta Jura yaşlı volkano-tortul kayaçlar [29–31], Erken-Geç Jura yaşlı intrüzif kayaçlar [32–34] ve Geç Jura-Erken Kretase yaşlı karbonatlı kayaçlardan [35] oluşur.

Geç Kretase yaşlı plütonik ve volkanik kayaçlar Kuzey Zonda baskın litolojiyi teşkil ederken [7,10,15,18,19,21,26,31,36–43], güney zonda tortul kayaçlar egemendir.

Bölgede Geç Kretase sonrası birimler ise başlıca Geç Paleosen-Erken Eosen yaşlı adakitik kayaçlar [44], Orta Eosen yaşlı volkanik-subvolkanik kayaçlar [42,45–54], Orta Eosen yaşlı plutonik kayaçlar [40,43,55–62], Neojen yaşlı volkanik kayaçlar [61,63], Geç Miosen ve Pliyo–Kuvaterner yaşlı adakitik volcanik-subvolkanik kayaçlardan [52,64] oluşurlar. Bölgenin en yaşlı kayaçlarını Kuvaterner yaşlı traverten ve alüvyonlar oluşturur.

Doğu Pontid Tektonik Birliği Kuzey Zonu'nda yer alan ve genelde volkanik ve plutonik kayaçların egemen olduğu çalışma alanında, en yaşlı kayaçları Geç Kretase yaşlı killi-kumlu kireçtaşı ve kırmızı kireçtaşı ara katkılı bazalt, andezit ve piroklastları oluşturur. Bu birim üzerine killi kireçtaşı, kumlu kireçtaşı ve kırmızı kireçtaşı ara katkılı dasit, riyolit ve piroklastları gelir. Bu birimleri kireçtaşı, kumtaşı ve kırmızı kireçtaşı ara katkılı andezit ve piroklastleri üstlerler. Sarıosman plutonu tüm bu birimleri kesmiştir (Görsel 1).

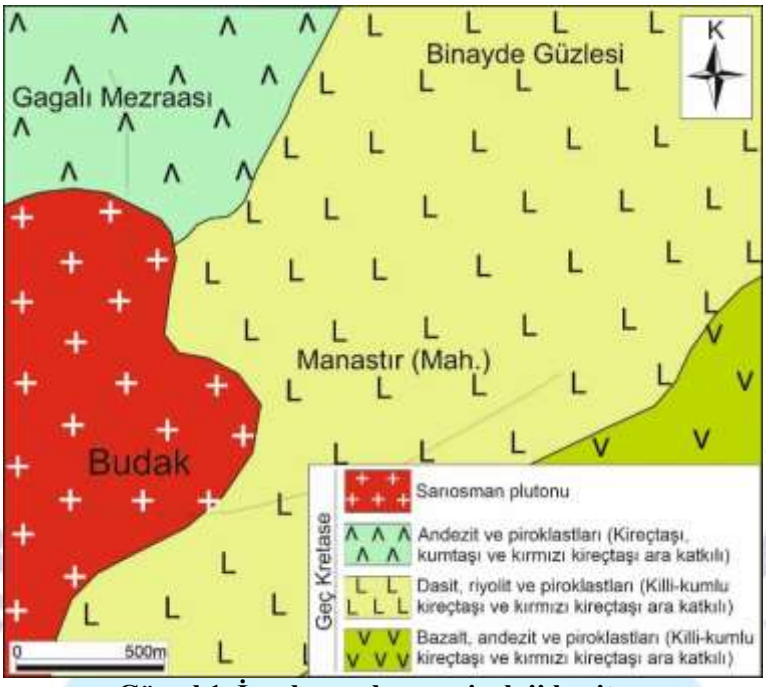

Görsel 1. İnceleme alanının jeoloji haritası

3. ANALİTİK YÖNTEMLERİ

Bu çalışmada, araziden derlenen kayaç örneklerinin ince kesitleri hazırlanmış ve polarizan mikroskopta ayrıntılı petrografik özellikleri belirlenmiştir. İnceleme alanına ait 6 adet kayaç örneğin ana, iz ve nadir toprak element analizleri Kanada'da Vancouver, BC Analiz (ACME) Laboratuvarı'nda yapılmıştır. Ana ve iz elementler ICP (Inductively Coupled Plasma) yöntemiyle, nadir toprak elementler (NTE) ise ICP-MS (Inductively Coupled Plasma–Mass Spectrometry) yöntemiyle ile analiz edilmiştir. Ana ve iz element analizleri için 0.2 gr toz örnek 1.5 gr $LiBO_2$ ile karıştırılarak, % 5 HNO_3 içeren bir sıvı içinde çözündürülmesinden itibaren analiz edilirken, nadir toprak element analizleri için 0.250 gr toz örnek dört farklı asit içinde çözündürülmüş ve analiz edilmiştir.

4. MİNERALOJİ VE PETROGRAFİ

Budak volkanitlerine ait dasit ve riyolitlerin dokusal özellikleri ile mineralojik-petrografik bileşimleri incelenmiştir. Dasitler ve riyolitler mikroskobik incelemelerde porfirik, mikrogrönü porfirik ve kısmende sferolitik doku gösterirler (Görsel 2).

Plajiyoklaslar iri levhamsı kristaller, hamurda da küçük kristaller halindedir. İri kristaller öz ve yarı öz şekilli olup, bazılarında zonlu yapı görülür. Bazı kristallerde albit, bazılarında da polisentetik ikizlenme belirgindir. Plajiyoklaslar andezin-oligoklas (An_{26-36}) bileşimindedirler. En yaygın bozuşma ürünlerini kalsit ve serizit oluşturur. Kuvarslar öz ve yarı öz şekilli iri kristaller, hamurda da küçük taneler halinde bulunur. İri kristallerin kenarları hamur tarafından yenmiş olarak bulunur. Bazı minerallerde dalgalı sönme belirgindir ve genellikle çatlaklı yapıdadır. Alkali feldispatlar iri levhamsı prizmatik kristaller, hamurda da küçük kristaller halindedir. İri kristaller öz ve yarı öz şekilli olup, karlsbad ikizi belirgindir. Genelde ayrışmış

olup killeşmiştir. Biyotitler öz ve yarı öz şekilli iri levhamsı kristaller, hamurda da küçük taneler halinde görülür. İri kristaller genellikle dilinimleri boyunca ve kenarlardan itibaren kloritleşme gösterir. Bazı mineraller bükülmüş lameller halindedir. X istikametindeki pleokroizma kırmızımsı kahverengi, y istikametindeki pleokroizma sarımsı kahverengi'dır. (100) dilinimleri belirgin ve bu dilinimlerine göre paralel sönme gösterir. Hornblendler hem iri hem de küçük kristaller halinde ve kesitlerde az oranda görülür. Pleokroizma renkleri kahverengimsi yeşil ve açık sarı yeşildir. (010) yüzeyine paralel kesitlerde maksimum sönme açıları yaklaşık 14-15 derecedir. Genelde kalsite ayrışmış ve kenar kısımlarda opak mineraller gelişmiştir. Opak mineraller hem ayrışma ürünü olarak hem de hamurda küçük ve iri taneler halinde dağınık olarak bulunurlar. İkincil mineraller kalsit, klorit, epidot, serizit ve kil minerallerinden oluşurlar. Hamur, yukarıdaki minerallerinin mikro ve kripto kristallerinden ve opak mineral tanelerinden oluşur (Görsel 2).

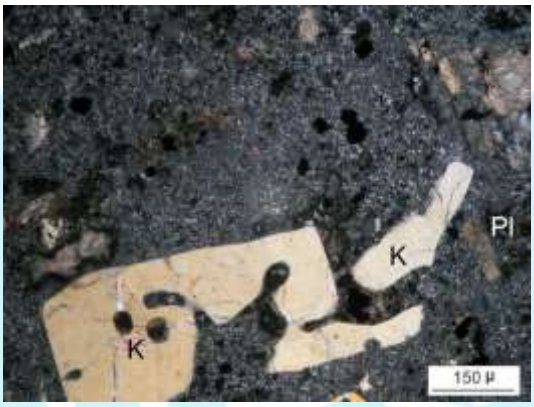

Görsel 2. Budak volkanitlerine ait korrode olmuş kuvars mineralleri (Ç.N., Pl: Plajiyoklas, K: Kuvars)

5. TÜM-KAYAÇ JEOKİMYASI

5.1. Ana ve İz Elementler

SiO_2'ye karşı (Na_2O+K_2O) diyagramında [65] Budak volkanitlerinin subalkalen karakterli bazaltik dasit ve riyolitbileşimli kayaçlardan oluştuğu görülür (Görsel 3a). Winchester ve Floyd [66]'un Nb/Y'ye karşı $Zr/TiO_2*0.0001$ kimyasal adlandırma diyagramında volkanik kayaçlar dasit/riyolit bileşimli kayaçlardan oluşur (Görsel 3b).

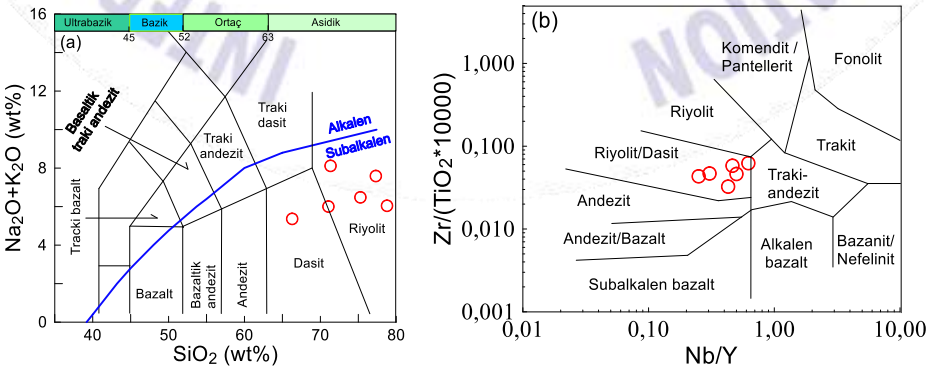

Görsel 3. Budak volkanitlerine ait örneklerin a) SiO_2'e karşı toplam alkali (Na_2O+K_2O) diyagramı [65] **(Alkali/Subalkali ayrımı eğrisi Irvine ve Baragar,** [67]**'den alınmıştır), b) Nb/Y'e karşı Zr/TiO_2 sınıflama diyagramı** [66]

Kayaç örnekleri K_2O-SiO_2 diyagramına [65,68] düşürüldüğünde, örneklerin yüksek-potasyum içeriğine sahip olduğu görülür (Görsel 4a). AFM diyagramında örneklerin tümü kalk-alkalen karakterlidir (Görsel 4b).

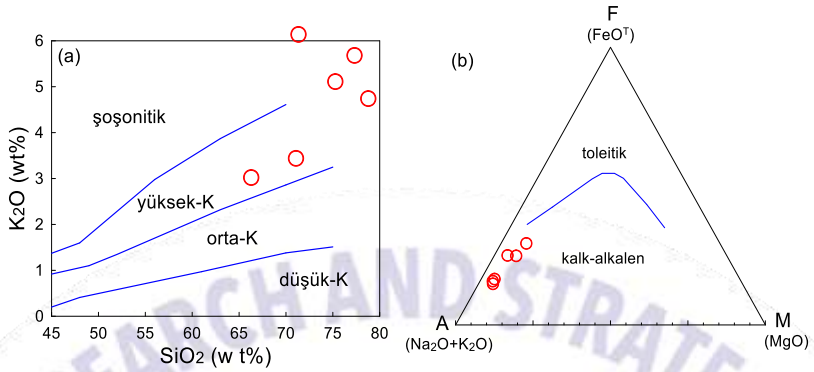

Görsel 4. Budak volkanitlerine ait örneklerin, a) SiO_2 - (Na_2O+K_2O) sınıflama [69] **diyagramı, b) AFM diyagramı (Toleyitik-kalk alkali ayrımı eğrisi Irvine ve Baragar,** [67]**'den alınmıştır)**

SiO_2'ye karşı ana element değişim diyagramlarının (Görsel 5) bir kısmında düzensiz dağılımlar gözlenmekle birlikte, yer yer iyi korelasyonlar vermeleri, Geç Kretase yaşlı volkanitlerin gelişiminde fraksiyonel kristallenmenin oldukça önemli bir rol oynadığına işaret etmektedir. SiO_2'ye karşı ana element değişim diyagramlarında; SiO_2 değerleri arttıkça Na_2O, CaO, MgO, Al_2O_3, $Fe_2O_3^T$, TiO_2 ve P_2O_5 azalarak iyi derecede negatif bir ilişki gösterirler (Görsel 5). K_2O değerlerinde ise SiO_2 artışına paralel olarak pozitif bir korelasyon gözlenir (Görsel 5).

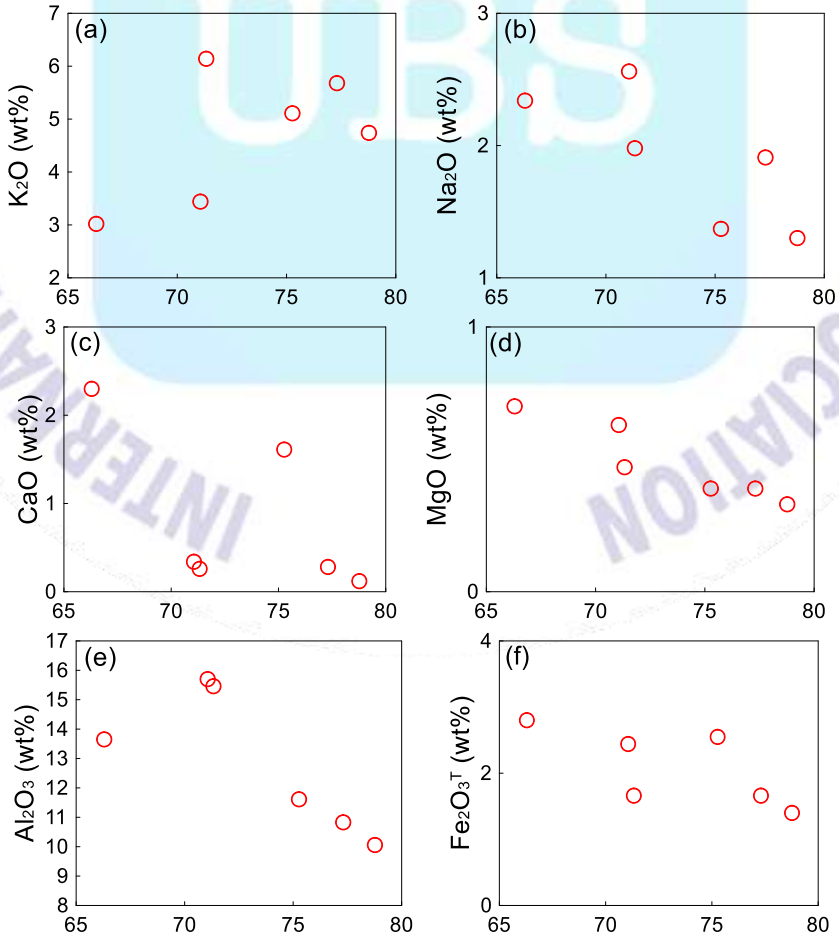

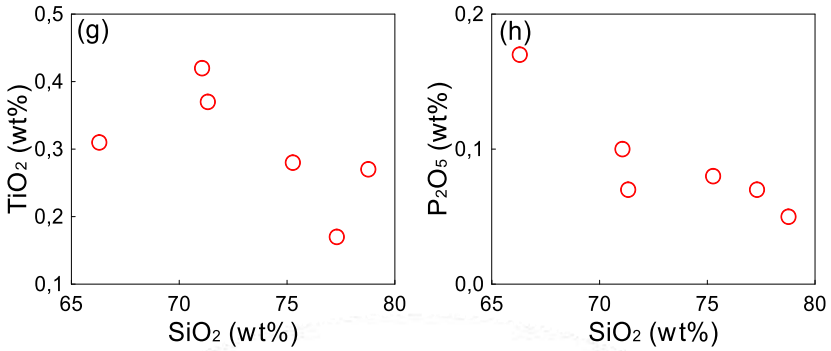

Görsel 5. Budak volkanitlerine ait kayaç örneklerinin SiO_2'ye karşı ana element değişim diyagramları

SiO_2'ye karşı iz element değişim diyagramlarında; SiO_2 arttıkça Ba ve Rb değerlerinde pozitif bir ilişki gözlenirken; Sr, Zr, Y ve Ni'de negatif bir ilişki gözlenir (Görsel 6).

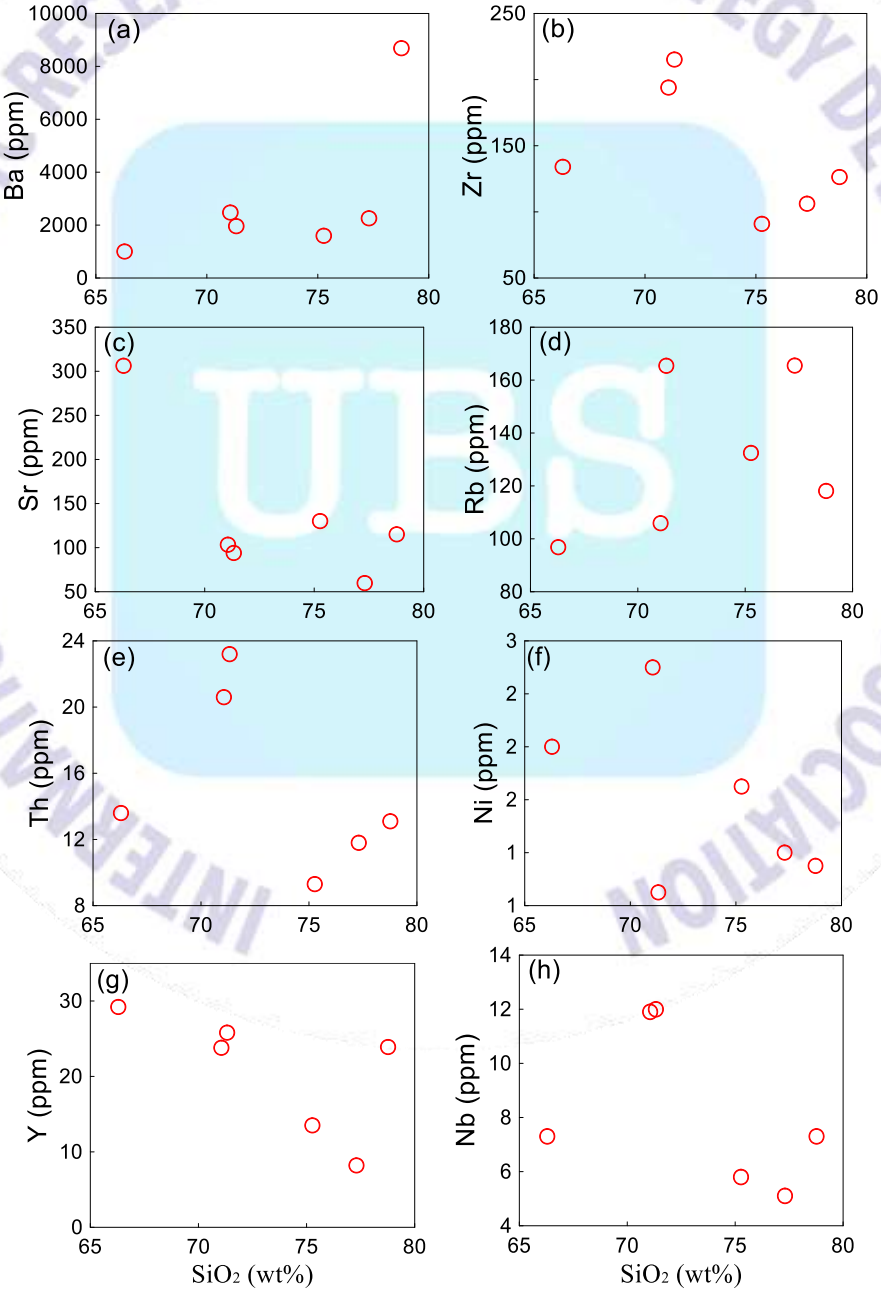

Görsel 6. Budak volkanitlerine ait kayaç örneklerinin SiO_2'ye karşı iz element değişim diyagramları

Örneklerin ilksel mantoya [70] göre normalleştirilmiş olan iz element değişim diyagramında K, Rb, Ba, Th, U, Pb ve Nd konsantrasyonları bakımından zenginleşme gözlenirken; Nb, Ta, P ve Ti bakımından fakirleşme izlenmektedir (Görsel 7a). Özellikle Th, U ve Rb gibi elementlerdeki zenginleşme kabuk etkisini yansıtmaktadır. Negatif Nb ve Ta anomalisi, kayaçların ana magmasının gelişiminde, yitim bileşeninin etken bir rol oynadığını göstermektedir.

İncelenen volkanitlerin kondrite [71] normalize edilmiş nadir toprak element dağılımları genel olarak birbirine benzerlik göstermektedir (Görsel 7b). Bu durum, inceleme alanındaki volkanitleri oluşturan kayaçların aynı/benzer manto kaynağından türediklerini işaret etmektedir. Volkanik kayaç örneklerinin kondrite normalize edilmiş nadir toprak element dağılım diyagramlarında (Görsel 7b), hafif nadir toprak elementler, ağır nadir toprak elementlere göre daha fazla zenginleşmiştir.

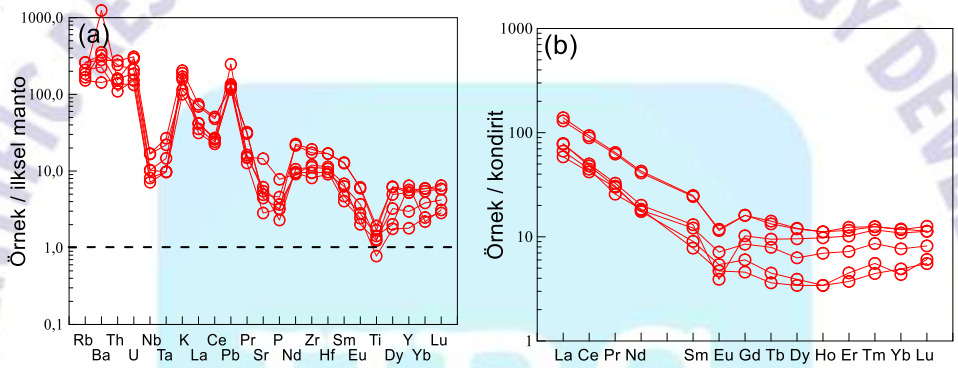

Görsel 7. Budak volkanitlerine ait kayaçların (a) ilksel mantoya göre [70] **(b) kondirite** [71]**göre normalize edilmiş iz element dağılım diyagramları**

5.2. Tektonik Konum

İncelenen volkanitlerin, alterasyondan fazla etkilenmediği bilinen elementlerin birbirleriyle ilişkilerine göre tektonik ortamları belirlenmeye çalışılmıştır. Nb'ye karşı Nb/Th [72] tektonik ayırtman diyagramına göre, örnekler yay volkanitleri alanına düşmektedir (Görsel 8a). Sr/Y-Y [73] ayırtman diyagramında örnekler normal yay volkanik serisi alanına düşmektedir (Görsel 8b).

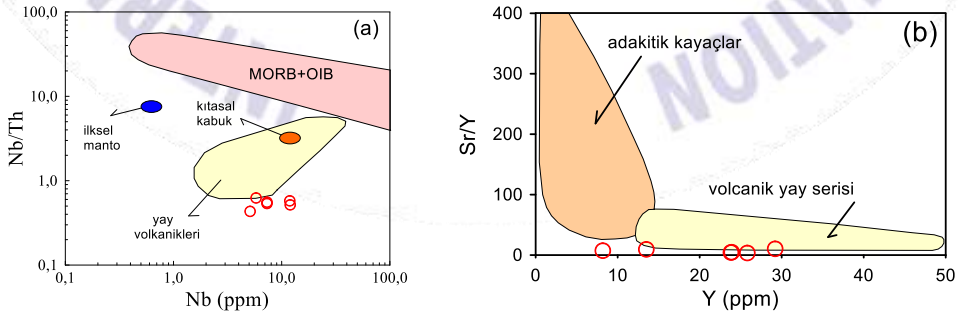

Görsel 8. Budak volkanitlerine ait tektonik ayırtman diyagramları. (a) Nb (ppm)'ye karşı Nb/Th diyagramı (ilksel manto değerleri Hofmann, [74]'den, kıtasal bazalt-OOSB+OAB ve yay volkanitleri alanları Schmidberger ve Hegner, [75]'den alınmıştır). (b) Sr/Y-Y ayırtman diyagramı [73]

6. TARTIŞMA VE SONUÇLAR

Tüm kayaç ana, iz ve nadir toprak element verileri dikkate alındığında (Görsel 5-7), volkanitlerin gelişiminde amfibol, plajiyoklas ve Fe-Ti oksit fraksiyonel kristalleşmesinin önemli olduğu görülür. Artan SiO_2 içeriğine karşılık TiO_2 ve $Fe_2O_3^T$ içeriklerinin giderek azalması Fe-Ti oksitlerin ayrımlaşmasına işaret etmektedir. SiO_2'ye karşı CaO, $Fe_2O_3^T$ ve MgO daki negatif ilişkiler plajiyoklas fazların ana magmadan ayrımlaştığına işaret etmektedir. SiO_2'ye karşı P_2O_5 değişim diyagramında gözlenen negatif korelasyon ise apatit fraksiyonlaşmasını yansıtmaktadır.

SiO_2'ye karşı Y/Nb oranlarında gözlenen negatif yönsemeler, magma gelişimi esnasında kabuksal kirlenmeye işaret eder (Görsel 9a). Th/Yb ve Ta/Yb oranları, kaynak bileşimi ve kabuksal kirlenmenin tayininde etkili bir şekilde kullanılması, kabuksal kirlenmede Ta ve Yb'ye nazaran Th elementinin daha fazla etkilenmesinden kaynaklanmaktadır [76]. Th/Yb'ye karşı Ta/Yb diyagramı (Görsel 9b), incelenen kayaçların gelişiminde AFC proseslerinin önemli bir rol oynadığını ve volkanitlerin oluşumuna kaynaklık eden magmanın ilksel mantoya göre yitim zonu zenginleşmesine uğradığını gösterir.

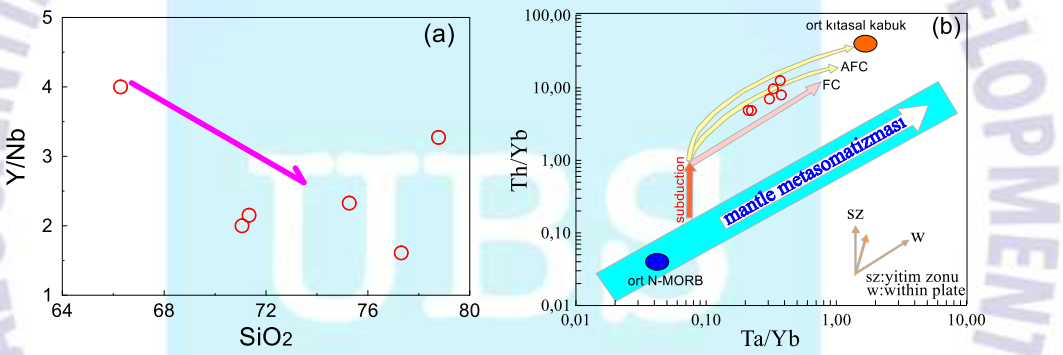

Görsel 9. Budak volkanitlerinin, a) SiO_2'ye karşı Y/Nb diyagramı, b) Ta/Yb'a karşı Th/Yb diyagramı [76], (yitim zenginleşmesi ve manto metasomatizmasını gösterir vektörler Pearce vd., [76]'dan alınmıştır, N-tipi OOSB ve ortalama üst kabuk değerleri Sun ve McDonough, [70] ve Taylor and McLennan, [71]'ten alınmıştır)

Budak volkanik kayaçlarında gözlenen LILE element zenginleşmesi, yüksek Th/Yb oranları, volkanitlerin ana magmasının litosferik manto kaynağından türemiş olabileceğini gösterir [77,78]. Ayrıca, çalışılan volkanik kayaçlarda gözlenen LILE elementlere nazaran Nb ve Ta tüketilmesi, sedimentler ya da yiten levhadan türeyen sıvıların metazomatizmasıyla etkilenmiş, yitimle ilişkili magma kaynağının özelliğini ifade eder [78,79].

Ce/Pb'ye karşı Ce diyagramında (Görsel 10a), çalışılan volkanik kayaçlara ait örnekler yay volkanikleri alanı ve civarında yer alırlar. Örneklerde gözlenen düşük Ce/Pb oranları, okyanusal bazaltlardan [74] farklı olup, bu durum çalışılan volkanik kayaçların astenosferik manto kaynağından türemediğini gösterir. Yüksek Nb/La oranları (>1) okyanus adası bazalt (OIB) benzeri astenosferik manto kaynağını, düşük oranlar (<0.5) ise litosferik manto kaynağına işaret eder [80]. Bu nedenle, Nb/La ve La/Yb oranları volkanik kayaçlarda kısmı ergime derecesi ve kaynak bileşiminin belirlenmesinde faydalıdır [81]. İncelenen volkanik kayaçlarının Nb/La ve La/Yb oranları litosferik manto kaynağına işaret eder (Görsel 10b).

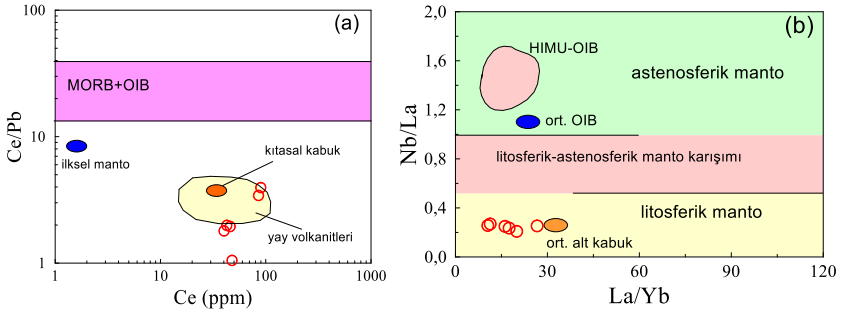

Görsel 10. Budak volkanitlerinin; (a) Ce/Pb karşı Ce diyagramı (ilksel manto değerleri Hofmann, [74]'den, kıtasal kabuk, MORB, OIB ve yay volkanitleri Schmidberger ve Hegner, [75]'dan alınmıştır). (b) La/Yb'ye karşı Nb/La diyagramı (OAB değerleri, Fitton vd., [82]'den, ortalama alt kabuk değerleri, Chen ve Arculus, [83]'den, HIMU+OAB alanları, Weaver vd., [84]'den, astenosferik, litosferik ve karışım manto alanlarını ayıran çizgi Smith vd., [80]'dan alınmıştır)

Sonuç olarak, incelenen Geç Kretase yaşlı Budak volkanitlerinin ana ve iz element karakteristikleri, volkanik kayaçları oluşturan ana magmanın, yitim ile ilişkili bir jeodinamik ortamda, sıvılar ve/veya sedimentlerce zenginleştirilmiş bir litosferik manto kaynağından türemiş olabileceğini gösterir.

KAYNAKÇA

[1] Çamur MZ, Güven İH, Er M. Geochemical characteristics of the eastern Pontide volcanics: an example of multiple volcanic cycles in arc evolution. Turkish Journal of Earth Sciences 1996:123–44.

[2] Arslan M, Tüysüz N, Korkmaz S, Kurt H. Geochemistry and petrogenesis of the eastern Pontide volcanic rocks, Northeast Turkey. Chemie der Erde Geochemistry 1997;57:157–87.

[3] Yılmaz S, Boztuğ D. Space and time relations of three plutonic phases in theEastern Pontides, Turkey. International Geology Review 1996;38:935–56.

[4] Kaygusuz A, Aydınçakır E. Mineralogy, whole-rock and Sr–Nd isotope geochemistry of mafic microgranular enclaves in Cretaceous Dagbasi granitoids, Eastern Pontides, NE Turkey: Evidence of magma mixing, mingling and chemical equilibration. Geochemistry 2009;69:247–77. https://doi.org/10.1016/j.chemer.2008.08.002.

[5] Liu Z, Zhu D-C, Wang Q, Eyuboglu Y, Zhao Z-D, Liu S-A, vd. Transition From Low-K to High-K Calc-Alkaline Magmatism at Approximately 84 Ma in the Eastern Pontides (NE Turkey): Magmatic Response to Slab Rollback of the Black Sea. Journal of Geophysical Research: Solid Earth 2018;123:7604–28. https://doi.org/10.1029/2018JB016026.

[6] Sipahi F, Kaygusuz A, Saydam Eker Ç, Vural A, Akpınar İ. Late Cretaceous arc igneous activity: the Eğrikar Monzogranite example. International Geology Review 2018;60:382–400. https://doi.org/10.1080/00206814.2017.1336120.

[7] Temizel İ, Arslan M, Yücel C, Yazar EA, Kaygusuz A, Aslan Z. U-Pb geochronology, bulk-rock geochemistry and petrology of Late Cretaceous syenitic plutons in the Gölköy (Ordu) area (NE Turkey): Implications for magma generation in a continental

arc extension triggered by slab roll-back. Journal of Asian Earth Sciences 2019;171:305–20. https://doi.org/10.1016/j.jseaes.2019.01.004.
[8] Kaygusuz A, Şen C. Calc-alkaline I-type plutons in the eastern Pontides, NE Turkey: U-Pb zircon ages, geochemical and Sr-Nd isotopic compositions. Chemie der Erde - Geochemistry 2011;71:59–75. https://doi.org/10.1016/j.chemer.2010.07.005.
[9] Kaygusuz A, Aydinçakir E. Petrogenesis of a Late Cretaceous composite pluton from the eastern Pontides: the Dağbaşi pluton, NE Turkey. Neues Jahrbuch für Mineralogie - Abhandlungen 2011;188:211–33. https://doi.org/10.1127/0077-7757/2011/0201.
[10] Kaygusuz A, Siebel W, Şen C, Satir M. Petrochemistry and petrology of I-type granitoids in an arc setting: the composite Torul pluton, Eastern Pontides, NE Turkey. International Journal of Earth Sciences 2008;97:739–64. https://doi.org/10.1007/s00531-007-0188-9.
[11] Kaygusuz A, Chen B, Aslan Z, Siebel W, Şen C. U-Pb SHRIMP zircon ages, geochemical and Sr-Nd isotopic compositions of the late cretaceous I-type Sariosman pluton, Eastern Pontides, NE Turkey. Turkish Journal of Earth Sciences 2009;18:549–81. https://doi.org/10.3906/yer-0806-1.
[12] Kaygusuz A, Sipahi F, Ilbeyli N, Arslan M, Chen B, Aydinçakir E. Petrogenesis of the late Cretaceous Turnagöl intrusion in the eastern Pontides: Implications for magma genesis in the arc setting. Geoscience Frontiers 2013;4:423–38. https://doi.org/10.1016/j.gsf.2012.09.003.
[13] Kaygusuz A, Arslan M, Siebel W, Sipahi F, İlbeyli N, Temizel İ. LA-ICP MS zircon dating, whole-rock and Sr-Nd-Pb-O isotope geochemistry of the Camiboğazı pluton, Eastern Pontides, NE Turkey: Implications for lithospheric mantle and lower crustal sources in arc-related I-type magmatism. Lithos 2014;192–195:271–90.
[14] Kaygusuz A, Aydınçakır E, Yücel C, Atay HE. Petrographic and geochemical characteristics of carboniferous plutonic rocks around Erenkaya (Gümüşhane, NE Turkey). Journal of Engineering Research and Applied Science 2021;10:1774–88.
[15] Karslı O, Dokuz A, Uysal I, Aydin F, Chen B, Kandemir R, vd. Relative contributions of crust and mantle to generation of Campanian high-K calc-alkaline I-type granitoids in a subduction setting, with special reference to the Harşit Pluton, Eastern Turkey. Contributions to Mineralogy and Petrology 2010;160:467–87. https://doi.org/10.1007/s00410-010-0489-z.
[16] Bektas O, Sen C, Atici Y, Köprübasi, Koprubasi N. Migration of the Upper Cretaceous subduction-related volcanism towards the back-arc basin of the eastern Pontide magmatic arc (NE Turkey). Geological Journal 1999;34:95–106. https://doi.org/10.1002/(SICI)1099-1034(199901/06)34:1/2<95::AID-GJ816>3.0.CO;2-J.
[17] Sipahi F, Sadıklar MB, C. Ş. The geochemical and Sr-Nd isotopic characteristics of Murgul (Artvin) volcanics in the Eastern Black Sea region (NE Turkey). Chemie der Erde 2014;74:331–342.
[18] Özdamar Ş. Geochemistry and geochronology of late Mesozoic volcanic rocks in the northern part of the Eastern Pontide Orogenic Belt (NE Turkey): Implications for the closure of the Neo-Tethys Ocean. Lithos 2016;248–252:240–56.
[19] Eyüboğlu Y. Late Cretaceous high-K volcanism in the eastern Pontide orogenic belt: Implications for the geodynamic evolution of NE Turkey. vol. 52. 2010. https://doi.org/10.1080/00206810902757164.
[20] Alan İ, Balcı V, Keskin H, Altun İ, Böke N, Demirbağ H, vd. Tectonostratigraphic characteristics of the area between Çayeli (Rize) and İspir (Erzurum). Bulletin of the Mineral Research and Exploration 2019;158:1–29.
[21] Aydin F, Dokuz A, Kandemir R, Karsli O. Temporal , geochemical and geodynamic

evolution of the Late Cretaceous subduction zone volcanism in the eastern Sakarya Zone , NE Turkey : implications for mantle-crust interaction in an arc setting 2020. https://doi.org/10.1016/j.jseaes.2019.104217.

[22] Topuz G, Altherr R, Schwarz WH, Dokuz A, Meyer HP. Variscan amphibolite-facies rocks from the Kurtoğlu metamorphic complex (Gümüşhane area, Eastern Pontides, Turkey). International Journal of Earth Sciences 2007;96:861–73. https://doi.org/10.1007/s00531-006-0138-y.

[23] Dokuz A. A slab detachment and delamination model for the generation of Carboniferous high-potassium I-type magmatism in the Eastern Pontides, NE Turkey: The Köse composite pluton. Gondwana Research 2011;19:926–44. https://doi.org/10.1016/j.gr.2010.09.006.

[24] Kaygusuz A, Arslan M, Siebel W, Sipahi F, Ilbeyli N. Geochronological evidence and tectonic significance of Carboniferous magmatism in the southwest Trabzon area, eastern Pontides, Turkey. International Geology Review 2012;54:1776–800. https://doi.org/10.1080/00206814.2012.676371.

[25] Kaygusuz A, Arslan M, Sipahi F, Temizel İ. U-Pb zircon chronology and petrogenesis of Carboniferous plutons in the northern part of the Eastern Pontides, NE Turkey: Constraints for Paleozoic magmatism and geodynamic evolution. Gondwana Research 2016;39:327–46.

[26] Kaygusuz A, Arslan M, Temizel İ, Yücel C, Aydınçakır E. U–Pb zircon ages and petrogenesis of the Late Cretaceous I-type granitoids in arc setting, Eastern Pontides, NE Turkey. Journal of African Earth Sciences 2021;174:104040. https://doi.org/10.1016/j.jafrearsci.2020.104040.

[27] Vural A, Kaygusuz A. Petrology of the Paleozoic Plutons in Eastern Pontides: Artabel Pluton (Gümüşhane, NE Turkey). Journal of Engineering Research and Applied Science 2019;8:1216–28.

[28] Kaygusuz A. Geochronological age relationships of Carboniferous Plutons in the Eastern Pontides (NE Turkey). Journal of Engineering Research and Applied Science 2020;9:1299–307.

[29] Kandemir R, Yılmaz C. Lithostratigraphy, facies, and deposition environment of the lower Jurassic Ammonitico Rosso type sediments (Arts) in the Gümüşhane area, NE Turkey: Implications for the opening of the northern branch of the Neo-Tethys Ocean. Journal of Asian Earth Sciences 2009;34:586–98.

[30] Şen C. Jurassic volcanism in the Eastern Pontides: Is it rift related or subduction related? Turkish Journal of Earth Sciences 2007;16:523–39.

[31] Saydam Eker C. Petrography and geochemistry of Eocene sandstones from eastern Pontides (NE TURKEY): Implications for source area weathering, provenance and tectonic setting. Geochemistry International 2012;50:683–701. https://doi.org/10.1134/S001670291206002X.

[32] Dokuz A, Karsli O, Chen B, Uysal I. Sources and petrogenesis of Jurassic granitoids in the Yusufeli area, Northeastern Turkey: Implications for pre- and post-collisional lithospheric thinning of the eastern Pontides. Tectonophysics 2010;480:259–79. https://doi.org/10.1016/j.tecto.2009.10.009.

[33] Karslı O, A D, Kandemir R. Zircon Lu-Hf isotope systematics and U-Pb geochronology, whole-rock Sr-Nd isotopes and geochemistry of the early Jurassicssic Gokçedere pluton, Sakarya Zone-NE Turkey: a magmatic response to roll-back of the Paleo-Tethyan oceanic lithosphere. Contributions to Mineralogy and Petrology 2017;172:1–31.

[34] Aydınçakır E, Gündüz R, Yücel C. Emplacement conditions of magma(s) forming Jurassic plutonic rocks in Gümüşhane (Eastern Pontides, Turkey). Bulletin of Mineral

Research and Exploration 2020;162:175–196.
[35] Pelin S. Alucra (Giresun) Güneydoğu yöresinin petrol olanaklan bakımından jeolojik incelemesi. Trabzon: Karadeniz Teknik Üniversitesi Yayını, Yayın No. 87,; 1977.
[36] Altherr R, Topuz G, Siebel W, Şen C, Meyer HP, Satir M, vd. Geochemical and Sr-Nd-Pb isotopic characteristics of Paleocene plagioleucitites from the Eastern Pontides (NE Turkey). Lithos 2008;105:149–61. https://doi.org/10.1016/j.lithos.2008.03.001.
[37] Topuz G, Altherr R, Siebel W, Schwarz WH, Zack T, Hasözbek A, vd. Carboniferous high-potassium I-type granitoid magmatism in the Eastern Pontides: The Gümüşhane pluton (NE Turkey). Lithos 2010;116:92–110. https://doi.org/10.1016/j.lithos.2010.01.003.
[38] Sipahi F, Akpınar İ, Saydam Eker Ç, Kaygusuz A, Vural A, Yılmaz M. Formation of the Eğrikar (Gümüşhane) Fe–Cu skarn type mineralization in NE Turkey: U–Pb zircon age, lithogeochemistry, mineral chemistry, fluid inclusion, and O-H-C-S isotopic compositions. Journal of Geochemical Exploration 2017;182:32–52. https://doi.org/10.1016/j.gexplo.2017.08.006.
[39] Kaygusuz A, Saydam Eker Ç. Geochemical features and petrogenesis of Late Cretaceous subduction-related volcanic rocks in the Değirmentaşı (Torul/Gümüşhane) area, Eastern Pontides (NE Turkey). Journal of Engineering Research and Applied Science 2021;10:1689–702.
[40] Vural A, Kaygusuz A. Geochronology, petrogenesis and tectonic importance of Eocene I-type magmatism in the Eastern Pontides, NE Turkey. Arabian Journal of Geosciences 2021;14:467. https://doi.org/10.1007/s12517-021-06884-z.
[41] Vural A, Akpinar İ, Sipahi F. Mineralogical and Chemical Characteristics of Clay Areas, Gümüşhane Region (NE Turkey), and Their Detection Using the Crósta Technique with Landsat 7 and 8 Images. Natural Resources Research 2021;30:3955–85. https://doi.org/10.1007/s11053-021-09912-7.
[42] Kaygusuz A, Arslan A, Siebel W, Şen C. Geochemical and Sr-Nd Isotopic Characteristics of Post-Collisional Calc-Alkaline Volcanics in the Eastern Pontides (NE Turkey). Turkish Journal of Earth Sciences 2011;20:137–59. https://doi.org/10.3906/yer-1002-8.
[43] Kaygusuz A, Yücel C, Arslan M, Temizel İ, Yi K, Jeong Y-J, vd. Eocene I-type magmatism in the Eastern Pontides, NE Turkey: Insights into magma genesis and magma-tectonic evolution from whole-rock geochemistry, geochronology and isotope systematics. International Geology Review 2020. https://doi.org/doi.org/10.1080/00206814.2019.1647468.
[44] Topuz G, Altherr R, Schwarz WH, Siebel W, Satir M, Dokuz A. Post-collisional plutonism with adakite-like signatures: The Eocene Saraycik granodiorite (Eastern Pontides, Turkey). Contributions to Mineralogy and Petrology 2005;150:441–55. https://doi.org/10.1007/s00410-005-0022-y.
[45] Tokel S. Doğu Karadeniz bölgesinde Eosen yaşlı kalkalkalen andezitler ve jeotektonizma. Türkiye Jeoloji Kurultayı Büllteni 1977;20:49–54.
[46] Vural A, Akpınar İ, Kaygusuz A, Sipahi F. Petrological characteristics of Eocene volcanic rocks around Demirören (Gümüşhane, NE Turkey). Journal of Engineering Research and Applied Science 2021;10:1703–16.
[47] Aslan Z, Arslan M, Temizel I, Kaygusuz A. K-Ar dating, whole-rock and Sr-Nd isotope geochemistry of calc-alkaline volcanic rocks around the Gümüşhane area: Implications for post-collisional volcanism in the Eastern Pontides, Northeast Turkey. Mineralogy and Petrology 2014;108:245–67. https://doi.org/10.1007/s00710-013-0294-2.
[48] Kaygusuz A, Merdan-Tutar Z, Yucel C. Mineral chemistry, crystallization conditions

and petrography of Cenozoic volcanic rocks in the Bahçecik (Torul/Gumushane) area, Eastern Pontides (NE Turkey). Journal of Engineering Research and Applied Science 2017;6:641–51.

[49] Kaygusuz A, Gucer MA, Yucel C, Aydincakir E, Sipahi F. Petrography and crystallization conditions of Middle Eocene volcanic rocks in the Aydıntepe -Yazyurdu (Bayburt) area , Eastern Pontides (NE Turkey). Journal of Engineering Research and Applied Science 2019;8:1205–15.

[50] Temizel I, Arslan M, Ruffet G, Peucat JJ. Petrochemistry, geochronology and Sr-Nd isotopic systematics of the Tertiary collisional and post-collisional volcanic rocks from the Ulubey (Ordu) area, eastern Pontide, NE Turkey: Implications for extension-related origin and mantle source characteristi. Lithos 2012;128–131:126–47. https://doi.org/10.1016/j.lithos.2011.10.006.

[51] Arslan M, Temizel I, Abdioğlu E, Kolayli H, Yücel C, Boztuğ D, vd. 40Ar-39Ar dating, whole-rock and Sr-Nd-Pb isotope geochemistry of post-collisional Eocene volcanic rocks in the southern part of the Eastern Pontides (NE Turkey): Implications for magma evolution in extension-induced origin. Contributions to Mineralogy and Petrology 2013;166:113–42. https://doi.org/10.1007/s00410-013-0868-3.

[52] Yücel C, Arslan M, Temizel İ, Abdioğlu Yazar E, Ruffet G. Evolution of K-rich magmas derived from a net veined lithospheric mantle in an ongoing extensional setting: Geochronology and geochemistry of Eocene and Miocene volcanic rocks from Eastern Pontides (Turkey). Gondwana Research 2017;45:65–86.

[53] Kaygusuz A, Sahin K. Petrographical , geochemical and petrological characteristics of Eocene volcanic rocks in the Mescitli area , Eastern Pontides (NE Turkey). Journal of Engineering Research and Applied Science 2016;5:473–86.

[54] Kaygusuz A, Selvi D. Crystallization conditions and petrography of eocene volcanic rocks in the Gümüşdamla -Erikdibi area (Bayburt , NE Turkey). Journal of Engineering Research and Applied Science 2020;9:1529–37.

[55] Karslı O, Chen B, Aydin F, Şen C. Geochemical and Sr-Nd-Pb isotopic compositions of the Eocene Dölek and Sariçiçek Plutons, Eastern Turkey: Implications for magma interaction in the genesis of high-K calc-alkaline granitoids in a post-collision extensional setting. Lithos 2007;98:67–96. https://doi.org/10.1016/j.lithos.2007.03.005.

[56] Temizel İ, Abdioğlu Yazar E, Arslan M, Kaygusuz A, Aslan Z. Mineral chemistry, whole-rock geochemistry and petrology of Eocene I-type shoshonitic plutons in the Gölköy area (Ordu, NE Turkey). Bulletin of the Mineral Research and Exploration 2018;157:121–52.

[57] Temizel I, Arslan M, Yücel C, Abdioğlu Yazar E, Kaygusuz A, Aslan Z. Eocene tonalite–granodiorite from the Havza (Samsun) area, northern Turkey: adakite-like melts of lithospheric mantle and crust generated in a post-collisional setting. International Geology Review 2020;62:1131–58. https://doi.org/10.1080/00206814.2019.1625077.

[58] Çakmak G, Kaygusuz A. Petrography and crystallization conditions of the Pelitli Pluton in the Bayburt area, Eastern Pontides (NE Turkey). Journal of Engineering Research and Applied Science 2021;10:1658–69.

[59] Kaygusuz A, Öztürk M. Geochronology, geochemistry, and petrogenesis of the Eocene Bayburt intrusions, Eastern Pontide, NE Turkey: implications for lithospheric mantle and lower crustal sources in the high-K calc-alkaline magmatism. Journal of Asian Earth Sciences 2015;108:97–116.

[60] Eyüboğlu Y, Dudas FO, Thorkelson D, Zhu DC, Liu Z, Chatterjee N, vd. Eocene granitoids of northern Turkey: Polybaric magmatism in an evolving arc–slab window system. Gondwana Research 2017;50:311–45.

[61] Kaygusuz A, Yücel C, Arslan M, Sipahi F, Temizel İ, Çakmak G, vd. Petrography, mineral chemistry and crystallization conditions of Cenozoic plutonic rocks located to the north of Bayburt (Eastern Pontides, Turkey). Bulletin of the Mineral Research and Exploration 2018;157:75–102.
[62] Sipahi F, Saydam Eker Ç, Akpınar İ, Gücer MA, Vural A, Kaygusuz A, vd. Eocene magmatism and associated Fe-Cu mineralization in northeastern Turkey: a case study of the Karadağ skarn. International Geology Review 2022. https://doi.org/10.1080/00206814.2021.1941323.
[63] Aydin F, Karslı O, Chen B. Petrogenesis of the Neogene alkaline volcanics with implications for post-collisional lithospheric thinning of the Eastern Pontides, NE Turkey. Lithos 2008;104:249–66. https://doi.org/10.1016/j.lithos.2007.12.010.
[64] Yücel C, Arslan M, Temizel İ, Abdioğlu E. Volcanic facies and mineral chemistry of Tertiary volcanics in the northern part of the Eastern Pontides, northeast Turkey: implications for pre-eruptive crystallization conditions and magma chamber processes. Mineralogy and Petrology 2014;108:439–467.
[65] Le Maitre RW, Bateman P, Dudek A, Keller J, Lameyre J, Le Bas MJ, vd. A Classification of Igneous Rocks and Glossary of Terms: Recommendations of the International Union of Geological Sciences Subcommission on the Systematics of Igneous rocks. Blackwell Scientific Publications, Oxford, U.K.; 1989.
[66] Winchester JA, Floyd PA. Geochemical discrimination of different magma series and their differentiation products using immobile elements. Chemical Geology 1977;20:325–43. https://doi.org/10.1016/0009-2541(77)90057-2.
[67] Irvine TN, Baragar WRA. A guide to the chemical classification of the common volcanic rocks. Canadian Journal of Earth Sciences 1971;8:523–48.
[68] Rickwood PC. Boundary lines within petrologic diagrams which use oxides of major and minor elements. Lithos 1989;22:247–63. https://doi.org/10.1016/0024-4937(89)90028-5.
[69] Middlemost EAK. Naming materials in the magma/igneous rock system. Earth Science Reviews 1994;37:215–24. https://doi.org/10.1016/0012-8252(94)90029-9.
[70] Sun SS, Mcdonough WF. Chemical and isotopic systematics of oceanic basalts: implications for mantle composition and processes. Içinde: Saunders AD, Norry MJ, editörler. Magmatism in the Ocean Basins., London: Geological Society, Special Publications 42; 1989, s. 313–47.
[71] Taylor SR, McLennan SM. The Continental Crust; its Composition and Evolution Geoscience Text. Blackwell Scientific Publications, Oxford, U.K.; 1985.
[72] Pearce JA, Cann JR. Tectonic setting of basic volcanic rocks determined using trace element analyses. Earth and Planetary Science Letters 1973;19:290–300. https://doi.org/10.1016/0012-821X(73)90129-5.
[73] Drummond MS, Defant M. J. A model for trondhjemite-tonalite-dacite genesis and crustal growth via slab melting: Archean to modern comparisons. Journal of Geophysical Research 1990;95:21503–21521.
[74] Hofmann AW. Chemical differentiation of the Earth: the relationship between mantle, continental crust, and the oceanic crust. Earth Planet Sciences Letters 1988;90:297–314.
[75] Schmidberger S, Hegner E. Geochemistry and isotope systematics of calc-alkaline volcanic rocks from the Saar-Nahe basin (SW Germany). Implications for Late Hercynian orogenic development. Contributions to Mineralogy and Petrology 1999;135:373–85.
[76] Pearce JA, Bender JF, De Long SE, Kidd WSF, Low PJ, Güner Y, vd. Genesis of collision volcanism in Eastern Anatolia, Turkey. Journal of Volcanology and

Geothermal Research 1990;44:189–229. https://doi.org/10.1016/0377-0273(90)90018-B.

[77] Pearce JA, Peate DW. Tectonic implications of the composition of volcanic arc magmas. Annual Review of Earth and Planetary Sciences 1995;23:251–285.

[78] Elburg MA, Bergen MV, Hoogewerff J, Foden J, Vroon P, Zulkarnain I, vd. Geochemical trends across an arc-continent collision zone: magma sources and slab-wedge transfer processes below the Pantar Strait volcanoes, Indonesia. Geochimica et Cosmochimica Acta 2002;66:2771–2789.

[79] Hawkesworth CJ, Turner SP, McDermott F, Peate DW, Van Calsteren P. U-Th isotopes in arc magmas: Implications for element transfer from the subducted crust. Science 1997;276:551–5. https://doi.org/10.1126/science.276.5312.551.

[80] Smith EI, Sanchez A, Walker JD, Wang K. Geochemistry of mafic magmas in the Hurricane Volcanic field, Utah: implications for small- and large-scale chemical variability of the lithospheric mantle. Journal of Geology 1999;107:433–448.

[81] Jahn BM, Wu FY, Lo CH. Crust-mantle interaction induced by deep subduction of the continental crust: geochemical and Sr-Nd isotopic evidence from post-collisional mafic-ultramafic intrusions of the northern Dabie Complex, Central China. Chemical Geology 1999;157:119–46.

[82] Fitton JG, James D, Leeman WP. Basic magmatism associated with late Cenozoic extension in the western United States: compositional variations in space and time. Journal of Geophysical Research 1991;96. https://doi.org/10.1029/91jb00372.

[83] Chen W, Arculus RJ. Geochemical and isotopic characteristics of lower crustal xenoliths, San Francisco Volcanic Field, Arizona, U.S.A. Lithos 1995;36:203–25. https://doi.org/10.1016/0024-4937(95)00018-6.

[84] Weaver BL, Wood DA, Tarney J, Joron J. Geochemistry of ocean island basalt from the South Atlantic: Ascension, Bouvet, St. Helena, Gough and Tristan da Cunda. Içinde: Fitton J., Upton BGJ, editörler. Alkaline igneous rocks, Geological Society, London, Special Publications, 30,; 1987, s. 253–67.

YUMRUDAĞI VOLKANİKLERİNİN (ÇANAKKALE/TÜRKİYE) GENEL JEOLOJİSİ, PETROGRAFİSİ VE JEOKİMYASI

Doç.Dr. Alaaddin VURAL [1], Prof.Dr. Abdullah KAYGUSUZ [2]

[1] Gümüşhane Üniversitesi, orcid id: 0000-0002-0446-828X

[2] Gümüşhane Üniversitesi, orcid id: 0000-0002-6277-6969

ÖZET

Bu çalışmada Bayramiç (Batı Anadolu, Çanakkale) kuzeyinde yer alan Yumrudağı volkanitlerinin genel jeolojik, petrografik ve tüm kayaç jeokimyasal özellikleri incelenmiştir. İnceleme alanındaki başlıca birimler mikaşistler, ofiyolitik kayaçlar, plütonik kayaçlar, Yumrudağ volkanitleri ve Pliyo-Kuvaterner yaşlı genç çökellerden oluşur. İncelenen Yumrudağı volkanitleri andezit ve traki-andezit bileşiminde olup, başlıca plajiyoklas, amfibol ve Fe-Ti oksit minerallerinden oluşurlar. Volkanitler kalk-alkali karakterli olup, orta-yüksek K içeriğine sahiptirler. Büyük iyon yarıçaplı litofil elementler (LILE) ve hafif nadir toprak elementlerce (LREE) zenginleşmiş, yüksek çekim alanlı elementler (HFSE) bakımından tüketilmişlerdir. Kondrite normalize edilmiş nadir toprak element dağılımları, düşük-orta derecede zenginleşmeyle konkav şekilli olup (La_N/Lu_N=5-10), volkanitleri oluşturan kayaçların benzer kaynaktan itibaren oluştuklarını gösterirler. Volkanitlerin gelişiminde genelde fraksiyonel kristallenme rol oynamıştır. Tüm bu veriler, volkanitlerin köken magmasının litosferik manto kaynağı olabileceğini gösterir.

Anahtar Kelimeler : Yumrudağı volkanitleri, Petrografi, Tüm-kayaç Jeokimyası, Çanakkale.

GENERAL GEOLOGY, PETROGRAPHY AND GEOCHEMISTRY OF YUMRUDAĞI VOLCANICS (ÇANAKKALE/TURKEY)

ABSTRACT

In this study, the general geological, petrographic and whole-rock geochemical properties of Yumrudağı volcanics located in the north of Bayramiç (Western Anatolia, Çanakkale) were investigated. The main units in the study area consist of micaschists, ophiolitic rocks, plutonic rocks, Yumrudağ volcanics and Plio-Quaternary young sediments. The studied Yumrudağı volcanics are in andesite and trachy-andesite composition and consist mainly of plagioclase, amphibole and Fe-Ti oxide minerals. Volcanics have calc-alkaline character and have medium-

high K content. They are enriched with Large-Ion Lithophile Elements (LILE) and light rare earth elements (LREE) and depleted in high field strength element (HFSE). The chondrite normalized rare earth element distributions are concave with low to moderate enrichment (LaN/LuN=5-10), indicating that the volcanic rocks were formed from a similar source. Fractional crystallization generally played a role in the development of volcanics. All these data indicate that the origin magma of the volcanics may be the source of the lithospheric mantle.

Keywords: Yumrudağı volcanics, Petrography, Whole-rock Geochemistry, Çanakkale

1. GİRİŞ

Biga Yarımadası jeolojik çeşitliliği ve metalojenezi nedeniyle jeolojik ve maden jeolojisi açısından geçmişten beri bir çok çalışmaya konu olmuştur [1,2,11–19,3–10]. Çalışma sahasının içinde bulunduğu Yumrudağı ve çevresini de içine alan Batı Anadolu Volkanik ve Genişlemeli bölgesi (Görsel 1) Biga yarımadasında (KB Anadolu) bilinen metalojenik bölgeyi oluşturur [1,2,8–10,20] ki özelde Biga Yarımadası genelde ise tüm Batı Anadolu antik dönemlerden beri önemli madencilik faaliyetlerinin gerçekleştirildiği bölgelerin başında gelir [21–24]. Biga yarımadasını içine alan bölge hem Sakarya Zonu hem de Rodop Masifi dilimlerini kapsar. Kazdağ metamorfik kompleksi ve çok sayıda volkanik eşlenikleri ile birlikte yüzeylemiş magmatik kütleleri içeren Jura öncesi temel kayaçlar tüm Sakarya zonu içinde görülürler [25,26]. Bölgede Kazdağ Masifi'nin doğu kanadı boyunca yüzeyleyen Eybek plütonu, Eosen'den beri ilerleyen kısalma ve kabuk kalınlaşmasının bir sonucu olarak yükselimini sürdürmektedir Kazdağ Metamorfik çekirdek kompleksi ise tektonik olarak Karakaya Kompleksinin aktif kıtasal kenar sedimentlerinden oluşan dalma-batma yığışım birimleri tarafından üzerlenir [26]. Tektonik geçmişine bağlı yoğun magmatik faaliyetler Biga Yarımadası'nın cevherleşme potansiyelini artırmış, bölgeye dünya ölçeğinde epitermal altın yatakları ve prospeksiyon sahaları bahşetmiştir. Cevherleşmeler bölgenin dinamik çatısı ile de ilişkili olarak daha çok Senozoyik volkanik kayaçlar (Üst Miyosen; 11.68±0.25 ile 6.47±0.47 Ma aralığında [27–30]) içinde gözlenirler [1,20,31].

Bu çalışma kapsamında Bayramiç (Batı Anadolu, Çanakkale) kuzeyi Yumrudağı ve yakın çevresinin genel jeolojisi yanında birçok alterasyon alanı ve cevherleşmeye ev sahipliği yapan (Görsel 1) Yumrudağ volkaniklerinin petrografik ve jeokimyasal özellikleri incelenmiştir.

Görsel 3. Çalışma sahası yer bulduru haritası

2. ÇALIŞMA YÖNTEMLERİ

Sahadaki kayaçların mineralojik-petrografik tanımlamaları için ince kesitleri MTA Genel Müdürlüğü Mineraloji-Petrografi servisinde hazırlanan 28 adet örneğin, mineralojik-petrografik determinasyonları yapılmıştır. Ayrıca volkanik kayaçların kökenlerinin tespit edilmesi ve tektonikle ilişkilerinin ortaya konması amacıyla 8 adet örneğin tüm kayaç analizleri Kanada Acmelab'ta analiz ettirilmiştir. Kimyasal analizler için seçilen her biri yaklaşık 350-400 g kayaç örnekleri çeneli kırıcıda küçültülerek, Tungsten-karbit halkalı öğütücülerde 200 mesh boyutuna kadar öğütülmüş ve çeyrekleme yöntemiyle yaklaşık 50 gr toz örnek kimyasal analizler için ayrılmıştır. Ana element analizleri İndüktif Eşleşmiş Plazma (Inductivly Coupled Plasma)-Atomik Emisyon Spektrometri (ICP-AES); iz ve nadir toprak element (NTE) analizleri ise ICP-MS (Kütle Spektrometri) yöntemiyle yapılmıştır. Analitik detaylar Vural [1]'da yer almaktadır.

3. İNCELEME ALANININ GENEL JEOLOJİ

Çalışma sahası kuzeybatı Anadolu'da, Biga yarımadası sınırları içinde yeralmaktadır. Bölgedeki birimler, Okay et al., [26] tarafından Tersiyer öncesi ve sonrası birlik/birimler olarak ele alınmış olup, KD-GB yönünde Tersiyer öncesi üç tektonik zon ayırt edilmiştir Ezine Zonu, Ayvacık-Karabiga Zonu, Sakarya Zonu) (Şekil 2).

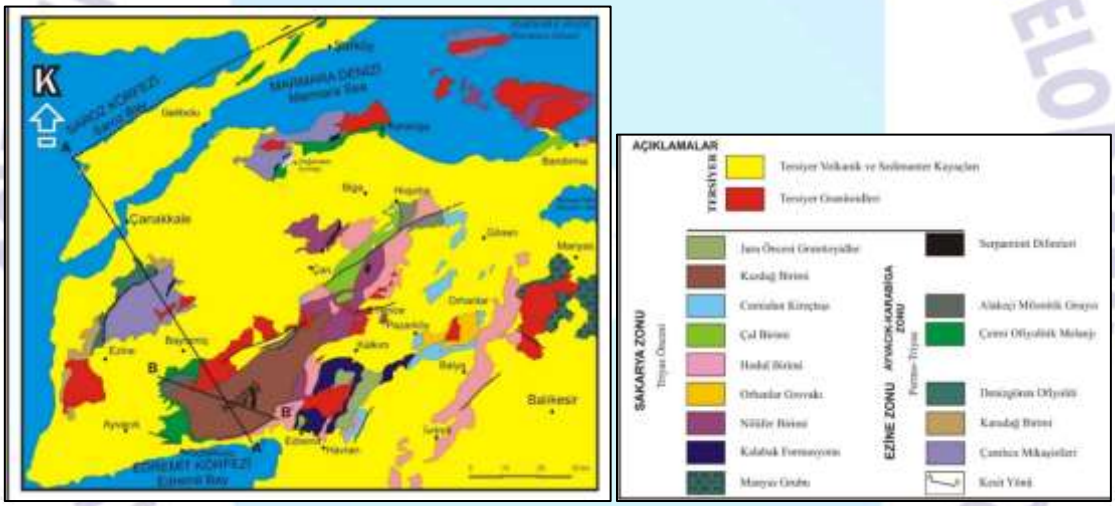

Görsel 4. Biga Yarımadası Bölgesel Jeolojisi (Okay vd. [26]'dan değiştirilerek alınmıştır)

Çalışma sahasında temelde Ezine Zonu'na ait mikaşistler ve ofiyolit kayaçları yeralmakta olup, bu birim/birlikler Tersiyer magmatikleri tarafından kesilmekte, volkanik ve sedimanter kayaçlar tarafından örtülmektedir (Görsel 3).

Sahadaki magmatik kayaçlar; plütonik, volkanik ve bunların piroklastik eşleniklerinden oluşur. Plütonik kayaçlar Kuşçayırı Plütonu, volkanik kayaçlar ise Yumrudağı Volkanikleri olarak adlandırılmıştır [1,4]. Yumrudağı Volkanikleri; Meydan Tepesi, Yumrudağı ve Kuşalıca Tepesi mevkilerinde yüzlek verir. Volkanikler, en altta andezit ve latit ve bunların piroklastik eşleniklerini içerir. Orta kesime doğru andezit ve dasitlerle ardalanır. Daha üst seviyelere doğru bazaltik trakiandezitler ve bazaltik andezitler, tüf, aglomera, andezitik silisleşmiş tüfler şeklinde

bir istif sunar [4,31–33]. Çalışma sahası daha kuzey kesimlerinde bu volkanik kayaçları keser konumda dasit porfirler de gözlenir [1] (Görsel 4).

Sahada Oligosen-Üst Pliyosen dönemine ait sedimanter kayaçlara rastlanmaktadır. Sedimanter kayaçlar daha çok, volkanik kayaçlarla yanal geçişli ve onları örter konumdadır. Oligosen-Alt Miyosen döneminde daha çok kumtaşı, silttaşı, çamurtaşı birimlerine rastlanmaktadır. Alt-Orta Miyosen döneminde ise daha çok gölsel kırıntılılar görülmektedir. Üst Miyosen-Pliyosen döneminde ise daha çok karasal kırıntılılara rastlanmaktadır.

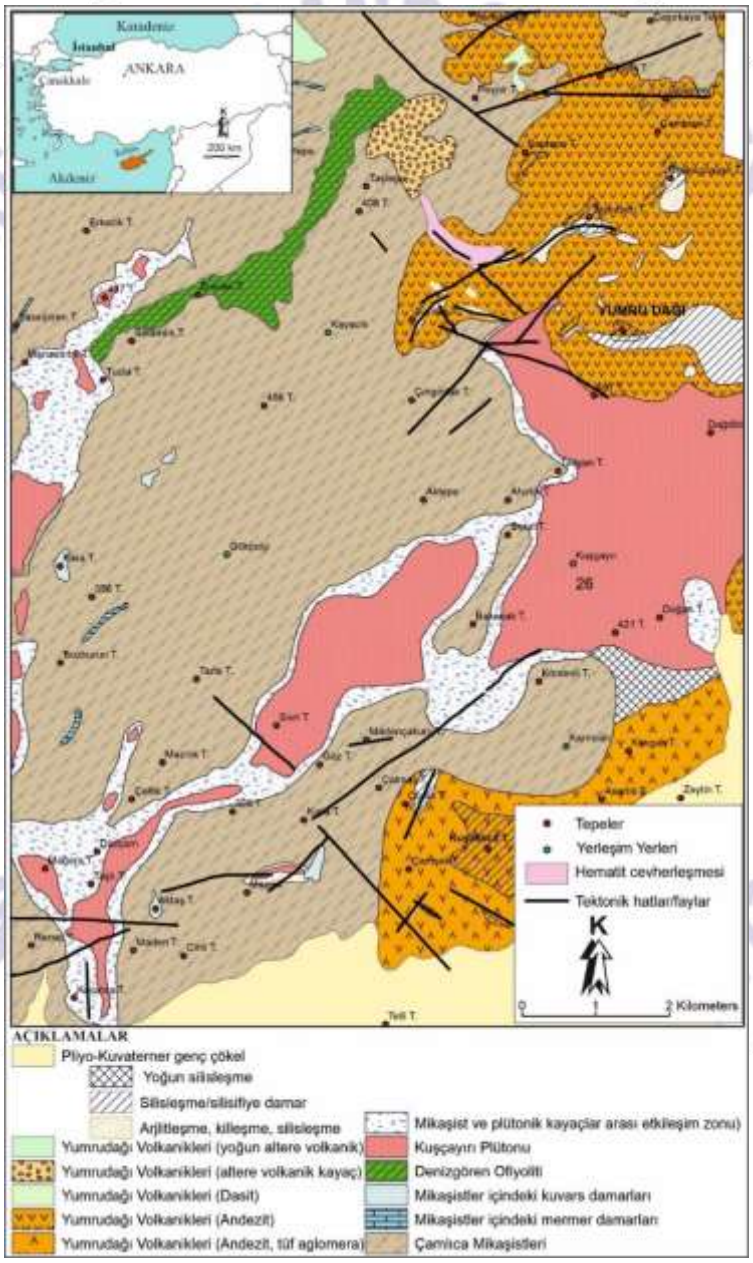

Görsel 5. Çalışma sahası jeoloji haritası (Vural [1]'dan değiştirilerek)

Görsel 6. Yumrudağı altere volkanik kayaçları (avk) ve onları keser konumdaki dasit porfirler (dp), (Kartaldağı, KD'ya bakış)

3.1. Yumrudağı Volkanitlerinin Mineralojik-Petrografik Özellikleri

Sahadan alınan volkanik kayaç örneklerine ait ince kesitlerin mikroskobik incelenmesi sonucu kayaçların dokusal özellikleri ile mineralojik-petrografik bileşimleri belirlenmiştir. Yumrudağı Volkanikleri genelde andezit bileşimlidir. Andezitlerin mikroskobik incelemesinde porfirik ve mikrolitik porfirik dokular gözlenir (Görsel 5). Başlıca mineraller plajiyoklaz ve amfibol fenokristallerinden oluşmakta olup, opak mineraller ile birlikte aynı minerallerin mikrolitlerinden oluşan bir hamur içinde yer alırlar. Plajiyoklaz 0.4 mm ile 4.5 mm arasında değişen tane boyunda, öz şekilli taneler halinde olup yer yer serisitleşmiş ve karbonatlaşmıştır. Bazı minerallerde albit ikizi, bazılarında da polisentetik ikiz görülür. Plajiyoklazlarda yer yer zonlu yapılar görülmektedir. (010) yüzeyine paralel kesitlerde yaklaşık 35-43 derece arasında sönme açıları göstermekte olup, andezin bileşimindedirler. Amfiboller iri öz ve yarı öz şekilli prizmatik kristaller, hamurda da küçük kristaller halinde görülür. Amfibol 0.2 mm ile 5.5 mm arasında değişen tane boyunda olup, öz şekilli olanlarda altı gen şekil net olarak gözlenmektedir. Bazı mineraller plajiyoklas ve opak mineral inklüzyonları içerirler. (010) yüzeyine paralel kesitlerde yaklaşık 24-25 derece arasında sönme açıları gösterirler. Opak mineraller irili ufaklı taneler halinde ve dağınık olarak bulunur. İkincil mineraller kalsit, klorit, serizit ve epidot minerallerinden oluşur. Kayaç, ilmenit ve ilmenomanyetit içermektedir. İlmenitler 45 mikron ile 100 mikron arasında değişen tane boyundadır. Örnekteki mafik mineraller içerisinde ufak taneler halinde hematit bulunmaktadır. Hamur plajiyoklas ve amfibol minerallerinin mikro ve kripto kristallerinden ve opak mineral tanelerinden oluşur (Görsel 5).

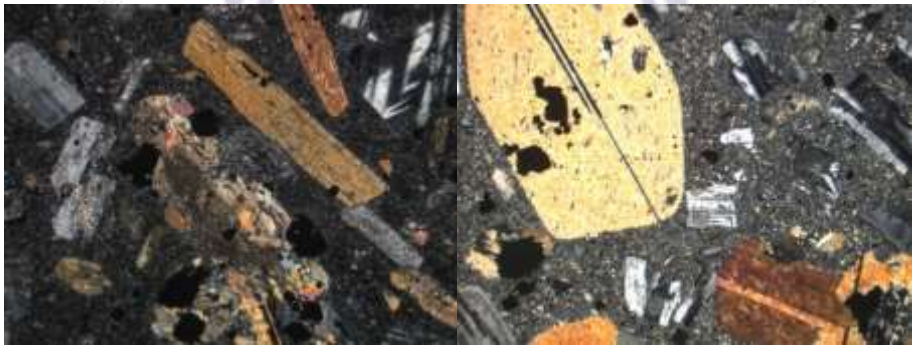

Görsel 7 (a-b)Andezitlere ait porfirik dokular ve iri amfibol mineralleri (ÇN, Pl: Plajiyoklas, Amf: Amfibol, Op: Opak mineral)

3.1. Yumrudağı Volkanitlerinin Jeokimyasal Özellikleri

Yumrudağı volkanitlerine ait örneklerin ana, iz element ve nadir toprak element (NTE) analizleri Vural [1; Ek-2]'da verilmiş olup, volkanitlerin SiO_2 içerikleri % 58-62, K_2O içerikleri 1.4-3.0, Fe_2O_3 içerikleri 4.8-7.4 ve Mg numaraları (Mg#) 41-52 arasında değişmektedir. Volkanitlerin K_2O/Na_2O oranları 0.5-1.2 arasındadır. SiO_2'ye karşı (Na_2O+K_2O) diyagramında [34], Yumrudağı volkanitlerinin subalkalen karakterli genelde andezit ve az oranda da traki-andezit bileşimli kayaçlardan oluştuğu görülür (Görsel 6a). Winchester ve Floyd [35]'un SiO_2-Zr/TiO_2 diyagramında örnekler genelde andezit ve az oranda da traki-andezit bileşimli kayaçlardan oluşur (Görsel 6b).

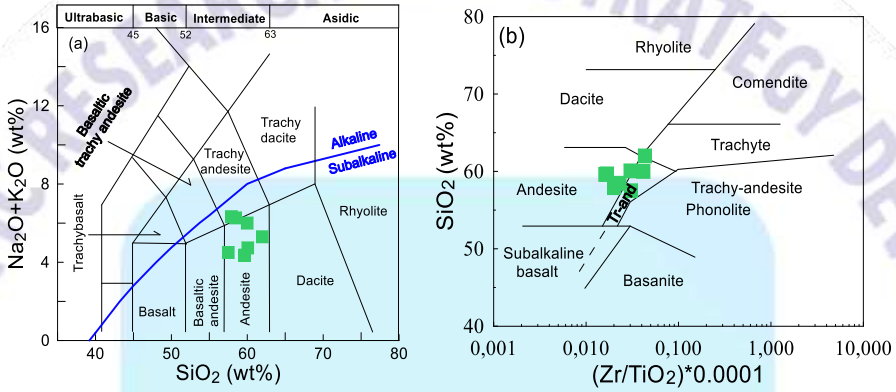

Görsel 8. Yumrudağı volkanitlerine ait örneklerin a) SiO_2'e karşı toplam alkali (Na_2O+K_2O) diyagramı [34] (Alkali/Subalkali ayrımı eğrisi Irvine ve Baragar, [36]'den alınmıştır), b) SiO_2-Zr/TiO_2 diyagramı [35]

Kayaç örnekleri K_2O-SiO_2 diyagramına [34 ve,37] düşürüldüğünde, orta-yüksek potasyum içeriğine sahip oldukları görülür (Görsel 7a). AFM diyagramında örneklerin tümü kalk-alkalen karakterlidir (Görsel 7b).

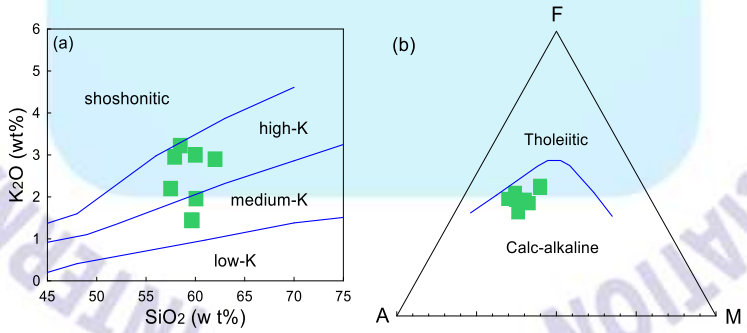

Görsel 9. Yumrudağı volkanitlerine ait örneklerin a) SiO_2'e karşı K_2O diyagramı [34], b) AFM diyagramı (Toleyitik-kalk alkali ayrımı eğrisi Irvine ve Baragar, [36]'den alınmıştır)

SiO_2'ye karşı ana element değişim diyagramlarının (Görsel 8) bir kısmında düzensiz dağılımlar gözlenmekle birlikte, yer yer iyi korelasyonlar vermeleri, volkanitlerin gelişiminde ayrımlaşmanın oldukça önemli bir rol oynadığına işaret etmektedir. Ana elementlerde SiO_2 değerleri arttıkça CaO, MgO, $Fe_2O_3^T$, TiO_2 ve P_2O_5 azalarak iyi derecede negatif bir ilişki gösterirler (Görsel 8c-e). Na_2O ve Al_2O_3'te SiO_2 arttıkça düzensiz bir ilişki görülür. K_2O değerlerinde ise SiO_2 artışına paralel olarak pozitif bir korelasyon gözlenir (Görsel 8).

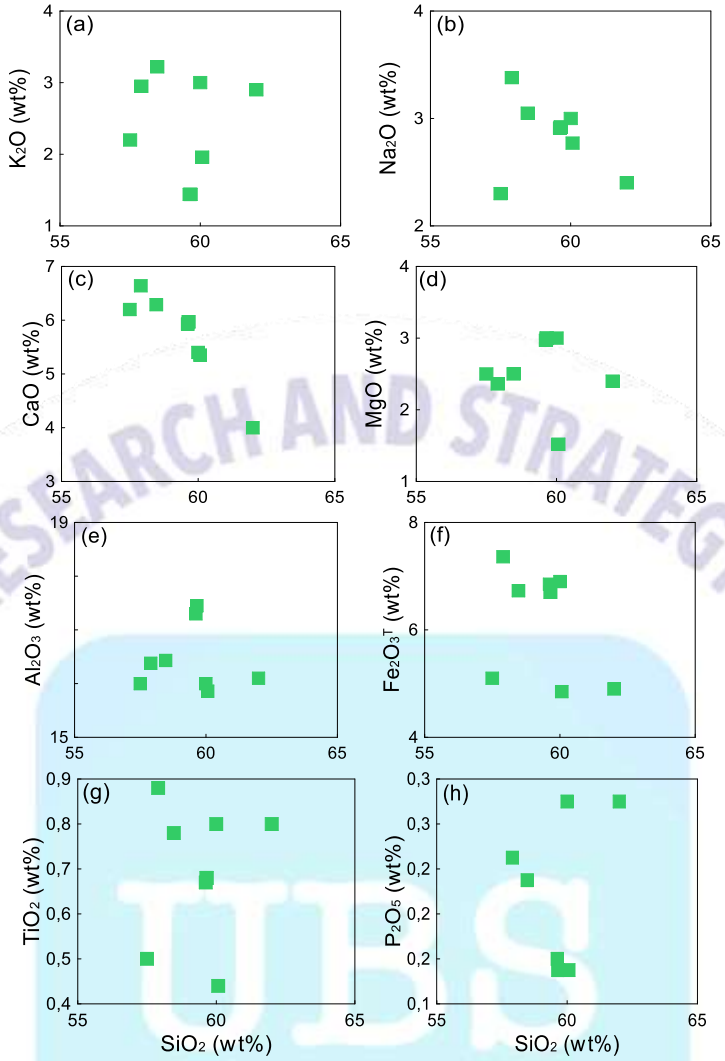

Görsel 10. Yumrudağı volkanitlerine ait kayaç örneklerinin SiO_2'ye karşı ana element değişim diyagramları

SiO_2'ye karşı iz element değişim diyagramlarında; SiO_2 arttıkça Zr, Rb ve Nb değerlerinde pozitif bir ilişki gözlenirken; Ba ve Sr'da negatif bir ilişki gözlenir (Görsel 9a-h).

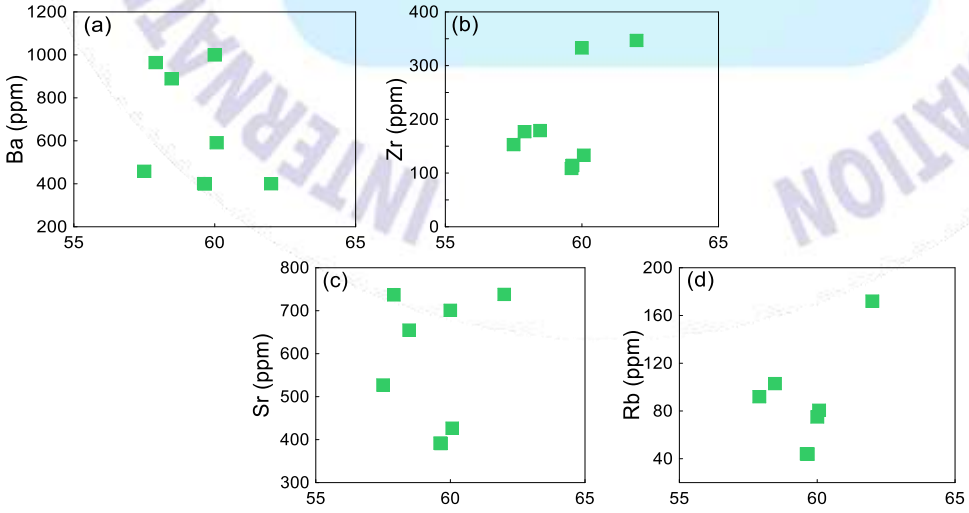

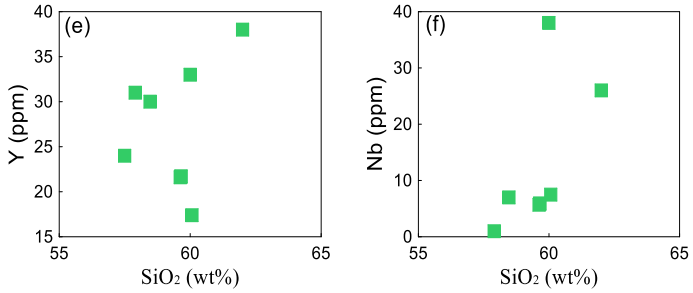

Görsel 11. Yumrudağı volkanitlerine ait kayaç örneklerinin SiO_2'ye karşı iz element değişim diyagramları

Örneklerin ilksel mantoya [38] göre normalleştirilmiş olan iz element değişim diyagramında Sr, K, Rb, Ba, Th, U, Pb ve Nd konsantrasyonları bakımından zenginleşme gözlenirken; Ti, Nb, Ce, Pr, P ve Ta bakımından fakirleşme izlenmektedir (Görsel 10a). İncelenen volkanitlerin kondrite [39] normalize edilmiş nadir toprak element (NTE) dağılımları genel olarak birbirine benzerlik göstermektedir (Görsel 10b). Bu durum, inceleme alanındaki volkanitleri oluşturan kayaçların benzer manto kaynağından türediklerini işaret etmektedir. Volkanik kayaç örneklerinin kondrite normalize edilmiş nadir toprak element dağılım diyagramlarında (Görsel 10b), hafif nadir toprak elementler, ağır nadir toprak elementlere göre daha fazla zenginleşmiştir. Örneklerin $(La/Lu)_N$ oranları 4.63-10.39 arasında değişir (Vural 2006, Ek-2). Örneklerin tümünde hafif negatif Eu anomalisi gözlenmemekte olup (Görsel 10b), $(Eu/Eu^*)_N$ oranları 0.82-0.93 arasındadır (Vural 2006, Ek-2).

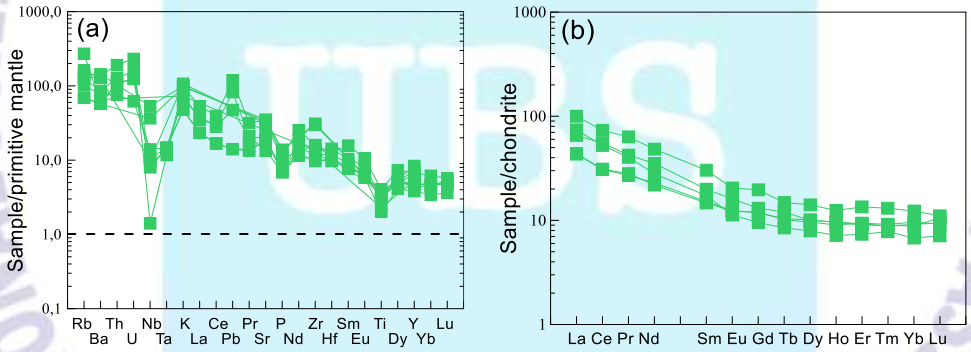

Görsel 12. Yumrudağı volkanitlerine ait kayaçların (a) ilksel mantoya göre [38] (b) kondirite [39] göre normalize edilmiş iz element dağılım diyagramları

Ce/Pb'ye karşı Ce diyagramında (Görsel 11a), çalışılan volkanik kayaçlara ait örnekler yay volkanikleri alanında yer alırlar. Örneklerde gözlenen düşük Ce/Pb oranları (3.2 ila 11.4), okyanusal bazaltlardan (20 ila 30) [40,41] farklı olup, bu durum çalışılan volkanik kayaçların astenosferik manto kaynağından türemediğini gösterir. Yüksek Nb/La oranları (>1) okyanus adası bazalt (OIB) benzeri astenosferik manto kaynağını, düşük oranlar (<0.5) ise litosferik manto kaynağına işaret eder [42,43]. Bu nedenle, Nb/La ve La/Yb oranları volkanik kayaçlarda kısmı ergime derecesi ve kaynak bileşiminin belirlenmesinde faydalıdır [44]. İncelenen volkanik kayaçlarının Nb/La oranları 0.03 ila 0.37 arasında ve La/Yb oranları 6.7 ila 16.1 arasında olup [1; Ek-2], spinel lerzolitik litosferik manto kaynağına işaret eder (Görsel 11b).

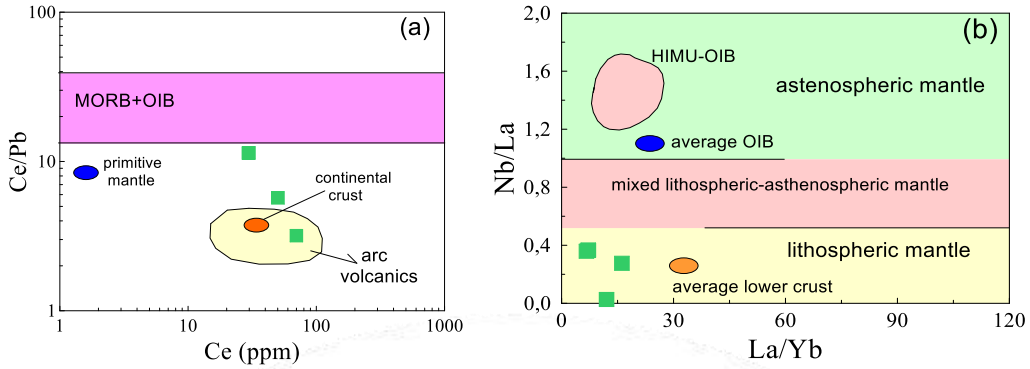

Görsel 13. Yumrudağı volkanitlerinin; (a) Ce/Pb karşı Ce diyagramı (ilksel manto değerleri Hofmann, [40]'den, kıtasal kabuk, OOSB, OAB ve yay volkanitleri Schmidberger ve Hegner, [45]'dan alınmıştır). (b) La/Yb'ye karşı Nb/La diyagramı (OAB değerleri, Fitton vd., [46]'den, ortalama alt kabuk değerleri, Chen ve Arculus, [47]'den, HIMU+OAB alanları, Weaver vd., [48]'den, astenosferik, litosferik ve karışım manto alanlarını ayıran çizgi Smith vd., [43]'dan alınmıştır)

Elde edilen veriler ışığında tüm kayaç ana, iz ve nadir toprak element verileri dikkate alındığında, volkanitlerin gelişiminde hornblend, plajiyoklas ve Fe-Ti oksit ayrımlaşmasının önemli olduğu görülür. Yumrudağı volkanik kayaçlarında gözlenen LILE element (K, Sr, Rb ve Ba), Th ve Ce zenginleşmesi, yüksek Th/Yb oranları, volkanitlerin ana magmasının litosferik manto kaynağından türemiş olabileceğini gösterir [49–53].

4. SONUÇLAR

- İnceleme alanında Permo-Triyas'dan Tersiyere kadar değişen yaşta kayaçlar yer alır.
- Yumrudağı volkanitlerini oluşturan andezit türü kayaçlar genellikle mikrolitik porfirik ve porfirik dokulu olup, başlıca mineraller plajiyoklas ve hornblend fenokristallerinden oluşur.
- Değişim diyagramlarında gözlenen iyi derecede pozitif ve negatif ilişkiler, kayaçların gelişiminde fraksiyonel kristallenmenin etkili olduğunu gösterir.
- Volkanitlerin ilksel mantoya göre normalize edilmiş iz element dağılımları, özellikle büyük iyon yarıçaplı litofil elementler (LILE) ve hafif nadir toprak elementler (LREE) bakımından zenginleşme, fakat yüksek çekim alanlı elementler (HFSE) bakımından fakirleşme göstermektedir.
- Kondrite göre normalize edilmiş nadir toprak element dağılımları, düşük-orta derecede zenginleşmeyle (La_N/Lu_N = 4.6 ila 10.4) konkav şekilli olup, genellikle birbirine paralel dağılım göstermeleri benzer kaynaktan itibaren oluştuğunu gösterir.
- İncelenen Yumrudağı volkanitlerin petrografik ve jeokimyasal özellikleri dikkate alındığında, volkanitlerin köken magmasının muhtemelen litosferik manto kaynağının kısmi ergimesi ile oluştuğunu göstermektedir.

Acknowledgment

Bu çalışma sorumlu yazarın doktora tezi verilerinden yararlanılarak üretilmiş olup, yazar Maden Tetkik ve Arama Genel Müdürlüğü çalışanlarına ve tez danışmanı Prof. Dr. Doğan Aydal'a teşekkür eder.

KAYNAKÇA

[1] Vural A. Bayramiç (Çanakkale) ve Çevresindeki Altın Zenginleşmelerinin Araştırılması. Ankara Üniversitesi, 2006.

[2] Vural A, Aydal D. Bayramiç ve Yakın Çevresindeki Altın Zenginleşmelerinin Araştırılması. 69. Türkiye Jeoloji Kurultayı, Ankara, Türkiye: Türkiye Jeoloji Kurultayı; 2016, s. 376–7.
[3] Aydal D, Vural A, Taşdelen Uslu İ, Aydal EG. Crosta Technique Application on Bayramiç (Alakeçi-Kısacık) Mineralized Area by Using Landsat 7 Etm+ Data. Journal of Engineering and Architecture Faculty of Selcuk University 2007;22:29–40.
[4] Aydal D, Vural A, Taşdelen Uslu İ, Aydal EG. Investigation of Kuşçayırı-Kartaldağı (Bayramiç-Çanakkale) mineral enhancement region by Crosta technique with LANDSAT 7 ETM+ bands. Technical University of İstanbul, First Remote Sensing Workshop and Panel, İstanbul, Türkiye: 2006, s. 11.
[5] Aydal D, Vural A, Polat O. Definition of the Base Metal and Gold Bearing Hydrotermally Altered Areas in Volcanic Rocks Using by Landsat 7 TM Imagery: Case Study from Bayramiç (Çanakkale). 57th Geology Congress, Ankara, Türkiye: 2004, s. 89–90.
[6] Vural A, Aydal D. Soil geochemical prospecting at listvenite area, Bayramiç, (Çanakkale Turkey). 34th National and the 2nd International Geosciences Congress, Tehran, Iran: 2016.
[7] Aydal D, Vural A, Taşdelen Uslu İ, Aydal EG. Crosta Technique Application on Bayramic (Alakeçi-Kisacik) Mineralized Area by Using Landsat 7 TM Data. 30th Anniversary Fikret Kurtman Geology Symposium, Konya, Türkiye: 2006, s. 195.
[8] Vural A, Aydal D. Using soil geochemistry for gold exploration:Ayvacık (Çanakkale-Northwest Turkey). 34th National and the 2nd International Geosciences Congress, Tehran, Iran: 2016.
[9] Vural A, Aydal D, Akpınar İ. A low sulphur epithermal gold mineralization in Kisacik-Ayvacik area (Çanakkale-Turkey). Goldschmidt Conference Abstracts, Prague, Czech Republic: 2011, s. 2105.
[10] Vural A, Aydal D. Soil geochemistry study of the listvenite area of Ayvacik (Çanakkale, Turkey). Caspian Journal of Environmental Sciences 2020;18:205–15.
[11] Aygen T. Balya bölgesi jeolojisinin incelenmesi. Ankara, Türkiye: 1956.
[12] Bingöl E. Geology of Biga Peninsula and some characteristics of Karakaya Formation. International Geodynamics Project, Report of Turkey, Ankara, Turkey: Maden Tetkik ve Arama Genel Müdürlüğü; 1975, s. 71–7.
[13] Geis H. Kuzey Kazdağ'ının Jeolojik yapısı. Ankara: 1953.
[14] Gözler MZ. Kazdağ batısı Mıhlı Dere Vadisinin jeolojik petrografik incelemesi. Geological Bulletin of Turkey 1986;29:133–42.
[15] Gümüş A. Important lead-zinc deposits of Turkey. Symposium on Mining Geology and the Base Metals, CENTO, Ankara, Turkey: 1964, s. 155–68.
[16] Kaaden G. Age relations of magmatic activüy and metamorphic processes in the northwestern part of Anatolia, Turkey. Bulletin of the Mineral Research and Exploration 1959;52:15–33.
[17] Kalafatçıoğlu A. Geology around Ezine and Bozcaada and the age of the li-mestones and serpentines. Bulletin of the Mineral Research and Exploration 1963;60:61–70.
[18] Okay Aİ, Satır M, Maltiski H, Siyako M, Metzger R, Akyüz S. Paleo- and Neo-Tethyan events in Northwest Turkey: geoiogical and geochronological constraints. Tectonics of Asia, Cambridge University Pres; 1996, s. 420–1.
[19] Schuiling RD. Kazdağ kristalerinin arz Pre-Hersiniyen iltiva safhası hakkında. Bulletin of the Mineral Research and Exploration 1959;53:87–91.
[20] Yigit O. Gold in Turkey - A missing link in Tethyan metallogeny. Ore Geology Reviews 2006;28:147–79. https://doi.org/10.1016/j.oregeorev.2005.04.003.
[21] Vural A, Kaya S, Başaran N, Songören OT. Anadolu Madenciliğinde İlk Adımlar.

Ankara, Türkiye: Maden Tetkik ve Arama Genel Müdürlüğü, MTA Kültür Serisi-3; 2009.
[22] Vural A. Güneyköy ve Çevresi (Eşme-Uşak) Arsenopirit Cevherleşmelerinin Maden Jeolojisi. Ankara Üniversitesi, 1998.
[23] Vural A, Ünlü T. Güneyköy ve Çevresindeki Kalıntı Altınlı Arsenopirit Cevherleşmelerinin Maden Jeolojisi Açısından İncelenmesi. 69. Türkiye Jeoloji Kurultayı, Ankara, Türkiye: Türkiye Jeoloji Kurultayı; 2016, s. 374–5.
[24] Vural A, Ünlü T. The geology and mineralogical / petrographic features of Umurbabadağ and its surroundings (Eşme , Uşak - Turkey). Journal of Engineering Research and Applied Science 2020;9:1561–87.
[25] Cavazza W, Okay Aİ, Zattin M. Rapid early-middle Miocene exhumation of the Kazdag Massif (western Anatolia). International Journal of Earht Sciences 2009;98:1935–47.
[26] Okay Aİ, Siyako M, Bürkan KA. Biga yarımadasının jeolojisi ve tektonik evrimi. Türkiye Petrol Jeologları Derneği Bülteni 1990;2:83–121.
[27] Aldanmaz E. Mantle source characteristics of alkali basalts and basanites in an extensional intracontinental plate setting, Western Anatolia, Turkey: Implications for multi-stage melting. International Geology Review 2002;44:440–57. https://doi.org/10.2747/0020-6814.44.5.440.
[28] Ercan T, Satir M, Steinitz G, Dora A, Sarifakioglu E, Adis C, vd. Characteristic of Tertiary volcanism in the Biga Peninsula and Gökçeada, Bozcaada and Tavşan islands (NW Anatolia). Bull Miner Res Explor Inst Turk 1995;117:55–86.
[29] Genç ŞC. Evolution of the Bayramiç magmatic complex, Northwestern Anatolia. Journal of Volcanology and Geothermal Research 1998;85:233–49.
[30] Karacik Z, Yilmaz Y. Geology of the ignimbrites and the associated volcano-plutonic complex of the Ezine area, northwestern Anatolia. Journal of Volcanology and Geothermal Research 1998;85:251–64. https://doi.org/10.1016/S0377-0273(98)00058-4.
[31] Vural A, Aydal D. Determination of Lithological Differences and Hydrothermal Alteration Areas by Remote Sensing Studies: Kısacık (Ayvacık-Çanakkale, Biga Peninsula, Turkey). Journal of Engineering Research and Applied Science 2020;9:1341–57.
[32] Vural A, Kaygusuz A. Alakeçi-Kısacık volkanitlerinin Petrografisi ve Jeokimyası (KB Türkiye). 4th International European Conference on Interdisciplinary Scientific Research, Warsaw, Poland: 2021, s. 1–14.
[33] Vural A, Kaygusuz A. Kuşçayırı Plütonunun Petrografisi, Jeokimyası ve Petrolojisi (KB Türkiye). 4th International European Conference on Interdisciplinary Scientific Research, Warsaw, Poland: 2021, s. 51–69.
[34] Le Maitre RW, Bateman P, Dudek A, Keller J, Lameyre J, Le Bas MJ, vd. A Classification of Igneous Rocks and Glossary of Terms: Recommendations of the International Union of Geological Sciences Subcommission on the Systematics of Igneous rocks. Blackwell Scientific Publications, Oxford, U.K.; 1989.
[35] Winchester JA, Floyd PA. Geochemical discrimination of different magma series and their differentiation products using immobile elements. Chemical Geology 1977;20:325–43. https://doi.org/10.1016/0009-2541(77)90057-2.
[36] Irvine TN, Baragar WRA. A guide to the chemical classification of the common volcanic rocks. Canadian Journal of Earth Sciences 1971;8:523–48.
[37] Rickwood PC. Boundary lines within petrologic diagrams which use oxides of major and minor elements. Lithos 1989;22:247–63. https://doi.org/10.1016/0024-4937(89)90028-5.

[38] Sun SS, McDonough WF. Chemical and isotopic systematics of oceanic basalts: Implications for mantle composition and processes. Geological Society Special Publication 1989;42:313–45. https://doi.org/10.1144/GSL.SP.1989.042.01.19.
[39] Taylor SR, McLennan SM. The Continental Crust; its Composition and Evolution Geoscience Text. Blackwell Scientific Publications, Oxford, U.K.; 1985.
[40] Hofmann AW. Chemical differentiation of the Earth: the relationship between mantle, continental crust, and the oceanic crust. Earth Planet Sciences Letters 1988;90:297–314.
[41] Hofmann AW. Mantle geochemistry: The message from oceanic volcanism. Nature 1997;385:218–29. https://doi.org/10.1038/385218a0.
[42] Bradshaw TK, Smith EI. Polygenetic Quaternary volcanism at Crater Flat, Nevada. Journal of Volcanology and Geothermal Research 1994;63:165–82. https://doi.org/10.1016/0377-0273(94)90072-8.
[43] Smith EI, Sanchez A, Walker JD, Wang K. Geochemistry of mafic magmas in the Hurricane Volcanic field, Utah: implications for small- and large-scale chemical variability of the lithospheric mantle. Journal of Geology 1999;107:433–448.
[44] Jahn BM, Wu FY, Lo CH. Crust-mantle interaction induced by deep subduction of the continental crust: geochemical and Sr-Nd isotopic evidence from post-collisional mafic-ultramafic intrusions of the northern Dabie Complex, Central China. Chemical Geology 1999;157:119–46.
[45] Schmidberger S, Hegner E. Geochemistry and isotope systematics of calc-alkaline volcanic rocks from the Saar-Nahe basin (SW Germany). Implications for Late Hercynian orogenic development. Contributions to Mineralogy and Petrology 1999;135:373–85.
[46] Fitton JG, James D, Leeman WP. Basic magmatism associated with late Cenozoic extension in the western United States: compositional variations in space and time. Journal of Geophysical Research 1991;96. https://doi.org/10.1029/91jb00372.
[47] Chen W, Arculus RJ. Geochemical and isotopic characteristics of lower crustal xenoliths, San Francisco Volcanic Field, Arizona, U.S.A. Lithos 1995;36:203–25. https://doi.org/10.1016/0024-4937(95)00018-6.
[48] Weaver BL, Wood DA, Tarney J, Joron J. Geochemistry of ocean island basalt from the South Atlantic: Ascension, Bouvet, St. Helena, Gough and Tristan da Cunda. Içinde: Fitton J., Upton BGJ, editörler. Alkaline igneous rocks, Geological Society, London, Special Publications, 30,; 1987, s. 253–67.
[49] Pearce JA, Peate DW. Tectonic implications of the composition of volcanic arc magmas. Annual Review of Earth and Planetary Sciences 1995;23:251–285.
[50] Churikova T, Dorendorf F, Worner G. Sources and fluids in the mantle wedge below Kamchatka, Evidence from across-arc geochemical variation. Journal of Petrology 2001;42:1567–1593.
[51] Elburg MA, Bergen MV, Hoogewerff J, Foden J, Vroon P, Zulkarnain I, vd. Geochemical trends across an arc-continent collision zone: magma sources and slab-wedge transfer processes below the Pantar Strait volcanoes, Indonesia. Geochimica et Cosmochimica Acta 2002;66:2771–2789.
[52] McDermott F, Delfin FG, Defant MJ, Turner S, Maury R. The petrogenesis of magmas from Mt. Bulusan and Mayon in the Bicol arc, the Philippines. Contributions to Mineralogy and Petrology 2005;150:652–70.
[53] Zellmer GF, Annen C, Charlier BLA, George RMM, Turner SP, Hawkesworth CJ. Magma evolution and ascent at volcanic arcs: Constraining petrogenetic processes through rates and chronologies. Journal of Volcanology and Geothermal Research 2005;140:171–91. https://doi.org/10.1016/j.jvolgeores.2004.07.020.

ADOMIAN'S DECOMPOSITION METHOD TO GENERALIZED MAGNETO-THERMOELASTICITY

Hamdy M. Youssef, Eman A. Al-Lehaibi

Department of Mathematics-Faculty of Education-Alexandria University, Egypt

Mathematics Department, Al-Lith College, Umm Al-Qura University, Al-Lith, KSA

Abstract:

Due to many applications and problems in the fields of plasma physics, geophysics, and other many topics, the interaction between the strain field and the magnetic field has to be considered. Adomian introduced the decomposition method for solving linear and nonlinear functional equations. This method leads to accurate, computable, approximately convergent solutions of linear and nonlinear partial and ordinary differential equations even the equations with variable coefficients. This paper is dealing with a mathematical model of generalized thermoelasticity of a half-space conducting medium. A magnetic field with constant intensity acts normal to the bounding plane has been assumed. Adomian's decomposition method has been used to solve the model when the bounding plane is taken to be traction free and thermally loaded by harmonic heating. The numerical results for the temperature increment, the stress, the strain, the displacement, the induced magnetic, and the electric fields have been represented in figures. The magnetic field, the relaxation time, and the angular thermal load have significant effects on all the studied fields.

Keywords: Adomian's Decomposition Method, magneto-thermoelasticity, finite conductivity, iteration method, thermal load.

NUMERICAL APPROACH TO A MATHEMATICAL MODELING OF BIOCONVECTION DUE TO GYROTACTIC MICRO-ORGANISMS OVER A NONLINEAR INCLINED STRETCHING SHEET

Madhu Aneja, Sapna Sharma

[2]School Of Mathematics, India
T.I.E.T, India

Abstract:

The water-based bioconvection of a nanofluid containing motile gyrotactic micro-organisms over nonlinear inclined stretching sheet has been investigated. The governing nonlinear boundary layer equations of the model are reduced to a system of ordinary differential equations via Oberbeck-Boussinesq approximation and similarity transformations. Further, the modified set of equations with associated boundary conditions are solved using Finite Element Method. The impact of various pertinent parameters on the velocity, temperature, nanoparticles concentration, density of motile micro-organisms profiles are obtained and analyzed in details. The results show that with the increase in angle of inclination δ, velocity decreases while temperature, nanoparticles concentration, a density of motile micro-organisms increases. Additionally, the skin friction coefficient, Nusselt number, Sherwood number, density number are computed for various thermophysical parameters. It is noticed that increasing Brownian motion and thermophoresis parameter leads to an increase in temperature of fluid which results in a reduction in Nusselt number. On the contrary, Sherwood number rises with an increase in Brownian motion and thermophoresis parameter. The findings have been validated by comparing the results of special cases with existing studies.

Keywords: Bioconvection, inclined stretching sheet, Gyrotactic micro-organisms, Brownian motion, thermophoresis, finite element method.

Classifying and Predicting Efficiencies Using Interval DEA Grid Setting

Yiannis G. Smirlis

University of Piraeus, School of Economics, Greece

Abstract:

The classification and the prediction of efficiencies in Data Envelopment Analysis (DEA) is an important issue, especially in large scale problems or when new units frequently enter the under-assessment set. In this paper, we contribute to the subject by proposing a grid structure based on interval segmentations of the range of values for the inputs and outputs. Such intervals combined, define hyper-rectangles that partition the space of the problem. This structure, exploited by Interval DEA models and a dominance relation, acts as a DEA pre-processor, enabling the classification and prediction of efficiency scores, without applying any DEA models.

Keywords: Data envelopment analysis, interval DEA, efficiency classification, efficiency prediction.

TOPOLOGICAL SENSITIVITY ANALYSIS FOR RECONSTRUCTION OF THE INVERSE SOURCE PROBLEM FROM BOUNDARY MEASUREMENT

Maatoug Hassine, Mourad Hrizi

Department of Mathematics, Faculty of Sciences Monastir, Tunisia.
Department of Mathematics, Faculty of Sciences Monastir, Tunisia

Abstract:
In this paper, we consider a geometric inverse source problem for the heat equation with Dirichlet and Neumann boundary data. We will reconstruct the exact form of the unknown source term from additional boundary conditions. Our motivation is to detect the location, the size and the shape of source support. We present a one-shot algorithm based on the Kohn-Vogelius formulation and the topological gradient method. The geometric inverse source problem is formulated as a topology optimization one. A topological sensitivity analysis is derived from a source function. Then, we present a non-iterative numerical method for the geometric reconstruction of the source term with unknown support using a level curve of the topological gradient. Finally, we give several examples to show the viability of our presented method.

Keywords: Geometric inverse source problem, heat equation, topological sensitivity, topological optimization, Kohn-Vogelius formulation.

MATERIAL CONCEPTS AND PROCESSING METHODS FOR ELECTRICAL INSULATION

Robert Sekula
ABB Corporate Research Center, Poland

Abstract:
Epoxy composites are broadly used as an electrical insulation for the high voltage applications since only such materials can fulfill particular mechanical, thermal, and dielectric requirements. However, properties of the final product are strongly dependent on proper manufacturing process with minimized material failures, as too large shrinkage, voids and cracks. Therefore, application of proper materials (epoxy, hardener, and filler) and process parameters (mold temperature, filling time, filling velocity, initial temperature of internal parts, gelation time), as well as design and geometric parameters are essential features for final quality of the produced components. In this paper, an approach for three-dimensional modeling of all molding stages, namely filling, curing and post-curing is presented. The reactive molding simulation tool is based on a commercial CFD package, and include dedicated models describing viscosity and reaction kinetics that have been successfully implemented to simulate the reactive nature of the system with exothermic effect. Also a dedicated simulation procedure for stress and shrinkage calculations, as well as simulation results are presented in the paper. Second part of the paper is dedicated to recent developments on formulations of functional composites for electrical insulation applications, focusing on thermally conductive materials. Concepts based on filler modifications for epoxy electrical composites have been presented, including the results of the obtained properties. Finally, having in mind tough environmental regulations, in addition to current process and design aspects, an approach for product re-design has been presented focusing on replacement of epoxy material with the thermoplastic one. Such "design-for-recycling" method is one of new directions associated with development of new material and processing concepts of electrical products and brings a lot of additional research challenges. For that, one of the successful products has been presented to illustrate the presented methodology.
Keywords: Curing, epoxy insulation, numerical simulations, recycling.

AN IMPLICIT METHODOLOGY FOR THE NUMERICAL MODELING OF LOCALLY INEXTENSIBLE MEMBRANES

Aymen Laadhari
Department of Information Technology
and Electrical Engineering, Swiss Federal Institute of Technology,Zurich

Abstract:
We present in this paper a fully implicit finite element method tailored for the numerical modeling of inextensible fluidic membranes in a surrounding Newtonian fluid. We consider a highly simplified version of the Canham-Helfrich model for phospholipid membranes, in which the bending force and spontaneous curvature are disregarded. The coupled problem is formulated in a fully Eulerian framework and the membrane motion is tracked using the level set method. The resulting nonlinear problem is solved by a Newton-Raphson strategy, featuring a quadratic convergence behavior. A monolithic solver is implemented, and we report several numerical experiments aimed at model validation and illustrating the accuracy of the proposed method. We show that stability is maintained for significantly larger time steps with respect to an explicit decoupling method.

Keywords: Finite element method, Newton method, level set, Navier-Stokes, inextensible membrane, liquid drop.

MICROSTRIP PATCH ANTENNA ENHANCEMENT TECHNIQUES

Ahmad H. Abdelgwad
Fayoum University

Abstract:
Microstrip patch antennas are widely used in many wireless communication applications because of their various advantages such as light weight, compact size, inexpensive, ease of fabrication and high reliability. However, narrow bandwidth and low gain are the major drawbacks of microstrip antennas. The radiation properties of microstrip antenna is affected by many designing factors like feeding techniques, manufacturing substrate, patch and ground structure. This manuscript presents a review of the most popular gain and bandwidth enhancement methods of microstrip antenna and reports a brief description of its feeding techniques.

Keywords: Gain and bandwidth enhancement, slotted patch, parasitic patch, electromagnetic band gap, defected ground, feeding techniques.

EMAIL BASED GLOBAL AUTOMATION WITH RASPBERRY PI AND CONTROL CIRCUIT MODULE: DEVELOPMENT OF SMART HOME APPLICATION

Lochan Basyal
Amritsar College of Engineering and Technology

Abstract:
Global Automation is an emerging technology of today's era and is based on Internet of Things (IoT). Global automation deals with the controlling of electrical appliances throughout the world. The fabrication of this system has been carried out with interfacing an electrical control system module to Raspberry Pi. An electrical control system module includes a relay driver mechanism through which appliances are controlled automatically in respective condition. In this research project, one email ID has been assigned to Raspberry Pi, and the users from different location having different email ID can mail to Raspberry Pi on assigned email address "raspberrypilochan96@gmail.com" with subject heading "Device Control" with predefined command on compose email line. Also, a notification regarding current working condition of this system has been updated on respective user email ID. This approach is an innovative way of implementing smart automation system through which a user can control their electrical appliances like light, fan, television, refrigerator, etc. in their home with the use of email facility. The development of this project helps to enhance the concept of smart home application as well as industrial automation.

Keywords: Control circuit, email, global automation, internet of things, Raspberry Pi.

EFFECT OF UREA DEEP PLACEMENT TECHNOLOGY ADOPTION ON THE PRODUCTION FRONTIER: EVIDENCE FROM IRRIGATION RICE FARMERS IN THE NORTHERN REGION OF GHANA

Shaibu Baanni Azumah, William Adzawla

PhD Student with the Department of Agricultural and Resource Economics, University for Development Studies, Ghana.
Agriculture Economist and a Climate Change Economics PhD. Student, Universite Cheikh Anta Diop, WASCAL GRP- CCE, BP 5683, Dakar, Senegal

Abstract:
Rice is an important staple crop, with current demand higher than the domestic supply in Ghana. This has led to a high and unfavourable import bill. Therefore, recent policies and interventions in the agricultural sub-sector aim at promoting various improved agricultural technologies in order to improve domestic production and reduce the importation of rice. In this study, we examined the effect of the adoption of Urea Deep Placement (UDP) technology by rice farmers on the position of the production frontier. This involved 200 farmers selected through a multi stage sampling technique in the Northern region of Ghana. A Cobb-Douglas stochastic frontier model was fitted. The result showed that the adoption of UDP technology shifts the output frontier outward and also move the farmers closer to the frontier. Farmers were also operating under diminishing returns to scale which calls for redress. Other factors that significantly influenced rice production were farm size, labour, use of certified seeds and NPK fertilizer. Although there was an opportunity for improvement, the farmers were highly efficient (92%), compared to previous studies. Farmers' efficiency was improved through increased education, household size, experience, access to credit, and lack of extension service provision by MoFA. The study recommends the revision of Ghana's agricultural policy to include the UDP technology. Agricultural Extension officers of the Ministry of Food and Agriculture (MoFA) should be trained on the UDP technology to support IFDC's drive to improve adoption by rice farmers. Rice farmers are also encouraged to expand their farm lands, improve plant population, and also increase the usage of fertilizer to improve yields. Mechanisms through which credit can be made easily accessible and effectively utilised should be identified and promoted.
Keywords: Efficiency, rice farmers, stochastic frontier, UDP technology.

STRATEGY IN CONTROLLING RICE-FIELD CONVERSION IN PANGKEP REGENCY, SOUTH SULAWESI, INDONESIA

Nurliani, Ida Rosada

Indonesian Moslem University

Abstract:

The national rice consumption keeps increasing along with raising income of the households and the rapid growth of population. However, food availability, particularly rice, is limited. Impacts of rice-field conversion have run cumulatively, as we can see on potential losses of rice and crops production, as well as work opportunity that keeps increasing year-by-year. Therefore, it requires policy recommendation to control rice-field conversion through economic, social, and ecological approaches. The research was a survey method intended to: (1) Identify internal factors; quality and productivity of the land as the cause of land conversion, (2) Identify external factors of land conversion, value of the rice-field and the competitor's land, workforce absorption, and regulation, as well as (3) Formulate strategies in controlling rice-field conversion. Population of the research was farmers who applied land conversion at Pangkep Regency, South Sulawesi. Samples were determined using the incidental sampling method. Data analysis used productivity analysis, land quality analysis, total economic value analysis, and SWOT analysis. Results of the research showed that the quality of rice-field was low as well as productivity of the grains (unhulled-rice). So that, average productivity of the grains and quality of rice-field were low as well. Total economic value of rice-field was lower than the economic value of the embankment. Workforce absorption value on rice-field was higher than on the embankment. Strategies in controlling such rice-field conversion can be done by increasing rice-field productivity, improving land quality, applying cultivation technique of specific location, improving the irrigation lines, and socializing regulation and sanction about the transfer of land use.

Keywords: Land conversion, quality of rice-field, land economic value, strategy in controlling.

JIGGER FLEA (TUNGA PENETRANS) INFESTATIONS AND USE OF SOIL-COW DUNG-ASH MIXTURE AS A FLEA CONTROL METHOD IN EASTERN UGANDA

Gerald Amatre, Julius Bunny Lejju, Morgan Andama

Gerald Amatre, Kyambogo University, Kampala-Uganda
Julius Bunny Lejju, Mbarara University of Science and Technology
Morgan Andama, Mbarara University of science and Technology.

Abstract:
Despite several interventions, jigger flea infestations continue to be reported in the Busoga sub-region in Eastern Uganda. The purpose of this study was to identify factors that expose the indigenous people to jigger flea infestations and evaluate the effectiveness of any indigenous materials used in flea control by the affected communities. Flea compositions in residences were described, factors associated with flea infestation and indigenous materials used in flea control were evaluated. Field surveys were conducted in the affected communities after obtaining preliminary information on jigger infestation from the offices of the District Health Inspectors to identify the affected villages and households. Informed consent was then sought from the local authorities and household heads to conduct the study. Focus group discussions were conducted with key district informants, namely, the District Health Inspectors, District Entomologists and representatives from the District Health Office. A GPS coordinate was taken at central point at every household enrolled. Fleas were trapped inside residences using *Kilonzo traps.* A *Kilonzo Trap* comprised a shallow pan, about three centimetres deep, filled to the brim with water. The edges of the pan were smeared with Vaseline to prevent fleas from crawling out. Traps were placed in the evening and checked every morning the following day. The trapped fleas were collected in labelled vials filled with 70% aqueous ethanol and taken to the laboratory for identification. Socio-economic and environmental data were collected. The results indicate that the commonest flea trapped in the residences was the cat flea (*Ctenocephalides felis*) (50%), followed by Jigger flea (*Tunga penetrans*) (46%) and rat flea (*Xenopsylla Cheopis*) (4%), respectively. The average size of residences was seven squire metres with a mean of six occupants. The residences were generally untidy; with loose dusty floors and the brick walls were not plastered. The majority of the jigger affected households were headed by peasants (86.7%) and artisans (13.3%). The household heads mainly stopped at primary school level (80%) and few at secondary school level (20%). The jigger affected households were mainly headed by peasants of low socioeconomic status. The affected community members use soil-cow dung-ash mixture to smear floors of residences as the only measure to control fleas. This method was found to be ineffective in controlling the insects. The study recommends that home improvement campaigns be continued in the affected communities to improve sanitation and hygiene in residences as one of the interventions to combat flea infestations. Other cheap, available and effective means should be identified to curb jigger flea infestations.

Keywords: Cow dung-soil-ash mixture, infestations, Jigger flea, Tunga penetrans.

FISH CATCH COMPOSITION FROM GOBIND SAGAR RESERVOIR DURING 2006-2012

Krishan Lal, Anish Dua

NSCBM Govt. College, India
Aquatic Biology Lab., Guru Nanak Dev University, India

Abstract:
Gobind Sagar Reservoir has been created in Himachal Pradesh, India (31° 25′ N and 76 ° 25′E) by damming River Sutlej at village Bhakra in 1963. The average water spread area of this reservoir is 10,000 hectares. Fishermen have organized themselves in the form of co-operative societies. 26 fisheries co-operative societies were working in Gobind Sagar Reservoir up till 2012. June and July months were observed as closed season, no fishing was done during this period. Proper record maintaining of fish catch was done at different levels by the state fisheries department. Different measures like minimum harvestable size, mesh size regulation and prohibition of illegal fishing etc. were taken for fish conservation. Fishermen were actively involved in the management. Gill nets were used for catching fishes from this reservoir. State fisheries department is realizing 15% royalty of the sold fish. Data used in this paper is about the fish catch during 2006-2012 and were obtained from the state fisheries department, Himachal Pradesh. *Catla catla*, *Labeo rohita*, *Cirrhinus mrigala*, *Sperata seenghala*, *Cyprinus carpio*, *Tor putitora*, *Hypophthalmichthys molitrix*, *Labeo calbasu*, *Labeo dero* and *Ctenopharyngodon idella* etc., were the fish species exploited for commercial purposes. Total number of individuals of all species caught was 3141236 weighing 5637108.9 kg during 2006-2012. *H. molitrix* was introduced accidently in this reservoir and was making a good share of fish catch in this reservoir. The annual catch of this species was varying between 161279.6 kg, caught in 2011 and 788030.8 kg caught in 2009. Total numbers of individuals of *C. idella* caught were 8966 weighing 64320.2 kg. The catch of *Cyprinus carpio* was varying between 144826.1 kg caught in 2006 and 214480.1 kg caught in 2010. Total catch of *Tor putitora* was 180263.2 kg during 2006-2012. Total catch of *L. dero, S. seenghala* and *Catla catla* remained 100637.4 kg, 75297.8 kg and 561802.9 kg, respectively, during 2006-2012. Maximum fish catch was observed during the months of August (after observing Closed Season). Maximum catch of exotic carps was from Bhakra area of the reservoir which has fewer fluctuations in water levels. The reservoir has been divided into eight beats for administrative purpose, to avoid conflicts between operating fisheries co-operative societies for area of operation. Fish catch was more by co-operative societies operating in the area of reservoir having fewer fluctuations in water level and catch was less by co-operative societies operating in the area of more fluctuations in water level. Species-wise fish catch by different co-operative societies from their allotted area was studied. This reservoir is one of most scientifically managed reservoirs.
Keywords: Co-operative societies, fish catch, fish species, reservoir.

EFFECT OF STITCHING PATTERN ON COMPOSITE TUBULAR STRUCTURES SUBJECTED TO QUASI-STATIC CRUSHING

Ali Rabiee, Hessam Ghasemnejad
Cranfield University

Abstract:
Extensive experimental investigation on the effect of stitching pattern on tubular composite structures was conducted. The effect of stitching reinforcement through thickness on using glass flux yarn on energy absorption of fiber-reinforced polymer (FRP) was investigated under high speed loading conditions at axial loading. Keeping the mass of the structure at 125 grams and applying different pattern of stitching at various locations in theory enables better energy absorption, and also enables the control over the behaviour of force-crush distance curve. The study consists of simple non-stitch absorber comparison with single and multi-location stitching behaviour and its effect on energy absorption capabilities. The locations of reinforcements are 10 mm, 20 mm, 30 mm, 10-20 mm, 10-30 mm, 20-30 mm, 10-20-30 mm and 10-15-20-25-30-35 mm from the top of the specimen. The effect of through the thickness reinforcements has shown increase in energy absorption capabilities and crushing load. The significance of this is that as the stitching locations are closer, the crushing load increases and consequently energy absorption capabilities are also increased. The implementation of this idea would improve the mean force by applying stitching and controlling the behaviour of force-crush distance curve.

Keywords: Through-thickness, stitching, reinforcement, Tulbular composite structures, energy absorption.

NUMERICAL HEAT TRANSFER PERFORMANCE OF WATER-BASED GRAPHENE NANOPLATELETS

Ahmad Amiri, Hamed K. Arzani, S. N. Kazi, B. T. Chew

Abstract:

Since graphene nanoplatelet (GNP) is a promising material due to desirable thermal properties, this paper is related to the thermophysical and heat transfer performance of covalently functionalized GNP-based water/ethylene glycol nanofluid through an annular channel. After experimentally measuring thermophysical properties of prepared samples, a computational fluid dynamics study has been carried out to examine the heat transfer and pressure drop of well-dispersed and stabilized nanofluids. The effect of concentration of GNP and Reynolds number at constant wall temperature boundary condition under turbulent flow regime on convective heat transfer coefficient has been investigated. Based on the results, for different Reynolds numbers, the convective heat transfer coefficient of the prepared nanofluid is higher than that of the base fluid. Also, the enhancement of convective heat transfer coefficient and thermal conductivity increase with the increase of GNP concentration in base-fluid. Based on the results of this investigation, there is a significant enhancement on the heat transfer rate associated with loading well-dispersed GNP in base-fluid.

Keywords: Nanofluid, turbulent flow, forced convection flow, graphene, annular, annulus.

BIOCONTROL EFFECTIVENESS OF INDIGENOUS TRICHODERMA SPECIES AGAINST MELOIDOGYNE JAVANICA AND FUSARIUM OXYSPORUM F. SP. RADICIS LYCOPERSICI ON TOMATO

Hajji Lobna, Chattaoui Mayssa, Regaieg Hajer, M'Hamdi-Boughalleb Naima, Rhouma Ali, Horrigue-Raouani Najet

High Agronomic Institute of Chott Mariem, Tunis

Abstract:

In this study, three local isolates of *Trichoderma* (Tr1: *T. viride*, Tr2: *T. harzianum* and Tr3: *T. asperellum*) were isolated and evaluated for their biocontrol effectiveness under *in vitro* conditions and in greenhouse. *In vitro* bioassay revealed a biopotential control against *Fusarium oxysporum* f. sp. *radicis lycopersici* and *Meloidogyne javanica* (RKN) separately. All species of *Trichoderma* exhibited biocontrol performance and (Tr1) *Trichoderma viride* was the most efficient. In fact, growth rate inhibition of *Fusarium oxysporum* f. sp. *radicis lycopersici* (FORL) was reached 75.5% with Tr1. Parasitism rate of root-knot nematode was 60% for juveniles and 75% for eggs with the same one. Pots experiment results showed that Tr1 and Tr2, compared to chemical treatment, enhanced the plant growth and exhibited better antagonism against root-knot nematode and root-rot fungi separated or combined. All *Trichoderma* isolates revealed a bioprotection potential against *Fusarium oxysporum* f. sp. *radicis lycopersici*. When pathogen fungi inoculated alone, Fusarium wilt index and browning vascular rate were reduced significantly with Tr1 (0.91, 2.38%) and Tr2 (1.5, 5.5%), respectively. In the case of combined infection with Fusarium and nematode, the same isolate of *Trichoderma* Tr1 and Tr2 decreased Fusarium wilt index at 1.1 and 0.83 and reduced the browning vascular rate at 6.5% and 6%, respectively. Similarly, the isolate Tr1 and Tr2 caused maximum inhibition of nematode multiplication. Multiplication rate was declined at 4% with both isolates either tomato infected by nematode separately or concomitantly with Fusarium. The chemical treatment was moderate in activity against *Meloidogyne javanica* and *Fusarium oxysporum f. sp. radicis lycopersici* alone and combined.

Keywords: Trichoderma spp., Meloidogyne javanica, Fusarium oxysporum f.sp. radicis lycopersici, biocontrol.

A SIMULATION MODEL AND PARAMETRIC STUDY OF TRIPLE-EFFECT DESALINATION PLANT

[1]Maha BenHamad, [2]Ali Snoussi, [3]Ammar Ben Brahim

[1]National engineering school of Gabes, Tunisia

[2,3] National engineering school of Gabes, Tunisia

Abstract:

A steady-state analysis of triple-effect thermal vapor compressor desalination unit was performed. A mathematical model based on mass, salinity and energy balances is developed. The purpose of this paper is to develop a connection between process simulator and process optimizer in order to study the influence of several operating variables on the performance and the produced water cost of the unit. A MATLAB program is used to solve the model equations, and Aspen HYSYS is used to model the plant. The model validity is examined against a commercial plant and showed a good agreement between industrial data and simulations results. Results show that the pressures of the last effect and the compressed vapor have an important influence on the produced cost, and the increase of the difference temperature in the condenser decreases the specific heat area about 22%.

Keywords: Steady-state, triple effect, thermal vapor compressor, MATLAB, Aspen HYSYS.

A MULTIOBJECTIVE DAMPING FUNCTION FOR COORDINATED CONTROL OF POWER SYSTEM STABILIZER AND POWER OSCILLATION DAMPING

Jose D. Herrera, Mario A. Rios

Universidad de los Andes, Bogata, Colombia

Abstract:

This paper deals with the coordinated tuning of the Power System Stabilizer (PSS) controller and Power Oscillation Damping (POD) Controller of Flexible AC Transmission System (FACTS) in a multi-machine power systems. The coordinated tuning is based on the critical eigenvalues of the power system and a model reduction technique where the Hankel Singular Value method is applied. Through the linearized system model and the parameter-constrained nonlinear optimization algorithm, it can compute the parameters of both controllers. Moreover, the parameters are optimized simultaneously obtaining the gains of both controllers. Then, the nonlinear simulation to observe the time response of the controller is performed.

Keywords: Balanced realization, controllability Grammian, electromechanical oscillations, FACTS, Hankel singular values, observability Grammian, POD, PSS.

EXERGY BASED PERFORMANCE ANALYSIS OF A GAS TURBINE UNIT AT VARIOUS AMBIENT CONDITIONS

Idris A. Elfeituri

Department of Mechanical Engineering, University of Benghazi, Benghazi City, P.O.

Abstract:

This paper studies the effect of ambient conditions on the performance of a 285 MW gas turbine unit using the exergy concept. Based on the available exergy balance models developed, a computer program has been constructed to investigate the performance of the power plant under varying ambient temperature and relative humidity conditions. The variations of ambient temperature range from zero to 50 ºC and the relative humidity ranges from zero to 100%, while the unit load kept constant at 100% of the design load. The exergy destruction ratio and exergy efficiency are determined for each component and for the entire plant. The results show a moderate increase in the total exergy destruction ratio of the plant from 62.05% to 65.20%, while the overall exergy efficiency decrease from 38.2% to 34.8% as the ambient temperature increases from zero to 50 ºC at all relative humidity values. Furthermore, an increase of 1 ºC in ambient temperature leads to 0.063% increase in the total exergy destruction ratio and 0.07% decrease in the overall exergy efficiency. The relative humidity has a remarkable influence at higher ambient temperature values on the exergy destruction ratio of combustion chamber and on exergy loss ratio of the exhaust gas but almost no effect on the total exergy destruction ratio and overall exergy efficiency. At 50 ºC ambient temperature, the exergy destruction ratio of the combustion chamber increases from 30% to 52% while the exergy loss ratio of the exhaust gas decreases from 28% to 8% as the relative humidity increases from zero to 100%. In addition, exergy analysis reveals that the combustion chamber and exhaust gas are the main source of irreversibility in the gas turbine unit. It is also identified that the exergy efficiency and exergy destruction ratio are considerably dependent on the variations in the ambient air temperature and relative humidity. Therefore, the incorporation of the existing gas turbine plant with inlet air cooling and humidifier technologies should be considered seriously.

Keywords: Destruction, exergy, gas turbine, irreversibility, performance.

DETERMINATION OF THE OPTIMAL DG PV INTERCONNECTION LOCATION USING LOSSES AND VOLTAGE REGULATION AS ASSESSMENT INDICATORS CASE STUDY: ECG 33 KV SUB-TRANSMISSION NETWORK

Ekow A. Kwofie, Emmanuel K. Anto, Godfred Mensah
Electricity Company of Ghana, System Planning Division,Ghana
Kwame Nkrumah University of Science and Technology, Department of Electrical/Electronic Engineering, PMB, University Post Office, KNUST - Kumasi, Ghana
Electricity Company of Ghana, System Planning Division, Ghana

Abstract:
In this paper, CYME Distribution software has been used to assess the impacts of solar Photovoltaic (PV) distributed generation (DG) plant on the Electricity Company of Ghana (ECG) 33 kV sub-transmission network at different PV penetration levels. As ECG begins to encourage DG PV interconnections within its network, there has been the need to assess the impacts on the sub-transmission losses and voltage contribution. In Tema, a city in Accra - Ghana, ECG has a 33 kV sub-transmission network made up of 20 No. 33 kV buses that was modeled. Three different locations were chosen: The source bus, a bus along the sub-transmission radial network and a bus at the tail end to determine the optimal location for DG PV interconnection. The optimal location was determined based on sub-transmission technical losses and voltage impact. PV capacities at different penetration levels were modeled at each location and simulations performed to determine the optimal PV penetration level. Interconnection at a bus along (or in the middle of) the sub-transmission network offered the highest benefits at an optimal PV penetration level of 80%. At that location, the maximum voltage improvement of 0.789% on the neighboring 33 kV buses and maximum loss reduction of 6.033% over the base case scenario were recorded. Hence, the optimal location for DG PV integration within the 33 kV sub-transmission utility network is at a bus along the sub-transmission radial network.

Keywords: Distributed generation photovoltaic, DG PV, optimal location, penetration level, sub-transmission network.

OPTIMAL DESIGN OF MULTIMACHINE POWER SYSTEM STABILIZERS USING IMPROVED MULTI-OBJECTIVE PARTICLE SWARM OPTIMIZATION ALGORITHM

Badr M. Alshammari, T. Guesmi
University of Hail, Saudi Arabia

Abstract:
In this paper, the concept of a non-dominated sorting multi-objective particle swarm optimization with local search (NSPSO-LS) is presented for the optimal design of multimachine power system stabilizers (PSSs). The controller design is formulated as an optimization problem in order to shift the system electromechanical modes in a pre-specified region in the s-plan. A composite set of objective functions comprising the damping factor and the damping ratio of the undamped and lightly damped electromechanical modes is considered. The performance of the proposed optimization algorithm is verified for the 3-machine 9-bus system. Simulation results based on eigenvalue analysis and nonlinear time-domain simulation show the potential and superiority of the NSPSO-LS algorithm in tuning PSSs over a wide range of loading conditions and large disturbance compared to the classic PSO technique and genetic algorithms.

Keywords: Multi-objective optimization, particle swarm optimization, power system stabilizer, low frequency oscillations.

TREATMENT OF LOW-GRADE IRON ORE USING TWO STAGE WET HIGH-INTENSITY MAGNETIC SEPARATION TECHNIQUE

Moses C. Siame, Kazutoshi Haga, Atsushi Shibayama
Akita University in the Graduate School of International Resource Science, Japan
Assistant Professor and Atsushi Shibayama is the professor at Akita University in the Graduate School of Engineering and
Resource Science, Japan

Abstract:

This study investigates the removal of silica, alumina and phosphorus as impurities from Sanje iron ore using wet high-intensity magnetic separation (WHIMS). Sanje iron ore contains low-grade hematite ore found in Nampundwe area of Zambia from which iron is to be used as the feed in the steelmaking process. The chemical composition analysis using X-ray Florence spectrometer showed that Sanje low-grade ore contains 48.90 mass% of hematite (Fe2O3) with 34.18 mass% as an iron grade. The ore also contains silica (SiO2) and alumina (Al2O3) of 31.10 mass% and 7.65 mass% respectively. The mineralogical analysis using X-ray diffraction spectrometer showed hematite and silica as the major mineral components of the ore while magnetite and alumina exist as minor mineral components. Mineral particle distribution analysis was done using scanning electron microscope with an X-ray energy dispersion spectrometry (SEM-EDS) and images showed that the average mineral size distribution of alumina-silicate gangue particles is in order of 100 μm and exists as iron-bearing interlocked particles. Magnetic separation was done using series L model 4 Magnetic Separator. The effect of various magnetic separation parameters such as magnetic flux density, particle size, and pulp density of the feed was studied during magnetic separation experiments. The ore with average particle size of 25 μm and pulp density of 2.5% was concentrated using pulp flow of 7 L/min. The results showed that 10 T was optimal magnetic flux density which enhanced the recovery of 93.08% of iron with 53.22 mass% grade. The gangue mineral particles containing 12 mass% silica and 3.94 mass% alumna remained in the concentrate, therefore the concentrate was further treated in the second stage WHIMS using the same parameters from the first stage. The second stage process recovered 83.41% of iron with 67.07 mass% grade. Silica was reduced to 2.14 mass% and alumina to 1.30 mass%. Accordingly, phosphorus was also reduced to 0.02 mass%. Therefore, the two stage magnetic separation process was established using these results.

Keywords: Sanje iron ore, magnetic separation, silica, alumina, recovery.

Human Sustainable Development: Welfare and Happiness in Iran

Ehsan Shahghasemi

Associate Professor of Communication at the University of Tehran,

ABSTRACT

After almost eight decades of the global project of development that yielded a great leap in heightening life standards, it is time to see if the development project has been able to meet its ultimate goal: to end human misery. With a special focus on Iran, my argument in this paper is that since the Development Paradigm mainly mistook happiness with welfare, technological advancement, and material wealth, it has failed to end human misery. Even worse, people in the developed sections of Iranian society seem to be much more unhappy than their predecessors. Development has produced great expectations, individualism, and consumerism and all of these are great sources of discontent. A sustainable development paradigm can go one step further and add another human dimension to other dimensions of the development. Indeed, to start taking a human dimension into account, the sustainable development paradigm should have a clear and correct image of what human is.

Keywords: Sustainable Development; Happiness; Iran; Development Paradigm

Introduction

James Basset who was an American Presbyterian missionary in Iran's 19th century traveled from Urmia in northwestern Iran to the capital city of Tehran to evaluate the possibility of new developments and expansions of the American mission. His account of the 1872 famine in Iran is daunting: "Four miles beyond TurkmanTchai (sic), we passed the ruins of a village which a few months previous contained one hundred families. It was now reduced by the famine to fifteen households. Men, women, and children were met on the way slowly traveling westward. Many sat by the way eating herbs and roots which they had dug up" (Bassett, 1886, p. 71). He added:

> "The famine had been very severe during the winter. At first only refugees from other places died from this cause, but later many of the citizens died. In the nine months preceding, five thousand six hundred and thirty dead bodies were carried out of one gate for burial, and one thousand one hundred in the last forty-six days. In the same period of nine months there had been borne through another city gate five thousand dead bodies. It was thought that the water had become polluted, since some of the water courses passed near or under the cemeteries." (Bassett, 1886, quoted in Shahghasemi, 2017: 51).

I teach a course on Human Communication in which I allocate one whole session on "pain." Here I try to tell my students how their forefathers and foremothers lived harsh just a few decades ago and throughout history. I tell freshmen that we live in the Middle East and this is one of the most dangerous regions in the world (See for example Shahghasemi and Prosser, 2019). I read the above quotations from Basset and other resources and I show scenes from Merian C. Cooper's *Grass: A Nation's Battle for Life* (1925) in which Bakhtiari nomads in southwest Iran work barefoot in freezing snow for five others to create a trail for the rest of the tribe to pass -also barefoot- and get to the other side of the ragged *Zard-a-Koh*. What shocks them and they always confront me over that is that these people were happier than us.

My argument in this paper is that in order to have a sustainable development, we need cutting-edge technology, and we should pursue the latest and the most advanced technologies, but we should take into account the very premises and necessities of human happiness and understand how *technology* can help it.

Technology-Intensive Approach

WWII created a watershed for economic growth. Some wealthy nations took this opportunity while otherss were busy trying to get their independence. This time is generally known as *the golden age of capitalism* or *the postwar boom* (Marglin and Schor, 2011). A reasonable evaluation by prosperous nations -and most notably the US- was that without developing poor nations, some problems would occur to the global economy, and this created a widespread development project. One approach was to help developing nations get the advanced technologies they needed; this way, this group of thinkers believed, technologies would be used by a large or small group of people inside those societies and all of the people will benefit more or less. It constituted the core of the industrialization prescribed for developing countries. More often than not, capital- and machine-intensive technologies substituted for labor that was abundantly available in poor countries. The badly needed capital for the new technologies was provided by national governments and often supplemented by loans from bilateral/multilateral agencies and transnational corporations (Melkote and Steeves, 2019). The crucial tool for greater productivity in the agricultural sector was seen as a migration from human/animal labor-intensive techniques to a technology-intensive approach, as in the Western and other developed countries. Technical and management-intensive programs such as the Green Revolution were vigorously pursued in many countries in Asia (Melkote and Steeves, 2019) and produced some favorable results.

The most tragic experience of the technology-intensive development approach happened in communist China. Mao in his Great Leap Forward program aimed at converting the very poor country of China into an advanced nation, and a model of a communist society (Wemheuer, 2015). The results of this industry-intensive strategy were horrendous. It is estimated that over 40 million Chinese people were killed, committed suicide, or died of starvation from 1958 to 1962. More people were killed in China in this period, than in WWII.

Technology-Intensive Development in Iran

Iran started to cooperate with Western powers and imported their technologies to confront the mighty Ottoman empire from Safavid onwards. In early 19th century, after the Russia-Iran war which culminated in a humiliating defeat of Iran, Abbas Mirza planned a program to import technology and science from the West. In 1888, Naser el-din Shah sent Haj Husayn Quli Khan Sadr al-Saltana to be the first Iranian envoy to the United States. On October 5, 1888, he presented a letter by Naser el-din Shah to President Cleveland. In this letter, the Shah made an impassioned plea for American help to save Persia from Britain and Russia. The shah even pleaded to have his country's resources exploited by America in the hope of a treaty of alliance:

> The government of Persia, which is an old established and independent kingdom of the world, have special message to her young and prosperous and powerful sister. . . But we have two great neighbors which instead of assisting us . . . always internally endeavoring to prevent us . . . you help us with your sicences (sic) and industries and send your companies and merchand (sic) and manufacturies (sic) to our country . . . Hoping that our reqist (sic) for the present will be strictly secret from any person besides your highness . . . (Yeselson, 1956, quoted in Shahghasemi, 2017: 83).

There were other efforts to industrialize Iran, but the first effective one was that of Reza Shah. He was an uneducated military commander but as clever as he was, he came to understand that to end the Iranian people's misery, one should industrialize Iran. He took several strategies after he seized power through terror and cunning, and one of these strategies was a technology-intensive approach.

Reza Shah reigned Iran for 16 years. He extorted, tortured, and suppressed, but the country he gave to his son was completely different from the country he had when he came to the throne. He built thousands of kilometers of roads, made a cross-country railroad, and created a centralized and strong government. When he was forced to resign in 1942, he had built over

680 big factories; he even built a fighter plane factory and delivered many fighters to the Iranian air force.

As a result of continuous industrialization, the urban population grew rapidly from 31% of the whole population in 1956 to 38% in 1966, to 47% in 1976 (currently, this figure is 75%). The oil crisis of the 1970s was a big economic and technological opportunity for Iran. A flood of money ran toward Iran and the country started to show interest in the most advanced technologies. The shah of Iran built both the Aryamehr Steel Mill complex at Isfahan and the Machine Tools Factory at Tabriz and came to the conclusion that it was necessary to build technical schools attached to the factories in order to obtain qualified workers (Hetherington, 1982).

But, instead of furthering the modernization of the country in a natural way, the shah, like his father, based his power on the three Pahlevi pillars: the armed forces, the court patronage network, and the vast state bureaucracy (Abrahamian, 1982). This created a watershed for corruption and at the end of the Pahlavi regime, the level of corruption had become intolerable (Hetherington, 1982).

On the military front, the shah continued to treat the military establishment as his central support. He increased its size from 200,000 men in 1963 to 410,000 in 1977: the army went from 180,000 to 200,000; the gendarmerie from 25,000 to 60,000; the air force from 7,500 to 100,000; the navy from 2,000 to 25,000; the elite commando unit from 2,000 to 17,000; and the elite force of Imperial Guard, which was supposed to guard the royal establishment, from 2,000 to 8,000. Moreover, he increased the annual military budget from $293 million in 1963 to $1.8 billion in 1973, and, after the quadrupling of oil revenues, to $7.3 billion in 1977 (Abrahamian, 1982). Buying more than $12 billion worth of Western-manufactured arms between 1970 and 1977 alone, the shah built up a vast high-tech arsenal that included, among other weapons, 20 F14 Tomcat fighter planes with long-range Phoenix missiles, 190 F4 Phantom fighter planes, 166 F5 fighter aircraft, 10 Boeing 707 transport planes, 800 helicopters, 28 hovercrafts, 760 Chieftain tanks, 250 Scorpion tanks, 400 M47 tanks, 460 M60 tanks, and 1 Spruance naval destroyer. By 1977, Iran had the largest navy in the Persian Gulf, the most advanced air force in the Middle East, and the fifth-largest military force in the world. As if this were not enough, the shah placed orders for another $12 billion worth of arms to be de livered between 1978 and 1980. Among items in this order were 202 helicopter gun ships, 326 troop-carrying helicopters, 160 F16s, 209 F4s, 7 Boeing planes, 3 Spruance destroyers, and 10 nuclear submarines (Abrahamian, 1982). Also, Iran's nuclear program which had started in the 1950s, got a very faster pace by the 1970s (Kibaroglu, 2006). In early 1979, in one of the most technologically

advanced countries of the Middle East and Asia, the *unhappy* people took part in a massive uprising and overthrew the Shah. More surprisingly, a majority of these unhappy people idolized a kind of lifestyle that belonged to fourteen hundred years ago.

After the revolution, however, the technological advancement of the Iranian society continued, because a devastating 8 years of war with Iraq and other incidents showed the Iranian clergy establishment that *faith* alone was not enough to save the regime and the country. Today Iran is still one of the most technologically advanced countries in the region. But has this advancement -that many people, especially many among the authorities, call *development*- made Iranians happy?

Technology and Happiness in Iran

Iran is currently a technologically advanced country and this is at odd with the current economic situation of this country. Iran is among the so-called *nuclear* countries. Iran is one of the few countries in the world that has space technology. In nano-technology, Iran is one of the leading countries in Asia. In aviation and military technology Iran has had her advancements. In medical technology Iran is self-sufficient in many less sophisticated technologies. In the *Dominant Paradigm of Development*, and in particular in the technology-intensive approach to development, Iran should be a happy and prosperous country, but it is not.

Despite its technological advancement, Iran is economically under pressure. A typical Iranian worker makes $150–300 a month, while the monthly salary for an average middle-class individual is about $400– 700. Since the living costs, especially food, have increased, Iranians' income generally no longer covers anything beyond life's necessities. Official statistics tell us that more than 50% of Iranian live in "absolute poverty" and the situation is worsening. The sanctions and inefficiency have undermined the Iranian economy and hence more Iranian middle-class people lose their socioeconomic status; denying their transfer into a low-class position, many resort to used items and as a result, a growing market of "used" branded commodities in Iran has emerged (Shahghasemi, 2021).

Despite technological advancements, Iranians are seemed to be specifically unhappy with their look. Iran is one of the leading cosmetic markets in the Middle East and Africa; experts believe Iran will be the fastest-growing market for cosmetics during the next eight years (Alliance Experts, 2021). Also, Iranians are very fond of cosmetic surgeries. Iran's medical system is an advanced one but the services it provides are very cheap. So many other people from other countries come to Iran to do surgeries and hence, Tehran is dubbed "the capital of nose job" (see for example Kaivanara, 2020).

Iranians are generally unhappy with their marriages. In the past decade, the rate of divorce among Iranian men and women has been on the rise. Among the wealthy and the well-educated, this rate has been higher. In comparison to four decades ago, now the possibility that a marriage ends up in divorce is three times more.

In the past decade, it seems the rate of drug abuse has been on the rise in Iran. In general, Iranians are highly idealist people and since the realization of their ideals seems almost impossible, some like to pursue it in an imaginary world. Also, the demise of religious and ideological values and the vacuum of new ideals has exacerbated this situation. Young people are more seeking pleasure, than redemption these days. Official figures say t million among 84 million Iranians are addicted to some kind of drug but based on my own experience, the real number is much higher.

Conclusion: A Sustainable Development Approach Towards Technology

I don't like discussions about the complete failure of the Development Paradigm. Development has done much for us. These days we are less likely to understand how life was harsh before the development project started. My argument is that the Development Paradigm equated technological development with happiness -just as most of us in the modern societies mistakenly see material wealth as happiness- but despite many successes in its planned goals, the Development Paradigm largely failed to make us happier. Despite its technological advancements, Iran is among the unhappiest nations in the world (See for example Faulders, 2014; Keyser, 2019; Chamlou, 2020).

The Sustainable Development Paradigm looks for a solution. This paradigm still aims at a more technologically advanced society, but would not end there. Humans are humans; they have their complexities and without properly addressing those complexities, all efforts would be fruitless or even counterproductive. With a Heideggerian approach, we should know that technologies should be seen as something far beyond mere tools. Using social and psychological sciences in planning will help us to have technologies, but at service of human happiness.

References

Abrahamian, E. (1982). *Iran between two revolutions*. New Jersey: Princeton University Press.

Alliance Experts (2021). The Iran cosmetics market: Opportunities in the skincare industry. Retrieved May 18, 2022 from https://www. allianceexperts.com/en/knowledge/countries/asia/iran-cosmetics- industry/.

Chamlou, N. (2020). Just how happy are Iranians with their lives? Retrieved May 21, 2022 from https://www.atlanticcouncil.org/blogs/iransource/just-how-happy-are-iranians-with-their-lives/

Faulders, K. (2014). Iraq, Iran Top World's Unhappiest Countries List. Retrieved May 21, 2022 from https://abcnews.go.com/blogs/politics/2014/06/iraq-iran-top-worlds-unhappiest-countries-list

Heidegger, M. (2013). *The question concerning technology, and other essays*. New York: Harper Perennial.

Hetherington, N. S. (1982). Industrialization and Revolution in Iran: Forced Progress or Unmet Expectation?. *Middle East Journal, 36,* 3, 362-373.

Kaivanara, M. (October 01, 2020). Geographies of Capital and Capital of Geographies: Reckoning the Embodied City of Tehran through Cosmetic Surgeries. *Current Anthropology, 61,* 5, 603-621.

Keyser, Z. (2019). Iran is one of the unhappiest countries in the world – report. Retrieved May 21, 2022 from https://www.jpost.com/middle-east/iran-is-one-of-the-most-unhappy-countries-in-the-world-report-584412

Kibaroglu, M. (2006). Good for the Shah, Banned for the Mullahs: The West and Iran's Quest for Nuclear Power. *Middle East Journal, 60,* 2, 207-232.

Marglin, S. A., Schor, J. (2011). *The Golden age of capitalism: Reinterpreting the postwar experience*. Oxford: Oxford University Press.

Melkote, S. R., Steeves, H. L. (2019). *Communication for development: Theory and practice for empowerment and social justice*. Los Angeles: SAGE.

Shahghasemi, E. (2017). Iranians in the Minds of Americans. New York: Nova Press.

Shahghasemi, E., Prosser, M. (2019). The Middle East: Social Media Revolution in Public and Private Communication. International Conference on Future of Social Sciences and Humanities, Warsaw.

Shahghasemi, E. (2021). "Rich Kids of Tehran: The Consumption of Consumption on the Internet in Iran". *Society*. doi : 10.1007/s12115-021-00626-3.

Wemheuer, F. (2015). *Famine politics in Maoist China and the Soviet Union*. New Haven: Yale University Press.

YENİ NESİL BİRLEŞTİRME TEKNOLOJİLERİ KENDİNDEN KİLİTLEMELİ PERÇİNLEME

OKTAY ÇAVUŞOĞLU [1], HAKAN AYDIN [2], HALUK DİNKCİ [3], AHMET GÜRKAN YILMAZOĞLU [4], UĞUR ÜZEL [5]

[1]TOFAŞ, Türk Otomotiv Fabrikası, Bursa, Türkiye; - 0000-0002-2826-1814

[2]Bursa Uludağ Üniversitesi, Mühendislik Fakültesi, - 0000-0001-7364-6281

[3]TOFAŞ, Türk Otomotiv Fabrikası, Bursa, Türkiye; - 0000-0001-7130-1941

[4]TOFAŞ, Türk Otomotiv Fabrikası, Bursa, Türkiye; - 0000-0002-1811-7827

[5]TOFAŞ, Türk Otomotiv Fabrikası, Bursa, Türkiye;– 0000-0001-5819-6841

ÖZET

Otomotiv sektöründe artan rekabet, ar-ge merkezleri yeni birleştirme teknolojilere yönlendirmiştir. Kendinden kilitlemeli perçinleme teknolojisi temel malzemeye ısı girdisi olmamasından dolayı diğer birleştirme yöntemlerinin önüne geçmektedir. Bu çalışmada, otomotiv sektöründe giderek yaygınlaşan yeni nesil birleştirme teknolojilerinden olan kendinden kilitlemeli perçinleme teknolojisi detaylı olarak incelenmiştir. Farklı malzeme kombinasyonları birleştirilerek mekanik özellikleri karşılaştırılmıştır. Mekanik testler 25 kN kapasiteli Zwick marke çekme test cihazından gerçekleştirilmiştir.

Anahtar Kelimeler: FEE 340, DC 04, Mekanik Özellikler, Malzeme Karakterizasyonu

NEXT GENERATION JOINING TECHNOLOGIES SELF PIERCE RIVETING

Abstract

Increasing competition in the automotive industry has directed R&D centers to new joinning technologies. Self-locking riveting technology can be preferred over other joining methods since there is no heat input to the base material. In this study, self-locking rivet technology, which is one of the new generation joining technologies that is becoming increasingly widespread in the automotive industry, is examined in detail. Different material combinations were combined and their mechanical properties were compared. Mechanical tests were carried out on a 25 kN capacity Zwick marke tensile testing machine.

Keywords: FEE 340, DC 04, Mechanical Properties, Material Characterization

1. GİRİŞ

Günümüzde teknolojinin gelişmesiyle birlikte, arzu edilen özelliklere sahip yeni malzemeler üretilmeye başlanmıştır. Yeni malzemelerin geliştirilmesiyle birlikte bu malzemelerin verimli bir şekilde birleştirilmesi temel konulardan biri haline gelmiştir. Diğer birleştirme yöntemlerinde istenmeyen kısıtlamaların bulunmasından dolayı kendinden kilitlemeli perçin

teknolojisi otomotiv sektöründe giderek yaygınlaşmaya başlamıştır [1]. Kendinden kilitlemeli perçin teknolojisi, farklı malzemelerin çoklu birleştirilmesini izin veren ve otomasyona uygunluğu nedenleriyle tercih edilmektedir [2]. İşlem farklı veya aynı malzemenin bir baskı kuvveti uygulayarak perçin yardımıyla birleştirilmesi esasına dayanmaktadır. Perçin malzemeye batırılırken genişleyerek kendinden kilitleme işlemini gerçekleştirmiş olmaktadır [3,4]. Kendinden kilitleme perçinleme; düşük enerji ihtiyacı, statik ve kırılma dayanımı sağlamaktadır [5,6].

Literatürde bu alanda çeşitli çalışmalar yer almaktadır. Chun-yu Zhang ve diğ. çelik ve alüminyum parçaların kendinden kilitlemeli perçinleme teknolojiyle birleştirmiş. Çekme ve yorulma testlerine gerçekleştirmiş. Kuvvet-Yer değiştirme ve S/N eğrileri oluşturarak, bunlara etki eden parametreleri incelemiştir [7]. Kim, W.Y. ve diğ. Helisel perçin kullanarak çelik ve alüminyum malzemelere birleştirmiş elde ettiği sonuçları simüle etmiştir [8].

Bu çalışmada 1,5 mm kalınlığında DC 04 ve 1,5 mm kalınlığında FEE 340 sac malzemelerini birleştirilmiştir. Daha sonra sabit sıcaklık ve hız altında mekanik özellikleri karşılaştırılmıştır.

2. MATARYEL VE YÖNTEM

Çalışmada kullanılan FEE 340 ve DC 04 malzemelerinin mekanik özellikleri Çizelge 1'de gösterilmiştir.

Çizelge 1. Mekanik Özellikler

Malzeme	Akma Dayanımı	Çekme Dayanımı	Kopma Uzaması
DC 04	140-210 MPa	270-350 MPa	%38
FEE 340	340-420 MPa	410 MPa min.	%22

Perçin şematik resimleri ve numunenin şematik resimleri Görsel 1 ve Görsel 2 'de gösterilmiş.

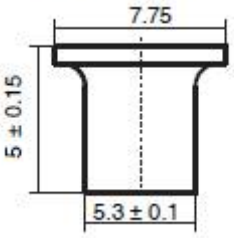

Görsel 1. Perçin Şematik Gösterimi

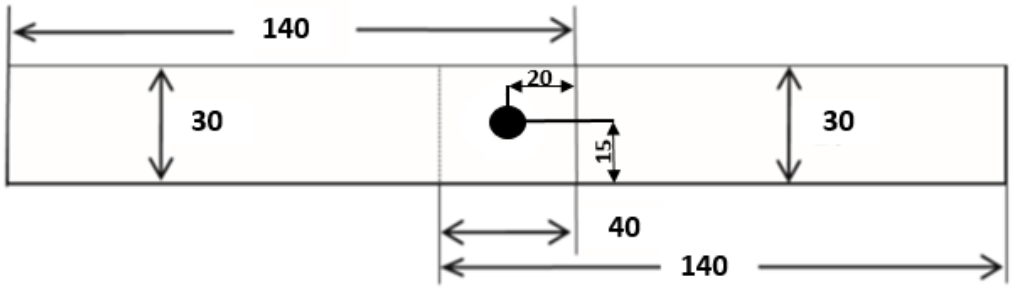

Görsel 2. Numunenin Şematik Gösterimi

Deney sırasında kullanılan malzeme kombinasyonları Görsel 3'te gösterilmiştir. Farklı ve benzer malzemelerin mekanik özelliklerini belirlemek için farklı malzeme kombinasyonları oluşturularak çekme testi uygulanmıştır.

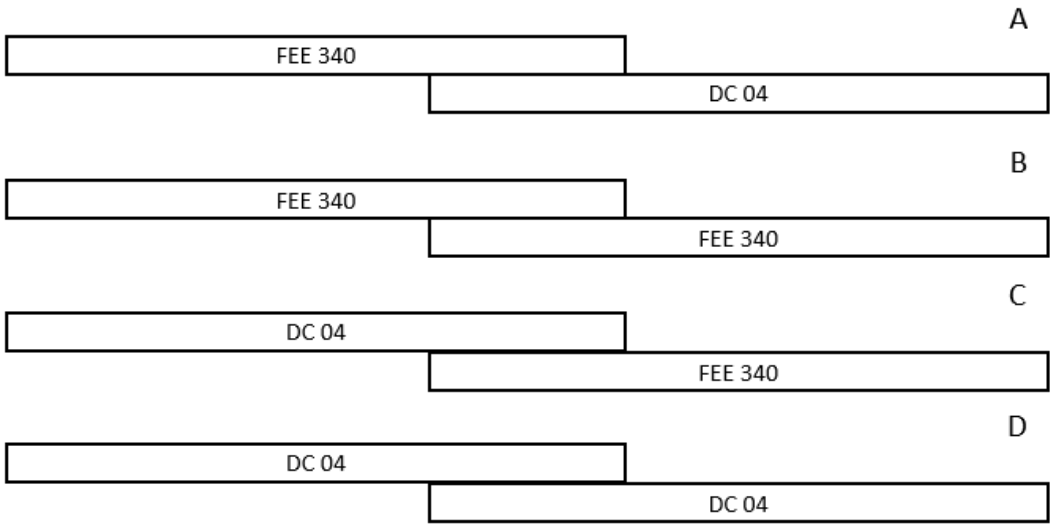

Görsel 3. Malzeme Kombinasyonları

Perçinleme işlemi Bollhoff marka kendinden kilitlemeli perçinleme cihazında gerçekleştirilmiştir. Çekme testi 25 kN kapasiteli Zwick marka çekme test cihazında, sabit oda sıcaklığında ve $6.7 \times 10^{-3}\ s^{-1}$ hız altında gerçekleştirilmiştir.

3. SONUÇLAR VE DEĞERLENDİRME

Görsel 4'te kendinden kilitleme perçinleme teknolojisiyle birleştirilmiş farklı malzeme kombinasyonların çekme testi eğrileri gösterilmiştir. En yüksek çekme kuvvet B Kombinasyonunda (FEE 340 – FEE 340) 6145,97 N olarak elde edilmiştir. En düşük çekme kuvveti D kombinasyonunda (DC 04 – DC 04) 4421,47 N olarak elde edilmiştir. A Kombinasyonunda (FEE 340 – DC 04) 5993,86 N , C Kombinasyonunda (DC 04 – FEE 340) 4954,13 N çekme kuvveti elde edilmiştir. Süneklik açısından karşılaştırıldığında en fazla uzama D kombinasyonunda (DC 04 - DC 04) , en düşük uzama ise B kombinasyonunda (FEE 340 – FEE 340) olarak gerçekleşmiştir.

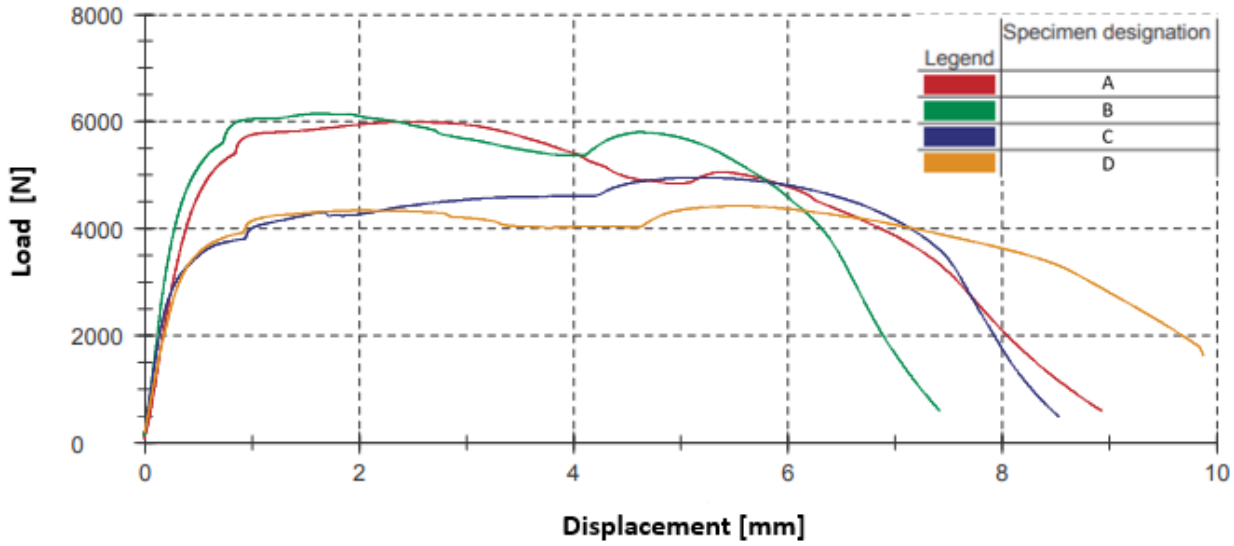

Görsel 4. Kuvvet – yer değişimi eğrileri

4. SONUÇLAR

Bu çalışmada, kendinden kilitleme perçinleme teknolojisiyle birleştirilmiş FEE 340 ve DC 04 çelik sacların birleştirme kombinasyonlarının mekanik özellikleri üzerindeki etkisi araştırılmıştır. Deneysel çalışmaların sonuçları şu şekilde özetlenebilir:

- Aynı malzeme kombinasyonlarından elde edilmiştir, A ve C kombinasyonlarından A kombinasyonu daha iyi bir kenetlenmek göstermiştir.
- Sert malzemenin üst katmanda yer almasının daha iyi bir kenetlenme sağladığı tespit edilmiştir.
- En yüksek kuvvet B kombinasyonunda elde edilmiştir. Ancak daha erken bir kopma görüşmüştür.
- D kombinasyonunda ise kuvvet çok yüksek olmamasına rağmen, daha fazla uzadığı görülmüştür.

KAYNAKÇA

[1] Mori, K.-I., Bay, N., Fratini, L., Micari, F., and Tekkaya, A. E., 2013, "Joining by Plastic Deformation," CIRP Ann. Manuf. Technol., 62(2), pp. 673–694.
[2] Zhang, J., & Yang, S. (2015). Self-piercing riveting of aluminum alloy and thermoplastic composites. Journal of Composite Materials, 49(12), 1493-1502.
[3] Liu, X., Lim, Y. C., Li, Y., Tang, W., Ma, Y., Feng, Z., & Ni, J. (2016). Effects of process parameters on friction self-piercing riveting of dissimilar materials. Journal of Materials Processing Technology, 237, 19-30.

[4] Ma, Y., Li, Y., Hu, W., Lou, M., & Lin, Z. (2016). Modeling of friction self-piercing riveting of aluminum to magnesium. Journal of Manufacturing Science and Engineering, 138(6).
[5] Li, D. (2017). Influence of aluminium sheet surface modification on the self-piercing riveting process and the joint static lap shear strength. The International Journal of Advanced Manufacturing Technology, 93(5), 2685-2695.
[6] Huang, L., Guo, H., Shi, Y., Huang, S., & Su, X. (2017). Fatigue behavior and modeling of self-piercing riveted joints in aluminum alloy 6111. International Journal of Fatigue, 100, 274-284.
[7] Zhang, C. Y., Gou, R. B., Yu, M., Zhang, Y. J., Qiao, Y. H., & Fang, S. P. (2017). Mechanical and fatigue properties of self-piercing riveted joints in high-strength steel and aluminium alloy. *Journal of Iron and Steel Research International*, *24*(2), 214-221.
[8] Kim, W. Y., Kim, D. B., Park, J. G., Kim, D. H., Kim, K. H., Lee, I. H., & Cho, H. Y. (2014). Design of Helical Self-Piercing Rivet for Joining Aluminum Alloy and High-Strength Steel Sheets. *Transactions of the Korean Society of Mechanical Engineers A*, *38*(7), 735-742.

BİR DÖKÜM FABRİKASINDA ÜRETİM KAPASİTESİNİ VE VERİMLİLİĞİNİ ARTTIRMA ÇALIŞMASI

MİHRİCAN ERDOĞAN[1], Dr. Öğr. Üyesi TÜLAY KORKUSUZ POLAT [2]

[1] Sakarya Üniversitesi, Mühendislik Fakültesi, ORCID ID: 0000-0002-2495-9449

[2] Sakarya Üniversitesi, Mühendislik Fakültesi, , ORCID ID: 0000-0001-6693-7873

ÖZET

Rekabetin gittikçe arttığı iş dünyasında firmalar karlılıklarını devam ettirebilmek için daha verimli üretim yapmak zorundadırlar. İşletmeler özellikle üretim/satış/işgücü konularında gerçekçi planlamalar yapabilmek için neyi ne kadar sürede ve ne kadar işgücü ile üretebildiklerini bilmelidirler. Verimliliğin arttırılması için israfların ve kayıp zamanların ortadan kaldırılması büyük önem taşımaktadır. İş etüdü uygulamaları, yapılan işlerin standart zamanlarının hesaplanmasını sağlayarak kapasite planının daha doğru şekilde yapılmasına, siparişlerin teslim sürelerine daha iyi uyulmasına yardımcı olmaktadır. İş etüdü uygulamaları Özellikle küçük ve orta büyüklükteki işletmelerde (KOBİ) standart zaman çalışmaları oldukça etkili sonuçlar sağlamaktadır. Bu çalışmada KOBİ statüsünde olan ve alüminyum enjeksiyon döküm yapan bir fabrikada siparişlerin zamanında teslim edilememesi probleminin çözümünde üretim verimliliğini ve kapasiteyi arttırmak için yapılan faaliyetler ele alınmaktadır. Metal enjeksiyonu yapan fabrikada işçilerin kayıp zamanlarının fazla olması problemi yaşanmaktadır. Bu da verimliliğin beklenenin çok altında olmasına neden olmaktadır. Problemin bir sonucu olarak ürünler müşteriye zamanında teslim edilememektedir. Bu çalışmada işçilerin kayıp zamanlarının fazla olmasından kaynaklanan bu problemin çözümü için yapılan standart zaman çalışmaları anlatılmaktadır. Uygulama için öncelikle standart zaman hesabı yapılarak olması gereken üretim kapasitesi hesaplanmıştır. Daha sonra simülasyon modeli ile üretilen parçaların belli bir zaman diliminde istenilen gerçek karakteristiklerini tahmin etmek için bir model kurulmuştur. Verimliliği arttırmaya yönelik maliyet analizi yapılarak kaç işçi çalıştırılması gerektiği, yeni bir makine alınmasına gerek olup olmadığı konularında da analiz yapılmıştır.

Anahtar Kelimeler: İş Etüdü, Standart Zaman Hesabı, Kapasite, Verimlilik

1. GİRİŞ

Üretim kapasitesini arttırarak verimliliği yükseltmek işletmelerin rekabet avantajlarını devam ettirebilmeleri için sıklıkla seçtiği bir yöntemdir. Verimliliği arttırmak için işletmedeki tüm israfı azaltmak önemlidir. Buna kayıp zamanları azaltmak da dahildir. Kayıp zamanların azaltılmasında ve darboğazların belirlenmesinde kullanılan yöntemlerden birisi iş etüdü yöntemleridir. İş Etüdü,

iyileştirme sağlamak için belirli bir faaliyeti etkileyen tüm kaynak ve bileşenleri araştıran bir tekniktir (Ceyhun Sabır ve Dönmez, 2013). İş etüdü çalışmaları metot etüdü ve iş ölçümü olmak üzere iki grupta incelenebilir (Adem ve ark., 2021).

İş etüdü uygulamalarına hem literatürde hem de pratikte sıklıkla rastlanmaktadır. Dizdar ve Özen (2001) çalışmalarında ahşap mobilya sanayisinde faaliyet gösteren bir işletme için üretim verimliliğini arttırmak istemişler ve iş etüdü uygulaması yapmışlardır. Gündüz Cengiz ve Orbak (2010) çalışmalarında süt ürünleri üretimi yapan bir işletmede verimliliği arttırmak için zaman etüdü çalışması yapmışlardır. Çolak ve arkadaşları (2016), beyaz eşya yan sanayi imalatçısı olan bir işletmede üretim süresini iyileştirerek verimliliği arttırmak için metot zaman ölçümü yöntemi kullanmışlardır. Şenyiğit ve arkadaşları (2021), bir mobilya işletmesinde iş etüdü yöntemi uygulamışlar ve verimlilik analizi yapmışlardır. Kumaş ve arkadaşları (2016), bir konfeksiyon işletmesinin verimliliği için iş etüdü yöntemini kullanmışlardır. Deste ve İlhan Küçük (2021) çalışmalarında sac kesim işlemleri gerçekleştiren bir işletmede iş etüdü uygulaması yapmışlardır.

Bu çalışmada alüminyum enjeksiyon yapan bir işletmedeki siparişlerin zamanında teslim edilememesi problemi ele alınmaktadır. Bunun için öncelikle mevcut sistem incelenmiş ve birim parça çevrim süreleri hesaplanmıştır. Daha sonra normal zaman ve standart zamanlar hesaplanarak kayıp zamanlar bulunmuştur. Üretim kapasitesinin belirlenebilmesi için Promodel programı ile simülasyon modeli oluşturulmuştur. Son olarak maliyet analizi yapılarak sonuçlar karşılaştırılmıştır.

2. UYGULAMA

Alüminyum enjeksiyon fabrikasındaki siparişlerin yetişmemesi probleminin çözümü için verimlilik ve kapasiteyi arttırmaya yönelik olarak yapılacak çalışmalar şekil 1'de gösterilmektedir.

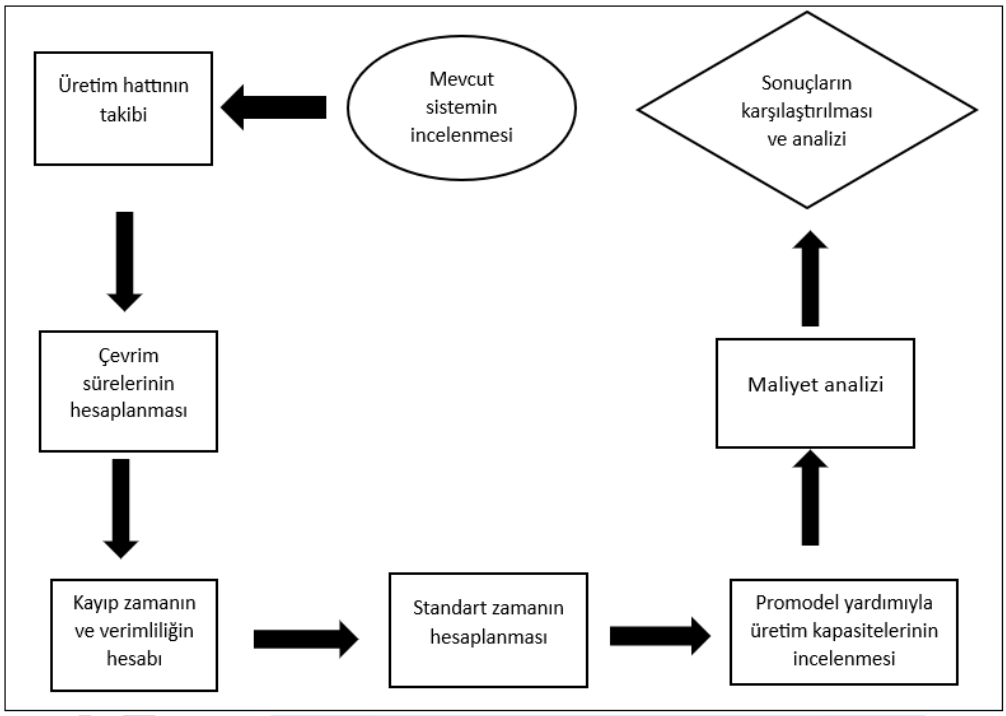

Şekil 1: Uygulama için akış şeması

2.1. Mevcut Durumun İncelenmesi

Ele alınan alüminyum enjeksiyon döküm fabrikasının üretim akışı şekil 2'de gösterilmektedir.

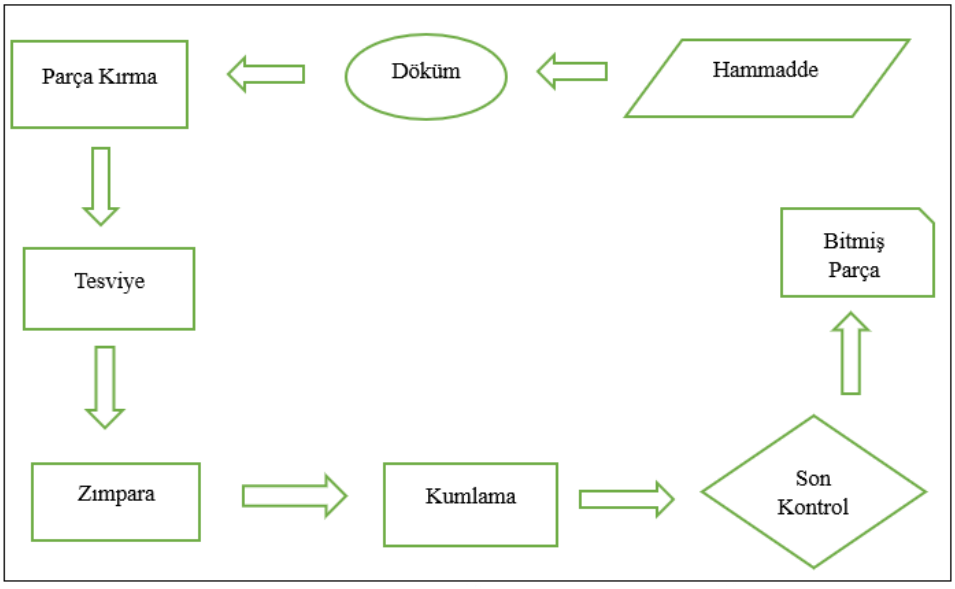

Şekil 2: Üretim akışı

Üretim akışı için birim parça çevrim süreleri hesaplandığında Döküm aşaması: 10 dk., Parça kırma aşaması: 10 dk., Tesviye aşaması: 20 dk., Zımpara aşaması: 15 dk., Kumlama aşaması: 10 dk. Olarak bulunmuştur. Çevrim sürelerine bakıldığında birim parça için toplam çevrim süresi 65 dk.'dır.

Mevcut durumda operatör olarak 1 işçi, parça kırma için 1 işçi, tesviye için 1 işçi, zımpara için 1 işçi, kumlama için 1 işçi çalışmaktadır.

2.2. Normal Zaman ve Standart Zaman Hesabı

Tempo değeriyle hesaplanan normal zaman tablo 1'de gösterilmektedir.

Aşama	Tempo	Gözlenen Zaman (dk)	Normal Zaman (dk)
Döküm	95	10	9,5
Parça Kırma	105	10	10,5
Tesviye	105	20	21
Zımpara	110	15	16,5
Kumlama	105	10	10,5

Standart Zaman Formülü: Normal Zaman+ (1+ (Tolerans/100))

İşçi tolerans puanlarını hesaplayabilmek için dinlenme payları kullanılmıştır.

- Döküm için tolerans puanı hesabı;

Kişisel ihtiyaçlar: 3 puan,

Çalışma sırasında duruş pozisyonu; ayakta: 2 puan,

Bedensel çaba yoğunluğu ve beceri; çok hafif: 2 puan,

Gürültü; konuşmak için sesi yükseltmek:1 puan,

Çevre koşulları; aşırı sıcak ve soğuk yerler: 6 puan,

TOPLAM =3+ 2+2+1+6 = 14 puan

- Parça kırma için tolerans puanı hesabı;

Kişisel ihtiyaçlar: 2 puan,

Bedensel çaba yoğunluğu ve beceri; hafif ve ustalık isteyen: 4 puan,

Çalışma sırasında duruş pozisyonu; eğilme veya uzanma: 4 puan,

Gürültü; düzensiz, sürekli normal gürültü:1 puan,

TOPLAM= 2+4+4+1= 11 puan

- Tesviye için tolerans puanı hesabı;

Kişisel ihtiyaçlar: 3 puan,

Bedensel çaba yoğunluğu ve beceri; hafif ve ustalık isteyen: 4 puan,

Çalışma sırasında duruş pozisyonu; oturma: 1 puan,

Gürültü; konuşmak için sesi yükseltmek: 1 puan,

TOPLAM= 3+4+1+1 = 9 puan

- Zımpara için tolerans puanı hesabı;

Kişisel ihtiyaçlar: 2 puan,

Bedensel çaba yoğunluğu ve beceri; hafif ve ustalık isteyen: 4 puan,

Çalışma sırasında duruş pozisyonu; oturma:1 puan,

Gürültü; konuşmak için sesi yükseltmek: 1 puan,

TOPLAM= 2+4+1+1 = 8 puan

- Kumlama için tolerans puanı hesabı;

Kişisel ihtiyaçlar: 2 puan,

Bedensel çaba yoğunluğu ve beceri; çok hafif: 2 puan,

Çalışma sırasında duruş pozisyonu; ayakta: 2 puan,

TOPLAM= 2+2+2 = 6 puan

Tolerans puanları da dikkate alınarak yapılan standart zaman hesabı tablo 2'de gösterilmektedir.

Aşama	Tempo	Gözlenen Zaman (dk)	Normal Zaman (dk)	Tolerans	Standart Zaman
Döküm	95	10	9,5	14	10,64
Parça Kırma	105	10	10,5	11	11,61
Tesviye	105	20	21	9	22,09
Zımpara	110	15	16,5	8	17,58
Kumlama	105	10	10,5	6	11,56

Standart sürelerin toplamı 73,48 dk.'dır. Bu süre, bir parçanın üretimi için yeterli ve gerekli olan süredir.

2.3 Kayıp Zaman ve Verimlilik Hesabı

Günlük alınan verilere göre hesaplanan döküm kayıp zamanları tablo 3'de gösterilmektedir.

Saat	Planlanan Adet	Gerçekleşen Adet	Kayıp Zaman	Açıklama	Verimlilik
08:00 – 09:00	6	3	30 dk	Kalıp değişimi yapıldı.	%50
09:00 – 10:00	6	5	10 dk	-	%83,3
10:00 – 11:00	6	4	20 dk	10 dk çay molası	%66,6

11:00 – 12:00	6	6	-	-	%100
12:00 – 13:00	6	2	40 dk	12:30 – 13:00 öğle arası	%33,3
13:00 – 14:00	6	6	-	-	%100
14:00 – 15:00	6	5	10 dk	-	%83,3
15:00 – 16:00	6	6	-	-	%100
16:00 – 17:00	6	4	20 dk	10 dk çay molası	%66,6
17:00 – 18:00	6	5	10 dk	-	%83,3

2.4. Mevcut Durum için Simülasyon Modelinin Oluşturulması

Promodel programı aracılığı ile oluşturulan simüasyon modelinde 1 döküm operatörü, 1 parça kırma işçisi, 1 tesviyeci, 1 zımparacı, 1 kumlama işçisi olmak üzere toplam 5 üretim kalemi belirlenmiştir. Oluşturulan model şekil 3'de gösterilmektedir.

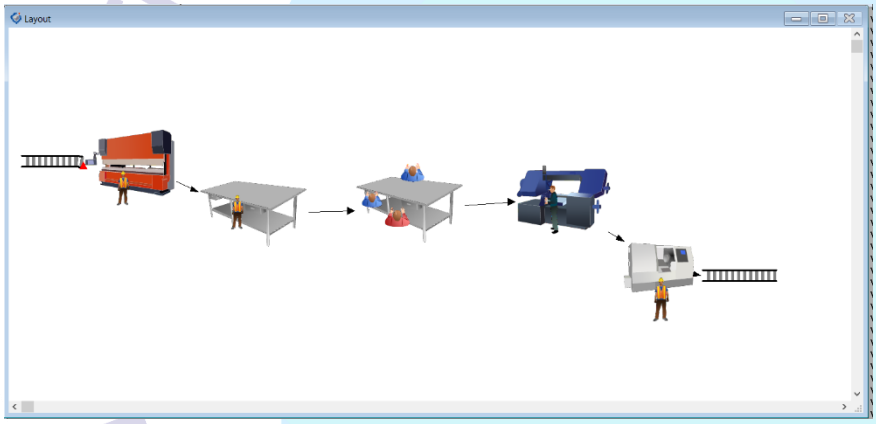

Şekil 3: Mevcut durum için simülasyon modeli

Promodel'da oluşturulan simülasyon modeli için kullanılan veriler şekil 4'de gösterilmektedir.

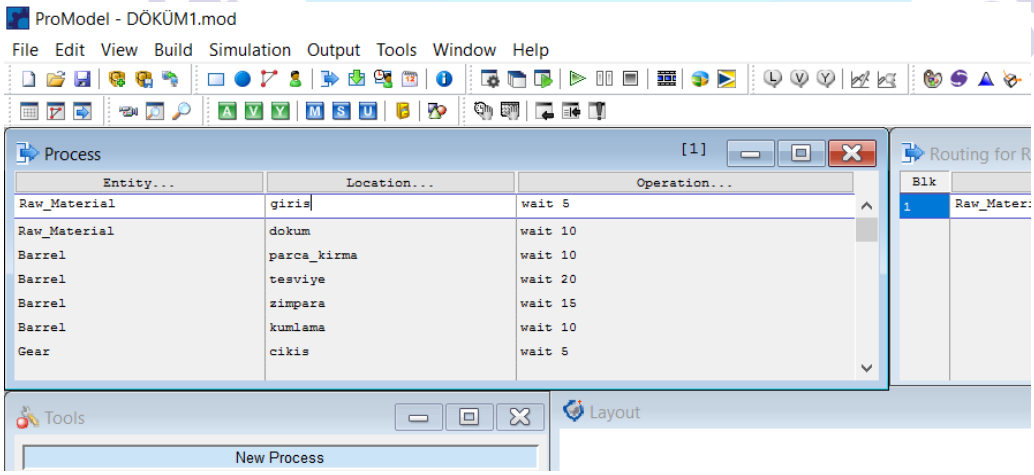

Şekil 4: Simülasyon modeli için kullanılan veriler

Çevrim süreleri, fabrika yerleşimi, üretim sırası verileri de modele girildiğinde şekil 5'de gösterilen üretim kapasitesi elde edilmiştir.

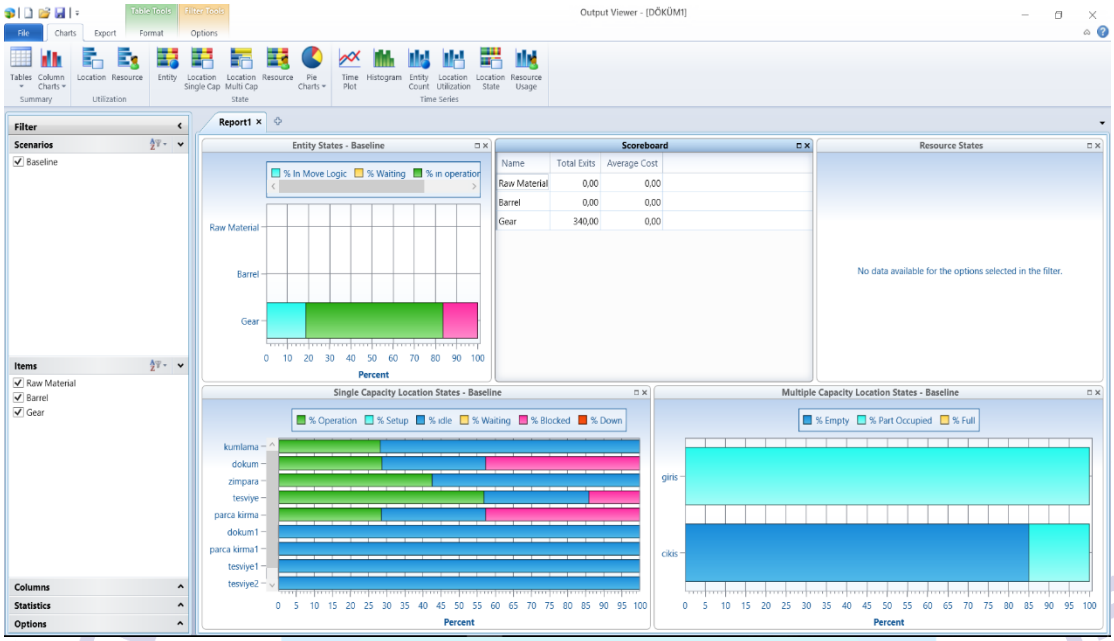

Şekil 5: Mevcut durumun üretim kapasitesi

İşçiler günlük 9 saat ve ayda 22 gün çalışmayla ayda 198 saat çalışmaktadır. Şekil 5, 5 işçi ile çalışılan mevcut durumdaki üretim kapasitesini göstermektedir. Çıkan sonuç göz önüne alındığında, mevcut durumda ayda 340 adet marş motoru kapağı üretilmektedir.

2.5. İyileştirme Sonrası için Simülasyon Modeli

5 personel ile çalışılan mevcut duruma, siparişlerin yetişmesi için 1 döküm operatörü ve 1 adet tesviyeci alındığında işçi dağılımı: operatör: 2 işçi, parça kırma: 1 işçi, tesviye: 2 işçi, zımpara: 1 işçi, kumlama: 1 işçi şeklinde olacaktır. 7 işçi için oluşturulan simülasyon modeli şekil 6'da gösterilmektedir.

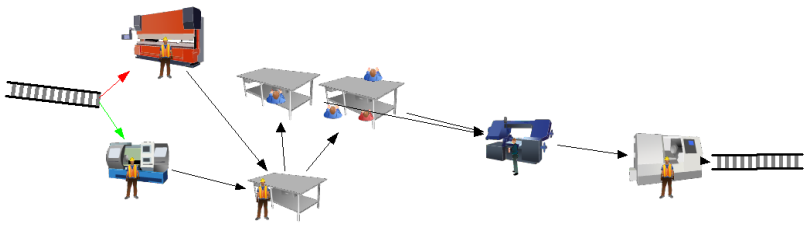

Şekil 6: İyileştirme sonrası durum için simülasyon modeli

Promodel'da oluşturulan iyileştirme sonrası durumunun simülasyon modeli için kullanılan veriler şekil 7'de gösterilmektedir.

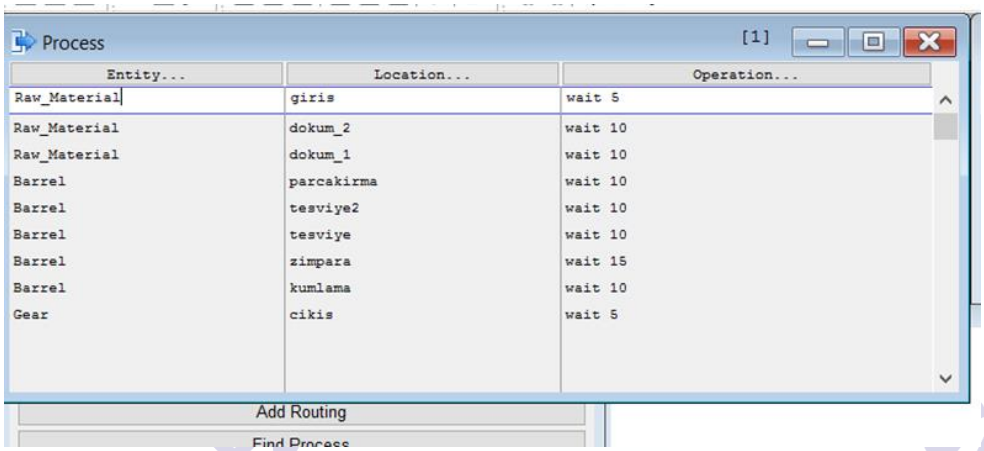

Şekil 7: İyileştirme sonrası için Simülasyon modeli için kullanılan veriler

İyileştirme sonrası durum için çevrim süreleri, fabrika yerleşimi, üretim sırası verileri de modele girildiğinde şekil 8'de gösterilen üretim kapasitesi elde edilmiştir.

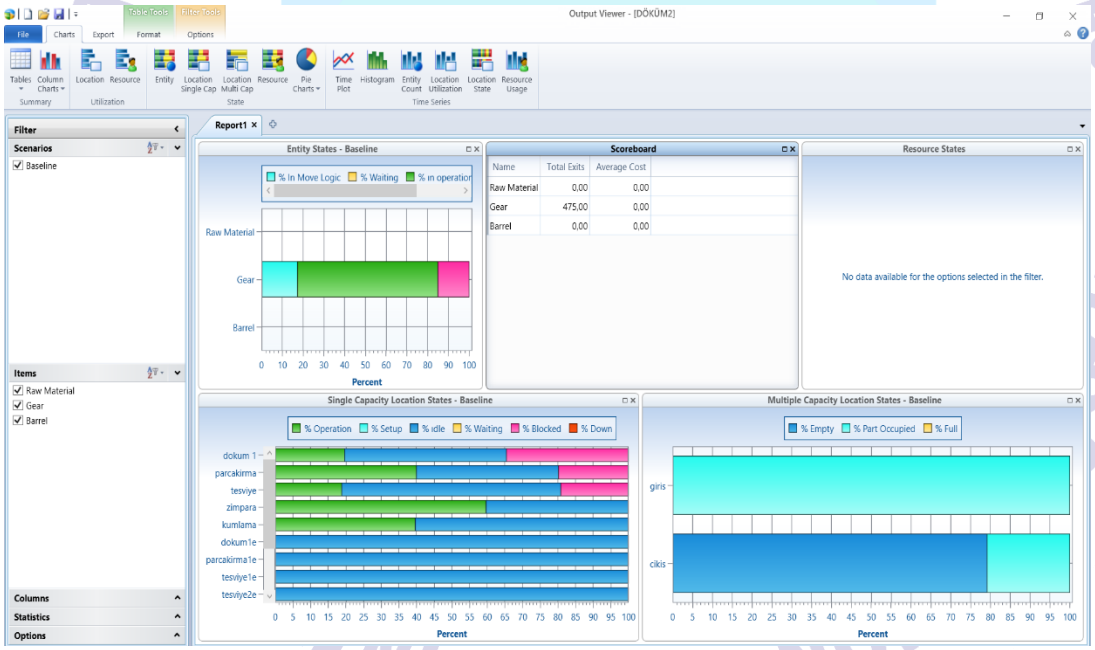

Şekil 8: İyileştirme sonrası için üretim kapasitesi

İşçiler günlük 9 saat ve ayda 22 gün çalışmayla ayda 198 saat çalışmaktadır. Şekil 8, 7 işçi ile çalışılan iyileştirilmiş durumdaki üretim kapasitesini göstermektedir. Çıkan sonuç göz önüne alındığında, mevcut durumda ayda 475 adet marş motoru kapağı üretilmektedir.

3. SONUÇLAR VE DEĞERLENDİRME

Bu çalışmada alüminyum enjeksiyon üretimi yapan bir işletmenin üretiminde kayıp zamanının fazla olması ve dolayısıyla verimliliğinin düşük olması problemi ele alınmıştır. Yapılan çevrim

süresi, kayıp zaman ve verimlilik hesaplamalarından sonra oluşturulan simülasyon modeli ile görülmüştür ki 2 yeni işçi işe almak ve 1 döküm makinesi satın almak ile üretim kapasitesi ve verimlilik artmaktadır. Simülasyon modelinden elde edilen bilgiler ışığında maliyet analizi yapıldığında iyileştirme sonrası üretim kapasitesinin arttığı ve parça birim maliyetlerinin düşürülerek daha fazla kar elde edildiği ortaya konulmuştur. Yeni döküm makinesinin maliyeti fazla olmasına rağmen elde edilen sonuca bakılarak karlı bir yatırım olacağı sonucuna varılabilir.

KAYNAKÇA

[1] Ceyhun Sabır, E., Dönmez, U. İplik İşletmesinde İş Etüdü Uygulaması, Tekstil ve Mühendis, 20: 92, sayfa 11-26, 2013

[2] Adem, A., Yılmaz Kaya, B., Çakıt, E., Dağdeviren, M. Üretim sistemlerindeki dijital dönüşümün iş etüdü teknikleri üzerindeki etkisi. Verimlilik Dergisi, Özel Sayı, sayfa 110-122, 2021.

[3] Dizdar, E.N., Özen, R. Ahşap Mobilya Endüstrisinde Üretim Verimliliği için İş Etüdü Uygulamaları, Teknoloji, sayı 1-2, 1-9, 2001.

[4] Gündüz Cengiz, T., Orbak, A.Y. Bir Süt ve Süt Ürünleri İşletmesinde İş ve Zaman Etüdü Çalışması ile Verimliliğin Arttırılması, International Journal of Engineering Research and Development, vol 2, no 2, June, 2010.

[5] Çolak, M., Aydın Keskin, G., Çelik, B., Avcı, S. Metot Zaman Ölçümü (MZÖ) yöntemi ile üretim süresinin iyileştirilmesi: beyaz eşya yan sanayisinde bir uygulama, SAÜ Fen Bilimleri Dergisi, cilt 20, sayı 3, sayfa 417-427, 2016.

[6] Şenyiğit, E., Karakaş, S., Uçar, S., Akbal, S. Bir mobilya işletmesinde Kurumsal Kaynak Planlaması için iş etüdü-verimlilik uygulamasının analizi: örnek olay, Avrupa Bilim ve Teknoloji Dergisi, Özel Sayı 28, sayfa 476-480, Kasım 2021.

[7] Kumaş, Z., Ceyhun Sabır, E., Duru Baykal, P., Konfeksiyon işletmesinin verimliliği için iş etüdü tekniğinin kullanımı, Çukurova Üniversitesi Mühendislik ve Mimarlık Fakültesi Dergisi, 31(1), sayfa 175-179, Haziran 2016.

[8] Deste, M., İlhan Küçük, H. Sac kesim için yeni makine seçiminde iş etüdü yaklaşımı ile bir uygulama, Ekonomi, İşletme ve Maliye Araştırmaları Dergisi, cilt 3, sayı 2, sayfa 167-179, 2021.

TREYLER ÜRETİMİ YAPAN BİR İŞLETMEDE ÜRETİM PLANLAMA İÇİN İYİLEŞTİRME ÇALIŞMASI

SENA NUR ASLAN[1], Dr. Öğr. Üyesi TÜLAY KORKUSUZ POLAT [2]

[1] Sakarya Üniversitesi, Mühendislik Fakültesi, ORCID ID: 0000-0002-9167-6326

[2] Sakarya Üniversitesi, Mühendislik Fakültesi, ORCID ID: 0000-0001-6693-7873

ÖZET

Teknolojinin hızlı gelişmesi ile birlikte üretim sektöründeki gelişim de ivmelenmiştir. Gelişim ve değişim sadece üretimde değil aynı zamanda da müşteri isteklerinde de olmaktadır. Üretim sektöründe rekabetin çok yoğun olması dolayısı ile müşteri isteklerinin zamanında karşılanmaması özellikle ürünlerin zamanında teslim edilememesi müşterilerin rakip işletmeleri tercih etmesine neden olmaktadır. Teslim sürelerine daha fazla uyulması için işletmelerin üretimlerini daha fazla kontrol altında tutmaları gerekmektedir. Ama kontrol her zaman mümkün olamamaktadır. Özellikle sipariş tipi üretimlerde malzeme planı yapılması ve ihtiyaç duyulan malzemenin geç gelmesinden dolayı üretimde gecikmeler meydana gelebilmektedir. Bu çalışmada sipariş tipi olarak treyler üretimi yapan bir işletmede yaşanan ürünlerin zamanında teslim edilememesi problemi ele alınmaktadır. Proje bazlı sipariş tipi üretim yapan işletmede üretilen her treyler için müşterinin verdiği şartnameye göre farklılıklar olmaktadır. İşletme siparişe göre mühendislik ilkesiyle müşteri talebine yönelik projelendirme yapmaktadır. Bu nedenle işletmenin üretim hacmi düşük, çeşitlilik miktarı ise yüksektir. Her proje için şartnameye göre baştan planlama yapılması zorunluluğu proje takibini zorlaşmaktadır. Aynı zamanda planlama doğru şekilde yapılamadığında ürün teslim süreleri de tam olarak belirlenememektedir. Planlama eksikliğinden dolayı üretime başladıktan sonra dahi siparişi verilmeyen malzemeler ya da hala tedarikçiden gelmeyen malzemeler olmaktadır. Bu çalışmada projelerin takibinin kolaylaşması için bir çözüm sunulacaktır. Problemin çözümü için üretim ve malzeme planı yapılarak optimum sonuç elde edilmeye çalışılmıştır. Öncelikle ilgili şartnamelere göre malzeme istekleri belirlenmiştir. Daha sonra proje faaliyetleri belirlenerek şebeke diyagramı oluşturulmuştur. Çalışmada PERT tekniği ile projeler için olası başlangıç ve

bitiş süreleri belirlenmiştir. Yapılan bu çalışma ile projenin üretim ve malzeme planı takibinin daha kolay yapılması hedeflenmiştir.

Anahtar Kelimeler: Malzeme Planlama, Üretim Planlama, Şebeke Diyagramı, PERT Tekniği

1. GİRİŞ

Müşteri tarafından tercih edilebilirliği arttıran önemli kriterlerden birisi zamanında teslimdir. Bu nedenle projelerin zamanında teslimi işletmeler açısından oldukça önemlidir. Zamanında teslim yapabilmek için ilgili proje için zaman, işgücü ve malzeme gibi kaynakların doğru planlanması gerekmektedir. Bu nedenle proje yönetimi teknikleri işletmelerin sıklıkla kullandığı tekniklerdendir. Proje yönetimi, belirli bir projede belirlenen amaçlara (zamanında teslim, belirli bir miktarda üretim gibi) ulaşabilmek için gereken kaynakların planlanması, organizasyonu, tedariki ve yönetilmesi ile ilgilenen bir disiplindir. Proje yönetimi teknikleri sayesinde işletmeler, planlanan veya beklenmedik durumların gelecekteki etkilerini tahmin ederek önceden önlem alabilmektedirler (Ertuğrul ve Karakaşoğlu, 2008).

PERT (Proje Değerlendirme ve Gözden Geçirme Tekniği) üretimdeki gecikmeleri, aksamaları ve çeşitli çatışmaları minimuma indirmek için uygulanan ve projenin çeşitli kısımlarını bir arada yürüten ve bunlar arasında düzenli bir koordinasyon sağlayan ve projelerin tamamlanmasını hızlandıran bir yöntemdir (Temiz ve Cingöz, 2015).

Proje yönetimi uygulamalarına, proje çalışması yapılan tüm sektörlerde sıklıkla rastlamak mümkündür. Özer (2020) çalışmasında, şebeke analizinin Türkiye ormancılığındaki kullanım durumunu incelemiş ve CPM (Critical Path Method) ve PERT tekniklerinin uygulanmasında kullanılan istatistiksel formülleri ve yöntemleri sıralamıştır. Kılıç ve Özgürel (2005) çalışmalarında, tersiyer kanal düzeyindeki bir sulama ünitesinde kaynak seviyeleme ve sulama optimizasyonu yapabilmek için CPM ve PERT yöntemlerini kullanmışlardır. Şimşek ve Akçay Kasapoğlu (2006) çalışmalarında inşaat sektörü için proje yönetimi uygulaması yapmışlar ve ek olarak müteahhit seçimi için gerekli kriterleri Analitik Hiyerarşi Yöntemi ile belirlemişlerdir. Kömürlü ve Toltar (2018) çalışmalarında inşaat projelerinde proje yönetiminin kullanımını ve proje yönetiminin projenin başarısına etkisini incelemişlerdir. Bozoğlu (2005) çalışmasında AB hibe projeleri için proje yönetim

tekniklerini uygulamıştır. Köktepe Karahüseyinoğlu ve Karahüseyinoğlu (2021) çalışmalarında sağlık sektöründe yapılan proje yönetimi uygulamalarını incelemişlerdir.

Bu çalışmada öncelikle müşterinin siparişinin şartnamesine göre gerekli istekler belirlenerek hazırlanacak projenin faaliyetleri tanımlanmıştır. Daha sonra şebeke diyagramı oluşturulmuş ve PERT tekniği ile problem için çözüm yolu üretilmiştir.

2. UYGULAMA

Bu çalışma sipariş tipi üretim yapan bir treyler üreticisinde yapılmıştır. Sipariş tipi üretim yapan işletmede üretilen her treyler için müşterinin verdiği şartname değişiklik gösterebilmektedir. İşletme siparişe göre mühendislik ilkesiyle müşteri talebine yönelik projelendirme yapmaktadır. Bu nedenle üretim hacmi düşük, ürün çeşitlilik miktarı ise yüksektir. Her proje için baştan planlama yapılması zorunluluğu sipariş takibini zorlaştırmaktadır. Planlama eksikliklerinden dolayı da malzeme teslim süreleri tam olarak belirlenememektedir. Üretim süreci esnasında dahi siparişi verilmeyen malzemeler ya da henüz gelmeyen malzemeler olmaktadır. Bu çalışmada projenin takibinin kolaylaşması için bir çözüm önerisi sunulacaktır.

2.1 Proje Şartnamesine göre İsteklerin Belirlenmesi

Bu aşama proje başlamadan önce, müşteri talep ve isteklerini belge (şartname) halinde sunar. Bu şartnamede; elektrik, su, taşıyabileceği ağırlık kapasitesi vb. gibi istekler yer almaktadır. Tasarımdan sorumlu AR-GE birimi ilk önce bu şartnameyi en ince ayrıntısına kadar okur ve şartnameye göre tasarım ortaya çıkarır. Şartnamede net olmayan durumlar var ise müşteri ile iletişime geçirilir. Şartname ilgili üretim bölümlerine göre ayrılır.

2.2 Hazırlanan Proje için Faaliyetlerin Belirlenmesi

Proje tasarımı bittikten sonra proje hazırlanmasından ve planlamasından sorumlu mühendisler toplantı yapar. Buradaki en önemli nokta; her projenin özel olması ve projelerin birbirinden bağımsız olmasıdır. Bu yüzden her projenin tasarımı/planlanması/satın alınması gereken malzemeleri birbirinden farklı olabilmektedir. Bunun için her projenin planlaması kendine özgü ve diğerlerinden ayrı olarak yapılmaktadır. Bu toplantılar ve bilgi aktarımı sonucunda proje planlama birimi yapılacak işleri gruplara böler ve iş faaliyetlerini oluşturur. Uygulama için sac kasa üretimi seçilmiştir. Sac kasa projesinin faaliyetleri tablo 1'de gösterilmektedir.

Tablo 1: Faaliyetler

	Faaliyetler	İş Adımları
A	1-2	NPU'ların kesilmesi
B	2-3	Alt şasi montajı
C	2-4	Yan, arka kapakların profillerin kesilmesi
D	3-7	Televrelerin montajı (Şaşinin alt yapısında kullanılan bükümlü demir.)
E	7-8	Ön direklerin montajı
F	4-6	Ön üst profil kesimi
G	4-11	Yan ve arka kapak hazırlanması
H	4-5	Arka kapak menteşe hazırlığı
I	8-9	Ön direğin ön saca montajı
J	6-9	Ön üst profil birleştirilmesi
K	6-10	Taban sacı kesilmesi
L	10-11	Taban sacı montajı
M	9-12	Ön üst profilin ön direğe montajı
N	12-13	Ön z sac + z büküm profil destek
O	13-14	Baba omegaların montajı (Kapakların destek aldığı iskelet yapısı)
P	14-15	Omega kapatma sacı (iç)
R	15-11	Arka omega üst kapama + ön direk üst kapama
S	11-16	Tutamak ve yan menteşe montajı
T	5-16	Arka kapak menteşe montajı
U	16-17	Baba erkeği + arka baba erkeği montajı
V	17-18	Kapakların takılması
Y	18-19	Boya
Z	19-20	Kalite

2.3 Şebeke Diyagramın Oluşturulması

Bu aşamaya kadar faaliyetler hazırdır. Hazırlanan faaliyetlerin diyagramı oluşturulur. Diyagram oluştururken çalıştırılacak kişi sayısının, ekipmanın, eş zamanlı yapılabilecek ve yapılamayacak faaliyetlerin dikkate alınması gerekmektedir. Projenin şebeke ağ diyagramı şekil 1'de gösterilmektedir.

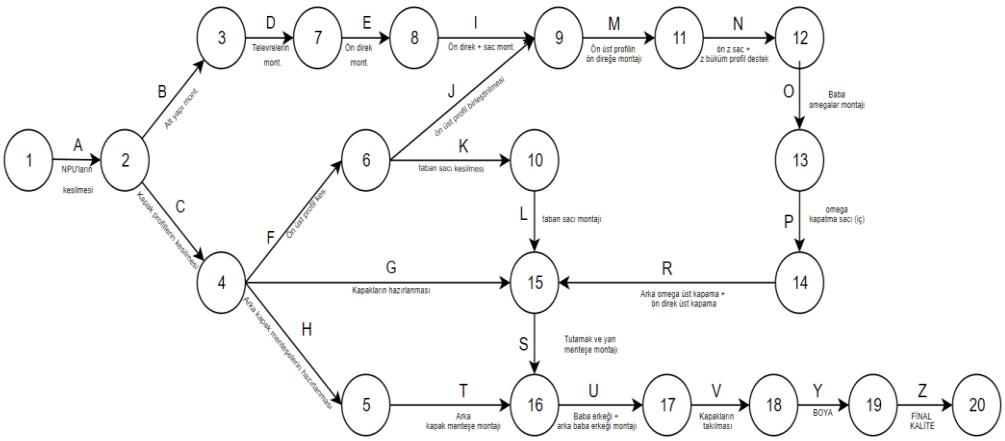

Şekil 1: Şebeke ağ diyagramı

Şekil 1'de gösterilen şebeke ağ diyagramında A harfi ile gösterilen faaliyet NPU'ların kesilmesidir. NPU'ların kesilmesinden sonra eş zamanlı olarak B ve C faaliyetleri gerçekleşebilmektedir. Böylelikle şebeke ağ diyagramı Z faaliyetine kadar sürmektedir.

2.4 PERT Tekniği ile Problemin İncelenmesi

PERT tekniğindeki verilen sürelerin gerçek faaliyetlerle yakın olması en önemli aşamadır. PERT tekniğinde olasılıklar doğrultusunda hareket edilecek her faaliyet için üç süre girilmelidir. Faaliyetlerin süresi ve şebeke ağ diyagramı belirledikten sonra çözüme geçilir.

İlk öncelikle beklenen ortalama süre (t) hesaplanır. Beklenen ortalama süresi hesapladıktan sonra her faaliyetin varyans hesaplaması yapılır. Tablo 2'de PERT tekniğinin aşamaları gösterilmektedir.

Tablo 2: PERT tekniği aşamaları

Faliyetler		İş Adımları	a (en iyimser süre)	m (en olası süre)	b (en kötümser süre)
A	1-2	NPU'ların kesilmesi	110	114	115
B	2-3	Alt şasi montajı	506	610	706
C	2-4	Yan, arka kapakların profillerin kesilmesi	55	58	60
D	3-7	Televrelerin montajı	310	313	315
E	7-8	Ön direklerin montajı	100	102	103
F	4-6	Ön üst profil kesimi	10	12	14
G	4-15	(profillerin birleştrilmesi + sac)	243	255	280
H	4-5	Arka kapak menteşe hazırlığı	123	210	238
I	8-9	Ön direğin ön saca montajı	55	74	80
J	6-9	Ön üst profil birleştirilmesi	50	54	58
K	6-10	Taban sacı kesilmesi	17	18	19
L	10-15	Taban sacı montajı	45	86	90
M	9-11	Ön üst profilin ön direğe montajı	4	5	6
N	11-12	Ön z sac + z büküm profil destek	75	76	77
O	12-13	Baba omegalar montajı	457	500	549
P	13-14	Omega kapatma sacı (iç)	35	35	40
R	14-15	Arka omega üst kapama + ön direk üst kapama	6	8	10
S	15-16	Tutamak ve yan menteşe montajı	262	260	284
T	5-16	Arka kapak menteşe montajı	158	159	225
U	16-17	Baba erkeği + arka baba erkeği montajı	50	52	55
V	17-18	Kapakların takılması	276	296	319
Y	18-19	Boya	450	465	480
Z	19-20	Kalite	110	135	120

Tablo 2'de A olarak faaliyet gösterilmektedir. 1-2 olarak gösterim ise A faaliyetinin başlangıç-bitiş noktalarını gösterir. Tablo 2'deki süreler dakika cinsinden gösterilmiştir. A faaliyeti için problem olmadığı durumda yapılabilen en iyi süre 110 dakikadır. 114 dakika en olası süreyi ve 115 dakika ise en kötümser süreyi vermektedir.

Şekil 2'de şebeke ağ diyagramındaki faaliyetlerin kendi süreleri gösterilmektedir.

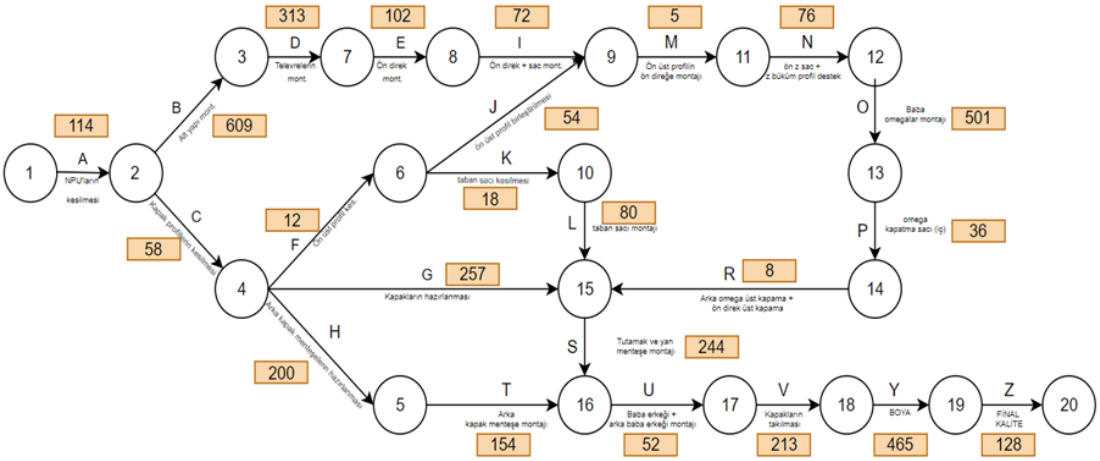

Şekil 4: Şebeke ağ diyagramındaki faaliyetlerin süreleri

A faaliyeti için toplam süre 114 dakika sürmektedir. B faaliyeti 609 dakika sürmektedir. Bu gösterim faaliyetler arasındaki kümülatif gösterim değildir. Bu diyagramda faaliyetin daha kolay gösterimi için her faaliyetin üstünde beta dağılımıyla hesaplanan t süreleri gösterilmiştir.

2.5 PERT Tekniği ile Problemin Çözümlenmesi

PERT tekniğini çözmek için en iyimser, en olası ve en kötümser süreler ile beta dağılımlı t süresi hesaplanır. Beklenen t süresi hesaplandıktan sonra varyanslar hesaplanır. Bu bilgi ve veri kümesi ile istenen başlama ve bitirme sürelerini hesaplanabilmektedir. Problemin çözümlenmesi ve sonuçları tablo 3'de gösterilmektedir.

Tablo 3: Sonuçlar

Faliyetler		İş Adımları	t	varyans^2	ES DAKİKA (En erken başlama)	EF DAKİKA (En erken bitirme)	LS DAKİKA (En geç başlama)	LF DAKİKA (En geç bitirme)	S (Boş) SAAT
A	1-2	NPU'ların kesilmesi	114	0,69	0	114	0	114	0,000
B	2-3	Alt şasi montajı	609	1111,11	114	723	114	723	0,000
C	2-4	Yan, arka kapakların profillerin kesilmesi	58	0,69	114	172	1668	1726	25,900
D	3-7	Televrelerin montajı	313	0,69	723	1036	723	1036	0,000
E	7-8	Ön direklerin montajı	102	0,25	1036	1138	1036	1138	0,000
F	4-6	Ön üst profil kesimi	12	0,44	172	184	1144	1156	16,200
G	4-15	(profillerin birleştrilmesi + sac)	257	38,03	172	429	1579	1836	23,450
H	4-5	Arka kapak menteşe hazırlığı	200	367,36	172	372	1636	1836	24,400
I	8-9	Ön direğin ön saca montajı	72	17,36	1138	1210	1138	1210	0,000
J	6-9	Ön üst profil birleştirilmesi	54	1,78	184	238	1156	1210	16,200
K	6-10	Taban sacı kesilmesi	18	0,11	184	202	1738	1756	25,900
L	10-15	Taban sacı montajı	80	56,25	202	282	1756	1836	25,900
M	9-11	Ön üst profilin ön direğe montajı	5	0,11	1210	1215	1210	1215	0,000
N	11-12	Ön z sac + z büküm profil destek	76	0,11	1215	1291	1215	1291	0,000
O	12-13	Baba omegalar montajı	501	235,11	1291	1792	1291	1792	0,000
P	13-14	Omega kapatma sacı (iç)	36	0,69	1792	1828	1792	1828	0,000
R	14-15	Arka omega üst kapama + ön direk üst kapama	8	0,44	1828	1836	1828	1836	0,000
S	15-16	Tutamak ve yan menteşe montajı	264	13,44	1836	2080	1816	2080	0,000
T	5-16	Arka kapak menteşe montajı	170	124,69	372	526	1910	2080	25,900
U	16-17	Baba erkeği + arka baba erkeği montajı	52	0,69	2080	2132	2080	2132	0,000
V	17-18	Kapakların takılması	297	51,36	2132	2345	2049	2345	0,000
Y	18-19	Boya	465	25,00	2429	2810	2345	2810	0,000
Z	19-20	Kalite	128	2,78	2894	2938	2810	2938	0,000

Kritik faaliyetler, S (boş) sürelerinde otomatik olarak çıkmaktadır. Boş (S) süreleri sıfır olan değerler kritik faaliyetlerdir. Bu kritik faaliyetler ne erken ne de geç başlayabilir. Planlanan zaman da yapılmalıdır. Eğer bu kritik noktalarda sapma olursa hazırlanan planda zaman kaymaları söz konusu olacaktır. Dolayısıyla sipariş istenilen zamanda teslim edilemeyebilir. Ya da daha fazla mesai ihtiyacı oluşabilir.

En erken başlama, bitirme ve en geç başlama, bitirme süreleri hesaplanmıştır. Böylece her faaliyetin süreleri bulunmuştur. Planlanan bu faaliyetler başlamadan önce üretimde kullanılacak malzemelerin de temin edilmesi gerekmektedir. Şartnameye göre belirlenen malzeme listesi (BOM-Bill Of Material) her faaliyete göre gruplandırılarak istenilen malzemenin en erken ve en geç ne zaman teslim edilmesi gerektiğinin takibi daha kolay şekilde yapabilmektedir. Malzeme ve teslim süreleri tablo 4'de gösterilmektedir.

Tablo 4: Malzeme teslim süreleri

Faliyetler		İş Adımları	t	varyans^2	ES DAKİKA (En erken başlama)	LS DAKİKA (En geç başlama)	En Erken Teslim Tarihi	En Geç Teslim Tarihi
A	1-2	NPU'ların kesilmesi	114	0,69	0	0	1.gün	1.gün
B	2-3	Alt şasi montajı	609	1111,11	114	114	1.gün	2.gün
C	2-4	Yan, arka kapakların profillerin kesilmesi	58	0,69	114	1668	1.gün	4.gün
D	3-7	Televrelerin montajı	313	0,69	723	723	2.gün	3.gün
E	7-8	Ön direklerin montajı	102	0,25	1036	1036	3.gün	3.gün
F	4-6	Ön üst profil kesimi	12	0,44	172	1144	1.gün	3.gün
G	4-15	(profillerin birleştrilmesi + sac)	257	38,03	172	1579	1.gün	4.gün
H	4-5	Arka kapak menteşe hazırlığı	200	367,36	172	1636	1.gün	4.gün
I	8-9	Ön direğin ön saca montajı	72	17,36	1138	1138	3.gün	3.gün
J	6-9	Ön üst profil birleştirilmesi	54	1,78	184	1156	1.gün	3.gün
K	6-10	Taban sacı kesilmesi	18	0,11	184	1738	1.gün	4.gün
L	10-15	Taban sacı montajı	80	56,25	202	1756	1.gün	4.gün
M	9-11	Ön üst profilin ön direğe montajı	5	0,11	1210	1210	3.gün	3.gün
N	11-12	Ön z sac + z büküm profil destek	76	0,11	1215	1215	3.gün	3.gün
O	12-13	Baba omegalar montajı	501	235,11	1291	1291	3.gün	4.gün
P	13-14	Omega kapatma sacı (iç)	36	0,69	1792	1792	4.gün	4.gün
R	14-15	Arka omega üst kapama + ön direk üst kapama	8	0,44	1828	1828	4.gün	4.gün
S	15-16	Tutamak ve yan menteşe montajı	264	13,44	1836	1816	4.gün	5.gün
T	5-16	Arka kapak menteşe montajı	170	124,69	372	1910	1.gün	5.gün
U	16-17	Baba erkeği + arka baba erkeği montajı	52	0,69	2080	2080	5.gün	5.gün
V	17-18	Kapakların takılması	297	51,36	2132	2049	5.gün	5.gün
Y	18-19	Boya	465	25,00	2429	2345	6.gün	6.gün
Z	19-20	Kalite	128	2,78	2894	2810	7.gün	7.gün

Malzeme listesi, her malzemenin kullanılacağı faaliyete göre gruplandırılmıştır. Bir günlük çalışma sekiz saat olarak kabul edilmiştir. Her sekiz saat ile gün ataması yapılmıştır. Örneğin bir faaliyet 7. saat de gerçekleşiyor ise 1. gün gerçekleşecektir. 19. saat ise 3. gün gerçekleşecektir. Excel'de eğer formülü kullanılarak fer faaliyetin gerçekleşme günleri elde edilmiştir.

Daha sonrasında düşey ara formülünden yararlanılarak tablo 4'deki faaliyet numaraları tablo 5'de verilen malzemelerin en erken teslim tarihi ve en geç teslim tarihine göre ilgili gün bulunarak otomatik olarak çekilebilmektedir.

Tablo 5: Malzeme listesi ve teslim günleri

Malzeme Listesi

Faaliyetler	Parça Adı		Adet	En Erken Teslim Tarihi	En Geç Teslim Tarihi
A	100 lük profil		1	1.gün	1.gün
	100 lük profil		1		
	65 lik profil		7		
	65 lik profil		1		
	65 lik profil		10		
B	ALT ŞASİ DESTEK L1		2	1.gün	2.gün
	ALT ŞASİ DESTEK L2		2		
	ALT ŞASİ DESTEK L3		2		
C	YAN KAPAK ON SOL	1_RECTANGULAR_TUBE_29	1	1.gün	4.gün
		1_RECTANGULAR_TUBE_30	1		
		1_RECTANGULAR_TUBE_31	1		
		1_RECTANGULAR_TUBE_32	1		
		YAN_KAPAK_SAC	1		
	ARKA YAN KAPAK SOL	1_RECTANGULAR_TUBE_33	1		
		1_RECTANGULAR_TUBE_34	1		
		1_RECTANGULAR_TUBE_35	1		
		1_RECTANGULAR_TUBE_36	1		
		YAN_KAPAK_SACI_2	1		
	ARKA YAN KAPAK SAĞ	1_RECTANGULAR_TUBE_33	1		
		1_RECTANGULAR_TUBE_34	1		
		1_RECTANGULAR_TUBE_35	1		
		1_RECTANGULAR_TUBE_36	1		
		YAN_KAPAK_SACI_2_MIR	1		
	YAN KAPAK ON SAG	1_RECTANGULAR_TUBE_29	1		
		1_RECTANGULAR_TUBE_30	1		
		1_RECTANGULAR_TUBE_31	1		
		1_RECTANGULAR_TUBE_32	1		
		YAN_KAPAK_SAC_MIR	1		
	ARKA KAPAK	1_RECTANGULAR_TUBE_29	1		
		1_RECTANGULAR_TUBE_30	1		
		1_RECTANGULAR_TUBE_31	1		
		1_RECTANGULAR_TUBE_32	1		
		ARKA_KAPAK_SAC	1		
D	YAN TELEVRE		2	2.gün	3.gün
	ÖN TELEVRE_2		1		
	ARKA TELEVRE 2		1		
E	DİREK_TELEVRE		1	3.gün	3.gün
	ÖN_DİREK_2		1		
	ÖN_DİREK_KAPATMA		1		
	ÖN_DİREK_SAC_2		1		
	ÖN_DİREK_KAPAMA_SACI_2		1		
	ÖN_DİREK_KAPAMA_2		1		
F	ÖN ÜST PROFİL	1_RECTANGULAR_TUBE_24	1	1.gün	3.gün
		1_RECTANGULAR_TUBE_25	1		
		1_RECTANGULAR_TUBE_26	1		
		1_RECTANGULAR_TUBE_27	1		
		1_RECTANGULAR_TUBE_28	1		
G	Yan_Kapak_Menteşe_Sacı		1	1.gün	4.gün
	Arka_Kapak_Kapama_Sacı(2)		2		
	Arka Kapak Sac		1		
H	Arka Kapak Burç(2)		2	1.gün	4.gün
	Arka Kapak Menteşe Sacı_22 (4)		4		
I	ÖN DUVAR SAC		1	3.gün	3.gün
K	taban sacı		1	1.gün	4.gün
N	Z_UST_KAPAMA		1	3.gün	3.gün
	ÖN Z SAC (1)		1		
	ÖN Z_2 (1)		1		
	Z_Destek Alt Sac (2)		2		
O	YAN BABA OMEGA SOL	YAN_OMEGA	1	3.gün	4.gün
		BABA_YUVA BABA_2	1		
		BABA_YUVA BABA_2	1		
		ARKA_OMEGA	1		
	YAN BABA OMEGA SAĞ	BABA_YUVA_MIR	1		
		BABA_2_MIR	1		
		YAN_OMEGA_MIR	1		
		BABA_YUVA_MIR	1		
		BABA_2_MIR	1		
		ARKA_OMEGA_MIR	1		
		ARKA_OMEGA_KAPAMA_M	1		
		ARKA_OMEGA_KAPAMA_M	1		
P	YAN BABA OMEGA SOL	YAN_BABA_KAPAMA_SACI	1	4.gün	4.gün
		ARKA_OMEGA_KAPAMA	1		
R	ARKA BABA OMEGA SOL		1	4.gün	4.gün
S	YAN MENTEŞE	MENTEŞE_1 (8)	8	4.gün	5.gün
S		MENTEŞE_2 (8)	8	4.gün	5.gün
	EL_TUTAMAĞI		1		
U	KONİK BABA ERKEĞİ		8	5.gün	5.gün
	LAMA (10)		10		
	KAMA(10)		10		
Y	BOYA		3 Kutu	6.gün	6.gün

Tablo 5'de, A faaliyeti için 100'lük ve 65'lik profil gerekmektedir. A faaliyeti birinci gün yapılacağı için birinci gün sabahında işe başlamadan önce bu malzemelerin getirilmesi gerekmektedir. Yani bir gün önceden hazırlığı yapılmalıdır.

Aynı şekilde A, B ve C faaliyetlerin en erken bitirme süreleri birinci gündür. Bu 3 faaliyetin malzemeleri proje başlamadan önce hazırlanması istenmektedir. Ama en geç olasılıkla B faaliyeti için 2. gün ve C faaliyeti 4. gün teslim edilebilir. Malzemelerin teslim süreleri en geç teslim edilme sürelerinden sonra teslim edilirse üretimde aksaklıklar ve istenilen zamanda üretilmeme gibi problemler ortaya çıkabilir.

3. SONUÇLAR VE DEĞERLENDİRME

Ele alınan problem treyler üretimde plansız üretime başlanmasıdır. Problemin çözümü için PERT tekniği ile yapılacak olan işleri gruplara bölüp, üretim faaliyetlerini belirledikten sonra şebeke ağ diyagramı ile faaliyetler planlanmıştır. Hazırlanan şebeke ağ diyagramı ile her faaliyetin en erken ve en geç başlama, bitirme süreleri hesaplanmıştır ve sonucunda kritik noktalar bulunmuştur.

PERT uygulaması ile projedeki kritik faaliyetler bulunmuştur. Projenin tamamlanma süresi 7 gün olarak elde edilmiştir. Bu proje üretiminde dar boğaz oluşabilecek faaliyetler için mesai ve işgünü artırımına gidilerek projenin istenilen sürede bitmesi hedeflenmiştir. Üretimde kullanılacak malzemelerin ne zaman teslim alınması gerektiği, satın almadan sorumlu kişiye bildirilir ve teslim sürelerine göre satın alma gerçekleşir.

Uygulama ile, proje yöneticilerinin malzeme eksikliğinden dolayı üretimi bekletme ihtimali düşürülmüş ve boş zaman kayıpları eş zamanlı üretim ile minimum hale getirilmiştir.

KAYNAKÇA

[1] Ertuğrul, İ., Karakaşoğlu, N. Bulanık PERT yaklaşımlarının makine üretim sürecinde karşılaştırılması, Dokuz Eylül Üniversitesi İktisadi ve İdari Bilimler Fakültesi Dergisi, cilt 23, sayı 1, sayfa 109-124, 2008.

[2] Temiz, N., Cingöz, K. İşgören seçim sürecindeki kritik faaliyetlerin analitik hiyerarşi süreci ile değerlendirilmesi, Dokuz Eylül Üniversitesi Sosyal Bilimler Enstitüsü Dergisi, cilt 17, sayı 4, sayfa 531-553, 2015.

[3] Özer, N. Şebeke analizinin Türkiye ormancılığındaki durumu, JENAS Journal to Environmental and Natural Studies, vol 2, issue 2, pages 96-101, Fall, 2020.

[4] Kılıç, M., Özgürel, M. Tersiyer kanal düzeyindeki bir sulama ünitesinde kaynak seviyeleme ve sulamanın optimizasyonu, Ege Üniversitesi Ziraat Fakültesi Dergisi, 42 (2), sayfa 97-108, 2005.

[5] Şimşek, U.T., Akçay Kasapoğlu, Ö. Analitik Hiyerarşi Prosesi tekniği ile bir proje yönetimi uygulaması, Öneri, cilt 7, sayı 25, sayfa 141-149, Ocak 2006.

[6] Kömürlü, R., Toltar, L. İnşaatta proje yönetimi; projenin başarısına etkisi, Mimarlık ve Yaşam Dergisi, 3(2), sayfa 249-258, 2018.

[7] Bozoğlu, G. Proje Yönetimi ve PERT, CPM tekniklerinin AB Hibe Projesine Uygulanması, Marmara Üniversitesi Sosyal Bilimler Enstitüsü Ekonometri Anabilim Dalı Yöneylem Araştırması Bilim Dalı, Yüksek Lisans Tezi

[8] Köktepe Karahüseyinoğlu, E., Karahüseyinoğlu, F. Sağlık kurumlarında proje yönetimi, Eurasia Summit, 2nd International Social Science Congress, Haziran 2021 https://www.avrasyakongresi.org/_files/ugd/7cf5ba_2fbb57d47512425da890a513c41838d8.pdf#page=68

DOĞAL DİL İŞLEME YÖNTEMLERİ İLE SOSYAL MEDYA PAYLAŞIMLARINDA DEPRESYON TESPİTİ

DEPRESSION DETECTION IN SOCIAL MEDIA SHARES VIA NATURAL LANGUAGE PROCESSING TECHNIQUES

Recep YILDIRIM[1], Dr. Öğr. Üyesi, Sinem AKYOL[2]

[1]Fırat Üniversitesi, Mühendislik Fakültesi, 180290030@firat.edu.tr - 0000-0002-6653-3593

[2]Fırat Üniversitesi, Mühendislik Fakültesi, sakyol@firat.edu.tr - 0000-0001-9308-3500

ÖZET

Depresyon, en yaygın zihinsel rahatsızlıkların başında gelmektedir. Kişinin duygu durumunu etkileyen bu zihinsel rahatsızlık tedavi edilmediği takdirde intihara varana dek geniş bir yelpazede kötü sonuçlar doğurabilmektedir. Bu sebeple kişinin davranışları incelenerek depresyon içerisinde olup olmadığının belirlenmesi hayati öneme sahiptir. Sosyal medya kullanımının oldukça yaygınlaşması ve insanların duygu ve düşüncelerini özgür bir şekilde bu tarz platformlarda ifade edebilmeleri, sözü edilen platformlardaki aktivitelerin analiz edilerek kişinin hastalık durumunun tespit edilebilirliğini gündeme getirmiştir. Depresyon halinin çoğunlukla kendini sözlü olarak belli etmesi ve sözlü iletişimin sosyal medyadaki yazılı iletişime karşılık gelmesi gözleri sosyal medya platformlarındaki metinsel paylaşımlara çevirmiştir. Yapılan paylaşımlar bir araya getirilerek veri setlerinin oluşturulabilir ve bu veri setleri sayesinde doğal dil işleme (DDİ) teknikleri ile kişinin depresyon durumu tespit edilebilir. Bu çalışma kapsamında bahsedilen veri setine benzer bir veri seti kullanılmış, 4 farklı yapıda 4 doğal dil işleme modeli eğitilmiştir ve bu modeller sayesinde sosyal medya üzerindeki metinsel paylaşımlar kullanılarak paylaşımı yapan kullanıcının depresyon içerisinde olup olmadığının tespiti gerçekleştirilmiştir.

Veri seti olarak, Reddit platformu üzerindeki kullanıcıların paylaşımları kullanılmıştır. 116,037'si "*suicide*" ve 116,037'si "*non-suicide*" olmak üzere toplamda 232,074 veriden oluşan veri setine, Bidirectional modellerin getirdiği hesaplama yükünü azaltmak adına kullanılması önerilen Unidirectional modelleri eğitebilmek için her bir girdi verisinin ters sırada yeniden oluşturulduğu yeni bir veri seti eklenmiştir. Eğitilen modeller *Bidirectional LSTM, Bidirectional GRU, Unidirectional LSTM* ve *Unidirectional GRU* modelleridir ve sinir ağları tabanlı olup, çoğunlukla metinsel ve/veya zaman serisinden oluşan verilerin işlenmesinde kullanılırlar. Oluşturulan modeller *accuracy, precision, recall, f1-score, sensitivity* ve *specificity* metrikleri kullanılarak incelenmiştir, hız farkları karşılaştırılmıştır. Karşılaştırma sonunda %96.6 doğruluk oranı ile en yüksek doğruluğu *Bidirectional LSTM* modeli göstermiştir. Verilerin tersine çevrilmiş hallerini de barındıran veri seti ile eğitilmiş modeller de ise bu oranlar *LSTM* modeli için %96.2 ve *GRU* modeli için %96.0'dır. Buradan da anlaşılacağı üzere sunulan teknik benzer doğruluk oranlarına yarıya düşürülmüş parametre sayısı ile erişilmesini mümkün kılmıştır.

Anahtar Kelimeler: Depresyon Tespiti, Sosyal Medya Analizi, Derin Öğrenme, Doğal Dil İşleme

ABSTRACT

Depression is one of the most common mental illnesses. This illness that affects the person's state of mind in a bad way may end up in the suicide of the person himself/herself when it is not treated. Therefore, the detection of depression by the inspection of a person's behaviours is vital. The highly increasing social media usage and the freedom served by these social media platforms to persons to share their feelings easily revealed potential ability for the detection of depression by analysing that activity in their social media accounts. Textual shares in social media attract attention since depression mostly appears as verbally and text shares are equivalents of these verbal communications in social media. These shares can be collected in a dataset and depression in a person can be detected with the help of natural language processing (NLP) techniques. A dataset which is similar to just mentioned one has been used to train 4 natural language processing models in 4 different types within the scope of this work and with the aid of models a person's proneness to depression has been detected by using the person's textual social media shares.

User shares on the Reddit platform have been used as a dataset. The dataset contains 232,074 shares and 116,037 shares of the dataset belong to the "suicide" class and 116,037 shares of the dataset belong to the "non-suicide" class. The reverse order of the shares has been created to train the Unidirectional models which are used as an alternative to alleviate the computing complexity of the Bidirectional models as an addition to the dataset and this dataset composed of reverse order shares is added to the original dataset. At a glance, trained models are Bidirectional LSTM, Bidirectional GRU, Unidirectional LSTM and Unidirectional GRU. All models are based on neural networks and they are used mostly to process sequences like textual data or time series. The built models have been examined according to their accuracy, precision, recall, f1-score, sensitivity and specificity metrics results, speed differences have been compared. The Bidirectional LSTM model has had the highest accuracy value in comparison to the other models with 96.6% accuracy. The Unidirectional LSTM and GRU models which have been trained on the dataset that also contains the reversed data have reached the 96.2% and 96.0% accuracy values, respectively. This is the proof that our technique allowed the Unidirectional models which have halved parameters in comparison to Bidirectional models to reach almost the same accuracy values as the Bidirectional models.

Keywords: Depression Detection, Social Media Analysis, Deep Learning, Natural Language Processing

1. GİRİŞ

Günümüzde, gelişen teknoloji ve internete olan kolay erişim sosyal medya kullanımını oldukça yaygınlaştırmıştır. İnsanlığın yarıya yakını, günlük zamanının azımsanamayacak bir

miktarını sosyal medya platformlarında geçirmekte tüm insani iletişimini sanal olarak gerçekleştirmektedir. Öyleki İnternet ve Sosyal Medya Kullanıcı İstatistiklerinin (Internet and Social Media User Stats) 2018 yılında yayınladığı rapora göre dünyadaki toplam nüfusun %42'si (3.196 milyar) sosyal medya platformlarını kullanmaktadır [1]. Raporda yayınlanan veriler ışığında, internete erişimi olan insan miktarının %53 (4.021 milyar) olduğu göz önünde bulundurularak, erişimi olan bu insanların yaklaşık %79'unun (3.176 milyar) aktif bir şekilde sosyal medya platformlarını kullandığı ortaya çıkmaktadır. Yine aynı rapora göre sosyal medya kullanımı 2017-2018 yılları arasında %10'luk bir artış göstermiştir.

Hiç şüphesiz bu kullanım oranları tüm dünyayı etkileyen COVID-19 salgını sebebiyle daha da artmış, sosyal medya kullanımı daha da yaygınlaşmıştır. İletişimin bu iki boyuta indirgenmiş ve geçmişe göre kolaylaşmış hali insanların yalnızlaşmasına yol açmıştır. Zaman içerisinde hastalıklı düşünceler kişi üzerinde zihinsel/davranışsal bozukluklar olarak kendini göstermekte ve anksiyete, obsesif kompulsif bozukluk, depresyon gibi çok daha ciddi ve tedavi edilmesi gereken, edilmediği takdirde kişinin kendine zarar vermesi ve/veya daha ileri giderek intihar etmesi gibi sonuçları doğurmaktadır. Dünya Sağlık Örgütü'nün yaptığı bir araştırmaya göre depresyon, dünya çapında 300 milyondan fazla kişiyi etkileyen en yaygın zihinsel bozukluktur [2]. Depresyon ayrıca her yıl en çok ölüme neden olan ikinci ya da üçüncü sebeptir [3]. Amerika Psikiyatri Derneğinin tanımladığı şekli ile depresyon, kişinin nasıl hissettiğini, nasıl düşündüğünü ve nasıl davrandığını kötü yönde etkileyen yaygın ve ciddi bir tıbbi rahatsızlıktır [4].

Depresyonun bu kadar yaygın olması ve ölüme yol açması, depresyon belirtilerinin önceden tespitine hayati bir önem kazandırmıştır. Günümüz dünyasında, insanların zamanlarını sosyal medyada harcamaları; yaşantılarını, yaşadıklarını, düşünce ve duygularını da yine sosyal medya platformlarında paylaşmaları, dikkatleri bu platformlardaki paylaşımlara ve bu çalışmanın da konusunu oluşturan paylaşımların analizine çekmiştir.

Son yıllarda, metinsel sosyal medya paylaşımlarının analizi ile ilgili birçok çalışma yapılmıştır. Michael Mesfin Tadesse ve arkadaşları, yaptıkları bir çalışmada *LSTM* ağı, *CNN* ağı ve *LSTM-CNN* ağlarının bir araya getirilmesiyle oluşturulan bir başka ağ tabanlı 3 farklı model inşa etmiş ve *Reddit* platformu üzerinde yapılan metinsel paylaşımlardan oluşturulan bir veri seti üzerinde bu modelleri eğiterek sırasıyla %91.7, %90.6 ve %93.8 oranında doğruluk değerlerine ulaşmışlardır [5]. Bir başka çalışmada ise Li-Chen Cheng ve Song-Lin Tsai film eleştirilerinden oluşan bir veri seti üzerinde *LSTM, Bi-LSTM* ve *GRU* tabanlı modeller eğitmiş, sırasıyla %80.83, %87.11 ve %64.92 oranında başarı elde etmişlerdir [6]. Önceki çalışmadan farklı olarak Li-Chen Cheng ve Song-Lin Tsai yaptıkları çalışmada *Word2Vec* yöntemi yerine bu çalışmada da kullanılan *Word Embeddings* yöntemini kullanmışlardır [7]. Aynı şekilde *Reddit* platformu üzerinden toplanan 60000 veri ile oluşturulmuş bir başka veri setinde Pratyaksh Jain ve arkadaşları derin öğrenme yöntemlerinden ziyade geleneksel makine öğrenmesi modelleri kullanarak probleme çözüm aramışlardır. Çalışmaları kapsamında *Logistic Regression, Naïve bayes, Support vector machine* ve *Random forest* modellerini eğitmiş ve sırasıyla %79, %76, %77 ve %77 başarı oranlarını elde etmişlerdir [8].

Bu çalışmada da sosyal medya platformlarındaki kullanıcıların metinsel içerikli paylaşımları analiz edilmiş ve derin öğrenme modeli ve tekniklerinden faydalanılarak kişinin depresyon durumu ve intihara olan eğilimi tespit edilmeye çalışılmıştır. 2. Bölüm olan *Yöntemler* bölümünde, kullanılan derin öğrenme modellerinden bahsedilmiştir. Özet olarak, modellerin neler olduğu, neden kullanıldığı, kaç parametreden oluştuğu, model yapısı, birbirlerinden ne gibi farklılıkları olduğu ve artı ve eksileri gibi konular ele alınmıştır. 3. Bölüm (*Veri Seti*), tespit için kullanılan modellerin eğitiminde yararlanılan veri setinin özelliklerini barındırmaktadır. 4. Bölümde (*Deneysel Sonuçlar*) eğitilen modellerin ürettiği sonuçlar yaygın bazı metrikler üzerinden sunulmuş, modellerin eğitim/çıkarım hızları karşılaştırılmış ve çalışma kapsamında önerilen teknik ile eğitilen modellerin performansları, halihazırda var olan teknikler ile eğitilmiş modellerin performansları ile kıyaslanmıştır. Son olarak 5. Bölümde (*Sonuç*) ise çalışmanın güçlü/zayıf yönleri ele alınmış ve gelecekte yapılabilecek yeni çalışmalardan bahsedilmiştir.

2. YÖNTEMLER

Bu çalışma kapsamında metinsel sosyal medya paylaşımlarından kullanıcıların depresyon ve intihar belirtisi gösterip göstermediğini tespit etmek amacıyla 4 farklı derin öğrenme modeli kullanılmıştır. Kullanılan modeller, uzun dizileri işleme konusundaki kabiliyetinden dolayı *RNN* (*Recurrent Neural Network*) temelli *LSTM* (*Long Short-Term Memory*) ve *GRU* (*Gated Recurrent Unit*) ağları etrafında şekillenmiştir [9][10]. Kullanılan modellerin listesi Çizelge *1*'de verilmiştir:

Çizelge 1. Derin Öğrenme modelleri listesi

Bidirectional LSTM
Bidirectional GRU
LSTM
GRU

Doğal dil işlemede, modelin *N* anındaki girdi verisini işlerken yalnızca o andaki değeri değil de *N+1, N+2* gibi sonraki değerleri de işlemesi model doğruluğu açısından önemli olduğundan dolayı modellerin direkt kullanılması yerine iki farklı türevi kullanılmıştır. Bunlardan ilki girdi olarak verilen katmanın kopyasını oluşturup girdi verileri üzerinde ters sırada işleyen *Bidirectional* model yapısı iken ikincisi alışılagelmiş *Unidirectional* model yapısıdır [11]. Fakat sonraki girdi verilerini işlemenin önemi sebebiyle Unidirectional modeller

eğitilirken girdi verisi ters çevrilerek tekrar modele girdi olarak verilmiş ve böylelikle *Unidirectional* modellerin de yüksek doğruluk oranları üretmesi beklenmiştir. Bu tarz bir yaklaşımın ana sebebi modelin parametre sayısını düşürmektir. Bu yolla modelin eğitim ve çıkarım süresinin azaltılması hedeflenmiştir.

Tüm modellerde ek olarak bir *Embedding* katmanı kullanılmıştır. Bu katmanın eklenme sebebi ise, metin içerisindeki kelimeleri temsil edecek sayı değerlerinin problem bazında öğrenilmesinin istenmesidir. Bu yolla kelimeler için model doğruluğunu düşürmeye müsait sabit sayı değerlerinden ziyade geri yayılım algoritması sayesinde eğitim boyunca model parametreleri ile beraber öğrenilebilen, kelimenin daha iyi bir temsili olan sayı değerleri elde edilmiştir. Oluşturulan modellerin mimarileri Görsel 1 ve 2'de sunulmaktadır:

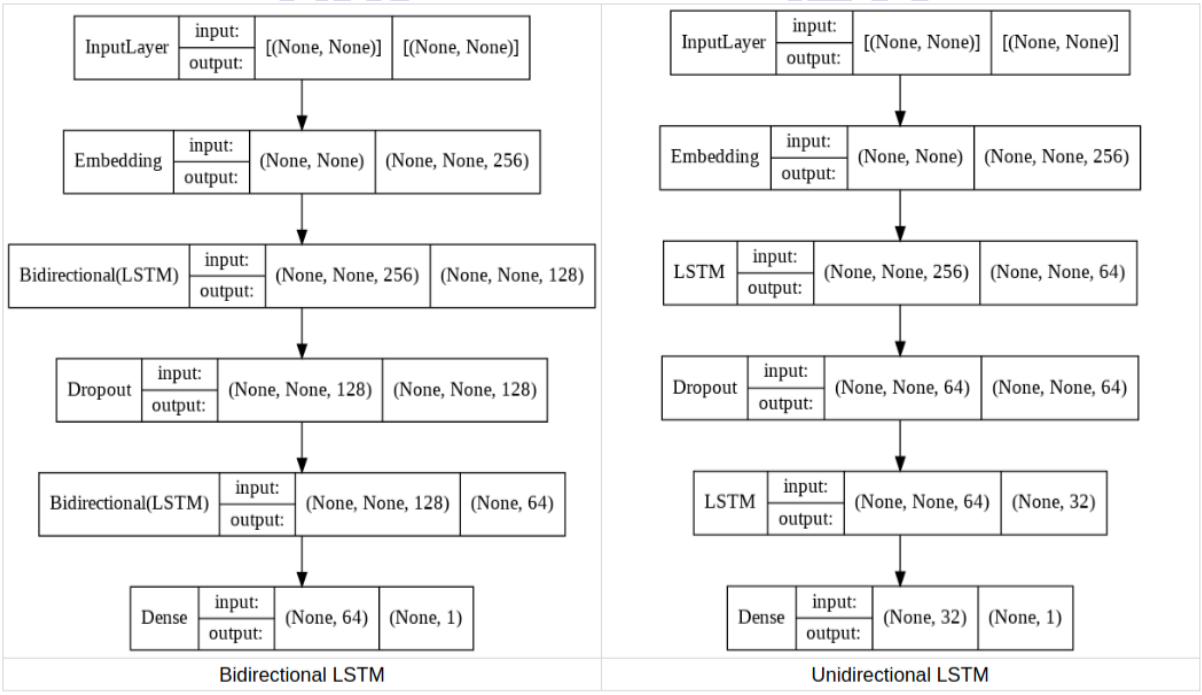

Görsel 1. LSTM Modelleri

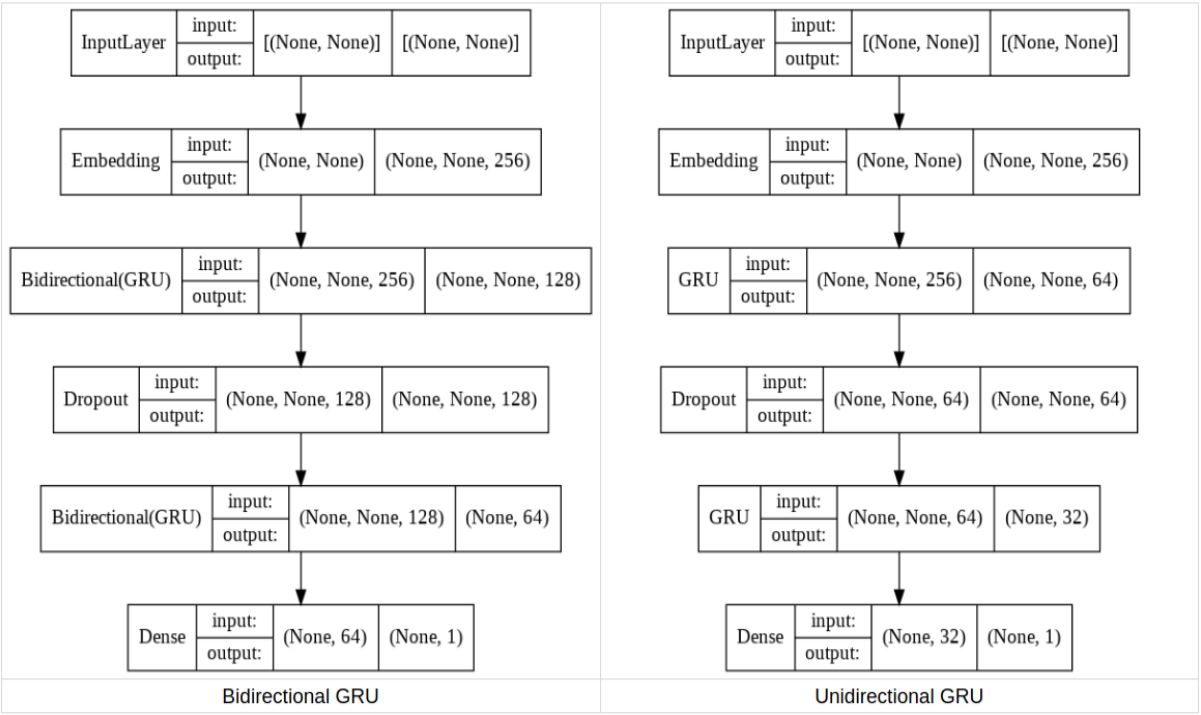

Görsel 2. GRU Modelleri

Görsel 2'de de görüldüğü üzere kullanılan 4 modelin de katman sayıları aynıdır. Her bir model, ilk katman olarak bir *Embedding* katmanı kullanır (*InputLayer* olarak tasvir edilen katman(lar) hiçbir parametre ve işlem içermeyip yalnızca modele girdi olarak verilen verilerin boyutunu temsil etmektedir). *Embedding* katmanı en basit haliyle satır sayısının veri setindeki benzersiz kelimelerin sayısına yakın bir sayı olarak ayarlandığı, sütun sayısının ise eldeki probleme göre ayarlanabilir bir parametre olduğu bir matris olarak düşünülebilir. Bu problem özelinde satır sayısı 30,000 sütun sayısı ise 256 olarak seçilmiş ve bu değerler tüm modellerde kullanılmış *Embedding* katmanları için aynıdır. *Embedding* katmanının devamında ise her modele özgü olan *RNN* temelli katmanlar eklenmiştir. Tüm modellerdeki ilk *RNN* katmanı olan bu katmanda nöron sayısı 64 olarak seçilmiştir. *Unidirectional* modellerde bu katman yalnızca bir katmandan oluşuyor iken *Bidirectional* modellerde bu katman özünde birbirinden bağımsız iki katman eş katmandan oluşmaktadır. Bu ikinci eş katman, gelen girdi verisi üzerinde ilk eş katmanda olduğu gibi soldan sağa değil de sağdan sola olacak şekilde girdi verilerini işlemektedir. İkinci eş katmanın eklenmesiyle ilgili katmandaki nöron sayısı iki katına çıkmış ve bu nedenle parametre sayısı da aynı oranda artmıştır.

Aktivasyon fonksiyonu olarak ise model farketmeksizin ilgili katman için *tanh* (*hyperbolic tangent*) aktivasyon fonksiyonu kullanılmıştır. *RNN* temelli modele özgü katmanın devamında modelin aşırı uyumunu (*overfitting*) engellemek adına tüm modellerde değeri 0.5 olarak ayarlanmış bir *Dropout* katmanı kullanılmıştır. *Dropout* katmanı her bir tekrarlamada modelin, verilen orana göre bazı parametrelerini eğitimin dışında tutarak modelin aşırı uyumunu engeller. *Dropout* katmanından sonra ise tekrar *RNN* temelli modele özgü katman kullanılmıştır. Bu katman da önceki *RNN* temelli katmanla aynı yapıda olup yalnızca 64 nöron yerine 32 nörondan oluşmaktadır ve yine aynı şekilde aktivasyon fonksiyonu olarak *tanh* fonksiyonunu kullanmaktadır. Çözülmek istenen problem bir ikili sınıflandırma problemi

olduğundan son katman olarak tüm modellerde 1 nörondan oluşan tam bağlı sinir ağı (*fully connected neural network*) katmanı kullanılmıştır. Bu katmanda kullanılan aktivasyon fonksiyonu ise *sigmoid* aktivasyon fonksiyonudur. *Embedding* katmanı dahil edilmediğinde, modellerin parametreleri Çizelge 2'de gösterildiği şekildedir:

Çizelge 2. Model Parametreleri Sayısı

	Bidirectional	Unidirectional
LSTM	205,633	94,625
GRU	154,817	71,265

Çizelgeden de görüldüğü gibi *Bidirectional* modellerdeki ikinci eş katmanların varlığı modellerin parametrelerini *Unidirectional* eşitlerine kıyasla yaklaşık olarak ikiye katlamıştır. Bazı problemler düşünüldüğünde model parametrelerinin çok olması bir avantaj iken bu varsayım her problem için geçerli değildir. Aksine bazı problemlerde parametre sayısı arttıkça modelin doğruluk oranı düşmektedir. Ayrıca parametre sayısı arttıkça modelin eğitim ve çıkarım süresi de doğru orantılı biçimde artmaktadır. Çizelge 2'de gösterilen parametrelere ilave olarak tüm modellerin başına birebir aynı yapıda olan bir *Embedding* katmanı eklendiği için her bir modelin toplam parametre sayısı *30,000 x 256 = 7,680,000* parametre daha artmıştır.

3. VERİ SETİ

Çalışma kapsamında kullanılan modelleri eğitmek için *Kaggle* platformu üzerinden alınan *Suicide and Depression Detection* veri seti kullanılmıştır [12]. Bu veri seti *Pushshift API* kullanılarak *Reddit* platformu üzerinde 16 Aralık 2008'den 2 Haziran 2021'e kadar olan "*SuicideWatch*" ve 1 Haziran 2009'dan 2 Haziran 2021'e kadar olan "*depression*" gönderilerinden toplanmıştır [13]. Veri seti, 116,037 adet "*suicide*" sınıfına ve 116,037 adet "*non-suicide*" sınıfına ait olan toplamda 232,074 adet metinsel veriden oluşmaktadır. Bu verilerin 156649 tanesi eğitim (*train*), 58019 tanesi çıkarım (*test*) ve 17406 tanesi ise doğrulama (*validation*) seti olarak kullanılmıştır.

Bidirectional modellerde bu veri seti olduğu gibi kullanılırken, *Unidirectional* modellerde doğruluğu artırmak adına veri setinde bulunan metinsel veriler ters sırada tekrar oluşturulup tersini oluşturmak için kullanılan asıl veriden hemen sonra gelecek veri olacak şekilde veri setine eklenmiştir. İşlem tamamlandıktan sonra veri setindeki toplam veri adedi *2 x 232,074 = 464,148* olmuş, eğitim, çıkarım ve doğrulama setleri de aynı oranda artmıştır. Bu yolla *Unidirectional* modellerin de girdi verilerini ters sırada işleyerek, var olan katmana eş ikinci bir *RNN* katmanı içermeden, *Bidirectional* modeller ile aynı veya yakın doğruluk oranlarını üretmesi hedeflenmiştir. Bu sayede daha az sayıda parametre içeren, eğitim ve

çıkarım süreleri daha kısa fakat doğruluk oranları benzer modellerin inşa edilmesi amaçlanmaktadır.

4. DENEYSEL SONUÇLAR

Modellerin eğitim aşamasında sonra karşılaştırılabilmeleri ve aralarındaki farkların daha iyi görülebilmesi için *Accuracy*, *Precision*, *Recall*, *F1-Score*, *Sensitivity* ve *Specificity* olmak üzere toplamda 6 adet metrik kullanılmıştır. Uygulanan bu metriklerin ürettiği sonuçlar Çizelge 3'te gösterilmiştir:

Çizelge 3. Metrikler

	Bidirectional LSTM	Bidirectional GRU	Unidirecitonal LSTM	Unidirectional GRU
Accuracy	96.6%	96.5%	96.2%	96.0%
Precision	96.0%	95.5%	96.0%	95.2%
Recall	97.2%	97.2%	96.3%	96.8%
F1-Score	96.6%	96.4%	96.2%	96.0%
Sensitivity	97.2%	97.2%	96.3%	96.8%
Specificity	96.0%	95.8%	96.0%	95.3%

Görüleceği üzere *LSTM* modelleri *GRU* modellerine kıyasla ihmal edilebilir düzeyde daha iyi performans göstermiştir. Aynı şekilde *Bidirectional* modeller, *Unidirectional* olan eşitlerine göre görece daha iyi performans göstermişlerdir. Ama asıl dikkat edilmesi gereken ve amaçlanan yakın doğruluk düzeylerinde alınan hız değerleridir. Modellerin eğitim süreleri Çizelge 4'te gösterilmiştir:

Çizelge 4. Model Eğitim ve Çıkarım Süreleri

	Bidirectional LSTM	Bidirectional GRU	Unidirectional LSTM	Unidirectional GRU
Adım Başına Eğitim Süresi	312ms	298ms	141ms	137ms
Adım Başına Çıkarım Süresi	113ms	111ms	49ms	50ms

Hız bakımından değerlendirilecek olunursa Çizelge 2'de görüldüğü gibi *GRU* modellerinin parametre sayıları *LSTM* modellerinin parametre sayılarının ¾'ü kadar olduğundan aynı GPU üzerinde eğitildiklerinde *GRU* modellerinin eğitim süreleri *LSTM* modellerinin eğitim sürelerinden daha kısa sürmüştür. Daha az parametreli modellerde ve/veya daha az veri içeren veri setlerinde Çizelge 4'te görülen hız değerleri fark edilemeyecek düzeyde yakın olsa da çok veri içeren veri setlerinde ve çok daha fazla parametreden oluşan modellerde hissedilebilir düzeyde bir hız artışı olacaktır. Örneğin 20 milyon veriden oluşan bir veri seti kullanıldığında (her bir adımda 32 adet veri kullanılmaktadır - *batch size* 32) *epoch* başına *Bidirectional LSTM* modeli *Bidirectional GRU* modeline kıyasla 2 saat 25 dakika daha uzun sürecektir. Bu süre Denklem 1'de eğitim verisi olarak 20 milyon ve *batch size* olarak 32 kullanıldığında hızlıca hesaplanabilir. Burada dikkat edilmesi gereken nokta Denklem 1'in yaklaşık bir süre verdiği, eğitimin gerçekleştirildiği makinenin farklı zamanlarda farklı işlemleri yürütmesinden dolayı eğitim sürelerinde farklılıklar oluşabileceğidir.

$$(Eğitim\ verisi\ \div\ Batch\ size)\ \times Adım\ Süresi(ms)\ \div (1{,}000\ \times\ 60 \times 60) \quad (1)$$

Dikkat edilmesi gereken husus *Unidirectional* modellerin *Bidirectional* eşitlerine göre gösterdiği hız farkıdır. *Unidirectional* modeller eğitim aşamasında 2 kat hızlı gibi görünse de bu modeller ile kullanılan veri seti *Bidirectional* modellerde kullanılan veri setinden 2 kat daha fazla veri içerdiğinden yaklaşık eğitim süreleri ile sonuçlanmıştır (*Unidirectional* modeller eğitilirken her bir eğitim verisinin hem soldan sağa hem de sağdan sola şekilde iki kez kullanıldığı hatırlanmalıdır). Fakat çıkarım safhasında, *Unidirectional* modeller *Bidirectional* eşitlerine göre 2 kat daha hızlı sonuç üretmiş ve neredeyse aynı başarı sonuçlarını göstermiştir. Buradan hareketle, bu problem özelinde, *Bidirectional* modeller kullanarak çıkarım sürelerini uzatmak yerine verilerin ters sıradaki eşitlerini de içeren iki kat daha büyük bir veri seti ile eğitilmiş *Unidirectional* modeller kullanılması daha uygun görülmektedir. Ayrıca, yine bu problem özelinde, *LSTM* modelleri yerine *GRU* modellerinin kullanılması, Denklem 1 kullanılarak hesaplandığı gibi büyük veri setleri ile çalışıldığında eğitim sürelerini kayda değer ölçüde azaltmaktadır. Bu sonuçlardan hareketle en uygun model görüleceği üzere *Unidirectional GRU* modelidir. Modellerin başarı oranlarını görsel olarak da betimlemek amacıyla karmaşıklık matrisi Görsel 3'te görüldüğü üzere oluşturulmuştur:

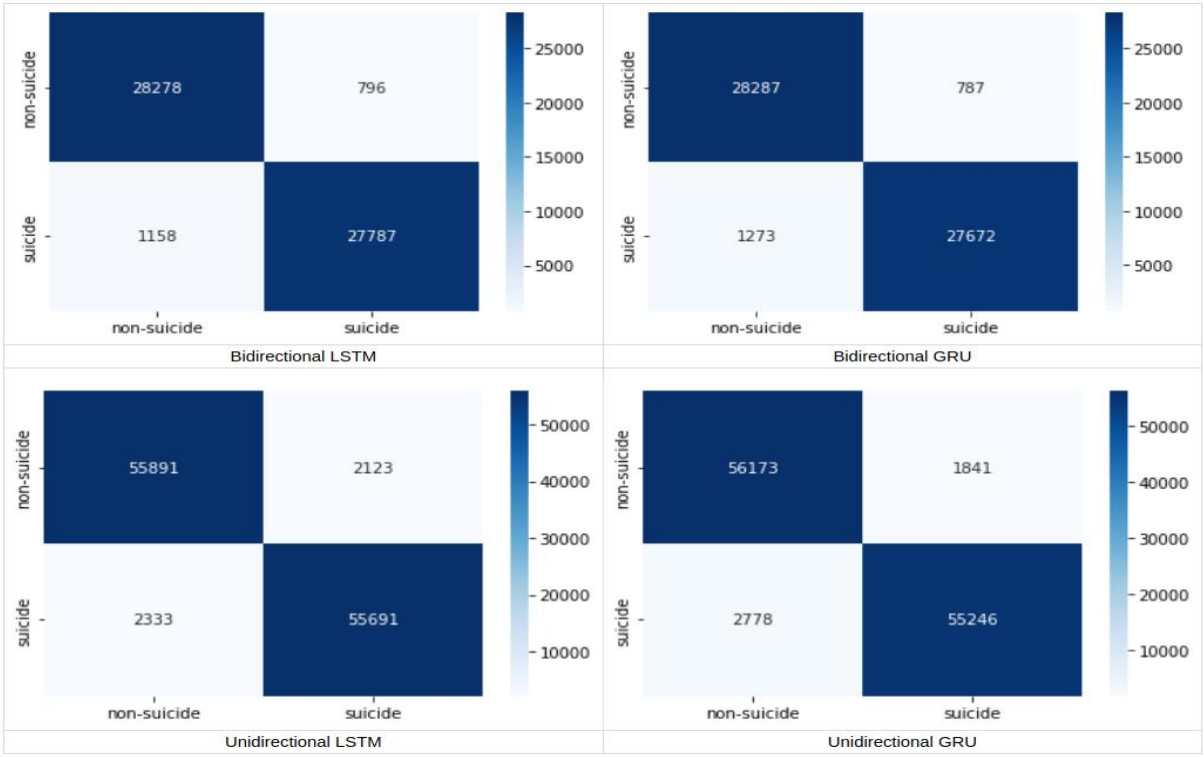

Görsel 3. Modellerin Karmaşıklık Matrisleri

Karmaşıklık matrisinden de anlaşılacağı gibi eğitilen modellerin tamamı, veri setindeki sınıfları başarılı bir şekilde sınıflandırabilmiştir. Bu değerler ışığında Çizelge 3'te paylaşılan diğer metrikler de kolayca hesaplanabilmektedir. Karmaşıklık matrisine ek olarak ROC-AUC eğrisi değerleri ise Görsel 4'te görüldüğü gibi olmaktadır:

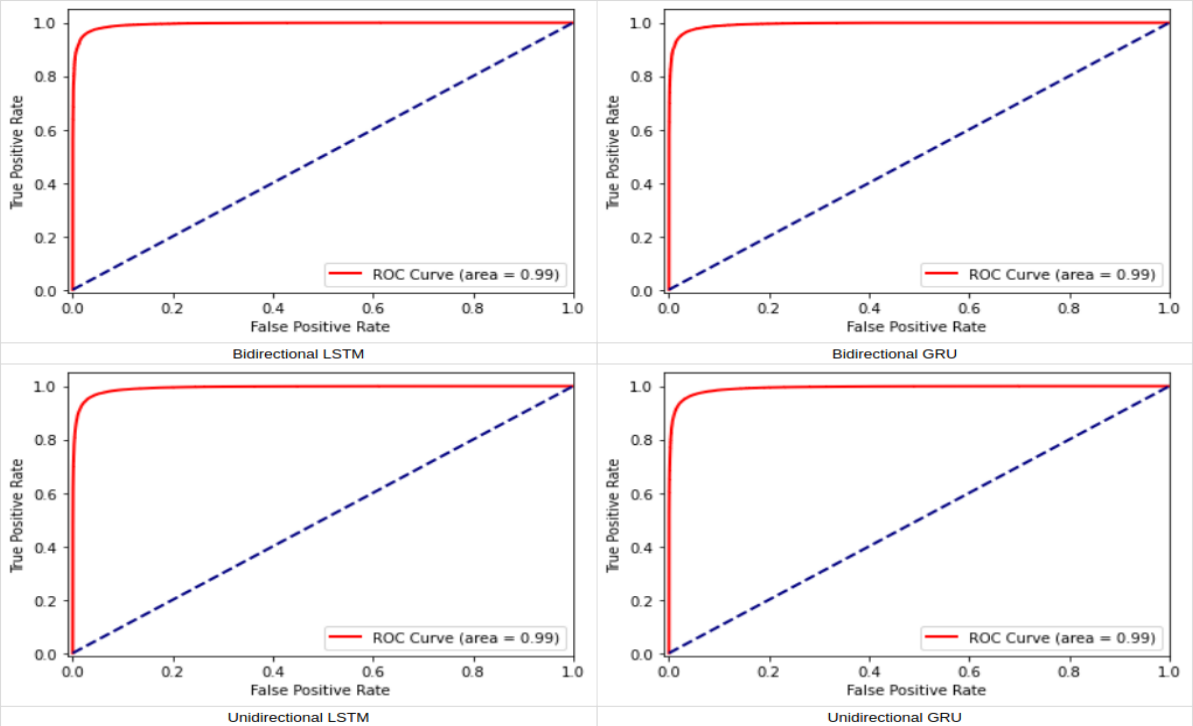

Görsel 4. ROC-AUC Eğrisi Değerleri

Aynı şekilde, Görsel 4 ile de modellerin başarı düzeyleri rahatlıkla görülebilmektedir. Eğitilen tüm modeller benzer doğruluk değerleri gösterdiğinden, ROC-AUC eğrisi değerleri de birbirinin aynısı (%99) olarak sonuçlanmıştır.

5. SONUÇ

Depresyon, artık günümüz dünyasının önemli bir problemi haline gelmiştir. Bu durumun önceden tespiti ise tartışmasız bir şekilde bugünde olduğu gibi gelecekte de önemini koruyacaktır.

Bu çalışma ile modern derin öğrenme mimarileri ve teknikleri sayesinde depresyon belirtisi gösteren kişilerin sosyal medya platformlarındaki metinsel paylaşımları kullanılarak depresyon hallerinin tespiti gerçekleştirilmiştir. Hali hazırda var olan tekniklere ek olarak çalışma kapsamında daha az parametreli ve bu sayede hızlı çalışan ama buna oranla çok parametreli modeller kadar başarı gösteren modellerin eğitimi için kullanılabilecek bir veri artırma tekniği de kullanılmıştır. Her ne kadar bu teknik çalışmanın konusunu oluşturan problemin çözümünde başarı göstermiş olsa da tekniğin başka benzer problemler üzerinde aynı başarı itkisi görevini göreceği henüz net olarak ortaya konulmamıştır. Bu sebeple bahsi geçen teknik *Bidirectional* modellerin kullanılabildiği ve/veya cümle içerisindeki kelimelerin sırasının etkili olduğu birçok problemde uygulanabilir olsa da beklenildiği üzere problemi çözmeyi garanti etmez. Bir doğruluk artışı sağlamadığı gibi hali hazırda var olan hesaplama yüküne ilave bir yük de ekleyebileceği unutulmamalıdır. Fakat problemin yapısı, oluşturulan makine öğrenmesi/derin öğrenme modelinin mimarisi, eldeki veri seti gibi bazı koşullar doğru bir şekilde sağlandığı takdirde, tekniğin sağladığı yarar göz ardı edilesi değildir.

Her ne kadar depresyon, sosyal medya üzerinde kendini sıklıkla metinsel paylaşım yoluyla gösterse de metin paylaşımından ziyade başka iletişim yöntemlerinin daha yoğunlukta olduğu sosyal medya platformlarında da depresyon tespiti yapılması yararlı olacaktır. Örneğin kişinin sesli ve/veya görüntülü, görsel, video ve benzeri paylaşımlarından da depresyon tespiti yapılması mümkündür. Hatta etkileşime girdiği diğer paylaşımlar bile depresyon tespiti için kullanılabilir olmaktadır. Bu çalışma kapsamında, sosyal medyadaki paylaşımların çoğunluğunu oluşturan metinsel paylaşımlar tercih edilmiş olsa da gelecek çalışmalarda bahsi geçen diğer veriler de kullanılıp farklı modeller bir araya getirilerek daha kesin ve net bir sınıflandırma yapılabilir, yapılması daha uygun düşecektir.

Sonuç olarak makine öğrenmesi artık günlük yaşantının vazgeçilmez bir parçası haline gelmeye başlamıştır. Yalnızca depresyon tespitinde değil, hayatın birçok başka noktasında kolaylaştırıcı çözümler üretebilme potansiyelini de içerisinde taşımaktadır ve bu potansiyel ile umut vadeden bir gelecek inşa etmek mümkündür.

KAYNAKÇA

[1] We are Social. Digital in 2018. (Erişim Tarihi: 28.04.2022)

[2] A. Priya, S. Garg, N.P. Tigga, Predicting anxiety, depression and stress in modern life using machine learning algorithms, Procedia Computer Science 167 (2020)1258–1267. April, 16, 4, 2020

[3] N.S. Srimadhur, S. Lalitha, An end-to-end model for detection and assessment of depression levels using speech, Procedia Computer Science 171 (2020) 12–21, June, 4, 6, 2020

[4] What Is Depression. (Erişim Tarihi: 28.04.2022)

[5] Michael Mesfin Tadesse, Hongfei Lin, Bo Xu and Liang Yang, Detection of Suicide Ideation in Social Media Forums Using Deep Learning, December, 24, 12, 2019

[6] Li-Chen Cheng and Song-Lin Tsai, Deep Learning for Automated Sentiment Analysis of Social Media, August, 27-30, 8, 2019

[7] Tomas Mikolov, Kai Chen, Greg Corrado, Jeffrey Dean, Efficient estimation of word representations in vector space, [cs.CL] September, 7, 8 2013

[8] Depression and Suicide Analysis Using Machine Learning and NLP, Pratyaksh Jain et al 2022 J. Phys.: Conf. Ser. 2161 012034

[9] Sepp Hochreiter, Jürgen Schmidhuber, Long Short-Term Memory, Neural Computation 9(8):1735-1780, November, 1, 11, 1997

[10] Dzmitry Bahdanau, KyungHyun Cho, Yoshua Bengio, Neural machine translation by jointly learning to align and translate, ICLR 2015, May, 19, 5, 2016

[11] Mike Schuster and Kuldip K. Paliwal, Bidirectional recurrent neural networks, IEEE Transactions on Signal Processing 45(11):2673 - 2681, December, 1, 12, 1997

[12] Suicide and Depression Detection dataset, Kaggle (Erişim Tarihi: 05.04.2022)

[13] Pushshift.io, Learn About Big Data and Social Media Ingest and Analysis